UNIVERSITA' DEGLI STUDI DI MILANO

DIPARTIMENTO DI CHIMICA
PhD COURSE IN INDUSTRIAL CHEMISTRY, XXXI CYCLE

Rational design and synthesis of small molecules targeted against neurodegenerative processes and diseases

CHIM/06 Organic Chemistry

Davide GORNATI
R11404

Tutor: Prof. Dr. Pierfausto SENECI (Università degli studi di Milano)
Co-Tutor: Dr. Leonardo MANZONI (CNR-Istituto di Scienze e Tecnologie Molecolari)

Co-ordinator: Prof. Dr. Maddalena PIZZOTTI

A.Y. 2017/2018

GENERAL INTRODUCTION

Improved sanitary conditions, disease prevention (e.g., vaccinations) and treatment (e.g., antibiotics) have increased life expectancy, up to the 67.2 years value in 2010 [1]. Unfortunately, living longer a poor life does not represent anyone's dream, mostly due to neurodegenerative diseases (NDDs). Alzheimer's Disease International (ADI) estimates in its 2013 report [2] that there are more than 35 million people with dementia worldwide as of 2010, and that this number will double by 2030 and triplicate by 2050. In industrialized countries the prevalence of Parkinson's disease (PD) is about 1% for people over 60, with estimates of up to 4% for people in the highest age groups [3]. In 2016 the Centres for Disease Control and Prevention estimated that between 14,000 - 15,000 Americans suffered from Amyotrophic Lateral Sclerosis (ALS).

These and other NDDs are the result of neurodegenerative processes [4], that entail the progressive loss of structure or function of neurons, eventually causing their death. Symptomatic treatment strategies available on the market for NDDs are inadequate, as they offer only temporary relief without changing the ultimate NDD outcome [5].

Reduction in the activity of the cholinergic neurons, for instance, is a well-known feature of Alzheimer's disease (AD) [6], so that the most common approach against the progression of AD is based on acetylcholinesterase inhibitors (donepezil **1,** tacrine **2**, rivastigmine **3** and galantamide **4**) to increase the concentration of acetylcoline (ACh) in the brain and balance its loss caused by the death of cholinergic neurons [7]. Excitotoxicity is observed in AD and other NDDs such as Parkinson disease (PD) and multiple sclerosis (SM) [6], entailing the overstimulation of glutamate receptors (also known as *N*-methyl-D-aspartate receptors, NMDArs), by glutamate, an excitatory neurotransmitter of the nervous system. Memantine **5** is a non-competitive NMDAr able to reversibly block these receptors and to inhibit their overstimulation [8, 9].

Tetrabenazine **6** [10] was the first approved drugs in 2000 as a symptomatic treatment of hyperkinetic movement disorders in Huntington disease [11]. Benzodiazepines and neuroleptics are other symptomatic drugs that help to reduce chorea, the abnormal involuntary movement disorder [12].

Medications, surgery, and physical treatment can provide relief for PD patients. Motor symptoms of PD result from reduced dopamine production in the brain's basal ganglia. Levodopa **7** (a precursor of dopamine) has been widely used as a symptomatic PD treatment for over 40 years [13]. Another approach is based on dopamine agonists that bind to dopamine receptors in the brain with similar effects to levodopa [13]. Among them, bromocryptine **8**, pergolide **9**, pramipexole **10**, ropinirole **11**, Pyribedil **12** and cabergoline **13**. Dopamine levels may be increased by inhibiting the activity of monoamine oxidase B (MAO-B), an enzyme which breaks down dopamine, or of catechol-*O*-methyltransferase (COMT, an enzyme that degrades catecholamines and other catechols) [14]. Tolcapone **14** and entacapone **15** are COMT inhibitors, while safinamide **16**, selegiline **17** and rasagiline **18** are inhibitors of MAO-B.

ALS is a severe, poorly addressable NDD [15]. Riluzole **19** has been found to modestly extend survival by about 2-3 months [16, 17]. It seems to decrease the release of the excitatory neurotransmitter glutamate from pre-synaptic neurons, with a poorly understood mechanism of action (MoA) [18]. Edaravone **20** was approved for ALS in the US in 2017, based on a small randomized controlled clinical trial with early-stage ALS patients in Japan. The drug is an antioxidant, and oxidative stress has been hypothesized to be part of the process that kills neurons in ALS patients [19, 20].

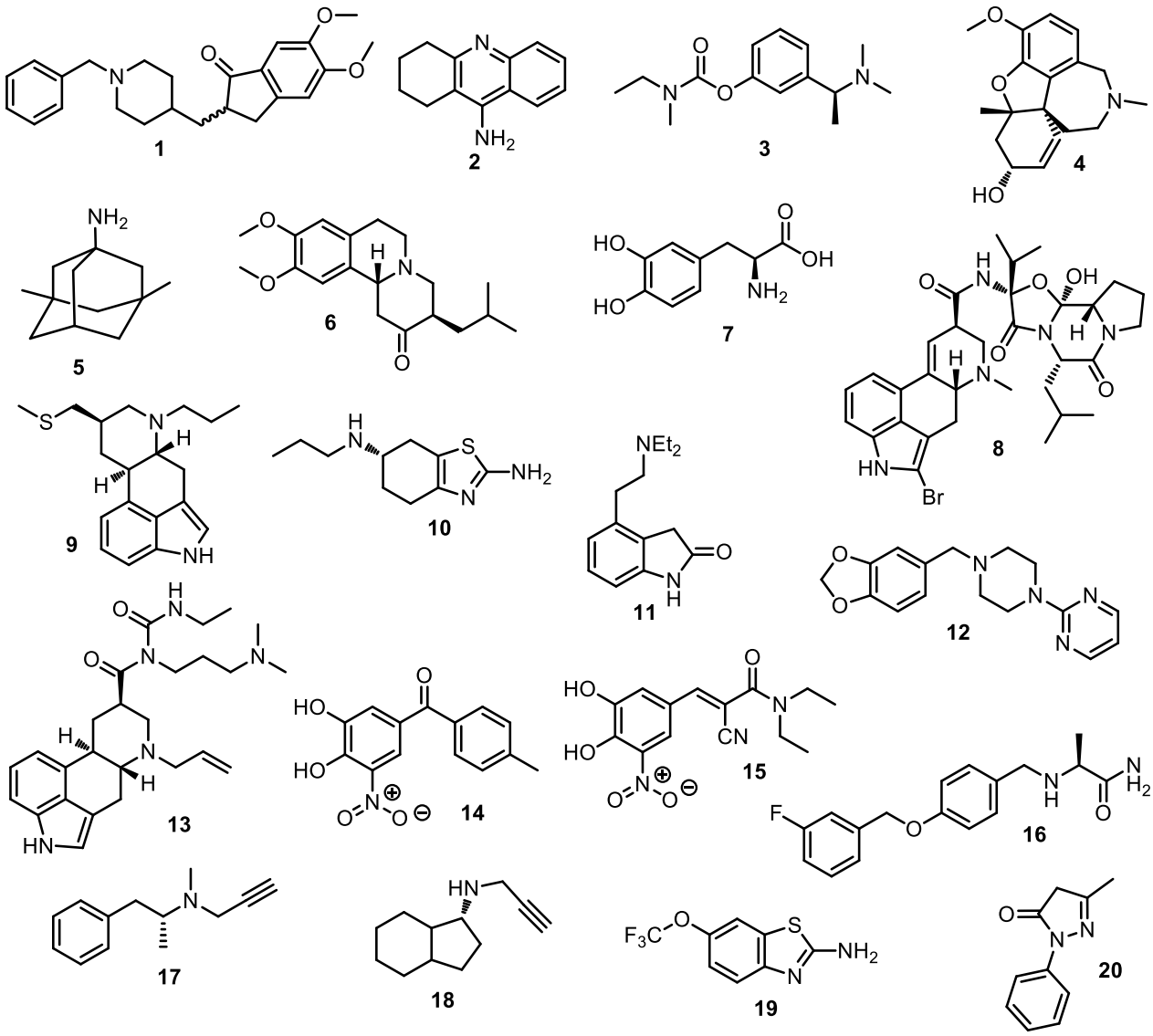

Figure 1. Symptomatic treatments of common NDDs.

Effective treatment of NDDs should be based on small molecules able to modulate disease-modifying pathways involved in the development and/or the progression of NDDs, to cause their remission. In my Ph.D. work I focused on four different pathways (each described in a Chapter) involved in the development of multiple NDD. With the aim to therapeutically modulate them by promoting and/or inhibiting those targets I've rationally designed and synthetized several classes of compounds. My research group established a multi-disciplinary approach in collaboration with bioinformatics, biologists, pharmacologists and clinicians; thus, my putative NDD treatments were tested by our co-workers in different Universities and Institutes (CIBIO, university of Trento; San Raffaele Research Institute, Milan; Department of Neuroscience, Federico II University, Naples).

The first chapter of my Ph.D. thesis (pg. 05-87) focuses on the modulation of the vesicular delivery system between endosomes and the trans-Golgi network (TGN), a pathway dysregulated in several NDDs [21]. Starting from a recently discovered small molecule modulator, and assisted by computational studies (IBF-CNR, Milan, Dr. Milani), I have synthetized a family of novel small molecules able to stabilize a protein complex involved in this MoA, thus increasing cell-survival in a cellular model of ALS (San Raffaele Research Institute, Dr. Muzio). A lead compound was submitted to in vivo PK/PD and efficacy testing in a mouse model

of ALS, with promising preliminary results. A patent was recently filed by San Raffaele Research Institute and UniMI.

Chapter 2 (pg. 88-127) focuses on the modulation of the rate and the quality of protein synthesis, a crucial affected mechanism in most of the ≈600 characterized NDDs, in order to avoid the accumulation, aggregation and precipitation of mis-folded amyloidogenic proteins [22, 23]. I've targeted the design and synthesis of putative disease-modifying agents targeting two validated MoAs, to possibly synergize their action and influence the pathogenic process. Thus, I've synthetized three different hybrids that contain two portions active as protein misfolding/aggregation preventers through different MoAs. Their biological characterization is under way (CIBIO – Trento University, Prof. Piccoli), and preliminary results will be discussed.

Chapter 3 (128-172) is focused on the induction of the autophagy, a well-know self-degradation process of cellular components suitable to promote the clearance of amyloidogenic proteins [23]. This strategy initially focused on trehalose [24, 25], a naturally occurring disaccharide with known anti-aggregating properties, that was modified in order to both clarify its molecular chaperone MoA, and to increase its bioavailability (in collaboration with CIBIO, Trento University, Prof. Piccoli). Eventually, other putative autophagy inducers were identified and characterized, leading to the identification of a putative new molecular target for a well-known small molecule with neuroprotective activity.

In the last Chapter (173-227) I've focused on a validated biological target family, named Acid Sensitive Ionic Channels (ASICs) [26], that are not usually pursued against NDDs. However, as the effect of ASICs in pathological conditions (acidosis for instance, observed in different NDDs) could enhance the degeneration of neuronal cells [27], and I rationally designed (with computational support from IBF-CNR, Dr. Mastrangelo) synthesized a small library of novel ASICs antagonists, based on a known ASIC inhibitor. These compounds were characterized in collaboration with the Neuroscience Dept. At Federico II University (Prof. Annunziato). Very promising preliminary results were obtained and will be described here.

Each Chapter in this Ph.D. thesis is divided in five Sections:

1) A short introduction on the pathway and of the biological targets involved;

2) The description of the chemical routes used for the preparation of the small molecules;

3) Their virtual and tangible characterization (in-silico docking, in vitro and sometimes in vivo profiling);

4) A critical evaluation of project results, and planned future activities;

5) An experimental part reporting in details the synthesis, the purification and the analytical characterization of each intermediate and of each final, targeted small molecule.

[1]. https://www.cia.gov/library/publications/the-world-factbook/rankorder/2102rank.html
[2]. http://www.alz.co.uk/research/WorldAlzheimerReport2013ExecutiveSummary.pdf
[3]. De Lau, L.M.; Breteler, M.M. Epidemiology of Parkinson's disease. *Lancet Neurol*. **2006**, 5, 525-535.
[4]. Nieoullon, A. Neurodegenerative diseases and neuroprotection: current views and prospects. *J. Appl. Biomed*. **2011**, 9, 173-183.
[5]. Seneci, P. Molecular targets in protein misfolding and neurodegenerative disease. *Academic Press,* San Diego, **2014**, 314 pages.
[6]. Geula, C.; Mesulam, M.M. Cholinesterases and the pathology of Alzheimer disease. *Alzheimer Dis. Assoc. Disord.* **1995**, 9 Suppl. 2, 23–28.
[7]. Stahl, S.M. The new cholinesterase inhibitors for Alzheimer's disease, part 2: illustrating their mechanisms of action. *J. Clin. Psyc*. **2000**, 61, 813–814.
[8]. Lipton, S.A. Paradigm shift in neuroprotection by NMDA receptor blockade: memantine and beyond. *Nat. Rev. Drug Discov.* **2006**, 5, 160–170.
[9]. "Memantine". *US National Library of Medicine (Medline),* **2004**.
[10]. Huntington's Disease Information Page: National Institute of Neurological Disorders and Stroke (NINDS)". NINDS, **2016.**
[11]. Jankovic, J.; Beach, J. Long-term effects of tetrabenazine in hyperkinetic movement disorders. *Neurology* **1997**, 48, 358–362.
[12]. Huntington Disease. *Gene Reviews bookshelf*. University of Washington, **2007.**
[13]. The National Collaborating Centre for Chronic Conditions. "Symptomatic pharmacological therapy in Parkinson's disease". *Parkinson's Disease*. Royal College of Physicians., London, **2006**, 59–100.
[14]. Axelrod, J.; Tomchick, R. Enzymatic O-methylation of epinephrine and other catechols. *J. Biol. Chem*. **1958**, 233, 702–705.
[15]. Amyotrophic Lateral Sclerosis (ALS) Fact Sheet. *Nat. Inst. of Neurol. Disorders and Stroke*. **2014.**
[16]. Miller, R.G.; Mitchell, J.D.; Moore, D.H. Riluzole for amyotrophic lateral sclerosis (ALS)/motor neuron disease (MND). *Cochrane Database Syst. Rev.* **2012**, Issue 3.
[17]. Carlesi, C.; *et al.* Strategies for clinical approach to neurodegeneration in amyotrophic lateral sclerosis. *Arch. Ital. Di Biol.* **2011,** 149, 151–167.
[18]. Hardiman, O.; *et al.* Amyotrophic lateral sclerosis. *Nat. Rev. Dis. Prim.* **2017**, 3, 17071.
[19]. Miyaji, Y.; *et al*. Effect of edaravone on favorable outcome in patients with acute cerebral large vessel occlusion: subanalysis of RESCUE-Japan Registry. *Neurol. Med. Chir.* **2015**, 55, 241–247.
[20]. Petrov, D.; Mansfield, C.; Moussy, A.; Hermine, O. ALS Clinical Trials Review: 20 years of failure. Are we any closer to registering a new treatment? *Front. Aging Neurosci*. **2017**, 9, 68.
[21]. Schreji, A.M.; Fon, E.A.; Mc Pherson P.S. Endocytic membrane trafficking and neurodegenerative disease. *Cell. Mol. Life Sci*. **2016**, 73, 1529-1545.
[22]. Bossy-Wetzel, E.; Scharzenbacher, R.; Lipton, S.A. Molecular pathways to neurodegeneration. *Nat. Med*. **2014**, 10, S2-S9.
[23]. Forman, M.S.; Trojanowski, J.Q.; Lee, V.M.-Y. Neurodegenerative diseases a decade of discoveries paves the way for therapeutic breakthroughs. *Nat. Med.* **2004**, 10, 1055-1063.
[24]. Sarkar, S.; Davies, J.E.; Huang, Z.; Tunnacliffe, A.; Rubinsztein, D.C. Trehalose, a novel MTOR independent autophagy enhancer, accelerates the clearance of mutant huntingtin and a-synuclein. *J. Biol. Chem.* **2007**, 282, 5641-5652.
[25]. Mardones, D.; Rubinsztein, C.; Hetz, C. Mystery solved: Trehalose kickstarts autophagy by blocking glucose transport. *Sci. Signal*. **2016**, 9, fs2.
[26]. Waldmann, R.; Champigny, G.; Bassilana, F.; Heurteaux, C.; Lazdunski, M. A proton-gated cation channel involved in acid-sensing. *Nature* **1997**, 386, 173–177.
[27]. Vergo, S.; *et al.* Acid-sensing ion channel 1 is involved in both axonal injury and demyelination in multiple sclerosis and its animal model. *Brain*, **2011**, 134, 571-584.

Chapter I

Small molecules as neuroprotective retromer-stabilizing agents

INDEX

INTRODUCTION

1.1.1. The endosomal network: sorting and delivery of intra- and extra-cellular cargos

Eukaryotic cells are sectioned by distinct membrane-enclosed compartments containing their own characteristic set of enzymes and molecules. The functionality of each compartment is determined by the proteins within, and can be used to classify the role of each organelle. Hence, a finely regulated transport system is required to deliver macromolecules and substances to the correct organelle.

There are diverse strategies to distribute different types of proteins towards their destination within the cell. Sorting signals defined by amino acids sequences are essential to address correctly each organelle [1].

Endocytosis is the general term defining the internalization of fluid, solutes, macromolecules, plasma membrane components and particles by invagination of the plasma membrane and formation of vesicles and vacuoles through membrane fission [2]. This process is involved in numerous pathways in the cell, regulating the sorting, processing, recycling, storing and degrading of various substances and macromolecules. Due to the significance of endocytosis in cell metabolism, a fine tuning and regulations evolved to properly sort the vesicles and their cargos [2].

1.1.2. The logistics of the endosome system

Vesicles are formed by an enlargement of an existing membrane containing the cargo, and then by merging with another compartment. The fusion only occurs in topologically equivalent compartments recognized by sorting receptors on the cytosolic surface of the membrane. A single protein can contain different signal sequences which can interact with complementary receptors on the membrane surface. Each signal sequence specifies a precise destination in the cell. Most transport vesicles bud off with proteins covering their cytosolic surface and forming a distinctive cage. The coat performs two main functions, by selecting the appropriate molecules for transport and sculpting the forming vesicle [1].

The endocytic pathway can be partitioned in a *recycling* circuit for plasma membrane components and their ligands, and a *degradative* system for digestion of macromolecules. Both are connected by a unidirectional feeder pathway, transporting selected membrane components from the recycling circuit to the degradative system. The feeder function is mediated by endosomes, which also exchange lysosomal components from the trans Golgi network (TGN) to lysosomes [2].

Early endosomes (EE) are defined as the first endocytic compartments to accept incoming cargo internalized from the plasma membrane (PM), and are highly dynamic structures. They are composed by thin tubular extensions and large vesicles that have membrane invaginations shaping them to a multi-vesicular appearance. The junction of endosomes between endocytic and biosynthetic pathways is determined by retrograde transport of cargo to the TGN [3].

Most cargos internalized by endocytosis within EEs are recycled back to the plasma membrane (top, Figure 1, *recycling endosome*), so that the transport to lysosomes via late endosomes (LEs) is a minor pathway limited to a relatively small fraction of internalized membrane components. Also, LEs transport new lysosomal hydrolases and membrane proteins to lysosomes for maintenance and amplification of the degradative compartment. The transition from EEs to lysosomes depends on the cargo. The EEs' content being processed is retained within the vesicle, completing the EE to LE transformation, while the other

compounds and macromolecules are recycled back at the beginning of the process. The functionality of EEs is defined by associated proteins on the cytosolic surface of the vesicle. Maturation of the EEs require the exchange of proteins, such as hydrolases, which are provided by TGN through bidirectional vesicle exchange [2].

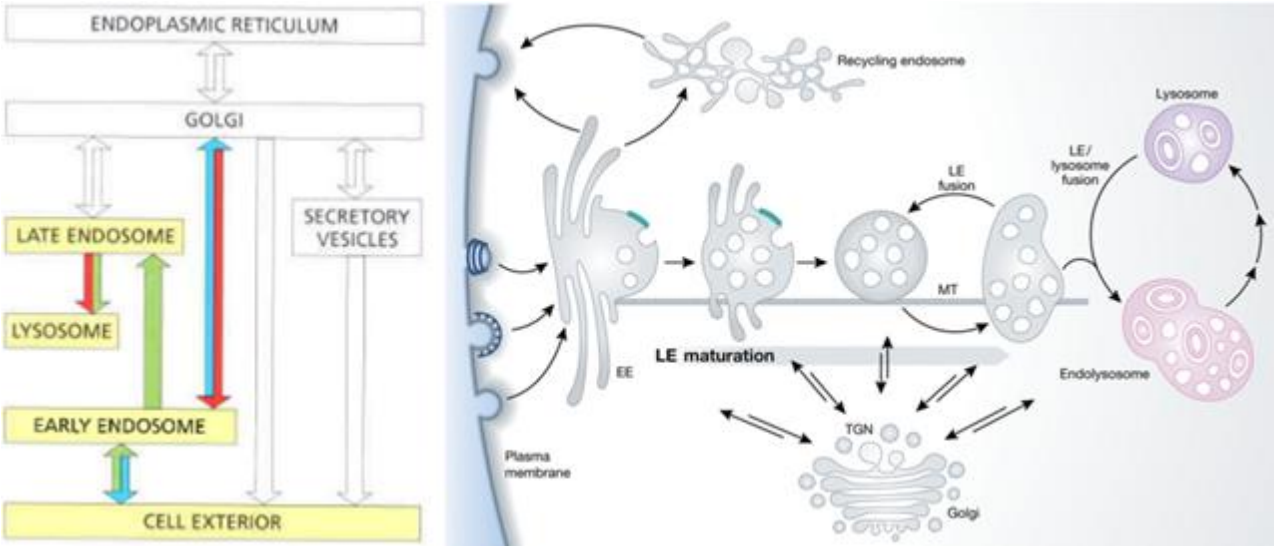

Figure 1. Left: presumed exchange pathways between endosomes and the trans-Golgi network (TGN). Right: endocytic pathways associated with maturation of early endosomes (EEs) to late endosomes (Les) and lysosomes.

The path from EEs to the TGN is nevertheless mediated by specialized protein coat assemblies that form patches dedicated to specific cargo proteins. One of the most characterized complexes is the retromer, which returns acid hydrolase receptors such as the mannose-6-phosphate receptor (M6P) [4] and other proteins from endosomes to TGN or to the cell membrane, and will be explained in details later. The exchange of substances between TGN and EEs is continuously ongoing, defining a central role of TGN in EEs maturation. The pathway is elusive because the organelles are scattered, and undergo continuous maturation, transformation, fusion, and fission [2]. To ensure a coordinated flow of vesicular traffic, specific surface markers, like Rab proteins, identify vesicles according to their origin and type of cargo, and target membranes displaying complementary receptors by assembling different regions on the membrane. Subsequently to the recognition of the matching membrane, SNARE proteins mediate the fusion of the lipid bilayers.

Rab proteins are the biggest GTPase subfamily and each of them is associated with one or more membrane enclosed organelles [5]. Each organelle shows at least one Rab protein on its cytosolic surface. Due to their distribution and specificity, Rab proteins are ideal molecular markers to identify membranes involved in the vesicular traffic. Rab proteins bind to membranes using GTP-bound lipids as anchors, which upon binding recruit other proteins named Rab effectors, and carry out vesicle transport, membrane tethering and fusion.

The transition from EEs to LEs can be followed by monitoring the exchange of Rab5 to Rab7. Rab5 assembles on endosomal membranes and mediates the capture of clathrin-coated vesicles from the plasma membrane [2]. Another function of Rab5 is the activation of PI3-kinase, which locally converts phosphatidylinositol (PtdIns) to phosphatidylinositol-3 phosphate (PtdIns3P), allowing the binding Rab effectors to establish functionally distinct membrane domains that fulfil different functions within a fully formed membrane.

The retromer complex is recruited during the exchange between Rab5 and Rab7 [6], recognizing unbound M6Ps. This indicates that the cargo is released within the vesicle, so that the receptor must be retrieved back to the TGN to deliver another cargo [1]. It is reasonable to assume that this mechanism involving retromer

and M6Ps is common to all retromer cargos. During the maturation to LEs, the vesicles move from the peripheral cytoplasm to the nuclear area, finally becoming lysosomes [2].

Dysfunction in endocytic membrane trafficking is a recurrent theme in NDDs [7]. The morphology of neurons, consisting of long processes extending far beyond the cell soma, requires an accurate and coordinated delivery of proteins and lipids to their final destination. Proximal and distal dendrites, axonal growth cones, and synapses rely on controlled membrane trafficking from the biosynthetic and endosomal compartments. Functional alterations in membrane trafficking proteins may cause dysfunctions in downstream membrane trafficking, and an accumulation of dysfunctional proteins and organelles, followed by neuronal vulnerability and cell death.

1.1.3. The Retromer complex: molecular insights

The retromer is a protein coat that mediates endosomal protein sorting and trafficking between cell compartments (Figure 2). It assembles during the transition from EEs to Les [6], and forms tubular vesicles in membranes rich of phosphatidylinositol 3,5-diphosphate (PtdIns(3,5)P2) [3] that return specific trans-membrane proteins to the plasma membrane or to the TGN [8].

The retromer is composed by an heterotrimeric Vps26 (38 KDa), Vps29 (20 KDa) and Vps35 (92 KDa) complex named Cargo Selective Complex (CSC) [9], and by different combinations of sorting nexin (SNX) proteins that contribute to membrane recruitment and formation of the recycling tubules [10] (Figure 2 and 3).

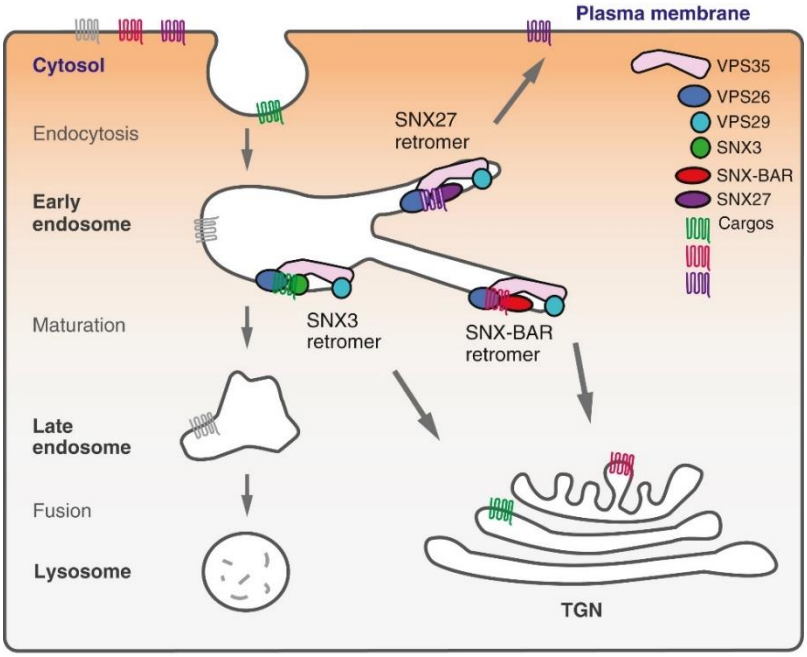

Figure 2. Schematic representation of retromer trafficking between cell compartments.

The association of the cargo recognition core with endosomes follows the assembly of SNXs [10]. In mammals, only six SNXs are known to interact with retromer: SNX1 and SNX2 [10], SNX3 [11], SNX5 and SNX6 [12], and SNX27 [13]. Whereas SNXs can be recruited to endosomes independently from the CSC, they are essential for the retrieval of the associated cargo [10]. SNX3 presents a phox-homology (PX) domain which interacts primarily with phosphatidylinositol 3-phosphate (PtdIns3P). This phospholipid is enriched in EE-directing recruitment of cytosolic proteins. SNX1, SNX2, SNX5 and SNX6 contain a membrane-curvature-sensing the Bin-amphiphysin Rvs (BAR) domain, which is important for the correct engagement of the retromer complex and tubulation (Figure 3) [8].

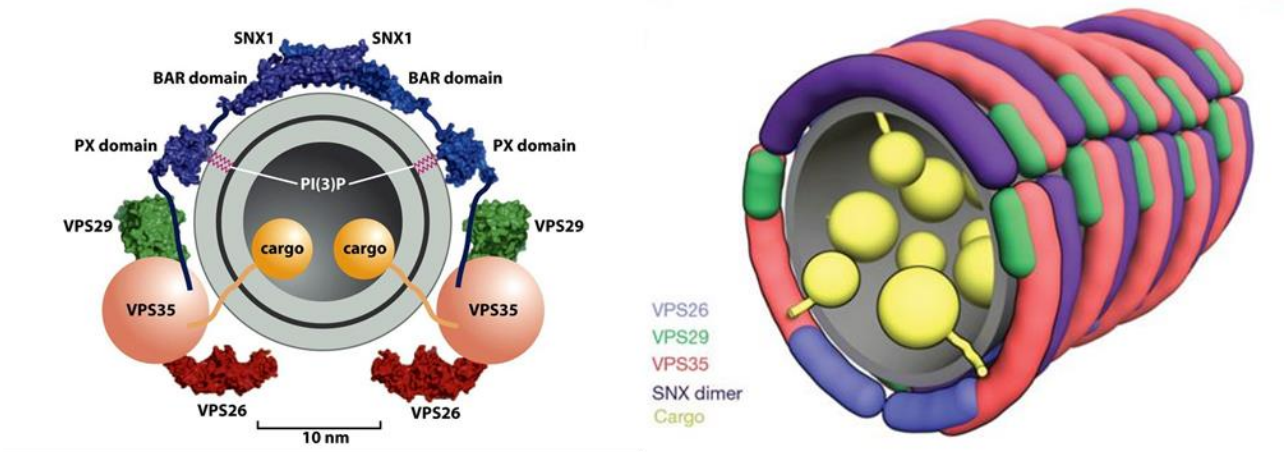

Figure 3. Representation of the assembly of the retromer complex during tubulation.

Each SNX is involved in different trafficking pathways, selecting the cargo transported by the retromer. Cargos include cellular transmembrane proteins, such as signalling receptors, ion channels, transporters, or enzymes. The association of SNXs to their cargo is defined by sorting signals in the amino acidic sequence. For example, SNX1 and SNX2 interact with CIMPR and sortilin [10, 14], SNX27 interacts with β2-adrenergic receptor (β2AR), and with cargos presenting FERM-like and PDZ domains [15], and so on [16].

Due to crystallographic analysis and electron microscopy (Figure 4), further information about the cargo recognition core are available. The equimolar Vps26:Vps29:Vps35 complex is arranged in an elongated structure. The structure of Vps35 exhibits some structural flexibility in the mid-section, and Vps26 and Vps29 can bind to Vps35 independently of one another. This flexibility suggests that the retromer could adapt to the shape of curved tubulovesicular membranes [9].

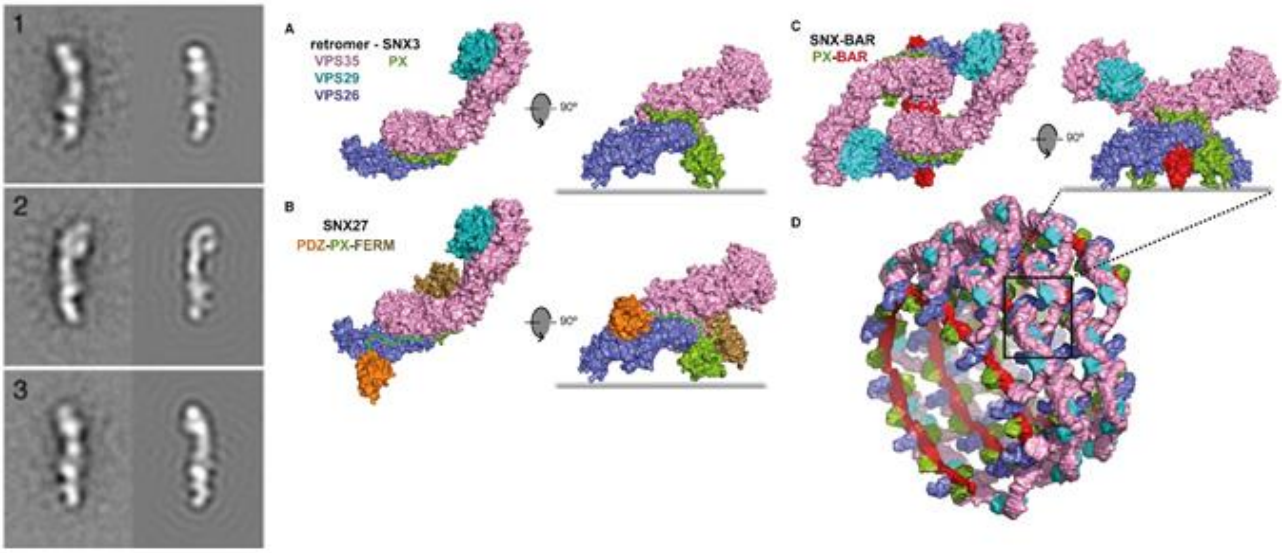

Figure 4. Left: electron microscopy images of the elongated conformation of the CSC complex. Right: retromer structural model obtained from multiple electron density structures.

Vps35 is unstable when expressed without Vps26 or Vps29, and therefore it cannot be crystallized alone. To overcome the problem, a portion of Vps35 was crystallized with either Vps29, or Vps26. The electron density of the Vps29:Vps35 subcomplex, containing ≈40% of the C-terminal Vps35 subunit, highlights the helical solenoid conformation of Vps35 [9]. This type of conformation is recurrent in proteins involved in coated vesicles trafficking and adaptors. The disposition of the alpha helices and their aminoacidic residues highly

suggests potential cargo binding sites, reminiscent of the cation-independent mannose 6-phosphate receptor (CIMPR) binding site [9, 17]. CIMPR contains multiple sorting motifs that direct the transport of membrane proteins between various compartments. This protein binds lysosomal hydrolases, and can be sorted to the endosome by clathrin-coated vesicles with adaptor protein 1 (AP-1), structurally similar to Vps35 [9], and then returned to TGN by the retromer [17].

Vps29 has a phosphoesterase fold which can dephosphorylate the serine residue in the SDEDLL motif of the CIMPR cytoplasmic tail [17]. Vps35 interacts with this region, covering the entire metal-binding site. However, the metal-binding site is not involved in any in vitro (with exception of CIMPR) or in vivo enzymatic activity, rather acting as a scaffold for the stability of Vps29 and the retromer complex [9]. It is also reported that SNX1 and SNX2 interact with Vps29 and Vps35 [10], suggesting their binding to other retromer components.

The Vps26 crystal structure has been solved with the remaining ≈60% portion of Vps35 [18]. SNX3 was required to crystallize such complex. The structure of Vps35 is in agreement with the structure obtained when complexed with Vps29, confirming that the solenoid conformation is maintained throughout the entire protein. Vps26 interacts at the N-terminal tail of Vps35, and SNX3 binds simultaneously both Vps26 and Vps35. It is known that SNX3 interacts with PtdIns3P using its PX domain [19], which is opposite to the interface between Vps26 and Vps35. This is consistent with the role of SNX3 in retromer recruitment to endosomal membranes. The interaction involves both flexible extensions and rigid segments of the PX domain in a multi-interface association with the Vps26 and Vps35 subunits.

1.1.4. The retromer complex as a putative target against NDDs

The balance between protein degradation and recycling is crucial to cellular homeostasis. There are two options for membrane proteins that enter endosomes: they either remain in the endosomes, which ultimately will lead to lysosomal degradation; or they are recycled.

Retromer malfunctioning can cause several pathological conditions depending on its cargo, placing the retromer activity within a much broader physiological context. The retromer complex was first linked to NDDs by analyzing Alzheimer's disease (AD) brain tissues showing reduced levels of Vps26 and Vps35 [20]. Soon after, other components of the retromer complex were associated to AD such as SNX3 and Rab7 [21] and different sortilin family members [22,23] leading to accumulation of amyloid precursor protein (APP) [24]. Moreover, an involvement of the retromer was found in PD; for example, the D620N mutation of Vps35 in late-onset PD impairs trafficking of cathepsin D, a CIMPR cargo, D due to failure in WASH recruitment [25,26], and in Rab7 leads to sorting defects and deficiency of Vps35 [27].

Altogether, those associations between retromer and NDDs suggest a general mechanism where retromer malfunctioning reduces trafficking of the amyloid precursor peptide (APP) out of endosomes [28]. Hence, cargos reside for longer time in the endosome and are pathogenically processed into neurotoxic fragments [20,24]. With those assumptions is possible to consider the retromer complex as a disease-modifying target for drug discovery against NDDs.

We hypothesize, as others, that increasing the interaction between individual retromer proteins could increase complex stability [29], and could enhance retromer-mediated trafficking and transport. Thus, stabilizing the retromer structure protects it from degradation and increases its steady-state concentration in the cell [30]. As to therapeutic indications, our research team (and in particular, the group at San Raffaele

Research Institute, led by Dr. L. Muzio) was interested to evaluate the potential of retromer stabilizing agents against Amyotrophic Lateral Sclerosis (ALS).

1.1.5. R55: a small molecule stabilizer of the retromer complex with neuroprotective properties

Recently, a small molecule was found to stabilize the retromer complex in vitro [31]. Namely, the bis isothiourea R55 (left, Figure 5) was discovered as a pharmacological chaperone enhancing retromer stability and functionality.

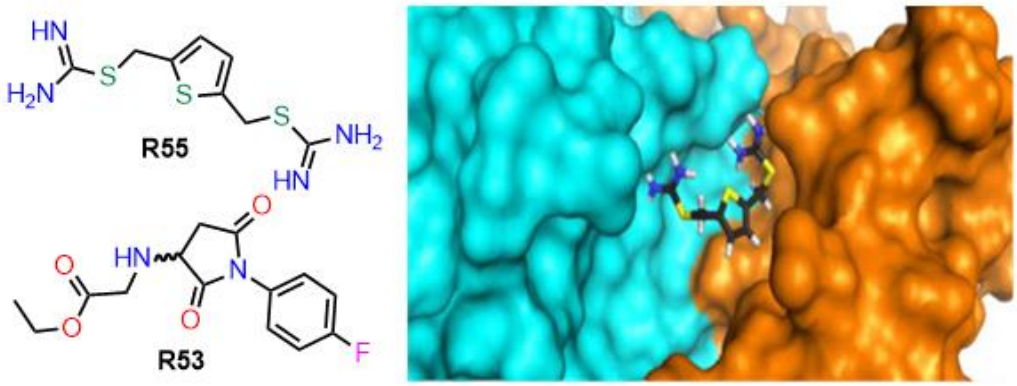

Figure 5. Left: structure of R55 and R53. Right: putative binding mode of R55 at the Vps35-Vps29 interface.

R55 stabilizes CMC *in vitro* (≈10°C increase in denaturation temperature of CMC compared with an inactive compound named R53, Figure 6, left). This is comparable with the thermal stabilization obtained for pharmacological chaperones in clinical trials for the treatment of Gaucher, Fabry and Pompe lysosomal diseases [32]. The ≈10°C increase does not happen with single CMC proteins or with CMC containing a binding site-mutated Vps35 (Figure 6, right).

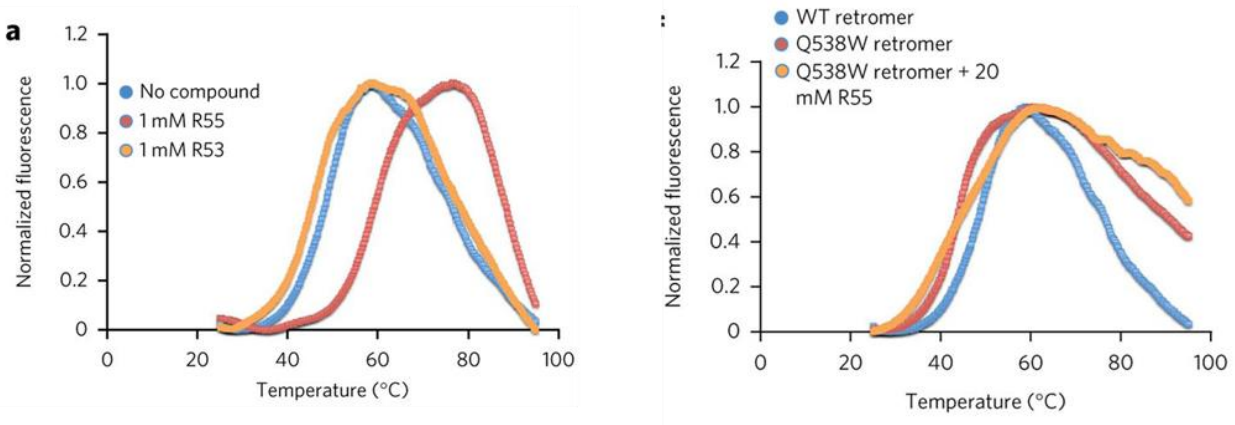

Figure 6. Denaturation temperatures of wild type (WT, left) and binding site-mutated CMC (right) in presence of R55 (active) and R53 (inactive).

In a cell-based assay performed on hippocampal neurons, R55 does not show toxicity up to 50μM, and at 5μM it increases the levels of both Vps35 (≈180%) and Vps26 (≈150%). Furthermore, the mRNA levels of Vps proteins are not affected by R55, indicating that the increase of retromer complex are not due to their expression.

Increased Vps35 levels by genetic manipulation reduce Aβ accumulation [20], due to trafficking of its APP precursor. Accordingly, treatment of either wild-type (WT) hippocampal neurons (Figure 7, left) and hippocampal neurons bearing a pathogenic double APP mutation [33] (Figure 7, right) with R55 (5μM) show significant reduction of pathological $A\beta_{40}$ (respectively 24% and 44%) and $A\beta_{42}$ (respectively 28% and 39%) peptide levels.

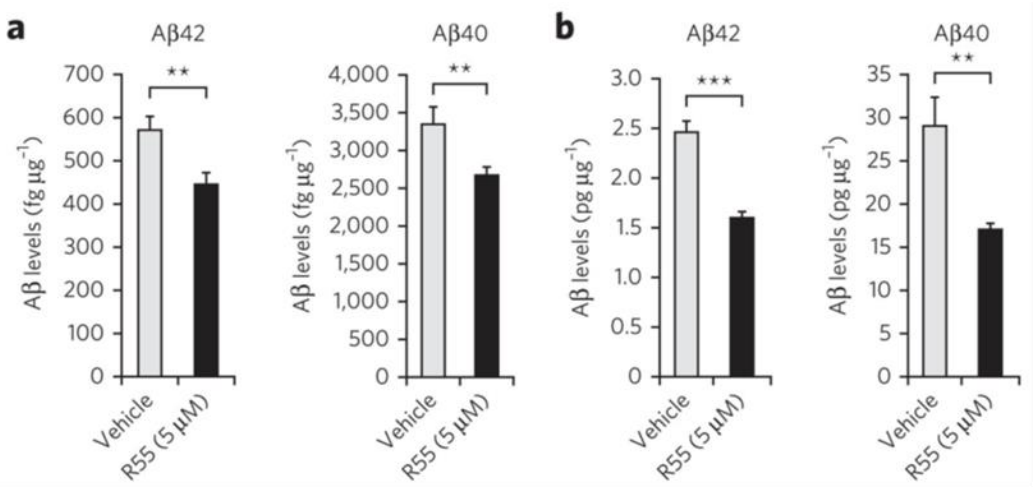

Figure 7. (a) $A\beta_{42}$ and $A\beta_{40}$ levels in WT and (b) APP mutation-bearing hippocampal neurons treated with vehicle, or with R55.

1.1.6. First goal: R55-inspired aryl aminoguanidyl hydrazones as putative CMC stabilizer agents

The structure of putative CMC stabilizer agents reported in this Chapter is inspired by the R55 scaffold, and by its putative binding site; changes were made so to create novel and patentable retromer stabilizers.

Computational studies performed in collaboration with Dr. Mario Milani at IBF-CNR Milan studied the interaction of R55 within the Vps35-Vps29 interface of the retromer complex (retromer complex cohordinates were extracted from a published X-ray structure [31]). This interaction, graphically shown in Figure 8 (two poses of R55 in its binding pocket at the Vps35-Vps29 interface) suggested us i) the importance of a disubstituted ring spacer between the two isothioureas in R55, ii) the possibility to insert substituents on the isothioureas- and/or on the (hetero)aromatic spacer, and iii) the possibility to replace the isothioureas with a positively charged group at physiological pH.

We started by studying the influence of variously disubstituted ring spacers (point i), and the replacement of isothioureas (point iii).

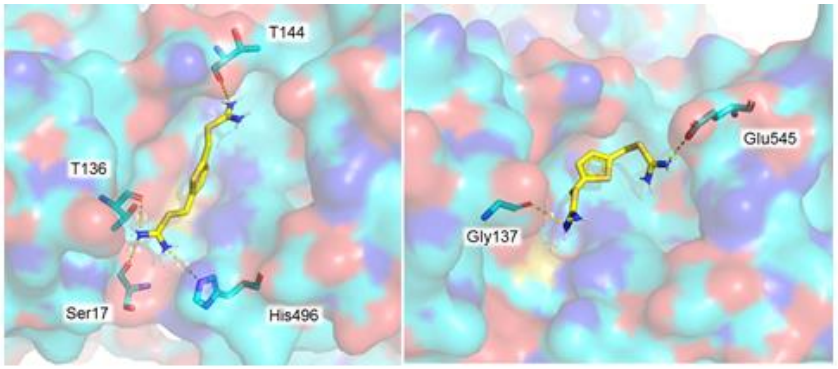

Figure 8. R55 binding to the retromer complex: two binding poses at the Vps35-Vps29 interface.

Accordingly, a small group of molecules was initially synthesized, and in-vitro characterized to select the single, novel scaffold for more systematic future modifications (Figure 9).

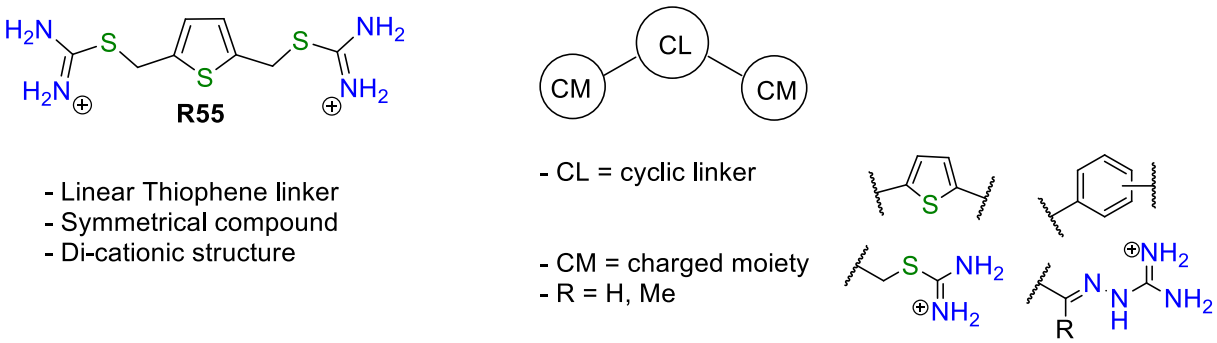

Figure 9. R55 (left), and general structure of putative novel retromer stabilizers (right): structural comparison.

As shown in Figure 8, right, we kept two charged moieties (CM, isothiourea as in R55 or aminoguanidyl hydrazone) spaced with a rigid, conformation-constraining monocyclic (hetero)aromatic linker (CL, 2,5-disubstituted thiophene as in R55 or either m or p-substituted phenyl rings). Aminoguanidyl hydrazones were chosen due to their pKa = 7.9 (i.e., similar to isothioures and bioavailability compliant), their stability and synthetic accessibility, and – most important – their recurrence in biologically active, BBB-permeable drugs (see for example guanabenz [34] and sephin1 [35], Chapter 2). Similar charged moieties such as guanidines or amines were not considered, due to their high pKa values (respectively ≈13 and ≈9).

Six compounds were initially made, by studying the structural variations shown in Figure 8 (their structure and synthesis is reported in Paragraph 1.2.1). They were tested in vitro at San Raffaele Research Institute (Dr. L. Muzio) as Vps35/retromer stabilizers (the biological assay, and the results for these and other putative retromer stabilizers is reported in Paragraph 1.3.1). Out of them, phenyl m-disubstituted aminoguanidyl hydrazone **AG1** (Figure 10, left) resulted to be most active, and was selected as starting point for the synthesis of a small library of novel retromer complex stabilizers. The general structure of 1-inspired m-phenyl aminoguanidyl hydrazones (AGs from now on) is shown in Figure 10, right.

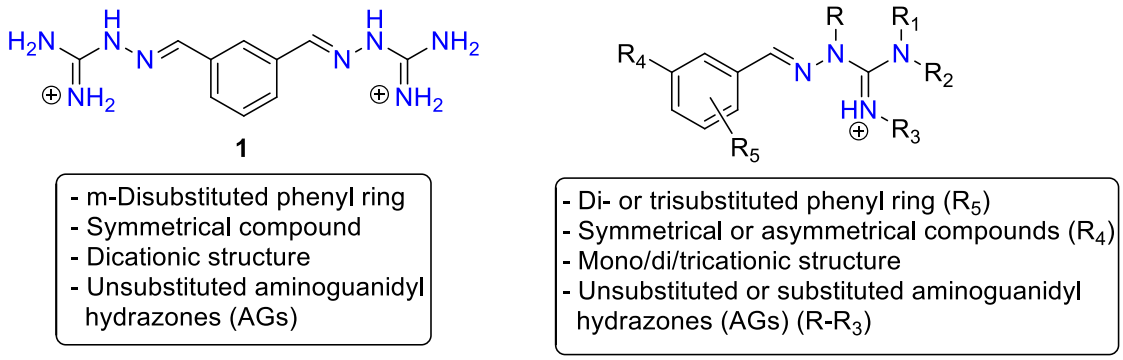

Figure 10. Unsubstituted phenyl aminoguanidyl hydrazone **AG1** (left) and a library of **AG1**-inspired putative retromer stabilizer derivatives (right): structural comparison.

We rationally designed and synthesized seventeen **AG1**-inspired analogues bearing an additional substituent on the m-phenyl ring spacer ($R_5 \neq H$); six analogues bearing substituted AGs (one or more among $R\text{-}R_3 \neq H$), and three asymmetrical analogues to check the need for two charged moieties in **AG1** ($R_4 \neq$ AG, Figure 10).

The whole set of 32 putative retromer stabilizer agents inspired by R55 shown in Figures 9 and 10 (see Paragraphs 1.2.1 to 1.2.4 for their synthesis) were sent to biological in-vitro profiling at San Raffaele Research Institute, and were in-silico docked at IBF-CNR to check their virtual affinity for the retromer complex;

biological and computational procedures, assays and results regarding **AG1**-inspired analogues are respectively detailed in Paragraphs 1.3.1 and 1.3.2.

Among them, parent, unsubstituted **AG1** proved to be a potent, in vivo active, bioavailable, non toxic retromer stabilizer (see Paragraph 1.3.3). Due to this and, in general, to the appeal of the entire structural class of AG-containing retromer stabilizers as putative treatments against neurodegenerative diseases (NDDs) caused by protein misfolding, we recently filed a patent application. Two full papers (one centered around the whole class/in vitro testing, targeted for J. Med. Chem.; another, centered around the in vivo active advanced AG lead **1**, targeted for a Nature journal) are currently being written, and will shortly follow.

1.1.7. Second goal: 2-Aryl-4-aminoquinazolines as rationally designed CMC stabilizer agents

The wealth of information acquired with the rational design, the synthesis, the structural and the biological characterization of a library of R55-inspired, AG-containing retromer stabilizers prompted us to search for another, structurally different, equally patentable class of compounds binding at the same binding site / Vps35-Vps29 interface of the retromer complex.

This effort started with a virtual HTS campaign [36], performed by Dr. Milani at IBF-CNR. The putative binding side at Vps35-Vps29 interface identified for R55, and validated for **AG1** and its analogue library, was used as a structural model for *in-silico* screen / docking of a virtual-library made by 30000 compounds, from small synthetic molecules to natural compounds [37]. As results of this virtual campaign, a few prospective scaffolds were identified/contained in virtual hits (some examples are shown in Figure 11). Among them, we focused our attention on the 2-4 disubstituted quinazoline scaffold, a rigid structure easy to be synthetized and modified, with a moderate MW, and most important present in multiple hits (general structure in Figure 11, in blue; see R and R_1 for identified hits).

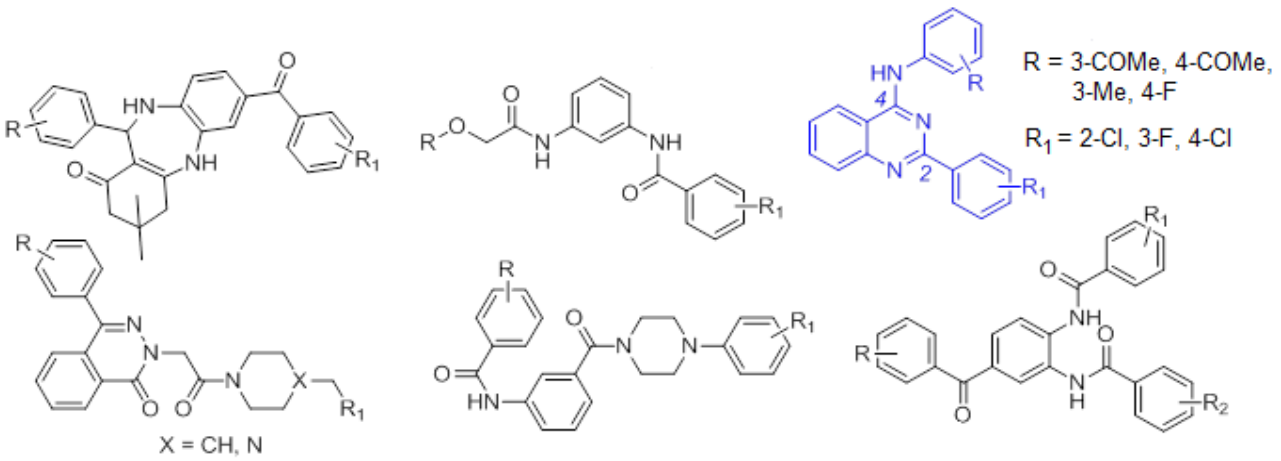

Figure 11. Chemical structure of virtual hits identified from virtual screening on the R55/**AG1** binding site on the retromer complex (2-aryl 4-amino quinazoline scaffold in blue).

At first, we checked through our co-workers at IBF-CNR (Dr. Milani) if small molecules based on the same scaffold could assume different, and possibly more fitting orientations in the binding site. We thought that the electronic properties and the bulkiness of the R/R_1-substituents (i.e., substitution patterns on both 2- and 4-aryl rings) could further influence orientation and – most important – potency of binding to the retromer complex.

Scaffold exploration, to acquire a SAR around the 2-aryl-4-aminoaryl quinazoline scaffold, and synthetic feasibility with limited efforts in a combinatorial library synthesis formats were our drivers. Among the virtual hits, compound **2a** (Figure 12, left) was selected as a starting point due to synthetic accessibility and reagent availability in our lab. In silico docking suggested that the substitution pattern (small F or Me groups) on both phenyl rings allows it to assume two different conformations shown in Figure 12, middle and right. They differ by the positioning of the aryl rings, and both show an interesting Energy binding (Eb) value between -9 and -10 Kcal/mol.

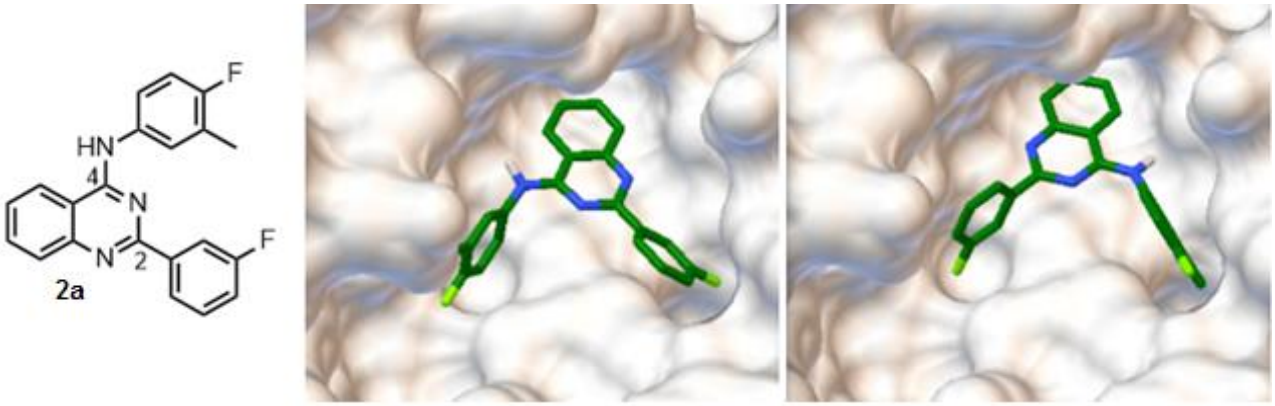

Figure 12. Chemical structure and docking poses of N-(4-fluoro-3-methylphenyl)-2-(3-fluorophenyl)quinazolin-4-amine **2a.**

In order to validate predictions on substituted 2-aryl-4-aminoaryl quinazolines, starting from compound **2a**, we designed and synthetized two small libraries where one of the two aryl substitution patterns were kept constant, while changing the nature and the size of the substituent in positions "**2**" or "**4**". The synthetic efforts are respectively reported in Paragraphs 1.2.5 and 1.2.6, leading to 22 compounds: nine "**2**"-modified 2-aryl-4-aminoaryl quinazolines **2b-i** (left, Figure 13) and thirteen "**4**"-modified 2-aryl-4-aminoaryl quinazolines **3a-m** (right, Figure 13).

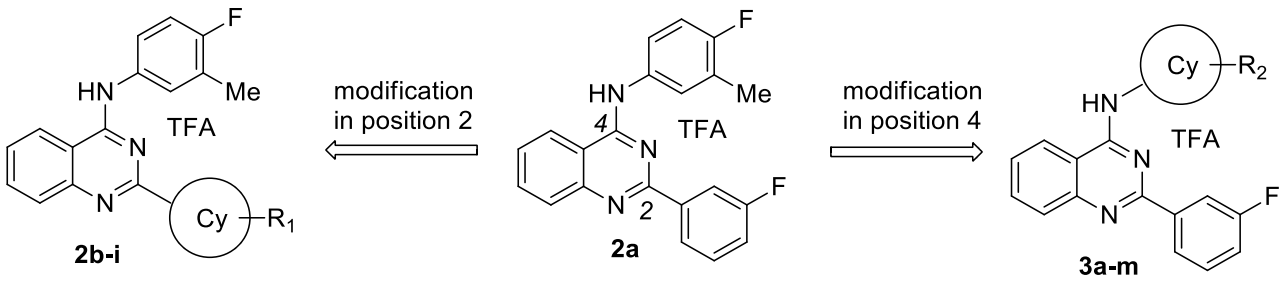

Figure 13. Small arrays of 2-aryl-4-aminoaryl quinazolines from standard **2a**: "2" modified **2b-i**, left, and "4"-modified **3a-m.**

Thus, in total twenty-two compounds were synthetized during my stage at Promidis S.r.l. (supervisor: Dr. Bertuolo). In the next future they will be in-silico docked (IBF-CNR Milan, Dr. Milani), and their biological activity will be evaluated at San Raffaele Research Institute (Dr. Muzio).

1.2. CHEMISTRY

1.2.1. Synthesis of R55 inspired retromer stabilizer agents: first array, compounds AG1, 4a,b, 5 and 6a,b

As previously mentioned, a 6-membered small array of compounds was designed to study the influence of either replacing the thiophene linker, or the isothiourea groups in R55 (respectively CL and CM, Figure 9). Their structure is shown in Figure 14.

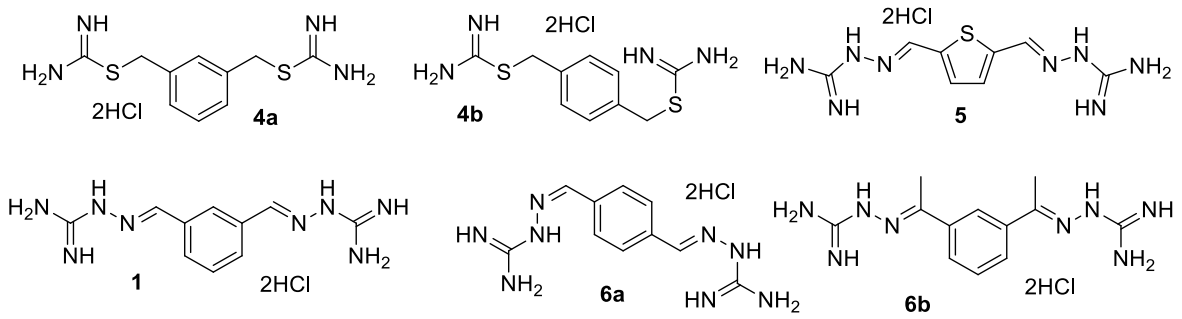

Figure 14. First library of R55 analogues: compounds **AG1, 4a,b** , **5** and **6a,b**.

Phenyl di-isothioureas **4a** (meta) and **4b** (para) were selected to study the thiophene-phenyl switch, and the best positioning of the CM-bearing side chains. They were synthesized in good yields with through a nucleophilic substitution on di-(chloromethyl) benzene reported in literature [38], and shown in Scheme 1.

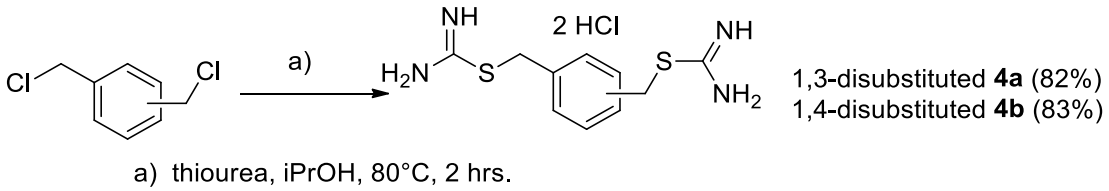

Scheme 1. Synthesis of compounds **4a,b**.

Thiophene di-aminoguanidyl hydrazone (AG) **5** was chosen to study the influence of the isothiourea-AG switch on biological activity. Then, phenyl di-AGs **AG1** (meta) and **6a** (para) were chosen because they bear both replacements (CL and CM) with different substitution patterns. Finally, the phenyl dimethyl AG analogue **6b** was chosen to study the influence of substitution on the alpha position.

Compounds **AG1**, **5**, **6a,b** were synthesized as shown in Scheme 2.

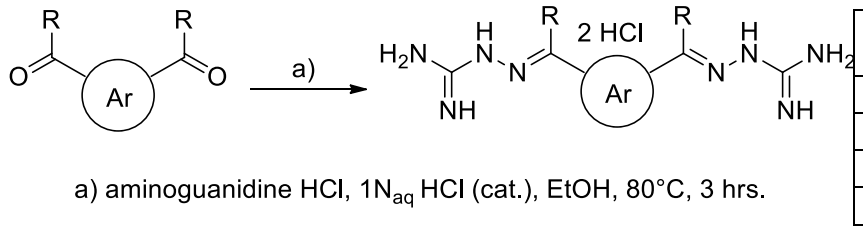

Name	Ar	R	Yield (%)
5	Thienyl	H	75
1	*m*-phenyl	H	88
6a	*p*-phenyl	H	87
6b	*m*-phenyl	Me	78

Scheme 2. Synthesis of compounds **1, 5**and **6a,b**.

The condensation between a dicarbonyl compound (a dialdehyde for **1**, **5**, **6a**; a diketone for **6b**) and commercially available aminoguanidine dihydrochloride (step a, Scheme 2) was performed in refluxing ethanol, and was catalyzed by a few drops of aqueous HCl. The target compounds were insoluble after cooling to RT, and were collected after simple filtration in high yields and purities (Scheme 2, right).

A single variation (the replacement of isothioureas with AGs – **5**, and of 2,5-substituted thiophene with 1,3-substituted benzene – **4a**), and their combination (**AG1**) led to retromer stabilizers (see Chapter 1.3.1 for more details on their potency, and on biological assays). Conversely, 1,4-substituted phenyls bearing isothioureas (**4b**) and aminoguanidine hydrazones (**6a**), and 1,3-substituted dimethyl phenyl compound **6b** were completely inactive. Eventually, **AG1** was selected as the scaffold for further synthetic efforts among active compounds due to its higher potency in vivo (1 week experiment in WT C57BL6 mice, Vps35 stabilization), indicating a better bioavailability than similarly in vitro active compounds **4a** and R55.

The following Paragraphs will sequentially describe the synthesis of several sub-classes of **AG1** analogues. Please note that their synthesis often progressed in parallel during my Ph.D.

1.2.2. Synthesis of Ph-substituted aryl aminoguanidyl lhydrazones 1a-q

A first array of **AG1** analogues contains a third substituent on the phenyl ring, in order to determine a preliminary structure-activity relationship (SAR) around the ring. The whole set of 17 putative retromer stabilizer agents is shown in Figure 15.

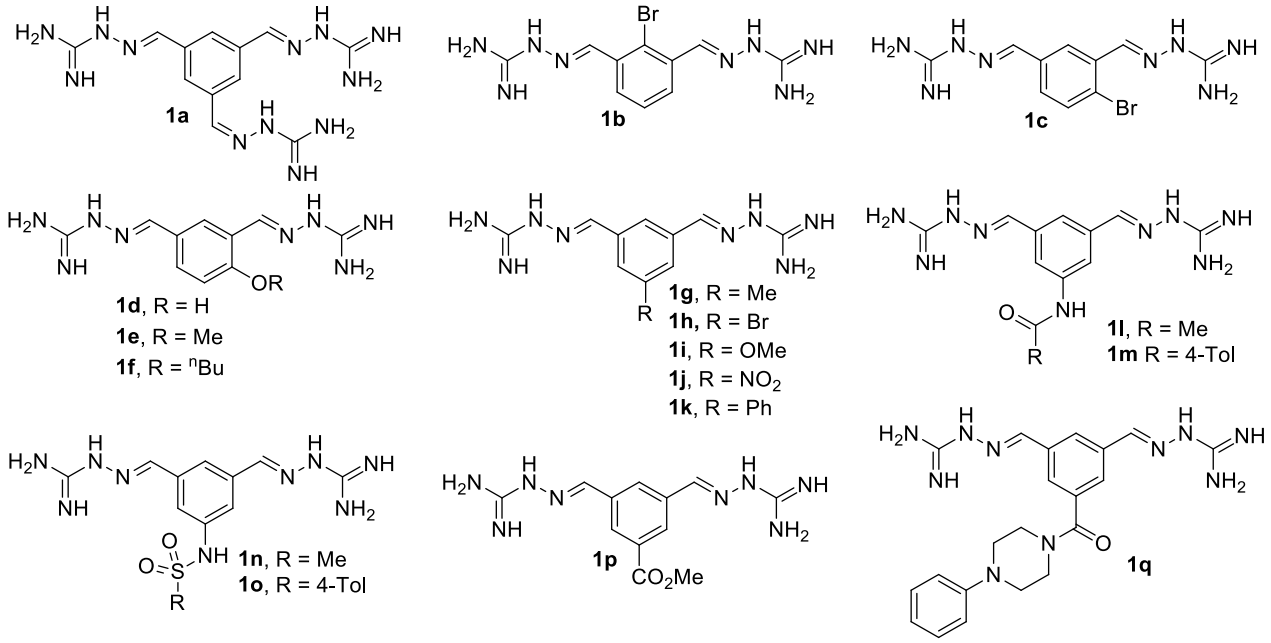

Figure 15. Phenyl trisubstituted **AG1** analogues: compounds **1a-q**.

The retrosynthetic approach devised for phenyl aminoguanidyl hydrazones (AGs) **1a-q** is shown in Scheme 2.

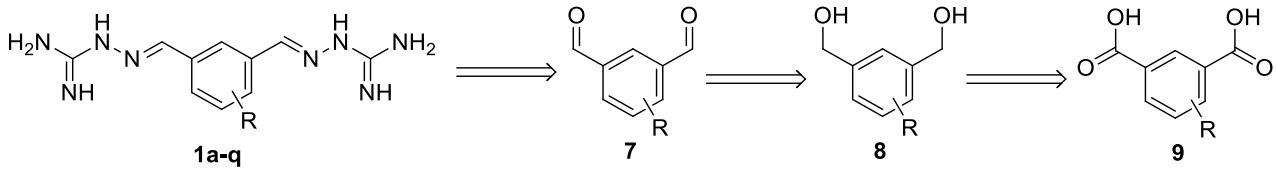

Scheme 2. Retrosynthetic analysis for the synthesis on compound **1a-q**.

AGs **1a-q** were invariably obtained by condensation of aminoguanidine on the corresponding substituted isophthalic aldehydes **7**. In a few cases, such aldehydes were commercially available; in most cases they were obtained by reduction of the corresponding isophtalic acids **9** to bis benzyl alcohols **8** and partial oxidation to aldehydes **7**. As to R groups, some of them were stable in the devised synthetic strategy, and were present

in commercially available aldehyde or acid precursors; some others needed to be built through additional, compound-specific synthetic steps. Their synthesis is shown in this Section.

Tri-AG **1a** was obtained as a trihydrochloride salt according with Scheme 3 in 78% yield from commercially available 1,3,5-benzene tricarboxaldehyde **7a** after condensation with aminoguanidine hydrochloride (step a). Similarly to **AG1**, compound **1a** was obtained in high yield and purity by simple filtration.

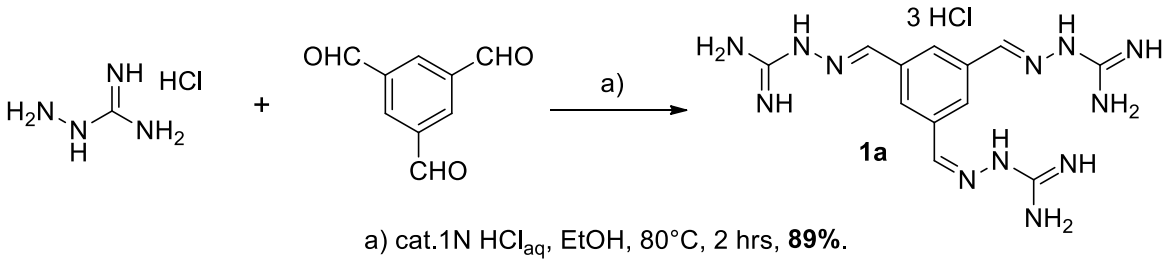

a) cat.1N HCl_{aq}, EtOH, 80°C, 2 hrs, **89%**.

Scheme 3. Synthesis of tri-AG **1a**.

2-Br- di-AG **1b** was prepared as a dihydrochloride salt by condensation of commercially available 2-bromo-1,3-isophthalaldehyde **7b** with aminoguanidine hydrochloride in good yields and purity after simple filtration, as shown in Scheme 4.

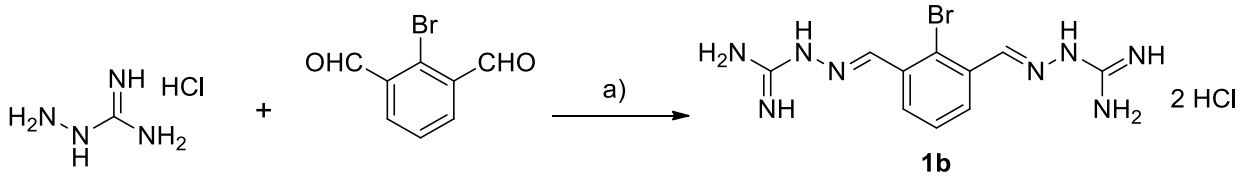

a) cat.1N HCl_{aq}, EtOH, 80°C, 2 hrs, **89%**.

Scheme 4. Synthesis of 2-Br-di-AG **1b**.

4-Br- di-AG **1c** was prepared as a dihydrochloride salt in a three steps synthesis from commercially available 4-bromo-1,3-isophthalic acid **9c**, as shown in Scheme 5.

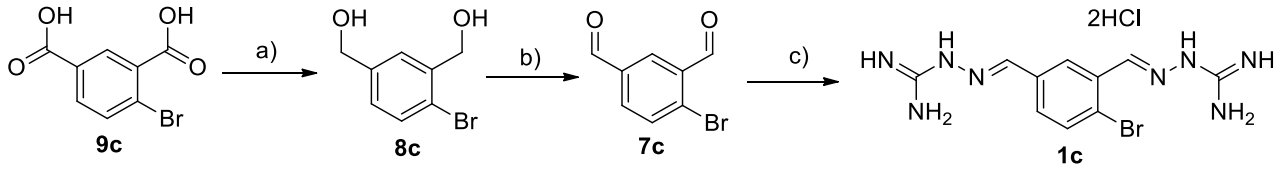

a) 1M BH_3-THF, dry THF, N_2, 0°C to RT, 48hrs, **86%**; b) MnO_2, chloroform, 70°C, 16hrs; **86%**; c) aminoguanidine HCl, cat. 1N HCl_{aq}, EtOH, 80°C, 4hrs, **88%**.

Scheme 5. Synthesis of 4-Br-di-AG **1c**.

2-Bromoisophthalic acid **9c** was first reduced to 2-bromo-1,3 bis-(hydroxymethyl) benzene **8c** with borane (step a), then partially oxidized to 2-bromoisophthalaldehyde **7c** with MnO_2 (step b). Condensation between **7c** and aminoguanidine hydrochloride in standard conditions (step c, Scheme 5) led 4-Br-di-AG **2c** as a dihydrochloride salt in excellent yields and purity after simple filtration.

4-OH- (**1d**), 4-OMe (**1e**) and 4-O^{n}Bu-di-AG **1f** were prepared in good yields as dihydrochloride salts from commercially available 4-hydroxy-1,3-isophthalaldehyde **7d**, as shown in Scheme 6. Please note that, from here onwards, we will keep constant the 1,3-di-AG numbering, even when a heteroatom-based substituent would have priority as here (i.e., we call them 4-O di-AGs rather than 1-O di-AGs).

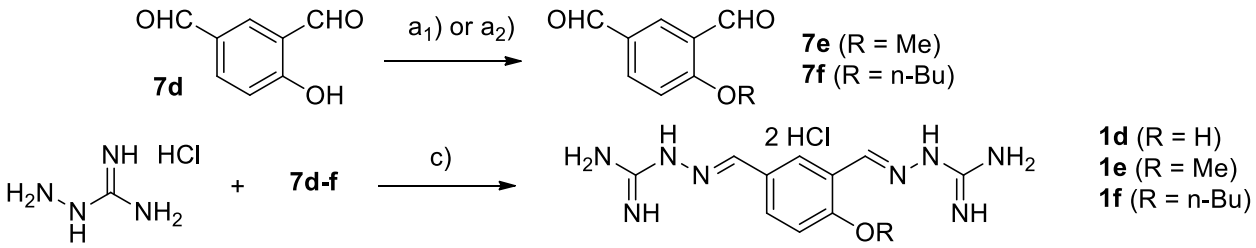

a_1) MeI, K_2CO_3, dry DMF, N_2, RT, 24 hrs, **60%**; a_2) ^{n}BuBr, K_2CO_3, dry DMF, N_2, 85°C, 24 hrs, **75%**;
b) cat. 1N HCl_{aq}, EtOH, 80°C, 8hrs, 77% (**1d**), **79%** (**1e**), **80%** (**1f**).

Scheme 6. Synthesis of 4-OH-, 4-OMe- and 4-OnBu-di-AGs **1d-f**.

4-OH-di-AG **1d** was made by condensation of **7d** with aminoguanidine hydrochloride in standard conditions (step b, Scheme 6). 4-OMe- and 4-OnBu-di AGs **1e** and **1f** required the alkylation of phenoxyaldehyde **7d** with an appropriate halide (steps a_1 or a_2) to synthesize the condensation reagents **7e** and **7f**. 4-OH-, 4-OMe- and 4-OnBu-di-AGs **1d-f** were obtained in good purity after simple filtration from EtOH, similarly to **AG1**.

5-Me- (**1g**), 5-Br- (**1h**), 5-OMe (**1i**) and 5-NO_2-di-AG **1j** were prepared as dihydrochloride salts in good to excellent yields in a three steps synthesis from commercially available *m*-substituted 1,3-isophthalic acids **9g-9j**, as shown in Scheme 7.

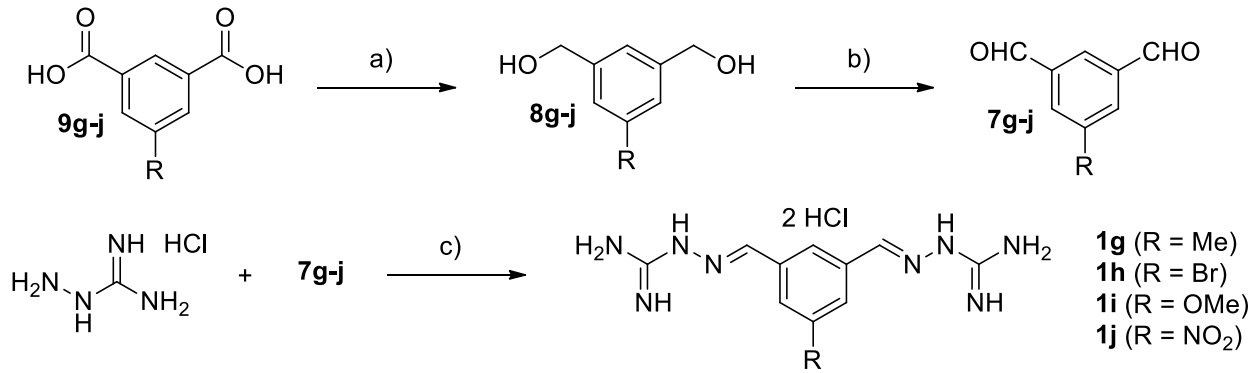

(a) 1M BH_3 in THF, dry THF, N_2, 0°C to RT, 48 hrs, **80** to **88%**; (b) MnO_2, $CHCl_3$, 70°C, 16 hrs, **77** to **92%**;
(c) cat. HCl, EtOH, 80°C, 2 to 8 hrs, **77%** (**1g**), **88%** (1h), **81%** (**1i**) or **80%** (**1j**).

Scheme 7. Synthesis of 5-Me-, 5-Br-, 5-OMe- and 5-NO_2-di-AGs **1g-j**.

Reaction conditions and yields are similar to steps a to c in Scheme 5. 5-Me-, 5-Br, 5-OMe- and 5-NO_2-di-AGs **1g-j** were obtained in good purity after simple filtration from EtOH, similarly to **AG1**.

5-Bromo-1,3-bis(hydroxymethyl)benzene **8h**, shown in Scheme 7, was used to prepare in good yields 5-phenyl-1,3-AG **1k** as a dihydrochloride salt through a three steps synthesis (Scheme 8).

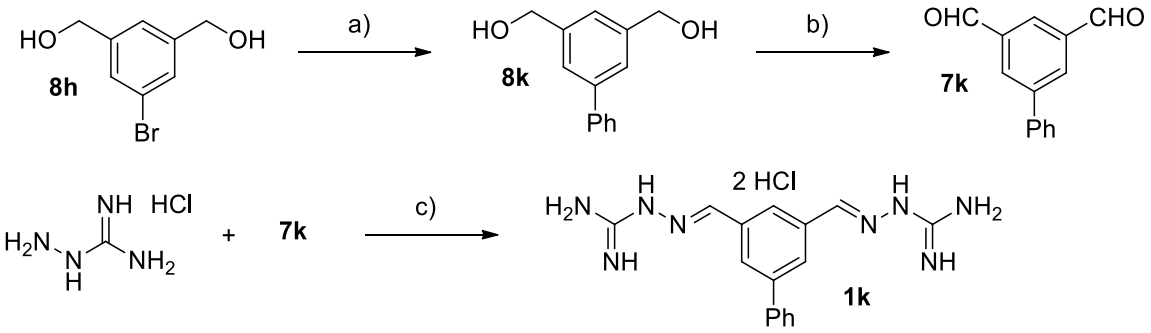

a) $PhB(OH)_2$, $Pd(PPh_3)_4$, 2N aq. Na_2CO_3, dioxane, 105°C, 6 hrs, **82%**; b) MnO_2, $CHCl_3$, 70°C, 16 hrs, **81%**; c) cat. HCl, EtOH, 80°C, 8 hrs, **79%.**

Scheme 8. Synthesis of 5-Ph-diAG **1k**.

Suzuki coupling of **8h** with phenylboronic acid (step a) yielded 5-phenyl-1,3-(hydroxymethyl) benzene **8k**. Partial oxidation (step b) and condensation with aminoguanidine hydrochloride (step c, Scheme 8) were performed as in standard conditions. Due to its higher EtOH solubility, pure 5-Ph-di-AG **1k** required reverse phase chromatography to be obtained as a dihydrochloride salt after lyophilization.

5-Nitro-1,3-(hydroxymethyl)benzene **8j**, shown in Scheme 7, was used to prepare in moderate to good yields 5-NHAc- (**1l**) and 5-NHp-MeBz-di-AG **2m** as dihydrochloride salts (Scheme 9).

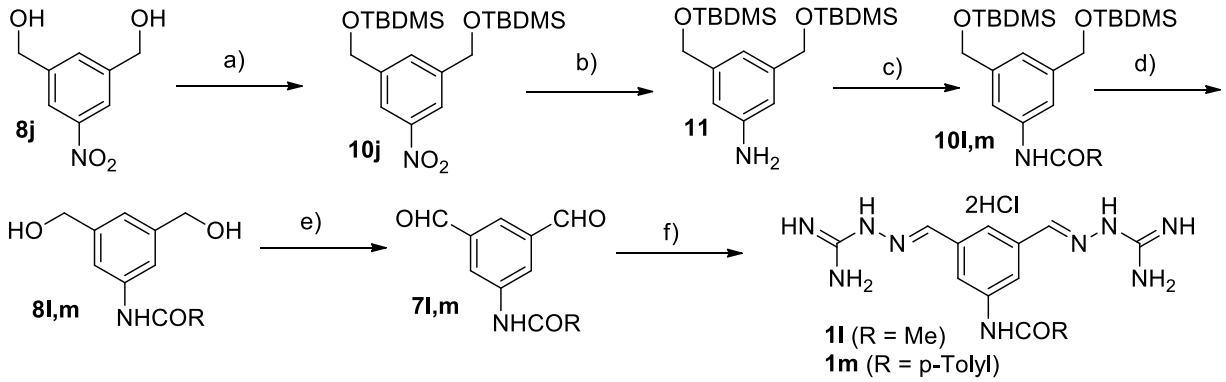

a) TBSCl, 1H-imidazole, CH_2Cl_2, 0°C to RT, 3 hrs; b) cat. 10% Pd/C, H_2, EtOH, RT, 24 hrs, **78%** (2 steps); c) acylating agent, TEA, DMAP, CH_2Cl_2, 0°C to RT, 1 to 2 hrs, **67%** (**10m**); d) AcCl, dry MeOH, N_2, 0°C, 30 min; e) MnO_2, $CHCl_3$, 70°C, 16 hrs, **74%** (**7l**, 3 steps) or **83%** (**7m,** 2 steps); f) aminoguanidine HCl, cat. HCl, EtOH, 80°C, 4 to 6 hrs, **85%** (**1l, 1m**).

Scheme 9. Synthesis of 5-NHAc and 5-NHpMeBz-di-AGs **1l,m**.

Protection of the hydroxyl groups in **8j** with a bulky sylil group (step a, **10j**) and catalytic hydrogenation of the nitro group (step b) led to the key 5-amino intermediate **11**. Its acylation with the appropriate reagent (step c, **10l,m**) was followed by silyl deprotection (step d, **8l,m**) in good overall yields. Then, partial oxidation (step e, **7l,m**) and condensation with aminoguanidine hydrochloride (step f, Scheme 8) in standard conditions led to target, 5-NHAc- and 5-NHpMeBz-di-AGs **1l** and **1m**. They were both obtained in pure form after simple filtration from EtOH, similarly to **AG1**.

1-amino-3,5-(t-butyldimethylsilyloxy-methyl)benzene **11**, shown in Scheme 9, was used to prepare 5-NHMs- (**1n**) and 5-NHTos-diAG **1o** as dihydrochloride salts in moderate to good yields (Scheme 10).

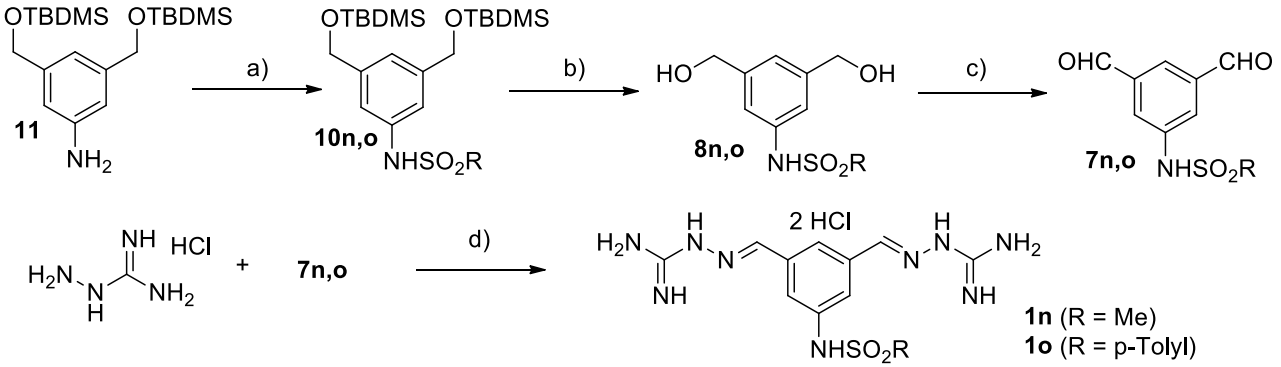

a) sulfonylating agent, pyridine, DMAP, CH_2Cl_2, 0°C to rt, 16 hrs, **85%** (**10o**); b) AcCl, dry MeOH, N_2, 0°C, 30 min, **81%** (**8o**); c) MnO_2, $CHCl_3$, 70°C, 16 hrs, **68%** (**7n**, 3 steps) or **90%** (**7o**); d) cat. HCl, EtOH, 80°C, 4 hrs, **83%** (**1n**) or **79%** (**1o**).

Scheme 10. Synthesis of 5-NHMs- and 5-NHTos-di-AGs **1n,o**.

Sulfonylation of the amine in **11** with the appropriate reagent (step a, **10n,o**) was followed by silyl deprotection (step b, **8n,o**) in good overall yields. Then, partial oxidation (step c, **7n,o**) and condensation with aminoguanidine hydrochloride (step d, Scheme 10) in standard conditions led to target, 5-NHMs- and 5-NHpTos-di-AGs **1n** and **1o**. They were both obtained in pure form after simple filtration from EtOH, similarly to **AG1**.

5-COOMe-di-AG **1p** was prepared as a dihydrochloride salt in moderate yields from commercially available trimethyl 1,3,5-benzenetricarboxylate, as shown in Scheme 11.

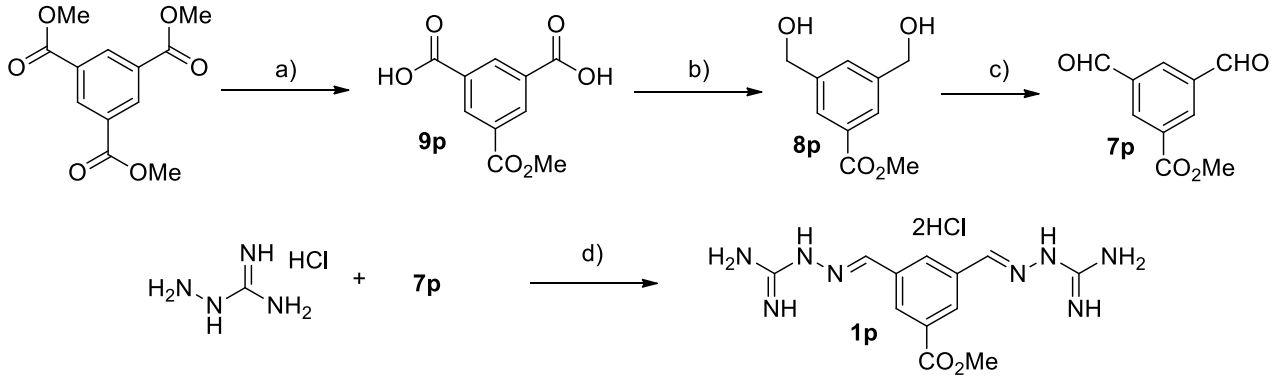

a) 1.8M aq. NaOH, MeOH, rt, 24 hrs; b) 1M BH_3 in THF, dry THF, N_2, 0°C to rt, 24 hrs, **54%** (2 steps); c) MnO_2, $CHCl_3$, 70°C, 16 hrs, **85%**; d) cat. HCl, EtOH, 80°C, 4 hrs, **71%.**

Scheme 11. Synthesis of 5-COOMe-di-AG **1p**.

The diacid, monoester **9p** was prepared by carefully controlled basic hydrolysis of two ester groups of the tricarboxylate (step a). Reduction of free carboxylic acids (step b, **8p**), partial oxidation (step c, **7p**) and condensation with aminoguanidine hydrochloride (step d, Scheme 10) in standard conditions led to pure 5-COOMe-di-AG **1p** after simple filtration.

Finally, 1-carbomethoxy isophthaldehyde **7p**, shown in Scheme 11, was used to prepare 1-(4'-phenylpiperazinyl)-3,5-bis-aminoguanidyl phenyl hydrazone (5-CONPip-di-AG) **1q** as a trihydrochloride salt in low, unoptimized yields as shown in Scheme 12

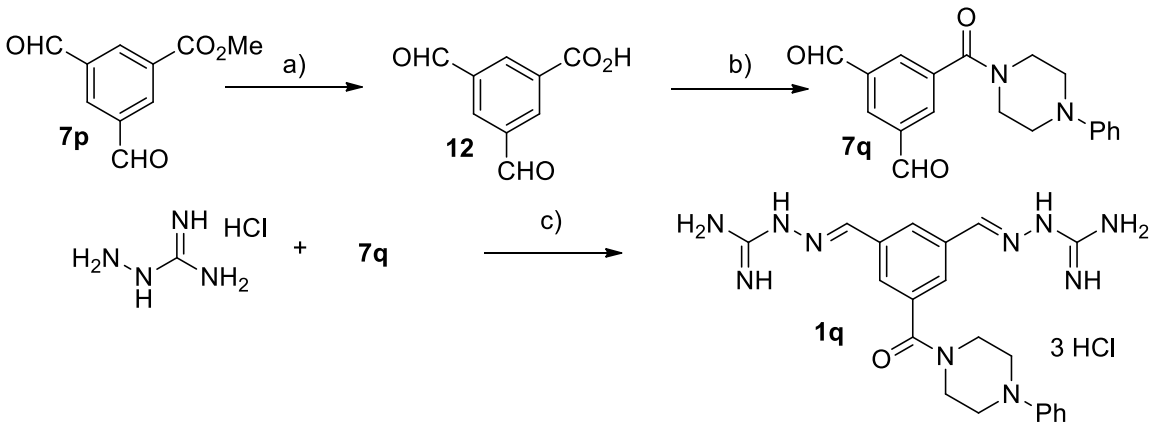

a) NaOH, water/THF, rt, 24 hrs; b) 4-Ph-piperazine, EDC, HOBt, TEA, dry CH_2Cl_2, N_2, rt, 24 hrs, **30%** (2 steps); c) cat. HCl, EtOH, 80°C, 4 hrs, **72%**.

Scheme 12. Synthesis of 5-CONPip-di-AG **1q**.

The poor 2-step yield for ester hydrolysis (step a, **12**) and amidation (step b, **7q**) is likely due to the crude from the former reaction, that could not be easily purified and was submitted as such to amidation. Then, condensation with aminoguanidine hydrochloride in standard conditions (step c, Scheme 11) yielded pure 5-CONPip-di-AG **1q** as a dihydrochloride salt after reverse phase chromatography and lyophilization, due to its higher solubility in EtOH.

1.2.3. Synthesis of N-substituted aryl aminoguanidyl hydrazones 13a-f

A second array of **AG1** analogues contains N-substituted aminoguanidines, in order to determine a preliminary SAR around the side chains. The set of 6 putative retromer stabilizer agents, obtainable through condensation between a substituted aminoguanidine and isophthalaldehyde, is shown in Figure 16.

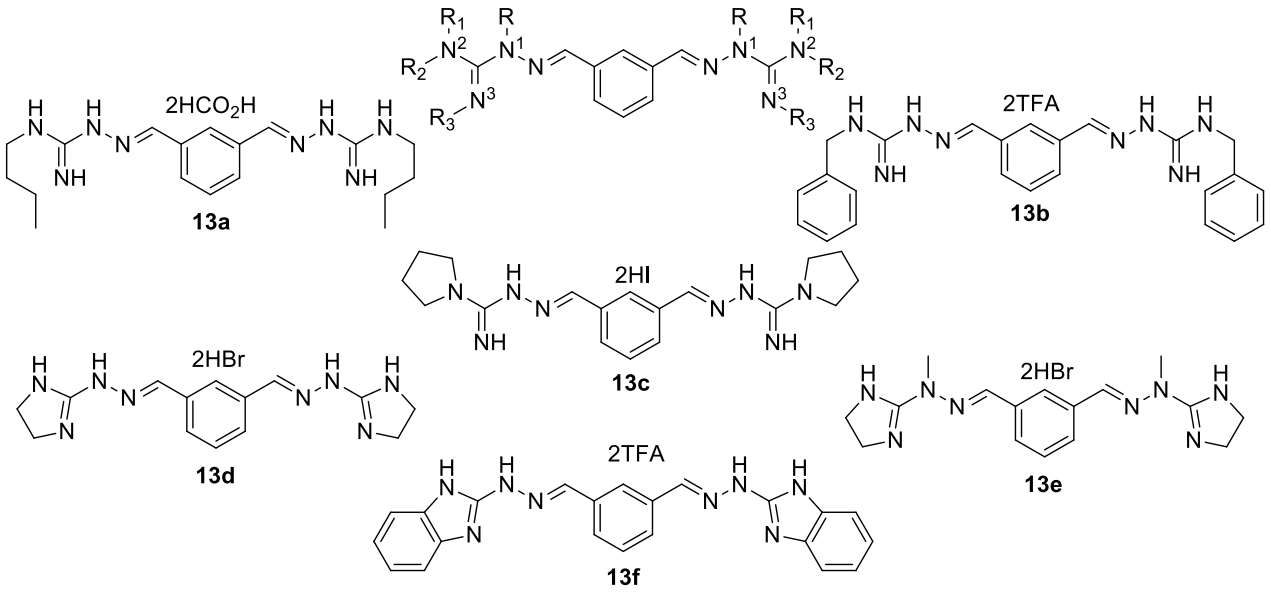

Figure 16. Phenyl **AG1** analogues bearing N-substituted aminoguanidyl hydrazones: compounds **13a-f**.

1,3-Bis-(N_2-*n*-butylaminoguanidyl) phenyl hydrazone (N_2-nBu-di-AG) **13a**, 1,3-bis-(N_2-benzylaminoguanidyl) phenyl hydrazone (N_2-Bn-di-AG) **13b** and 1,3-bis-(N_2-pyrrolidinoguanidyl) phenyl hydrazone (N_2-Pyrr-di-AG)

13c were prepared in good to excellent yields in a two steps synthesis culminating in the condensation between isophthalaldehyde and N-alkylated aminoguanidine hydroiodides **14a-c** as shown in Scheme 13.

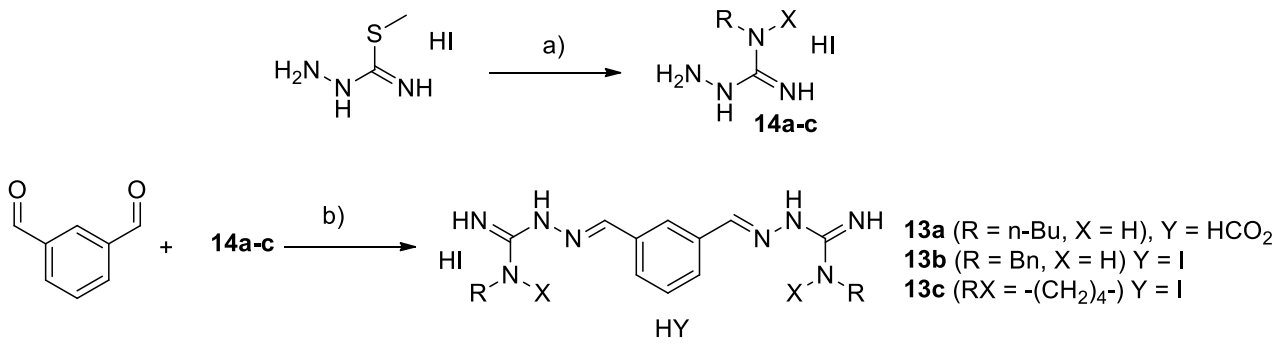

a) n-$BuNH_2$ (**14a**), $BnNH_2$ (**14b**) or pyrrolidine (**14c**), MeOH, rt, 72 hrs, **99%** (**14a**), **60%** (**14b**) or **89%** (**14c**);
b) EtOH, 80°C, 16 hrs, **53%** (**13a**), **70%** (**13b**) or **80%** (**13c**).

Scheme 13. Synthesis of N_2-nBu-, N_2-Bn- and N_2-Pyrr-di-AGs **13a-c**.

N-alkylated aminoguanidine hydroiodides **14a-c** were prepared from commercially available S-methyl isothiosemicarbazide dihydroiodide, that was reacted with the appropriate primary or secondary amine (step a) to provide acyclic N_2-*n*-butyl- (**14a**) or N_2-benzyl-aminoguanidine (**14b**), and cyclic N_2-*n*-pyrrolidinoguanidine (**14c**) as dihydroiodide salts. Standard condensation between isophthalaldehyde and crude **14a-14c** (step b, Scheme 13) yielded target N_2-substituted di-AGs **13a-c**. Among them, pure compound **13c** was obtained as a dihydroiodide salt after simple filtration from EtOH, similarly to **AG1**; conversely, compounds **13a,b**, due to their higher solubility in EtOH, required reverse phase chromatography for their purification as diformate (**13a**) or dihydroiodide salt (**13b**).

1,3-Bis-(N_2N_3-imidazolinyl) phenyl hydrazone (N_2N_3-Im-di-AG) **13d** and 1,3-bis-(N-methyl-N_2N_3-imidazolinyl) phenyl hydrazine (N-Me-N_2N_3-Im-di-AG) **13e** were prepared in good yields by the condensation between isophthalaldehyde and the corresponding, commercially available 2-hydrazino imidazoline hydrobromides (step a, Scheme 14).

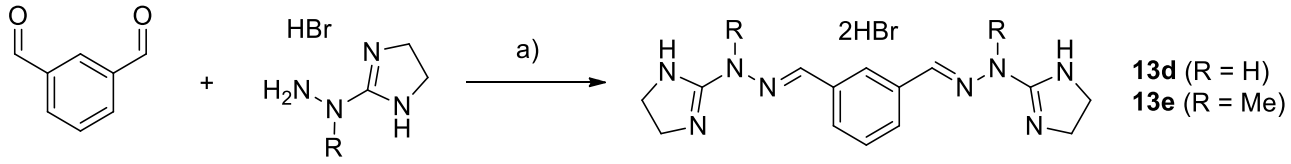

a) EtOH, 80°C, 16 hrs, **82%** (**13d**, **13e**).

Scheme 14. Synthesis of N_2N_3-Im- and N-Me-N_2N_3-Im-di-AGs **13d,e**.

Both pure compounds were obtained as dihydrobromide salts by simple filtration from EtOH, similarly to **AG1**.

Finally, 1,3-bis-(N_2N_3-benzimidazolyl) phenyl hydrazone (N_2N_3-Bzim-di-AG) **13f** was prepared in good yields by the condensation between isophthalaldehyde and commercially available 2-hydrazino benzimidazole (step a, Scheme 15).

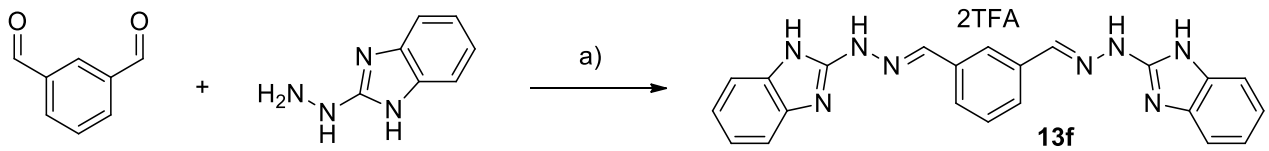

a) cat. AcOH, EtOH, 80°C, 2 hrs, **66%.**

Scheme 15. Synthesis of N_2N_3-BzIm-di-AG **13f**.

A catalytic amount of acetic acid was used to promote the reaction, and pure **13f** was obtained as a ditrifluoroacetate salt after reverse phase chromatography.

1.2.4. Synthesis of Ph-substituted aryl mono-aminoguanidyl hydrazones 15a-c

A third array of **AG1** analogues contains a single aminoguanidyl hydrazone, in order to determine the need for both AG groups. The set of 3 putative retromer stabilizer agents, bearing a polar acylaminoacidic substituent, is shown in Figure 17.

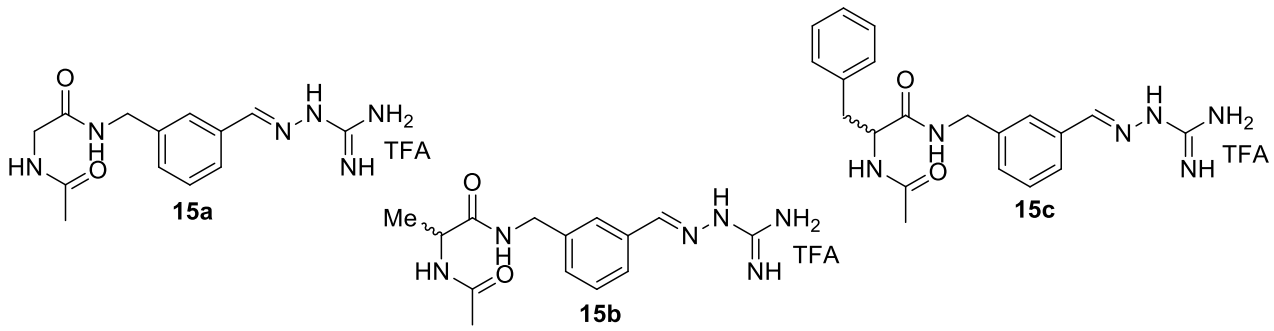

Figure 17. Phenyl **AG1** analogues bearing a single aminoguanidyl 26ydrazine: compounds **15a-c**.

We chose the simplest N-acetyl glycine group (**15a**, Gly-mono-AG), that does not contain chiral centres and bears the smallest possible capping group, and two incrementally larget side chains corresponding to alanine and phenylalanine (respectively **15b**, Ala-mono-AG, and **15c**, Phe-mono-AG) to check the effect of one AG replacement, and – if activity would have been preserved – to study the influence of larger amino acid side chains on potency and bioavailability. Racemic aminoacids were used to test evaluate both enantiomers in a single experiment.

The planned and executed synthetic route to compounds **15ac** is shown in Scheme 16.

Commercially available 3-cyanobenzoic acid was reduced to the corresponding (3-(aminomethyl)phenyl) methanol **16** using borane (step a), and the hydroxybenzyl moiety was protected (step b) yielding benzylamine **17** in good yields. Acylation with three corresponding, commercially available N-acetyl aminoacids in standard conditions (step c, **18a-c**) was followed by sylil deprotection (step d), leading to benzyl alcohols **19a-c** in excellent yields. Finally, IBX oxidation (step e, **20a-c**) and condensation with aminoguanidine hydrochloride in standard condition (step f, Scheme 16) provided mono-AGs **15a-c**. Their increased lipophilicity required work up and reverse phase chromatography for their final purification.

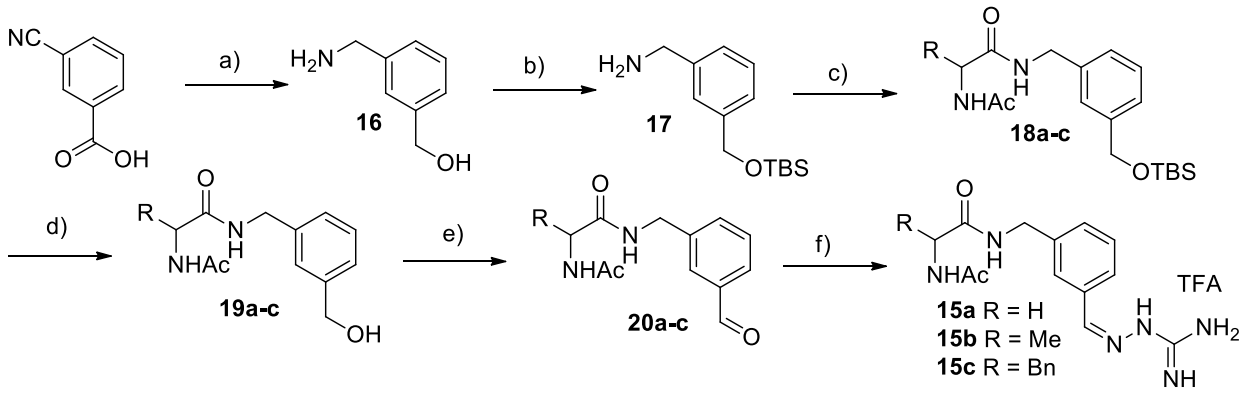

a) 1M BH_3-THF, dry THF, N_2, 0°C to RT, 4hrs; b) TBSCl, 1H-imidazole, dry DCM, 0°C to RT, 6hrs, **72%** over two steps; c) H-Acetyl-aminoacid, EDCI, HOBt, DIPEA, dry DCM, RT, 16hrs; d) cat. AcCl, dry MeOH, 0°C, 30min,**82-86%** over two steps; e) IBX, dry MeCN, 80°C, 3hrs; f) amminoguanidine HCl, cat. 1N HCl_{aq}, EtOH, 80°C, 3hrs, **60-65%** over two steps.

Scheme 16. Synthesis of Gly-, Ala- and Phe-mono-Ags **15a-c**.

The 32 compound-set of putative retromer stabilizer agents inspired by R55, and shown in Figure 12, 14, 15 and 17 was sent to biological in-vitro profiling at the San Raffaele Research Institute, Milan (Dr. Luca Muzio). The results of biological profiling are reported in Paragraph 1.3.1.

1.2.5. Synthesis of "2"-modified-N-(4-fluoro-3-methylphenyl)quinazolin-4-amines 2a-k

As previously mentioned, a virtual HTS searching for a structurally different, equally patentable class of compounds binding at the same binding site / Vps35-Vps29 interface of the retromer complex, led to the identification of the 2-4 disubstituted quinazoline scaffold, a rigid structure easy to be synthetized and modified, in multiple hits. Among them, compound **2a** (Figure 18, left) was selected due to its synthetic accessibility, and to its good fit in the binding site/Vps35-Vps29 interface (Figure 18, right).

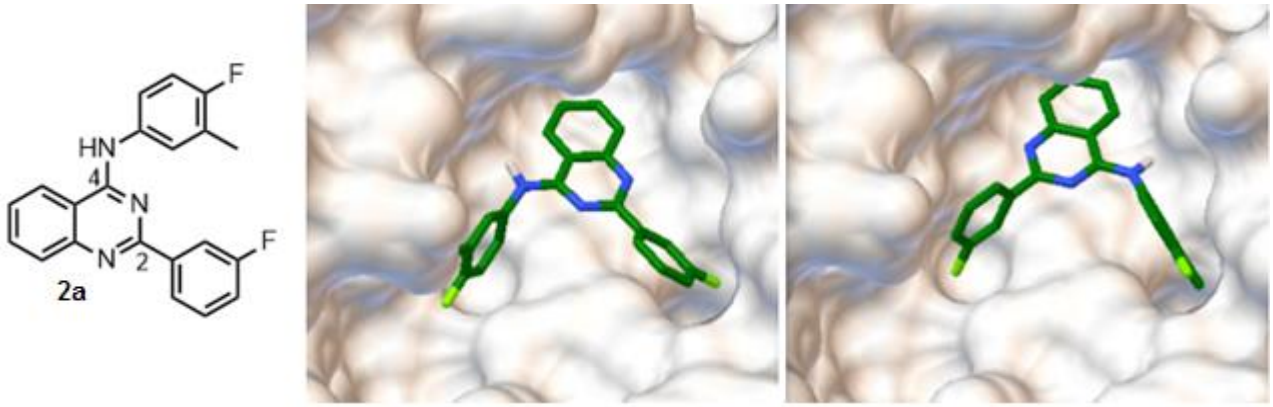

Figure 18. Chemical structure and docking poses of N-(4-fluoro-3-methylphenyl)-2-(3-fluorophenyl)quinazolin-4-amine **2a.**

The synthesis of compound **2a** from commercially available 2,4-dichloro quinazoline is shown in Scheme 17.

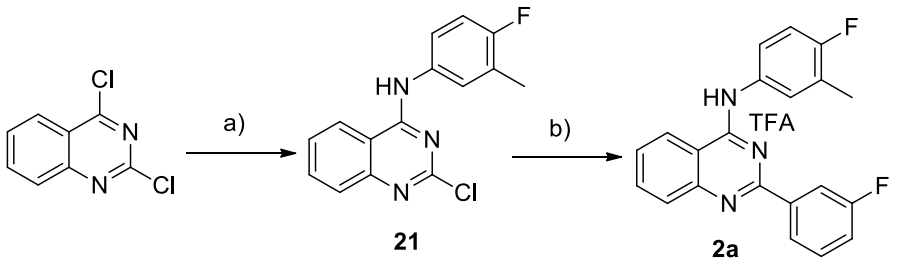

a) 4-Fluoro-3-methylaniline, TEA, THF, 80°C, 8hrs, **74%**; 3-Fluorobenzeneboronic acid, $Pd(PPh_3)_4$, 2M aq. Na_2CO_3, dioxane, 105°C, 6hrs, **71%.**

Scheme 17. Synthesis of N-(4-fluoro-3-methylphenyl)-2-(3-fluorophenyl)quinazolin-4-amine **2a.**

The most reactive, 4-chlorine atom in 2,4-dichloro quinazoline was selectively functionalized in a nucleophilic substitution with 4-fluoro-3-methylaniline (step a), with good yields. Then, a Suzuki coupling protocol was used on 2-chloro intermediate **21**, using 3-fluorobenzene boronic acid (step b, Scheme 17). Pure target compound **2a** was obtained in good yields after purification.

A first small library of **2a** analogues with different substituent patterns on the 2-aryl ring ("**2**"-modified array) was then conceived. They could be easily prepared from intermediate **21** (Scheme 17), simply by changing the boronic acid used in step b. The structures of ten rationally selected components of the "**2**"-modified array (compounds **2b-k**) is shown in Figure 19.

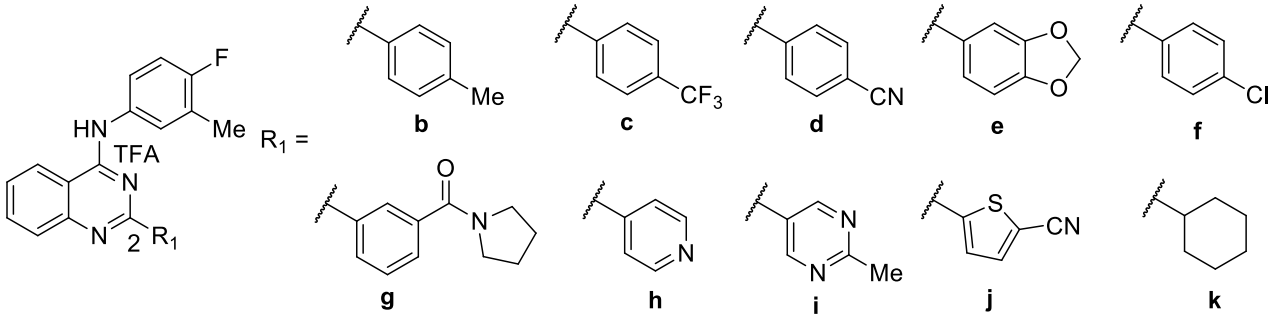

Figure 19. "**2**"-Modified array: chemical structures, compounds **2b-k**.

Their synthesis, and the synthesis of another array of 2,4-substituted quinazolines (see next Paragraph), was carried out during a stage at organic/medicinal chemistry-oriented Promidis Srl (Milan), in order to access analytical and synthetic equipments for high throughput organic synthesis.

The results of array synthesis for compounds **2b-k** are reported in Table 1.

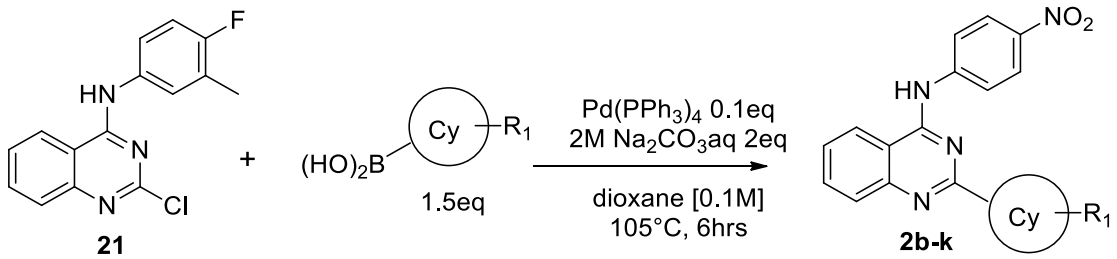

Table 1. "2"-Modified array: compounds **2b-k.**

Cpd.	Cy	R_1	Yield % (Isolated)	Product/SM ratio (UPLC-MS)	Purity % (UPLC-MS)
2b	Phenyl	4-Me	65	100:0	99.6
2c	Phenyl	4-CF_3	57	100:0	99.7
2d	Phenyl	4-CN	50	>95:5	98.4
2e	Phenyl	3,4-dioxolanyl	77	100:0	99.6
2f	Phenyl	4-Cl	48	>90:10	98.6
2g	Phenyl	3-COPyrrolidinyl	41	>95:5	98.5
2h	4-Pyridyl	-	64	>90:10	98.3
2i	3,5-Pyrimidinyl	4-Me	61	>95:5	98.8
2j	2-Thienyl	3-CN	0	25:75[a]	-
2k	Cyclohexyl	-	0	0:100	-

[a], 24 hours. SM = starting material

Eight out of ten attempted reactions (**2b-i**) showed almost complete disappearance (UPLC-MS) of starting material **21**, and yielded after purification moderate to good yields of pure compounds **2b-i** (see Table 1, and Paragraph 1.5 for detailed experimental protocols). Thus, either electron-rich (**2b,e**), -poor (**2c,d**) and N-containing heteroaromatic boronic acid (**2h,i**) provided good synthetic results. Conversely, poor conversion (less than 25%) was observed by UPLC-MS, even increasing the reaction time to 24 hours, during the synthesis of thiophene-containing **2j**; unfortunately, its purification failed either using direct or reverse phase chromatography. Finally, using an aliphatic boronic acid (compound **2k**), only unreacted starting material **21** was observed.

"2"-modified compounds **2b-i,** together with parent compound **2a**, were obtained with a ≥97% purity as trifluoroacetate salts after reverse phase preparative HPLC.

1.2.6. Synthesis of "4"-modified 2-(3-fluorophenyl)- quinazolin-4-amines 3a-m

A small library of **2a** analogues with different substituent patterns on the 4-aryl ring ("**4**"-modified array) was also conceived. The structures of thirteen rationally selected components of the "**4**"-modified array (compounds **3a-m**) is shown in Figure 20.

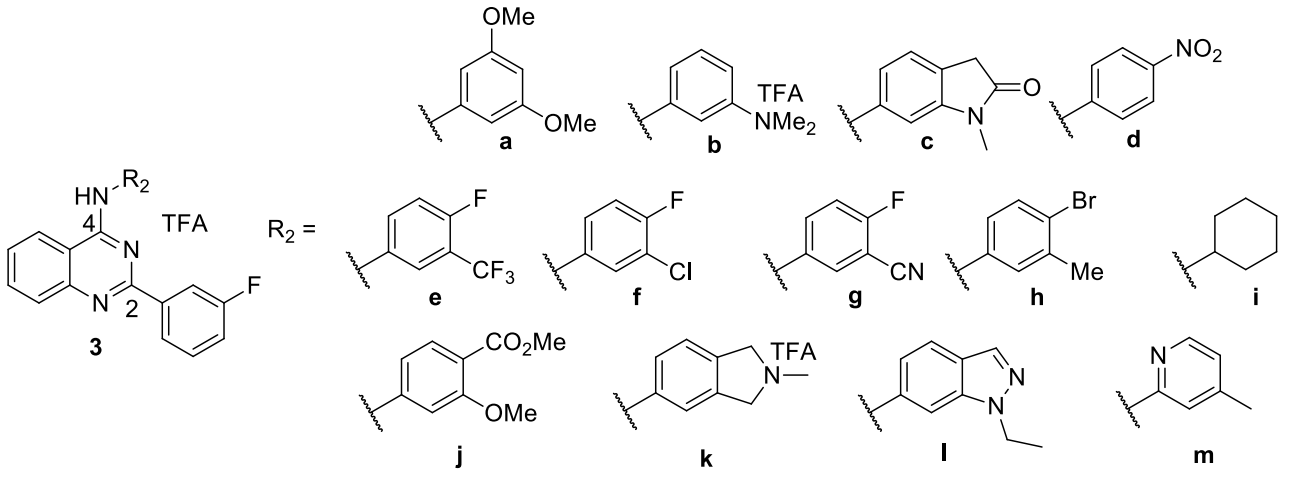

Figure 20. "**4**"-Modified array: chemical structures, compounds **3a-m**.

In order to be suitable for parallel synthesis, the synthetic pathway used for compounds **2a-i** had to be modified as shown in Scheme 18.

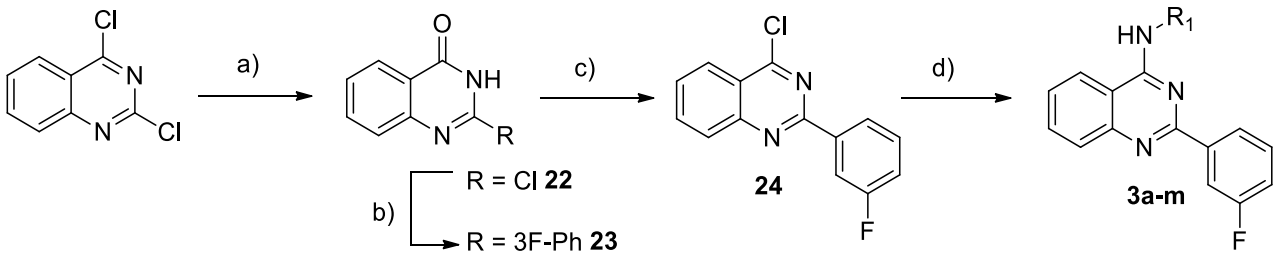

a) NaOH, H_2O, RT, 3hrs, **84%**; b) 3-Fluorobenzeneboronic acid, $Pd(PPh_3)_4$, 2M aq. Na_2CO_3aq, dioxane, 105°C, 7hrs; c) $SOCl_2$, DMF, 75°C, 30min, **70%** over two steps; d) NH_2R_1, TEA, THF, 80°C, 8hrs.

Scheme 18. "**4**"-Modified array: synthesis of compounds **3a-m**.

In order to mask the higher reactivity of the 2-position of 2,4-dichloro quinolone, it was hydrolysed to the corresponding amide **22** (step a). Then, Suzuki coupling with 3-Fluorophenylboronic acid in standard conditions (step b) was followed by chlorination of amide **23** (step c), in good overall yields. The nucleophilic substitution at position 4 on compound **24** was initially performed as reported for dichloro quinazoline (step a, Scheme 17; step d, Scheme 19).

Most reactive, electron-rich array members **3a-c** could be prepared with this experimental procedure, but less reactive/electron-poor compound **3d** could not be obtained in high yields. Thus, an extensive optimization of the nucleophilic substitution conditions was carried out on such transformation, as shown in Table 2.

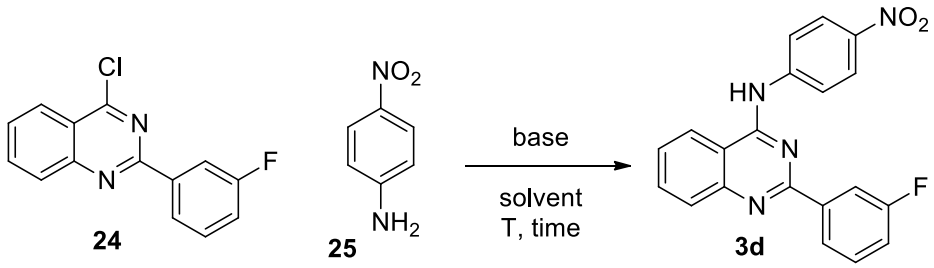

Table 2. Synthesis of compound **3d** from chloro quinazoline **24** (1 eq): chemistry assessment.

Entry	**25** (eq)	Base (eq)	Solvent [0.1M]	T (°C)	Time (hrs)	% conversion (measured by UPLC-MS)
1	1.1	TEA (1.5 eq)	THF	80	6	<10
2	3	TEA (3 eq)	THF	80	8	<20
3	1.1	TEA (1.5 eq)	dioxane	105	8	<45
4	1.1	K_2CO_3 (1.5 eq)	dioxane/H_20 4:1	105	8	<45
5	1.1	K_2CO_3 (1.5 eq)	dioxane/H_20 4:1	105, µW	3	≈50
6	1.1	LiHMDS (1 eq)	THF	25	10 min	≈60
7	1.1	LiHMDS (2 eq)	THF	25	20 min	100

Poor conversions of starting chloride **24** were observed by using an excess of aniline **25** (entry 2). A THF to dioxane switch allowed a 25°C temperature increase, with a moderate improvement in the conversion of **24** to **3d**, either using TEA (entry 3) or an inorganic base (entry 4). Using microwave irradiation, a similar, ≈50% conversion was observed (entry 5).

These discouraging results prompted us to consider a stronger base, so to deprotonate aniline **24**, thus increasing its nucleophilicity. A stoichiometric amount of a [1M] solution of lithium bis(trimethylsilyl)amide (LHMDS) in THF was added dropwise at room temperature, and 10 minutes after the addition ≈60% conversion was detected (entry 6). By just doubling the LHDMS equivalents and time (entry 7), quantitative conversion from **24** to **3d** was detected by UPLC-MS. The target compound **3d** was obtained in high yields and purity after solvent removal and reverse phase chromatography. Please note that the use of LHMDS in such transformation is unprecedented.

The revised nucleophilic substitution protocol (entry 7) was successfully used to synthesize the whole 13-member "**4**"-modified array shown in Figure 20. The results are reported in Table 3.

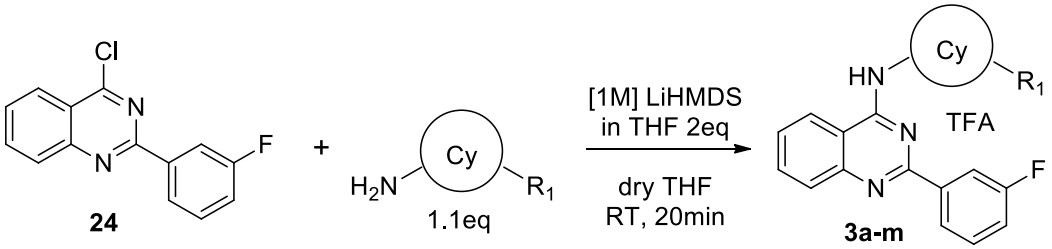

Table 3. Synthesis of "4" modified array from chloro quinazoline **24** (1 eq): chemistry assessment.

Entry	Cy	R_1	Yield % (Isolated)	Product/SM ratio (UPLC-MS)	Purity % (UPLC-MS)
3a	Phenyl	3,5-Ome	82	100:0	98.2
3b	Phenyl	3-Nme_2	77	100:0	97.6
3c	6-indazolin-2-one	N-Methyl	0	Complex mixture, degradation	-
3d	Phenyl	4-NO_2	80	100:0	98.8
3e	Phenyl	4-F, 5-CF_3	81	100:0	97.4
3f	Phenyl	4-F, 5-Cl	79	100:0	99.8
3g	Phenyl	4-F, 5-CN	81	100:0	98.6
3h	Phenyl	4-Br, 5-Me	76	100:0	99.0
3i	Cyclohexyl	-	86	100:0 (1eq of LiHMDS)	99.6
3j	Phenyl	3-Ome, 4-CO_2Me	66	80:10+10 side-products (0°C)	97.0
3k	5-Isoindoline	N-Methyl	83	100:0	99.2
3l	6-Indazole	N_1-Ethyl	84	100:0	99.8
3m	2-Pyridine	5-Methyl	89	100:0	99.6

Halogen, ether, nitrile and tertiary amine groups were well tolerated with this milder reaction protocol, and even "tricky" reagents could be adjusted by further softening the protocol (one LHMDS equivalent for aliphatic amines/**3i**; 0°C for trans-amidation-sensitive aniline ester/**3j**, Table 3). Conversely, a complex degradation mixture was obtained by using the aniline **3c** bearing acidic protons. A needed optimization of the reaction conditions (temperature, amount of base) was not performed, due to time constraints.

The 22 compound-set of putative retromer stabilizer agents built on the 2-aryl-4-arylamino quinazoline scaffold, and shown in Figure 18 to 20, was recently sent to biological in-vitro profiling at the San Raffaele Research Institute, Milan (Dr. Luca Muzio). The results of their biological profiling will be available soon, and will be compared with the similarly ongoing computational prediction for their binding potency.

1.3. ACTIVITY PROFILING: BIOLOGICAL AND VIRTUAL ASSAYS

1.3.1. Preliminary in vitro profiling: identification of AG1

The first array of R55-inspired compounds (**AG1**, **4a,b**, **5** and **6a,b**, Figure 12) was tested at San Raffaele Research Institute. Namely, each compound (10 μM) was incubated with Neuro2A cells, and its effect on Vps35 was determined. First, R55 was used as a standard control, that efficiently and dose-dependently increased Vps35 levels (≈1.8 increase) after 48 hours of incubation (Western blot A, histogram B and Table C Figure 21).

The same test was then executed in triplicate for each tested compound, cells lysates were established after 48 hours' incubation, and levels of Vps35 were normalized on the housekeeping gene β-actin. The fold change/stabilization of Vps35 of the cells treated with these compounds are reported in Table C, Figure 21.

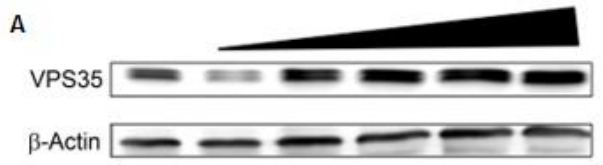

C

COMPOUND	FOLD CHANGE
R55	1.80
4a	2.15
4b	≈ 1
AG1	1.95
5	1.70
6a	≈ 1
6b	≈ 1

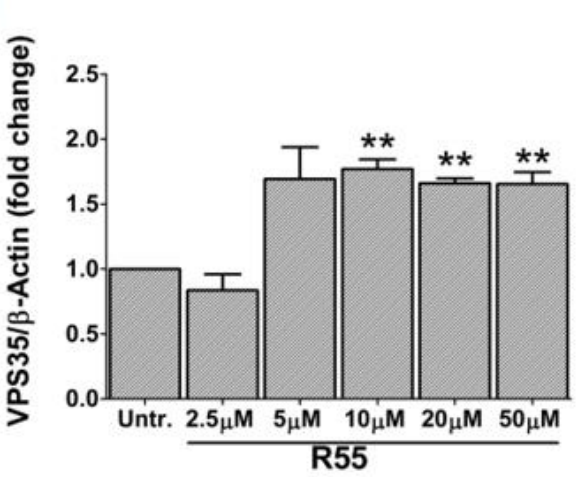

Figure 21. A, B) biochemical effects of R55 on Vps35 in Neuro2A cells. Histogram shows mean ± s.d. values (n=3 for each group). **P < 0.01 determined using Student's t-test. C). Tabulated biochemical effects of compounds **4a,b**, **AG1**, **5** and **6a,b** on Vps35 in Neuro2A cells compared to R55.

As previously mentioned, a single variation (the replacement of isothioureas with Ags – **5**, and of 2,5-substituted thiophene with 1,3-substituted benzene – **4a**), and their combination (**AG1**) led to retromer stabilizers. Conversely, 1,4-substituted phenyls bearing isothioureas (**4b**), aminoguanidine hydrazones (**6a**), and 1,3-substituted dimethyl phenyl compound **6b** were completely inactive.

An in vivo experiment was then performed on spinal cord of WT C57BL6 mice treated with our compounds. C57BL6 mice were intraperitoneally injected daily with either vehicle, standard R55, **4a** and **AG1** (10 mg/kg). After one-week, mice were perfused with saline and their lumbar spina cords dissected and processed to obtain protein extracts. The results are shown in the graph in Figure 22.

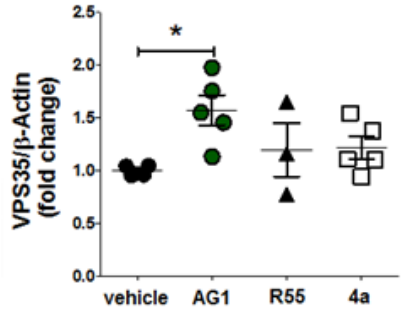

Figure 22. Fold changes of Vps35 measured of spinal cord extracts from mice receiving vehicle, R55 and **AG1.** Each dot represents a single animal. One way ANOVA following Tukey's multiple comparison test. * p<0.05.

No signs of toxicity were observed in each case. As previously mentioned in Paragraph 1.2.1, the most in-vitro active **4a** and **R55** showed only a negligible Vps35 fold increase, conversely to **AG1.** We hypothesized a better bioavailability for **AG1**, that prompted us to select it as a scaffold onto which to expand a detailed SAR toward retromer stabilizing agents.

1.3.2. In-vitro characterization of mono- and di-AGs 1a-q, 13a-f and 15a-c.

The 26-member set of **AG1**-inspired derivatives prepared as in Paragraphs 1.2.2.-1.2.4 was tested for effects on Vps35 levels in the same in vitro assay described in Paragraph 1.3.1. Table 4 shows the mean fold changes/increase of Vps35 (second and fifth columns) ± standard deviation (s.d., third and sixth column) from independent cultures (assays in triplicate, n=3) receiving each **AG1**-derivative at 10 μM for 48 hours. Fold changes are calculated over Vps35 levels measured in vehicle-treated cells, with **AG1** used as a standard.

COMPOUND	FOLD CHANGE	Standard deviation	COMPOUND	FOLD CHANGE	Standard deviation
Vehicle	1.00	-	**1n**	1.28	0.16
AG1	1.95	0.03	**1o**	1.50	0.32
1a	1.15	0.34	**1p**	1.58	0.28
1b	1.30	0.52	**1q**	1.78	0.37
1c	1.62	0.39			
1d	2.48	1.61	**13a**	toxic	-
1e	2.08	x	**13b**	toxic	-
1f	1.42	0.98	**13c**	1.98	0.69
1g	2.08	0.73	**13d**	inactive	x
1h	inactive	x	**13e**	inactive	x
1i	1.30	0.25	**13f**	1.10	x
1j	inactive	x			
1k	inactive	x	**15a**	**15a**	**15a**
1l	1.67	0.13	**15b**	**15b**	**15b**
1m	0.98	0.15	**15c**	**15c**	**15c**

Table 4. In vitro and in silico profiling data for di-AGs **1a-q** and **13a-f**, and for mono-AGs **15a-c**. x: single experiment (n=1), no standard deviation.

Most compounds were able to increase the levels of Vps35 (sometimes even better than **AG1**; see for example 4-OMe/**1d,** 4-OnBu/**1e** and **5**-Me/**1g**), although with a certain variability. To this regard, **AG1** was tested several tens of times, though the test s.d. is extremely low, and its reliability is solid; the other values – as indicated by much higher s.d. – are less reliable, but still indicate a SAR among compounds.

In particular, little or no activity (fold change ≤1.30) was observed for 2-substituted **2**-Br/**1b** and for mono-AGs **14a-c**.

4-Substitutions appear to be promising, as all four 4-substituted di-AGs **1c-f** show fold change activity, and either the phenol 4-OH/**1d** and the small ether 4-OMe/**1e** should be more potent than **AG1**.

5-Substitutions (12 compounds, tri-AG **1a** and di-AGs **1g-q**) offer a complex SAR picture. Seven (bulky substituents, 5-Br/**1h**, 5-Ph/**1k**, 5-NO_2/**1j** and 5-NHpMeBz/**1m**, but also 5-OMe/**1i**, 5-NHMs/**1n** and tri-AG/**1a**) show little or no activity. Four (5-COOMe/**1p**, and hydrophilic 5-NHAc/**1l**, NHTos/**1o**, and 5-CONPip/**1q**) show comparable/slightly lower activity than **AG1**, while only 5-Me/**1g** should be more potent than **AG1**.

N-Substitutions (6 compounds, **13a-f**) also span the activity spectrum. Namely, three of them (**13d-f**, sharing a N_2N_3-cyclized substitution) were substantially inactive; N_2-pyrr/**13c**, containing a cyclic N_2 substituent, showed a comparable/possibly higher potency than **AG1**; and **13a,b**, containing an acyclic, lipophilic N_2 substituent, showed significant toxicity at the tested 10μM concentration.

While the 26-membered set of compounds could not fully explore the SAR around the phenyl di-AG scaffold, and the assay reliability is not ideal, some preliminary indications can be extracted, and hypotheses – to be confirmed by future work/analogues – can be formulated.

As to phenyl ring substitutions (**1a-q**), the most exploited position 5/meta to both AGs appears either to be detrimental, or neutral to biological activity; only the small 5-Me/**1g** compound is promising, so that further 5-substituted di-AGs should not be a priority. As to position 4/adjacent to an AG, small hydrophilic/electron-rich groups (4-OH/**1d**, 4-OMe/**1e**) are potent analogues, while either a longer ether or a bulky hydrophobic group (4-OnBu/**1f**, 4-Br/**1c**) are less active; a deeper exploration of small, hydrophilic substituents (i.e., amines, amides) is thus warranted. As to position 2/orto to both AGs, the inactive 2-Br/**1b** may not be the best substituent, and a few small substituents with different properties (i.e., 2-Me, 2-OMe) should be made. As to AG substitutions (**13a-f**), a cyclization between two AG nitrogens (N_2N_3, **13d-f**) is detrimental. Conversely, the introduction of lipophilic substituents on one nitrogen (N_2, **13a-c**) either is activity-neutral (cyclic N_2 substituent, **13c**), or induces toxicity in Neuro2A cells (lipophilic, acyclic N_2 substituents, **13a,b**). As toxicity could also be an indication of higher potency, N_2-Bu-di-AG/**13a** was also tested at lower concentrations; toxicity was observed even at 2.5 μM, but interesting biological activity was observed at sub-micromolar concentrations (0.6 μM).

These results warrant the synthesis of additional N_2-substituted di-AGs, to further expand their SAR; and suggest to consider putatively synergistic substitutions (i.e., N^2-Bu-5-OR-di-AG) to check their biological activity. Furthermore, we plan to use our recently established computational model for the **AG1** – Vps35-Vps29 interface interaction to try to rationalize current and future activity data for **AG1**-based retromer stabilizers. Images of the three most populated and potent docking poses of **AG1** in its binding site are reported in Figure 23.

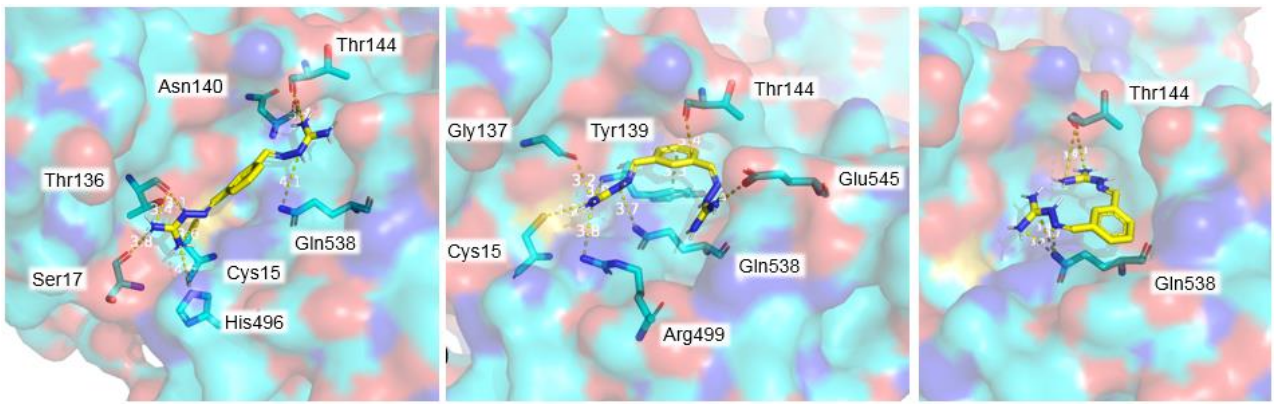

Figure 23. **AG1** docking at the Vps35-Vps29 interface: three preferred poses

.

1.3.3. Detailed in-vitro and in-vivo characterization of AG1

While the synthesis of mono- and di-AGs was continuing, the research team for the retromer project decided to select **AG1** as a lead, and to further characterize in vitro and in vivo as a putative safe and bioavailable retromer stabilizer/ALS treatment.

At first, we verified if the observed fold change/increase of Vps35 depends on its stabilization by **AG1**, or if the compound influences the expression of Vps35/other retromer proteins. Thus, neuro2A cells received vehicle, **AG1** or R55 at 10µM for 48 hours (n=5 for each group), and cell lysates were processed to purify total messenger RNAs (mRNAs) of the retromer components Vps26, Vps29 and Vps35. Real time polymerase chain reaction (PCR) was used to quantify these mRNAs, and the results are summarized in Figure 24.

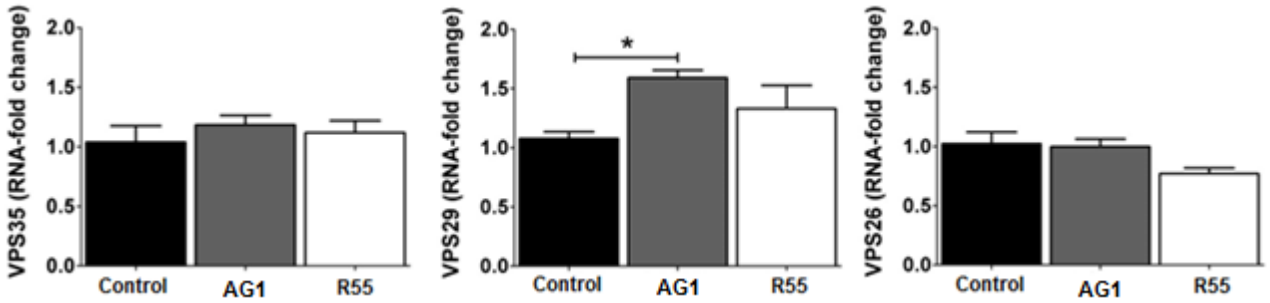

Figure 24. Real time PCR on Vps35, Vps29 and Vps26 mRNA levels from Neuro2A cells treated with vehicle, **AG1** or R55 (10 µM). RNA fold changes are calculated on expression levels measured in untreated cells. Data are visualized as mean ± S.D. One way ANOVA following Tukey's multiple comparison test.

In general, mRNA levels of Vps proteins were not affected by either **AG1**, or by R55. A small, statistically non significant expression increase for Vps29 mRNA was not considered to be relevant.

Then, to start evaluating the effect of retromer increase on pathology/ALS in vitro models, we assayed cell survival of Neuro2A cells transfected with G93A mutated Superoxide Dismutase 1 (SOD), a gene that stimulates an ALS-like phenotype, and eventually causes cell death. In details, SOD1-G93A-transfected Neuro2A cells, or LacZ-transfected Neuro2A/control cells were treated with 10 µM of **AG1**, and incubated for 48 hours; then, their viability/survival was measured. The results are summarized in histogram a, Figure 25.

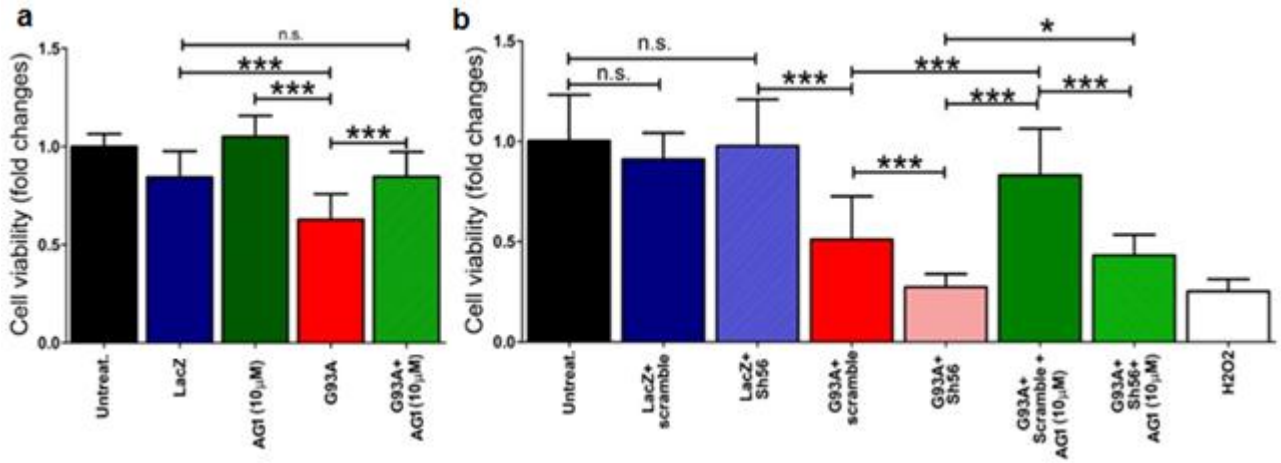

Figure 25. a) Cell survival (fold changes over untreated, mean values ± s.d.) established in Neuro2A transfected with G93A plasmids in the presence/absence of **AG1**. b) Cell survival of Neuro2A cells in a short interference assay.

As expected, no toxicity was detected in untreated, and in LacZ-transfected/control cells (black and blue bars). Treatment of LacZ-transfected cells with **AG1** (10 μM) did not influence viability, indirectly showing its lack of aspecific toxicity (dark green bar). Conversely, SOD G93A-expressing Neuro2A cells showed limited survival (red bar), that was almost completely prevented **AG1** treatment (10 μM, light green bar).

To further correlate the protective effect shown for AG**1** on SOD G93A-expressing Neuro2A cells with the stabilization of the retromer complex, we run a Vps35 short interference RNA (siRNA) assay in Neuro2A cells, where a Vps35-specific, Sh56 siRNA was used to reduce Vps35 levels. Transfected Neuro2A cells were thus treated with either Sh56 or with a scramble/control siRNA, with or without **AG1**; the results are summarized in histogram b, Figure 28.

The reduction of Vps35 levels in LacZ transfected/ control Neuro2A cells did not affect their survival (light blue bar) when compared with untreated cells (black bar). As expected, cell survival was reduced in SOD G93A-expressing Neuro2A cells (red bar), but treatment with Vps35-specific, Sh56 siRNA increased the toxic effect of the SOD G93A mutation (pink bar). While **AG1** (10 μM) confirmed its neuroprotective effect on SOD G93A-expressing Neuro2A cells (dark green bar), its effect was completely abolished by the presence of Vsp35-reducing Sh56 siRNA (light green bar). This definitely proves that the neuroprotective effect of **AG1** on SOD G93A-expressing Neuro2A cells is Vps35-retromer-dependent.

Before moving to in vivo efficacy testing in mice, **AG1** (10mg/kg) was daily injected in heathy mice, to check its pharmacokinetic (PK) profile. Brain and blood samples were collected after 12 hrs, 48 hrs and 7 days. The concentrations of **AG1** were determined in both biological samples using mass spectrometry. We did not observe any **AG1** in blood, possibly pointing to a fast elimination (likely, due to its hydrophilic/charged nature); this bodes well to avoid long term, aspecific toxicity. Conversely, detectable levels of **AG1** were measured in brain extracts - i.e., where the molecular target of **AG1** is located. According to Figure 26, its concentration was 1.4 (±0.5) ng/mg in brain extracts from mice sacrificed after 12 hours, growing to 2.14 (±0.3) ng/mg after 48 hours and to 6.73 (±3.3) ng/mg after 7 days. No signs of gross toxicity were observed in sacrificed mice.

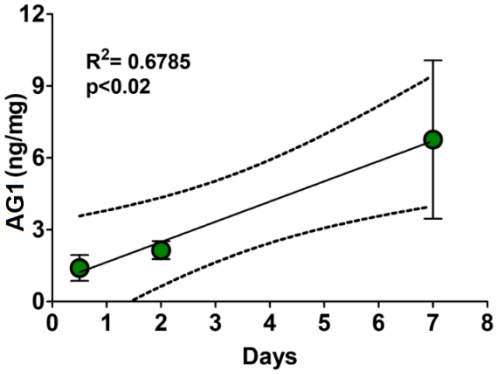

Figure 26. Quantification of **AG1** in WT mice brains.

To address whether retromer stabilization can exert a neuroprotective effect in motor neurons (MNs, the main targets of AL pathologyS) of SOD1 G93A-expressing ALS mice a preclinical experiment in mice was performed to evaluate the amount of **AG1** able to cross the blood brain barrier (BBB).

Due to the interesting *in-vitro* results, the absence of toxicity in vivo, and the limited but accumulation-prone/growing amount of **AG1** found in the brain of mice, a 70 days' preclinical efficacy experiment on SOD1 G93A transgenic mice was performed. Starting from day 30 of age (pre-symptomatic phenotype), SOD1 G93A mice and WT controls were daily injected with **AG1** (10 mg/kg) or vehicle; treatment was blind, so to not influence the evaluation of results. Mice receiving **AG1** displayed a small drop of their body weight, when compared with mice receiving vehicle, but the reduction did not reach statistical significance and did not indicate toxicity (Figure 27A). Rather, SOD1 G93A mice receiving **AG1** displayed a substantial amelioration of the locomotion performances, indicated by increased latency to fall in accelerating rotarod tests (Figure 27B, green dots). This impressive result shows a performance stabilization, juxtaposed to a typical, ALS-like

deterioration for vehicle-treated SOD1 G93A mice (red dots), which is close to the WT mice performance (not shown), thus suggest that a stabilization of the retromer complex can foster protective effects in vivo in ALS-like phenotypes.

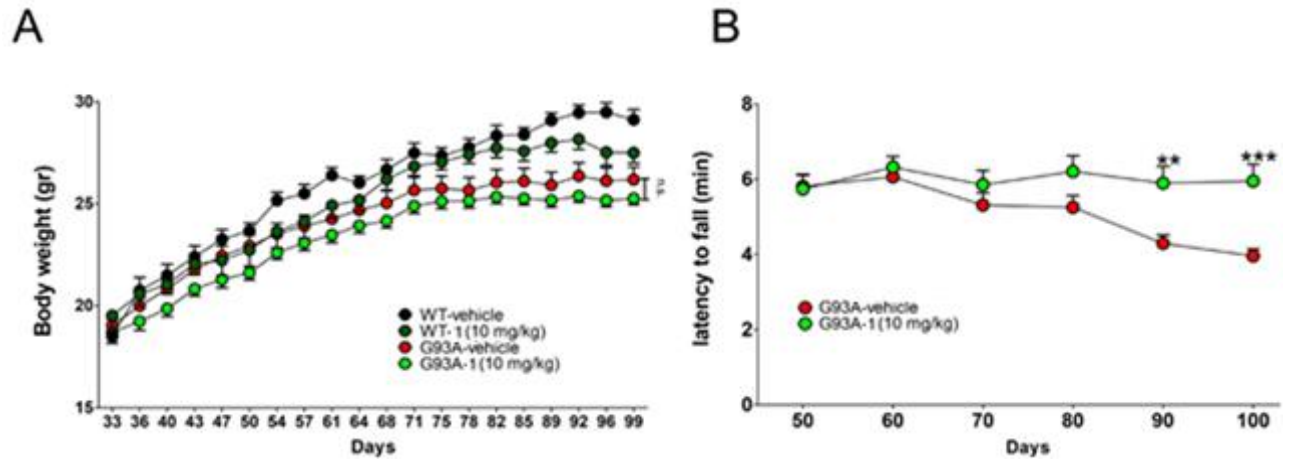

Figure 27. A). Body weight of WT and SOD1 G93A mice receiving **AG1** (10 mg/kg from day 30 to day 100, labelled as **1** in the Figure). B). Latency to fall in SOD1 G93A mice receiving **AG1** (10 mg/kg), (n=15 for each group, symbols indicate means ± s.e.m.). **P < 0.01, ***P<0.001 determined using two way ANOVA followed by Bonferroni multiple comparisons test.

SOD1 G93A mice were sacrificed at day 100, and their lumbar spinal cords assayed for studying MNs cell morphology and numbers. We initially scored neuronal nuclear antigen-positive ($NeuN^+$) neurons in the ventral horn of the spinal cord to monitor bona fide MNs. Mice receiving **AG1** displayed a significantly higher numbers of MNs than vehicle-treated SOD1 G93A mice (Figure 28A, green spots, better shown in the dotted histogram, compare green vs. red dots); similar results were observed scoring the number of choline acetyltransferase-positive ($ChAT^+$, another MN marker) MNs on parallel sections (Figure 28B, red spots, once more better shown in the dotted histogram, compare green vs. red dots).

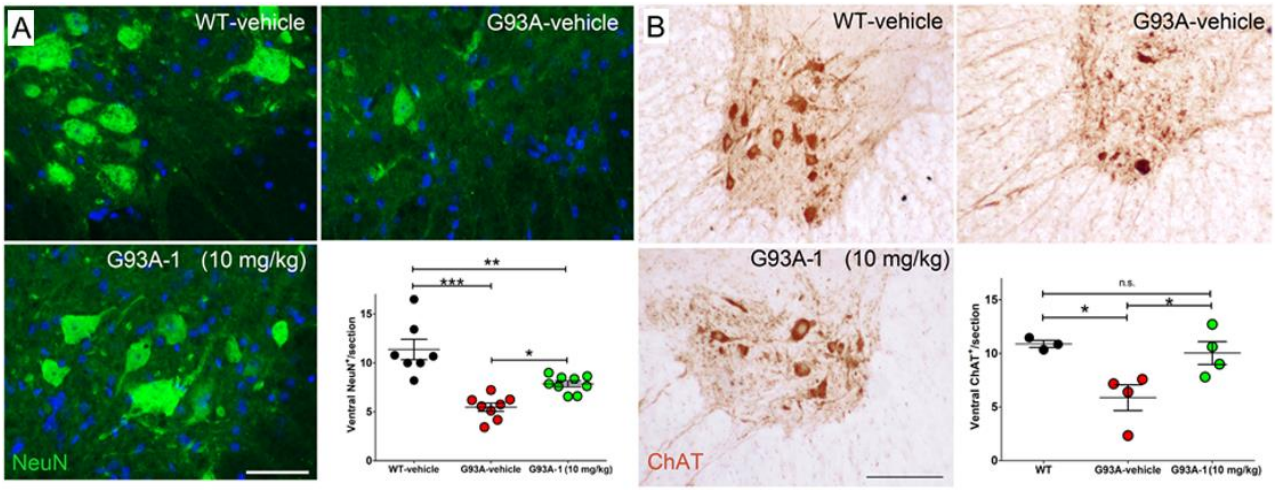

Figure 28. A) Immunofluorescence for NeuN in vehicle-treated WT mice and G93A mice receiving vehicle or **AG1** (10 mg/kg, labelled as **1** in the Figure). Quantifications at day 100 of $NeuN^+$ cells in the ventral horn of lumbar spinal cords are plotted on the histogram (mean values± s.e.m.). B Adjacent sections labelled for ChAT. Quantifications of $ChAT^+$ MNs are shown in the histogram. Each dot in both histograms represent a single animal. *P < 0.05, **P < 0.01, ***P<0.001 determined using one way ANOVA followed by Tukey's Multiple Comparison Test. Scale bar 30µM

Finally, histopathological analysis of sciatic nerves from WT/control and SOD1 G93A mice receiving **AG1** or vehicle was performed. Consistent with the advanced stage of the ALS phenotype, SOD1 G93A mice at day

100 displayed axonal degeneration in sciatic nerves (Figure 29B) when compared with WT/healthy mice (Figure 29A). On the other hand, SOD1 G93A mice treated with **AG1** showed a significant protection of peripheral nerve fibers that was mirrored by a reduction of fibers undergoing degeneration (Figure 29C, D better shown in the dotted histogram, compare green vs. red dots).

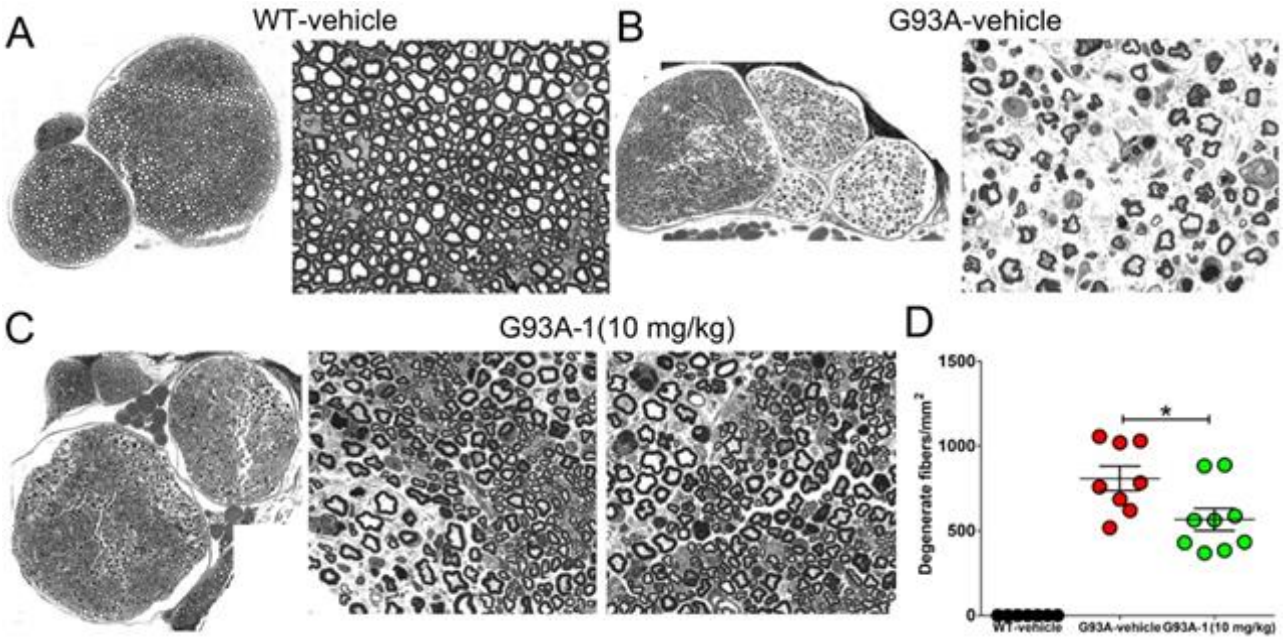

Figure 29. (A)Transverse semi-thin sciatic sections of fibers in WT mice receiving vehicle, (B) in SOD1 G93A mice receiving the vehicle, and (C) in SOD1 G93A mouse receiving **AG1** (10 mg/kg, labelled as **1** in the Figure). Quantifications of degenerating fibers are plotted in the histogram of panel D. Each symbol represents a single animal while the histogram shows the mean value ± s.d. (*P < 0.05 determined using one way ANOVA followed by Tukey's Multiple Comparison).

Clearly, in vitro and in vivo profiling of **AG1** shows its potential in the treatment of retromer-dependent NDDs in general, and ALS in particular. We believe that, by further characterizing either other available **AG1** analogues or new ones to be prepared, the chance of finding even more potent compounds is significant.

1.4 CONCLUSIONS AND FUTURE PERSPECTIVES

In conclusion, as a main goal, starting from bis-isothioureas R55 and using a ligand-based approach, bis-aminoguanidine hydrazone **AG1** was synthetized, in-vitro characterized at San Raffaele Institute and found to be more potent and bioavailable than the isothiourea. Taking advantage of this validation, a small array of more than 20 AG**1**-inspired mono- and bis-aminoguanidine hydrazones (AGs) was rationally designed, synthetized and in vitro characterized (Figure 30).

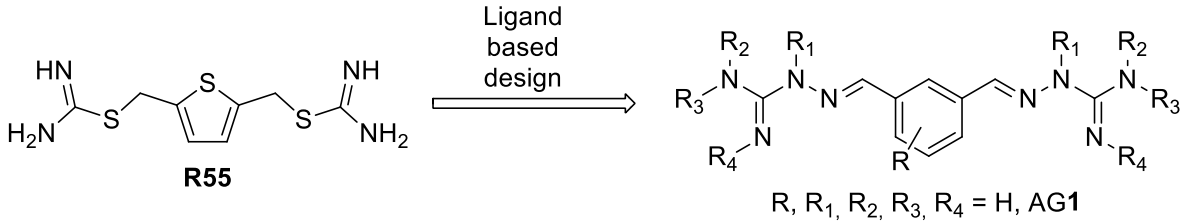

Figure 30. Novel, patentable retromer stabilizers: my strategy.

As shown in the previous Section, two AGs are required for the biological activity, while modification both on the phenyl spacer and on the charged moiety are well tolerated and - if suitably chosen to establish new molecular interactions in the binding site – may even increase the biological activity of the AGs. In conclusion, my efforts led to the identification of a new bis-aminoguanidyl phenyl hydrazone-based chemotype suitable as retromer stabilizer that was protected in a patent application filed by San Raffaele Institute and the University of Milan. Starting from the acquired data around AGs, several other compounds will be synthetized in the next future to establish a clear Structure-Activity-Relationship (SAR).

Compound **AG1**, in particular was selected for intensive in vitro and in vivo characterization. It was found able to significantly increase Vps35 levels and, as a consequence, the retromer functioning in Neuro2A cells transfected with plasmids encoding the ALS-recapitulating G93A mutant form of the SOD1 protein. In a preclinical experiment, administering **AG1** to G93A mice, we observed a retromer increase-dependent reduction of MN degeneration, as well as a decreased peripheral fibers' loss. Treated ALS-like mice, then, displayed increased locomotion performances. These findings open a new avenue for the disease-modifying treatment of ALS. Among planned future modifications on the **AG1** scaffolds, some will be directed to increase its pharmacokinetic profile (half-life, general bioavailability, BBB permeability, and so on).

As a second goal, taking advantage of the putative binding side of R55- and **AG1**-like pharmacological chaperones on the retromer complex, a novel putative class of retromer stabilizer were identified from a virtual HTS campaign at CNR. Starting from virtual hit **2a**, , 21 different 2,4 disubstituted quinazolines (**2b-i**, **3a-m**, Figure 31) were rationally designed and synthetized using two fully-optimized, convergent approaches suitable for high throughput organic synthesis (HTOS) of larger, similar libraries.

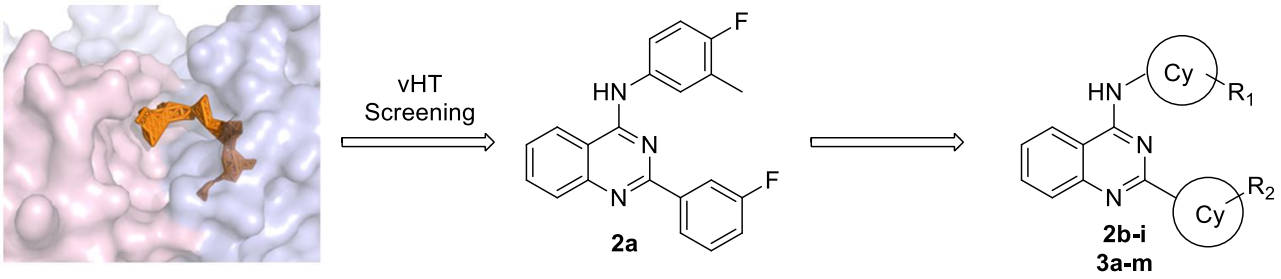

Figure 31. 2,4-Disubstituted quinazolines as retromer stabilizers: my rational strategy.

Their biological characterization in terms of retromer stabilization is ongoing at San Raffaele Institute, and depending on the results our research group will consider the possibility to expand the diversity of virtual hit **2a** analogues, either working on the same scaffold or introducing additional, computational chemistry-suggested chemical modifications.

1.5. EXPERIMENTAL PART: Synthesis and analytical characterization of intermediates and final compounds

1.5.1 GENERAL SYNTHETIC PROCEDURES

1.5.1.1. METHOD A: reduction of substituted isophthalic acids to substituted m-xylene-α,α′-diols

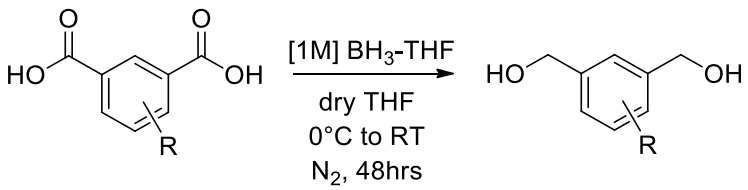

Under nitrogen atmosphere, a suspension of substituted isophthalic acid (1 eq.) in anhydrous THF (1 mL/mmol) was vigorously stirred and cooled to 0°C. A solution of 1M BH_3 in THF (4 eq.) was added dropwise in 1 hr. The reaction mixture was allowed to warm slowly to RT and was stirred for additional 48 hrs. MeOH was added dropwise to quench the reaction mixture, and the solvent was then evaporated under reduced pressure. Addition of MeOH and evaporation was repeated three times. Then, the residue was redissolved in EtOAc (40 mL), washed with saturated aq. $NaHCO_3$ (2 x 20 mL) and brine (10 mL). The organic layer was dried with anhydrous Na_2SO_4, filtered and evaporated. The resulting solid was purified by flash chromatography on silica gel (eluant mixture: n-hexane/EtOAc) to afford the corresponding pure substituted **m-xylene-α,α′-diol**.

1.5.1.2. METHOD B: oxidation of substituted m-xylene-α,α′-diols to substituted isophthalaldehydes

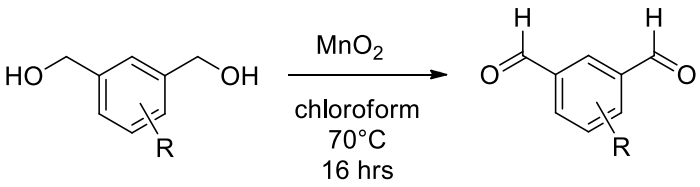

Solid MnO_2 (5-10 eq.) was added under vigorous stirring to a solution of **m-xylene-α,α′-diol** (0.5-2 mmoles, 1 eq.) in chloroform (5-10 mL/mmol), and the reaction mixture was heated at reflux. After overnight reflux/stirring, the reaction mixture was cooled to RT, and filtered through a Celite pad. The pad was washed with CH_2Cl_2 or EtOAc (40 mL), the combined organic phase was concentrated in vacuo, and the residue was purified by flash chromatography on silica gel (eluant mixture: n-hexane/EtOAc) to afford the corresponding pure substituted isophthalaldehyde.

1.5.1.3 METHOD C: Condensation between substituted m-dicarbonyl arenes and N-unsubstituted aminoguanidines

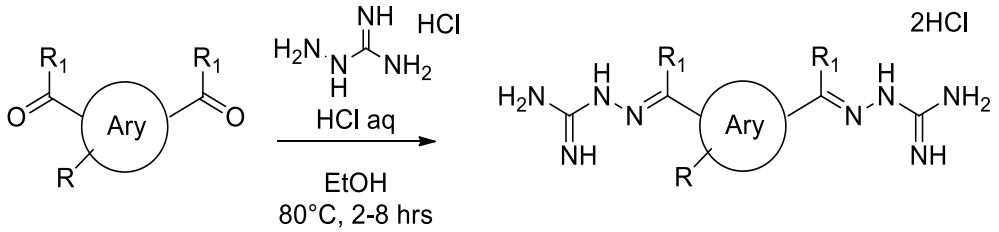

Aminoguanidine hydrochloride (1 eq.) and 1N aq. HCl (3-5 drops, catalytic) were sequentially added to a warm, vigorously stirred solution of substituted *m*-dicarbonyl arene (1 eq.) in absolute EtOH (3-10 mL/mmol). The reaction mixture was refluxed, with TLC monitoring (eluant mixture: CH_2Cl_2/MeOH 8:2 with a few AcOH drops). Precipitation of a white solid was often observed. After 2-8 hours, the reaction mixture was cooled to RT, the solid product was filtered, washed with cold EtOH (10 mL), with Et_2O (10 mL), and dried in vacuum to yield the corresponding pure N-unsubstituted phenyl 1,3-bisaminoguanidyl hydrazone.

1.5.1.4. METHOD D: Condensation between isophthalaldehyde and N-substituted aminoguanidines

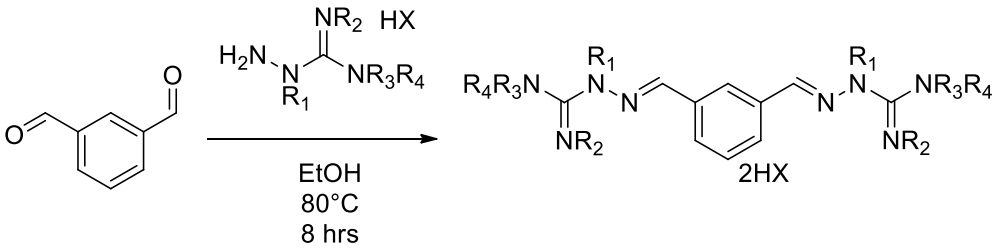

An appropriate aminoguanidine salt (2 eq.) was added to a warmed, vigorously stirred solution of isophthalaldehyde (1 eq.) in absolute EtOH (7.5 mL/mmol). The reaction mixture was refluxed, with TLC monitoring (eluant mixture: CH_2Cl_2/MeOH 8:2 with a few AcOH drops). Precipitation of a white solid was often observed. After 8 hours, the reaction mixture was cooled to RT, the solid product was filtered, washed with cold EtOH (10 mL), with Et_2O (10 mL, and dried in vacuum to yield the corresponding pure N-substituted phenyl 1,3-bisaminoguanidyl hydrazone.

1.5.1.5. METHOD E: Suzuki cross-coupling on intermediate 21

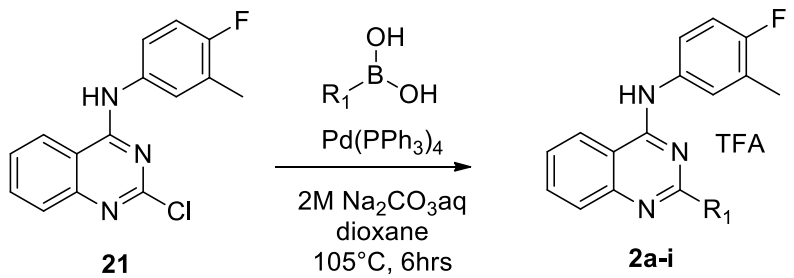

21 **2a-i**

2-chloro-N-(4-fluoro-3-methylphenyl)quinazolin-4-amine **1** (35-52 mg), the appropriate boronic acid (1.5 eq) and $Pd(PPh_3)_4$ (0.1 eq) were weighed in a microwave vial. The vial was capped and a stream of N_2 was bubbled for 5 minutes to remove the air. Degassed dioxane (c.a 0.12M, 0.8 - 1.2 mL) was added, followed by 2M aq. Na_2CO_3 (2 eq). The yellow mixture was stirred at 105°C for 6 hrs, then cooled to RT, diluted with AcOEt (20 mL), washed with 0.5M NaOH (2 x 10 mL) and with brine (10 mL). The organic phase was dried over anhydrous Na_2SO_4, filtered and concentrated. The crude was chromatographed on silica gel (eluant mixture: petroleum ether/AcOEt) to rapidly remove the phosphine oxide. The required purity threshold was reached by preparative HPLC using H_20/MeCN and 0.05% of TFA as solvents, to yield the corresponding 2-substituted-N-(4-fluoro-3-methylphenyl)quinazolin-4-amines.

1.5.1.6. METHOD F: Aromatic substitution on 4-chloro-2-(3-fluorophenyl)quinazoline 23

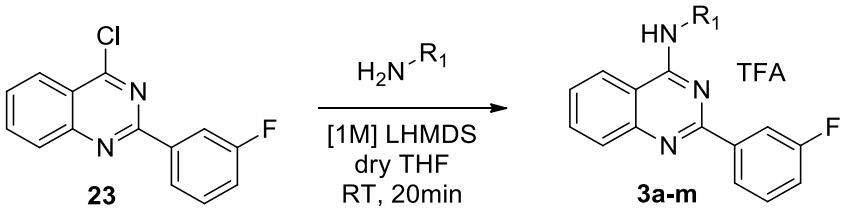

Under nitrogen atmosphere, 1M LHMDS in THF(2eq) was slowly added dropwise to a stirred mixture of 4-chloro-2-(3-fluorophenyl)quinazoline **23** (1 eq) and the corresponding aniline (1.1-1.2 eq) in dry THF (20 mL/mmol). The reaction mixture was stirred for further 20 minutes, then TFA (5eq) was added. The reaction mixture was stirred for further 5 minutes, then it was concentrated under vacuum. The crude was purified by reverse phase chromatography (eluant mixture: H_20/MeCN + 0.1% TFA), to yield the corresponding 2-(3-fluorophenyl)-N-substituted quinazolin-4-amines.

1.5.2. Synthesis of 1,3-phenyl di-aminoguanidyl hydrazone hydrochloride AG1

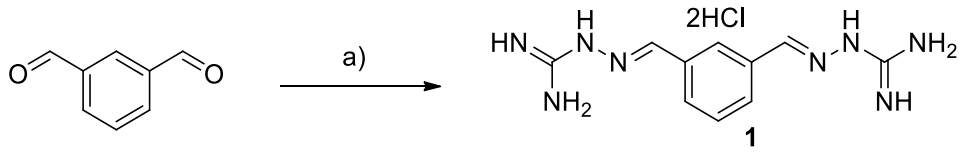

a) aminoguanidine-HCl, cat. 1N HCl_{aq}, EtOH, 80°C, 4hrs, **88%**.

The reaction was performed according to **METHOD C**, using isophthalaldehyde (400 mg, 3.00 mmoles), aminoguanidine hydrochloride (663.3 mg, 6.00 mmoles) and absolute EtOH (10 mL). Pure 1,3-bisamidino phenylhydrazone hydrochloride **AG1** (839.7 mg ,2.64 mmoles) was obtained as a white solid in **88%** yield.

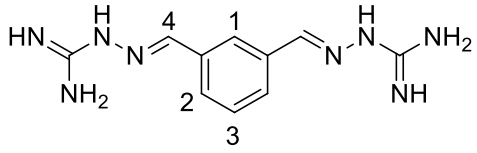

Characterization: m.p. = 200-204 °C

^{1}H NMR (400 MHz, DMSO-d_6) δ: 12.26 (bs, 2H, NH), 8.32 (s, 1H, H1), 8.22 (s, 2H, H4), 8.15-7.58 (bs, 6H, NH), 7.96 (d, J = 7.6 Hz, 2H, H2), 7.53 (t, J = 7.6 Hz, 1H, H3).

^{13}C NMR (100 MHz, D_2O) δ: 154.7, 147.3, 133.2, 129.2, 126.6.

MS (ESI), m/z: calcd for $C_{10}H_{14}N_8$·246.13, found 247.20 ($M+H^+$).

1.5.3. Synthesis of 2,5 thienyl di-aminoguanidyl hydrazone hydrochloride 5

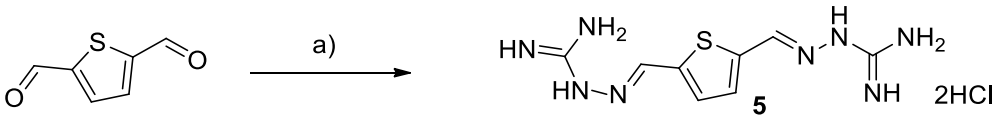

a) aminoguanidine-HCl, cat. 1N HCl_{aq}, EtOH, 80°C, 4hrs, **75%**

The reaction was performed according to **METHOD C**, using 2,5-thiophenedicarboxaldehyde (132 mg, 0.94 mmoles), aminoguanidine (207 mg, 1.88 mmoles) and absolute EtOH (5 mL). Pure 1,3-bisamidino thiophenyl hydrazone hydrochloride **5** (229.2 mg, 0.71 mmoles) was obtained as a yellow solid in 75% yield.

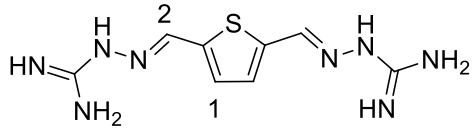

Characterization: m.p. = 290-296 °C dec.

^{1}H NMR (400 MHz, DMSO-d_6) δ: 12.22 (bs, 2H, NH), 8.41 (s, 2H, H2), 8.00-7.60 (m, 6H, NH), 7.50 (s, 2H, H1).

^{13}C NMR (100 MHz, DMSO-d_6) δ: 156.6, 143.2, 141.5, 133.2.

MS (ESI), m/z: calcd for $C_8H_{12}N_8S$·252.09, found 253.14 ($M+H^+$).

1.5.4. Synthesis of 1,4-phenyl di-aminoguanidyl hydrazine hydrochloride 6a

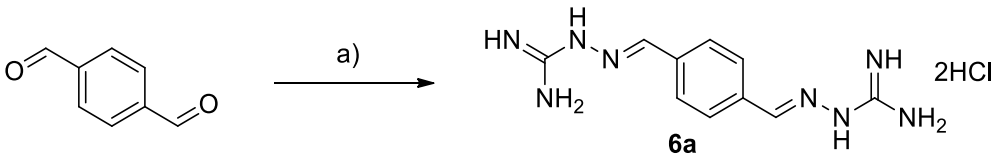

a) aminoguanidine HCl, cat. 1N HCl_{aq}, EtOH, 80°C, 4hrs, **80%**

The reaction was performed according to **METHOD C**, using terephthalaldehyde (290 mg, 2.16 mmoles), aminoguanidine hydrochloride (500 mg, 4.32 mmoles) and absolute EtOH (7 mL). Pure 1,4-bisamidino phenylhydrazone hydrochloride **6a** (551.6 mg, 1.72 mmoles) was obtained as a white solid in **80%** yield.

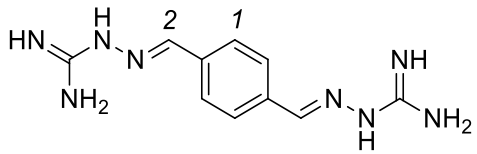

Characterization: m.p. = 337-340 ° dec.

^{1}H NMR (400 MHz, DMSO-d_6) δ: 12.31 (bs, 2H, NH), 8.21 (s, 2H, H2), 7.94 (s, 4H, H1), 7.60-8.20 (bs, 8H, NH).

^{13}C NMR (100 MHz, DMSO-d6) δ: 155.5, 146.0, 135.2, 127.8.

MS (ESI), m/z: calcd for $C_{10}H_{14}N_8$·246.13, found 247.14 ($M+H^+$).

1.5.5. Synthesis of 1,3-phenyl di-aminoguanidyl methyl-hydrazone hydrochloride 6b

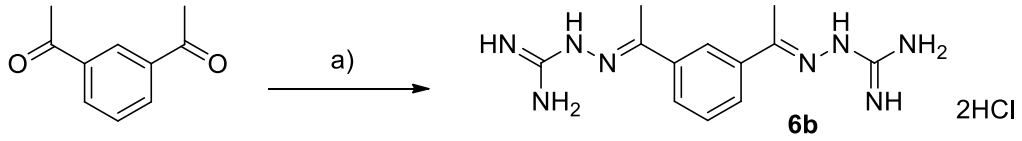

a) aminoguanidine-HCl, cat. 1N HCl_{aq}, EtOH, 80°C, 4hrs, **70%**

The reaction was performed according to **METHOD C**, using 1,3-diacetylbenzene (170 mg, 1.05 mmoles), aminoguanidine hydrochloride (231.8 mg, 2.10 mmoles) and absolute EtOH (5 mL). Pure 1,3-bisamidino phenyl α-methylhydrazone hydrochloride **6b** (274.2 mg, 0.73 mmoles), that precipitated only after cooling at RT, was obtained as a white solid in **70%** yield.

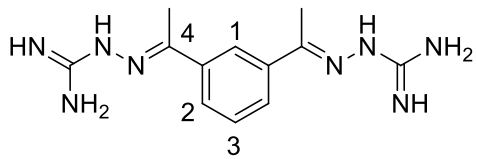

Characterization: m.p. 328-330°C dec.

^{1}H NMR (400 MHz, D_2O) δ: 7.70 (d, J = 9.2 Hz, 2H, H2), 7.35 (s, 1H, H1), 7.29 (t, J = 9.2 Hz, 1H, H3), 1.95 (s, 6H, H4).

^{13}C NMR (100 MHz, D_2O) δ: 155.3, 152.7, 136.0, 128.6, 127.6, 124.0, 13.3.

MS (ESI), m/z: calcd for $C_{12}H_{18}N_8$ 274.17, found 275.23 ($M+H^+$).

1.5.6. Synthesis of 1,3,5-phenyl tri-aminoguanidyl hydrazone hydrochloride 1a

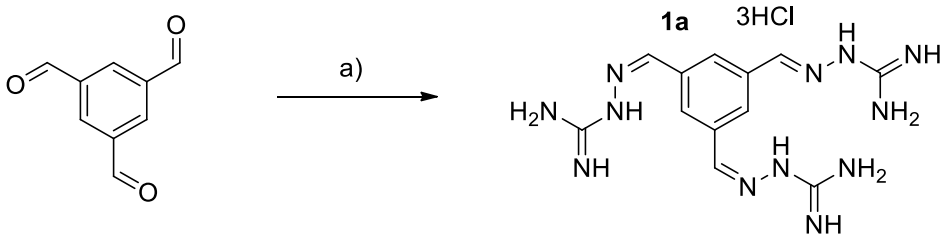

a) aminoguanidine-HCl, cat. 1N HCl_{aq}, EtOH, 80°C, 4hrs, **78%**

The reaction was performed according to **METHOD C**, using benzene-1,3,5-tricarboxaldehyde (50 mg, 0.308 mmoles), aminoguanidine hydrochloride (112.5 mg, 1.018 mmoles) and absolute EtOH/H_20 9:1 (5 mL). Pure 1,3,5-trisamidino phenylhydrazone hydrochloride **1a** (105.2 mg, 0.240 mmoles) was obtained as a white solid in **78**% yield.

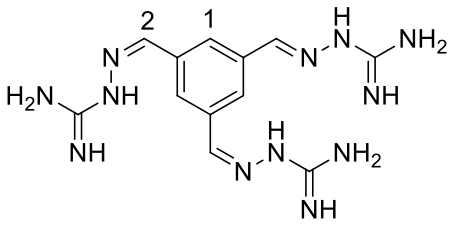

Characterization: m.p. > 350 °C

^{1}H NMR (400 MHz, D_2O) δ: 7.57 (s, 3H, H2), 7.30 (s, 3H, H1).

^{13}C NMR (100 MHz, D_2O) δ: 154.5, 146.3, 133.4, 127.6.

MS (ESI), m/z: calcd for $C_{12}H_{18}N_{12}$·330.178, found 330.23 ($M+H^+$).

1.5.7. Synthesis of 2-Br-1,3-phenyl di-aminoguanidyl hydrazone hydrochloride 1b

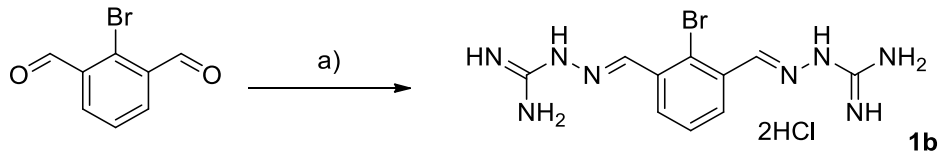

a) aminoguanidine-HCl, cat. 1N HCl_{aq}, EtOH, 80°C, 2hrs, **89%**

The reaction was performed according to **METHOD C**, using 2-bromoisophthalaldehyde (197 mg, 0.93 mmoles), aminoguanidine hydrochloride (205 mg, 1.86 mmoles) and absolute EtOH (9 mL). Pure 2-bromo-1,3-bisamidino phenylhydrazone hydrochloride **1b** (330 mg, 0.84 mmoles) was obtained as a white solid in **89%** yield.

Characterization: m.p. = 244-246 °C

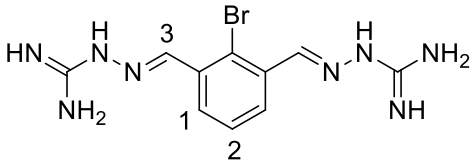

^{1}H NMR (400 MHz, DMSO-d_6) δ: 12.22 (bs, 2H, NH), 8.65 (s, 2H, H3), 8.38 (d, J = 7.7 Hz, 2H, H1), 8.30-7.60 (bs, 6H, NH), 7.51 (t, J = 7.7 Hz, 1H, H2).

^{13}C NMR (100 MHz, D_2O) δ: 155.6, 146.7, 132.9, 130.0, 126.9.

MS (ESI), m/z: calcd for $C_{10}H_{13}BrN_8$·324.04, found 325.14 ($M+H^+$).

1.5.8. Synthesis of 4-Br-1,3-phenyl di-aminoguanidyl hydrazone hydrochloride 1c

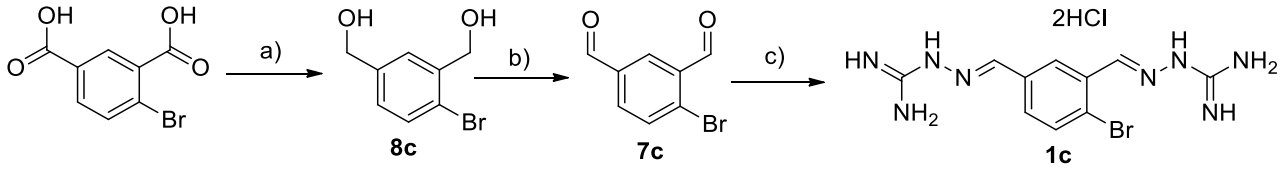

a) 1M BH_3-THF, dry THF, N_2, 0°C to RT, 48hrs, **86%**; b) MnO_2, chloroform, 70°C, 16hrs; **86%**; c) aminoguanidine HCl, cat. 1N HCl_{aq}, EtOH, 80°C, 4hrs, **88%**.

(4-Bromo-1,3-phenylene)dimethanol 8c

The reaction was performed according to **METHOD A**, using 4-bromo-isophthalic acid (590 mg, 2.41 mmoles), 1M BH_3 in THF (10 ml, 10.00 mmoles) and THF (2.5 mL). Pure 4-bromo ,3-xylene-α,α'-diol **8c** (455 mg, 2.10 mmoles) was obtained as a white solid in **86%** yield.

The analytical characterization of this intermediate is not available.

4-Bromoisophthalaldehyde 7c

The reaction was performed according to **METHOD B**, using 4-bromo-1,3-xylene-α,α'-diol (128 mg, 0.59 mmoles), solid MnO_2 (257 mg, 2.95 mmoles) and chloroform (3 mL). Pure 4-bromo isophthalaldehyde **7c** (108.0 mg, 0.508 mmoles) was obtained as a white solid in **86%** yield.

The analytical characterization of this intermediate is not available.

4-Br-1,3-Phenyl di-aminoguanidyl hydrazone hydrochloride 1c.

The reaction was performed according to **METHOD C**, using 4-bromoisophthalaldehyde (108 mg, 0.51 mmoles), aminoguanidine hydrochloride (112 mg, 1.02 mmoles) and absolute EtOH (5 mL). Pure 4-bromo-1,3-bisamidino phenylhydrazone hydrochloride **1c** (178 mg, 0.44 mmoles) was obtained as a white solid in **88%** yield.

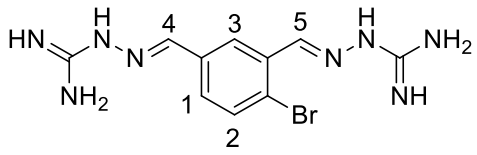

Characterization: m.p. = 310-314 °C

^{1}H NMR (400 MHz, DMSO-d_6) δ: 12.40 (bs, 2H, NH), 8.58 (d, J = 2.0 Hz, 1H, H3), 8.54 (s, 1H, H4 or H5), 8.20 (s, 1H, H5 or H4), 8.20-7.60 (bs, 6H, NH), 7.98 (dd, J = 2.0 Hz, J = 8.4 Hz, H1), 7.78 (d, J = 8.4 Hz, 1H, H2).

^{13}C NMR (100 MHz, DMSO-d_6) δ: 157.0, 156.8, 146.3, 145.8, 134.8, 134.7, 133.8, 131.1, 128.5, 126.5.

MS (ESI), m/z: calcd for $C_{10}H_{13}BrN_8$·324.04, found 325.14 ($M+H^+$).

1.5.9. Synthesis of 4-OH-1,3-phenyl di-aminoguanidyl hydrazone hydrochloride 1d

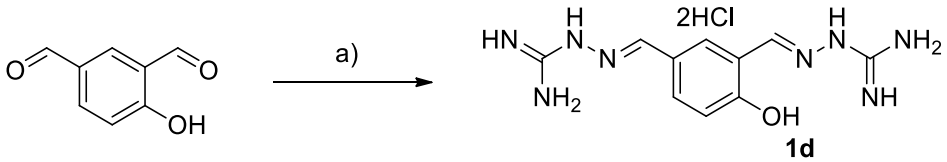

a) aminoguanidine-HCl, cat. 1N HCl_{aq}, EtOH, 80°C, 2hrs, **77%**

The reaction was performed according to **METHOD C**, using 4-hydroxyisophthalaldehyde (132 mg, 0.87 mmoles), aminoguanidine hydrochloride (193 mg, 1.75 mmoles) and absolute EtOH (8 mL). Pure 4-hydroxy-1,3-bisamidino phenylhydrazone hydrochloride **1d** (224 mg, 0.67 mmoles), that precipitated only after cooling at RT, was obtained as a white solid in **77%** yield.

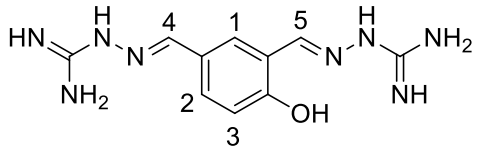

Characterization: m.p. = 189-195 °C

^{1}H NMR (400 MHz, DMSO-d_6) δ: 12.05 (bs, 2H), 10.95 (bs, 1H, OH), 8.52 (s, 1H, H4 or H5), 8.48 (d, J = 1.8 Hz, 1H, H1), 8.12 (s, 1H, H5 or H4), 8.20-7.40 (bs, 6H, NH), 7.95 (dd, J = 8.6 Hz, J = 1.8 Hz, 1H, H3), 7.05 (d, J = 8.6 Hz, 1H, H2).

^{13}C NMR (100 MHz, D_2O) δ: 158.8, 155.7, 155.4, 148.4, 147.4, 131.6, 129.4, 126.1, 119.3, 117.7.

MS (ESI), m/z: calcd for $C_{10}H_{14}N_8O$·262.13, found 263.21 ($M+H^+$).

1.5.10. Synthesis of 4-OMe- and 4-OnBu-1,3-phenyl di-aminoguanidyl hydrazone hydrochloride 1e and 1f

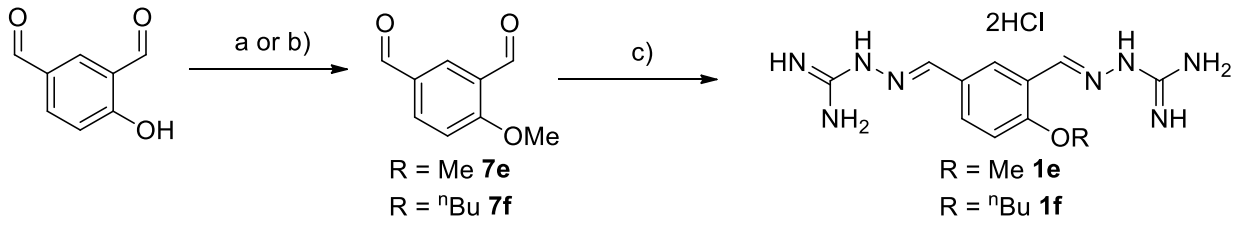

a) MeI, K_2CO_3, dry DMF, N_2, RT, 24 hrs, **60%**; b) BuBr, K_2CO_3, dry DMF, N_2, 85°C, 24 hrs, **75%**; c) aminoguanidine HCl, cat. 1N HCl_{aq}, EtOH, 80°C, 8hrs, **79%** (**1e**), **80%** (**1f**).

4-Methoxyisophthalaldehyde 7e

Methyl iodide (0.13 mL, 2 mmoles, 2 eq.) was added to a stirred mixture of 4-hydroxyisophthalaldehyde (150 mg, 1 mmol, 1 eq.) and K_2CO_3 (420 mg, 3 mmoles, 3 eq.) in dry DMF (5 mL) under nitrogen atmosphere. The reaction mixture was stirred at RT for 24 h, then the solvent was removed at reduced pressure. The crude was suspended in EtOAc (30 mL), washed with 5% aqueous NaOH (3 x 20 mL) and with brine (10 mL). The combined organic layer was dried with anhydrous Na_2SO_4, filtered and evaporated. 4-Methoxyisophthalaldehyde **7e** (105 mg, 0.60 mmoles) was obtained with a **60%** yield as a white solid that was pure enough to be used without further purification.

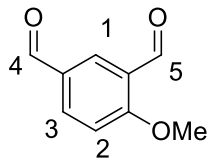

Characterization:

^{1}H NMR (400 MHz, $CDCl_3$) δ: 10.50 (s, 1H, H4 or H5), 10.01 (s, 1H, H5 or H4), 8.35 (d, J = 2.0 Hz, 1H, H1), 8.12 (dd, J = 2.0 Hz, J = 9.1 Hz, 1H, H3), 7.15 (d, J = 9.1 Hz, 1H, H2), 4.00 (s, 3H, OMe).

4-Butoxyisophthalaldehyde 7f

n-BuBr (0.22 mL 2 mmoles, 2 eq.) was added to a stirred mixture of 4-hydroxyisophthalaldehyde (150 mg, 1 mmol, 1 eq.) and K_2CO_3 (420 mg, 3 mmoles) in dry DMF (5 mL) under nitrogen atmosphere. The reaction mixture was heated under stirring at 85°C for 24 hrs, then cooled to RT. The solvent was removed at reduced pressure. The crude was suspended in EtOAc (30 mL), washed with 5% aqueous NaOH (3 x 20 mL) and with brine (10 mL). The combined organic layer was dried with anhydrous Na_2SO_4, filtered and evaporated. 4-Buthoxyisophthalaldehyde **7f** (155 mg, 0.75 mmoles) was obtained with a **75%** yield as a white solid that was pure enough to be used without further purification.

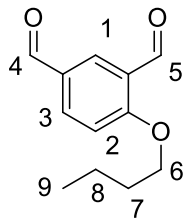

Characterization:

^{1}H NMR (400 MHz, $CDCl_3$) δ: 10.5 (s, 1H, H4 or H5), 10.0 (s, 1H, H5 or H4), 8.35 (d, J = 2.0 Hz, 1H, H1), 8.12 (dd, J = 2.0 Hz, J = 9.1 Hz, 1H, H3), 7.15 (d, J = 9.1 Hz, 1H, H2), 4.23 (t, J = 2.4 Hz, 2H, H6), 1.91 (m, 2H, H7), 1.56 (m, 2H, H8), 1.04 (t, J = 7.8 Hz, 3H, H9).

4-Methoxy-1,3-phenyl di-aminoguanidyl hydrazone hydrochloride 1e

The reaction was performed according to **METHOD C**, using 4-methoxyisophthalaldehyde (75 mg, 0.46 mmoles), aminoguanidine hydrochloride (101 mg, 0.92 mmoles) and absolute EtOH (4.6 mL). Pure 4-methoxy-1,3-bisamidino phenylhydrazone hydrochloride **1e** (126 mg, 0.36 mmoles) was obtained as a white solid in **79%** yield.

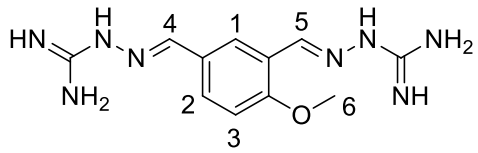

Characterization: m.p. = 301-306 °C dec

^{1}H NMR (400 MHz, DMSO-d_6) δ: 12.12 (bs, 2H, NH), 8.51 (s, 1H, H4 or H5), 8.49 (s, 1H, 1), 8.19 (s, 1H, H4 or H5), 8.20-7.40 (m, 6H, NH), 8.00 (d, J = 6.6 Hz, 1H, H3), 7.12 (d, J = 6.6 Hz, 1H, H2), 3.92 (s, 3H, H6).

^{13}C NMR (100 MHz, DMSO-d_6) δ: 160.1, 156.9, 147.2, 142.7, 132.2, 127.4, 127.0, 123.0, 114.2, 56.2.

MS (ESI), m/z: calcd for $C_{11}H_{16}N_8O$·276.14, found 277.22 ($M+H^+$).

4-^{n}Butoxy-1,3-phenyl di-aminoguanidyl hydrazone hydrochloride 1f

The reaction was performed according to **METHOD C**, using 4-butoxyisophthalaldehyde (110 mg, 0.53 mmoles), aminoguanidine hydrochloride (118 mg, 1.06 mmoles) and absolute EtOH (5 mL). Pure 4-butoxy-1,3-bisamidino phenylhydrazone hydrochloride **1f** (166 mg, 0.42 mmoles) was obtained as a white solid in **80%** yield.

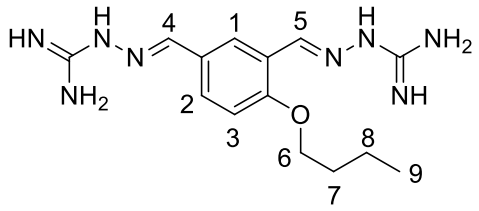

Characterization: m.p. = 292-298 °C dec

^{1}H NMR (400 MHz, DMSO-d_6) δ: 12.12 (bs, 2H, NH), 8.51 (s, 2H, H4 or H5, H1), 8.16 (s, 1H, H5 or H4), 8.20-7.40 (bs, 6H, NH), 8.00 (d, J = 8.7 Hz, 1H, H3), 7.12 (d, J = 8.7 Hz, 1H,H2), 4.15 (t, J = 2.4 Hz, 2H, H6), 1.80 (m, 2H, H7), 1.52 (m, 2H, H8), 0.99 (t, J = 7.8 Hz, 3H, H9).

^{13}C NMR (100 MHz, DMSO-d_6) δ: 160.1, 156.9, 147.2, 142.7, 132.2, 127.4, 127.0, 123.0, 114.2, 69.1, 31.3, 19.3, 14.3.

MS (ESI), m/z: calcd for $C_{14}H_{22}N_8O$·318.19, found 319.26 ($M+H^+$).

1.5.11. Synthesis of 5-mthyle-1,3-phenyl di-aminoguanidyl hydrazone hydrochloride 1g

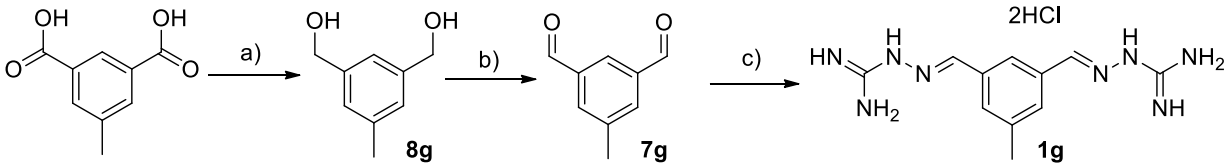

a) 1M BH_3-THF, dry THF, N_2, 0°C to RT, 48hrs, **81%**; b) MnO_2, chloroform, 70°C, 16hrs; **77%**; c) aminoguanidine HCl, cat. 1N HCl_{aq}, EtOH, 80°C, 4hrs, **77%**.

5-Methyl-3-xylene-α,α'-diol 8g

The reaction was performed according to **METHOD A**, using 5-methyl-isophthalic acid (600 mg, 3.33 mmoles), 1M BH_3 in THF (13 mL, 13.3 mmoles) and THF (3 mL). Pure 5-methyl ,3-xylene-α,α'-diol **8g** (410 mg, 2.70 mmoles) was obtained as a pale yellow oil in **81%** yield.

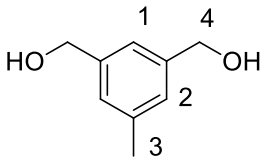

Characterization:

^{1}H NMR (400 MHz, $CDCl_3$) δ: 6.96 (s, 1H, H1), 6.80 (s, 2H, H2), 4.62 (s, 4H, H4), 3.81 (s, 3H, H3), 2.11 (bs, 2H, OH).

5-Methylisophthalaldehyde 7g

The reaction was performed according to **METHOD B**, using 5-methyl-1,3-xylene-α,α'-diol (200 mg, 1.32 mmoles), solid MnO_2 (571 mg, 6.57 mmoles) and chloroform (6.5 mL). Pure 5-methyl isophthalaldehyde **7g** (150.9 mg, 1.02 mmoles) was obtained as a white solid in **77%** yield.

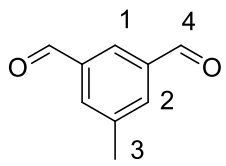

Characterization:

^{1}H NMR (400 MHz, $CDCl_3$) δ: 10.15 (s, 2H, H4), 8.25 (s, 1H, H1), 8.00 (s, 2H, H2), 2.53 (s, 3H, H3).

5-Methyl-1,3-phenyl di-aminoguanidyl hydrazone hydrochloride 1g

The reaction was performed according to **METHOD C**, using 5-methylisophthalaldehyde (104 mg, 0.70 mmoles), aminoguanidine hydrochloride (155 mg, 1.40 mmoles) and absolute EtOH (7 mL). Pure 5-methyl-1,3-bisamidino phenylhydrazone hydrochloride **1g** (179 mg, 0.54 mmoles) was obtained as a white solid in **77%** yield.

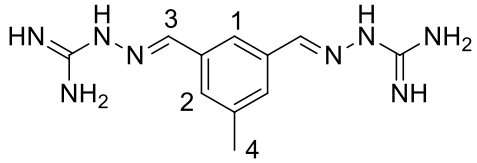

Characterization: m.p. = 292-298 °C dec

^{1}H NMR (400 MHz, DMSO-d_6) δ: 12.25 (bs, 2H, NH), 8.21 (s, 2H, H4), 8.10 (s, 1H, H1), 8.00-7.50 (bs, 6H, NH), 7.82 (s, 2H, H2), 2.41 (s, 3H, H3).

^{13}C NMR (100 MHz, DMSO-d_6) δ: 156.9, 147.4, 139.9, 135.2, 130.9, 125.5, 21.4.

MS (ESI), m/z: calcd for $C_{11}H_{16}N_8O$·260.15, found 261.20 ($M+H^+$).

1.5.12. Synthesis of 5-bromo-1,3-phenyl di-aminoguanidyl hydrazone hydrochloride 1h

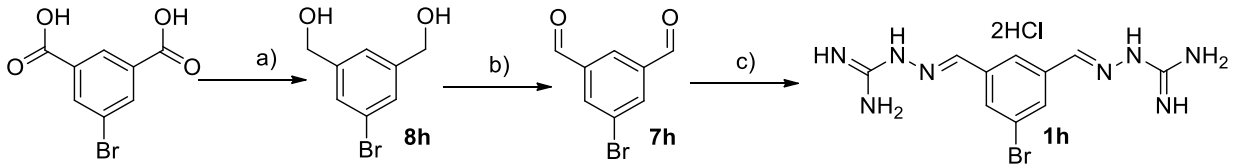

a) 1M BH_3-THF, dry THF, N_2, 0°C to RT, 48hrs, **88%**; b) MnO_2, chloroform, 70°C, 16hrs, **77%**;
c) aminoguanidine HCl, cat. 1N HCl_{aq}, EtOH, 80°C, 4hrs, **88%**

5-Bromo-3-xylene-α,α'-diol 8h

The reaction was performed according to **METHOD A**, using 5-bromo-isophthalic acid (610 mg, 2.49 mmoles), 1M BH_3 in THF (10 ml, 10.00 mmoles) and THF (2.5 mL). Pure 5-bromo, 3-xylene-α,α'-diol **8h** (475 mg, 2.19 mmoles) was obtained as a white solid in **88%** yield.

The analytical characterization of this intermediate is not available.

5-Bromoisophthalaldehyde 7h

The reaction was performed according to **METHOD B**, using 5-bromo-1,3-xylene-a,a'-diol (128 mg, 0.59 mmoles), solid MnO_2 (257 mg, 2.95 mmoles) and chloroform (3 mL). Pure 5-bromo isophthalaldehyde **7h** (97 mg, 0.454 mmoles) was obtained as a white solid in **77%** yield.

The analytical characterization of this intermediate is not available.

5-Bromo-1,3-phenyl di-aminoguanidyl hydrazone hydrochloride 1h

The reaction was performed according to **METHOD C**, using 5-bromoisophthalaldehyde (75 mg, 0.35 mmoles), aminoguanidine hydrochloride (78 mg, 0.70 mmoles) and absolute EtOH (3.5 mL). Pure 5-bromo-1,3-bisamidino phenylhydrazone hydrochloride **1h** (133.1 mg, 0.334 mmoles) was obtained as a white solid in **88%** yield.

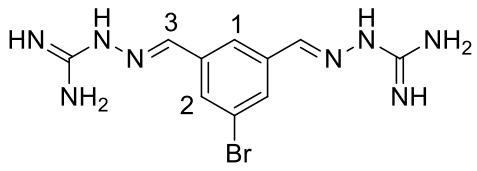

Characterization: m.p. = 310-315 °C dec.

^{1}H NMR (400 MHz, DMSO-d_6) δ: ^{1}H NMR (400 MHz, DMSO-d_6) δ: 12.31 (bs, 2H, NH), 8.27 (d, J = 1.2Hz, 2H, H2), 8.22 (t, J = 1.2Hz, 1H, H1), 8.17 (s, 2H, H3), 8.20-7.60 (bs, 6H, NH).

^{13}C NMR (100 MHz, DMSO-d_6) δ: 156.9, 145.8, 137.5, 132.0, 127.8, 124.1.

MS (ESI), m/z: calcd for $C_{10}H_{13}BrN_8$·324.04, found 325.19 ($M+H^+$).

1.5.13. Synthesis of 5-methoxy-1,3-phenyl di-aminoguanidyl hydrazone hydrochloride 1i

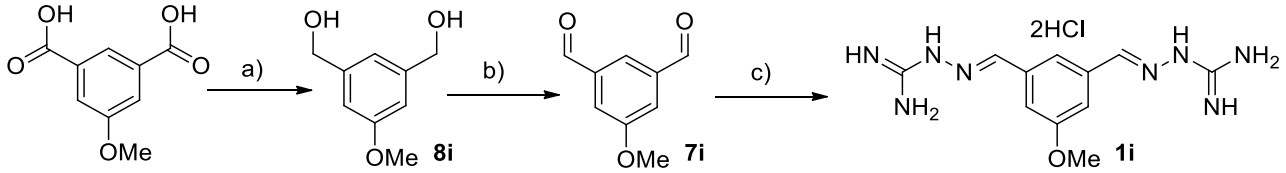

a) 1M BH_3-THF, dry THF, N_2, 0°C to RT, 48hrs, **80%**; b) MnO_2, chloroform, 70°C, 16hrs, **92%**;
c) aminoguanidine HCl, cat. 1N HCl_{aq}, EtOH, 80°C, 8hrs, **81%.**

5-Methoxy-3-xylene-α,α'-diol 8i

The reaction was performed according to **METHOD A**, using 5-methoxy-isophthalic acid (550 mg, 2.80 mmoles), 1M BH_3 in THF (11.2 mL, 11.2mmoles) and THF (2.8 mL). Pure 5-methoxy, 3-xylene-α,α'-diol **8i** (377 mg, 2.24 mmoles) was obtained as a white solid in **80%** yield.

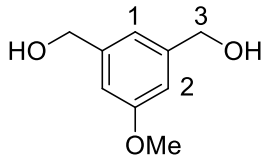

Characterization:

^{1}H NMR (400 MHz, $CDCl_3$) δ: 6.96 (s, 1H, H1), 6.80 (s, 2H, H2), 4.62 (s, 4H, H3), 3.81 (s, 3H, OMe), 2.11 (s, 2H, OH).

5-Methoxyisophthalaldehyde 7i

The reaction was performed according to **METHOD B**, using 5-methoxy-1,3-xylene-α,α-diol (330 mg, 1.97 mmoles), solid MnO_2 (867 mg, 10 mmoles) and chloroform (10 mL). Pure 5-methoxy isophthalaldehyde **7i** (297 mg, 1.81 mmoles) was obtained as a white solid in **92%** yield.

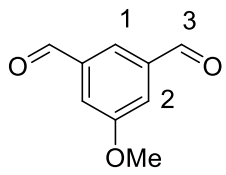

Characterization:

^{1}H NMR (400 MHz, $CDCl_3$) δ: 10.3 (s, 2H, H3), 7.96 (s, 1H, H1), 7.61 (s, 2H, H2), 3.99 (s, 3H, OMe).

5-Methoxy-1,3-phenyl di-aminoguanidyl hydrazone hydrochloride 1i

The reaction was performed according to **METHOD C**, using 5-methoxyisophthalaldehyde (93 mg, 0.57 mmoles), aminoguanidine hydrochloride (125 mg, 1.13 mmoles) and absolute EtOH (6 mL). Pure 5-methoxy-1,3-bisamidino phenylhydrazone hydrochloride **1i** (161 mg, 0.46 mmoles) was obtained as a white solid in **81%** yield.

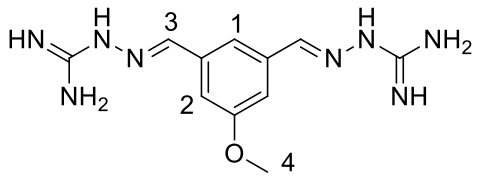

Characterization: m.p. = 300-307 °C dec

^{1}H NMR (400 MHz, DMSO-d_6) δ: 12.25 (bs, 2H, NH), 8.22-7.61 (bs, 6H, NH), 8.17 (s, 2H, H4), 7.83 (t, J = 1.08 Hz, 1H, H1), 7.59 (d, J = 1.08 Hz, 2H, H2), 3.82 (s, 3H, H3).

^{13}C NMR (100 MHz, DMSO-d_6) δ: 160.3, 155.9, 146.3, 135.7, 120.6, 114.7, 56.2.

MS (ESI), m/z: calcd for $C_{11}H_{16}N_8O$·276.15, found 277.22 ($M+H^+$).

1.5.14. Synthesis of 5-nitro-1,3-phenyl di-aminoguanidyl hydrazone hydrochloride 1j

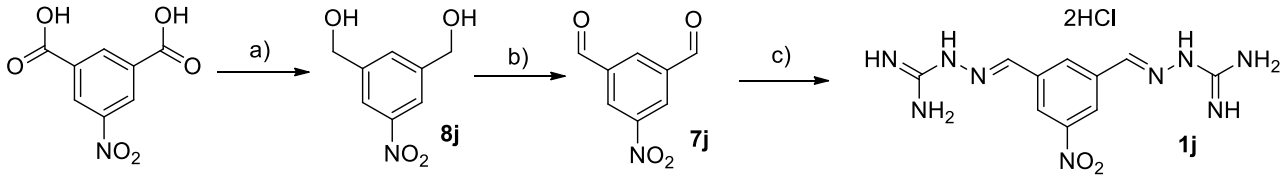

a) 1M BH_3-THF, dry THF, N_2, 0°C to RT, 48hrs, **83%**; b) MnO_2, chloroform, 70°C, 16hrs; **78%**; c) aminoguanidine HCl, cat. 1N HCl_{aq}, EtOH, 80°C, 2hrs, **80%**.

5-Nitro-3-xylene-α,α'-diol 8j

The reaction was performed according to **METHOD A**, using 5-nitro-isophthalic acid (700 mg, 3,32 mmoles), 1M BH_3 in THF (13 mL, 13 mmoles) and THF (3 mL). Pure 5-nitro-3-xylene-α,α'-diol **8j** (504 mg, 2.75 mmoles) was obtained as a pale yellow solid in **83%** yield.

The analytical characterization of this intermediate is not available.

5-Nitroisophthalaldehyde 7j

The reaction was performed according to **METHOD B**, using 5-nitro-1,3-xylene-α,α'-diol (123 mg, 0.67 mmoles), solid MnO_2 (291 mg, 3.35 mmoles) and chloroform (4 mL). Pure 5-nitro isophthalaldehyde **7j** (94 mg, 0.53 mmoles) was obtained as a light yellow solid in **78%** yield.

The analytical characterization of this intermediate is not available.

5-Nitro-1,3-phenyl di-aminoguanidyl hydrazone hydrochloride 1j

The reaction was performed according to **METHOD C**, using 5-nitroisophthalaldehyde (94 mg, 0.53 mmoles), aminoguanidine hydrochloride (117 mg, 1.06 mmoles) and absolute EtOH (5 mL). Pure 5-nitro-1,3-bisamidino phenylhydrazone hydrochloride **1j** (154 mg, 0.42 mmoles) was obtained as a white solid in **80%** yield.

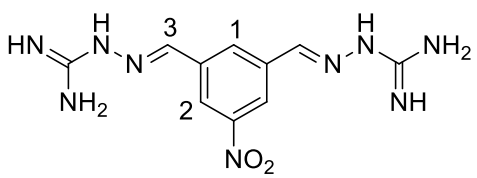

Characterization: m.p. = 310-315 °C dec

^{1}H NMR (400 MHz, DMSO-d_6) δ: 12.44 (bs, 2H, NH), 8.80 (d, J = 1.6 Hz, 2H, H2), 8.75 (t, J = 1.6 Hz, 1H, H1), 8.34 (s, 2H, H3), 8.25-7.75 (bs, 6H, NH).

^{13}C NMR (100 MHz, DMSO-d_6) δ: 156.0, 149.4, 144.5, 136.3, 132.7, 123.2.

MS (ESI), m/z: calcd for $C_{10}H_{13}N_9O_2$·291.12, found 292.21 ($M+H^+$).

1.5.15. Synthesis of 5-Ph-1,3-phenyl di-aminoguanidyl hydrazone hydrochloride 1k

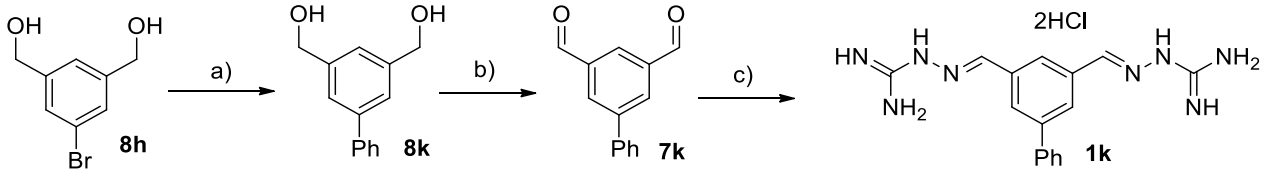

a) $PhB(OH)_2$, $Pd(PPh_3)_4$, 2N Na_2CO_3aq, dioxane 105°C, 6hrs. **82%**; b) MnO_2, chloroform, 70°C, 16hrs, **81%**;
c) amminoguanidine HCl, cat. 1N HCl_{aq}, EtOH, 80°C, 8hrs; **79%.**

5-Phenyl-3-xylene-α,α'-diol 8k

2M aq. Na_2C0_3 (1.86 mL) was added under nitrogen atmosphere to a vigorously stirred mixture of 5-bromo-3-xylene-α,α'-diol (270 mg, 1.24 mmoles), benzene boronic acid (177 mg, 1.45 mmoles) and $Pd(PPh_3)_4$ (143 mg, 0.124 mmoles) in 1 ,4-dioxane (8 mL). The reaction mixture was heated at reflux for 6 hours. The reaction was then cooled to RT, diluted with EtOAc (40 mL), washed with sat. aq. $NaHC0_3$ (20 mL) and brine (15 mL). The organic layer was evaporated, and the crude product was purified by flash chromatography (eluant mixture: n-hexane/EtOAc 3:1) to yield pure 5-phenyl, 3-xylene-α,α'-diol **8k** (220 mg, 1.02 mmoles) as a white solid in **82%** yield.

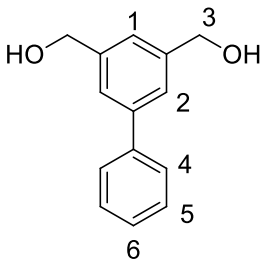

Characterization:

^{1}H NMR (400 MHz, $CDCl_3$) δ: 7.62 (d, J = 7.2 Hz, 2H, H4), 7.54 (s, 2H, H2), 7.46 (t, J = 7.2 Hz, 2H, H5), 7.38 (m, 2H, H1, H6), 4.79 (s, 4H, H3), 1.86 (bs, 2H, OH).

5-Phenylisophthalaldehyde 7k

The reaction was performed according to **METHOD B**, using 5-phenyl-1,3-xylene-α,α'-diol (170 mg, 0.79 mmoles), solid MnO_2 (343 mg, 3.95 mmoles) and chloroform (4 mL). Pure 5-phenyl isophthalaldehyde **7k** (135 mg, 0.64 mmoles) was obtained as a white solid in **81%** yield.

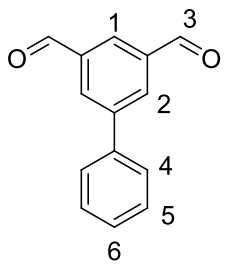

Characterization:

^{1}H NMR (400 MHz, $CDCl_3$) δ: 10.21 (s, 2H, H3), 8.39 (dd, J = 1.5 Hz, 2H, H2), 8.37 (t, J = 1.5 Hz, 1H, H1), 7.71 (dd, J = 8.6 Hz, J = 1.5 Hz, 2H, H4), 7.54 (dt, J = 8.6 Hz, J = 7.3 Hz, 2H, H5), 7.48 (dt, J = 7.3 Hz, J = 1.5 Hz, 1H, H6).

5-Phenyl-1,3-phenyl di-aminoguanidyl hydrazone hydrochloride 1k

The reaction was performed according to **METHOD C**, using 5-phenylisophthalaldehyde (127 mg, 0.61 mmoles), aminoguanidine hydrochloride (134 mg, 1.22 mmoles) and absolute EtOH (6 mL). After solvent removal, reverse phase chromatography (eluant mixture: H_2O/MeOH 95:5 to 100:0, 1‰ HCOOH), followed by dissolution in 0.5N HCl and lyophilization led to pure 5-phenyl-1,3-bisamidino phenylhydrazone hydrochloride **1k** (190 mg, 0.48 mmoles) as a white solid in **79%** yield.

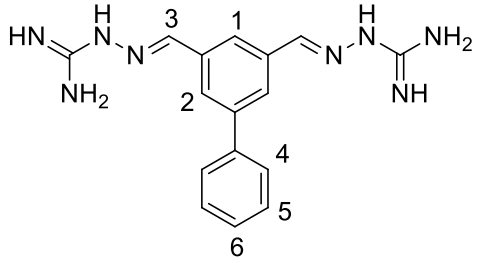

Characterization: m.p. = 215-220 °C

^{1}H NMR (400 MHz, DMSO-d_6) δ: 12.35 (bs, 2H, NH), 8.28 (m, 5H, H1, H2, H3), 8.20-7.60 (bs, 6H, NH), 7.83 (d, J = 8.4 Hz, 2H, H4), 7.53 (t, J = 8.4 Hz, 2H, H5), 7.44 (t, J = 8.4 Hz, 1H, H6).

^{13}C NMR (100 MHz, DMSO-d_6) δ: 156.0, 146.4, 1411.7, 139.3, 135.1, 129.4, 128.5, 127.5, 126.4.

MS (ESI), m/z: calcd for $C_{16}H_{18}N_8$ 322.17, found 323.19 ($M+H^+$).

1.5.16. Synthesis of 5-acetamido- and 5-(p-methyl)benzamido-1,3-phenyl di-aminoguanidyl hydrazone hydrochloride 1l and 1m

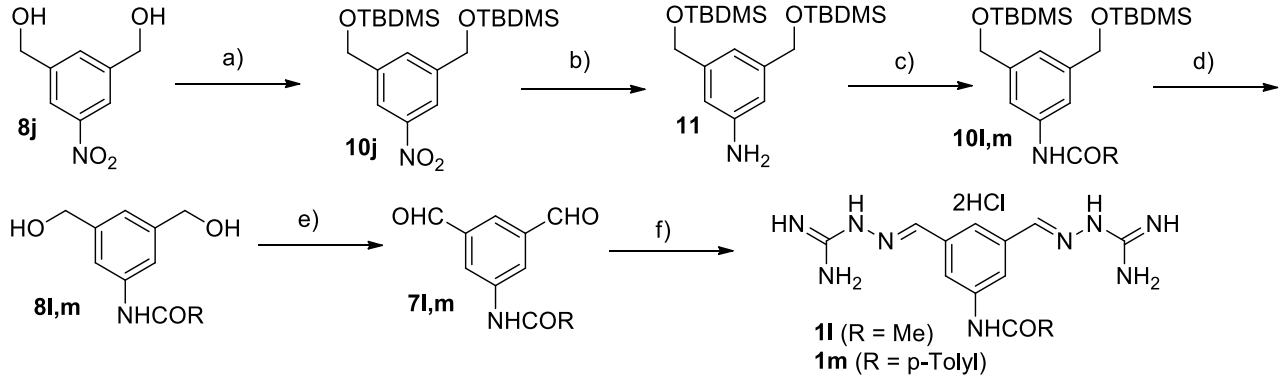

a) TBSCl, 1H-imidazole, CH_2Cl_2, 0°C to RT, 3 hrs; b) cat. 10% Pd/C, H_2, EtOH, RT, 24 hrs, **78%** (2 steps); c) acylating agent, TEA, DMAP, CH_2Cl_2, 0°C to RT, 1 to 2 hrs, **67%** (**10m**); d) AcCl, dry MeOH, N_2, 0°C, 30 min; e) MnO_2, $CHCl_3$, 70°C, 16 hrs, **74%** (**7l**, 3 steps) or **83%** (**7m,** 2 steps); f) aminoguanidine HCl, cat. HCl, EtOH, 80°C, 4 to 6 hrs, **85%** (**1l, 1m**).

(((5-Nitro-1,3-phenylene)bis(methylene))bis(oxy))bis(tert-butyldimethylsilane) 10j

5-Nitro-1,3-xylene-α,α'-diol (450 mg, 2.45 mmoles, 1 eq.) and 1H-imidazole (500 mg, 7.35 mmoles, 1.5 eqs.) were dissolved in CH_2Cl_2 (12 mL) at RT. Then the solution was cooled at 0°C, and t-butyldimethylsilyl chloride (930 mg, 6.12 mmoles, 1.25 eq.) was added. The reaction mixture was slowly warmed to RT and stirred for another 3 hrs. The solution was then diluted with CH_2Cl_2 (15 mL), washed with 5% aqueous citric acid (15 mL), 5% aqueous NaOH (15 mL) and brine (15 mL). The organic layer was dried with anhydrous Na_2SO_4, filtered and evaporated at reduced pressure. Crude (((5-nitro-1,3-phenylene)bis(methylene))bis (oxy))bis(tert-butyldimethylsilane) **10j**, obtained as a yellow oil (797 mg), was used without further purification in the next step.

3,5-Bis(((tert-butyldimethylsilyl)oxy)methyl)aniline 11

Crude diprotected nitro diol **10j** (797 mg) was dissolved in EtOH (10 mL). 10% Pd/C (80 mg) was added and the reaction mixture was stirred at 35 °C under hydrogen atmosphere for 24 hrs. The reaction mixture was filtered through a path of celite using MeOH (60 mL). The crude was purified by flash chromatography on silica gel (eluant mixture: DCM/EtOAc from 100:0 to 95:5), to afford pure diprotected aminodiol **11** (729 mg, 1.91 mmoles) as a light yellow oil in a **78%** yield over two steps.

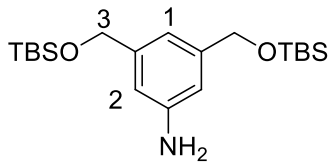

Characterization:

^{1}H NMR (400 MHz, $CDCl_3$) δ: 6.68 (s, 1H, H1), 6.59 (s, 2H, H2), 4.65 (s, 4H, H3), 4.00 (bs, 2H, NH), 0.98 (s, 18H, tBu), 0.1 (s, 12H, Me).

N-(3,5-Bis(((tert-butyldimethylsilyl)oxy)methyl)phenyl)acetamide 10l

Diprotected aminodiol **11** (300 mg, 0.79 mmoles) and TEA (0.55 mL, 4 mmoles) were dissolved in CH_2Cl_2 (8 mL). Then, acetic anhydride (0.223 mL, 2.36 mmoles) and a catalytic amount of dimethylaminopyridine (DMAP) were added, and the solution was stirred at RT for 2 hrs. After dilution with CH_2Cl_2 (15 mL) the solution was washed with 5% aqueous citric acid (10 mL), saturated aqueous $NaHCO_3$ (10 mL) and brine (10 mL). The organic layer was dried with anhydrous Na_2SO_4, filtered and evaporated at reduced pressure. N-(3,5-bis(((tert-butyldimethylsilyl)oxy)methyl)phenyl)acetamide **10l**, obtained as a pale yellow oil (350 mg), was used without further purification.

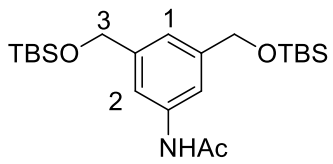

Characterization:

^{1}H NMR (400 MHz, $CDCl_3$) δ: 7.33 (s, 2H, H2), 7.28 (bs, 1H, NH), 7.08 (s, 1H, H1), 4.74 (s, 4H, H3), 2.22 (s, 3H, Ac), 0.98 (s, 18H, tBu), 0.1 (s, 12H, Me).

N-(3,5-Bis(((tert-butyldimethylsilyl)oxy)methyl)phenyl)-4-methylbenzamide 10m

At 0°C, diprotected aminodiol **11** (310 mg, 0.812 mmoles) and TEA (0.23 mL, 1.63 mmoles) were dissolved in CH_2Cl_2 (8 mL). Then, 4-methylbenzoyl chloride (0.14 mL, 1.06 mmoles) was added, and the solution was stirred at the same temperature for 1 hr. Excess of 4-methylbenzoyl chloride was quenched with MeOH (1 mL). After dilution with CH_2Cl_2 (15 mL) the solution was washed with 5% aqueous citric acid (10 mL), saturated aqueous $NaHCO_3$ (10 mL) and brine (10 mL). The organic layer was dried with anhydrous Na_2SO_4, filtered and evaporated at reduced pressure. The crude was purified by flash chromatography on silica gel (eluant mixture: DCM/EtOAc from 100:0 to 95:5), to afford pure O-protected amidodiol **10m** (262 mg, 0.525 mmol) as a pale yellow oil in a **67%** yield.

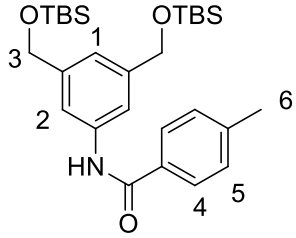

Characterization:

^{1}H NMR (400 MHz, acetone-*d*6) δ: 9.29 (bs, 1H, NH), 7.75 (d, *J* = 8.2Hz, 2H, H4) 7.59 (s, 2H, H2), 7.18 (d, *J* = 8.2 Hz, 2H, H5), 7.01 (s, 1H, H1), 4.64 (s, 4H, H3), 2.27 (s, 3H, H6), 0.82 (s, 18H, tBu), 0.00 (s, 12H, Me).

N-(3,5-Bis(hydroxymethyl)phenyl)acetamide 8l

O-Protected acetamidodiol **10l** was dissolved in dry MeOH (8 mL) under nitrogen atmosphere. The solution was cooled under stirring at 0°C, and acetyl chloride (20 µL, 0.262 mmoles) was added. The reaction mixture was stirred at 0° for 30 minutes, and a white precipitate was formed. The solvent was then removed under reduced pressure. The crude was triturated in acetone (10 mL) and filtered. The white solid was washed with acetone (3 x 8 mL) and dried to give pure N-(3,5-bis(hydroxymethyl) phenyl)acetamide **8l** (130 mg), obtained as a white solid that was used without further purification.

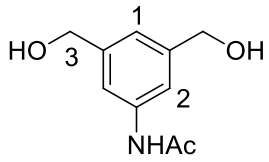

Characterization:

^{1}H NMR (400 MHz, DMSO-d_6) δ: 9.92 (s, 1H, NH), 7.45 (s, 2H, H2), 6.90 (s, 1H, H1), 5.18 (bs, 2H, OH), 4.41 (s, 4H, H3), 2.00 (s, 3H, Ac).

N-(3,5-Bis(hydroxymethyl)phenyl)-4-methylbenzamide 8m

Protected amidodiol **10m** (256.0 mg, 0.512 mmol, 1eq) was dissolved in dry MeOH (10mL) under nitrogen atmosphere. The solution was cooled under stirring at 0°C, and acetyl chloride (20 µL, 0.262 mmoles) was added. The reaction mixture was stirred at 0° for 30 minutes (TLC reaction monitoring, eluant: AcOEt). The solvent was then removed under reduced pressure to give pure N-(3,5-bis(hydroxymethyl) phenyl)-4-methylbenzamide **8m** (140 mg), obtained as a white solid that was used without further purification.

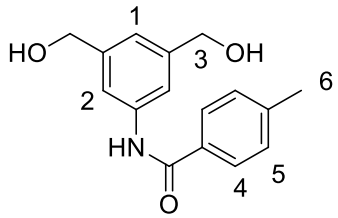

Characterization;

^{1}H NMR (400 MHz, acetone-*d*6) δ: 9.40 (bs, 1H, NH), 7.95 (d, *J* = 8.2Hz, 2H, H4) 7.75 (s, 2H, H2), 7.33 (d, *J* = 8.2 Hz, 2H, H5), 7.12 (s, 1H, H1), 4.64 (s, 4H, H3), 2.42 (s, 3H, H6).

5-Acetamido isophthalaldehyde 7l

The reaction was performed according to **METHOD B**, using 5-acetamido-1,3-xylene-α,α'-diol (128 mg, 0.26 mmoles), solid MnO_2 (268 mg, 3.10 mmoles) and chloroform (10 mL). Pure 5-acetamido isophthalaldehyde **7l** (104 mg, 0.54 mmoles) was obtained as a white solid in **69%** yield over three steps.

Characterization:

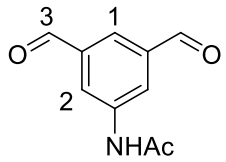

^{1}H NMR (400 MHz, CD_3CN) δ: 10.01 (s, 2H, H3), 8.65 (bs, 1H, NH), 8.72 (s, 2H, H2), 8.02 (s, 1H, H1), 2.09 (s, 3H, Ac).

5-(4'-Methyl)phenylamido isophthalaldehyde 7m

The reaction was performed according to **METHOD B**, using 5-tolylamido-1,3-xylene-α,α'-diol (140 mg, 0.51 mmoles), solid MnO_2 (340 mg, 5.20 mmoles) and chloroform (10 mL). Pure 5-tolylamido isophthalaldehyde **7m** (113.2 mg, 0.42 mmoles) was obtained as a white solid in **83%** yield over two steps.

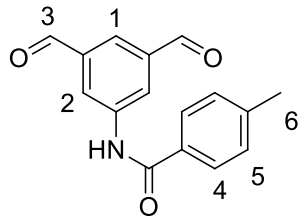

Characterization:

^{1}H NMR (400 MHz, acetone-*d*6) δ: 10.18 (s, 2H, H3), 9.96 (bs, 1H, NH), 8.73 (d, *J* = 4.1 Hz, 2H, H2), 8.22 (t, J = 4.1Hz, 1H, H1), 8.00 (d, *J* = 8.2Hz, 2H, H4), 7.38 (d, *J* = 8.2 Hz, 2H, H5), 2.44 (s, 3H, H6).

5-Acetamido-1,3-phenyl di-aminoguanidyl hydrazone hydrochloride 1l

The reaction was performed according to **METHOD C**, using 5-acetamido isophthalaldehyde (97 mg, 0.51 mmoles), aminoguanidine hydrochloride (113 mg, 1.02 mmoles) and absolute EtOH (5 mL). Pure 5-acetamido-1,3-bisamidino phenylhydrazone hydrochloride **1l** (163 mg, 0.43 mmoles) was obtained as a white solid in **85%** yield.

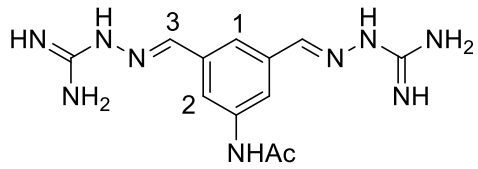

Characterization: m.p. = 332-338 °C dec

^{1}H NMR (400 MHz, DMSO-d_6) δ: 12.18 (bs, 2H, NH), 10.22 (s, 1H, NH), 8.19 (s, 2H, H3), 8.17 (s, 1H, H1), 8.00-7.75 (m, 6H, NH), 7.94 (s, 2H, H2), 2.08 (s, 3H, Ac).

^{13}C NMR (100 MHz, DMSO-d_6) δ: 170.2, 156.8, 147.6, 141.2, 135.6, 122.1, 121.4, 24.4.

MS (ESI), m/z: calcd for $C_{12}H_{17}N_9O$ ·303.16, found 304.26 ($M+H^+$).

5-(p-methyl)benzamido-1,3-phenyl di-aminoguanidyl hydrazone hydrochloride 1m

The reaction was performed according to **METHOD C**, using 5-(4'-methyl)phenylamido isophthalaldehyde (47 mg, 0.18 mmoles), aminoguanidine hydrochloride (41 mg, 0.37 mmoles) and absolute EtOH (2 mL). Pure 5-tolylamido-1,3-bisamidino phenylhydrazone hydrochloride **1m** (69 mg, 0.15 mmoles) was obtained as a white solid in **85%** yield.

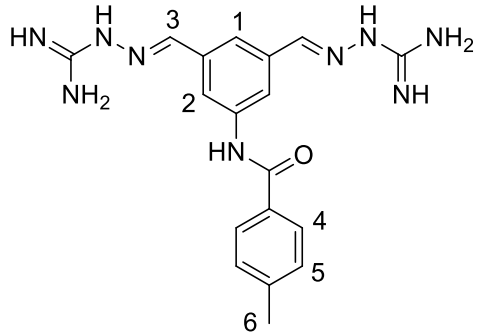

Characterization: m.p. = 296-300 °C dec

^{1}H NMR (400 MHz, DMSO-d_6) δ: 12.15 (bs, 2H, NH), 10.43 (bs, 1H, NH), 8.23 (s, 2H, H3), 8.20 (s, 1H, H1), 8.17 (s, 2H, H2), 7.95 (d, *J* = 8.2 Hz, 2H, H4), 7.83 (bs, 6H, NH), 7.37 (d, *J* = 8.2 Hz, 2H, H5), 2.41 (s, 3H, H6).

^{13}C NMR (100 MHz, DMSO-d_6) δ: 165.9, 155.9, 146.6, 142.4, 140.3, 134.8, 131.9, 129.5, 128.2, 122.9, 121.6, 21.5.

MS (ESI), m/z: calcd for $C_{18}H_{21}N_9O$·379.19, found 402.18 ($M+Na^+$).

1.5.17. Synthesis of 5-mesylamido- and 5-p-tosylamido-1,3-phenyl di-aminoguanidyl hydrazone hydrochloride 1n and 1o

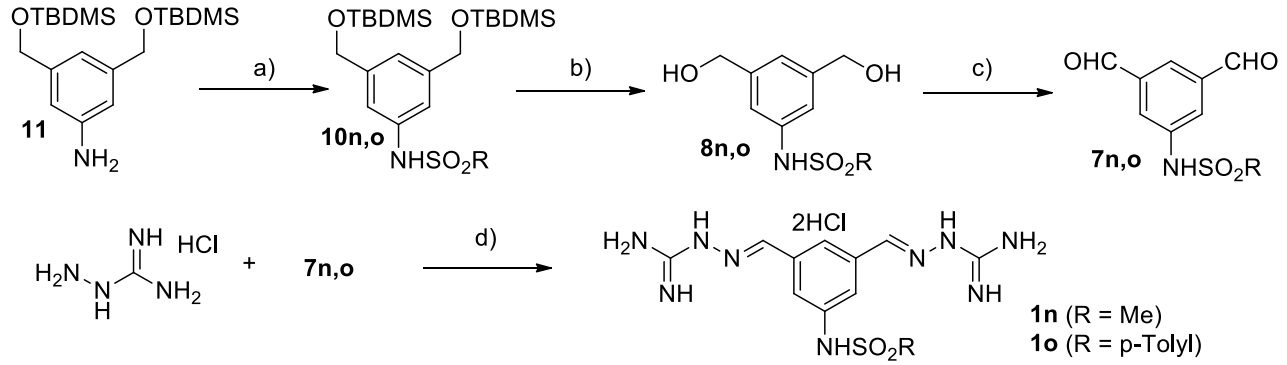

a) sulfonylating agent, pyridine, DMAP, CH_2Cl_2, 0°C to rt, 16 hrs, **85%** (**10o**); b) AcCl, dry MeOH, N_2, 0°C, 30 min; c) MnO_2, $CHCl_3$, 70°C, 16 hrs, **68%** (**7n**, 3 steps) or **71%** (**7o**, 2steps); d) cat. HCl, EtOH, 80°C, 4 hrs, **83%** (**1n**) or **79%** (**1o**).

N-(3,5-Bis(((tert-butyldimethylsilyl)oxy)methyl)phenyl)methanesulfonamide 10n

At 0°C, O-protected aminodiol **11** (166 mg, 0.434 mmoles) and pyridine (0.72 mL, 0.87 mmoles) were dissolved in CH_2Cl_2 (4 mL). Then, 4-methansulfonyl chloride (0.50 mL, 0.65 mmoles) was added, the solution was stirred at the same temperature for 1 hr and at RT for other 15hrs (TLC monitoring, eluant mixture: DCM/AcOEt 95:5). After dilution with CH_2Cl_2 (15 mL) the solution was washed with water (10 mL) and brine (10 mL). The organic layer was dried with anhydrous Na_2SO_4, filtered and evaporated at reduced pressure. The crude was filtered on a small path of silica gel (eluant mixture: DCM/EtOAc 98:2), to afford N-(3,5-bis(((tert-butyldimethylsilyl)oxy)methyl)phenyl)methanesulfonamide **10n** (199.7 mg) as a pale yellow oil that was used as such in the next reaction step.

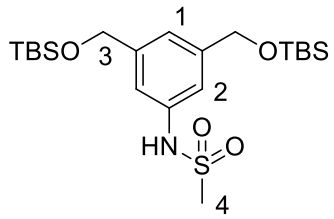

Characterization:

^{1}H NMR (400 MHz, acetone-d_6) δ: 8.44 (bs, 1H, NH), 7.12 (s, 2H, H2), 7.01 (s, 1H, H1), 4.64 (s, 4H, H3), 2.84 (s, 3H, H6), 0.83 (s, 18H, H5), 0.00 (s, 12H, H5).

N-(3,5-Bis(((tert-butyldimethylsilyl)oxy)methyl)phenyl)-4-methylbenzenesulfonamide 10o

At 0°C, O-protected aminodiol **11** (166 mg, 0.434 mmoles) and pyridine (0.72 mL, 0.87 mmoles) were dissolved in CH_2Cl_2 (5 mL). Then, 4-toluensolfonyl chloride (0.124 mg, 0.65 mmoles, 1.5 eqs.) was added, the solution was stirred at the same temperature for 1 hr and at RT for other 6hrs (TLC monitoring, eluant mixture: DCM/AcOEt 98:2). After dilution with CH_2Cl_2 (15 mL) the solution was washed with sat $NaHCO_3$ (10 mL) and brine (10 mL). The organic layer was dried with Na_2SO_4, filtered and evaporated at reduced pressure. The crude was purified on silica gel by flash chromatography (eluant mixture: DCM/EtOAc from 100:0 to 95:5), to afford pure N-(3,5-bis(((tert-butyldimethylsilyl)oxy)methyl)phenyl)-4-methylbenzenesulfonamide **10o** (195.7 mg, 0.366 mmol) as a white solid in **85%** yield.

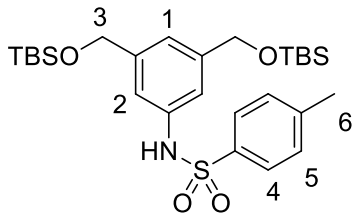

Characterization:

^{1}H NMR (400 MHz, acetone-d_6) δ: 8.87 (bs, 1H, NH), 7.61 (d, *J* = 8.2 Hz, 2H, H6), 7.22 (d, J = 8.2Hz, 2H, H7), 7.06 (s, 2H, H2), 6.93 (s, 1H, H1), 4.60 (s, 4H, H3), 2.28 (s, 3H, H8), 0.85 (s, 18H, H5), 0.00 (s, 12H, H5).

N-(3,5-Bis(hydroxymethyl)phenyl)methanesulfonamide 8n

The O-diprotected mesyldiol **10n** (199.7 mg) was dissolved in dry MeOH (8 mL) under nitrogen atmosphere. The solution was cooled under stirring at 0°C, and acetyl chloride (20 µL, 0.262 mmoles) was added. The reaction mixture was stirred at 0° for 30 minutes, and monitored by TLC (eluant: AcOEt). The solvent was then removed under reduced pressure to give the deprotected mesyldiol **8n** (100 mg) that was used in the next step without further purification.

N-(3,5-Bis(hydroxymethyl)phenyl)-4-methylbenzenesulfonamide 8o

The O-diprotected tosyldiol **10o** (196 mg, 0.366 mmol) was dissolved in dry MeOH (8 mL) under nitrogen atmosphere. The solution was cooled under stirring at 0°C, and acetyl chloride (10 µL, 0.131 mmoles) was added. The reaction mixture was stirred at 0° for 2 hrs, and monitored by TLC (eluant mixture: AcOEt/n-hexane 7:3). The solvent was then removed under reduced pressure to give the deprotected tosyldiol **8o** (112 mg) that was characterized and used in the next step without further purification.

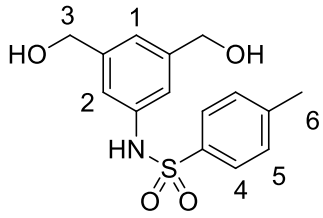

Characterization:

^{1}H NMR (400 MHz, acetone-d_6) δ: 8.72 (bs, 1H, NH), 7.57 (d, *J* = 8.2 Hz, 2H, H4), 7.18 (d, J = 8.2Hz, 2H, H5), 7.00 (s, 2H, H2), 6.89 (s, 1H, H1), 4.39 (s, 4H, H3), 4.03 (s, 2H, OH), 2.22 (s, 3H, H6).

^{13}C NMR (400 MHz, acetone-d_6) from HSQC δ: 129.4, 127.1, 120.3, 116.6, 63.4, 29.1.

N-(3,5-diformylphenyl)methanesulfonamide 7n

The reaction was performed according to **METHOD B**, using crude diol **8n** (100 mg), MnO_2 (300 mg, 4.33 mmoles, 10eq c.a.) and chloroform (6 mL). Pure N-(3,5-diformylphenyl)methanesulfonamide **7n** (65 mg, 0.29 mmoles) was obtained as a white solid in **68%** yield over three steps after filtration on celite using 50 ml of EtOAc as solvent and chromatographic purification (eluant hexane:AcOEt 1:1).

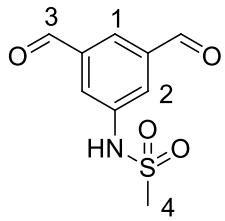

Characterization:

^{1}H NMR (400 MHz, acetone-d$_6$) δ: 10.02 (s, 2H, H3), 9.02 (bs, 1H, NH), 8.09 (s, 1H, H1), 8.01 (s, 2H, H2), 3.01 (s, 3H, H4).

^{13}C NMR (400 MHz, acetone-d_6) from HSQC δ: 191.1, 125.7, 124.0, 39.0.

N-(3,5-Diformylphenyl)-4-methylbenzenesulfonamide 7o

The reaction was performed according to **METHOD B**, using crude diol **8o** (112 mg), MnO_2 (200 mg, 2.32 mmoles) and chloroform (6 mL). Pure N-(3,5-diformylphenyl)-4-methylbenzenesulfonamide **7o** (79 mg, 0.26 mmoles) was obtained as a white solid in **71%** yield over two steps after filtration on celite with EtOAc (50 mL) and chromatographic purification on silicagel (eluant mixture: n-hexane/AcOEt from 8:2 to 6:4).

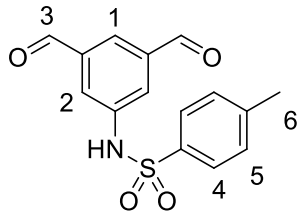

Characterization:

^{1}H NMR (400 MHz, acetone-d_6) δ: 9.95 (s, 2H, H3), 8.02 (s, 1H, H1), 7.90 (s, 2H, H2), 7.63 (d, *J* = 8.2 Hz, 2H, H4), 7.22 (d, J = 8.2Hz, 2H, H5), 2.22 (s, 3H, H6). ^{13}C NMR (400 MHz, acetone-d_6) from HSQC δ: 190.9, 129.8, 127.0, 126.0, 124.3, 29.1.

5-Mesylamido-1,3-phenyl di-aminoguanidyl hydrazone hydrochloride 1n

The reaction was performed according to **METHOD C**, using N-(3,5-diformylphenyl)methanesulfonamide **7n** (65 mg, 0.29 mmoles), aminoguanidine hydrochloride (63 mg, 0.58 mmoles) and absolute EtOH (3 mL). Pure 5-methansulfonamido phenyl-1,3-bisaminoguanidyl hydrazone hydrochloride **1n** (100 mg, 0.24 mmoles) was obtained as a white solid in **83%** yield.

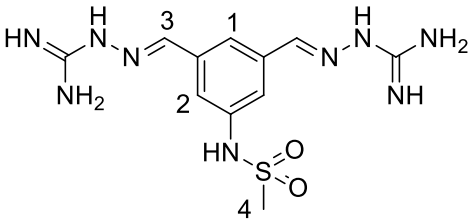

C**haracterization:** m.p. = 329-332 °C dec

^{1}H NMR (400 MHz, DMSO-d_6) δ: 12.25 (bs, 2H, NH), 10.01 (s, 1H, NH), 8.24 (s, 1H, H1), 8.21 (s, 2H, H3), 7.86 (bs, 6H, NH), 7.60 (s, 2H, H2), 3.10 (s, 3H, H4).

^{13}C NMR (100 MHz, DMSO-d_6) δ: 155.9, 146.3, 149.6, 135.4, 122.1, 121.4, 39.98

MS (ESI), m/z: calcd for $C_{11}H_{17}N_9O_2S$ 339.12, found 362.14 ($M+Na^+$).

5-pTosylamido-1,3-phenyl di-aminoguanidyl hydrazone hydrochloride 1o

The reaction was performed according to **METHOD C**, using 5-toluensulfonamido isophthalaldehyde (64 mg, 0.21 mmoles), aminoguanidine hydrochloride (46 mg, 0.42 mmoles) and absolute EtOH (2 mL). Pure 5-toluensulfonamido phenyl-1,3-bisaminoguanidyl hydrazone hydrochloride **1o** (80 mg, 0.16 mmoles) was obtained as a white solid in **79%** yield.

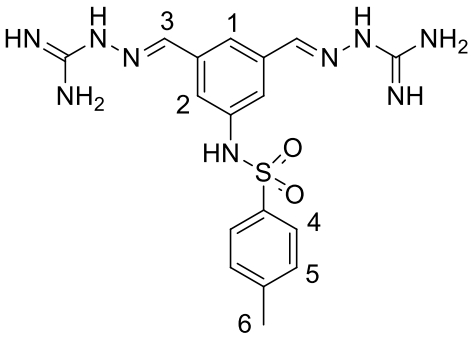

Characterization: m.p. = 286-290 °C dec

^{1}H NMR (400 MHz, DMSO-d_6) δ: 12.15 (bs, 2H, NH), 10.56 (s, 1H, NH), 8.17 (s, 1H, H1), 8.12 (s, 2H, H3), 7.82 (bs, 6H, NH), 7.71 (d, J = 8.2 Hz, 2H, H4), 7.46 (s, 2H, H2), 7.36 (d, J = 8.2 Hz, 2H, H5), 2.34 (s, 3H, H6).

^{13}C NMR (100 MHz, DMSO-d_6) δ: 155.4, 145.8, 143.5, 138.8, 136.6, 134.9, 129.8, 126.8, 121.2, 120.7, 21.0.

MS (ESI), m/z: calcd for $C_{11}H_{17}N_9O_2S$ 415.154, found 416.23 ($M+H^+$).

1.5.18. Synthesis of 5-carbomethoxy-1,3-phenyl di-aminoguanidyl hydrazone hydrochloride 1p

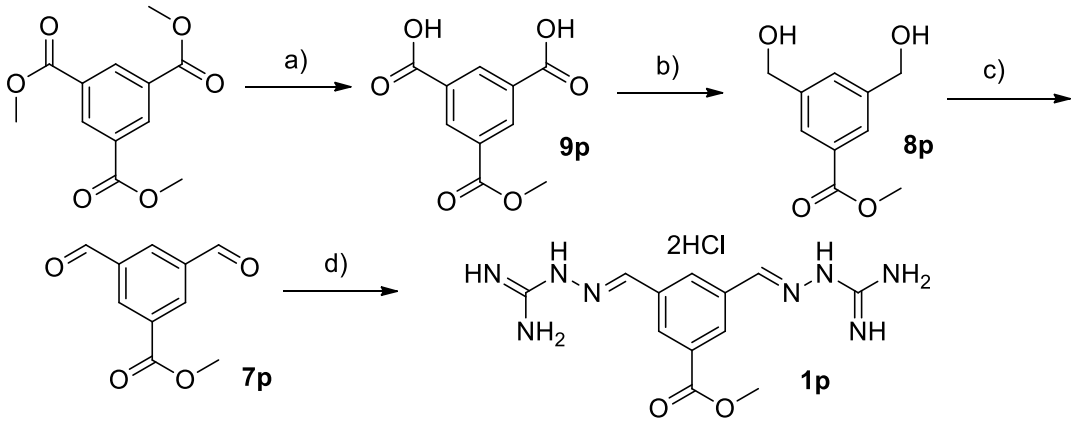

a) 2.07eq $NaOH_{aq}$, MeOH, RT, 24hrs; b) BH_3, THF, 0°C to 30°C, 24hrs, **54%** over two steps; c) MnO_2, chloroform, 70°C, 16hrs, **85%,** d) amminoguanidine HCl, cat. 1N HCl_{aq}, EtOH, 50°C, 4hrs, **71%.**

5-(Methoxycarbonyl)isophthalic acid 9p

1.8M aq. NaOH (9.1 mL, 16.38 mmoles) was added dropwise under stirring to a suspension of 1,3,5-benzenetricarboxylic acid trimethyl ester (2.0 g, 7.93 mmol) in MeOH (64 mL). The resulting cloudy mixture was stirred vigorously at RT, slowly becoming a clear solution over 5 hrs. After 15 hrs, MeOH was removed under reduced pressure. Water (25 mL) was then added and the solution was acidified (pH 2.0) with 6 M HCl, yielding a white dispersion. Extraction with EtOAc (2 x 25 mL) and solvent evaporation, after drying with Na_2SO_4, led to crude acid **9p** (1.5 g, impure of monoacid/bis-ester) as a white solid, that was used without further purification.

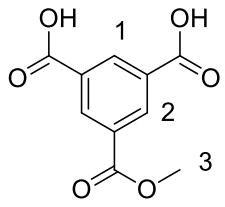

Characterization:

^1H NMR (400 MHz, DMSO-d_6) δ: 13.64 (bs, 2H, CO_2H), 8.66 (T, J = 2.2 Hz, 1H, H1), 8.65 (d, J = 2.2 Hz, 2H, H2), 3.94 (s, 3H, H3).

Methyl 3,5-bis(hydroxymethyl)benzoate 8p

The reaction was performed according to **METHOD A**, using crude 1,3,5-benzenetricarboxylic acid **9p** (1.5 g), 1M BH_3 in THF (33 mL, 33 mmoles) and THF (3 mL). Pure 3,5-bis(hydroxymethyl)benzoic acid methyl ester **8p** (773 mg, 3.94 mmoles) was obtained as a white solid in **54%** yield over two steps.

The analytical characterization of this intermediate is not available.

Methyl 3,5-diformylbenzoate 7p

The reaction was performed according to **METHOD B**, using 3,5-bis(hydroxymethyl)benzoic acid methyl ester **8p** (773 mg, 3.94 mmol), solid MnO_2 (1.9 g, 19.5 mmoles) and chloroform (20 mL). Pure methyl 3,5-diformylbenzoate **7p** (643 mg, 3.35 mmoles) was obtained as a white solid in **85%** yield after filtration on celite with EtOAc (50 mL), and used without further purification.

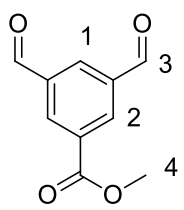

Characterization:

^{1}H NMR (400 MHz, $CDCl_3$) δ: 10.19 (s, 2H, H3), 8.81 (d, J = 2.2 Hz, 2H, H2), 8.60 (t, J = 2.2 Hz, 2H, H1), 4.04 (s, 3H, H4).

5-Carbomethoxy-1,3-phenyl di-aminoguanidyl hydrazone hydrochloride 1p

The reaction was performed according to **METHOD C**, using methyl 3,5-diformylbenzoate **7p** (78 mg, 0.407 mmoles), aminoguanidine hydrochloride (90 mg, 0.81 mmoles) and absolute EtOH (4 mL) at 50°C for 4 hrs. Pure 5-CO_2Me-1,3-phenyl di-aminoguanidyl hydrazone hydrochloride **1p** (109 mg, 0.29 mmoles) was obtained as a white solid in **71%** yield.

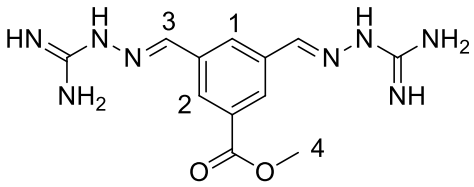

Characterization: m.p. = 322-324 °C dec

^{1}H NMR (400 MHz, DMSO-d_6) δ: 12.30 (bs, 2H, NH), 8.64 (s, 1H, H1), 8.44 (s, 2H, H3), 8.30 (s, 2H, H2), 7.91 (bs, 6H, NH), 3.92 (s, 3H, H4).

^{13}C NMR (100 MHz, DMSO-d_6) δ: 166.1, 156.0, 145.7, 135.1, 131.5, 130.7, 130.0, 53.0.

MS (ESI), m/z: calcd for $C_{12}H_{16}N_8O_2$ 304.14, found 327.31 ($M+Na^+$).

1.5.19. Synthesis of 5-(N-phenylpiperazinamido)-1,3-phenyl di-aminoguanidyl hydrazone hydrochloride 1q

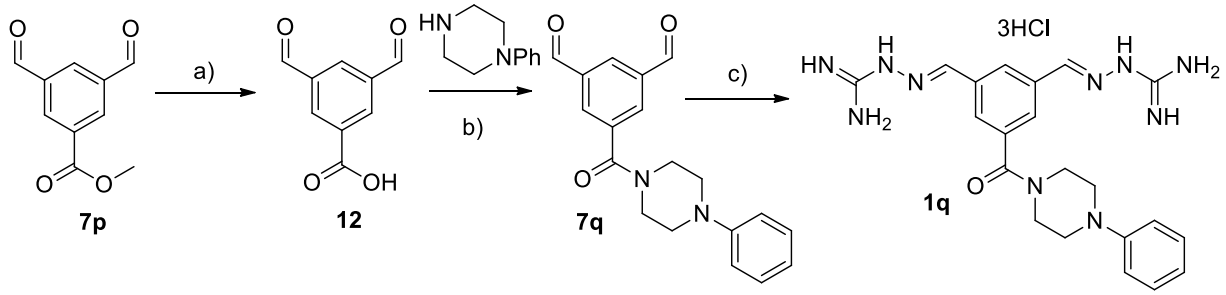

a) 2M $NaOH_{aq}$, MeOH, RT, 24hrs; b) EDCI, HOBt, TEA, DCM, RT, 24hrs, **30%** over two steps
aminoguanidine-HCl cat. 1N HCl_{aq}, EtOH, 80°C, 4hrs, **72%**

3,5-diformylbenzoic acid 12

2M aq. NaOH (0.47 mL, 0.94 mmoles) was added under stirring to a suspension of methyl 3,5-diformylbenzoate **7p** (174 mg, 0.90 mmoles) in MeOH (10 mL). The resulting mixture was stirred vigorously at RT until complete dissolution of starting material and formation of a white precipitate. After 24 hrs, MeOH was removed under reduced pressure, and crude acid **12** (161 mg) was used without further purification.

5-(4-Phenylpiperazine-1-carbonyl)isophthalaldehyde 7q

HOBt (162 mg, 1.2 mmoles) and EDC (230 mg, 1.2 mmoles) were sequentially added under stirring to a suspension of 3,5-diformylbenzoic acid **12** (161 mg, 0.90 mmoles) in dry DCM (10 mL). The resulting mixture was stirred vigorously at RT for 15 minutes. Then, 4-phenyl-1-piperazine (195 mg, 1.2 mmoles) and TEA (0.28

mL, 1.8 mmoles) were sequentially added. The reaction mixture was stirred at RT for 24 hrs, then was concentrated under reduced pressure. The residue was taken up with EtOAc (20 mL) and washed with 5% aq. citric acid (10 mL), sat. $NaHCO_3$ (10 mL) and brine (5 mL). The organic phase was dried over Na_2SO_4, filtered and concentrated under reduced pressure. Pure 5-(4-phenylpiperazine-1-carbonyl)isophthalaldehyde **7q** (90 mg, 0.28 mmoles) was obtained in **30%** yield after chromatographic purification (eluant mixture: n-hexane/AcOEt 4:6 + 1% TEA).

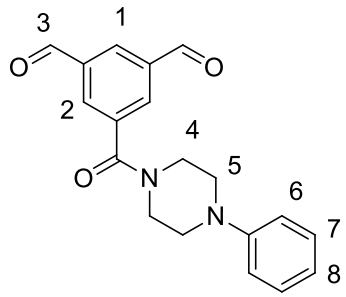

Characterization:

^{1}H NMR (400 MHz, acetone-d_6) δ: 10.15 (s, 2H, H3), 8.46 (s, 1H, H1), 8.23 (s, 2H, H2), 7.32 (m, 2H, H7), 6.94 (m, 3H, H6, H8), 3.99 (bs, 2H, H4b), 3.61 (bs, 2H, H4a), 3.30 (bs, 2H, H5b), 3.18 (bs, 2H, H5a).

5-(N-phenylpiperazinamido)-1,3-phenyl di-aminoguanidyl hydrazone hydrochloride 1q

The reaction was performed according to **METHOD C**, using 5-(4-phenylpiperazine-1-carbonyl)isophthalaldehyde **7q** (90 mg, 0.28 mmoles), aminoguanidine hydrochloride (76 mg, 0.68 mmoles) and absolute EtOH (3 mL). Pure 5-CONPip-1,3-phenyl di-aminoguanidyl hydrazone trihydrochloride **1q** (110 mg, 0.20 mmoles) was obtained as a light orange solid in **72%** yield after solvent concentration at reduced pressure, reverse phase chromatography (eluant mixture: water/MeOH from 100:0 to 0:100 + 1% formic acid), and lyophilization from an HCl solution.

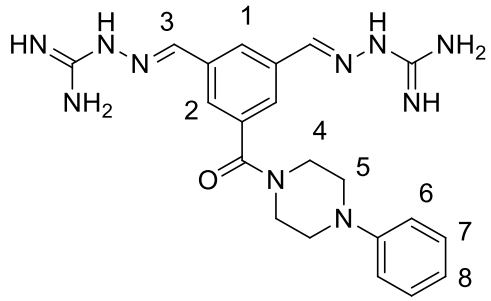

Analytical characterization: m.p. = 150-152 °C

^{1}H NMR (400 MHz, DMSO-d_6) δ: 12.32 (bs, 2H, NH), 8.35 (s, 1H, H1), 8.25 (s, 2H, H3), 8.09 (s, 2H, H2), 7.85 (bs, 6H, NH), 7.32 (m, 2H, H7), 7.21 (m, 2H, H6), 6.98 (m, 1H, H8), 3.92 (bs, 2H, H4b), 3.57 (bs, 2H, H4a), 3.28 (bs, 2H, H5b), 3.17 (bs, 2H, H5a).

^{13}C NMR (100 MHz, DMSO-d_6) δ: 168.5, 156.0, 145.7, 137.3, 134.9, 129.7, 128.2, 127.4, 121.2.

MS (ESI), m/z: calcd for $C_{21}H_{26}N_{10}O$·434.23, found 457.30 ($M+Na^+$).

1.5.20. Synthesis of 1,3-bis-(N^2-n-butyl)-phenyl di-aminoguanidyl hydrazone (N^2-nBu-di-AG) formiate 13a

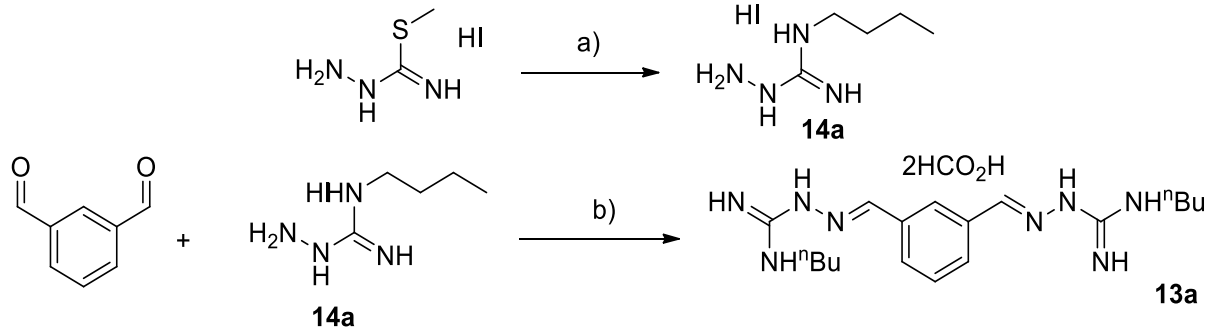

a) n-$BuNH_2$, MeOH, RT, 72 hrs, **99%**; b) EtOH, 80°C, 16hrs, **53%**

N^2-n-Butyl-aminoguanidine hydroiodide 14a

S-methyl isothiosemicarbazide hydroiodide (511.6 mg, 2.20 mmoles) was dissolved in MeOH (5 mL). Then n-butyl amine (0.33 mL, 3.30 mmoles) was added and the pale yellow solution was stirred at RT for 72 hrs. Then, the solvent was concentrated under reduced pressure. N-butyl aminoguanidine hydroiodide **14a** (526.8 mg) was obtained in quantitative yield as a red oil and used without further purification.

1,3-Bis-(N^2-n-butyl)-phenyl di-aminoguanidyl hydrazone (N2-nBu-di-AG) formiate 13a

The reaction was performed according to **METHOD D**, using isophthalaldehyde (110 mg, 0.82 mmoles), N-n-butylaminoguanidine hydroiodide **14a** (487 mg, 1.89 mmoles) and absolute EtOH (5 mL). Pure 1,3-bis-(N_2-n-butyl)-phenyl di-aminoguanidyl hydrazone formiate **13a** (198 mg, 0.44 mmoles) was obtained as a light yellow solid in **53%** yield after solvent concentration at reduced pressure and reverse phase chromatography (eluant mixture: H_2O/MeOH from 95:5 to 0:100 + 0.2% HCOOH).

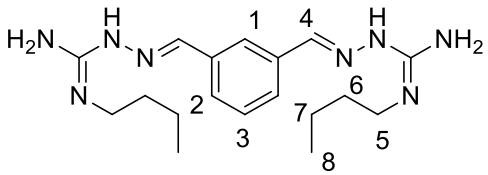

Characterization: m.p. = 100-105 °C

^{1}H NMR (400 MHz, DMSO-d_6) δ: 8.34 (s, 2H, HCOOH), 8.20 (s, 1H, H1), 8.13 (s, 2H, H4), 7.86 (d, J = 8.1 Hz, 2H, H2), 7.46 (t, J=8 Hz, 1H, H3), 3.23 (m, 4H, H5), 1.54 (m, 4H, H6), 1.35 (m, 4H, H7), 0.92 (t, J = 7.12 Hz, 6H, H8).

^{13}C NMR (100 MHz, DMSO-d_6) δ: 154.4, 146.5, 134.5, 129.6, 127.5, 41.3, 31.1, 19.7, 14.1.

MS (ESI), m/z: calcd for $C_{18}H_{30}N_8$·358.26, found 359.27 ($M+H^+$).

1.5.21. Synthesis of 1,3-bis-(N^2-benzyl)-phenyl di-aminoguanidyl hydrazone (N^2-Bn-di-AG) hydroiodide 13b

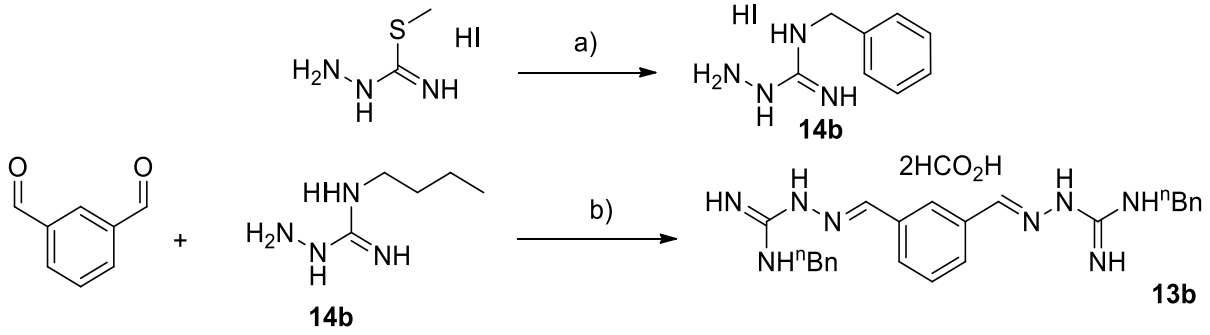

a) $BnNH_2$, MeOH, RT, 72 hrs, **60%**; b) EtOH, 80°C, 16hrs, **70%**

N^2-n-Benzyl-aminoguanidine hydroiodide 14b

S-methyl isothiosemicarbazide hydroiodide (511.6 mg, 2.20 mmoles) was dissolved in MeOH (5 mL). Then benzyl amine (0.36 mL, 3.30 mmoles) was added and the pale yellow solution was stirred at RT for 72 hrs. Then, the solvent was concentrated under reduced pressure. After solvent evaporation, the light red solid was suspended in Et_2O (10 mL), filtered and washed with 1:1 Et_2O/EtOAc (20 mL). After drying, crude N^2-n-benzyl-aminoguanidine hydroiodide **14b** (425.3 mg 1.32 mmoles) was used without further purifications (**60%** yield).

1,3-Bis-(N^2-benzyl)-phenyl di-aminoguanidyl hydrazone (N^2-Bn-di-AG) hydroiodide 13b

The reaction was performed according to **METHOD D**, using isophthalaldehyde (50 mg, 0.37 mmoles), N-benzylaminoguanidine hydroiodide **14b** (250 mg, 0.86 mmoles) and absolute EtOH (5 mL). Pure 1,3-bis-(N^2-benzyl)-phenyl di-aminoguanidyl hydroiodide **13b** (177 mg, 0.26 mmoles) was obtained as a yellow solid in **70%** yield after solvent concentration at reduced pressure and reverse phase chromatography (eluant mixture: H_2O/MeCN 95:5 to 40:60).

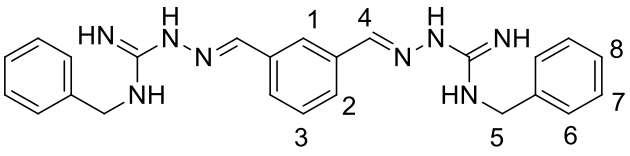

Characterization: m.p. = 100-105 °C

^{1}H NMR (400 MHz, DMSO-d_6) δ: 11.60 (bs, 2H, NH), 8.57 (bs, 2H, NH), 8.27 (m, 3H, H1, H4), 8.05 (bs, 2H, NH), 8.00 (m, 2H, H2)7.55 (t, J = 7.8 Hz, 1H, H3), 7.35 (m, 10H, H6, H7, H8), 4.60 (d, J = 5.4 Hz, 4H, H5).

^{13}C NMR (100 MHz, DMSO-d_6). δ: 154.7, 146.9, 137.5, 134.5, 129.6, 129.0,1128.0, 127.7, 127, 5, 44.5.

MS (ESI), m/z: calcd for $C_{24}H_{26}N_8$·426.23, found 427.22 ($M+H^+$).

1.5.22. Synthesis of 1,3-bis-(N^2-pyrrolidino)-phenyl di-aminoguanidyl hydrazone (N^2-Pyrr-di-AG) hydrochloride 13c

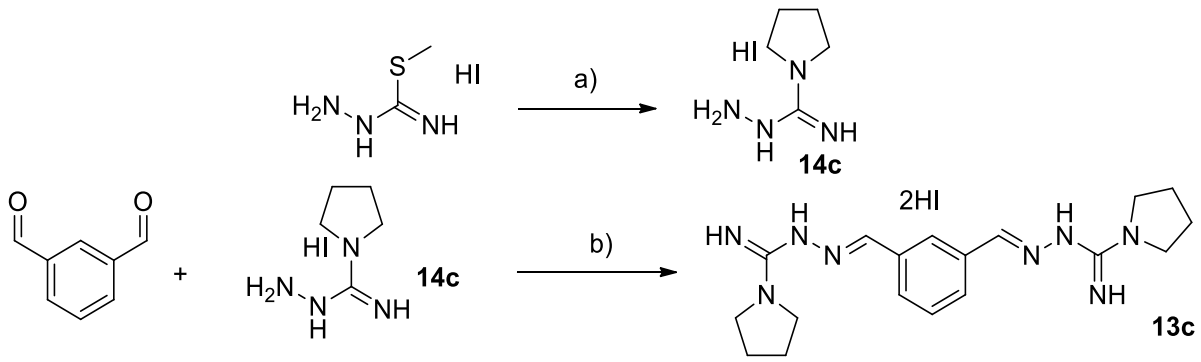

a) Pyrrolidine, MeOH, RT, 72 hrs, **89%**; b) EtOH, 80°C, 16hrs, **70%**

N^2-Pyrrolidin-aminoguanidine hydroiodide 14c

S-methyl isothiosemicarbazide hydroiodide (511.6 mg, 2.20 mmoles) was dissolved in MeOH (5 mL). Then pyrrolidine (0.271 mL, 3.30 mmoles) was added and the pale yellow solution was stirred at RT for 72 hrs. Then, the solvent was concentrated under reduced pressure. After solvent evaporation, the light pink solid was suspended in Et_2O (10 mL), filtered and washed with 1:1 Et_2O/EtOAc (20 mL). After drying, crude N^2-pyrrolidin-aminoguanidine hydroiodide **14c** (501.4 mg 1.96 mmoles) was used without further purifications (**89%** yield).

1,3-Bis-(N^2-pyrrolidino)-phenyl di-aminoguanidyl hydrazone (N^2-Pyrr-di-AG) hydroiodide 13c

The reaction was performed according to **METHOD D**, using isophthalaldehyde (40 mg, 0.30 mmoles), N-pyrrolidinaminoguanidine hydroiodide **14c** (168 mg, 0.66 mmoles) and absolute EtOH (3 mL). Pure 1,3-bis-(N^2-pyrrolidino)-phenyl di-aminoguanidyl hydrazone hydroiodide **13c** (128 mg, 0.21 mmoles) was obtained as an off-white solid in **70%** yield.

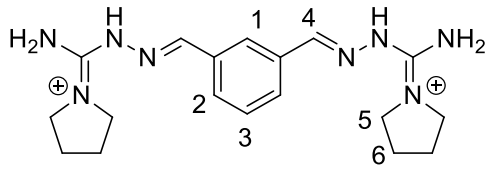

Characterization: m.p. = 191-196 °C dec

^{1}H NMR (400 MHz, DMSO-d_6) δ: 11.31 (bs,2H, 2H), 8.43 (s, 2H, H4), 8.28 (s, 1H, H1), 8.06 (d, J = 7.84 Hz, 2H, H2), 7.97 (bs, 4H, NH), 7.57 (t, J = 7.84 Hz, 1H, H3), 3.50 (t, J = 6.4 Hz, 8H, H5), 2.00 (t, J = 6.4 Hz, 8H, H6).

^{13}C NMR (100 MHz, DMSO-d_6) δ: 152.3, 147.1, 134.5, 129.8, 129.7, 127.4, 48.1, 25.1.

MS (ESI), m/z: calcd for $C_{18}H_{26}N_8$·354.23, found 355.22 ($M+H^+$).

1.5.23 Synthesis of 1,3-bis-(N^2N^3-imidazolin)-phenyl di-aminoguanidyl hydrazone hydrobromide 13e

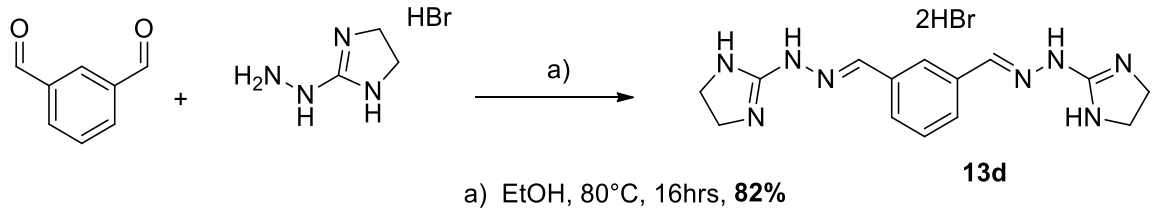

13d

a) EtOH, 80°C, 16hrs, **82%**

The reaction was performed according to **METHOD D**, using isophthalaldehyde (70 mg, 0.52 mmoles), N,N'-imidazolinaminoguanidine hydrobromide (198 mg, 1.10 mmoles) and absolute EtOH (3.5 mL). Pure 1,3-bis-N^2N^3-imidazolin)-phenyl di-aminoguanidyl hydrazone hydrobromide **13d** (196 mg, 0.43 mmoles) was obtained as a white solid in **82%** yield.

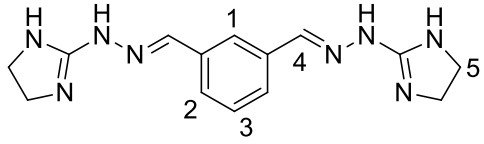

Characterization: m.p. = 281-289 °C

^{1}H NMR (400 MHz, DMSO-d_6) δ: 12.42 (bs, 2H, NH), 8.75 (bs, 4H, NH), 8.27 (s, 2H, H4), 8.22 (s, 1H, H1), 7.99 (d, J = 7.79 Hz, 2H, H2), 7.59 (t, J = 7.79 Hz, 1H, H3), 3.77 (s, 8H, H5).

^{13}C NMR (100 MHz, DMSO-d_6) δ: 158.5, 147.6, 134.5, 129.7, 129.4, 127.5, 43.2.

MS (ESI), m/z: calcd for $C_{14}H_{18}N_8$·298.17, found 299.18 ($M+H^+$).

1.5.24. Synthesis of 1,3-bis-(N^1-methyl-N^2N^3-imidazolin)-phenyl di-aminoguanidyl hydrazone hydrobromide 13e.

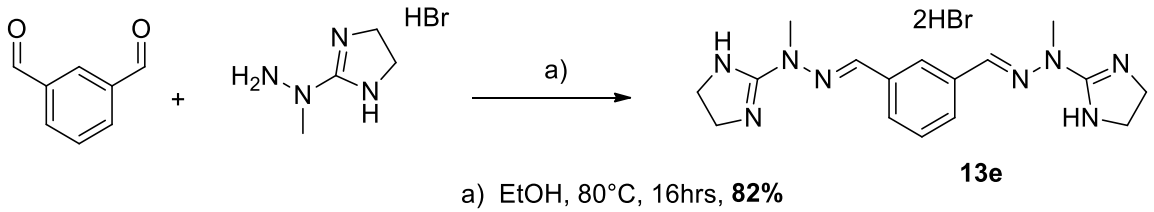

13e

a) EtOH, 80°C, 16hrs, **82%**

The reaction was performed according to **METHOD D**, using isophthalaldehyde (69 mg, 0.52 mmoles), N-methyl-N',N"-imidazolinaminoguanidine hydrobromide (213 mg, 1.09 mmoles) and absolute EtOH (3.5 mL). Pure 1,3-bis-(N^1-methyl-N^2N^3-imidazolin)-phenyl di-aminoguanidyl hydrazone hydrobromide **13e** (208 mg, 0.43 mmoles) was obtained as a white solid in **82%** yield.

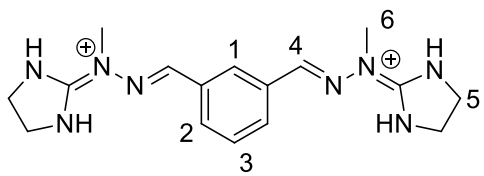

Characterization: m.p. = 340-346 °C dec

^{1}H NMR (400 MHz, DMSO-d_6) δ: 9.02 (bs, 4H, NH), 8.38 (s, 1H, H1), 8.19 (s, 2H, H4), 8.05 (d, J = 7.75 Hz, 2H, H2), 7.60 (t, J = 7.75 Hz, 1H, H3), 3.81 (s, 6H, H6), 3.75 (s, 8H, H5).

^{13}C NMR (100 MHz, DMSO-d_6) δ: 159.5, 144.4, 134.5, 130.0, 129.7, 128.3, 43.6, 33.2.

MS (ESI), m/z: calcd for $C_{16}H_{22}N_8$·326.20, found 327.20 ($M+H^+$).

1.5.25. Synthesis of 1,3-bis-(N^2N^3-benzimidazolin)-phenyl di-aminoguanidyl hydrazone trifluoroacetate 13f

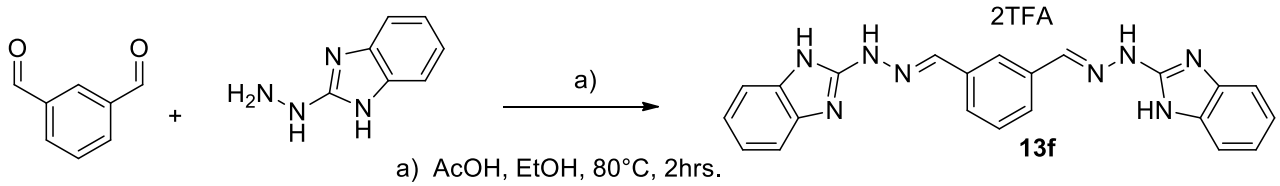

a) AcOH, EtOH, 80°C, 2hrs.

1-(1H-Benzimidazol-2-yl)hydrazine (109.6 mg, 0.74 mmoles) and AcOH (50 µL) were sequentially added under stirring to a solution of isophthalaldehyde (45.6 mg, 0.34 mmoles) in EtOH (5 mL) . The mixture was refluxed for 2 hrs. The reaction mixture was then allowed to cool to RT and filtered. The precipitate was washed with H_2O (20 mL), dried and purified by reverse phase chromatography (eluant mixture: water/MeCN from 95:5 to 40:60 + 0.1% TFA) to afford pure 1,3-bis-benzimidazolin)-phenyl di-aminoguanidyl hydrazone trifluoroacetate **13f** (124.5 mg, 0.20 mmoles) as a white solid in **59**% yield.

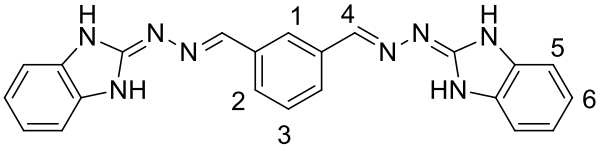

Characterization: m.p. = 200-207°C

^{1}H NMR (300 MHz, DMSO-d_6) δ: 13.11 (bs, 4H, NH), 8.36 (s, 2H, H4), 8.23 (s, 1H, H1), 8.09 (d, J = 7.8 Hz, 2H, H2), 7.65 (t, J = 7.7 Hz, 1H, H3), 7.50 (dd, J = 5.9, 3.2 Hz, 4H, H6), 7.30 (dd, J = 5.9, 3.2 Hz, 4H, H5).

^{13}C NMR (75 MHz, DMSO-d_6) δ: 149.8, 146.5, 134.9, 131.7, 129.7, 128.9, 127.4, 123.6, 112.6.

MS (ESI), m/z: calcd for $C_{22}H_{20}N_8$·396.18, found 397.21 ($M+H^+$).

1.5.26. Synthesis of 1,3-phenyl mono-aminoguanidyl hydrazones 15a-c

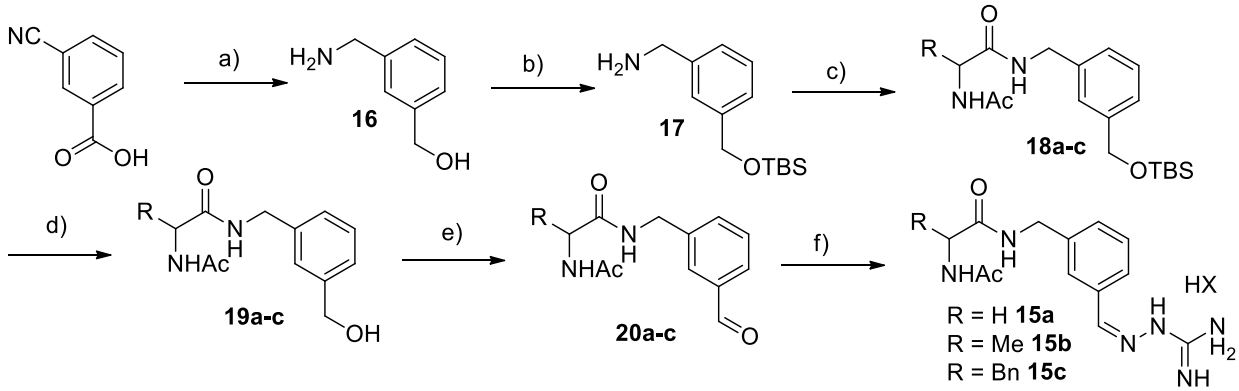

a) 1M BH_3-THF, dry THF, N_2, 0°C to RT, 4hrs; b) TBSCl, 1H-imidazole, dry DCM, 0°C to RT, 6hrs, **72%** over two steps; c) H-Acetyl-aminoacid, EDCI, HOBt, DIPEA, dry DCM, RT, 16hrs; d) cat. AcCl, dry MeOH, 0°C, 30min,**82-86%** over two steps; e) IBX, dry MeCN, 80°C, 3hrs; e) amminoguanidine HCl, cat. 1N HCl_{aq}, EtOH, 80°C, 3hrs, **60-65%** over two steps.

3-(Aminomethyl)phenyl methanol 16

3-Cyanobenzoic acid (1 g, 6.8 mmoles) was suspended in dry tetrahydrofuran (THF, 5 mL). 1M Borane-THF complex in THF (25 mL, 25 mmoles) was added dropwise over 1 hr at RT, and the mixture was stirred at the same temperature for additional 3 hrs. The reaction was quenched with 6M aqueous HCl (11 mL) to cleave the borate ester complex. THF was then removed under reduced pressure, and NaOH pellets were added till pH 12. The aqueous phase was then extracted with Et_2O (4 x 40mL). The ether phase was dried over $MgSO_4$ and concentrated under reduced pressure to give 885 mg of 3-(aminomethyl)benzyl alcohol **16** as a light-colored oil that was used without further purification.

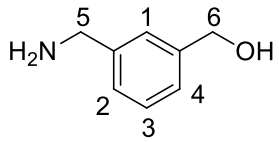

Characterization:

^{1}H NMR (300 MHz, $CDCl_3$) δ: 7.31-7.15 (m, 4H, H1, H2, H3, H4), 4.61 (s, 2H, H6), 3.77 (s, 2H, H5), 2.37 (bs,3H, NH, OH).

3-(((tert-Butyldimethylsilyl)oxy)methyl)phenyl methanamine 17

3-(Aminomethyl)benzyl alcohol **16** (885 mg, 6.8 mmoles) and 1H-imidazole (1.39 g, 20.4 mmoles) were dissolved in DCM (23 mL) at RT. Then the solution was cooled at 0°C, and t-butyldimethylsilyl chloride (2.05 g, 13.6 mmoles) was added. The reaction mixture was slowly warmed to RT and stirred for further 5 hrs. The solution was then diluted with DCM (20 mL), washed with water (20 mL) and brine (15 mL). The organic layer was dried with anhydrous Na_2SO_4, filtered and evaporated under reduced pressure. The resulting oil (2.0 g) was purified by flash chromatography on silica gel (eluant mixture: DCM/MeOH 95:5 to 85:15) to afford 1.23 g of pure 3-(((tert-butyldimethylsilyl)oxy)methyl)phenyl methanamine **17** as a colorless oil (4.89 mmoles, **72%** yield over two steps).

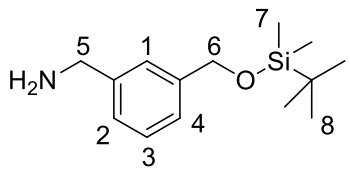

Characterization:

^{1}H NMR (300 MHz, DMSO-d6) δ: 7.32-7.15 (m, 4H, H1, H2, H3, H4), 4.71 (s, 2H, H6), 3.73 (s, 2H, H5), 1.94 (bs, 2H, NH), 0.93 (s, 9H, H8), 0.10 (s, 6H, H7).

2-Acetamido-N-(3-(((tert-butyldimethylsilyl)oxy)methyl)benzyl)acetamide 18a

N-Acetyl glycine (128.8 mg, 1.1 mmoles), EDCI (230.1 mg, 1.2 mmoles) and anhydrous HOBt (162.1 mg, 1.2 mmol, 1.2eq) were suspended under nitrogen atmosphere in dry DCM (7 mL). (3-(((tert-butyldimethylsilyl)oxy)methyl)phenyl) methanamine **17** (250 mg, 1mmoles) and DIPEA (0.35 mL, 2 mmol) dissolved in dry DCM (3mL) were added dropwise. The reaction mixture was stirred at RT and monitored by TLC (eluant mixture: DCM/MeOH 9:1). After 16 hrs the solvent was concentrated under reduced pressure, the residue was redissolved in EtOAc (30 mL) and washed with 10% citric acid solution (20 mL), saturated aq. $NaHCO_3$ (20 mL) and brine (10 mL). The organic layer was dried with anhydrous Na_2SO_4, filtered and evaporated. Crude 2-acetamido-N-(3-(((tert-butyldimethylsilyl)oxy)methyl)benzyl)acetamide **18a** (colourless oil, 371.5 mg) was used without further purification.

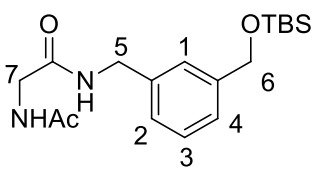

Characterization:

^{1}H NMR (300 MHz, DMSO-d_6) δ: 8.39 (t, J= 6.0 Hz, NH), 8.15 (t, J= 7.1 Hz, NH), 7.30 (m, 1H, H3), 7.19 (m, 3H, H1, H2, H4), 4.70 (s, 2H, H6), 4.30 (d, J = 6.0 Hz,

1H, H5), 3.73 (d, J = 7.1 Hz, 2H, H7), 1.88 (s, 3H, Ac), 0.93 (s, 9H, ^{t}Bu), 0.10 (s, 6H, Me).

2-Acetamido-N-(3-(hydroxymethyl)benzyl)acetamide 19a

Crude 2-acetamido-N-(3-(((tert-butyldimethylsilyl)oxy)methyl)benzyl)acetamide **18a** (371.5 mg, theor. 1 mmol) was dissolved in dry MeOH (10 mL) under nitrogen atmosphere. The solution was cooled under stirring at 0°C, and AcCl (11 µL, 0.15 mmoles) was added. The reaction mixture was stirred at 0°C for 2 hrs and monitored by TLC (eluant mixture: 9:1 DCM/MeOH). Pure 2-acetamido-N-(3-(hydroxymethyl)benzyl)acetamide **19a** (193.7 mg, 0.82 mmoles) was obtained in **82%** yield (over two steps) as a white solid after solvent concentration and purification on silica gel (eluant mixture: DCM/MeOH from 95:5 to 9:1).

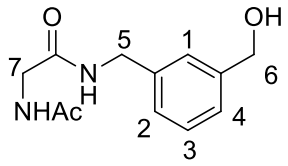

Characterization:

^{1}H NMR (300 MHz, DMSO-d_6) δ: 8.37 (t, J = 5.9 Hz, NH), 8.22 – 8.01 (m, NH), 7.42 – 7.01 (m, 4H, H1, H2, H3, H4), 5.19 (t, J = 5.6 Hz, OH), 4.48 (d, J = 5.6 Hz, 2H, H6), 4.28 (d, J = 6.0 Hz, 2H, H7), 3.72 (d, J = 5.9 Hz, 2H, H5), 1.87 (s, 3H, Ac).

^{13}C NMR (75 MHz, DMSO-d_6) δ: 169.7, 169.0, 142.5, 139.2, 128.0, 125.6, 125.4, 124.9, 62.9, 48.6, 42.1, 42.1, 22.6.

2-Acetamido-N-(3-formylbenzyl)acetamide 20a

A suspension of 2-acetamido-N-(3-(hydroxymethyl)benzyl)acetamide **19a** (112.68 mg, 0.477 mmoles) and IBX (200 mg, 0.716 mmoles) in acetonitrile (5 mL) was stirred vigorously at 80°C. The reaction progress was monitored by TLC (eluant mixture: 9:1 DCM/MeOH). After reaction completion (4 hrs), the resulting mixture was filtered through a short path of celite using 1:1 MeCN/AcOEt (50 mL). Crude 2-acetamido-N-(3-formylbenzyl)acetamide **20a** (95 mg) was obtained as a white solid after solvent concentration, and used without further purification.

2-acetamido-N-(3-((2-carbamimidoylhydrazono)methyl)benzyl)acetamide trifluoroacetate 15a

Aminoguanidine hydrochloride (58 mg, 0.524 mmoles) and 1N aq. HCl (3 drops, catalytic) were sequentially added to a warm, vigorously stirred solution of 2-acetamido-N-(3-formylbenzyl)acetamide **20a** (95 mg, theor. 0.477 mmoles) in absolute EtOH (5 mL). The reaction mixture was refluxed, with periodical TLC monitoring (eluant mixture: 8:2 CH_2Cl_2/MeOH, with a few AcOH drops). After 3 hours, the reaction mixture was cooled to RT, and concentrated in vacuum. Pure 2-acetamido-N-(3-((2-carbamimidoyl hydrazono)methyl)benzyl)acetamide trifluoroacetate **15a** (125.4 mg, 0.31 mmoles) was obtained as a white solid after reverse phase chromatography (eluant mixture: H_2O/MeCN from 95:5 to 0:100 + 0.1%) (**65**% yield over two steps).

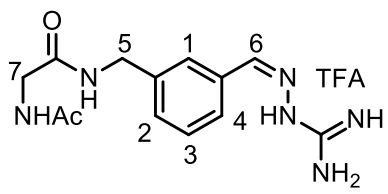

Characterization:

^{1}NMR (300 MHz, DMSO-d_6) δ: 11.86 (bs, 1H, NH), 8.46 (t, J = 5.9 Hz, 1H, NH), 8.36 (t, J = 5.4 Hz, NH), 8.17 (s, 1H, H6), 8.11 – 7.51 (m, 25H, NH, H4, H1), 7.50 – 7.28 (m, 2H, H3, H2), 4.35 (d, J = 5.9 Hz, 2H, H5), 3.71 (d, J = 5.7 Hz, H7), 1.91 (s, 3H, Ac).

^{13}C NMR (75 MHz, DMSO-d_6) δ: 170.3, 169.2, 155.4, 146.9, 140.2, 133.4, 129.1, 128.6, 126.7, 124.9, 42.6, 41.6, 22.4.

(±) 2-Acetamido-N-(3-(((tert-butyldimethylsilyl)oxy)methyl)benzyl)propenamide 18b

(±) 2-Acetamidopropanoic acid (144.2 mg, 1.1 mmoles), EDCI (230.1 mg, 1.2 mmoles) and anhydrous HOBt (162.1 mg, 1.2 mmoles) were susvigorously stirredpended under nitrogen atmosphere in dry DCM (7 mL). A solution of (3-(((tert-Butyldimethylsilyl)oxy)methyl)phenyl) methanamine **17** (250 mg, 1mmol) and DIPEA (0.35 mL, 2 mmoles) in dry DCM (3mL) was added dropwise. The reaction mixture was stirred at RT and monitored by TLC (eluant mixture: 9:1 DCM/MeOH). After 16 hrs, the solvent was concentrated under reduced pressure; the residue was redissolved in EtOAc (30 mL) and washed with 10% citric acid solution (20 mL), saturated aq. $NaHCO_3$ (20 mL) and brine (10 mL). The organic layer was dried with anhydrous Na_2SO_4, filtered and evaporated under reduced pressure. Crude (±) 2-acetamido-N-(3-(((tert-butyldimethylsilyl)oxy)methyl)benzyl)propenamide **18b** (white solid, 348.2 mg) was characterized and used without further purification.

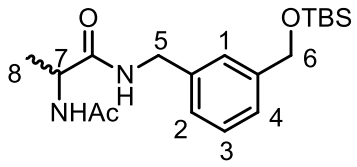

Characterization:

^{1}H NMR (300 MHz, DMSO-d6) δ: 8.40 (t, J= 6.0 Hz, NH), 7.06 (d, J= 7.1 Hz, NH), 7.30 (m, 1H, H3), 7.15 (m, 3H, H1, H2, H4), 4.70 (s, 2H, H6), 4.29 (m, 3H, H7, H5), 1.86 (s, 3H, Ac), 1.23 (d, J = 8.1 Hz, 3H, H8), 0.93 (s, 9H, ^{t}Bu), 0.09 (s, 6H, Me).

(±) 2-Acetamido-N-(3-(hydroxymethyl)benzyl)propenamide 19b

Crude (±) 2-acetamido-N-(3-(((tert-butyldimethylsilyl)oxy)methyl)benzyl)propenamide **18b** (348.2 mg, theor. 1 mmol) was dissolved in dry MeOH (10 mL) under nitrogen atmosphere. The solution was cooled under stirring at 0°C, and AcCl (11 µL, 0.15 mmoles) was added. The reaction mixture was stirred at 0° Cfor 2, hrs and monitored by TLC (eluant mixture: 9:1 DCM/MeOH). Pure (±) 2-acetamido-N-(3-(hydroxymethyl)benzyl) propenamide **19b** (215.3 mg, 0.86 mmoles) was obtained in **86%** yield over two steps as a white solid after solvent concentration and purification on silica gel (eluant mixture: DCM/MeOH from 95:5 to 9:1).

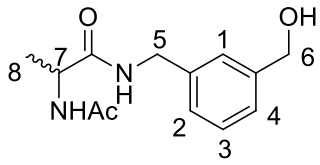

Characterization:

^{1}H NMR (300 MHz, DMSO-d_6) δ: 8.39 (t, J = 5.7 Hz, NH), 8.04 (d, J = 7.2 Hz, NH), 7.33 – 7.09 (m, 4H, Ar), 5.26 – 5.12 (t, J = 5.6 Hz, OH), 4.50 (d, J = 5.6 Hz, 2H, H6), 4.39 – 4.20 (m, 3H, H7, H5), 1.87 (s, 3H, Ac), 1.24 (d, J = 7.1 Hz, 3H, H8).

(±) 2-Acetamido-N-(3-formylbenzyl)propenamide 20b

A suspension of (±) 2-acetamido-N-(3-(hydroxymethyl)benzyl) propenamide **19b** (116.8 mg, 0.466 mmoles) and IBX (195.7 mg, 0.699 mmoles) in acetonitrile (5 mL) was stirred vigorously at 80°C. The reaction was monitored by TLC (eluant mixture: 9:1 DCM/MeOH). After reaction completion (4 hrs), the resulting mixture was filtered through a short path of celite with 1:1 MeCN/AcOEt (50 mL). Crude (±) 2-acetamido-N-(3-formylbenzyl)propenamide **20b** (99 mg) was obtained as a white solid after solvent concentration and used without further purification.

(±) 2-Acetamido-N-(3-((2-carbamimidoylhydrazono)methyl)benzyl)propanamide trifluoroacetate 15b

Aminoguanidine hydrochloride (56.7 mg, 0.512 mmoles) and 1N aq. HCl (3 drops, catalytic) were sequentially added to a warm, vigorously stirred solution of (±) 2-acetamido-N-(3-formylbenzyl)propenamide **20b** (99 mg, 0.466 theor. mmoles) in absolute EtOH (5 mL). The reaction mixture was refluxed, with periodical TLC

monitoring (eluant mixture: 8:2 CH_2Cl_2/MeOH with a few AcOH drops). After 3 hours, the reaction mixture was cooled to RT, and concentrated in vacuum. Pure (±) 2-acetamido-N-(3-((2-carbamimidoylhydrazono)methyl)benzyl)propanamide trifluoroacetate **15b** (117.1 mg, 0.28 mmoles) was obtained as a white solid after reverse phase chromatography (eluant mixture: H_2O/MeCN from 95:5 to 0:100 + 0.1% TFA) (**60**% yield over two steps).

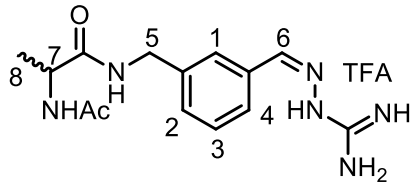

Characterization:

^{1}NMR (300 MHz, DMSO-d_6) δ: 11.92 (bs, 1H, NH), 8.48 (t, J = 6.0 Hz, 1H, NH), 8.25 (d, J = 6.3, 1H, NH Hz), 8.17 (s, 1H, H6), 8.11 – 7.50 (m, 5H, NH, H4, H1), 7.48 – 7.23 (m, 2H, N2, H3), 4.51 – 4.07 (m, 3H, H5, H7), 1.87 (s, 3H, Ac), 1.26 (d, J = 7.1 Hz, 2H, H8).

^{13}C NMR (75 MHz, DMSO-d_6) δ: 172.7, 169.8, 155.5, 146.8, 140.2, 133.5, 128.87, 128.6, 126.8, 124.6, 48.9, 41.5, 22.4, 17.6.

(±) 2-Acetamido-N-(3-(((tert-butyldimethylsilyl)oxy)methyl)benzyl)-3-phenylpropanamide 18 c

(±) 2-Acetamido-3-phenylpropanoic acid (228.0 mg, 1.1 mmoles), EDCI (230.1 mg, 1.2 mmoles) and anhydrous HOBt (162.1 mg, 1.2 mmoles) were vigorously stirred under nitrogen atmosphere in dry DCM (7 mL). A solution of (3-(((tert-butyldimethylsilyl)oxy)methyl)phenyl) methanamine **17** (250 mg, 1mmol) and DIPEA (0.35 ml, 2mmol) in dry DCM (3mL) was added dropwise. The reaction mixture was stirred at RT and monitored by TLC (eluant mixture: 9:1 DCM/MeOH). After 16 hrs, the solvent was concentrated under reduced pressure; the residue was redissolved in EtOAc (30 mL) and washed with 10% citric acid solution (20 mL), saturated aq. $NaHCO_3$ (20 mL) and brine (10 mL). The organic layer was dried with anhydrous Na_2SO_4, filtered and evaporated. Crude (±) 2-acetamido-N-(3-(((tert-butyldimethylsilyl)oxy)methyl)benzyl)-3-phenylpropanamide **18c** (colourless oil, 439.3 mg) was characterized and used without further purification.

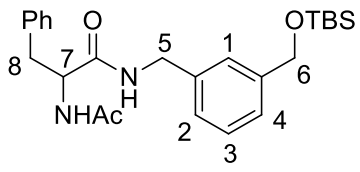

Characterization:

^{1}H NMR (300 MHz, $CDCl_3$) δ: 7.25-7.15 (m, 8H, H2, H3, H4, Ph), 7.04 (s, 1H, H1), 6.85 (m, 1H, NH), 6.48 (m, 1H, NH), 4.67 (m, 3H, H6, H7), 4.28 (m, 2H, H5), 3.04 (m, 2H, H8), 1.93 (s, 3H, Ac), 0.92 (s, 9H, ^{t}Bu), 0.09 (s, 6H, Me).

(±) 2-Acetamido-N-(3-(hydroxymethyl)benzyl)-3-phenylpropanamide 19c

Crude (±) 2-acetamido-N-(3-(((tert-butyldimethylsilyl)oxy)methyl)benzyl)-3-phenylpropanamide **18c** (439.3 mg, theor. 1 mmol) was dissolved in dry MeOH (10 mL) under nitrogen atmosphere. The solution was cooled under stirring at 0°C, and AcCl (11 µL, 0.15 mmoles) was added. The reaction mixture was stirred at 0°C for 2 hrs and monitored by TLC (eluant mixture: 9:1 DCM/MeOH). Pure (±) 2-acetamido-N-(3-(hydroxymethyl)benzyl)-3-phenylpropanamide **19c** (274.2 mg, 0.84 mmol) was obtained in **84%** yield (over two steps) as a white solid after solvent concentration and purification on silica gel (eluant mixture: DCM/MeOH from 95:5 to 9:1).

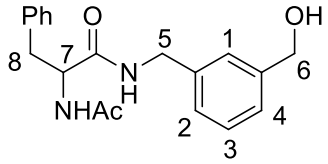

Characterization:

^{1}H NMR (300 MHz, DMSO-d_6) δ: 8.52 (t, J = 5.9 Hz, NH), 8.18 (d, J = 8.4 Hz, NH), 7.36 – 7.03 (m, 9H, Ar), 5.19 (t, J = 5.6 Hz, OH), 4.59 – 4.51 (m, 1H, H7), 4.49 (d, J = 5.6 Hz, 2H, H6), 4.28 (d, J = 5.9 Hz, 2H, H5), 3.02 (dd, J = 13.6, 5.1 Hz, 1H, $H8_B$), 2.79 (dd, J = 13.6, 9.5 Hz, 1H, $H8_A$), 1.79 (s, 3H, Ac).

^{13}C NMR (75 MHz, DMSO-d_6) δ: 171.3, 169.1, 142.5, 139.0, 138.1, 129.2, 128.1, 128.0, 126.3, 125.5, 125.3, 124.8, 62.9, 54.2, 42.1, 37.8, 22.5.

(±) 2-Acetamido-N-(3-formylbenzyl)-3-phenylpropanamide 20c

A suspension of (±) 2-acetamido-N-(3-(hydroxymethyl)benzyl)-3-phenylpropanamide **19c** (147.9 mg, 0.453 mmoles) and IBX (190.3 mg, 0.680 mmoles) in acetonitrile (5 mL) was stirred vigorously at 80°C. The reaction progress was monitored by TLC (eluant mixture: 9:1 DCM/MeOH). After reaction completion (4 hrs) the resulting mixture was filtered through a short path of celite using a with 1:1 MeCN/AcOEt. Crude (±) 2-acetamido-N-(3-formylbenzyl)-3-phenylpropanamide **20c** (120 mg) was obtained as a white solid after solvent concentration and used without further purification.

(±) 2-Acetamido-N-(3-((2-carbamimidoylhydrazono)methyl)benzyl)-3-phenylpropanamide trifluoroacetate 15c

Aminoguanidine hydrochloride (55.1 mg, 0.5 mmols) and 1N aq. HCl (3 drops, catalytic) were sequentially added to a warm, vigorously stirred solution of (±) 2-acetamido-N-(3-formylbenzyl)-3-phenylpropanamide **20c** (120 mg, 0.453 theor. mmol) in absolute EtOH (5 mL). The reaction mixture was refluxed, with periodical TLC monitoring (eluant mixture: 8:2 CH_2Cl_2/MeOH with a few AcOH drops). After 3 hours, the reaction mixture was cooled to RT, and concentrated in vacuum. Pure (±) 2-acetamido-N-(3-((2-carbamimidoylhydrazono) methyl)benzyl)-3-phenylpropanamide trifluoroacetate **15c** (143.4 mg, 0.29 mmoles) was obtained in a **64**% yield over two steps as a white solid after reverse phase chromatography (H_2O/MeCN from 95:5 to 0:100 + 0.1% TFA as eluents).

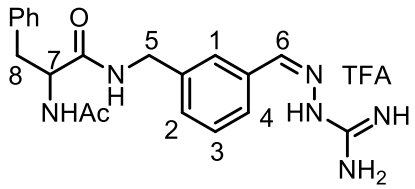

Characterization:

^{1}NMR (300 MHz, DMSO-d_6) δ: 12.04 (s, 1H, NH), 8.64 (t, J = 5.9 Hz, 1H, NH), 8.35 (d, J = 7.9 Hz, 1H, NH), 8.16 (s, 1H, H6), 7.80 (m, 4H, NH, H1), 7.67 (d, J = 7.7 Hz, 1H, H4), 7.39 (t, J = 7.6 Hz, 1H, H3), 7.35 – 7.13 (m, 6H, H2, Ph), 4.61 – 4.43 (m, 1H, H7), 4.43 – 4.17 (m, 2H, H5), 2.93 (ddd, J = 23.5, 13.7, 7.4 Hz, 2H, H8), 1.82 (s, 3H, Ac).

^{13}C NMR (75 MHz, DMSO-d6) δ: 171.5, 169.8, 155.3, 146.9, 140.0, 138.1, 133.4, 129.1, 128.6, 128.1, 126.6, 126.3, 125.0, 54.8, 41.6, 37.4, 22.4.

1.5.27. Synthesis of "2"-modified-N-(4-fluoro-3-methylphenyl)quinazolin-4-amines 2a-i

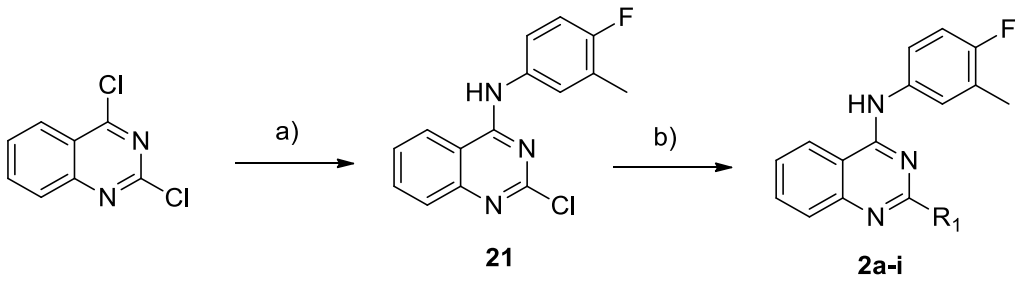

a) 4-Fluoro-3-Methylaniline 1eq, TEA, 1.5eq, THF, 80°C, 8hrs, **74%**; $R_1B(OH)_2$ 1.5eq, $Pd(PPh_3)_4$ 0.1eq, 2M Na_2CO_3aq 2eq, dioxane, 105°C, 6hrs, **41-77%.**

2-Chloro-N-(4-fluoro-3-methylphenyl)quinazolin-4-amine 21

Triethylamine (0.24 mL, 1.68 mmoles) was added to a stirred mixture of 2,4-dichloroquinazoline (223 mg, 1.12 mmoles) and 4-fluoro-3-methylaniline (145.7 mg, 1.12 mmoles) in THF (7 mL). The reaction mixture was heated at reflux and monitored by TLC (eluant mixture: petroleum ether/AcOEt 7:3). After 8 hrs the reaction was cooled to RT, and concentrated under reduced pressure. The crude was taken up with AcOEt (30 mL), washed with water (20 mL) and brine (10 mL). The organic phase was dried over anhydrous Na_2SO_4, filtered and concentrated. The crude (250.6 mg) was purified by flash chromatography (eluant mixture: petroleum ether/AcOEt from 8:2 to 6:4) to yield 224.1 mg of pure 2-chloro-N-(4-fluoro-3-methylphenyl)quinazolin-4-amine **21** as a white solid (0.831 mmoles, **74%** yield).

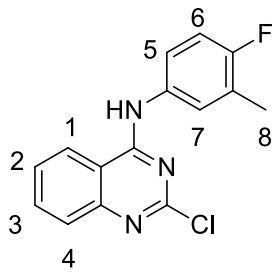

Characterization:

^{1}H NMR (300 MHz, $CDCl_3$): δ (ppm) 7.79-7.71 (m, 3H, Ar), 7.51 – 7.43 (m, 4H, Ar), 6.99 (t, J = 9.1 Hz, 1H, Ar), 2.28 (d, J = 3.0 Hz, 3H, H8).

^{13}C NMR (75 MHz, $CDCl_3$): δ (ppm) 160.2, 158.7, 157.0, 151.4, 133.9, 132.9, 128.4, 126.8, 125.9, 125.1, 121.1, 120.4, 115.3, 113.3, 14.8.

N-(4-Fluoro-3-methylphenyl)-2-(3-fluorophenyl)quinazolin-4-amine 2a

The reaction was performed according to **METHOD E**, using 2-chloro-N-(4-fluoro-3-methylphenyl)quinazolin-4-amine **20** (51.5 mg, 0.179 mmoles), 3-fluorobenzeneboronic acid (50.1 mg, 0.358 mmoles) and $Pd(PPh_3)_4$ (20.8 mg, 0.018 mmoles). Pure N-(4-fluoro-3-methylphenyl)-2-(3-fluorophenyl) quinazolin-4-amine trifluoroacetate **2a** (59.1 mg, 0.127 mmoles) was obtained as a yellow solid in **71%** yield.

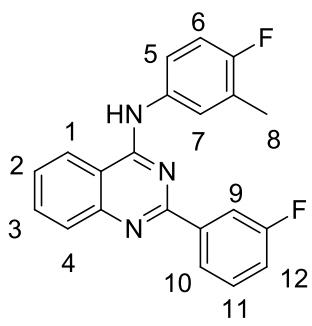

^{1}H NMR (300 MHz, DMSO-d_6): δ (ppm) 10.54 (bs, 1H, NH), 8.61 (d, J = 8.3 Hz, 1H, H1), 8.17 (d, J = 7.9 Hz, 1H, H10), 8.09 – 8.02 (m, 1H, H9), 8.02 – 7.91 (m, 2H, H3, H4), 7.81 (dd, J = 7.0, 2.3 Hz, 1H, H7), 7.77 – 7.56 (m, 3H, H2, H5, H11), 7.44 (td, J = 8.4, 2.1 Hz, 1H, H12), 7.28 (t, J = 9.2 Hz, 1H, H6), 2.33 (d, J = 1.4 Hz, 3H, H8).

^{13}C NMR (75 MHz, DMSO-d_6): δ (ppm) 164.4, 161.1, 158.5, 157.5, 146.7, 138.6, 135.0, 134.5, 131.4, 127.7, 126.9, 125.2, 124.8, 124.8, 123.9, 123.1, 118.8, 115.4, 115.1, 113.9, 14.8,

UPLC/MS (ESI$^+$): 348.38 [M+H$^+$] (mass calculated for $C_{21}H_{15}F_2N_3$: 347.12). Purity measured by UPLC/MS: 99.5%.

N-(4-Fluoro-3-methylphenyl)-2-(p-tolyl)quinazolin-4-amine 2b

The reaction was performed according to **METHOD E**, using 2-chloro-N-(4-fluoro-3-methylphenyl)quinazolin-4-amine **20** (35.9 mg, 0.125 mmoles), p-tolylboronic acid (34.0 mg, 0.25 mmoles) and $Pd(PPh_3)_4$ (15.0 mg, 0.013 mmoles). Pure N-(4-fluoro-3-methylphenyl)-2-(p-tolyl)quinazolin-4-amine trifluoroacetate **2b** (37.2 mg, 0.081 mmoles) was obtained as a yellow solid in **65%** yield.

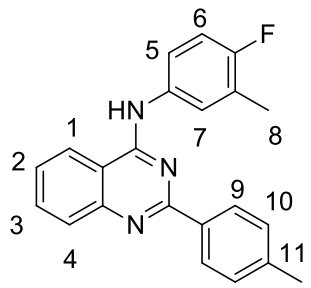

^{1}H NMR (300 MHz, DMSO-d_6): δ (ppm) 10.83 (s, 1H, NH), 8.64 (d, J = 8.3 Hz, 1H, H1), 8.21 (d, J = 8.2 Hz, 2H, H9), 8.00 (m, 2H, H3, H4), 7.83 – 7.72 (m, 2H, H2, H7), 7.69 (m, 1H, H5), 7.42 (d, J = 8.1 Hz, 2H, H10), 7.30 (t, J = 9.2 Hz, 1H, H6), 2.42 (s, 3H, H11), 2.33 (s, 3H, H8).

^{13}C NMR (75 MHz, DMSO-d_6): δ (ppm) 160.1, 159.0, 158.3, 156.9, 143.1, 135.5, 134.1, 130.0, 129.0, 127.8, 127.3, 127.2, 124.9, 124.7, 124.2, 123.6, 123.4, 115.7, 115.4, 113.4, 21.6, 14.8.

UPLC/MS (ESI$^+$): 344.26 [M+H$^+$] (mass calculated for $C_{22}H_{18}FN_3$: 343.15). Purity measured by UPLC/MS: 99.6%.

N-(4-Fluoro-3-methylphenyl)-2-(4-(trifluoromethyl)phenyl)quinazolin-4-amine 2c

The reaction was performed according to **METHOD E**, using 2-chloro-N-(4-fluoro-3-methylphenyl)quinazolin-4-amine **20** (36 mg, 0.126 mmoles), (4-(trifluoromethyl)phenyl)boronic acid (48.2 mg, 0.25 mmoles) and $Pd(PPh_3)_4$ (15.0 mg, 0.013 mmoles). Pure N-(4-fluoro-3-methylphenyl)-2-(p-tolyl)quinazolin-4-amine trifluoroacetate **2c** (37.1 mg, 0.072 mmoles) was obtained as an off-white solid in **57%** yield.

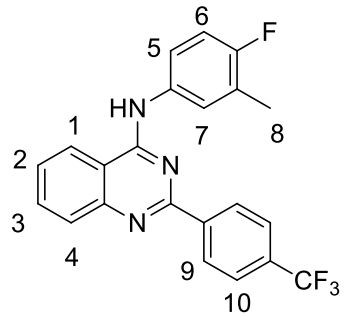

^{1}H NMR (300 MHz, DMSO-d_6): δ (ppm) 10.31 (s, 1H, NH), 8.60 (d, J = 8.3 Hz, 1H, H1), 8.54 (d, J = 8.1 Hz, 2H, H10), 7.94 (m, 4H, H3, H4, H9), 7.82 (dd, J = 7.0, 2.3 Hz, 1H, H7), 7.78 – 7.63 (m, 2H, H2, H5), 7.26 (t, J = 9.2 Hz, 1H, H6), 2.34 (d, J = 1.5 Hz, 3H, H8).

^{13}C NMR (75 MHz, DMSO-d_6): δ (ppm) 158.8, 157.7, 156.4, 148.4, 141.0, 134.8, 134.6, 131.1, 129.2, 127.5, 126.9, 126.6, 126.4, 126.1, 124.6, 123.8, 122.7, 115.5, 114.2, 14.8.

^{19}F NMR (282 MHz, DMSO-d_6): δ -61.20 (s, CF_3), -74.75 (m, TFA), -122.17 (s, 1F).

UPLC/MS (ESI$^+$): 398.36 [M+H$^+$] (mass calculated for $C_{22}H_{15}F_4N_3$: 397.12). Purity measured by UPLC/MS: 99.7%.

4-(4-((4-Fluoro-3-methylphenyl)amino)quinazolin-2-yl)benzonitrile 2d

The reaction was performed according to **METHOD E**, using 2-chloro-N-(4-fluoro-3-methylphenyl)quinazolin-4-amine **20** (35 mg, 0.122 mmoles), (4-cyanophenyl)boronic acid (35.9 mg, 0.244 mmoles) and $Pd(PPh_3)_4$ (15.0 mg, 0.013 mmoles). Pure 4-(4-((4-fluoro-3-methylphenyl)amino)quinazolin-2-yl)benzonitrile trifluoroacetate **2d** (29.0 mg, 0.061 mmoles) was obtained as a yellow solid in **50%** yield.

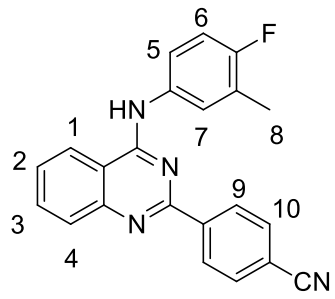

^{1}H NMR (300 MHz, DMSO-d_6): δ (ppm) 10.23 (s, 1H, NH), 8.60 (d, J = 8.3 Hz, 1H, H1), 8.51 (d, J = 8.4 Hz, 2H, H10), 8.02 (d, J = 8.4 Hz, 2H, H9), 7.97 – 7.90 (m, 2H, H3, H4), 7.80 (dd, J = 7.1, 2.3 Hz, 1H, H7), 7.71 (m, 2H, H2, H5), 7.26 (t, J = 9.2 Hz, 1H, H6), 2.32 (t, J = 9.0 Hz, 3H, H8).

^{13}C NMR (75 MHz, DMSO-d_6): δ (ppm) 159.4, 158.7, 157.6, 156.4, 141.8, 134.9, 134.5, 133.1, 129.1, 127.5, 126.6, 124.6, 123.7, 122.8, 119.2, 115.4, 115.2, 114.3, 14.9.

UPLC/MS (ESI$^+$): 355.33 [M+H$^+$] (mass calculated for $C_{22}H_{15}FN_4$: 354.13). Purity measured by UPLC/MS: 98.4%.

2-(Benzo[d][1,3]dioxol-5-yl)-N-(4-fluoro-3-methylphenyl)quinazolin-4-amine 2e

The reaction was performed according to **METHOD E**, using 2-chloro-N-(4-fluoro-3-methylphenyl)quinazolin-4-amine **20** (34.8 mg, 0.121 mmoles), benzo[d][1,3]dioxol-5-ylboronic acid (40.2 mg, 0.242 mmol) and $Pd(PPh_3)_4$ (14.2 mg, 0.012 mmoles). Pure 2-(benzo[d][1,3]dioxol-5-yl)-N-(4-fluoro-3-methylphenyl)quinazolin-4-amine trifluoroacetate **2e** (45.33 mg, 0.093 mmoles) was obtained as a yellow solid in **77%** yield.

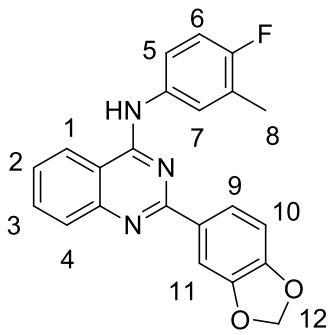

^{1}H NMR (300 MHz, DMSO-d_6): δ (ppm) δ 10.79 (bs, 1H, NH), 8.61 (d, J = 8.2 Hz, 1H, H1), 7.96 (m, 3H, H11, H10, H7), 7.74 (m, 3H, H2, H3, H4), 7.69 – 7.57 (m, 1H, H5), 7.27 (dd, J = 24.1, 15.0 Hz, 1H, H6), 7.15 (d, J = 8.3 Hz, 1H, H9), 6.18 (s, 2H, H12), 2.31 (bs, 3H, H8).

^{13}C NMR (75 MHz, DMSO-d_6): δ (ppm) 160.1, 158.9, 157.6, 156.9, 151.4, 148.4, 135.5, 134.0, 127.6, 127.4, 124.9, 124.7, 124.2, 123.6, 115.7, 115.4, 113.3, 109.1, 108.4, 102.6, 15.0.

UPLC/MS (ESI$^+$): 374.38 [M+H$^+$] (mass calculated for $C_{22}H_{16}FN_3O_2$: 373.12). Purity measured by UPLC/MS: 99.6%.

2-(4-Chlorophenyl)-N-(4-fluoro-3-methylphenyl)quinazolin-4-amine 2f

The reaction was performed according to **METHOD E**, using 2-chloro-N-(4-fluoro-3-methylphenyl)quinazolin-4-amine **20** (34.7 mg, 0.121 mmoles (4-chlorophenyl)boronic acid (37.8 mg, 0.242 mmoles) and $Pd(PPh_3)_4$ (14.1 mg, 0.012 mmoles). Pure 2-(4-chlorophenyl)-N-(4-fluoro-3-methylphenyl) quinazolin-4-amine trifluoroacetate **2f** (28.3 mg, 0.058 mmoles) was obtained as a yellow solid in **48%** yield.

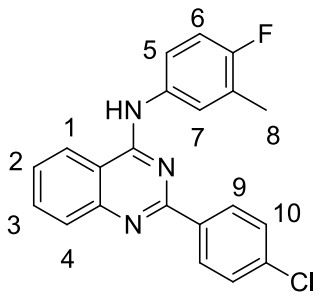

^{1}H NMR (300 MHz, DMSO-d_6): δ (ppm) δ 10.41 (s, 1H, NH), 8.60 (d, J = 8.2 Hz, 1H, H1), 8.35 (d, J = 8.6 Hz, 2H, H10), 8.06 – 7.84 (m, 2H, H4, H3), 7.80 (dd, J = 7.0, 2.3 Hz, 1H, H7), 7.75 – 7.66 (m, 2H, H5, H2), 7.65 (d, J = 8.6 Hz, 2H, H9), 7.27 (t, J = 9.2 Hz, 1H, H6), 2.33 (d, J = 1.5 Hz, 3H, H8).

^{13}C NMR (75 MHz, DMSO-d_6): δ (ppm) 159.8, 158.8, 158.0, 156.6, 136.7, 134.8, 134.7, 130.4, 129.3, 127.4, 126.8, 126.0, 124.8, 124.6, 123.8, 123.0, 115.4, 113.9, 14.9.

UPLC/MS (ESI$^+$): 364.24 [M+H$^+$] (mass calculated for $C_{21}H_{15}ClFN_3$: 363.09). Purity measured by UPLC/MS: 98.6%.

3-(4-((4-Fluoro-3-methylphenyl)amino)quinazolin-2-yl)phenyl)(pyrrolidin-1-yl)methanone 2g

The reaction was performed according to **METHOD E**, using 2-chloro-N-(4-fluoro-3-methylphenyl)quinazolin-4-amine **20** (35.1 mg, 0.123 mmoles), 3-(pyrrolidine-1-carbonyl)phenyl)boronic acid (55.2 mg, 0.246 mmoles) and $Pd(PPh_3)_4$ (14.2 mg, 0.012 mmoles). Pure (3-(4-((4-fluoro-3-methylphenyl)amino)quinazolin-2-yl)phenyl)(pyrrolidin-1-yl)methanone trifluoroacetate **2g** (40.9 mg, 0.050 mmoles) was obtained as a yellow solid in **41%** yield.

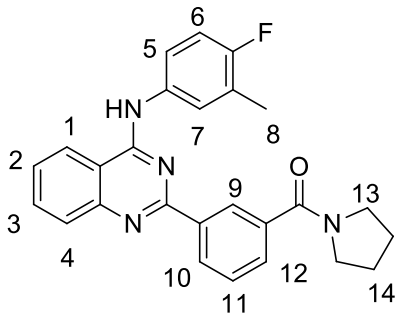

^{1}H NMR (300 MHz, DMSO-d_6): δ (ppm) δ 10.74 (s, 1H, NH), 8.64 (d, J = 8.3 Hz, 1H, H1), 8.46 (s, 1H, H9), 8.39 (d, J = 7.8 Hz, 1H, H10), 8.07 – 7.94 (m, 2H, H3, H4), 7.84 (dd, J = 7.0, 2.3 Hz, 1H, H7), 7.77 (m, 2H, H2, H12), 7.71 – 7.58 (m, 2H, H5, H11), 7.28 (t, J = 9.1 Hz, 1H, H6), 3.52 (t, J = 6.7 Hz, 2H, H13), 3.36 (t, J = 6.4 Hz, 2H, H13), 2.34 (d, J = 1.4 Hz, 3H, H8), 1.99 – 1.69 (m, 4H, H14).

^{13}C NMR (75 MHz, DMSO-d_6): δ (ppm) δ 168.1, 159.1, 157.9, 138.1, 135.4, 134.3, 130.8, 129.9, 129.3, 127.9, 127.7, 127.5, 124.9, 124.7, 124.1, 123.6, 123.5, 115.6, 115.3, 113.7, 49.5, 46.5, 26.5, 24.4, 14.8, 14.7.

UPLC/MS (ESI$^+$): 427.32 [M+H$^+$] (mass calculated for $C_{21}H_{22}FN_5$: 426.19). Purity measured by UPLC/MS: 98.5%.

N-(4-Fluoro-3-methylphenyl)-2-(pyridin-4-yl)quinazolin-4-amine 2h

The reaction was performed according to **METHOD E**, using 2-chloro-N-(4-fluoro-3-methylphenyl)quinazolin-4-amine **20** (40.0 mg, 0.139 mmoles), pyridin-4-ylboronic acid (34.2 mg, 0.278 mmoesl) and $Pd(PPh_3)_4$ (16.2 mg, 0.014 mmoles). Pure N-(4-fluoro-3-methylphenyl)-2-(pyridin-4-yl)quinazolin-4-amine trifluoroacetate **2h** (40.2 mg, 0.089 mmoles) was obtained as a yellow solid in **64%** yield.

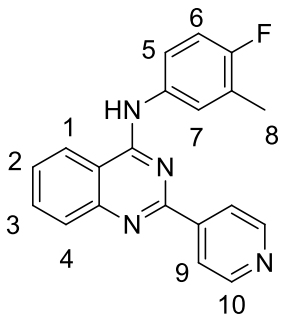

^{1}H NMR (300 MHz, DMSO-d_6): δ (ppm) 10.14 (s, 1H, NH), 8.90 (d, J = 4.5 Hz, 2H, H10), 8.62 (d, J = 8.3 Hz, 1H, H1), 8.48 (d, J = 6.0 Hz, 2H, H9), 7.96 (d, J = 3.8 Hz, 2H, H3, H4), 7.81 (dd, J = 7.0, 2.4 Hz, 1H, H7), 7.75 (m, 2H, H2, H5), 7.27 (t, J = 9.2 Hz, 1H, H6), 2.35 (d, J = 1.5 Hz, 3H, H8).

^{13}C NMR (75 MHz, DMSO-d_6): δ (ppm) 159.4, 158.8, 156.6, 156.0, 150.1, 149.2, 147.6, 135.3, 134.3, 128.7, 128.0, 126.5, 124.6, 123.7, 123.5, 122.6, 115.3, 114.8.

UPLC/MS (ESI$^+$): 331.35 [M+H$^+$] (mass calculated for $C_{20}H_{15}FN_4$: 330.13). Purity measured by UPLC/MS: 98.3%.

N-(4-Fluoro-3-methylphenyl)-2-(2-methylpyrimidin-5-yl)quinazolin-4-amine 2i

The reaction was performed according to **METHOD E**, using 2-chloro-N-(4-fluoro-3-methylphenyl)quinazolin-4-amine **20** (40 mg, 0.140 mmoles), 2-methylpyrimidin-5-ylboronic acid (38.5 mg, 0.279 mmoles) and $Pd(PPh_3)_4$ (16.4 mg, 0.014 mmoles). Pure N-(4-fluoro-3-methylphenyl)-2-(2-methylpyrimidin-5-yl)quinazolin-4-amine trifluoroacetate **2i** (39.6 mg, 0.085 mmoles) was obtained as an orange solid in **61%** yield.

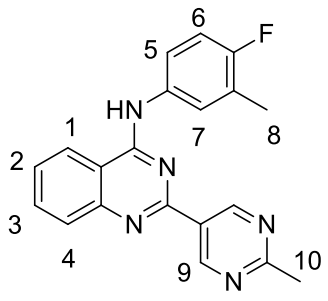

^{1}H NMR (300 MHz, DMSO-d_6): δ (ppm) 10.16 (s, 1H, NH), 9.46 (s, 2H, H9), 8.59 (d, J = 8.3 Hz, 1H, H1), 8.02 – 7.85 (m, 2H, H3, H4), 7.81 (dd, J = 7.0, 2.3 Hz, 1H, H7), 7.78 – 7.60 (m, 2H, H2, H5), 7.26 (t, J = 9.2 Hz, 1H, H6), 2.72 (s, 3H, H10), 2.32 (d, J = 1.5 Hz, 3H, H8).

^{13}C NMR (75 MHz, DMSO-d_6): δ (ppm) 169.2, 159.5, 158.6, 156.7, 156.2, 149.4, 134.97, 134.3, 128.4, 127.7, 127.3, 126.4, 124.4, 123.7, 122.6, 115.3, 114.5, 26.1, 14.9.

UPLC/MS (ESI$^+$): 346.28 [M+H$^+$] (mass calculated for $C_{20}H_{16}FN_5$: 345.14). Purity measured by UPLC/MS: 98.8%.

1.5.28. Synthesis of "4"-modified 2-(3-fluorophenyl)- quinazolin-4-amines 3a-m

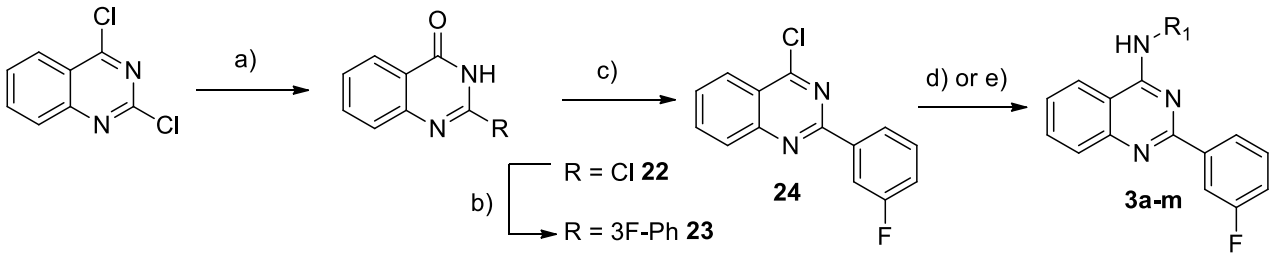

a) NaOH 3.3eq, H_2O, rt, 3hrs, **84%**; b) 3-FIuorobenzeneboronicacid 1.3eq, $Pd(PPh_3)_4$ 0.1eq, 2M Na_2CO_3aq 2eq, dioxane, 105°C, 7hrs; c) $SOCl_2$, DMF, 75°C, 30min, **70%** over two steps; d) NH_2R_1 1.1 eq, TEA 1.5eq, THF, 80°C, 8hrs; e) NH_2R_1 1.1 eq, LiHMDS 2eq, dry THF, RT, 20min.

2-Chloroquinazolin-4(3H)-one 22

2,4-Dichloroquinazoline (600 mg, 3.01 mmoles) was stirred at RT in 2% w/v NaOH (20 mL) till complete dissolution (3 hrs). The colorless solution was filtered to remove traces of insoluble materials, and the filtrate was neutralized by slow addition of AcOH till pH 4. The resulting white precipitate was filtered and dried under vacuum overnight to yield 485 mg of 2-chloroquinazolin-4(3H)-one **22** (2.547 mmoles, **85**% yield).

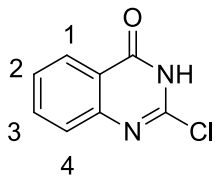

Characterization:

^{1}H NMR (300 MHz, DMSO-d_6) δ (ppm) 13.27 (s, 1H, NH), 8.10 (dd, J = 7.9, 1.1 Hz, 1H, H1), 7.87 – 7.79 (m, 1H, H3), 7.61 (d, J = 8.1 Hz, 1H, H4), 7.58 – 7.49 (m, 1H, H2).

^{13}C NMR (75 MHz, DMSO-d_6): δ (ppm) 162.8, 148.4, 144.3, 135.4, 127.6, 126.9, 126.7, 121.3.

2-(3-Fluorophenyl)quinazolin-4(3H)-one 23

2-Chloroquinazolin-4(3H)-one **22** (200 mg, 1.11 mmoles), 3-fluorobenzeneboronic acid (201.6 mg, 1.44 mmoles) and $Pd(PPh_3)_4$ (128 mg, 0.11 mmoles) were weighed in a microwave vial. The vial was sealed, and a stream of N_2 was bubbled for 5 minutes to remove the air. Then, degassed dioxane (4.4 mL) was added, followed by 2M aqueous Na_2CO_3 (1.1 mL). The yellow mixture was stirred at 105°C for 7 hrs, then cooled at RT. The resulting precipitate was diluted with water (5 mL) filtered, washed with water (10 mL), MeOH (10 mL) and Et_2O (10 mL). Crude 2-(3-fluorophenyl)quinazolin-4(3H)-one **23** (240.2 mg) was used without further purification.

4-Chloro-2-(3-fluorophenyl)quinazoline 24

DMF (0.5 mL) was added dropwise to a suspension of crude 2-(3-fluorophenyl)quinazolin-4(3H)-one **23** (240.2 mg, theor. 1.09 mmoles) in thionyl chloride ($SOCl_2$, 3 mL). The reaction mixture was heated at 75°C and stirred at the same temperature for 30 minutes. Then, the resulting red solution was concentrated under reduced pressure. The orange solid was taken up with DCM (30 mL), washed with sat. $NaHCO_3$ (20 mL) and brine (10 mL). The organic layer was dried over Na_2SO_4, filtered and concentrated under reduced pressure. The crude was purified by flash chromatography (eluant mixture: petroleum ether/AcOEt from 9:1 to 8:2), yielding 200.1 mg of pure 4-chloro-2-(3-fluorophenyl)quinazoline **24** as a white solid (0.777 mmoles, **70%** over two steps).

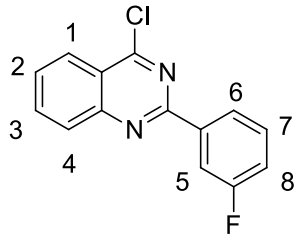

Characterization:

^{1}H NMR (300 MHz, DMSO-d_6) δ (ppm): 8.34 (t, J = 7.9 Hz, 2H, H1, H2), 8.25 – 8.11 (m, 3H, H6, H5, H4), 7.90 (ddd, J = 8.2, 5.5, 2.7 Hz, 1H, H3), 7.66 (td, J = 8.0, 6.0 Hz, 1H, H7), 7.47 (ddd, J = 8.4, 2.7, 1.4 Hz, 1H, H8).

^{13}C NMR (75 MHz, DMSO-d_6): δ (ppm) 164.7, 162.6, 161.5, 151.6, 139.0, 136.6, 131.6, 130.3, 129.1, 126.2, 124.8, 122.4, 118.8, 114.9.

N-(3,5-Dimethoxyphenyl)-2-(3-fluorophenyl)quinazolin-4-amine 3a

The reaction was performed according to **METHOD F**, using 4-chloro-2-(3-fluorophenyl)quinazoline **24** (34.6 mg, 0.133 mmoles), 3,5-dimethoxyaniline (25.3 mg, 0.165 mmoles) and 1M LHMDS in THF (270 µL). Pure N-(3,5-dimethoxyphenyl)-2-(3-fluorophenyl)quinazolin-4-amine trifluoroacetate **3a** (55.3 mg, 0.113 mmoles) was obtained as an off-white solid in **82%** yield.

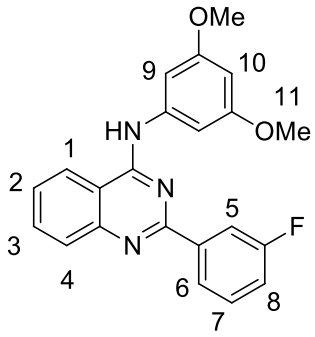

^{1}H NMR (300 MHz, DMSO-d_6): δ (ppm) 10.20 (bs, 1H, NH), 8.64 (d, J = 8.3 Hz, 1H, H1), 8.28 (d, J = 7.8 Hz, 1H, H6), 8.15 (d, J = 9.7 Hz, 1H, H5), 8.05 – 7.87 (m, 2H, H3, H4), 7.71 (ddd, J = 8.2, 5.5, 2.7 Hz, 1H, H2), 7.63 (dd, J = 14.1, 8.0 Hz, 1H, H7), 7.43 (td, J = 8.4, 2.1 Hz, 1H, H8), 7.28 (d, J = 2.1 Hz, 2H, H9), 6.39 (t, J = 2.1 Hz, 1H, H10), 3.82 (s, 6H, H11).

^{13}C NMR (75 MHz, DMSO-d_6): δ (ppm) 164.5, 161.2, 160.8, 158.6, 157.8, 140.8, 134.6, 131.1, 127.4, 126.8, 124.6, 123.8, 118.3, 115.0, 114.3, 101.0, 97.4, 55.7.

UPLC/MS (ESI$^+$): 376.30 [M+H$^+$] (mass calculated for $C_{22}H_{18}FN_3O_2$: 375.14). Purity measured by UPLC/MS: 98.2%.

N^1-(2-(3-Fluorophenyl)quinazolin-4-yl)-N^3,N^3-dimethylbenzene-1,3-diamine 3b

The reaction was performed according to **METHOD F**, using 4-chloro-2-(3-fluorophenyl)quinazoline **24** (42.4 mg, 0.164 mmoles), N^1,N^1-dimethylbenzene-1,3-diamine (24.6 mg, 0.180 mmoles) and 1M LHMDS in THF (330 µL). Pure N^1-(2-(3-fluorophenyl)quinazolin-4-yl)-N^3,N^3-dimethylbenzene-1,3-diamine bis-trifluoroacetate **3b** (75.7 mg, 0.126 mmoles) was obtained as a yellow solid in **77%** yield.

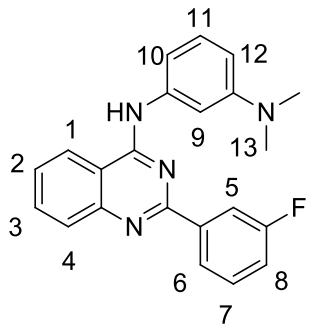

^{1}H NMR (300 MHz, DMSO-d_6): δ (ppm) 10.63 (bs, 1H, NH), 8.69 (d, J = 8.3 Hz, 1H, H1), 8.21 (d, J = 7.9 Hz, 1H, H6), 8.15 – 8.06 (m, 1H, H5), 8.06 – 7.88 (m, 2H, H3, H4), 7.76 (ddd, J = 8.2, 6.3, 1.9 Hz, 1H, H2), 7.65 (td, J = 8.0, 6.1 Hz, 1H, H7), 7.49 (dd, J = 10.6, 4.1 Hz, 2H, H8, H9), 7.35 (t, J = 8.1 Hz, 1H, H11), 7.25 (d, J = 8.1 Hz, 1H, H10), 6.76 (dd, J = 8.1, 1.8 Hz, 1H, H12), 3.01 (s, 6H, H13).

^{13}C NMR (75 MHz, DMSO-d_6): δ (ppm) 164.3, 161.1, 159.0, 157.3, 150.4, 145.6, 139.2, 138.0, 135.3, 131.3, 129.6, 127.9, 124.9, 124.7, 124.2, 119.2, 115.4, 113.9, 113.2, 110.9, 108.7, 41.3.

UPLC/MS (ESI$^+$): 359.34 [M+H$^+$] (mass calculated for $C_{22}H_{19}FN_4$: 358.16). Purity measured by UPLC/MS: 97.6%.

6-((2-(3-Fluorophenyl)quinazolin-4-yl)amino)-1-methylindolin-2-one 3c

Triethylamine (TEA, 0.038 µL, 0.250 mmolse) was added under stirring to a mixture of 4-chloro-2-(3-fluorophenyl)quinazoline **24** (26.8 mg, 0.104 mmoles) and 6-amino-1-methylindolin-2-one (36.9 mg, 0.228 mmoles) in THF (1 mL). The reaction mixture was heated at reflux and stirred for 8 hrs. After solvent concentration under reduced pressure, the crude was taken up with AcOEt (15 mL) and washed with sat. aqueous NH_4Cl (10 mL) and brine (10 mL). The organic layer was dried over anhydrous Na_2SO_4, filtered and concentrated. The crude was purified by reverse phase chromatography (eluant mixture: H_20/MeCN 95:5 to 40:60 + 0.1% TFA). Pure 6-((2-(3-fluorophenyl)quinazolin-4-yl)amino)-1-methylindolin-2-one trifluoroacetate **3c** (20.1 mg, 0.040 mmoles) was obtained as a dark yellow solid in **39%** yield.

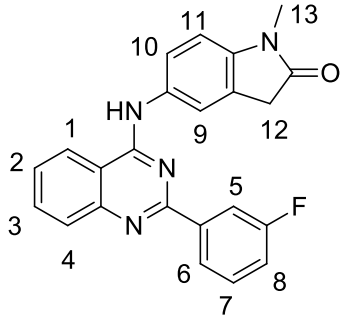

^{1}H NMR (300 MHz, DMSO-d_6): δ (ppm) 10.36 (s, 1H, NH), 8.61 (d, J = 8.3 Hz, 1H, H1), 8.20 (d, J = 7.9 Hz, 1H, H6), 8.08 (d, J = 9.8 Hz, 1H, H5), 7.93 (m, 2H, H3, H4), 7.80 – 7.75 (m, 2H, H9, H11), 7.75 – 7.58 (m, 2H, H7, H2), 7.42 (t, J = 7.2 Hz, 1H, H8), 7.11 (d, J = 8.2 Hz, 1H, H10), 3.67 (s, 2H, H12), 3.19 (s, 3H, H13).

^{13}C NMR (75 MHz, DMSO-d_6): δ (ppm) 174.8, 164.4, 161.3, 158.8, 157.7, 142.7, 134.8, 133.0, 131.3, 127.5, 125.9, 125.3, 124.8, 123.9, 123.2, 120.7, 118.6, 115.1, 114.1, 108.4, 35.9, 26.5.

UPLC/MS (ESI$^+$): 385.29 [M+H$^+$] (mass calculated for $C_{23}H_{17}FN_4O_3$: 384.14). Purity measured by UPLC/MS: 97.8%.

2-(3-Fluorophenyl)-N-(4-nitrophenyl)quinazolin-4-amine 3d

The reaction was performed according to **METHOD F**, using 4-chloro-2-(3-fluorophenyl)quinazoline **24** (32.4 mg, 0.125 mmoles), 4-nitroaniline (19.0 mg, 0.138 mmoles) and 1M LHMDS in THF (250 µL). Pure 2-(3-fluorophenyl)-N-(4-nitrophenyl)quinazolin-4-amine trifluoroacetate **3d** (48.0 mg, 0.100 mmoles) was obtained as a yellow solid in **80%** yield.

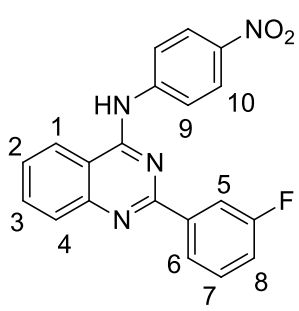

^{1}H NMR (300 MHz, DMSO-d_6): δ (ppm) 10.49 (bs, 1H, NH), 8.64 (d, J = 8.3 Hz, 1H, H1, H1), 8.38 (d, J = 9.3 Hz, 2H, H10), 8.29 (m, 3H, H9, H6), 8.15 (d, J = 9.7 Hz, 1H, H5), 7.97 (d, J = 3.8 Hz, 2H, H3, H4), 7.73 (dt, J = 8.3, 4.2 Hz, 1H, H4), 7.68 – 7.56 (m, 1H, H7), 7.40 (td, J = 8.3, 2.2 Hz, 1H, H8).

^{13}C NMR (75 MHz, DMSO-d_6): δ (ppm) 164.5, 161.3, 158.3, 158.0, 150.4, 146.2, 142.7, 140.5, 134.6, 131.2, 128.3, 127.4, 125.1, 124.6, 123.8, 121.8, 118.1, 114.8, 114.7.

UPLC/MS (ESI$^+$): 361.37 [M+H$^+$] (mass calculated for $C_{20}H_{13}FN_4O_2$: 360.10). Purity measured by UPLC/MS: 98.8%.

N-(4-Fluoro-3-(trifluoromethyl)phenyl)-2-(3-fluorophenyl)quinazolin-4-amine 3e

The reaction was performed according to **METHOD F**, using 4-chloro-2-(3-fluorophenyl)quinazoline **24** (22.8 mg, 0.088 mmoles), 4-fluoro-3-(trifluoromethyl)aniline (17.9 mg, 0.1 mmoles and 1M LHMDS in THF (180 µL). Pure N-(4-fluoro-3-(trifluoromethyl)phenyl)-2-(3-fluorophenyl)quinazolin-4-amine **3e** (37.64 mg, 0.071 mmoles) was obtained as an off-white solid in **81%** yield.

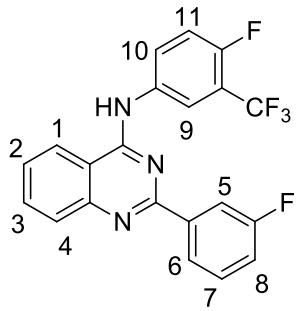

^{1}H NMR (300 MHz, DMSO-d_6): δ (ppm) 10.38 (s, 1H, NH), 8.66 (dd, J = 6.5, 2.6 Hz, 1H, H11), 8.60 (d, J = 8.3 Hz, 1H, H1), 8.26 (d, J = 7.9 Hz, 1H, H6), 8.22 – 8.14 (m, 1H, H10), 8.14 – 8.05 (m, 1H, H5), 8.02 – 7.90 (m, 2H, H3, H4), 7.80 – 7.52 (m, 3H, H2, H7, H9), 7.40 (td, J = 8.2, 2.0 Hz, 1H, H8).

^{13}C NMR (75 MHz, DMSO-d_6): δ (ppm) 164.5, 161.4, 158.5, 157.89, 157.0, 145.6, 140.5, 136.2, 134.5, 131.0, 128.7, 127.9, 127.4, 124.5, 123.6, 121.1, 118.1, 118.0, 114.8, 114.3.

^{19}F NMR (282 MHz, DMSO-d_6) δ: -60.22 (dd, J = 103.9, 12.6 Hz, CF_3), -73.55 – -76.46 (m, TFA), -113.18 (dd, J = 15.8, 9.1 Hz, 1F), -121.81 (s, 1F).

UPLC/MS (ESI$^+$): 402.35 [M+H$^+$] (mass calculated for $C_{21}H_{12}F_5N_3$: 401.10). Purity measured by UPLC/MS: 97.4%.

N-(3-Chloro-4-fluorophenyl)-2-(3-fluorophenyl)quinazolin-4-amine 3f

The reaction was performed according to **METHOD F**, using 4-chloro-2-(3-fluorophenyl)quinazoline **24** (45.8 mg, 0.177 mmoles), 3-chloro-4-fluoroaniline (27.9 mg, 0.194 mmoles) and 1M LHMDS in THF (345 µL). Pure N-(3-chloro-4-fluorophenyl)-2-(3-fluorophenyl)quinazolin-4-amine trifluoroacetate **3f** (68.0 mg, 0.140 mmoles) was obtained as a yellow solid in **79%** yield.

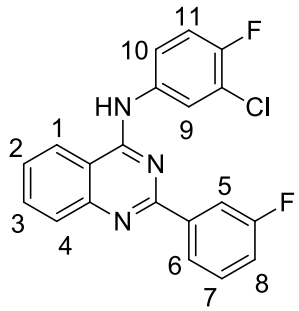

^{1}H NMR (300 MHz, DMSO-d_6): δ (ppm) 10.34 (bs, 1H, NH), 8.58 (d, J = 8.3 Hz, 1H, H1), 8.30 (dd, J = 6.9, 2.5 Hz, 1H, H9), 8.23 (d, J = 7.8 Hz, 1H, H6), 8.09 (d, J = 10.4 Hz, 1H, H5), 8.01 – 7.90 (m, 2H, H3, H4), 7.86 (ddd, J = 8.8, 4.1, 2.8 Hz, 1H, H10), 7.71 (ddd, J = 8.2, 5.5, 2.7 Hz, 1H, H2), 7.58 (m, 2H, H7, H11), 7.41 (td, J = 8.5, 2.2 Hz, 1H, H8).

^{13}C NMR (75 MHz, DMSO-d_6): δ (ppm) 164.5, 161.2, 158.6, 155.9, 152.6, 148.96, 139.9, 136.4, 134.6, 131.2, 127.4, 124.9, 124.5, 123.7, 123.5, 119.7, 118.3, 117.2, 114.8, 114.2.

UPLC/MS (ESI$^+$): 368.30 [M+H$^+$] (mass calculated for $C_{20}H_{12}ClF_2N_3$: 367.07). Purity measured by UPLC/MS: 99.8%.

2-Fluoro-5-((2-(3-fluorophenyl)quinazolin-4-yl)amino)benzonitrile 3g

The reaction was performed according to **METHOD F**, using 4-chloro-2-(3-fluorophenyl)quinazoline **24** (41.9 mg, 0.162 mmoles), 5-amino-2-fluorobenzonitrile (24.5 mg, 0.180 mmoles) and 1M LHMDS in THF (320 µL). Pure 2-fluoro-5-((2-(3-fluorophenyl)quinazolin-4-yl)amino)benzonitrile trifluoroacetate **3g** (64.1 mg, 0.131 mmoles) was obtained as a yellow solid in **81%** yield.

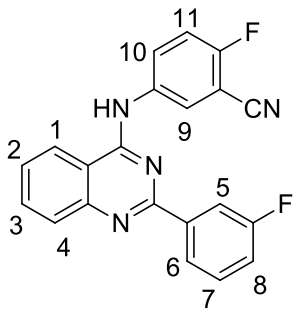

^{1}H NMR (300 MHz, DMSO-d_6): δ (ppm) 10.40 (s, 1H, NH), 8.54 (d, J = 8.3 Hz, 1H, H1), 8.47 (dd, J = 5.8, 2.7 Hz, 1H, H9), 8.27 – 8.16 (m, 2H, H10, H6), 8.05 (ddd, J = 10.6, 2.4, 1.4 Hz, 1H, H5), 8.01 – 7.89 (m, 2H, H3, H4), 7.72 (dt, J = 5.2, 4.6 Hz, 1H, H2), 7.69 – 7.61 (m, 1H, H11), 7.62 – 7.54 (m, 1H, H7), 7.39 (td, J = 8.3, 2.0 Hz, 1H, H8).

^{13}C NMR (75 MHz, DMSO-d_6): δ (ppm) 164.3, 160.8, 159.0, 158.0, 149.3, 140.2, 136.4, 134.6, 131.1, 130.4, 127.6, 127.4, 124.5, 123.6, 118.3, 117.3, 114.9, 114.1, 100.3.

UPLC/MS (ESI$^+$): 359.25 [M+H$^+$] (mass calculated for $C_{21}H_{12}F_2N_4$: 358.10). Purity measured by UPLC/MS: 98.6%.

N-(4-Bromo-3-methylphenyl)-2-(3-fluorophenyl)quinazolin-4-amine 3h

The reaction was performed according to **METHOD F**, using 4-chloro-2-(3-fluorophenyl)quinazoline **24** (21.5 mg, 0.083 mmoles), 4-bromo-3-methylaniline (16.9 mg, 0.091 mmoles) and 1M LHMDS in THF (170 µL). Pure N-(4-bromo-3-methylphenyl)-2-(3-fluorophenyl)quinazolin-4-amine trifluoroacetate **3h** (33.2 mg, 0.063 mmoles) was obtained as a yellow solid in **76%** yield.

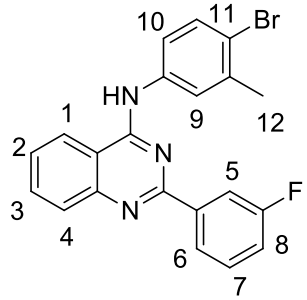

^{1}H NMR (300 MHz, DMSO-d_6): δ (ppm) 10.41 (bs, 1H, NH), 8.61 (d, J = 8.3 Hz, 1H, H1), 8.21 (d, J = 7.9 Hz, 1H, H6), 8.08 (dd, J = 10.1, 1.9 Hz, 1H, H5), 8.02 – 7.88 (m, 3H, H3, H4, H9), 7.83 – 7.66 (m, 3H, H2, H10, H11), 7.62 (m , 1H, H7), 7.43 (td, J = 8.4, 2.2 Hz, 1H, H8), 2.44 (s, 2H, H12).

^{13}C NMR (75 MHz, DMSO-d_6): δ (ppm) 164.3, 161.2, 158.6, 157.6, 147.7, 139.2, 138.4, 137.8, 134.8, 132.5, 131.2, 127.6, 126.4, 125.7, 124.7, 123.8, 122.8, 119.5, 118.5, 115.1, 114.2.

UPLC/MS (ESI$^+$): 408.36 [M+H$^+$] (mass calculated for $C_{21}H_{15}BrFN_3$: 407.04). Purity measured by UPLC/MS: 99.0%.

N-Cyclohexyl-2-(3-fluorophenyl)quinazolin-4-amine 3i

The reaction was performed according to **METHOD F**, using 4-chloro-2-(3-fluorophenyl)quinazoline **24** (34.7 mg, 0.134 mmoles), cyclohexanamine (16 µL, 0.147 mmoles) and 1M LHMDS in THF (135 µL). Pure N-cyclohexyl-2-(3-fluorophenyl)quinazolin-4-amine trifluoroacetate **3i** (50.2 mg, 0.115 mmoles) was obtained as a white solid in **86%** yield.

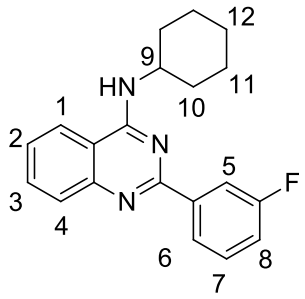

^{1}H NMR (300 MHz, DMSO-d_6): δ (ppm) 9.46 (bs, 1H, NH), 8.55 (d, J = 8.2 Hz, 1H, H1), 8.21 (d, J = 7.9 Hz, 1H, H6), 8.14 (dd, J = 10.0, 2.0 Hz, 1H, H5), 8.05 – 7.89 (m, 2H, H3, H4), 7.73 (ddd, J = 8.3, 7.1, 4.4 Hz, 2H, H4, H7), 7.58 (td, J = 8.5, 2.3 Hz, 1H, H8), 4.60 – 4.34 (m, 1H, H9), 2.04 (d, J = 10.0 Hz, 2H, H10), 1.85 (d, J = 12.1 Hz, 2H, H11), 1.71 (d, J = 12.4 Hz, 1H, H12), 1.65 – 1.35 (m, 4H, H10, H11), 1.25 (t, J = 12.2 Hz, 1H, H12).

^{13}C NMR (75 MHz, DMSO-d_6): δ (ppm) 164.3, 161.0, 159.6, 156.8, 147.6, 142.6, 135.7, 131.6, 128.0, 125.3, 124.5, 122.0, 120.0, 115.7, 113.0, 51.7, 32.0, 25.6, 25.3.

UPLC/MS (ESI$^+$): 322.37 [M+H$^+$] (mass calculated for $C_{20}H_{20}FN_3$: 321.16). Purity measured by UPLC/MS: 99.6%.

Methyl 4-((2-(3-fluorophenyl)quinazolin-4-yl)amino)-2-methoxybenzoate 3j

The reaction was performed according to **METHOD F**, using 4-chloro-2-(3-fluorophenyl)quinazoline **24** (29 mg, 0.112 mmoles), methyl 4-amino-2-methoxybenzoate (22.5 mg, 0.124 mmoles) and 1M LHMDS in THF (220 µL) at 0°C. Pure methyl 4-((2-(3-fluorophenyl)quinazolin-4-yl)amino)-2-methoxybenzoate trifluoroacetate **3j** (33.1 mg, 0.074 mmoles) was obtained as a yellow solid in **66%** yield.

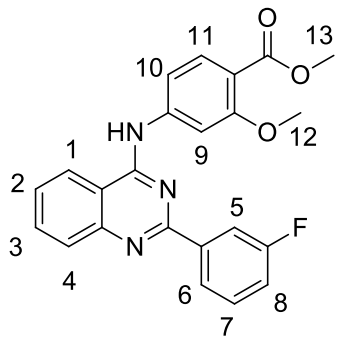

^{1}H NMR (300 MHz, DMSO-d_6): 10.25 (bs, 1H, NH), 8.66 (d, J = 8.4 Hz, 1H, H1), 8.32 (d, J = 7.9 Hz, 1H, H6), 8.19 (d, J = 9.5 Hz, 1H, H5), 8.00 (m, 1H, H9), 7.97 (m, 2H, H3, H4), 7.85 (d, J = 8.6 Hz, 1H, H11), 7.78 – 7.69 (m, 1H H2), 7.69 – 7.58 (m, 2H, H7, H10), 7.41 (td, J = 8.4, 2.4 Hz, 1H, H8), 3.92 (s, 3H, H12), 3.81 (s, 3H, H13).

^{13}C NMR (75 MHz, DMSO-d_6): δ (ppm) 166.0, 164.5, 161.3, 159.7, 158.4, 158.0, 144.7, 134.5, 132.3, 131.3, 128.1, 127.3, 124.5, 123.7, 118.1, 114.8, 114.6, 113.6, 105.9, 56.4, 52.0.

UPLC/MS (ESI$^+$): 404.31 [M+H$^+$] (mass calculated for $C_{23}H_{18}FN_3O_3$: 403.41). Purity measured by UPLC/MS: 97.0%

2-(3-Fluorophenyl)-N-(2-methylisoindolin-5-yl)quinazolin-4-amine 3k.

The reaction was performed according to **METHOD F**, using 4-chloro-2-(3-fluorophenyl)quinazoline **24** (22.5 mg, 0.087 mmoles), 2-methylisoindolin-5-amine (14.2 mg, 0.095 mmoles) and 1M LHMDS in THF (180 µL). Pure 2-(3-fluorophenyl)-N-(2-methylisoindolin-5-yl)quinazolin-4-amine bis-trifluoroacetate **3k** (43.3 mg, 0.072 mmoesl) was obtained as a white solid in **83%** yield.

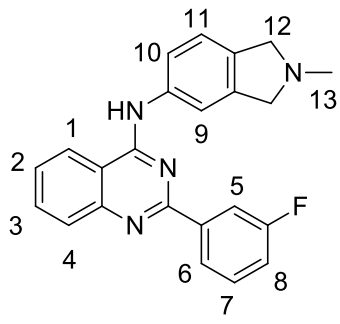

^{1}H NMR (300 MHz, DMSO-d_6): δ (ppm) 10.77 (bs, 1H, NH), 10.22 (s, 1H, NH$^+$), 8.61 (d, J = 8.3 Hz, 1H, H1), 8.26 (d, J = 7.8 Hz, 1H, H6), 8.11 (d, J = 9.6 Hz, 1H, H5), 8.01 (s, 1H, H9), 7.91 (m, 3H, H3, H4, H11), 7.69 (ddd, J = 8.3, 5.0, 3.2 Hz, 1H, H2), 7.64 – 7.49 (m, 2H, H7, H10), 7.39 (td, J = 8.3, 2.2 Hz, 1H, H8), 4.89 (t, J = 14.5 Hz, 2H, H12), 4.54 (t, J = 14.2 Hz, 2H, H12), 3.10 (s, 3H, H13).

^{13}C NMR (75 MHz, DMSO-d_6): δ (ppm) 164.5, 161.3, 158.5, 158.0, 150.0, 140.8, 139.7, 135.4, 134.3, 131.0, 130.5, 128.1, 127.1, 124.5, 123.7, 123.5, 123.4, 117.9, 117.4, 114.8, 114.5, 60.2, 41.0.

UPLC/MS (ESI$^+$): 371.48 [M+H$^+$] (mass calculated for $C_{23}H_{19}FN_4$: 370.16). Purity measured by UPLC/MS: 99.2%

N-(1-Ethyl-1H-indazol-6-yl)-2-(3-fluorophenyl)quinazolin-4-amine 3l

The reaction was performed according to **METHOD F**, using 4-chloro-2-(3-fluorophenyl)quinazoline **24** (23.0 mg, 0.089 mmoles), 1-ethyl-1H-indazol-6-amine (15.9 mg, 0.1 mmoles) and 1M LHMDS in THF (180 µL). Pure N-(1-ethyl-1H-indazol-6-yl)-2-(3-fluorophenyl)quinazolin-4-amine trifluoroacetate **3l** (37.2 mg, 0.075 mmoles) was obtained as a yellow solid in **84%** yield.

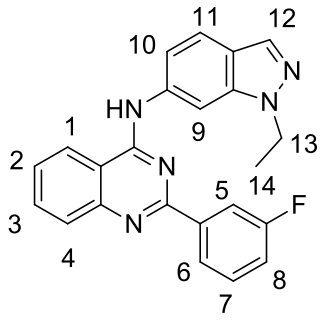

^{1}H NMR (300 MHz, DMSO-d_6): δ (ppm) 10.39 (bs, 1H, NH), 8.71 (d, J = 8.3 Hz, 1H, H1), 8.54 (s, 1H, H12), 8.31 (d, J = 7.8 Hz, 1H, H6), 8.17 (d, J = 9.6 Hz, 1H, H5), 8.07 (s, 1H, H9), 7.97 (m, 2H, H3, H4), 7.84 (d, J = 8.7 Hz, 1H, H10), 7.77 – 7.69 (m, 1H, H2), 7.59 (ddd, J = 11.4, 10.3, 4.8 Hz, 2H, H7, H11), 7.48 – 7.36 (m, 1H, H8), 4.49 (q, J = 7.2 Hz, 2H), 1.49 (t, J = 7.2 Hz, 3H).

^{13}C NMR (75 MHz, DMSO-d_6): δ (ppm) 164.6, 160.9, 159.0, 139.6, 137.7, 134.5, 133.9, 131.2, 127.4, 124.6, 123.8, 123.8, 121.3, 121.1, 118.2, 117.7, 115.0, 114.4, 102.7, 43.9, 15.4.

UPLC/MS (ESI$^+$): 384.45 [M+H$^+$] (mass calculated for $C_{23}H_{18}FN_5$: 383.15). Purity measured by UPLC/MS: 99.8%

2-(3-Fluorophenyl)-N-(4-methylpyridin-2-yl)quinazolin-4-amine 3m

The reaction was performed according to **METHOD F**, using 4-chloro-2-(3-fluorophenyl)quinazoline **24** (21.5 mg, 0.083 mmoles), 4-methylpyridin-2-amine (10.1 mg, 0.097 mmoles) and 1M LHMDS in THF (165 µL). Pure 2-(3-fluorophenyl)-N-(4-methylpyridin-2-yl)quinazolin-4-amine trifluoroacetate **3m** (33.1 mg, 0.074 mmoles) was obtained as an ivory solid in **89%** yield.

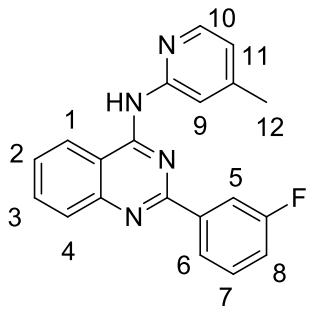

^{1}H NMR (300 MHz, DMSO-d6): δ (ppm) 10.81 (bs, 1H, NH), 8.71 (d, J = 8.2 Hz, 1H, H1), 8.40 (d, J = 5.3 Hz, 1H, H6), 8.29 – 8.27 (m, 2H, H10, H9), 8.14 (d, J = 9.8 Hz, 1H, H5), 7.96 (m, 2H, H3, H4), 7.75 – 7.57 (m, 2H, H2, H7), 7.43 (td, J = 8.3, 2.1 Hz, 1H, H8), 7.19 (d, J = 4.9 Hz, 1H, H11), 3.18 (s, 3H, H12).

^{13}C NRM (75 MHz, DMSO-d_6): δ (ppm) 164.5, 161.3, 158.4, 134.7, 131.3, 131.2, 127.6, 124.5, 124.2, 121.3, 118.0, 115.1, 114.8, 21.6.

UPLC/MS (ESI$^+$): 331.08 [M+H$^+$] (mass calculated for $C_{20}H_{15}FN_4$: 330.13). Purity measured by UPLC/MS: 99.6%.

1.6 BIBLIOGRAPHY

[1]. Alberts, B. Molecular Biology of the Cell. 6th Edition. New York, **2015**.

[2]. Huotari, J.; Helenius, A. Endosome maturation. *EMBO Journal* **2011**, 30, 3481–3500.

[3]. Jovic, M. *et al*. The early endosome: A busy sorting station for proteins at the crossroads. *Histol.Histopathol.* **2010**, 25, 99–112.

[4]. Arighi, C.N. *et al*. Role of the mammalian retromer in sorting of the cation-independent mannose 6-phosphate receptor. *J. Cell Biol*. **2004**, 165, 123–133.

[5]. Stenmark, H.; Olkkonen, V.M. The Rab GTPase family. *Gen. Biol.* **2001**, 2, REVIEWS3007.

[6]. Rojas, R. *et al*. Regulation of retromer recruitment to endosomes by sequential action of Rab5 and Rab7. *J. Cell Biol*. **2008**, 183, 513–526.

[7]. Schreji, A.M.; Fon, E.A.; Mc Pherson, P.S. Endocytic membrane trafficking and neurodegenerative disease. *Cell. Mol. Life Sci.* **2016**, 73, 1529-1545.

[8]. Lucas, M.; Hierro, A. Retromer. *Curr. Biol*. **2017**, 27, R687–R689.

[9]. Hierro, A. *et al*. Functional architecture of the retromer cargo-recognition complex. *Nature* **2007**, 449, 1063–1067.

[10]. Rojas, R. *et al*. Interchangeable but essential functions of SNX1 and SNX2 in the association of retromer with endosomes and the trafficking of mannose 6-phosphate receptors. *Mol. Cell. Biol.* **2007**, 27, 1112–1124.

[11]. Harterink, M. *et al*. A SNX3-dependent retromer pathway mediates retrograde transport of the Wnt sorting receptor Wntless and is required for Wnt secretion. *Nat. Cell Biol.* **2011**, 13, 914-923.

[12]. Wassmer, T. *et al*. A loss-of-function screen reveals SNX5 and SNX6 as potential components of the mammalian retromer. *J. Cell Sci*. **2006**, 120, 45–54.

[13]. Temkin, P. *et al*. SNX27 mediates retromer tubule entry and endosome-to-plasma membrane trafficking of signalling receptors. *Nat. Cell Biol.* **2011**, 13, 715–723.

[14]. Mari, M. *et al*. SNX1 defines an early endosomal recycling exit for sortilin and mannose 6 phosphate receptors. *Traffic* **2008**, 9, 380–393.

[15]. Steinberg, F. *et al*. A global analysis of SNX27-retromer assembly and cargo specificity reveals a function in glucose and metal ion transport. *Nat Cell. Biol.* **2003**, 15, 461–471.

[16]. Klinger, S.C.; Siupka, P.; Nielsen, M.S. Retromer-mediated trafficking of transmembrane receptors and transporters. *Membranes* **2015**, 5, 288–306.

[17]. Seaman, M.N.J. Identification of a novel conserved sorting motif required for retromer mediated endosome-to-TGN retrieval. *J. Cell Sci*. **2007**, 120, 2378–2389.

[18]. Lucas, M. *et al*. Structural mechanism for cargo recognition by the retromer complex. *Cell* **2016**, 167, 1623–1635.

[19]. Strochlic, T.I. *et al*. Grd19/Snx3p functions as a cargo-specific adapter for retromer-dependent endocytic recycling. *J. Cell Biol*. **2007**, 177, 115–125.

[20]. Small, S.A. *et al*. Model-guided microarray implicates the retromer complex in Alzheimer's disease. *Ann. Neurol.* **2005**, 58, 909–919.

[21]. Vardarajan, B.N. *et al*. Identification of Alzheimer disease-associated variants in genes that regulate retromer function. *Neurobiol. Aging* **2012**, 33, 2231.e15-2231.e30.

[22]. Liang, X. *et al*. Genomic convergence to identify candidate genes for Alzheimer disease on chromosome 10. *Human Mutation* **2009**, 30, 463–471.

[23]. Wen, Y. *et al*. SORL1 is genetically associated with neuropathologically characterized late-onset Alzheimer's disease. *J. Alzheimer's Dis.* **2013**, 35, 387–394.

[24]. Reitz, C. The role of the retromer complex in aging-related neurodegeneration: a molecular and genomic review. *Mol. Gen. Rev.* **2015**, 290, 413–427.

[25]. Follett, J. *et al*. The Vps35 D620N mutation linked to Parkinson's Disease disrupts the cargo sorting function of retromer. *Traffic* **2014**, 15, 230–244.

[26]. Zavodszky, E. *et al*. Mutation in VPS35 associated with Parkinson's disease impairs WASH complex association and inhibits autophagy. *Nat. Comm.* **2014**, 5, 3828.

[27]. MacLeod, D.A. *et al*. RAB7L1 Interacts with LRRK2 to modify intraneuronal protein sorting and Parkinson's disease risk. *Neuron* **2013**, 77, 425–439.
[28]. Bhalla, A. *et al*. The location and trafficking routes of the neuronal retromer and its role in amyloid precursor protein transport. *Neurobiol. Dis.* **2012**, 47, 126–134.
[29]. Norwood, S.J. *et al*. Assembly and solution structure of the core retromer protein complex. *Traffic* **2011**, 12, 56–71.
[30]. Ringe, D.; Petsko, G.A. What are pharmacological chaperones and why are they interesting? *J. Biol.* **2009**, 8, 80.1-80.4.
[31]. Mecozzi, V.J. *et al*. Pharmacological chaperones stabilize retromer to limit APP processing. *Nat. Chem. Biol.* **2014**, 10, 443–449.
[32]. Lieberman, R.L. *et al*. Structure of acid β-glucosidase with pharmacological chaperone provides insight into Gaucher disease. *Nat. Chem Biol.* **2007**, 3, 101–107.
[33]. Mucke, L. *et al*. High-level neuronal expression of Aβ 1–42 in wild-type human amyloid protein precursor transgenic mice: synaptotoxicity without plaque formation. *J. Neurosci.* **2000**, 20, 4050–4058.
[34]. Holmes, B.; Brogden, R.N.; Heel, R.C.; Speight, T.M.; Avery, G.S. Guanabenz. A review of its pharmacodynamic properties and therapeutic efficacy in hypertension. *Drugs* **1983**, 26, 212-229.
[35]. Das, I. *et al*. A. Preventing proteostasis diseases by selective inhibition of a phosphatase regulatory subunit. *Science* **2015**, 348, 239–242.
[36]. Rester, U. From virtuality to reality - Virtual screening in lead discovery and lead optimization: a medicinal chemistry perspective. *Curr. Opin. Drug Disc. Dev*. **2008**, 11, 559–568.
[37]. https://www.hit2lead.com/. Hit2Lead, ChemBridge Corporation, San Diego, US.
[38]. Tal, D.M.; Karlish, S.J.D. Synthesis of a novel series of arylmethylisothiouronium derivatives. *Tetrahedron* **1995**, 51, 3823-3830.

Chapter II

Sephin1-ISRIB hybrids as neuroprotective modulators of protein synthesis

INDEX

2.1. INTRODUCTION

2.1.1 The unfolded protein response (UPR): an endoplasmic reticulum-driven protein homeostasis mechanism

Despite the fact that in most neurodegenerative diseases (NDDs) any misfolded protein is located in the cytosol or nucleus, paradoxically one main consequence is interference with processes in the endoplasmic reticulum (ER), causing ER stress. This mechanism induces an adaptive response known as the unfolded protein response (UPR), with induction of ER chaperone expression and transient arrest in protein translation.

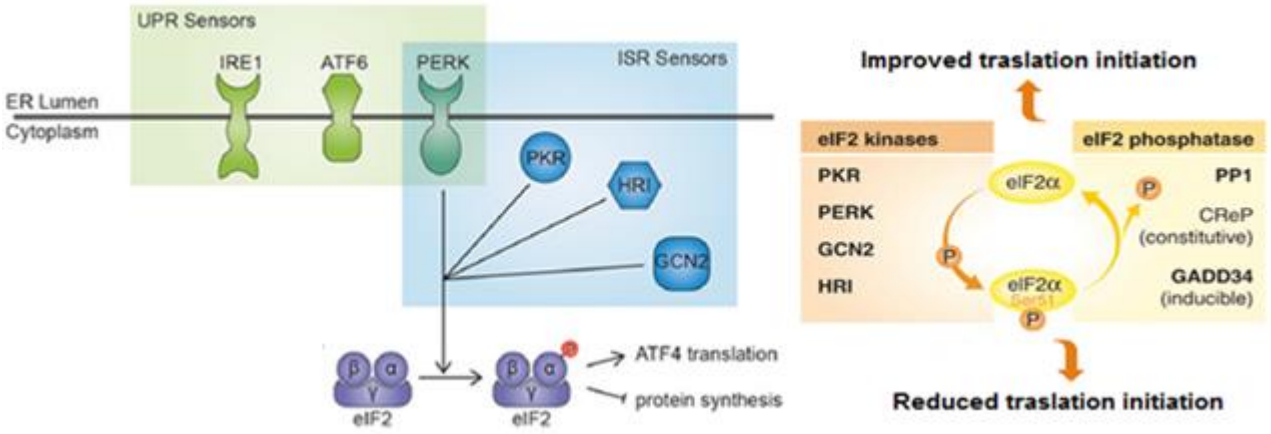

Figure 1. PERK-dependent UPR and ISR pathways. Left: attenuation in protein synthesis in the presence of mis-folded proteins mediated by UPR. Right: Phosphorylation of eukaryotic translation initiation factor 2 alpha (eIF2α) mediated by the integrated stress response (ISR).

The UPR (Figure 1, left) consists of three transmembrane ER proteins: protein kinase RNA (PKR)-like ER kinase (PERK) [1], inositol-requiring enzyme 1 (IRE1) [2] and activation transcription factor 6 (ATF6) [3]. In resting conditions, all three proteins form a complex with the chaperone GRP78/BiP [4]. When mis-folded proteins accumulate in the ER, BiP dissociates and binds to these misfolded proteins. Dissociation of BiP activates PERK, IRE1 and ATF6 [4]. Activation of PERK results in both attenuation of global protein synthesis and de-repression of activating transcription factor 4 (ATF4) mRNA translation via phosphorylation of Ser51 on the α-subunit of eIF2 (Figure 1, left). eIf2 (eukaryotic translation initiation factor 2) is a heterotrimer consisting of an alpha, a beta and a gamma subunit; it is an essential factor for protein synthesis that forms a ternary complex (TC) with GTP (guanosine-5'-triphosphate), a nucleoside triphosphate needed for RNA synthesis during the transcription process, and with the initiator Met-tRNA$_i^{Met}$. eIF2 is a crucial factor to make proteins in cells; and a decrease in its activity has been linked with memory loss in diseases such as Parkinson's and Alzheimer's disease [5, 6].

In addition to PERK, eIF2α-Ser51 phosphorylation is performed by three kinases: protein kinase double-stranded RNA-dependent (PKR) in response to viral infection, general control non-derepressible-2 (GCN2) in response to amino acid starvation, and heme-regulated inhibitor (HRI) in response to heme deficiency, oxidative stress, heat shock, or osmotic shock [7]. These various stress-induced signaling pathways that converge on eIF2α-P are collectively known as the integrated stress response (ISR) (right, Figure 1). The development of ER stress and induction of the UPR has been reported in different pathologies [8].

During protein mis-folding and aggregation, cytotoxicity is mostly reconducible to the soluble-pre-fibrillar stage. Large aggregates of amyloid fibrils are a last resort towards neuroprotection. Therefore, attempts to inhibit their formation is likely cell-damaging. Neurotoxic oligomeric species sequester many proteins affecting multiple cellular pathways. UPR modulation reduces significantly the toxicity in several protein mis-folding diseases, where ER stress is a causative factor. Novel drugs capable of reducing ER stress by modulating the UPR hold therapeutic promise against NDDs [9].

2.1.2 PERK-eIF2α and GADD34: a putative pathway and molecular target against NDDs

Upon dissociation of BiP, PERK dimerises, auto phosphorylates and phosphorylates the α-subunit of eukaryotic initiating factor 2 (eIF2α – Figure 2). Phosphorylating eIF2α disrupts the formation of the methionine-bearing ternary complex needed to initiate protein synthesis, thereby blocking the initiation of translation [10]. This translational repression halts protein synthesis to reduce the entrance of newly synthesised proteins into the ER and to relieve the protein load.

Activating transcription factor 4 (ATF4), a cAMP response element binding (CREB) transcription factor that regulates apoptosis, autophagy, aminoacid metabolism and antioxidant responses [11], escapes eIF2α-induced translational repression. Growth arrest and DNA-damage inducible protein (GADD34), the inducible eIF2α-P-specific phosphatase subunit of protein phosphatase 1 (PP1), is a target of ATF4. Stress-induced GADD34 promotes eIF2α dephosphorylation (Figure 2), removing the inhibition on the eIF2B methionine-bearing ternary complex, and allowing initiation of translation to be restored [12]. As such, GADD34 expression acts as a valuable negative feedback loop to protect the cell from sustained translational repression.

The UPR in general and the PERK branch in particular, must be at the right balance point to protect cells. Too high and prolonged eIF2α phosphorylation leads to depletion of essential short-lived proteins, and up-regulates translation of ATF4 leading to expression of downstream pro-apoptotic factors, such as CHOP. Conversely, too low levels of eIF2α phosphorylation lead to a continued protein load that does not alleviate ER stress. A mutation in CREP, the constitutive regulatory subunit of the PP1 complex that dephosphorylates eIF2αP, leads to diabetes and intellectual disability [13]. Lack of PERK activity through a PERK mutation in Wolcott-Rallison syndrome results in early-onset diabetes, epiphyseal dysplasias and neurodegeneration [14, 15]. Each cell type has its appropriate level of eIF2α phosphorylation. Striatal neurons have a very low level compared to other brain regions, which is increased upon expression of mutant Htt in cellular and mouse HD models [16]. Striatal neurons are the most sensitive in HD. Thus, both long-term inhibition of protein synthesis by phosphorylation of eIF2α (PERK branch activation) or prevention of eIF2α phosphorylation and consequent absence of transient translation inhibition (PERK branch inactivation) can be cytotoxic.

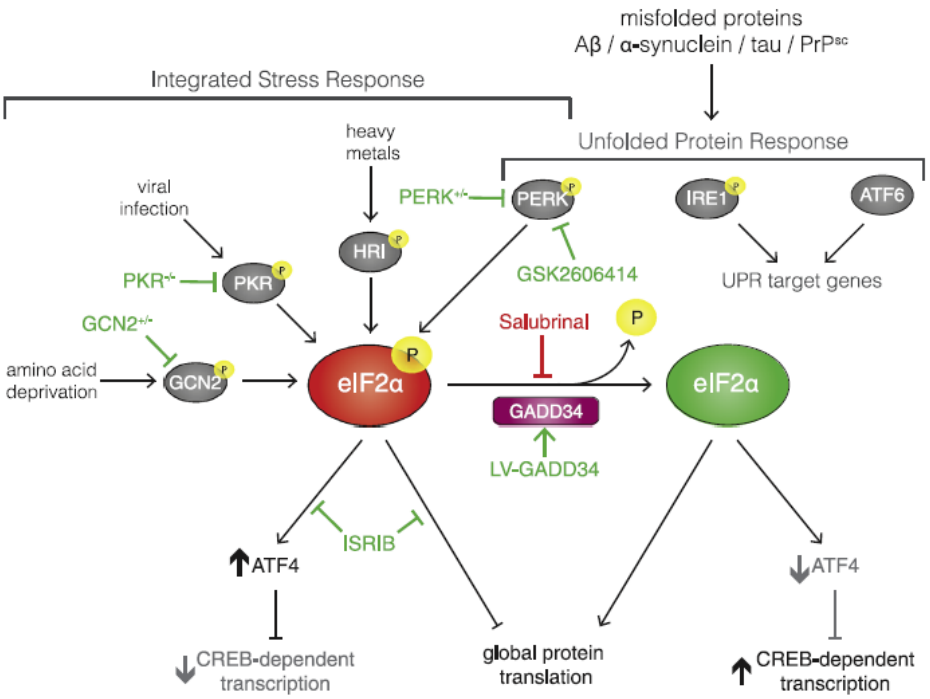

Figure 2. The PERK pathway: key phosphorylation of eIF2α.

Elevated amounts of UPR markers were shown in several protein mis-folding diseases and NDDs in particular [17]. This includes samples from post-mortem AD patients (increased amounts of BiP, activated IRE1, PERK and phosphorylated eIF2α) [18, 19], PD patients (increased amounts of PERK and phosphorylated eIF2α) [20]; and HD patients (increased amounts of BiP, CHOP and Herp) [21]. In animal models, UPR induction was observed in the brains of transgenic mice mimicking tau pathology- related AD [22], HD [23], ALS [24], PD [25], and prion disease [26]; that would point to inhibition of UPR/PERK/eIF2α phosphorylation for therapeutic purposes. Conversely, PERK-eIF2α signalling is neuroprotective in mutant SOD1 models in mice [27, 28] and in models of peripheral CMT1b neuropathy [28, 29]; that would point to stimulation of UPR/PERK/eIF2α phosphorylation for therapeutic purposes.

Involvement of the UPR/PERK branch is therefore common to many age-associated NDDs. It can be difficult to tease apart whether its activation is inherently cytoprotective or neurodegenerative – or both, at different disease stages, or through activation of different UPR branches. Activation or inhibition of one, or more UPR branches can have either beneficial or detrimental effects in different NDD models – or sometimes even in the same disease model at different progression stages. The roles of the UPR in NDD onset and progression, and the use of UPR modulation to treat age-associated neurodegeneration, are both highly important and a source of significant controversy [30].

2.1.3 Salubrinal, guanabenz and sephin 1: small molecule inhibitors of eIF2α dephosphorylation with neuroprotective properties

An HTS campaign on a ≈19,000 compound collection aimed towards compounds protecting the rat pheochromocytoma cell line PC12 from ER stress-induced apoptosis led, after hit reconfirmation and profiling, to the identification of a CCl_3-substituted asymmetric thiourea named salubrinal (**1**, Figure 3, left) [31].

Salubrinal inhibited ER stress-mediated apoptosis induced by the protein glycosylation inhibitor tunicamycin with an effective concentration (EC_{50}) of ≈15μM (Figure 3, middle), It reduced the processing of procaspase-7 (CT) to ER stress-activated caspase 7 (arrow, Figure 3, right), but it did not affect ER-unrelated apoptosis.

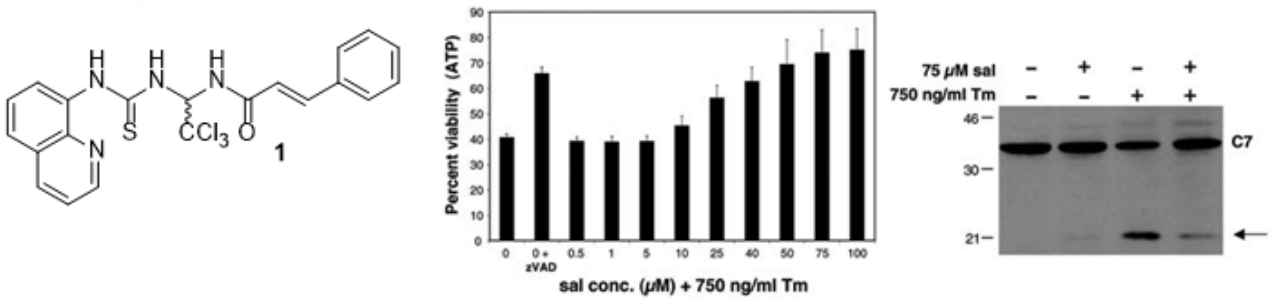

Figure 3. Chemical structure of salubrinal (**1**). Salubrinal: Inhibition of ER stress-activated apoptosis *in vitro*.

Salubrinal did not affect UPR through the IRE1 and ATF6 pathways. Conversely, it induced rapid and robust eIF2α phosphorylation without altering total eIF2α levels; Salubrinal acts indirectly, as it does not inhibit either PERK, or other known eIF2α kinases. Rather, salubrinal inhibited eIF2α dephosphorylation mediated by both constitutive/CREP and ER stress-induced/GADD34 phosphatase complexes namely. Salubrinal may induce eIF2α phosphorylation by binding and inhibiting directly the two eIF2α phosphatase complexes, or *via* other indirect mechanisms [32]. By inducing eIF2α phosphorylation in non-stressed cells, salubrinal might have undesirable effects because uncontrolled translation inhibition is deleterious. Moreover, salubrinal inhibited IκB kinase (IKK) complex phosphorylation and the subsequent NF-κB activation without affecting eIF2α phosphorylation [33]; it reduced the levels of phosphorylated IKK, NF-κB p65 and p38, without changing the level of phosphorylated eIF2α in chondrocytes treated with cytokines [34]; and protected Bcl-2 from inactivation caused by porphycene-induced photodamage in murine leukemia L1210 cells [35].

Salubrinal showed beneficial effects in a number of *in vivo* models related to neurodegeneration. They include PD [36], ALS [37, 38], Charcot-Marie-Tooth disease [29] and spinal cord injury [39]. Conversely, salubrinal showed detrimental in vivo effects in models of prion disease [26] and cognition [40].

The non-selective α2-adrenergic receptor antagonist guanabenz (**2/GA**, Figure 4, top left) [41] was identified as a hit capable of inhibiting the accumulation of two yeast prion proteins and of ovine Scrapie prion protein (Prp^{Sc}) in a dose-dependent manner, without affecting the non-pathological Prp^{C} species.

Guanabenz was later found to protect cells from ER-induced stress, acting selectively on the PERK pathway and attenuating tunicamycin-induced expression of several ER stress markers in a time-dependent manner (in particular CHOP, Figure 4, middle) [42]. Guanabenz inhibited eIF2α dephosphorylation by disrupting selectively the inducible PP1-GADD34/PPP1R15A phosphatase complex, while the constitutive PP1-CREB/PPP1R15B complex remained intact and active (right). Biotinylated guanabenz was used in a pull-down experiment, showing GADD34 to bind to bead-bound, while CREB was not extracted from cell lysates (Figure 4, bottom left) [42].

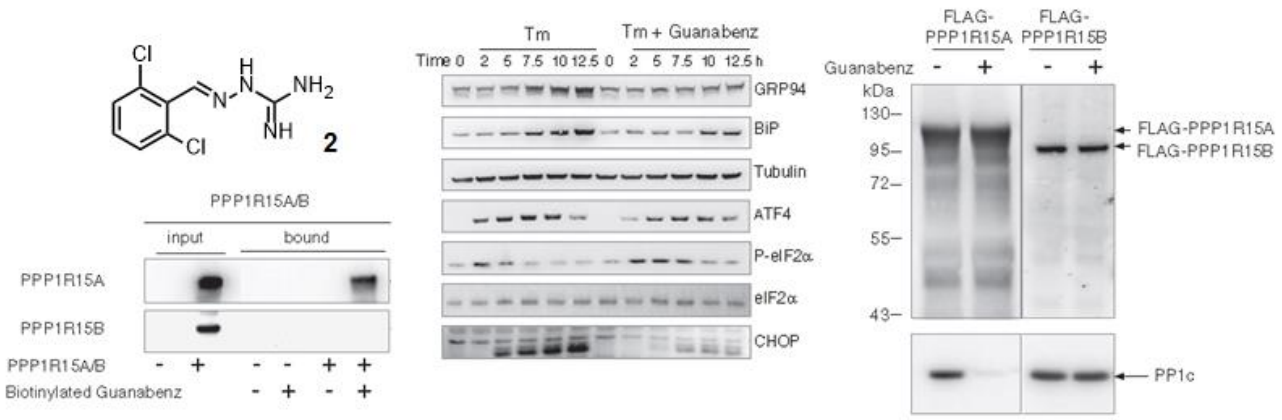

Figure 4. Guanabenz (**2**, GA): inhibition of inducible PP1-GADD34 dephosphorylation of eIF2α by binding with GADD34.

Guanabenz was tested and resulted to be protective in a few models related to mis-folding diseases and neurodegeneration. They include oculopharingeal muscular dystrophy [43], Bardet-Biedl syndrome [44], multiple sclerosis [45], and ALS [27, 38, 46]. A single report claimed neurotoxic in vivo effects for guanabenz in an ALS model [47], attributing study discrepancies to various experimental settings and to treatment of mutant mice at various disease progression times.

A study evaluating both salubrinal and guanabenz in models of TDP-43 induced neurotoxicity/ALS [38] showed stronger potency for the former compound, possibly due both to PERK/eIF2α-independent effects and to the inactivation of both inducible and constitutive phosphatase complexes. Although guanabenz should ensure more specificity and safety for in vivo testing, its adrenergic antagonist activity should cause side effects should cause drowsiness and coma, at high doses [48].

Later, mono-chlorinated guanabenz analogue **3** (Figure 5, top left) was presented as a potent inhibitor of inducible PP1-GADD34/PPP1R15A phosphatase complex and was named SElective holoPHosphatase Inhibitor 1 (**sephin1**) [28]. Its characterization confirmed its attenuating effects on tunicamycin-induced expression of several ER stress markers in a time-dependent manner (in particular CHOP, Figure 5, middle); its selective binding/sequestration of PP1-GADD34/PPP1R15A from cell lysates treated with its biotinylated analogue (bottom left); and its inability to antagonize any human α2-adrenergic receptor conversely to GA (Figure 5, right) [28].

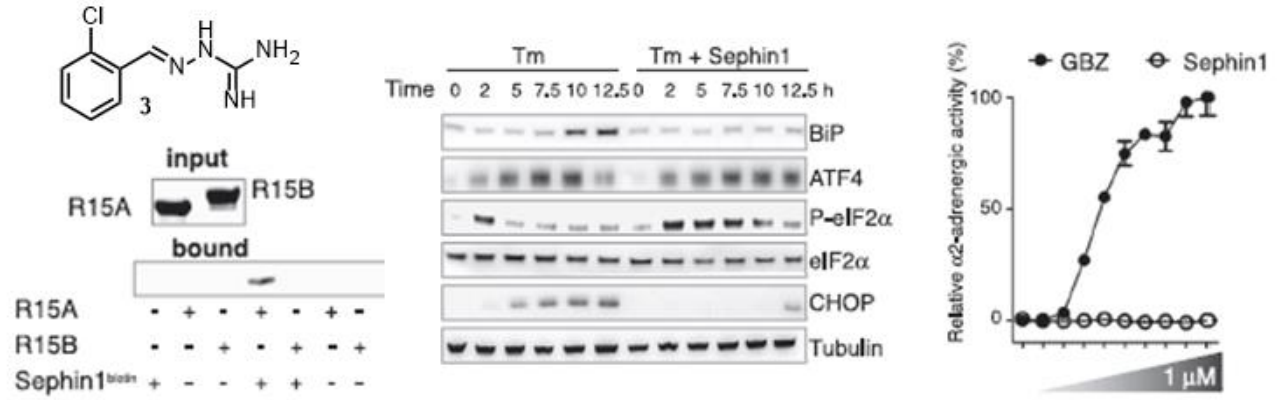

Figure 5. Sephin1: a selective inhibitor of PP1-GADD34/PPP1R15A phosphatase activity devoid of antagonism against human α2-adrenergic receptors.

Both guanabenz (100 μg/Kg dosage, IV) [28] and sephin1, administered orally at 1 or 10 mg/kg cross the blood-brain barrier (BBB) and show accumulation in the brain. In particular, sephin1 rapidly disappeared from plasma but concentrated in the nervous system, reaching concentrations 7 to 44 times higher in the brain and sciatic nerve (up to ≈1 μM) than in plasma.

Avoidance of human α2-adrenergic receptor antagonism should provide a cleaner in vivo activity profile for sephin1 in vivo. Sephin1 shows efficacy in two animal models of NDDs. Motor performance (Figure 5, top left) and biochemical evidence (myelin thickness, top right) were close to wild-type (WT) levels after 3 (top left) to 5 months (top right) of oral treatment at 1 mg/Kg in a mouse model of Charcot-Marie Tooth 1B (CMT1B) disease, a demyelinating neuropathy [29].

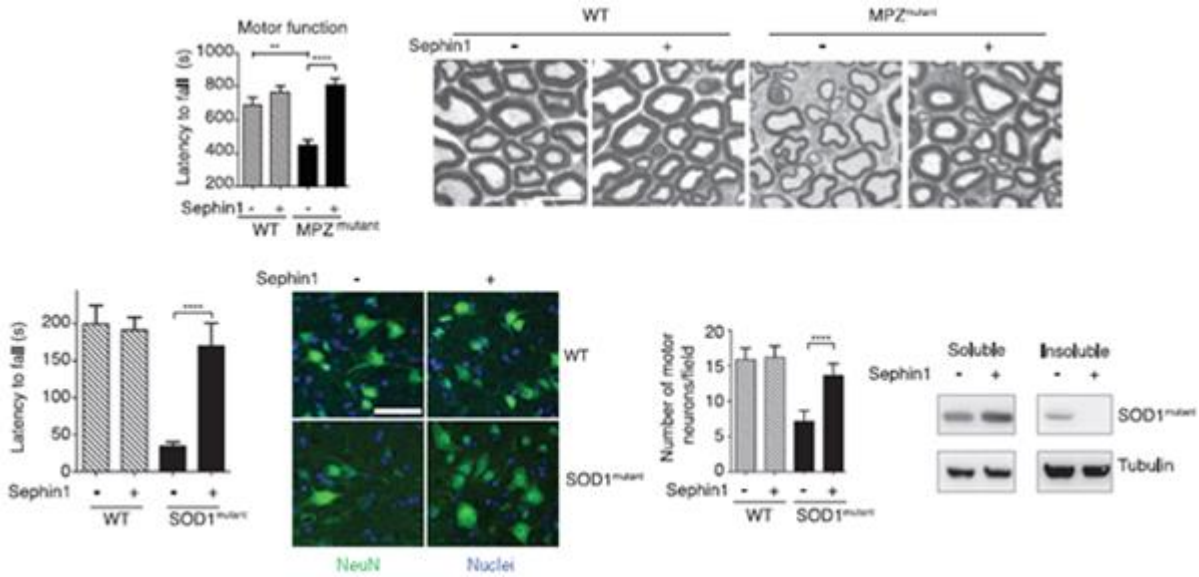

Figure 5. Sephin1: in vivo efficacy in models of CMT1B (top) and ALS (bottom).

Sephin1 also largely rescued motor performance deficits in superoxide dismutase 1 (SOD1) mutant mice in an ALS model (Figure 5, bottom left). It protected the animals from motor neuron loss (bottom centre, image and tabulated results), and reduced the insoluble fraction/protein aggregates composed by mutant SOD1 in spinal cord extracts (Figure 5, bottom right) [28].

2.1.4 EIF2B: a decameric protein complex involved in the progression of NDDs

The integrated stress response (ISR) has homeostatic functions that increase fitness. However, in some pathological circumstances, therapeutic benefit arises from attenuated signaling in the ISR [49]. Over-activation of the UPR has emerged as a major pathogenic mechanism involved in neurodegenerative diseases [50, 51].

High levels of activated PERK (PERK-P) and its downstream target, the phosphorylated alpha subunit of eukaryotic initiation factor 2 (eIF2α) are observed in brains of Alzheimer's and Parkinson's patients, in progressive supranuclear palsy and frontotemporal dementia (FTD) and in the rare prion disorders [20, 18, 52]. In these disorders, PERK-P and eIF2α-P accumulation are temporally and spatially associated with the deposition of disease specific misfolded proteins [52, 53].

In the brain, eIF2α represents a critical point for controlling rates of protein synthesis essential for learning and memory formation and for maintaining neuronal integrity in health and disease. Sustained over-activation of PERK/eIF2-P signalling causes chronic translational attenuation leading to synapse loss and neurodegeneration in prion-diseased and FTD mice [26, 54]. The synthesis of proteins in fact is an essential step in many biological processes, including memory, and drugs that inhibit protein synthesis are known to impair memory in rodents. It is believed that the brain needs these proteins to convert short-term memories into long-term memories through a process known as consolidation.

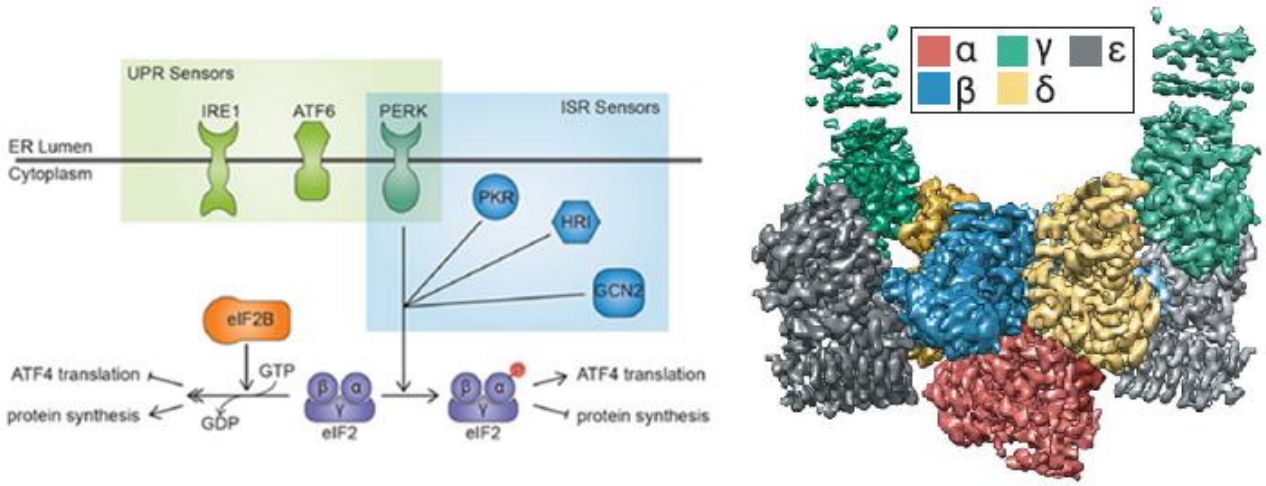

Figure 6. The dimeric/decameric structure of the eIF2B complex.

The eukaryotic translation initiation factor 2B (eIF2B) (Figure 6, right for a 3D model) is a hetero-decameric complex of two symmetrical sets of subunits a, b, c, d, and e. eIF2B act as the guanine nucleotide exchange factor for the eukaryotic initiation factor 2, and therefore converts its inactive eIF2-GDP form to the active eIF2-GTP (Figure 6, left). Phosphorylation of the alpha subunit of eIF2, leads to a stable eIF2α-P-GDP-eIF2B complex, that inhibits translation initiation [55, 56].

A 3D model of the eIF2α-P-GDP-eIF2B complex, and a cartoon depicting the different roles and conformations of the eIF2α-P-GDP-eIF2B complex are shown in Figure 7 (respectively left and right).

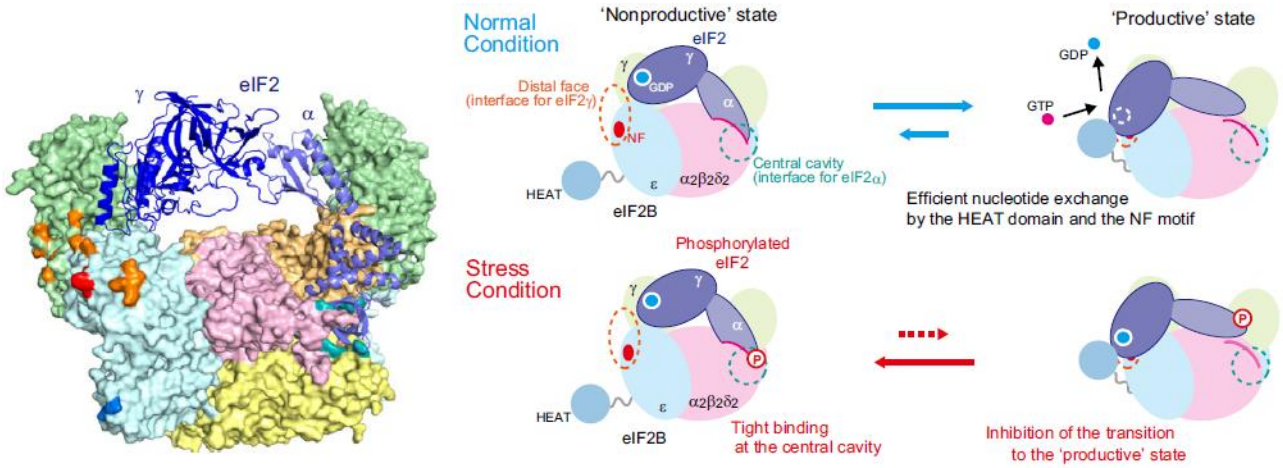

Figure 7. Left: Docking of eIF2 and eIF2B. Right: Schematic representation of the proposed mechanism of the stress-induced inhibition of the eIF2B nucleotide exchange activity [56].

2.1.5 ISRIB: Integrated Stress Response InhiBitor / stabilizer of eIF2B with neuroprotective properties

In 2013, a novel class of *trans*-symmetric bis-glycolamides able to restore protein synthesis during eIF2α phosphorylation, was identified [57]. The namesake, most potent compound **4** was named ISRIB (for Integrated Stress Response InhiBitor), and is reported in Figure 8, left.

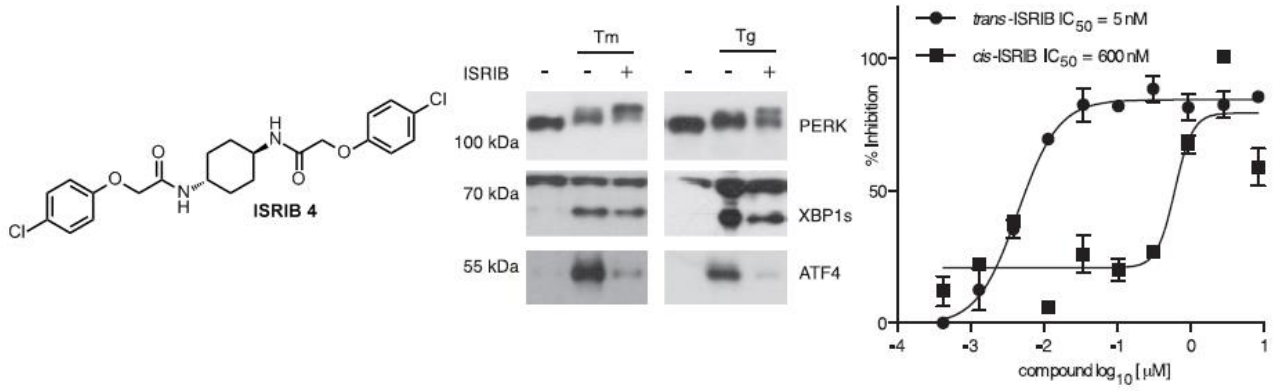

Figure 8. Structure and biological activity of ISRIB **4**.

In presence of thapsigargin or tunicamycin (ER STRESS inducers), ISRIB was able to block the production of endogenous ATF4 (Figure 8, middle), inhibiting the ATF4-luciferase reporter at low nM (IC_{50} = 5 nM; IC_{50cis} = 600 nM) (Figure 8, right). Interestingly, this compound was shown to act downstream of eIF2α phosphorylation, i.e. as an effective antagonist of the ISR pathway.

Using genetic, biochemical, and biophysical approaches, two groups [58, 59] independently identified the molecular target of ISRIB as eIF2B. In particular ISRIB was found able to stabilize the activated dimeric form of eIF2B [59].

In 2018, using a recombinant expression and purification protocol for all subunits of human eIF2B, cryo-electron microscopy (cryo-EM) and mutagenesis of different amino-acid residues, two groups [60, 61] identified a putative binding site for ISRIB at the interface between the b and d regulatory subunits of eIF2B (Figure 9).

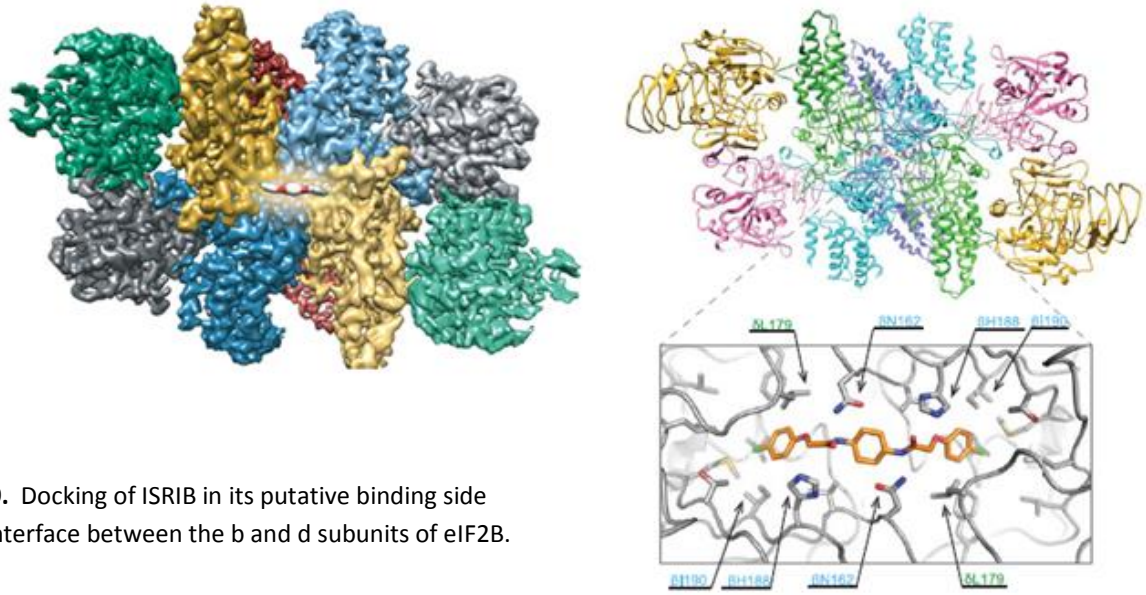

Figure 9. Docking of ISRIB in its putative binding side at the interface between the b and d subunits of eIF2B.

ISRIB is BBB-permeable, and shows efficacy against AD [62] and traumatic brain injury models [63]. Unfortunately, it is highly insoluble and unsuitable for use in humans as such.

2.1.6 ISRIB-sephin1 dual action compounds (DACs): putative disease modifiers against a variety of NDDs

The drug market as of today is dominated by small molecules. When dealing with complex diseases, inhibition of a molecular target may lead to a bypass of the target itself by the diseased cells-organs, and to resistance (e.g., penicillins and resistance to beta-lactamases [64]). Thus, there is an increasing need for multi-targeted therapies [65]. Multi-targeting may be achieved by administering a cocktail of active ingredients, and cocktails active against HIV are an example of clinical success [66]. However, effective drug combinations may require different administration routes, or different residence times in the human body [67]. Well tolerated drugs may become harmful in combination with other active principles, due to drug-drug interactions [68].

Typically, hybrid molecules or **dual action compounds** (DACs) contains the chemical functions required to interact with two molecular targets [69]. A connection is chosen for each pharmacophore unit, and a suitable spacer separates the two units without disturbing their biological activities. While cancer [70] and infectious diseases [71] are the areas where DACs are more popular and exploited, examples related to neurodegeneration have also been reported [72].

Disease-modifying agents against NDDs are not easily attainable, due either to the complexity of described patho-physiological mechanisms involved in neurodegeneration and PQC (Protein Quality Control), to the lack of fully validated therapeutic targets, and to their site of action – the brain, requiring BBB crossing. The similarities between the dimeric structure of ISRIB, and the monomeric structure of sephin1 (both reported in Figure 10, left) allowed us to design sephin1-ISRIB hybrid constructs. By acting on the same therapeutic areas in two different, and possibly opposite ways (ISRIB should promote protein synthesis through eIF2B stabilization, while sephin1 should decrease protein synthesis by increasing the phosphorylation of eIF2α), these hybrids could be useful in NDDs where to control the rate and the quality of protein synthesis is crucial.

A reported preliminary SAR on the ISRIB scaffold [73] showed the possibility to add or modify groups in m/p positions on one/both phenyl rings without significant loss in terms of biological activity. Similar SARs are lacking for the sephin1-GADD34 pair.

Initially, we planned to replace one (asymmetric) or two (symmetric) chloroaromatic moieties of ISRIB-**4** with the chloro-aminoguanidine hydrazine sephin1 pattern, maintaining the *trans*-symmetric bis-amide spacer (Figure 10, right). We also planned a limited study of the linker bond between the aryls and the spacer (X-Y Figure 10, right), keeping constant a 2-atom length as in ISRIB.

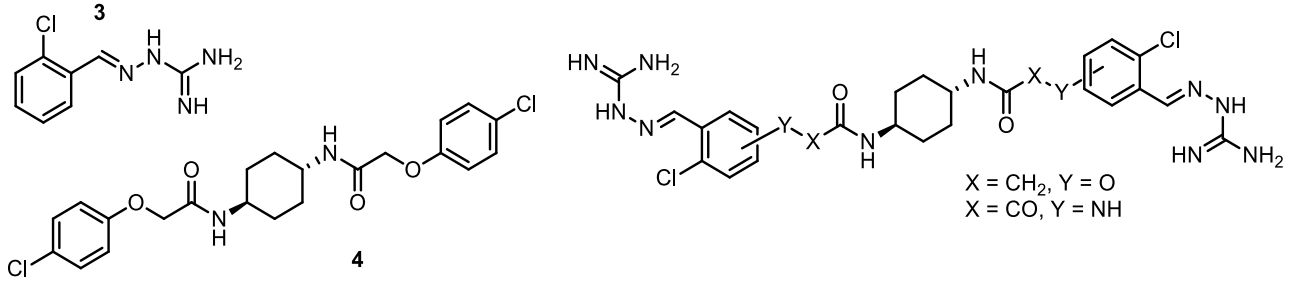

Figure 10. Left: structure of sephin1 **3** and ISRIB **4**. Right: general structure of sephin1-ISRIB DACs.

Firstly, we synthesized two pairs of sephin1 analogues bearing either a n-butyl ether (**5a** – meta with respect to the aminoguanidine; **5b** – para) and an acetamido (**6a** – meta; **6b** – para) substituent, shown in Figure 11; their synthesis is reported in the next paragraph 2.2.

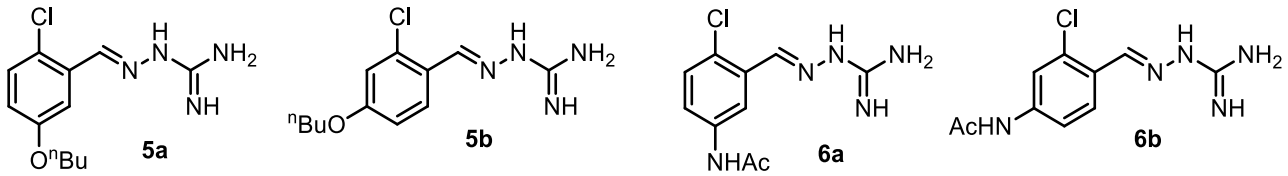

Figure 11. Sephin1 analogues bearing putative anchoring functions: chemical structures, compounds **5a,b** and **6a,b**.

We selected an ether and an amide connection due to their stability and synthetic accessibility; unfortunately, their biological testing by our collaborators at San Raffaele Hospital for GADD34 binding / inhibition (reported in paragraph 2.3) did not yield reliable results due to the low reproducibility of assay conditions. Considering that a para- ether connection is present in the active biotinylated analogue of sephin1 [28], and that a meta-substituted ether leads the chloro atom in para-position (as in ISRIB); we selected a **5a,b**-like connectivity on the phenyl ring of sephin1 for our hybrids (X = CH_2 and Y = O, according to Figure 10).

2.2 CHEMISTRY

2.2.1 Synthesis of trisubstituted sephin1 ether- analogues bearing putative anchoring functions for DAC synthesis

The synthesis of meta-substituted ether **5a** from commercially available meta-anthranilic acid is reported in Scheme 1.

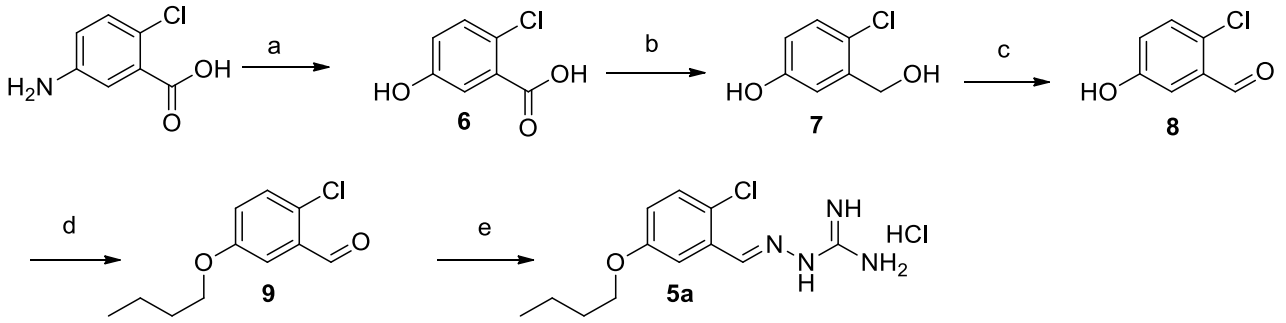

a) $NaNO_2$, H_2SO_4,H_2O, 5°C, then H_2O, active charcoal, 60°C, 3 hrs, **65%**; b) [1M] BH_3 in THF, dry THF, 0°C to 60°C, 4 hrs, **93%**; c) MnO_2, acetone, 60°C, 16 hrs, **68%**; d) n-BuBr, K_2CO_3, CH_3CN, 75°C, 24 hrs, **80%**; e) aminoguanidine-HCl, cat. HCl, EtOH, reflux, 16 hrs, **82%**.

Scheme 1. Synthesis of meta-substituted sephin1 ether derivative **5a**.

The aniline function in meta-anthranilic acid was replaced with a hydroxyl group via diazotization (step a, Scheme 1), using $NaNO_2$ in a sulfuric acid aqueous solution, followed by H_2O quenching to obtain meta hydroxybenzoic acid **6** in good yields [74]. Then, the carboxylic acid was reduced to aldehyde **8** in a 2-steps, high yielding procedure. Namely, reduction by a BH_3 solution in THF (step b) led to the dihydroxy compound **7**. Its partial oxidation to aldehyde **8** was carried out by using MnO_2 with good yield (step c), as reported in literature [75]. Standard O-alkylation was performed with n-BuBr and K_2CO_3 as base in CH_3CN (step d), obtaining high yields of n-butoxybenzaldehyde **9**. Finally, standard acid-catalyzed condensation with aminoguanidine hydrochloride led to target meta-substituted ether **5a**, obtained with high yield after flash chromatography with CH_2Cl_2/MeOH/AcOH and lyophilization from diluted aqueous HCl.

As to para-substituted ether **5b** (Scheme 2), its two-steps synthesis in good yields from 2-chloro,4-hydroxybenzaldehyde is carried out as seen for steps d, e in Scheme 1. Target para-substituted ether **5b** was obtained in high yields and purity by simple filtration from the crude reaction mixture.

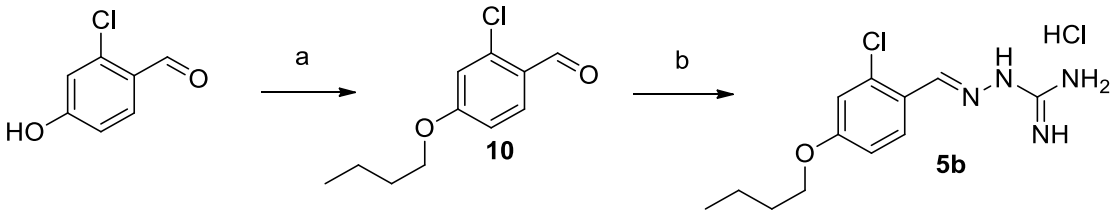

a) n-BuBr, K_2CO_3, CH_3CN, 75°C, 24 hrs, **90%**; b) aminoguanidine-HCl, cat. HCl, EtOH, reflux, 16 hrs, **85%**.

Scheme 2. Synthesis of para-substituted sephin1 ether derivative **5b**.

2.2.2 Synthesis of trisubstituted sephin1 acetamido analogues bearing putative anchoring functions for DAC synthesis

The synthesis of meta-substituted sephin1 acetamide **6a** from commercially available orto-chloro benzaldehyde is reported in Scheme 3.

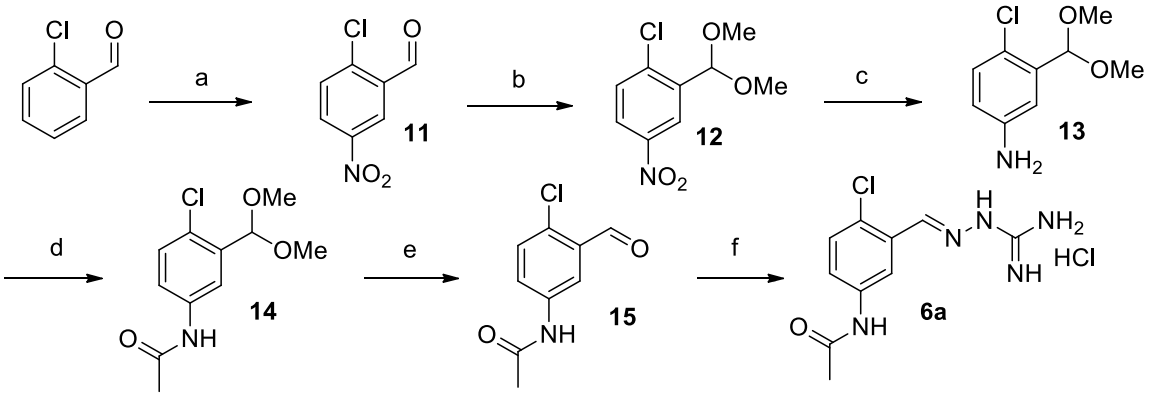

a) $NaNO_3$, H_2SO_4 0-5°C, 2hrs, **80%**; b) $CH(OMe)_3$, [1M] HCl in MeOH, dry MeOH, RT, 3hrs, **98%**; c) $Na_2S_2O_4$, K_2CO_3, TBAHS, 1:3 MeCN/H_2O, 35°C, 4hrs, **60%**; d) Ac_2O, TEA, DMAP, dry CH_2Cl_2, 0° to rt, 3hrs; e) aqueous HCl [1M], dioxane, 25°C, 1hr, **90%** over 2 steps; f) aminoguanidine HCl, cat. HCl, EtOH, 16 hrs, reflux, **89%.**

Scheme 3. Synthesis of meta-substituted acetamido sephin1 derivative **6a**.

A selective meta nitration (step a, Scheme 3) was performed with good yields using $NaNO_2$ in sulfuric acid. Then, I've protected the aldehyde function in **11** with $CH(OCH_3)_3$ and HCl [1M] in dry MeOH at RT (step b), obtaining nitroacetal **12** in quantitative yield. Sodium dithionite was used to reduce the nitro function (step c) in moderate yields, with K_2CO_3 as base and catalytic TBAHS, preventing the observed acetal deprotection with other experimental protocols. The resulting aminoacetal **13** was acetylated with Ac_2O, TEA and catalytic DMAP in dry CH_2Cl_2 (step d), and acetamidoacetal **14** was deprotected in standard aqueous acid conditions (step e) in excellent yields. Condensation between acetamidoaldehyde **15** and aminoguanidine hydrochloride in standard conditions produced the desired meta-substituted acetamide **6a** after filtration in good yields (step f).

As to para substituted acetamide **6b**, its synthesis from commercially available 2-chloro-4-nitrobenzoic acid is reported in Scheme 4.

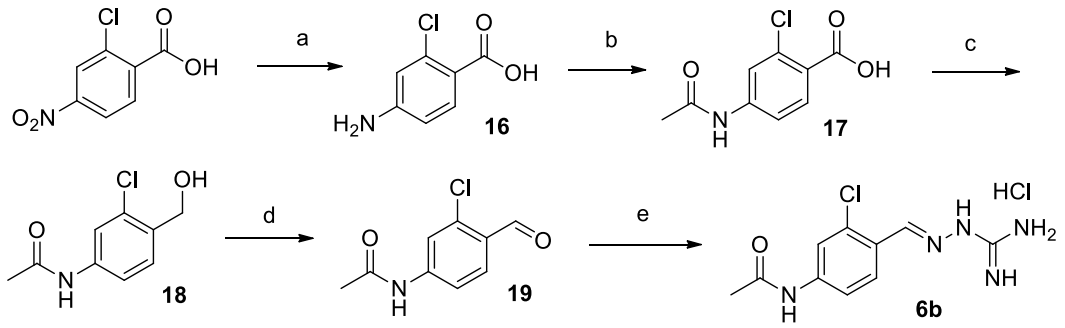

a) H_2, Pd/C, EtOAc, rt, 16hrs, 1atm, **85%**; b) Ac_2O, TEA, dry CH_2Cl_2, 30°C, 3hrs, **80%**; c) BOP, DIPEA, $NaBH_4$, THF, rt, 4hrs, **87%**; d) IBX, AcOH, dry CH_3CN, RT, 16hrs, **89%**; e) aminoguanidine-HCl, cat. HCl, rt, EtOH, 16 hrs, **90%.**

Scheme 4. Synthesis of para-substituted acetamido sephin1 derivative **6b**.

Catalytic hydrogenation of the nitro group with H_2 and Pd/C (step a, Scheme 4) led to the anthranilic acid **16**, then acetylated (step b) with Ac_2O and TEA as base in dry CH_2CL_2. Reduction of acetamido benzoic acid **17** (step c) was carried out with BOP, DIPEA and $NaBH_4$ as reducing agent in THF [76]. Acetamido alcohol **18** was partially oxidized (step d) with IBX in dry CH_3CN at RT (AcOH, was added to improve its solubility in the reaction mixture [77]). Finally, condensation between acetamido benzaldehyde **19** and aminoguanidine hydrochloride (step e) led to the desired para-substituted acetamide **6b**.

Despite the low reproducibility of the biological tests (see paragraph 2.3), due to reported data [28], we focused our attention onto the para- and the meta-substituted ether linkers (**5a, b**-like), to connect the sephin1 scaffold onto ISRIB.

2.2.3 Synthesis of standard ISRIB 4

The chemical structure of selected symmetric (**20**) and asymmetric (**21**, **22**) ISRIB-sephin1 synthetic targets is shown in Figure 12.

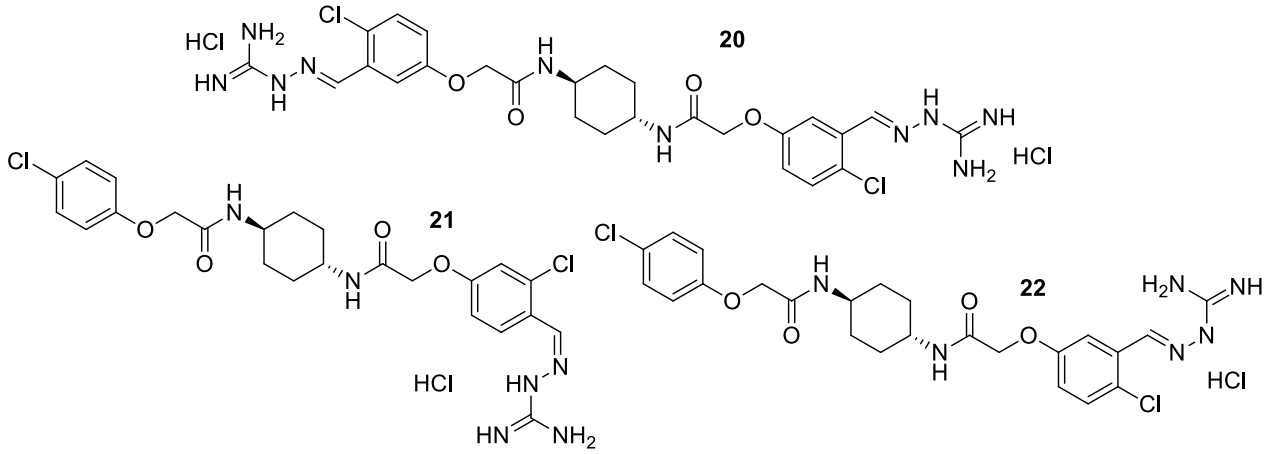

Figure 12. Structures of sephin1-ISRIB hybrids **20-22.**

The retrosynthesis of sephin1-ISRIB hybrids **20-22** shown in Scheme 5 was based on the same disconnection approach reported in literature [74]. Namely, the key step involves an amide coupling between *trans*-1,4-cyclohexanediamine **23** and various phenoxyacetates (Scheme 5).

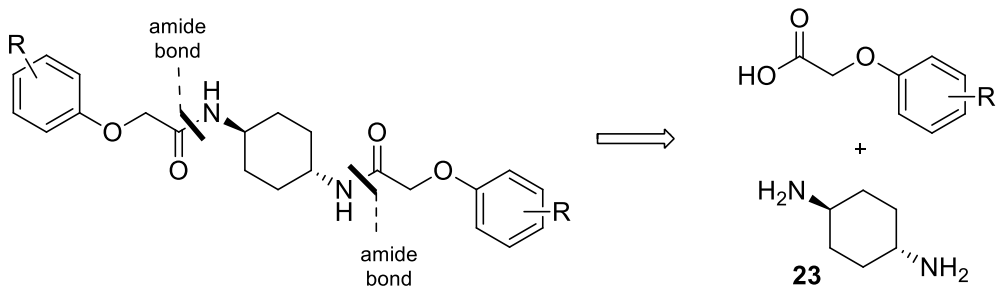

Scheme 5. Retrosynthetic pathway to sephin1-ISRIB hybrids **20**-**22**.

At first, I focused on the synthesis of standard ISRIB **4** (Scheme 6), in order to assess the reaction steps and evaluate the physico-chemical properties of the standard. ISRIB **4** was synthetized from commercially available p-chlorophenol via its O-alkylation using ethyl chloroacetate and K_2CO_3 as base in dry CH_3CN (step

a), to give chloroester **24** in high yields. The following quantitative ester hydrolysis (step b) was carried out using aqueous NaOH in THF at 50°C. The coupling reaction (step c) with phenoxyacetic acid **25** was carried out with EDC in a 1/1 CH_2Cl_2/DMF mixture, due to the low solubility of both reaction partners. Pure standard **4** was obtained after solvent concentration, suspension in acidic water (to dissolve water-soluble by-products), filtration and several washings with acidic and basic water. ISRIB **4** resulted to be poorly soluble, and required hot DMSO to be analytically characterized.

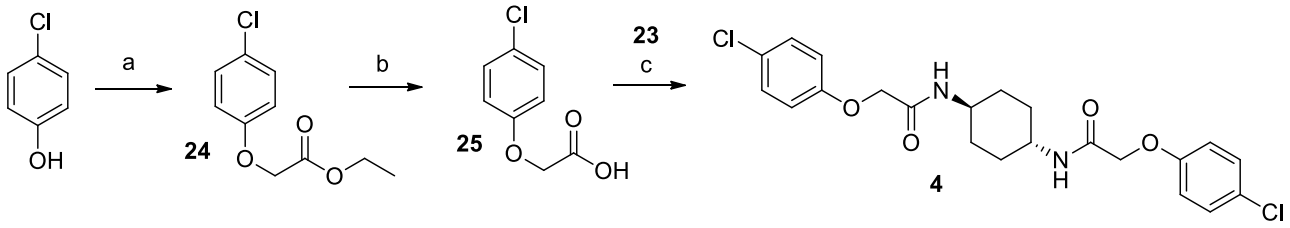

a) ethyl chloroacetate, K_2CO_3, dry CH_3CN, 75°C, 20 hrs, **95%**; b) 1M $NaOH_{aq}$, THF, 50°C, 1hr, **93%**; c) EDCI, HOBt, TEA, 1:1 dry CH_2Cl_2/DMF, 25°C, 20hrs, **67%.**

Scheme 6. Synthesis of standard ISRIB **4**.

2.2.4 Synthesis of the symmetric sephin 1-ISRIB hybrid 20

Using the same synthetic approach and varying the starting carboxylic acid derivative we obtained the target compound **20**. Its synthesis from already described phenol **8** (Scheme 1) is reported in Scheme 7.

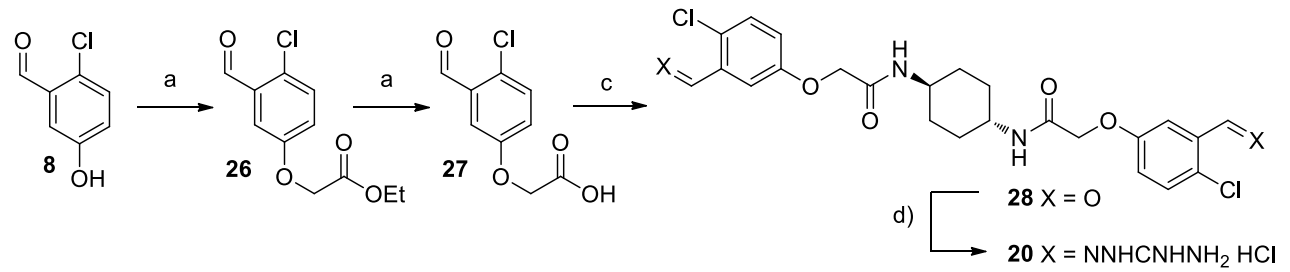

a) ethyl chloroacetate, K_2CO_3, dry CH_3CN, 75°C, 20 hrs, **80%**; b) [1M] $NaOH_{aq}$,THF, 50°C, 1hr, **81%**; c) **24**, EDCI, HOBt, TEA, 1:1 dry CH_2Cl_2/DMF, 25°C, 20hrs, **15%.** d) aminoguanidine-HCl, cat. HCl, EtOH, reflux, 16 hrs, **64%.**

Scheme 7. Synthesis of symmetric sephin1-ISRIB hybrid **20**.

Steps a-c in Scheme 7 to yield the symmetric dialdehyde **28** exactly mirror the same steps in Scheme 6. The yield in step c was extremely low, most likely due to the scarce solubility of the symmetric dialdehyde intermediate **28** that caused its precipitation during a direct phase column chromatography (eluant mixture: AcOEt/MeOH 9:1); the recovered **28** was nevertheless sufficient to complete the synthesis. The symmetric dialdehyde **28** was reacted with aminoguanidine hydrochloride (step d), and target pure symmetric sephin1-ISRIB hybrid **20** was obtained as a bis-hydrochloride by filtration from the cooled reaction mixture in good yields.

2.2.5 Synthesis of asymmetric sephin 1-ISRIB hybrids 21 and 22

The synthesis of para-substituted asymmetric sephin1-ISRIB hybrid **21** (para refers to the relationship between the aminoguanidine and the ether substitution in the trisubstituted phenyl ring) is shown in Scheme 8.

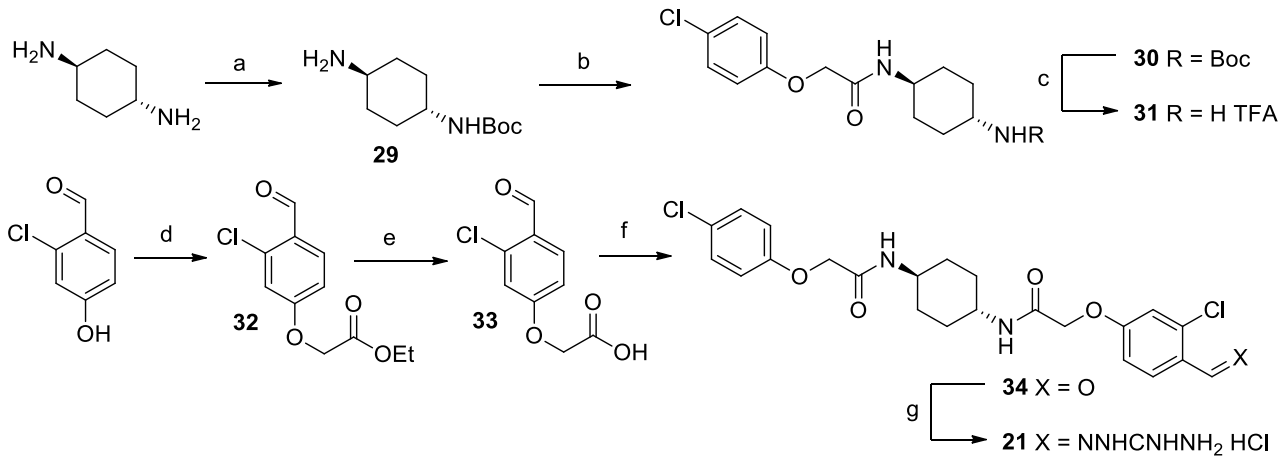

a) Boc_2O, TEA, dry $CHCl_3$, 25°C, 20 hrs, **53%**; b) **27**, EDCI, HOBt, TEA, 1:1 CH_2Cl_2/DMF, rt, 24 hrs, **83%**; c) triethylsilane, TFA, H_2O/DCM, rt, 16 hrs, **98%;** d) ethyl chloroacetate, K_2CO_3, dry CH_3CN, 75°C, 20 hrs, **75%**; e) [1M] NaOHaq.,THF, 50°C, 1 hr, **80%**; f) **31**, EDCI, HOBt, TEA, CH_2Cl_2/DMF 1:1, 25°C, 20 hrs, **11%**; g) aminoguanidine HCl, cat. HCl, EtOH, reflux, 16 hrs, **65%.**

Scheme 8. Synthesis of para-substituted asymmetric sephin1-ISRIB hybrid **21**.

The selective protection of one of the two amino groups of *trans*-1,4-cyclohexanediamine **64** (step a, Scheme 8) was carried out using a stoichiometric amount of Boc_2O and TEA, in $CHCl_3$. Mono-protected amine **29,** obtained in moderate yield after purification by flash chromatography, was then reacted with previously described chloro-phenoxy acetic acid **27** (step b) to yield protected amide **30** in high yields after filtration and washings with H_2O. Removal of the Boc protecting group (step c) was achieved in quantitative yield using triethylsilane and TFA in CH_2Cl_2 and leading to amine **31** as a trifluoroacetate salt. Trisubstituted phenoxyacetic acid **33** to be coupled with amine **31** was synthesized via O-alkylation of commercially available chloro-hydroxy benzaldehyde with ethyl chloroacetate acid using K_2CO_3 as base in dry CH_3CN (step d, ester **32**) and subsequent hydrolysis of the ester moiety (step e) in good yield.

The coupling reaction between **31** and **33** (step f, Scheme 8) was carried out as seen before, using EDCI and HOBt as coupling agents, TEA as base in dry CH_2Cl_2/DMF in order to solubilize the reagents. As seen for symmetric hybrid **20**, the reaction yield was extremely poor, most likely due to the extremely low solubility of the asymmetric para-aldehyde intermediate **34** that caused its precipitation during a direct phase column chromatography (eluant mixture: 9:1 AcOEt/MeOH); here too, enough adduct **34** was nevertheless obtained to complete the synthesis. At last (step d), condensation of asymmetric para-aldehyde **34** with aminoguanidine hydrochloride using the standard synthetic protocol led to the desired meta asymmetric sephin1-ISRIB hybrid **21** in good yields.

The synthesis of the meta-substituted asymmetric sephin1-ISRIB hybrid **22** is shown in Scheme 9.

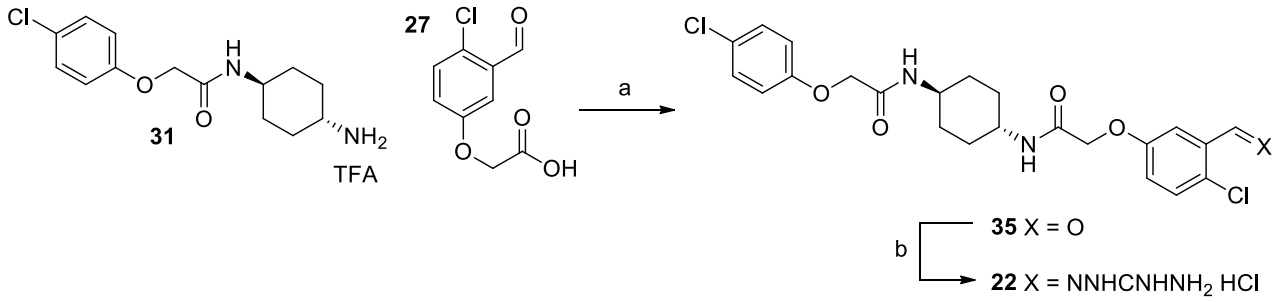

a) EDCI, HOBt, TEA, CH_2Cl_2/DMF 1:1, rt, 20 hrs, **40%**; g) aminoguanidine HCl, cat. HCl, EtOH, reflux, 16 hrs, **76%.**

Scheme 9. Synthesis of meta-substituted asymmetric sephin1-ISRIB hybrid **22**.

The synthesis of hybrid **22** required a coupling reaction between previously described amide **31** and para-trisubstituted phenoxyacetic acid **27** (step a, Scheme 9). The reaction was carried out with EDCI and HOBt as coupling agents, TEA as a base and mixture of dry CH_2Cl_2/DMF to solubilize the reagents. Filtration on a small path of silica gel replaced chromatography, and increased the yield to a moderate 40% of pure **35**. Finally, condensation with aminoguanidine hydrochloride in standard synthetic conditions (step b) led to the desired meta asymmetric sephin1-ISRIB hybrid **22** in good yield.

2.3. BIOLOGICAL CHARACTERIZATION

The linker-sephin1 constructs (ethers **5a,b** and acetamides **6a,b**) were to be profiled in terms of their putative action as selective inhibitors of PP1-GADD34/PPP1R15A phosphatase activity, using the reported assay format by Bertolotti [28] to identify which is the best position/group on the phenyl ring to preserve biological activity on the sephin1 target.

Biological testing for GADD34 binding / inhibition of **5a**, **6a** and **6b** measured their ability – and the ability of sephin1 as a positive standard – at a fixed concentration (50 μM) to foster eIF2α phosphorylation on HeLa cells, by measuring the relative phospho-eIF2α levels. The results are shown in Figure 13. The effects of the sephin1-linker construct **5b** could not be quantified, as any putative effects were masked by signs of toxicity on the cells at the tested concentration.

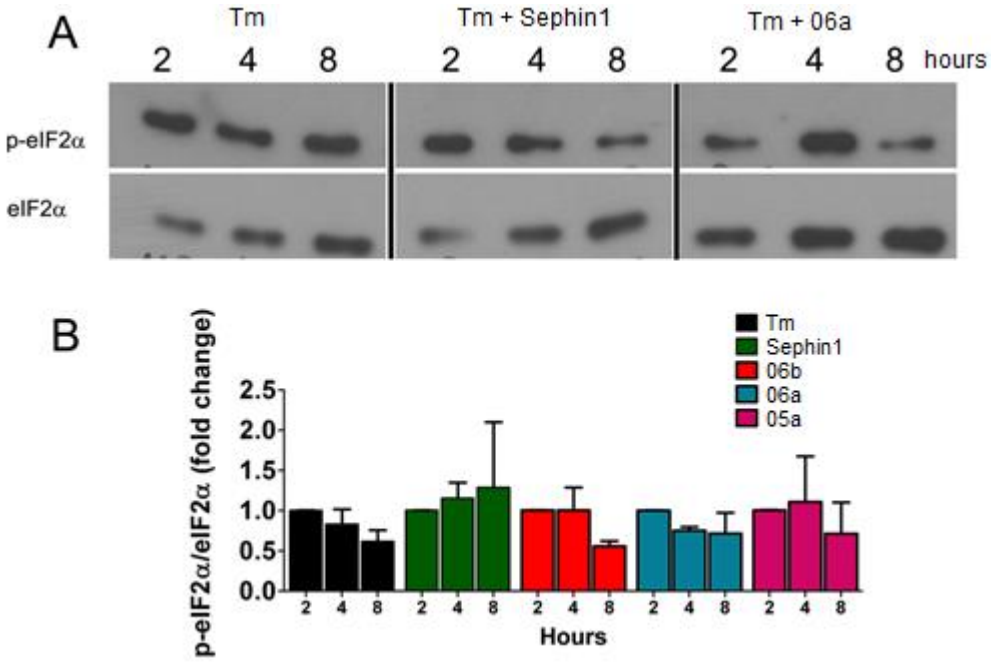

Figure 13. Biological testing of sephin1 **3** and sephin1-linker constructs **5a**, **6a** and **6b** for their effects on eIF2α phosphorylation.

Sephin1 rescues tunicamycin-induced ER stress by inhibiting phosphorylation of eIF2α (panel A, centre lane, and panel B, green bars, Figure 13). Unfortunately, neither among sephin1-linker constructs **5a** (panel B, fucsia bars), **6a** (panel B, blue bars) and **6b** (panel A, right lane, and panel B, red bars) showed any effect on phosphorylation of eIF2α. The low sensitivity and low reproducibility of assay conditions set up by our collaborators at the Neuroscience Department, San Raffaele Hospital (HSR, Dr. L. Muzio) prompted them and us to put on hold this assay format until technical issues could be solved. Thus, the selection of **5a,b**-like ether linkers to connect sephin1 with ISRIB was justified solely by literature data [28], as previously mentioned.

Due to ongoing attempts at HSR to optimize the assay, hybrids **20**, **21** and **22** have not been tested yet. As an alternative format, our co-workers are developing a viability test on HEK293 cells, and a cellular model based on mutated, aggregation-prone proteins related to ALS.

2.4. CONCLUSIONS AND FUTURE PERSPECTIVES

By acting on the same therapeutic areas in two different, and possibly opposite ways, dual action compounds (DACs) could be useful in NDDs where to control the rate and the quality of protein synthesis is crucial. ISRIB should promote protein synthesis through eIF2B stabilization; maximizing our experience on other NDD-impacting mechanisms exploited during my Ph. D. thesis, sephin1 should decrease protein synthesis by increasing the phosphorylation of eIF2α. Thus, we were interested to study the behaviour of such hydrids, once rationally designed and synthesized. Three symmetrical (compound **20**) or asymmetrical (compounds **21** / para-substituted and **22** / meta-substituted) sephin1-ISRIB hybrids were synthetized (Figure 14)

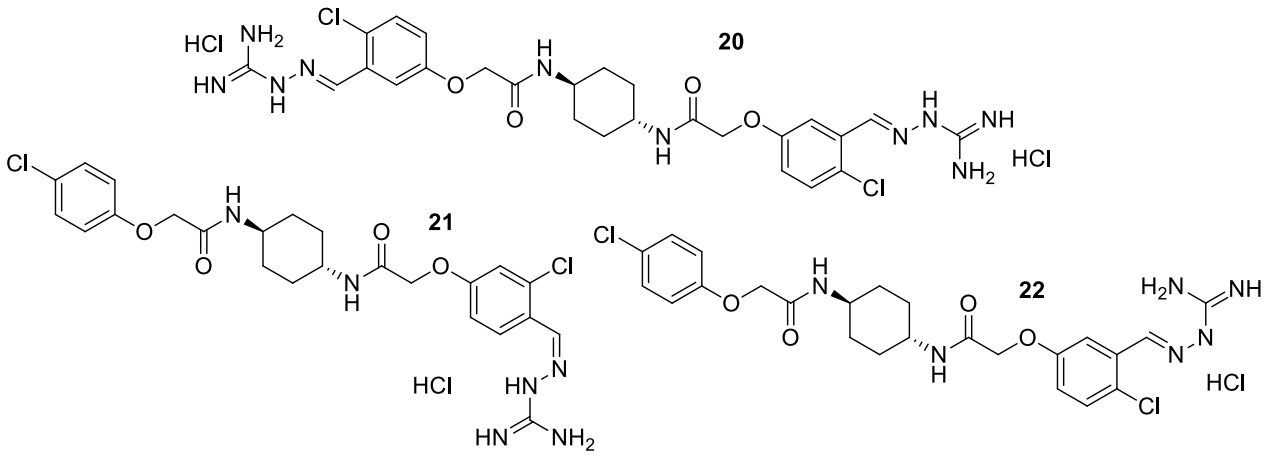

Figure 14. Structure of sephin1-ISRIB symmetrical (**20**) and unsymmetrical (**21**, **22**) DACs.

The connection between the ISRIB and the sephin1 moiety should have resulted from testing four tri-substituted sephin1 derivatives, shown in Figure 15.

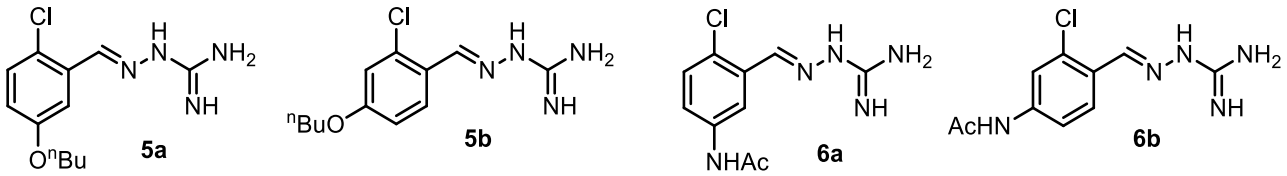

Figure 15. Structure of tri-substituted sephin1 derivatives **5a,b** and **6a,b**.

DACs were to be tested for their effects both on eIF2α and eIF2B (ISRIB, sephin1). Unfortunately, as is described in details in paragraph 2.3, biological testing for sephin1 activity still needs to be optimized (Dr. Muzio, HSR, and Prof. Piccoli, Trento University). More in details, we expect the set up of a viability test on HEK293 cells and a cellular model based on mutated, aggregation-prone proteins related to ALS to test our DAC hybrids. Once this set up will be completed, DACs **5a,b** and **6a,b** will be thoroughly profiled.

2.5 EXPERIMENTAL PART: Synthesis and analytical characterization of intermediates and final compounds

2.5.1 Synthesis of 2-(5-n-Butoxy-2-chlorobenzylidene) hydrazinecarboximidamide hydrochloride 5a

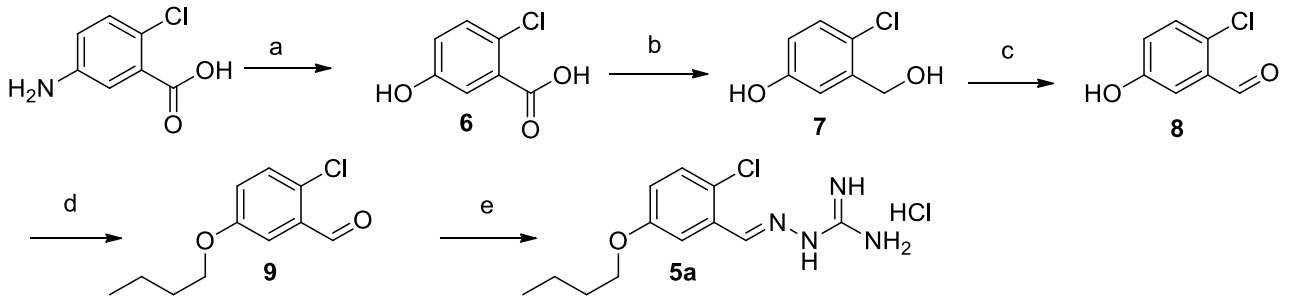

a) $NaNO_2$, H_2SO_4,H_2O, 5°C, then H_2O, active charcoal, 60°C, 3 hrs, **65%**; b) [1M] BH_3 in THF, dry THF, 0°C to 60°C, 4 hrs, **93%**; c) MnO_2, acetone, 60°C, 16 hrs, **68%**; d) n-BuBr, K_2CO_3, CH_3CN, 75°C, 24 hrs, **80%**; e) aminoguanidine-HCl, cat. HCl, EtOH, reflux, 16 hrs, **82%**.

2-Chloro-5-hydroxybenzoic acid 6

2-Chloro-5-aminobenzoic acid (1.290 g, 7.52 mmol, 1 eq) was suspended in 1% V/V aqueous H_2SO_4 (120 mL) and cooled to 5 °C in an ice-water bath while stirring. A solution of $NaNO_2$ (750 mg, 10.87 mmol, 1.5 eq) in H_2O (20 mL) was then added via a dropping funnel over a period of 15 min, maintaining the temperature between 0-5 °C. Then, the mixture was stirred for 3 hours until the solution became clear and was poured then into warm water (220 mL, 60°C). Decolourising charcoal (1 g) was added and the mixture was then refluxed for 30 min. After cooling to RT, the mixture was filtered, and the filtrate was extracted with EtOAc (3×250 mL). The collected organic extracts were dried with Na_2SO_4, filtered and the solvent was evaporated, yielding 837 mg of pure 2-chloro-5-hydroxybenzoic acid **6** as a light brown solid (4.89 mmol, 65% yield).

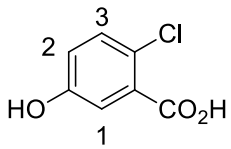

Characterization:

^{1}H NMR (300 MHz, DMSO): δ (ppm) 13.25 (s, 1H, COOH), 9.98 (s, 1H, OH), 7.30 (d, 1H, *J* = 8.7 Hz, H3), 7.14 (d, 1H, *J* = 3.0 Hz, H1), 6.90 (dd, 1H, *J* = 8.7, 3.0 Hz, H2).

4-Chloro-3-(hydroxymethyl)phenol 7

[1M] BH_3 in THF (12 mL, 12 mmol) was slowly added to a solution of 2-chloro-5-hydroxy benzoic acid **6** (837 mg, 4.85 mmol, 1 eq) in dry THF (12 mL) under nitrogen atmosphere. The suspension was stirred for 20 minutes at rt. The mixture was then refluxed for 3 hrs. The reaction mixture was allowed to cool to RT, then carefully quenched with methanol (10 mL). The mixture was stirred for another hour at RT. The solvent was evaporated, yielding 712 mg of pure 4-chloro-3-(hydroxymethyl)phenol **7** as a light yellow solid that was used without further purification (4.515 mmol, 93% yield).

2-Chloro-5-hydroxybenzaldehyde 8

4-Chloro-3-(hydroxymethyl)phenol **7** (712 mg, 4.52 mmol) was suspended in acetone (15 mL), then MnO_2 (2.11 g, 24.25 mmol, 5 eq) was added and the mixture was heated to 60°C for 16 hours (TLC monitoring: 7:3 hexane/AcOEt). The reaction mixture was cooled to room temperature and eluted through a celite path with AcOEt (50 mL). The solvent was removed under reduced pressure, and the crude product (750 mg) was

purified by flash chromatography (eluant: 8:2 hexane/EtOAc), yielding 480 mg of pure 2-chloro-5-hydroxybenzaldehyde **8** as a light yellow solid (3.07 mmol, 68% yield).

Characterization:

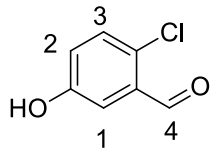

^{1}H NMR (300 MHz, $CDCl_3$): δ (ppm) 10.41 (s, 1H, H4), 7.41 (d, 1H, J = 3 Hz, H1), 7.34 (d, 1H, J = 9.0 Hz, H3), 7.07 (dd, 1H, J = 9.0 Hz, J = 3 Hz, H2), 5.97 (bs, 1H, OH).

5-n-Butoxy-2-chlorobenzaldehyde 9

2-Chloro-5-hydroxy benzaldehyde **8** (110 mg, 0.70 mmol, 1 eq) was dissolved in CH_3CN (3 mL). Then, BuBr (0.150 mL, 1.40 mmol, 2 eq) and K_2CO_3 (353.9 mg, 2.80 mmol, 4 eq) were added. The solution was heated to reflux and stirred for 20 hours (TLC monitoring: 9:1 hexane/AcOEt). After solvent evaporation, the reaction mixture was diluted with AcOEt (40 mL), washed with H_2O (15 mL) and with brine (10 mL). The crude product (188 mg) was purified by flash chromatography (eluant: 95:5 hexane/AcOEt), yielding 118.7 mg of pure 5-n-butoxy-2-chlorobenzaldehyde **9** as a white solid (0.56 mmol, 80% yield).

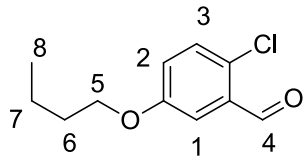

Characterization:

^{1}H NMR (300 MHz, $CDCl_3$): δ (ppm) 10.47 (s, 1H, H4), 7.48 (d, 1H, J = 2.8 Hz, H2), 7.36 (d, 1H, J = 8.7 Hz, H3), 7.09 (dd, 1H, J = 8.7 Hz, J = 2.8 Hz, H1), 3.96 (s, 2H, H5), 1.78 (m, 2H, H6), 1.46 (m, 2H, H7), 1.02 (t, 3H, J = 7.6 Hz, H8).

2-(5-n-Butoxy-2-chlorobenzylidene) hydrazinecarboximidamide hydrochloride 5a

5-n-Butoxy 2-chloro benzaldehyde **9** (127.1 mg, 0.597 mmol, 1 eq) and aminoguanidine hydrochloride (66.1 mg, 0.597 mmol, 1 eq) were dissolved in EtOH (6 mL), then cat. [1M] HCl (two drops) was added. The solution was heated to reflux and stirred for 16 hours (TLC monitoring: 9:1 CH_2Cl_2/MeOH). The solvent was then evaporated under vacuum and the crude was purified by flash chromatography (eluant: 9:1 CH_2Cl_2/MeOH, 1% AcOH). The white powder obtained was dissolved in dilute aqueous HCl and lyophilized yielding 151 mg of pure 2-(5-n-butoxy-2-chlorobenzylidene) hydrazinecarboximidamide **5a** as a hydrochloride salt (white solid, 0.490 mmol, 82% yield).

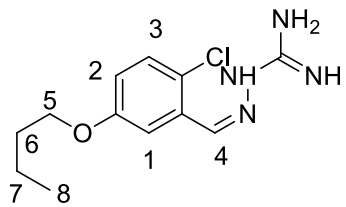

Characterization:

^{1}H NMR (300 MHz, DMSO): δ (ppm) 8.41 (s, 1H, H4), 7.78 (d, J = 3.1 Hz, 1H, H1), 7.32 (d, J = 9.0 Hz, 1H, H3), 7.28 (bs, 4H, NH_2), 6.94 (dd, J = 9.0 Hz, J = 3.1 Hz, 1H, H2), 4.06 (s, 2H, H5) 1.72 (m, 2H, H6), 1.44 (m, 2H, H7), 0.95 (t, 3H, J = 7.4 Hz, H8).

^{13}C NMR (75 MHz, DMSO): δ (ppm) 157.7, 157.4, 141.2, 132.5, 130.5, 124.1, 117.7, 112.0, 67.7, 30.7, 18.8, 13.7.

MS (ESI^+): 269.12 [$M+H^+$] (mass calculated for $C_{12}H_{17}ClN_4O$: 268.11).

2.5.2 Synthesis of 2-(4-n-Butoxy-2-chlorobenzylidene) hydrazinecarboximidamide hydrochloride 5b

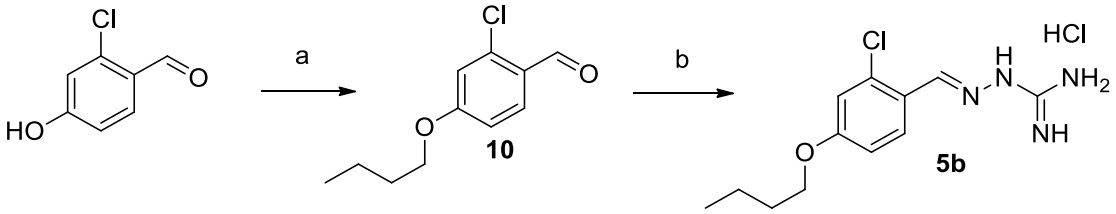

a) n-BuBr, K_2CO_3, CH_3CN, 75°C, 24 hrs, **90%**; b) aminoguanidine-HCl, cat. HCl, EtOH, reflux, 16 hrs, **85%**.

4-n-Butoxy-2-chlorobenzaldehyde 10

2-Chloro-4-hydroxy benzaldehyde (180.0 mg, 0.70 mmol, 1 eq) was dissolved in CH_3CN (5 mL). Then, BuBr (0.247 mL, 1.40 mmol, 2 eq) and K_2CO_3 (315 mg, 2.30 mmol, 3 eq) were added under stirring. The solution was heated to reflux and stirred for 24 hours (TLC monitoring: 9:1 hexane/AcOEt). The solvent was then evaporated, and the reaction mixture was diluted with AcOEt (40 mL), washed with H_2O (15 mL) and with brine (10 mL). The crude product (315 mg) was purified by flash chromatography (eluant: 95:5 hexane/AcOEt), yielding 220.6 mg of pure 4-n-butoxy-2-chlorobenzaldehyde **10** as a white solid (1.035 mmol, 90% yield).

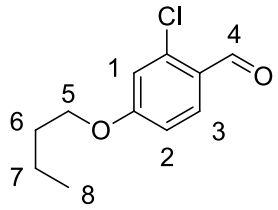

Characterization:

^{1}H NMR (300 MHz, $CDCl_3$): δ (ppm) 10.31 (s, 1H, H4), 7.86 (d, 1H, J = 8.5 Hz, H3), 6.87 (m, 2H, H1, H2), 4.02 (s, 2H, H5), 1.78 (m, 2H, H6), 1.46 (m, 2H, H7), 1.02 (t, 3H, J = 7.6 Hz, H8).

2-(4-n-Butoxy-2-chlorobenzylidene) hydrazinecarboximidamide hydrochloride 5b

4-n-butoxy-2-chlorobenzaldehyde **10** (67.9 mg, 0.344 mmol, 1 eq) and aminoguanidine hydrochloride (36 mg, 0.327 mmol, 0.95 eq) were dissolved in EtOH (2 mL), then cat. [1M] HCl (1 drop) was added. The solution was heated to 75°C and stirred for 16 hours. Then, the solvent was evaporated under reduced pressure and the crude was triturated with 1:10 cold EtOH/Et_2O (22 mL). After filtration and washing with Et_2O, 89.8 mg of pure 2-(5-n-butoxy-2-chlorobenzylidene) hydrazinecarboximidamide hydrochloride **5b** as a white solid were obtained (0.310 mmol, 90% yield).

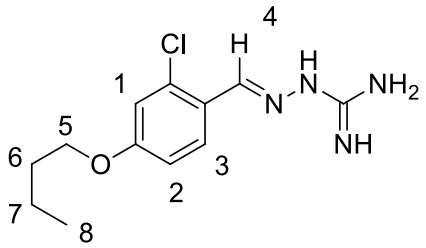

Characterization:

^{1}H NMR (300 MHz, DMSO): δ (ppm) 12.18 (s, 1H, NH), 8.41 (s, 1H, H4), 8.27 (d, 1H, J = 8.9 Hz, H3), 7.80 (bs, 3H, NH_2), 7.21 (d, 1H, J = 2.4 Hz, H1), 7.03 (dd, 1H, J = 8.9 Hz, J = 2.4 Hz, H2), 4.09 (s, 2H, H5) 1.72 (m, 2H, H6), 1.44 (m, 2H, H7), 0.95 (t, 3H, J = 7.4 Hz, H8).

^{13}C NMR (75 MHz, DMSO): δ (ppm) 161.0, 155.3, 142.6, 142.3, 134.4, 128.8, 123.0, 114.9, 114.6, 68.0, 30.6, 18.7, 13.7.

MS (ESI^+): 269.12 [$M+H^+$] (mass calculated for $C_{12}H_{17}ClN_4O$: 268.11).

2.5.3 Synthesis of (3-((2-carbamimidoylhydrazono)methyl)-4-chlorophenyl)acetamide hydrochloride 6a

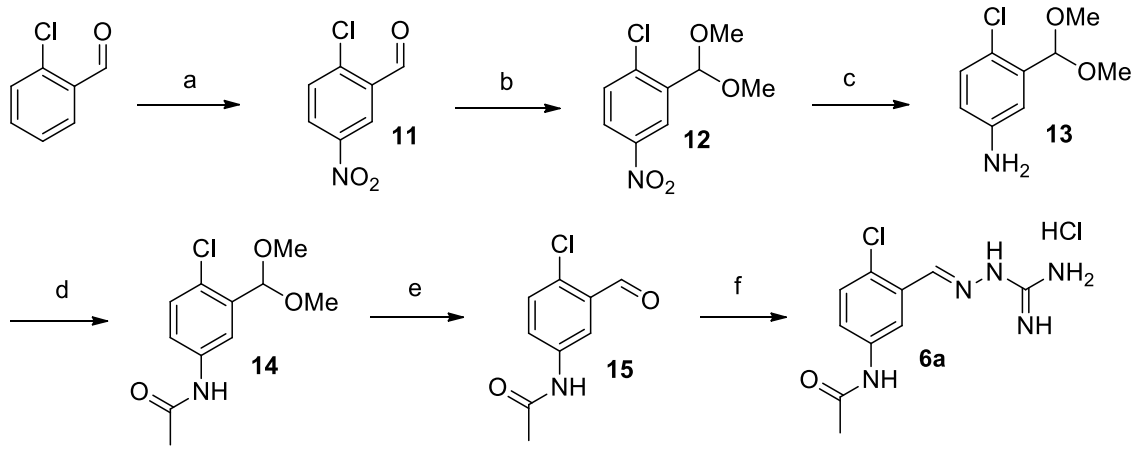

a) $NaNO_3$, H_2SO_4 0-5°C, 2hrs, **80%**; b) $CH(OMe)_3$, [1M] HCl in MeOH, dry MeOH, RT, 3hrs, **98%**; c) $Na_2S_2O_4$, K_2CO_3, TBAHS, 1:3 MeCN/H_2O, 35°C, 4hrs, **60%**; d) Ac_2O, TEA, DMAP, dry CH_2Cl_2, 0° to rt, 3hrs; e) aqueous HCl [1M], dioxane, 25°C, 1hr, **90%** over 2 steps; f) aminoguanidine HCl, cat. HCl, EtOH, 16 hrs, reflux, **89%**.

2-chloro-5-nitrobenzaldehyde 11

2-chlorobenzaldehyde (1.00 g, 7.12 mmol, 1 eq) was added under stirring at 0-5°C during 1 hour to a solution of sodium nitrate (665 mg, 7.84 mmol, 1.1 eq) in H_2SO_4 (6.4 mL). The reaction mixture was stirred for 1 hour, then was poured into an ice bath, and the solid product filtered off, washed with aqueous sodium bicarbonate until neutral pH, then dried in oven overnight. The crude solid (1.284 g) was crystallized by diluted aqueous AcOH, yielding 1.123 g of pure 2-chloro-5-nitrobenzaldehyde **11** as a white solid (5.696 mmol, 80% yield).

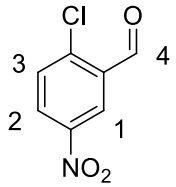

Characterization:

^{1}H NMR (400 MHz, $CDCl_3$): δ (ppm) 10.49 (s, 1H, H4), 8.75 (d, 1H, J = 2.8 Hz, H1), 8.38 (dd, 1H, J = 8.8 Hz, J = 2.8 Hz, H2), 7.68 (d, 1H, J = 8.8 Hz, H3).

1-chloro-2-(dimethoxymethyl)-4-nitrobenzene 12

[1M] HCl in MeOH (500 µL) and $CH(OMe)_3$ (1.302 g, 12.273 mmol, 3.5 eq) were sequentially added to a stirred solution of 2-chloro-5-nitrobenzaldehyde **11** (650.7 mg, 3.507 mmol, 1.0 eq) dissolved in dry MeOH (10 mL), under nitrogen atmosphere. The reaction mixture was stirred for 3 hours at RT (TLC monitoring: 8:2 hexane/AcOEt). After the disappearance of starting material, the reaction mixture was cooled to 0°C and TEA (4.5 mL) was added. The solvent was removed under reduced pressure, the crude residue was diluted with CH_2Cl_2 (35 mL) and sequentially washed with H_2O (20 mL) and brine (15 mL). The collected organic phases were dried over Na_2SO_4, filtered and the solvent was removed under reduced pressure, yielding 800.5 mg of pure 1-chloro-2-(dimethoxymethyl)-4-nitrobenzene **12** as a white solid (3.454 mmol, 98% yield).

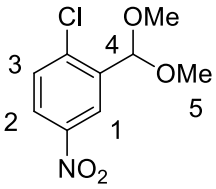

Characterization:

^{1}H NMR (400 MHz, $CDCl_3$): δ (ppm) 8.51 (d, 1H, J = 2.7 Hz, H1), 8.13 (dd, 1H, J = 8.8 Hz, J = 2.7 Hz, H2), 7.53 (d, 1H, J = 8.8 Hz, H3), 5.63 (s, 1H, H4), 3.39 (s, 6H, H5).

^{13}C NMR (100 MHz, $CDCl_3$): δ (ppm) 146.5, 139.9, 137.4, 130.7, 124.5, 123.8, 99.7, 53.8.

4-chloro-3-(dimethoxymethyl)aniline 13

Under nitrogen atmosphere, a solution of K_2CO_3 (2864.3 mg, 20.724 mmol, 6 eq) and $Na_2S_2O_4$ (4810.7 mg, 27.630 mmol, 8 eq) in H_2O (24 mL) was added dropwise to a solution of 1-chloro-2-(dimethoxymethyl)-4-nitrobenzene **12** (800.5 mg, 3.454 mmol, 1eq) and TBAHS (175.9 mg, 0.518 mmol, 0.15 eq) in CH_3CN (8 mL). The reaction mixture was stirred for 4 hours at 35°C (TLC monitoring: 7:3hexane/AcOEt). The organic solvent was removed under reduced pressure. The reaction mixture was extracted with AcOEt (4 x 25 mL). The organic phases were dried over Na_2SO_4, filtered and concentrated under reduced pressure. The resulting pale yellow oil (798 mg) was filtered through a short path of silica gel using AcOEt. The eluate was then concentrated under reduce pressure yielding 417.9 mg of pure 4-chloro-3-(dimethoxymethyl)aniline **13** (2.072 mmol, 60% yield).

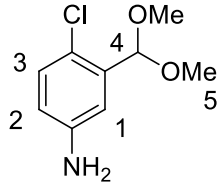

Characterization:

^{1}H NMR (400 MHz, $CDCl_3$): δ (ppm) 7.11 (d, 1H, J = 8.7 Hz, H3), 6.95 (d, 1H, J = 2.8 Hz, H1), 6.60 (dd, 1H, J = 8.7 Hz, J = 2.8 Hz, H2), 5.55 (s, 1H, H4), 3.97 (bs, 2H, NH_2), 3.36 (s, 6H, H5).

N-(4-chloro-3-(dimethoxymethyl)phenyl)acetamide 14

4-chloro-3-(dimethoxymethyl) aniline 13 (99.2 mg, 0.491 mmol, 1 eq) and TEA (2.5 eq) were dissolved in CH_2Cl_2 (5 mL). After 5 minutes' stirring, Ac_2O (70 μL, 0.738 mmol, 1.5 eq) was added. The reaction mixture was heated to 35°C and stirred for 4 hours (TLC monitoring: 7:3hexane/EtOAc). Then, the solvent was removed under reduced pressure, the crude residue was diluted with AcOEt (30 mL), washed with a 5% citric acid solution (2 x 10 mL) and with a sat. $NaHCO_3$ solution (2 x 10 mL). The organic layer was dried with Na_2SO_4, filtered and the solvent was removed under reduced pressure. Crude N-(4-chloro-3-(dimethoxymethyl) phenyl)acetamide **14** was used as such in the next step, without purification.

N-(4-chloro-3-formylphenyl)acetamide 15

Crude N-(4-chloro-3-(dimethoxymethyl)phenyl)acetamide **14** was dissolved in a 2:1 dioxane / [1M] HCl solution (1.5 mL). The reaction mixture was stirred at RT for 1 hr, then the solvent was removed under reduced pressure, yielding 90.1 mg of N-(4-chloro-3-formylphenyl)acetamide **15** (0.451 mmol, 90% yield).

Characterization

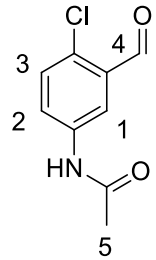

^{1}H NMR (400 MHz, DMSO): δ (ppm) 10.32 (s, 1H, H4), 8.15 (d, 1H, J = 2.8 Hz, H1), 7.88 (dd, 1H, J = 8.7 Hz, J = 2.8 Hz, H2), 7.58 (d, 1H, J = 8.7 Hz, H3), 2.09 (s, 3H, H5).

^{13}C NMR (100 MHz, DMSO): δ (ppm) 189.7, 168.9, 137.5, 132.5, 132.4, 131.3, 126.8, 119.5, 24.5.

MS (ESI^+): 220.123 [$M+Na^+$] (mass calculated for $C_9H_8ClNO_2$: 197.02).

N-(3-((2-carbamimidoylhydrazono)methyl)-4-chlorophenyl)acetamide hydrochloride 6a

N-(4-chloro-3-formylphenyl)acetamide **15** (79.9 mg, 0.404 mmol, 1 eq) and aminoguanidine hydrochloride (44.7 mg, 0.404 mmol, 1 eq) were dissolved in absolute EtOH (2 mL), then cat. [1M] HCl (2 drops) was added. The solution was heated to 75°C and stirred for 16 hours. Then after cooling to RT, the white precipitate formed was filtered and washed with cold EtOH, yielding 111.7 mg of pure N-(3-((2-carbamimidoylhydrazono)methyl)-4-chlorophenyl)acetamide hydrochloride **6a** (0.384 mmol, 95% yield).

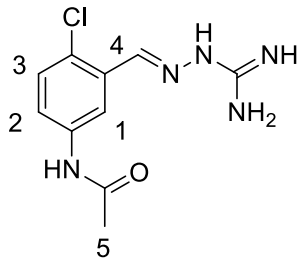

Characterization:

^{1}H NMR (400 MHz, DMSO): δ (ppm) 12.33 (bs, 1H, NH), 10.29 (s, 1H, NHAc), 8.54 (s, 1H, H4), 8.24 (d, 1H, J = 2.8 Hz, H1), 7.86 (bs, 3H, NH) 7.75 (dd, 1H, J = 8.7 Hz, J = 2.8 Hz, H2), 7.47 (d, 1H, J = 8.7 Hz, H3), 2.08 (s, 3H, H5).

^{13}C NMR (100 MHz, DMSO): δ (ppm) 168.6, 155.4, 143.3, 138.4, 130.7, 130.0, 127.1, 123.3, 118.4, 23.9.

MS (ESI^{+}): 254.08 [M+H^{+}] (mass calculated for $C_{10}H_{12}ClN_5O$: 253.07).

2.5.4 Synthesis of N-(4-((2-carbamimidoylhydrazono)methyl)-3-chlorophenyl)acetamide hydrochloride 6b

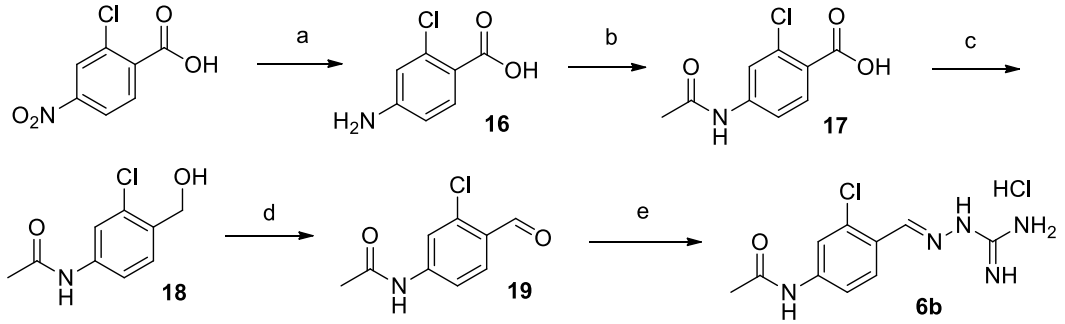

a) H_2, Pd/C, EtOAc, rt, 16hrs, 1atm, **85%**; b) Ac_2O, TEA, dry CH_2Cl_2, 30°C, 3hrs, **80%**; c) BOP, DIPEA, $NaBH_4$, THF, rt, 4hrs, **87%**; d) IBX, AcOH, dry CH_3CN, RT, 16hrs, **89%**; e) aminoguanidine-HCl, cat. HCl, rt, EtOH, 16 hrs, **90%.**

4-amino-2-chlorobenzoic acid 16

2-chloro-4-nitrobenzoic acid (1 g, 4.961 mmol, 1 eq) was dissolved in AcOEt (25 mL), then 10% Pd-C (200 mg) was added. The mixture was hydrogenated at 1 atm of pressure at 25°C under vigorous stirring for 16 hours, then it was filtered through a celite path with AcOEt (30 mL). The solvent was evaporated under reduced pressure, yielding 808.1 mg of pure 4-amino-2-chlorobenzoic acid **16** as a light green powder (4.217 mmol, 85% yield) that was used without further purification.

4-acetamido-2-chlorobenzoic acid 17

Crude 4-amino-2-chlorobenzoic acid **16** (245.0 mg, 1.428 mmol, 1 eq) was suspended in dry CH_2Cl_2 (3 mL). TEA (1.587 mL, 8 eq) and Ac_2O (0.202 mL, 1.5 eq) were sequentially added under vigorous stirring. The reaction mixture was stirred for 2 hours at 30°C (TLC monitoring: 8:2 AcOEt/hexane). The solvent was then evaporated, the oily residue was dispersed in [1M] HCl (10mL). The precipitate was filtered and thoroughly

washed with water, yielding 244.1 mg of pure 4-acetamido-2-chlorobenzoic acid **17** as a white solid (1.143 mmol, 80% yield) that was used without further purification.

N-(3-chloro-4-(hydroxymethyl)phenyl)acetamide 18

4-acetamido-2-chlorobenzoic acid **17** (292.7 mg, 1.303 mmol, 1 eq) was suspended in THF (6 mL), then TEA (272 µL, 1.565 mmol, 1.2 eq) and BOP (634.2 mg, 1.434 mmol, 1.1 eq) were added. The solution was stirred at RT for 15 min, then added dropwise under vigorous stirring to a suspension of $NaBH_4$ (74.0 mg, 1.955 mmol, 1.5eq) in THF (2 mL). After stirring for 4 hours, the solvent was evaporated, the residue was dissolved in AcOEt (30 mL) and sequentially washed with [1M] HCl (2 x 10 mL), saturated $NaHCO_3$ (2 x 10 mL) and brine (10 mL). The pooled aqueous phases were extracted with AcOEt (20 mL). The collected organic phases were dried with Na_2SO_4 and filtered. The solvent was removed under reduced pressure, yielding 226.3 mg of pure N-(3-chloro-4-(hydroxymethyl)phenyl)acetamide **18** as a white solid (1.134 mmol, 87% yield).

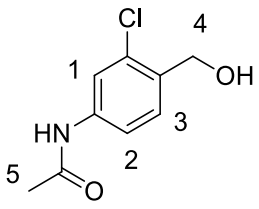

Characterization:

^{1}H NMR (300 MHz, DMSO): δ (ppm) 10.30 (s, 1H, NH), 7.85 (s, 1H, H1), 7.48 (s, 2H, H2, H3), 5.29 (t, 1H, J = 5.3 Hz, OH), 4.49 (d, 2H, J = 5.3 Hz, H4), 2.09 (s, 3H, H5).

^{13}C NMR (75 MHz, DMSO): δ (ppm) 168.6, 139.1, 133.8, 131.0, 128.5, 118.9, 117.4, 60.0, 24.0

N-(3-chloro-4-formylphenyl)acetamide 19

N-(3-chloro-4-(hydroxymethyl)phenyl)acetamide **18** (200.8 mg, 1.002 mmol, 1 eq) was suspended in MeCN (8 mL), then IBX (420.9 mg, 1.503 mmol, 1.5 eq) and AcOH (0.085 mL, 1.5 eq) were added under vigorous stirring. The reaction mixture was stirred for 16 hours at 30°C (TLC monitoring: 3:7 hexane/AcOEt). Solid $NaHCO_3$ (50 mg) was then added and the mixture was stirred for 10 minutes. The mixture was passed through a path of celite using AcOEt (30 mL) as eluant. The solvent was removed under reduced pressure, and the crude product was purified by flash chromatography (eluant: 4:6 hexane/EtOAc), yielding 176 mg of pure N-(3-chloro-4-formylphenyl)acetamide **19** as a white solid (0.891 mmole, 89% yield).

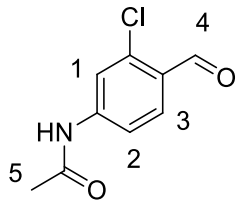

Characterization:

^{1}H NMR (400 MHz, DMSO): δ (ppm) 10.50 (s, 1H, NH), 10.22 (s, 1H, H4), 7.98 (s, 1H, H1), 7.85 (d, 1H, J = 8.8 Hz, H2), 7. 58 (d, 1H, J = 8.8 Hz, H3), 2.09 (s, 3H, H5).

^{13}C NMR (100 MHz, DMSO): δ (ppm) 188.4, 169.5, 145.4, 137.4, 130.7, 126.8, 119.1, 117.5, 24.3.

N-(4-((2-carbamimidoylhydrazono)methyl)-3-chlorophenyl)acetamide hydrochloride 6b

N-(3-chloro-4-formylphenyl)acetamide **19** (67.9 mg, 0.344 mmol, 1 eq) and aminoguanidine hydrochloride (38 mg, 0.344 mmol, 1 eq) were dissolved in EtOH (2 mL), then cat. [1M] HCl (1 drop) was added under stirring. The solution was heated to 75°C and stirred for 16 hours. Then, after cooling to RT the white precipitate formed was filtered and washed with cold EtOH. 89.8 mg of pure N-(4-((2-carbamimidoylhydrazono)methyl)-3-chlorophenyl)acetamide hydrochloride **6b** as a white solid were obtained (0.310 mmol, 90% yield).

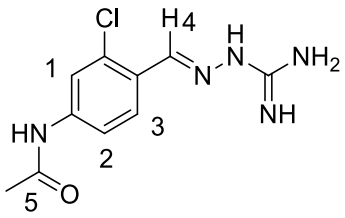

Characterization:

^{1}H NMR (300 MHz, DMSO): δ (ppm) 12.33 (bs, 1H, NH), 10.29 (s, 1H, NHAc), 8.48 (s, 1H, H4), 8.29 (d, 1H, J = 2.8 Hz, H1), 7.92 (d, 1H, J = 8.7 Hz, H3), 7.80 (sb, 3H, NH) 7.51 (d, 1H, J = 8.7 Hz, J = 2.8 Hz, H2), 2.08 (s, 3H, H5).

^{13}C NMR (75 MHz, DMSO): δ (ppm) 169.1, 155.3, 142.4, 142.3, 133.6, 128.0, 124.9, 118.7, 117.7, 24.2.

MS (ESI^{+}): 254.08 [M+H^{+}] (mass calculated for $C_{10}H_{12}ClN_5O$: 253.07).

2.5.5 Synthesis of standard ISRIB 4

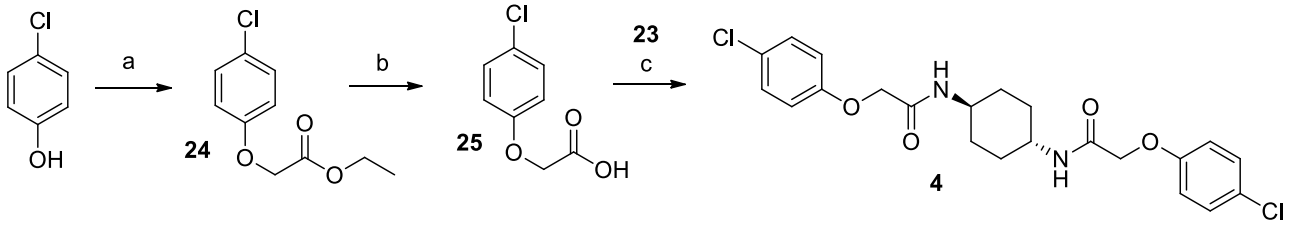

a) ethyl chloroacetate, K_2CO_3, dry CH_3CN, 75°C, 20 hrs, **95%**; b) 1M $NaOH_{aq}$, THF, 50°C, 1hr, **93%**; c) EDCI, HOBt, TEA, 1:1 dry CH_2Cl_2/DMF, 25°C, 20hrs, **67%.**

Ethyl 2-(4-chlorophenoxy)acetate 24

Chlorophenol (500 μL, 5.08 mmol, 1 eq) was dissolved in dry CH_3CN (6 mL). Then, ethyl chloroacetate (650μL, 6.095 mmol, 1.2 eq) and K_2CO_3 (842.4 mg, 1.17 mmol, 1.5 eq) were added. The reaction mixture was heated to 75°C and stirred for 20 hours (TLC monitoring: 85:15 hexane/EtOAc). The solvent was removed and the crude was dissolved in AcOEt (30 mL). The organic phase was washed with aqueous $NaHCO_3$ sat. (2 x 10 mL) and with brine (10 mL). The organic phase was dried with Na_2SO_4, filtered and the solvent removed under reduced pressure. The crude product (1.48 g) was purified by flash chromatography (eluant: 85:15 hexane/EtOAc), yielding 1.036 g of pure ethyl 2-(4-chlorophenoxy)acetate **24** as a light yellow solid (4.825 mmol, 95% yield).

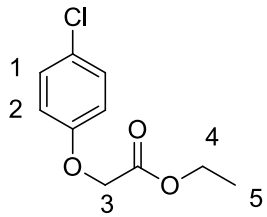

Characterization:

^{1}H NMR (400 MHz, $CDCl_3$): δ (ppm) 7.25 (d, 2H, J = 9.0 Hz, H1), 6.86 (d, 2H, J = 9.0, H2), 4.59 (s, 2H, H3), 4.29 (q, 2H, J = 7.2 Hz, H4), 1.30 (t, 3H, J = 7.9 Hz, H5).

The ^{1}H-NMR spectrum was consistent with those reported in literature [57].

2-(4-chlorophenoxy)acetic acid 25

Ethyl 2-(4-chlorophenoxy)acetate **24** (905 mg, 4.21 mmol, 1 eq) was dissolved in THF (10 mL), then a solution of [1M] NaOH (8.5 mL, 2 eq) was added. The reaction mixture was heated to 50 °C and stirred for 1 hour (TLC monitoring: 9:1 hexane/AcOEt). After THF evaporation, the aqueous solution was acidified with 1M HCl_{aq} under stirring until pH 2. The resulting precipitate was filtered, sequentially washed with H_2O (10 mL) and with Et_2O (10 mL), yielding 730 mg of pure 2-(4-chlorophenoxy)acetic acid **25** as a white solid (3.91 mmol, 93% yield).

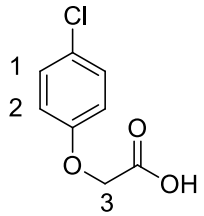

Characterization:

^{1}H NMR (400 MHz, DMSO): δ (ppm) 7.35 (d, 2H, *J* = 9.0 Hz, H2), 6.95 (d, 2H, J = 9.0 Hz, H3), 4.71 (s, 2H, H1), 3.38 (bs, 1H, OH).

The ^{1}H-NMR spectrum was consistent with those reported in literature [57].

ISRIB standard 4

2-(4-chlorophenoxy)acetic acid **25** (150 mg, 0.730 mmol, 2 eq) was suspended in a 1:1 mixture of dry CH_2Cl_2 and dry DMF (4 mL), and TEA (152.5 µL, 1.095mmol, 3 eq) was added. EDCI (167.90 mg, 0.876 mmol, 2.4 eq) and HOBt (118.36 mg, 0.876 mmol, 2.4 eq) were rapidly added under stirring to the homogeneous solution, and the reaction mixture was stirred at RT for 10 minutes. Then, trans-1,4-cyclohexanediamine **23** (41.72 mg, 0.365 mmol, 1 eq) was added. The solution was stirred at RT for 20 hours. Then, CH_2Cl_2 was removed, the oil was suspended in [1M] HCl, filtered and washed with sat $NaHCO_3$, water and finally with CH_2Cl_2. Pure ISRIB standard **4** (110.2 mg) was obtained as a white solid (0.244 mmol, 67% yield).

Characterization:

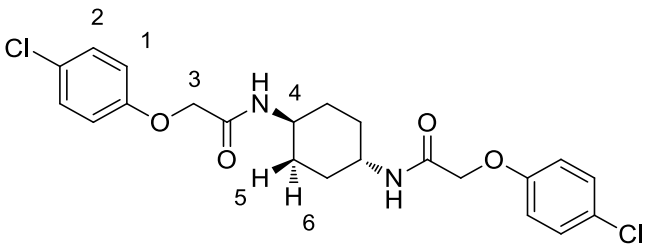

^{1}H NMR (400 MHz, DMSO): δ (ppm) 7.95 (d, 2H, J = 8.1 Hz, NH), 7.34 (d, 4H, J = 8.9 Hz, H2), 6.97 (d, 4H, J = 8.9 Hz, H1), 4.45 (s, 4H, H3), 3.59 (bs, 2H, H4), 1.77 (d, 4H, J = 6.0 Hz, H5), 1.34 (dd, 4H J = 10.6, 9.1 Hz, H6).

The ^{1}H-NMR spectrum was consistent with those reported in literature [57].

2.5.6 (E)-N,N'-((1r,4r)-cyclohexane-1,4-diyl)bis(2-(3-((E)-(2-carbamimidoylhydrazono)methyl)-4-chlorophenoxy)acetamide) dihydrochloride 20

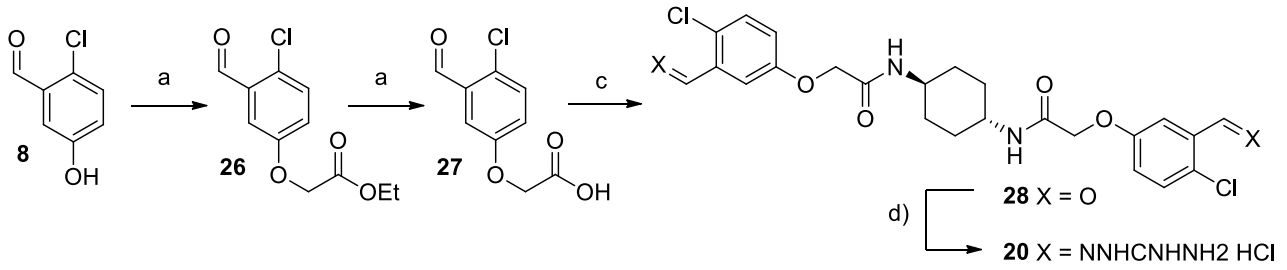

a) ethyl chloroacetate, K_2CO_3, dry CH_3CN, 75°C, 20 hrs, **80%**; b) [1M] $NaOH_{aq}$,THF, 50°C, 1hr, **81%**; c) **23**, EDCI, HOBt, TEA, 1:1 dry DCM/DMF, 25°C, 20hrs, **15%.** d) aminoguanidine-HCl, cat. HCl, EtOH, reflux, 16 hrs, **64%.**

Ethyl 2-(4-chloro-3-formylphenoxy)acetate 26

2-chloro-5-hydroxybenzaldehyde **8** (122.0 mg, 0.78 mmol, 1 eq) was dissolved in CH_3CN (4 mL). Then, chloroethyl acetate (143.5 mg, 1.17 mmol, 1.5 eq) and K_2CO_3 (161.2 mg, 1.17 mmol, 1.5 eq) were added under stirring. The reaction mixture was heated to 75°C and stirred for 20 hours (TLC monitoring: 85:15 hexane/EtOAc). The solvent was evaporated under reduced pressure and the crude was dissolved in AcOEt (30 mL). The organic phase was washed with aqueous sat. $NaHCO_3$ (2 x 10 mL) and with brine (10 mL). The organic phase was dried with Na_2SO_4, filtered and the solvent removed under reduced pressure. The crude product (197 mg) was purified by flash chromatography (eluant: 85:15 hexane/EtOAc), yielding 153.2 mg of pure ethyl 2-(4-chloro-3-formylphenoxy)acetate **26** as a slightly yellow solid (0.631 mmol, 80% yield).

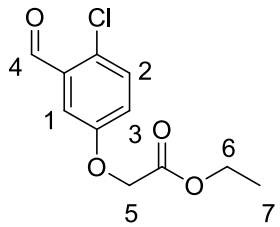

Characterization:

^{1}H NMR (400 MHz, DMSO): δ (ppm) 10.42 (s, 1H, H4), 7.37 (m, 2H, H1, H2), 7.16 (dd, 1H, J = 8.8, 3.1 Hz, H3), 4.65 (s, 2H, H5), 4.27 (q, 2H, J = 7.2 Hz, H6), 1.30 (m, 3H, H7).

2-(4-chloro-3-formylphenoxy)acetic acid 27

Ethyl 2-(4-chloro-3-formylphenoxy)acetate **26** (518.5 mg, 2.126 mmol, 1 eq) was dissolved in THF (5 mL), then [1M] NaOH (4.5 mL, 4.5 mmol, 2 eq) was added under stirring. The reaction mixture was heated to 50 °C and stirred for 1 hour (TLC monitoring: 9:1 hexane/AcOEt). THF was then evaporated under reduced pressure, and the aqueous solution was acidified with with [1M] HCl under stirring until pH 2. The resulting precipitate was filtered, washed with H_2O (10 mL) and with Et_2O (10 mL), yielding 340 mg of pure 2-(4-chloro-3-formylphenoxy)acetic acid **27** as a white solid (1.701 mmol, 81% yield).

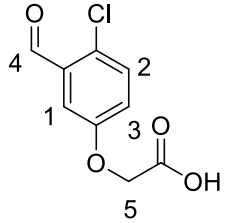

Characterization:

^{1}H NMR (400 MHz, DMSO): δ (ppm) 10.29 (s, 1H, H4), 7.55 (dd, 1H, *J* = 8.8, 1.4 Hz, H3), 7.31 (m, 2H, H1, H2), 4.80 (s, 2H, H5).

N,N'-((1r,4r)-cyclohexane-1,4-diyl)bis(2-(4-chloro-3-formylphenoxy)acetamide) 28

2-(4-chloro-3-formylphenoxy)acetic acid **27** (238 mg, 1.109 mmol, 2.2 eq) was suspended in a 1:1 mixture of dry CH_2Cl_2 and dry DMF (9 mL), under N_2, and TEA (210 µL, 1.512 mmol, 3 eq) was added. EDCI (231.9 mg, 1.210 mmol, 2.4 eq) and HOBt (163.51 mg, 1.210 mmol, 2.4 eq) were rapidly added to the homogeneous solution under stirring, and the reaction mixture was stirred at RT for 10 minutes. Then, trans-1,4-cyclohexanediamine **23** (57.6 mg, 0.504 mmol, 1 eq) was added. The resulting solution was stirred for 20 hours (TLC monitoring: 95:5 CH_2Cl_2/MeOH). Then, CH_2Cl_2 was removed, the oil was suspended in [1M] HCl, filtered and washed with sat $NaHCO_3$ and water. The crude product (168 mg) was purified by flash chromatography (eluant: AcOEt/MeOH from 100:0 to 9:1), yielding 37.2 mg of pure N,N'-((1r,4r)-cyclohexane-1,4-diyl)bis(2-(4-chloro-3-formylphenoxy)acetamide) **28** as a white solid (0.075 mmol, 15% yield). The compound has not been characterized due to its extreme insolubility in any solvent.

N,N'-((1r,4r)-cyclohexane-1,4-diyl)bis(2-(3-(((2-carbamimidoylhydrazono)methyl)-4-chlorophenoxy)acetamide) dihydrochloride 20

N,N'-((1r,4r)-cyclohexane-1,4-diyl)bis(2-(4-chloro-3-formylphenoxy)acetamide) **28** (24.7 mg, 0.049 mmol, 1 eq) was dissolved in absolute EtOH (2 mL). Then, aminoguanidine hydrochloride (10.76 mg, 0.097 mmol, 2 eq) was added under stirring. After the addition of cat. [1M] HCl (2 drops), the reaction mixture was heated to 80°C and stirred for 16 hours. After cooling to rt, the resulting precipitate was filtered, washed with absolute EtOH (5 mL) and with Et_2O (5 mL), yielding 22.1 mg of pure symmetrical sephin1-ISRIB hybrid **20** as a white solid (0.032 mmol, 64% yield).

Characterization:

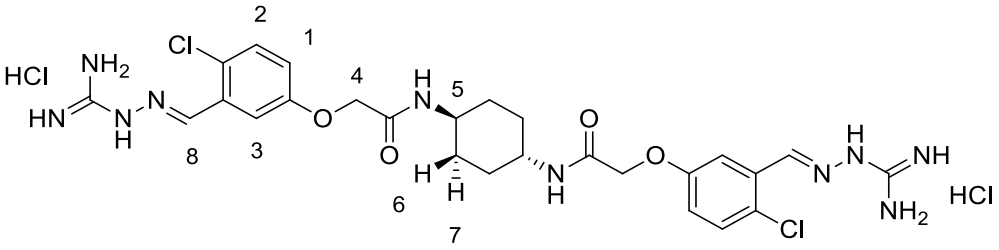

^{1}H NMR (400 MHz, DMSO): δ (ppm): 12.20 (s, 2H, NH), 8.50 (s, 2H, H8), 8.11 (d, *J* = 8.1 Hz, 2H, NHCO), 7.90 (bs, 6H, NH_2), 7.83 (d, *J* = 3.1 Hz, 2H, H3), 7.46 (d, *J* = 8.9 Hz, 2H, H2), 7.10 (dd, *J* = 8.9, 3.1 Hz, 2H, H1), 4.57 (s, 4H, H4), 3.60 (bs, 2H, H5), 1.78 (d, *J* = 6.0 Hz, 4H, H6), 1.36 (t, *J* = 9.9 Hz, 4H, H7).

^{13}C NMR (100 MHz, DMSO): δ (ppm): 166.8, 157.3, 155.4, 143.1, 131.7, 131.2, 125.9, 119.9, 112.2, 67.7, 47.4, 31.3.

HPLC/MS (ESI^+): 619.21 [$M+H^+$] (mass calculated for $C_{26}H_{32}Cl_2N_{10}O_4$: 618.20). Purity measured: 97.9%

2.5.7 Synthesis of 2-(4-((2-carbamimidoylhydrazono)methyl)-3-chlorophenoxy)-N-((1r,4r)-4-(2-(4-chlorophenoxy)acetamido)cyclohexyl)acetamide hydrochloride 21

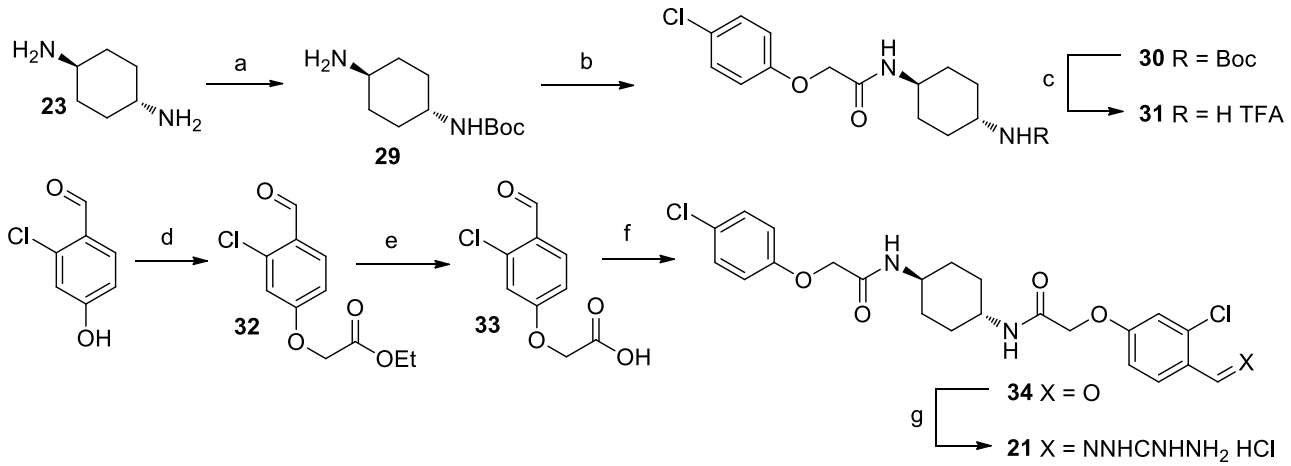

a) Boc_2O, TEA, dry $CHCl_3$, 25°C, 20 hrs, **53%**; b) **25**, EDCI, HOBt, TEA, 1:1 DCM/DMF, 25°C, 24 hrs, **83%**; c) triethylsilane, TFA, H_2O/DCM, 25°C, 16 hrs, **98%;** d) ethyl chloroacetate, K_2CO_3, dry CH_3CN, 75°C, 20 hrs, **75%**; e) [1M] NaOHaq.,THF, 50°C, 1 hr, **80%**; f) **31**, EDCI, HOBt, TEA, DCM/DMF 1:1, 25°C, 20 hrs, **11%**; g) aminoguanidine HCl, cat. HCl, EtOH, reflux, 16 hrs, **65%.**

tert-Butyl ((1r,4r)-4-aminocyclohexyl)carbamate 29

Trans-1,4-cyclohexandiamine **23** (500 mg, 4.378 mmol, 1 eq) was dissolved in $CHCl_3$ (18 mL), and TEA (0.608 mL, 2 eq) was added under stirring. The slow addition of Boc_2O (477.75 mg, 2.189 mmol, 1 eq) was carried out via a syringe in 1 hour under stirring. The reaction mixture stirred for 20 hours at rt (TLC monitoring: 9:1 CH_2Cl_2/MeOH). The solvent was evaporated under reduced pressure, the reaction mixture was diluted with a 5% citric acid solution (20 mL) and washed with CH_2Cl_2 (20 mL). The aqueous phase was basified to pH 10 and extracted with CH_2Cl_2 (3 x 15 mL). The collected organic phases were dried with Na_2SO_4, filtered and the solvent removed under reduced pressure. The crude product (490 mg) was purified by flash chromatography (eluant: CH_2Cl_2/MeOH from 9:1 to 85:15), yielding 433.6 mg of pure tert-butyl ((1r,4r)-4-aminocyclohexyl)carbamate **29** as a white solid (2.32 mmol, 53% yield).

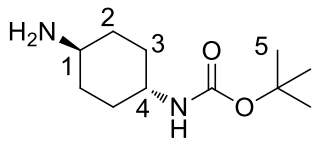

Characterization:

^{1}H NMR (400 MHz, $CDCl_3$): δ (ppm) 4.39 (s, 1H, NH), 3.39 (s, 1H, H1), 2.64 (s, 1H, H4), 2.00 (d, *J* = 10.6 Hz, 2H, H3), 1.87 (m, 2H, H3), 1.60 (s, 2H, NH_2), 1.45 (s, 9H, H5), 1.17 (m, 4H, H2).

The ^{1}H-NMR spectrum was consistent with those reported in literature [73].

tert-Butyl ((1r,4r)-4-(2-(4-chlorophenoxy)acetamido)cyclohexyl)carbamate 30

2-(4-chlorophenoxy)acetic acid **25** (239.30 mg, 1.117 mmol, 1 eq) was dissolved in a 2:1 CH_2Cl_2/DMF mixture (18 mL), and tert-butyl ((1r,4r)-4-aminocyclohexyl)carbamate **29** (229.3 mg, 1.229 mmol, 1.1 eq) was added under stirring. EDCI (321.19 mg, 1.676 mmol, 1.5 eq), HOBt (226.39 mg, 1.676 mmol, 1.5 eq) and TEA (466 µL, 3.351 mmol) were sequentially added and the reaction mixture was stirred at rt for 24 hours (TLC monitoring: 9:1 CH_2Cl_2/MeOH). Then, $CH_2Cl_2$was evaporated under reduced pressure, H_2O (20 mL) was added and the resulting precipitate was filtered under vacuum. The solid was washed with a 5% citric acid solution (15 mL), a sat. $NaHCO_3$ solution (15 mL) and a 1/1 CH_2Cl_2/Et_2O mixture (10 mL), yielding 355.3 mg of pure tert-butyl ((1r,4r)-4-(2-(4-chlorophenoxy)acetamido)cyclohexyl)carbamate **30** as a white solid (0.929 mmol, 83% yield).

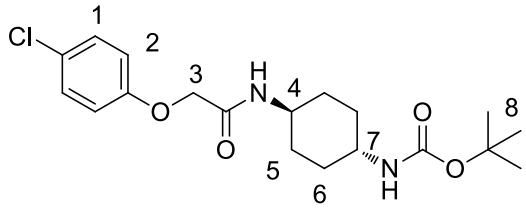

Characterization:

^{1}H NMR (400 MHz, DMSO): δ 7.93 (d, *J* = 7.9 Hz, 1H, NH), 7.34 (d, *J* = 8.9 Hz, 2H, H1), 6.97 (d, *J* = 9.0 Hz, 2H, H2), 6.72 (d, *J* = 7.8 Hz, 1H, NH), 4.44 (s, 2H, H3), 3.54 (m, 1H, H4), 3.17 (m, 1H, H7), 1.75 (t, *J* = 13.2 Hz, 4H), 1.38 (s, 9H, H8), 1.27 (m, 4H).

The ^{1}H-NMR spectrum was consistent with those reported in literature [73].

N-((1r,4r)-4-aminocyclohexyl)-2-(4-chlorophenoxy)acetamide 2,2,2-trifluoroacetate 31

Et_3SiH (0.088 mL, 0.57 mmol, 1.45 eq), TFA (0.902 mL, 11.8 mmol, 30 eq) and H_2O (60 µL) were sequentially added under stirring to a suspension of **30** (150 mg, 0.393 mmol, 1 eq) in CH_2Cl_2 (3 mL). The resulting solution was stirred at 25°C for 16 hours (TLC monitoring: 85:15 CH_2Cl_2/MeOH). Then, the solvent was evaporated under reduced pressure and the crude was diluted with Et_2O (10 mL). After 10 minutes' stirring, the precipitate was filtered and washed with Et_2O, yielding 152.1 mg of pure N-((1r,4r)-4-aminocyclohexyl)-2-(4-chlorophenoxy)acetamide 2,2,2-trifluoroacetate **31** (0.384 mmol, 97% yield).

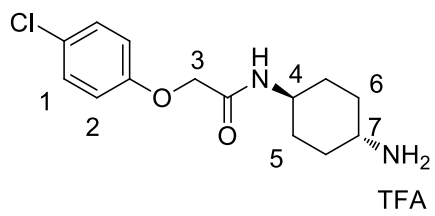

Characterization:

^{1}H NMR (400 MHz, DMSO): δ (ppm) 7.99 (d, *J* = 8.0 Hz, 1H, NH), 7.84 (bs, 2H, NH2), 7.35 (m, 2H, H1), 6.97 (m, 2H, H2), 4.46 (s, 2H, H3), 3.59 (bs, 1H, H4), 2.97 (bs, 1H, H7), 1.87 (m, 4H, H5), 1.35 (m, 4H, H6).

The ^{1}H-NMR spectrum was consistent with those reported in literature [73].

Ethyl 2-(3-chloro-4-formylphenoxy)acetate 32

2-Chloro-4-hydroxy benzaldehyde (500 mg, 3.192 mmol, 1 eq) was dissolved in CH_3CN (8 mL). Then, ethyl chloroacetate (604.4 mg, 4.748 mmol, 1.5 eq) and K_2CO_3 (690.4 mg, 4.748 mmol, 1.5 eq) were added under stirring. The reaction mixture was heated to 75°C and stirred for 20 hours (TLC monitoring: 85:15 hexane/EtOAc). The solvent was evaporated under reduced pressure and the crude was dissolved in AcOEt (30 mL). The organic phase was washed with aqueous sat. $NaHCO_3$ (2 x 10 mL) and with brine (10 mL). The organic phase was dried with Na_2SO_4, filtered and the solvent removed under reduced pressure. The crude product (690 mg) was purified by flash chromatography (eluant: 85:15 hexane/EtOAc), yielding 578 mg of pure ethyl 2-(3-chloro-4-formylphenoxy)acetate **32** as a yellow solid (2.339 mmol, 75% yield).

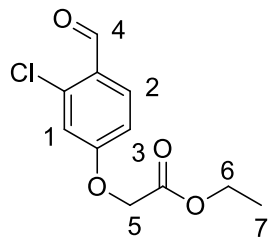

Characterization:

^{1}H NMR (400 MHz, $CDCl_3$): δ 10.36 (s, 1H, H4), 7.93 (d, *J* = 8.7 Hz, 1H, H2), 6.97 (d, *J* = 2.4 Hz, 1H, H1), 6.92 (dd, *J* = 8.7, 2.3 Hz, 1H, H3), 4.71 (s, 2H, H5), 4.31 (q, *J* = 7.1 Hz, 2H, H6), 1.33 (t, *J* = 7.1 Hz, 3H, H7).

2-(3-chloro-4-formylphenoxy)acetic acid 33

Ethyl 2-(3-chloro-4-formylphenoxy)acetate **32** (570.1 mg, 2.339 mmol, 1 eq) was dissolved in THF (5 mL), then [1M] NaOH (5 mL, 1.5 eq) was added under stirring. The reaction mixture was heated to 50 °C and stirred for 1 hour (TLC monitoring: 85:15 hexane/AcOEt). THF was evaporated under reduced pressure, the aqueous solution was acidified with 1M HCl_{aq} under stirring until pH 2. The resulting precipitate was filtered, washed with H_2O (10 mL) and Et_2O (10 mL), yielding 401.6 mg of pure 2-(3-chloro-4-formylphenoxy)acetic acid **33** as a light yellow solid (1.871 mmol, 80% yield).

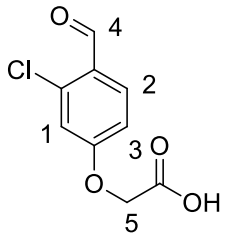

Characterization:

^{1}H NMR (400 MHz, DMSO): δ (ppm) 10.20 (s, 1H, H5), 7.84 (d, 1H, *J* = 8.8 Hz, H3), 7.19 (d, 1H, J = 2.4 Hz, H4), 7.08 (dd, 1H, J = 8.8 Hz, J = 2.4 Hz, H2), 4.89 (s, 2H, H1).

2-(3-chloro-4-formylphenoxy)-N-((1r,4r)-4-(2-(4-chlorophenoxy)acetamido)cyclohexyl)acetamide 34

Under N_2 atmosphere, N-((1r,4r)-4-aminocyclohexyl)-2-(4-chlorophenoxy)acetamide 2,2,2-trifluoroacetate **31** (203.4 mg, 0.513 mmol, 1 eq) was dissolved in a 1/1 mixture of dry CH_2Cl_2/DMF (6 mL), and 2-(3-chloro-4-formylphenoxy)acetic acid **33** (121.1 mg, 0.564 mmol, 1.1 eq) was added under stirring. EDCI (147.5 mg, 0.770 mmol, 1.5 eq), HOBt (104.0 mg, 0.770 mmol, 1.5 eq) and TEA (428 µL, 3.078 mmol) were sequentially added

under stirring. The reaction mixture was stirred at rt for 20 hours (TLC monitoring: 9:1 CH_2Cl_2/MeOH). $CH_2Cl_2$was evaporated under reduced pressure, the solution was diluted with H_2O (10 mL) under stirring, and the resulting precipitate was filtered under vacuum. The solid was sequentially washed with 5% HCl (10 mL), sat. $NaHCO_3$ (10 mL) and Et_2O (10 mL). The crude product (95 mg) was purified by flash chromatography (eluant: 98:2 AcOEt/MeOH), yielding 28.1 mg of pure 2-(3-chloro-4-formylphenoxy)-N-((1r,4r)-4-(2-(4-chlorophenoxy)acetamido)cyclohexyl)acetamide **34** as a white solid (0.059 mmol, 11% yield).

Characterization:

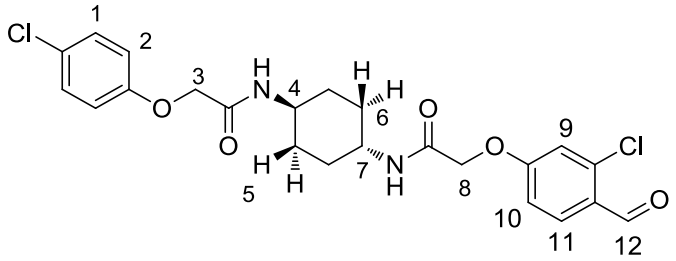

^{1}H NMR (400 MHz, $CDCl_3$): δ (ppm) 10.38 (s, 1H, H12), 7.96 (d, J = 8.7 Hz, 1H, H11), 7.30 (d, J = 9.0 Hz, 2H, H1), 7.03 (d, J = 2.3 Hz, 1H, H9), 6.97 (dd, J = 8.6, 2.0 Hz, 1H, H10), 6.88 (d, J = 9.0 Hz, 2H, H2), 6.36 (d, J = 8.2 Hz, 1H, NH), 6.27 (d, J = 8.1 Hz, 1H, NH), 4.55 (s, 2H, H3 or H8), 4.46 (s, 2H, H8 or H3), 3.89 (s, 2H, H4, H7), 2.09 (d, J = 6.1 Hz, 4H, H5,H6), 1.38 (t, J = 9.3 Hz, 4H, H5, H6).

^{13}C NMR (from HSQC, $CDCl_3$): δ (ppm) 188.1, 131.3, 129.7, 116.3, 116.0, 113.8, 67.6, 67.3, 47.2, 31.4, 31.3

2-(4-((2-carbamimidoylhydrazono)methyl)-3-chlorophenoxy)-N-((1r,4r)-4-(2-(4-chlorophenoxy)acetamido)cyclohexyl)acetamide hydrochloride 21

2-(3-chloro-4-formylphenoxy)-N-((1r,4r)-4-(2-(4-chlorophenoxy)acetamido)cyclohexyl)acetamide **34** (28.1 mg, 0.058 mmol, 1 eq) was dissolved in absolute EtOH (3 mL). Then, aminoguanidine hydrochloride (6.5 mg, 0.058 mmol, 1 eq) was added. After the addition of cat. [1M] HCl (1 drop), the reaction mixture was heated to reflux and stirred for 16 hours. After cooling to rt, the resulting precipitate was filtered, washed with absolute EtOH (5 mL), $CHCl_3$ (5 mL) and Et_2O (5 mL), yielding 20.5 mg of pure asymmetrical para-substituted sephin1-ISRIB hybrid **21** as a white solid (0.038 mmol, 65% yield).

Characterization:

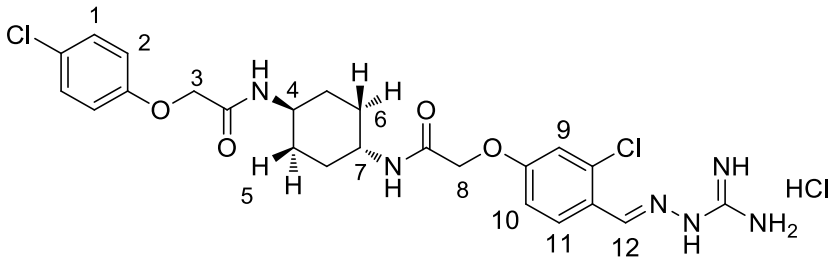

^{1}H NMR (400 MHz, DMSO): δ 12.02 (s, 1H, NH) 8.45 (s, 1H, H12), 8.23 (d, 1H, *J* = 8.9 Hz, H11), 8.03 (d, 1H, J = 8.1 Hz, NH), 7.96 (d, 1H, J = 8.1 Hz, NH), 7.67 (bs, 3H, NH), 7.34 (d, 2H, H1), 7.34 (d, J = 9.2 Hz, 2H, H1) 7.11 (d, 1H, *J* = 2.4 Hz, H9), 7.03 (dd, 1H, *J* = 8.9, 2.4 Hz, H10), 6.98 (d, 2H, *J* = 9.2 Hz, H2), 4.58 (s, 2H, H3), 4.46 (s, 2H, H8), 3.60 (bs, 2H, H4, H7), 1.79 (d, 4H, *J* = 6.1 Hz, H5), 1.35 (dd, 4H, *J* = 10.8, 9.0 Hz, H6).

^{13}C NMR (100 MHz, DMSO): δ (ppm) 166.5, 166.1, 160.0, 156.7, 155.4, 142.5, 134.1, 129.2, 128.7, 124.8, 123.8, 115.4, 114.9, 114.1, 67.2, 47.0, 30.9.

HPLC/MS (ESI$^+$): 538.41 [M+H$^+$] (mass calculated for $C_{24}H_{28}Cl_2N_6O_4$: 535.42). Purity measured: 98.8%.

2.5.8 Synthesis of 2-(3-((2-carbamimidoylhydrazono)methyl)-4-chlorophenoxy)-N-((1r,4r)-4-(2-(4-chlorophenoxy)acetamido)cyclohexyl)acetamide hydrochloride 22

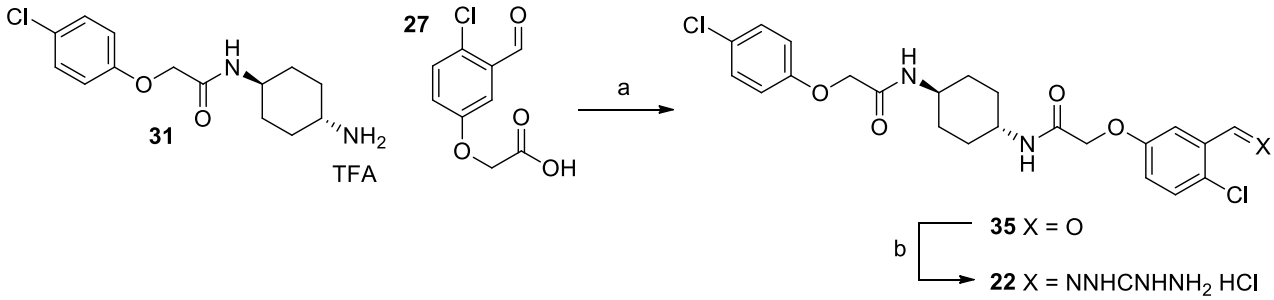

a) EDCI, HOBt, TEA, DCM/DMF 1:1, 25°C, 20 hrs, **40%**; g) aminoguanidine HCl, cat. HCl, EtOH, reflux, 16 hrs, **76%.**

2-(4-chloro-3-formylphenoxy)-N-((1r,4r)-4-(2-(4-chlorophenoxy)acetamido)cyclohexyl)acetamide 35

Under N_2 atmosphere, aminoamide **31** (146.5 mg, 0.368 mmol, 1 eq) was dissolved in a 1:1mixture of dry CH_2Cl_2/DMF (5 mL), and chloroformyl phenoxyacetic acid **27** (87.0 mg, 0.405 mmol, 1.1 eq) was added under stirring. EDCI (74.6 mg, 0.552 mmol, 1.5 eq), HOBt (105.9 mg, 0.552 mmol, 1.5 eq) and TEA (466 µL, 9 eq) were then sequentially added under stirring. The reaction mixture was stirred at rt for 20 hours (TLC monitoring: 9:1 CH_2Cl_2/MeOH). Then, $CH_2Cl_2$was evaporated under reduced pressure, H_2O (10 mL) was added and the resulting precipitate was filtered under vacuum. The solid was sequentially washed with a 5% HCl solution (10 mL), a sat. $NaHCO_3$ solution (10 mL) and Et_2O (10 mL). The crude product (174 mg) was filtered to a small path of silice (eluant: AcOEt/MeOH from 9:1), yielding 68.1 mg of pure 2-(4-chloro-3-formylphenoxy)-N-((1r,4r)-4-(2-(4-chlorophenoxy)acetamido)cyclohexyl)acetamide **35** as a white solid (0.142 mmol, 40% yield).

Characterization:

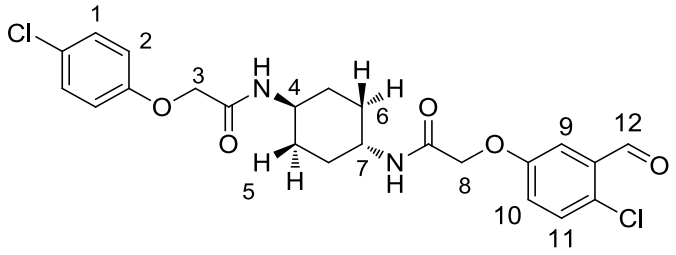

^{1}H NMR (400 MHz, DMSO-d6): δ (ppm) 10.30 (s, 1H, H12), 8.05 (d, J = 8.1 Hz, 1H, NH), 7.95 (d, J = 8.1 Hz, 1H, NH), 7.57 (d, J = 8.8 Hz, 1H, H11), 7.41 – 7.28 (m, 4H, H9, H10, H1), 6.97 (d, J = 9.0 Hz, 2H, H2), 4.56 (s, 2H, H3 or H8), 4.46 (s, 2H, H8 or H3), 3.60 (s, 2H, H4, H7), 1.77 (d, J = 6.0 Hz, 4H, H5, H6), 1.34 (dd, J = 10.8, 9.0 Hz, 4H, H5, H6).

^{13}C NMR (from HSQC, DMSO-d6): δ (ppm) 189.9, 132.0, 129.3, 123.2, 117.0, 114.6, 67.6, 67.5, 47.3, 31.3, 31.2.

2-(3-((2-carbamimidoylhydrazono)methyl)-4-chlorophenoxy)-N-((1r,4r)-4-(2-(4-chlorophenoxy)acetamido)cyclohexyl)acetamide hydrochloride 22

2-(4-chloro-3-formylphenoxy)-N-((1r,4r)-4-(2-(4-chlorophenoxy)acetamido)cyclohexyl)acetamide **35** (52.0 mg, 0.108 mmol, 1 eq) was dissolved in hot absolute EtOH (3 mL). Then, aminoguanidine hydrochloride (10.81 mg, 0.098 mmol, 0.9 eq) was added. After the addition of cat. [1M] HCl (2 drops), the reaction mixture was heated to reflux and stirred for 16 hours. After cooling at rt, the precipitate was filtered, sequentially washed with EtOH (5 mL), CH_2Cl_2 (5 mL) and Et_2O (5 mL), yielding 43.5 mg of pure 2-(3-((2-carbamimidoylhydrazono)methyl)-4-chlorophenoxy)-N-((1r,4r)-4-(2-(4-chlorophenoxy)acetamido)cyclohexyl)acetamide hydrochloride **22** as a white solid (0.076 mmol, 76% yield).

Characterization:

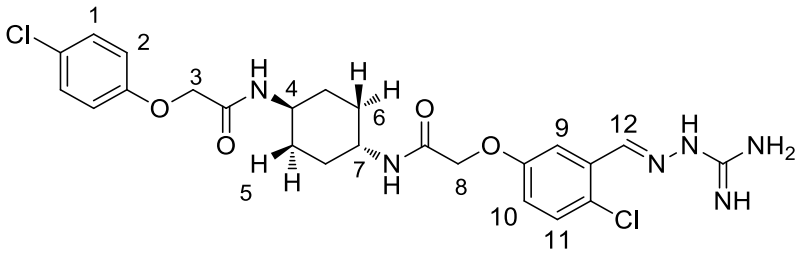

^{1}H NMR (400 MHz, DMSO-d6): δ 12.20 (s, 1H, NH), 8.50 (s, 1H, H12), 8.11 (d, *J* = 8.1 Hz, 1H, NH), 7.98 (d, *J* = 8.1 Hz, 1H, NH), 7.83 (bs, 3H, NH), 7.82 (d, *J* = 3.0 Hz, 1H, H3), 7.45 (d, *J* = 8.9 Hz, 1H, H11), 7.34 (d, *J* = 8.9 Hz, 2H, H1), 7.08 (dd, *J* = 8.9, 3.1 Hz, 1H, H10), 6.97 (d, *J* = 9.0 Hz, 2H, H2), 4.57 (s, 2H, H3 or H8), 4.45 (s, 2H, H8 or H3), 3.60 (bs, 2H, H4, H7), 1.78 (d, *J* = 6.0 Hz, 4H, H5), 1.35 (t, J = 9.5 Hz, 4H, H6).

^{13}C NMR (100 MHz, DMSO-d6): δ (ppm) 166.9, 166.8, 157.2, 157.1, 155.7, 143.0, 131.7, 131.2, 129.7, 125.9, 125.2, 119.8, 117.0, 112.7, 67.6, 47.4, 31.3.

HPLC/MS (ESI$^+$): 538.41 [M+H$^+$] (mass calculated for $C_{24}H_{28}Cl_2N_6O_4$: 535.42). Purity measured: 98.6%

2.6 BIBLIOGRAPHY

[1]. Cullinan, S.B.; Diehl, J.A. Coordination of ER and oxidative stress signaling: The PERK/Nrf2 signaling pathway. *Int. J. Biochem. Cell Biol*. **2006**, 38, 317-332.

[2]. Kaufman, R.J.; Cao, S. Inositol-requiring 1/X-box-binding protein 1 is a regulatory hub that links endoplasmic reticulum homeostasis with innate immunity and metabolism. *Embo Mol. Med*. **2010**, 2, 189-192.

[3]. Wang, Y.; Shen, J.; Arenzana, N.; Tirasophon, W.; Kaufman, R.J.; Prywes, R. Activation of ATF6 and an ATF6 DNA binding site by the endoplasmic reticulum stress response. *J. Biol. Chem*. **2000**, 275, 27013-27020.

[4]. Lai, E.; Teodoro, T.; Volchuk, A. Endoplasmic reticulum stress: signalling the unfolded protein response. *Physiol*. **2007**, 22, 193–201.

[5]. Hinnebusch, A.G. Translational regulation of GCN4 and the general amino acid control of yeast. *Annu. Rev. Microbiol.* **2006**, 59, 407–450.

[6]. Chang, R.C., Yu, M.S., Lai CS. Significance of molecular signaling for protein translation control in neurodegenerative diseases. *Neurosignals* **2006**, 15, 249–258.

[7]. Nika, J.; Rippel, S.; Hannig, E.M. Biochemical analysis of the eIF2beta gamma complex reveals a structural function for eIF2alpha in catalyzed nucleotide exchange. *J. Biol. Chem.* **2001**, 276, 1051–1056.

[8]. Oakes, S.A.; Papa, F.R. The role of endoplasmic reticulum stress in human pathology. *Annu. Rev. Pathol*. **2015**, 10, 173–194.

[9]. Roussel, B.D.; Kruppa, A.J.; Lomas, D.A.; Marciniak, S.J. Endoplasmic reticulum dysfunction in neurological disease. *Lancet Neurol*. **2013**, 12, 105–118.

[10]. Harding, H.P.; *et al.* translation initiation controls stress-induced gene expression in mammalian cells. *Mol. Cell* **2000**, 6, 1099–1108.

[11]. Blais, J.D.; et al. Activating transcription factor 4 is translationally regulated by hypoxic stress. *Mol. Cell. Biol*. **2004**, 24, 7469–7482.

[12]. Novoa, I.; Zeng, H.; Harding, H.P.; Ron, D. Feedback inhibition of the unfolded protein response by GADD34-mediated dephosphorylation of eIF2alpha. *J. Cell. Biol*. **2001**, 153, 1011–1022.

[13]. Abdulkarim, B.; et al. A missense mutation in PPP1R15B causes a syndrome including diabetes, short stature, and microcephaly. *Diabetes* **2015**, 64, 3951–3962.

[14]. Delepine, M.; et al. EIF2AK3, encoding translation initiation factor2-alpha kinase 3, is mutated in patients with Wolcott-Rallison syndrome. *Nat. Genet*. **2000**, 25, 406–409.

[15]. Biason-Lauber, A.; Lang-Muritano, M.; Vaccaro, T.; Schoenle, E.J. Loss of kinase activity in a patient with Wolcott- Rallison syndrome caused by a novel mutation in the EIF2AK3 gene. *Diabetes* **2002**, 51, 2301–2305.

[16]. Leitman, J.; et al. ER stress-induced eIF2-alpha phosphorylation underlies sensitivity of striatal neurons to pathogenic huntingtin. *PLoS One* **2014**, 9, e90803.

[17]. Hetz, C.; Mollereau, B. Disturbance of endoplasmic reticulum proteostasis in neurodegenerative diseases. *Nat. Rev. Neurosci*. **2014**, 15, 233–249.

[18]. Hoozemans, J.J.; et al. The unfolded protein response is activated in pretangle neurons in Alzheimer's disease hippocampus. *Am. J. Pathol*. **2009**, 174, 1241–1251.

[19]. O'Connor, T.; et al. Phosphorylation of the translation initiation factor eI- F2alpha increases BACE1 levels and promotes amyloidogenesis. *Neuron* **2008**, 60, 988–1009.

[20]. Hoozemans, J.J.; et al. Activation of the unfolded protein response in Parkinson's disease. *Biochem. Biophys. Res. Commun*. **2007**, 354, 707–711.

[21]. Carnemolla, A.; et al. Rrs1 is involved in endoplasmic reticulum stress response in Huntington disease. *J. Biol. Chem*. **2009**, 284, 18167–18173.
[22]. Kohler, C.; Dinekov, M.; Gotz, J. Granulovacuolar degeneration and unfolded protein response in mouse models of tauopathy and Abeta amyloidosis. *Neurobiol. Dis*. **2014**, 71, 169–179.
[23]. Cho, K.J.; et al. Inhibition of apoptosis signal-regulating kinase 1 reduces endoplasmic reticulum stress and nuclear huntingtin fragments in a mouse model of Huntington disease. *Neuroscience* **2009**, 163, 1128–1134.
[24]. Prell, T.; Lautenschläger, J.; Witte, O.W.; Carri, M.T.; Grosskreutz, J. The unfolded protein response in models of human mutant G93A amyotrophic lateral sclerosis. *Eur. J. Neurosci*. 2012, 35, 652–660.
[25]. Bellucci, A.; et al. Induction of the unfolded protein response by alpha-synuclein in experimental models of Parkinson's disease. *J. Neurochem*. **2011**, 116, 588–605.
[26]. Moreno, J.A.; et al. Sustained translational repression by eIF2alpha-P mediates prion neurodegeneration. *Nature* **2012**, 485, 507–511.
[27]. Wang, L.; Popko, B.; Tixier, E.; Roos, R.P. Guanabenz, which enhances the unfolded protein response, ameliorates mutant SOD1-induced amyotrophic lateral sclerosis. *Neurobiol. Dis*. **2014**, 71, 317–324.
[28]. Das, I.; et al. Preventing proteostasis diseases by selective inhibition of a phosphatase regulatory subunit. *Science* **2015**, 348, 239–242.
[29]. D'Antonio, M.; et al. Resetting translational homeostasis restores myelination in Charcot-Marie-Tooth disease type 1B mice. *J. Exp. Med*. **2013**, 210, 821–838.
[30]. Taylor, R.C. Aging and the UPR(ER). *Brain Res*. **2016**, 1648, 588-593.
[31]. Boyce, M.; et al. A selective inhibitor of eIF2α dephosphorylation protects cells from ER stress. *Science* **2005**, 307, 935-939.
[32]. Tsaytler, P.; Bertolotti, A. Exploiting the selectivity of protein phosphatase 1 for pharmacological intervention. *FEBS J*. **2013**, 280, 766-770.
[33]. Huang, X.; et al. Salubrinal attenuates β-amyloid-induced neuronal death and microglial activation by inhibition of the NF-κB pathway. *Neurobiol. Aging* **2012**, 33, 1007.e9-1007.e17.
[34]. Hamamura, K.; Lin, C.-C.; Yokota, H. Salubrinal reduces expression and activity of MMP13 in chondrocytes. *Osteoarthr. Cartil.* **2013**, 21, 764–772.
[35]. Kessel, D. Protection of Bcl-2 by salubrinal. *Biochem. Biophys. Res. Commun.* **2006**, 346, 1320–1323.
[36]. Colla, E.; et al. Endoplasmic reticulum stress is important for the manifestations of a-synucleinopathy in vivo. *J. Neurosci*. **2012**, 32, 3306-3320.
[37]. Zhang, Y.J.; et al. Aggregation-prone c9FTD/ALS poly(GA) RAN-translated proteins cause neurotoxicity by inducing ER stress. *Acta Neuropathol*. **2014**, 128, 505–524.
[38]. Vaccaro A.; et al. Pharmacological reduction of ER stress protects against TDP-43 neuronal toxicity in vivo. *Neurobiol. Dis*. **2013**, 55, 64-75.
[39]. Ohri, S.S.; Hetman, M.; Whittemore, S.R. Restoring endoplasmic reticulum homeostasis improves functional recovery after spinal cord injury. *Neurobiol. Dis*. **2013**, 58, 29–37.
[40]. Jian, M.; et al. eIF2a dephosphorylation in basolateral amygdala mediates reconsolidation of drug memory. *J. Neurosci*. **2014**, 34, 10010-10021.
[41]. Holmes, B.; Brogden, R.N.; Heel, R.C.; Speight, T.M.; Avery, G.S. Guanabenz. A review of its pharmacodynamic properties and therapeutic efficacy in hypertension. *Drugs* **1983**, 26, 212-229.
[42]. Tsaytler, P.; Harding, H.P.; Ron, D.; Bertolotti, A. Selective inhibition of a regulatory subunit of protein phosphatase 1 restores proteostasis. *Science* **2011**, 332, 91–94.
[43]. Barbezier, N.; et al. Antiprion drugs 6-aminophenanthridine and guanabenz reduce PABPN1 toxicity and aggregation in oculopharyngeal muscular dystrophy. *EMBO Mol. Med.* **2011**, 3, 35–49.

[44]. Mockel, A.; et al. Pharmacological modulation of the retinal unfolded protein response in Bardet-Biedl syndrome reduces apoptosis and preserves light detection ability. *J. Biol. Chem*. **2012**, 287, 37483-37494.
[45]. Way, S.W.; et al. Pharmaceutical integrated stress response enhancement protects oligodendrocytes and provides a potential multiple sclerosis therapeutic. *Nat. Commun*. **2015**, 6, 6532.
[46]. Jiang, H.Q.; et al. Guanabenz delays the onset of disease symptoms, extends lifespan, improves motor performance and attenuates motor neuron loss in the SOD1 G93A mouse model of amyotrophic lateral sclerosis. *Neuroscience* **2014**, 277, 132-138.
[47]. Vieira, F.G.; et al. Guanabenz treatment accelerates disease in a mutant SOD1 mouse model of ALS. *PLoS One* **2015**, 10, e135570.
[48]. Hall, A.H.; Smolinske, S.C.; Kulig, K.W.; Rumack, B.H. Guanabenz overdose. *Ann. Intern. Med*. **1985**, 102, 787–788.
[49]. Pakos-Zebrucka, K. et al. *EMBO Rep*. **2016**, 17, 1374–1395.
[50]. Hetz, C.; Chevet, E.; Harding, H.P. Targeting the unfolded protein response in disease. *Nat. Rev. Drug Discov*. **2013**, 12, 703-719.
[51]. Smith, H.L.; Mallucci, G.R. The unfolded protein response: mechanisms and therapy of neurodegeneration. *Brain* **2016**, 139, 2113-2121.
[52]. Stutzbach, L.D.; et al. The unfolded protein response is activated in disease-affected brain regions in progressive supranuclear palsy and Alzheimer's disease. *Acta Neuropathol. Commun.* **2013**,6, 1-31.
[53]. Nijholt, D.A.; van Haastert, E.S.; Rozemuller, A.J.; Scheper, W.; Hoozemans, J.J. The unfolded protein response is associated with early tau pathology in the hippocampus of tauopathies. *J. Pathol*. **2012**, 226, 693-702
[54]. Radford, H.; Moreno, J.A.; Verity, N.; Halliday, M.; Mallucci, G.R. PERK inhibition prevents tau-mediated neurodegeneration in a mouse model of frontotemporal dementia. *Acta Neuropathol*. **2015**, 130, 633-642.
[55]. Pavitt, G.D. eIF2B, a mediator of general and gene-specific translational control". *Biochem. Soc. Trans*. **2005**, 33, 1487–1492.
[56]. Kashiwagi, K.; Ito, T.; Yokoyama, S. Crystal structure of eIF2B and insights into eIF2–eIF2B interactions. *FEBS J*. **2017**, 284, 868-874.
[57]. Sidrauski, C.; et al. Parmaceutical brake-release of mRNA translation enhances cognitive memory. *Elife* **2013**, 2, e00498.
[58]. Sekine, Y.; et al. Mutations in a translation initiation factor identify the target of a memory-enhancing compound *Science* **2015**, 348, 1027–1030.
[59]. Sidrauski, C.; et al. Pharmacological dimerization and activation of the exchange factor eIF2B antagonizes the integrated stress response *Elife* **2015**, 4, e07314.
[60]. Tsai, J.C.; et al. Structure of the nucleotide exchange factor eIF2B reveals mechanism of memory-enhancing molecule. *Science* **2018,** 359, eaaq0939.
[61]. Zyryanova, A.F.; et al. Binding of ISRIB reveals a regulatory site in the nucleotide exchange factor eIF2B. *Science,* **2018**, 359, 1533–1536.
[62]. Hosoi, T.; Kakimoto, M.; Tanaka, K.; Nomura, J.; Ozawa, K. Unique pharmacological property of ISRIB in inhibition of A-induced neuronal cell death. *J. Pharmacol. Sci*., **2016**, 131, 292-295.
[63]. Chou, A.; et al. Inhibition of the integrated stress response reverses cognitive deficits after traumatic brain injury. *Proc. Natl. Acad. Sci. USA* **2017**, E6420-E6426.
[64]. Poole, K. Resistance to β-lactam antibiotics. *Cell. Mol. Life Sci.* **2004**, 61, 2200-2223.
[65]. Wermuth, C.G. Multitargeted drugs: the end of the "one-target-one-disease" philosophy? *Drug Discov. Today* **2004**, 9, 826-827

[66]. Larder, B.A.; Kemp, S.D.; Harrigan, P.R. Potential mechanism for sustained antiretroviral efficacy of AZT-3TC combination therapy. *Science* **1995**, 269, 696-699.

[67]. Duggan, S.T.; Chwieduk, C.M.; Curran, M.P.; Aliskiren. A review of its use as monotherapy and as combination therapy in the management of hypertension. *Drugs* **2010**, 70, 2011-2049.

[68]. *Drug-drug interactions, Second Edition*. Editor: A. D. Rodrigues. *CRC Press* **2008**, 768 pages.

[69]. Morphy, M.; Rankovic, R. Designed multiple ligands. An emerging drug discovery paradigm. *J. Med. Chem*. **2005**, 48, 6523-6543.

[70]. Chen, J.B.; et al. Design and synthesis of dual-action inhibitors targeting histone deacetylases and 3-hydroxy-3-methylglutaryl coenzyme A reductase for cancer treatment. *J. Med. Chem*. **2013**, 9, 56, 3645-3655.

[71]. Thaker, H.D.; et al. Synthetic mimics of antimicrobial peptides with immunomodulatory responses. *J. Am. Chem. Soc.* **2012**, 134, 11088-11091.

[72]. Wang, Z.; et al. Design, synthesis, and evaluation of orally available clioquinol- moracin M hybrids as multitarget-directed ligands for cognitive improvement in a rat model of neurodegeneration in Alzheimer's Disease. *J. Med. Chem.* **2015**, 58, 8616−8637.

[73]. Hearn, B.R.; et al. Structure–activity studies of bis-O-arylglycolamides: Inhibitors of the Integrated Stress Response. *ChemMedChem.* **2016**, 11, 870 – 880.

[74]. Gunosewoyo, H.; et al. Cubyl amides: Novel $P2X_7$ receptor antagonists. *Bioorg. Med. Chem. Lett*. **2008**, 18, 3720 – 3723.

[75]. Mathias, J.P.; Millan, D.S.; Lewthwaite, R.A.; Phillips, C. Preparation of triazolopyridinylsulfanyl derivatives as p38 MAP kinase inhibitors. **2006**, US2006/35922 A1.

[76]. McGeary, M.P. Facile and chemoselective reduction of carboxylic acids to alcohols using BOP reagent and sodium borohydride *Tetrahedron Lett*. **1998**, 39, 3319-3322.

[77]. Lin, C.-K.; Lu, T.J. A simple method for the oxidation of primary alcohols with o-iodoxybenzoic acid (IBX) in the presence of acetic acid. *Tetrahedron* **2010**, 66, 9688-9693

Chapter III

Trehalose-based compounds as autophagy inducers

INDEX

3.1. INTRODUCTION

3.1.1. Protein mis-folding and aggregation in NDDs

A mechanism shared by most of the ≈600 characterized NDDs is the aggregation and precipitation of mis-folded amyloidogenic proteins. Insoluble polymeric protein aggregates accumulate in the cytosolic and/or in the nuclear space of affected brain cells, or in the extracellular CNS space, in NDD- and protein-specific manner [1, 2].

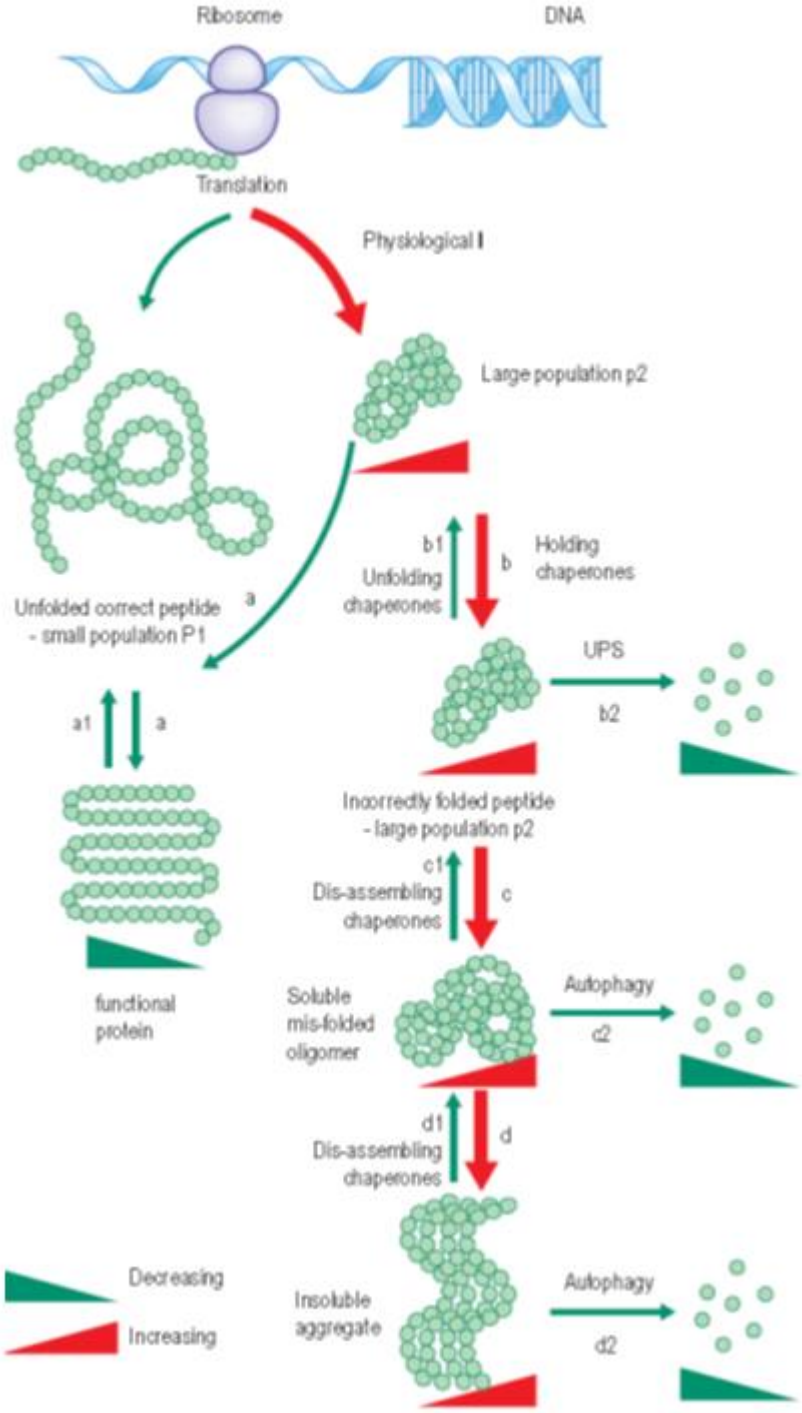

Figure 1. Ribosomal protein synthesis and PQC troubleshooting: Physiological and pathological conditions.

Unfolded proteins are synthesized by the ribosome, and require proper folding to assume unique three-dimensional structures [3]. Folding takes advantage of components of the protein quality control (PQC) machinery, and proceeds in parallel with protein synthesis [4]. The PQC network prevents aspecific interactions among abundant proteins (≈300 mg/mL overall concentration) in cells [5] and ensures their folding in physiological conditions [6].

Ribosomal protein synthesis is an error-prone process that under **basal/physiological** conditions creates a large population of correctly translated proteins (**P1**, Figure 1, left) [7]. Dynamic unfolding-refolding (**a^1**-**a**) is needed by **P1** proteins to reach specific cellular compartments or to perform specific functions, and the PQC machinery oversees the process [8].

Pathological conditions (i.e., inherited toxic mutations, a decrease in PQC efficiency) lead to the translation of increasingly large populations of folding-deficient proteins (**p2**, Figure 1, right). Proper folding to functional proteins (**a**, Figure 1) slowly decreases, while mis-folding to non-functional protein copies (**b**) increases [9]. The dynamic folding-unfolding equilibrium (**a^1** and **b^1**) contributes to the increase of **p2**/decrease of properly folded **P1** populations. Once mis-folded proteins exceed the capacity of holding and folding-unfolding chaperones, and of the UPS system (**b^2**) [10], mis-folded proteins aggregate first into soluble oligomeric complexes (**c**), then into insoluble aggregates (**d**).

Timelines are shortened when inherited genetic mutations cause the translation of a large **p2** population of mis-folded proteins [11]. Accumulation of mis-folded protein copies, of soluble oligomers and insoluble aggregates (respectively **b**, **c** and **d**) happens faster, while the corresponding PQC activities (respectively **b^1**, **c^1** and **d^1**) are rapidly impaired, and the capacity of UPS and autophagy (respectively **b^2**, **c^2** and **d^2**, Figure 1) is rapidly exceeded [12].

3.1.2. The autophagy machinery

Two main elimination pathways leading to protein disposal in cells are shown in Figure 1.

The ***ubiquitin-proteasome system*** (UPS) [13, 14] deals with most of regulated proteolytic events on soluble proteins. It is usually targeting relatively small and short-lived protein, that can access the 20S catalytic subunit of the proteasome [15].

Autophagy is a self-degradation process of cellular components – as small as proteins, up to whole organelles – known since many years [16]. Its crucial role, though, is fully appreciated since less than a decade [17, 18]. This pathway deals, *inter alia*, with long-lived proteins and insoluble/ubiquitin-proteasome system (UPS)-resistant aggregates [15]. Two different types of non-selective autophagy are known. *Macroautophagy* (MA from now on [16]) is the most common non-selective autophagic induced by stress stimuli [17]. *Micro-autophagy* [19] is a poorly characterized cellular process initiated by direct engulfment of cytoplasmic portions – smaller than in MA – by the lysosomal membrane, leading to their rapid degradation [20].

Five MA steps, reported in Figure 2 can be identified. 1) Initiation of autophagy, 2) nucleation to form phagophores/isolation membranes, 3) expansion to form autophagosomes (APs), 4) elongation, and finally 5) AP maturation and fusion with lysosomes yield fully degradative autolysosomes and complete MA [18-22].

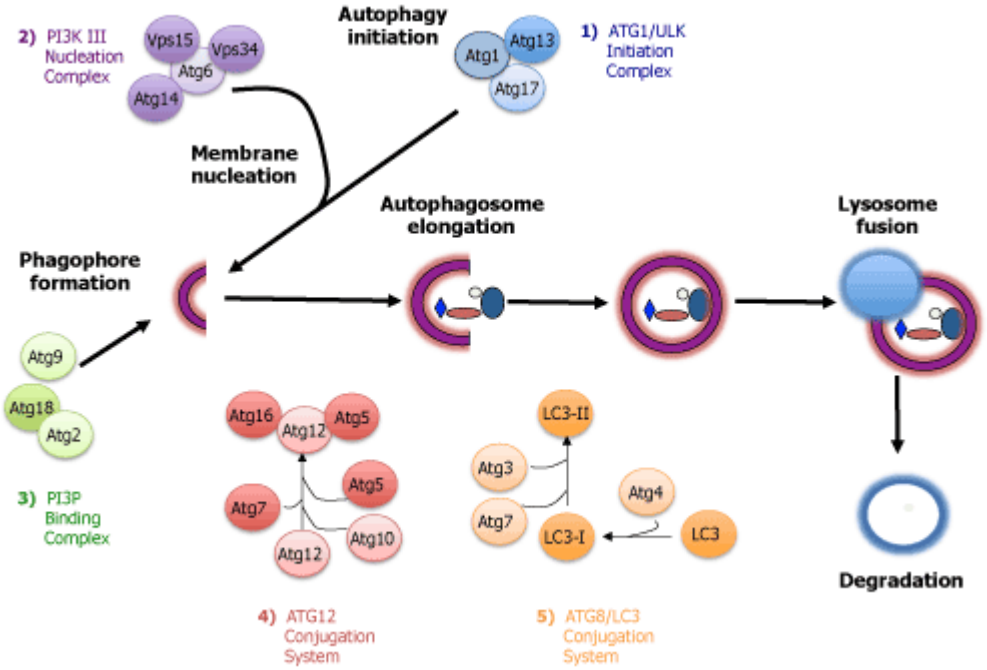

Figure 2. Macroautophagy: main steps.

1) Initiation starts at phagophore assembly sites (PASs [23]), and entails the assembly of vesicles and cellular material into pre-APs. It is achieved through the action of the UNC-51-like kinase (ULK) complex [24], whose translocation creates cytoplasmic PASs.

2) Nucleation depends on the PAS-bound class III phosphatidylinositol-3-kinase (PI3K) complex [25] to produce a phagophore/isolation membrane. The PI3K complex phosphorylates phosphatidylinositol (PI) to yield phosphatidylinositol-3-phosphate (PI3P), a promoter of membrane nucleation [26].

3) Expansion (phagophore formation) entails transport and incorporation of membrane material into the phagophore [27]. The trans-membrane protein carrier mammalian autophagy-related gene 9 (mAtg9) protein promotes ULK complex-dependent cycling of mAtg9-containing vesicles between *trans*-Golgi network and the endosome (ES) [28].

4) Elongation happens through two ubiquitin/UBQ-like (UBL) conjugating systems [29]. Atg5-Atg12-Atg16 multimeric complexes selectively associate to the pre-autophagosomal membrane, with a preference for PI3P-containing membranes [30]. Their role in elongation is due to the Atg12 UBL-like protein, and to two UBL domains on Atg5, that recruit and activate components needed for phagophore expansion and closure [31]. Among them, the complex centered around Atg8-like UBL proteins, such as the light chain 3 (LC3) protein [32]. The complex conjugates Atg8-like UBL proteins with the membrane phospholipid phosphatidylethanolamine (PE), forming an LC3-II conjugate [33]. LC3-II is an essential element in phagophore expansion and AP formation. The induction of autophagy is often measured by monitoring the ratio between LC3-II and LC3-I.

5) Maturation initiates with the removal of LC3-II from the outer surface of mature APs by the protease Atg4 [34]. Then, fully formed APs initiate a multi-step fusion process with one or more endosomal vesicles, to form an amphisome [35]. The final fusion step merges amphisomes with dense lysosomes (LSs), and the formation of fully degradative autolysosomes [36].

In pathological conditions, in particular during a NDD entailing the uncontrolled accumulation of mis-folded, aggregated proteins, the induction of autophagy could be beneficial. Any enzyme, receptor or protein complex involved in autophagy pathways may be considered a putative target to modulate (or more precisely, induce) autophagic activity in a damaged cellular environment. The majority of them have not been targeted yet in drug discovery projects, probably due to the lack of structural information or to the complexity of their biochemical pathways. In this work we have focused our attention on a specific molecule recently characterized as a pharmacological chaperone acting as an autophagy inducer.

3.1.3. Trehalose: a multi-purpose neuroprotective disaccharide

Trehalose **1** (drawn in three representations in Figure 3) is a disaccharide formed by a 1,1 linkage (refractory to glucosidase cleavage) between two D-glucose molecules [37].

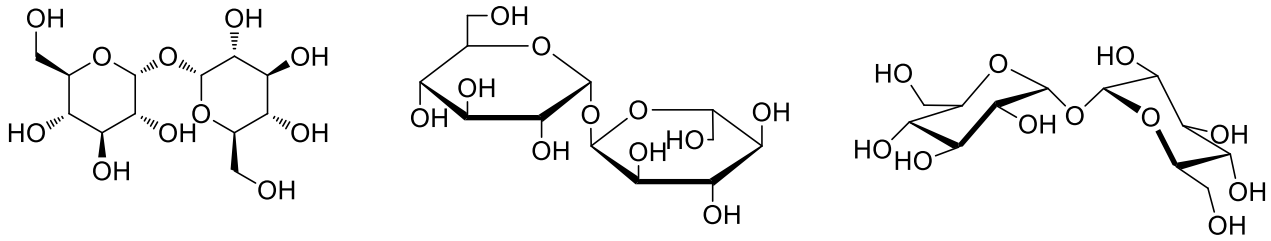

Figure 3. Chemical structure of trehalose **1**: different representations.

Trehalose is a non-reducing sugar, with good stability against acid hydrolysis. It is widely bio-synthesized in the biological world, but absent in mammals [38,39]. Trehalose performs different functions in lower organisms, such as acting as energy source during certain stages of development (i.e., germination of spores [40, 41]), or to perform specific tasks (i.e., flying in insects [41-43]. Mycobacteria incorporate trehalose into glycolipids to become part of their structural components [41, 44].

One of the more fascinating properties of trehalose in extremophile organisms is its participation in stabilizing life processes in extreme conditions (i.e., freezing or dehydration [37, 41, 45]). In various yeast species, for example, the accumulation of trehalose correlates with the ability of the organism to survive heat and desiccation stress [46, 47]. Accordingly, because of some inherent properties of trehalose, namely prevention of starch retrogradation and stabilization of proteins and lipids, it has proved quite useful in several industries including food processing, cosmetics and pharmaceutics [39, 48]

Trehalose recently emerged as a candidate for the reduction of protein misfolding and aggregation *in vitro* [49]. By acting as a chemical chaperone and solvating protein structures [50], at 50-100 mM, it protects them from mis-folding. The reduction of pathologic, aggregated proteins such as huntingtin (Huntington Disease) [49], synuclein (Parkinson Disease) and amyloid species (Alzheimer Disease) [51] was confirmed in several in vitro studies.

Recent studies have shown that some neuroprotective effects by trehalose in CNS / against NDDs arise via inducing autophagy, such as preventing neural tube defects [52], delaying the progression of amyotrophic lateral sclerosis [53], ameliorating dopaminergic and tau pathology [54], counteracting cellular prion infection [55] and accelerating the clearance of mutant huntingtin and alpha-synuclein [50, 56]. The induction of autophagy, as previously reported, was measured by monitoring the level of microtubule-associated LC3 [57]. The cytosolic form of LC3 (LC3-I) is converted to the phosphatidylethanolamine-conjugated form (LC3-

II) when autophagy occurs, and ≥100 mM trehalose **1** was shown to induce macroautophagy as shown in Figure 4.

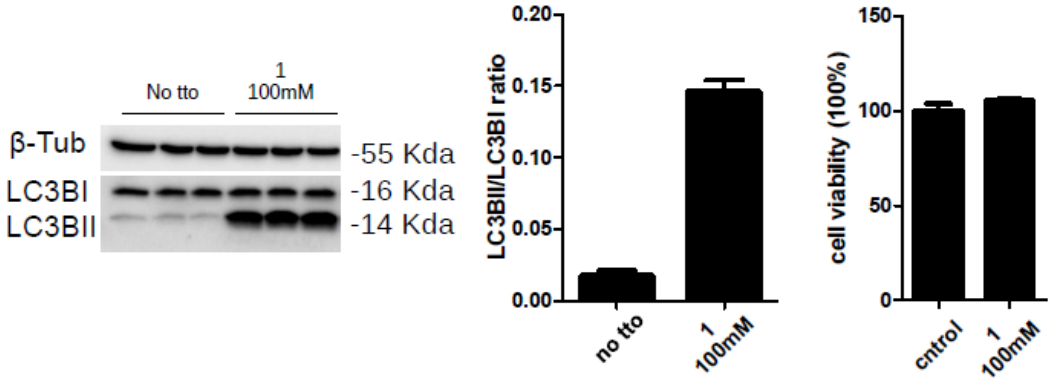

Figure 4. Autophagy activation by trehalose **1** (left, Western blot; middle, tabulation) and trehalose tolerability (right).

As it can be seen (Figure 4, Western blot, left, and tabulated, middle) the induction of autophagy by trehalose **1** was determined by measuring the increase of the concentration of the autophagy marker phospholipid-connected microtubule associated protein light chain 3 (LC3B-II), coupled with the decrease of its un-phospholipidated cytosolic LC3B-I form. We also gathered preliminary information on trehalose toxicity by testing its tolerability at high dosages in HEK293 cells (Figure 4, right), observing full viability/no toxicity up to 100 mM.

A putative mechanistic explanation of pro-autophagic effects of trehalose entailed the inhibition of cellular import of glucose and fructose through blockage of glucose transporters at the plasma membrane (GLUT), generating a starvation-like (low adenosine triphosphate) state that stimulates autophagy [58]. Unfortunately, this theory is not yet fully validated; thus, the goal of my Ph.D. work related to trehalose was also to gather information about its mechanism of action.

3.1.4. Aims of work

As previously mentioned, trehalose is endowed with multiple beneficial, protein-stabilizing, pharmacological chaperone effects. Despite its biological activity at high dosage (no less than 100 mM), thanks to its safety profile, its low cost and bioavailability from fermentation, trehalose itself is being currently used as a food additive, a protein stabilizer, and – most important – as a neuroprotective agent in preclinical and clinical studies.

Our main goal was to determine if, by limited chemical modifications unlikely to significantly increase their cost, trehalose derivatives could gain significant potency for their biological activities. Due to its extremely high hydrophilicity, trehalose would hardly permeate biological membranes. Even more importantly, trehalose is not naturally occurring in higher vertebrates, that express on their intestinal membrane enzymes required to hydrolyze trehalose (trehalases). These enzymes are found in the brush border cells of the epithelial membrane of the small intestine and in the proximal tubules of the kidneys [59, 60], and by splitting trehalose in two molecules of glucose they fully prevent the possibility to orally administer trehalose.

The fist aim of my Ph.D. work, concerning trehalose, was focused on the improvement of its pharmaco-kinetic profile in order to promote its oral administration and its delivery into higher organisms. By using well-known carbohydrate chemistry transformations assessed and executed on multi-gram scales, based on selective

protection and de-protection steps, we could synthesize three different trehalose prodrugs. Namely, we temporarily masked some of the hydroxyl groups in trehalose as acetates, as shown in Figure 5 (from right to left, a bis-, a tetra- and a hexa-acetyl trehalose).

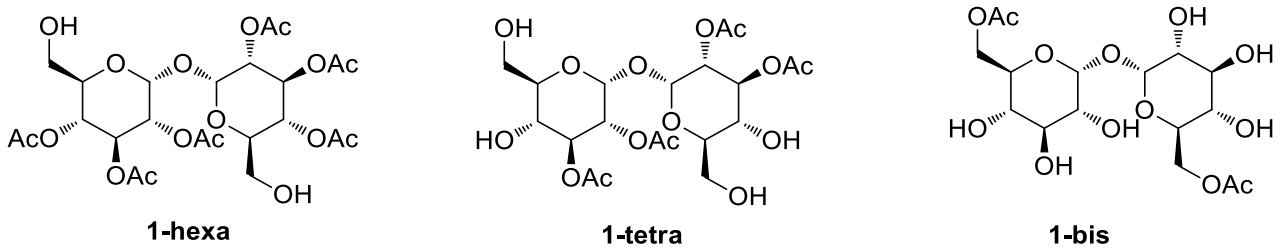

Figure 5. Chemical structure of synthetic targets: bis-, tetra- and hexa-acetyl trehalose.

The acetyl moiety was selected by us and others [61-64] because it is easy to insert, stable in acidic conditions (i.e., the stomach), is hydrolysed in men by ubiquitous esterases. Hopefully, then, we thought that acetylation could also have significantly decreased the binding affinity of trehalose for the trehalase enzymes, thus significantly increasing the concentration of trehalose in blood after oral administration of its acetylated prodrugs. We reasoned that the different number of acetyl/free hydroxyl groups in the three synthetic targets (Figure 5) were needed in order to evaluate which represents the best compromise between lipophilicity (cell- permeability) and water solubility (bioavailability in biological fluids).

The second aim of this work was to increase the biological activity of trehalose by permanent / non-prodrug modifications. As already described in Chapter 2, we considered the possibility to couple trehalose with another molecule suitable as autophagy inducer by using the double action compound (DAC) strategy.

As a clear SAR for trehalose is not established, due to the lack of at least one major, structurally characterized molecular target, the first hypothesized goal was the synthesis of different trehalose-based molecules bearing an anchor point for further functionalization in different positions of trehalose via regioselective chemical routes. We selected the azide moiety as a chemical handle for further coupling because it is suitable for a 3+2 cycloaddition (click reaction [65, 66], or alternatively can easily be converted into an amine using different approaches [67, 68]. In order to selectively exploit most of trehalose positions, the structure of 2- (compound **4**), 4- (compound **3**) and 6-monoazido trehalose (compound **2a**) were targeted, together with bis-6-azido trehalose **2b** (Figure 6).

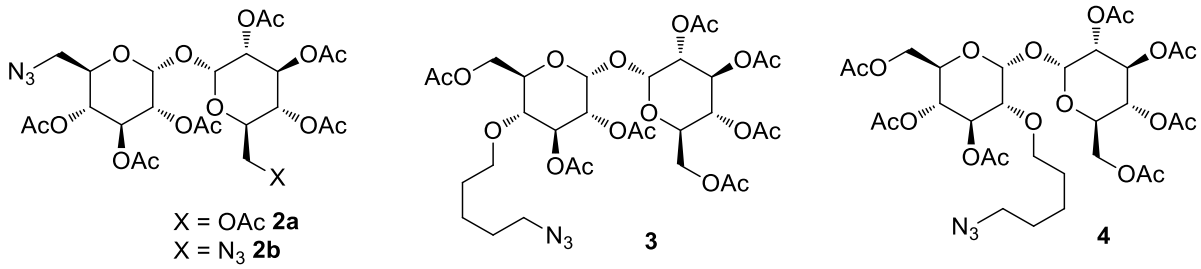

Figure 6. Chemical structure of regioselectively functionalized azido trehaloses **2a,b-4**.

More in details, 2- and 4-substituted azido trehaloses **4** and **3** were functionalized with a small, 5-carbon lypophilic linker ending with a primary/unhindered and reactive azido moiety. As to 6-azido trehaloses, mono-substituted **2a** derived from the replacement of one of the two primary alcohols by the azido moiety, while both of them were substituted with an azide in bis-substituted **2b**. All remaining hydroxyl group in

molecules **2a,b-4** were protected as acetyls, due to the orthogonality of this group with click reaction conditions and with amide coupling, to its relative stability but also to its easy removal in carefully controlled conditions.

Once synthetized, two among the four trehalose-based synthons were used to synthetize two DAC **5** and **6**, whose structure is reported in Figure 7. Namely, the azido moieties present in synthons **2a** and **2b** were successfully reacted in a click reaction with a close analogue of sephin-1 bearing a triple bond (see the previous Chapter for a detailed description of neuroprotective sephin-1).

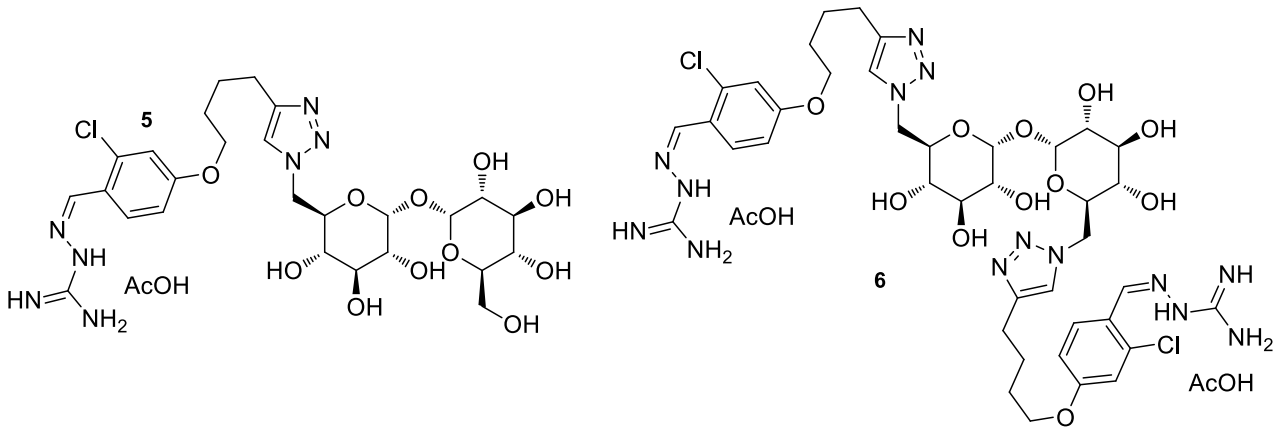

Figure 7. Trehalose-sephin-1 – based DACs: chemical structures, compounds **5**, **6**.

As previously mentioned in Chapter 2 (Figure 11 and related discussion), a third substitution / ether moiety on the sephin-1 scaffold and a short lipophilic linker were selected to couple sephin-1 and trehalose, due to the likelihood to preserve the biological activity of sephin-1.

Sephin 1 was selected due to a putative pro-autophagic role suggested by a research group at Trento University, led by Prof. G. Piccoli, with whom my research group collaborates. Sephin-1 acts as autophagy inducer at low μM concentration. Its induction of autophagy was measured as earlier described (Figure 8, left; see also Figure 4, left and middle). As it is tabulated in Figure 8, middle, sephin-1 resulted to be a potent autophagy inducer at ≈50 μM, and was well tolerated at the same concentration by HEK293 cells (Figure 8, right).

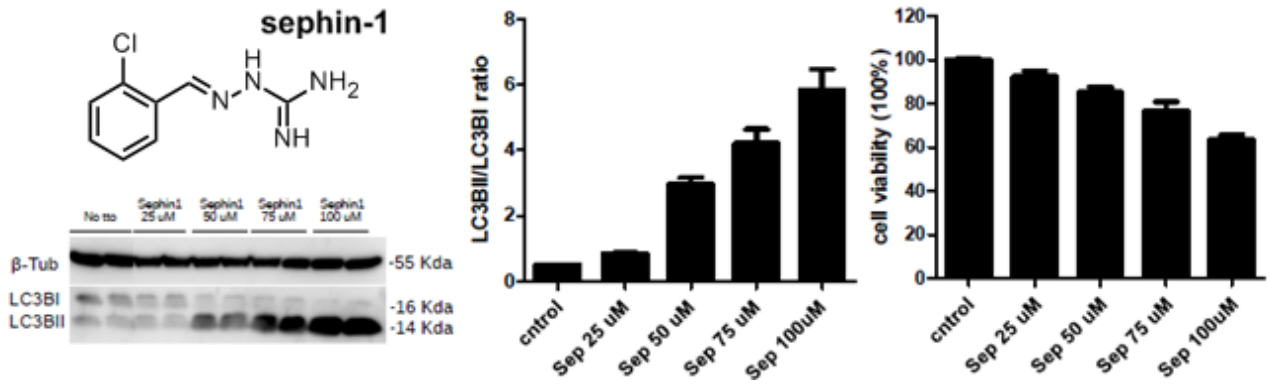

Figure 8. Sephin-1: induction of autophagy, tolerability by HEK293 cells. Cells were treated with sephin-1 for 24h. Protein lysates were resolved by western-blot using LC3B-I/II antibody 1:500 (ALX- 803-081) and β-Actin antibody 1:3000. β-Actin was used as control protein.

The next Paragraphs will describe in detail the synthetic pathways, starting from the preparation of **1-hexa**, **1-tetra** and **1-bis** trehalose prodrugs (Paragraph 3.2.1). While these compounds were previously reported

[64] the lack of experimental details about their preparation (i.e. stoichiometry, yields, work-up protocols and purifications) forced me to describe in details most reaction steps to their synthesis.

The protected azide derivatives **2a,b-4** (Paragraphs 3.2.2 – 3.2.4) and the two DACs **5** and **6** (Paragraph 3.2.5) are described. The prepared DACs were synthesized from mono- and bis-6-azido acetylated trehaloses **2a** and **2b**; the acetyl group was chosed as an ideal option in terms of protection and ease of removal after coupling with sephin-1 precursors. Coupling of sephin-1 analogues to 4- and 2-azido substituted trehaloses **3** and **4** will be carried out in future, to provide the correspondent DACs, in the lab where I spent my Ph.D. internship.

Either the successful attempts to intermediates and final compounds, and the failed experiments useful to understand synthetic behaviours and to eventually set up successful synthetic routes to target compounds, will be thoroughly described. Lastly, the biological profile of compounds **5** and **6** when tested as autophagy inducers is reported in Section 3.3.

3.2. CHEMISTRY

3.2.1. Synthesis of 1-hexa, 1-tetra and 1-bis acetylated trehalose prodrugs

The synthetic pathway used for the synthesis of hexa-acetylated trehalose **1-hexa** is reported in Scheme 1.

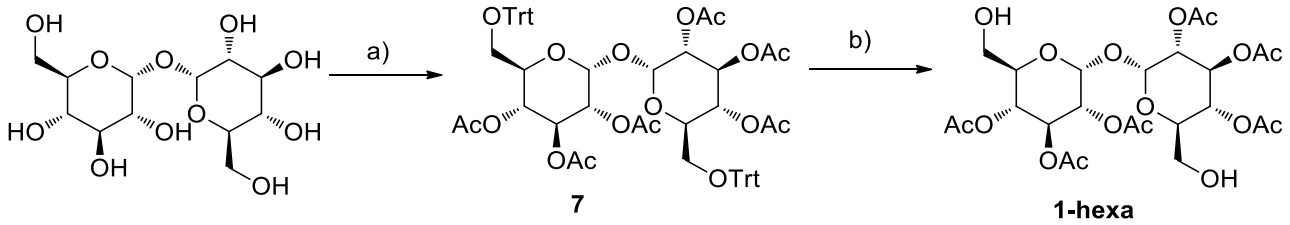

a) TrtCl, Py, 90°C, 24hrs then Ac_2O, RT, 16hrs, **72%**; b) DCA/DCM 1:1, 23°C, 30min, **90%**

Scheme 1. Synthesis of **1-hexa** from trehalose **1**.

Fully protected intermediate **7** was obtained as described in literature, using an excess of trityl chloride in hot pyridine (step a, Scheme 1) followed by a treatment with acetic anhydride (step b) [61]. The trityl groups were selectively removed using a 1:1 mixture of dichloroacetic acid (DCA) and methylene chloride as described in a patent [69] on a similarly protected carbohydrate. Compound **1-hexa** was obtained in good yield and purity after chromatographic purification.

The synthetic pathway used for the synthesis of tetra-acetylated **1-tetra** is reported in Scheme 2.

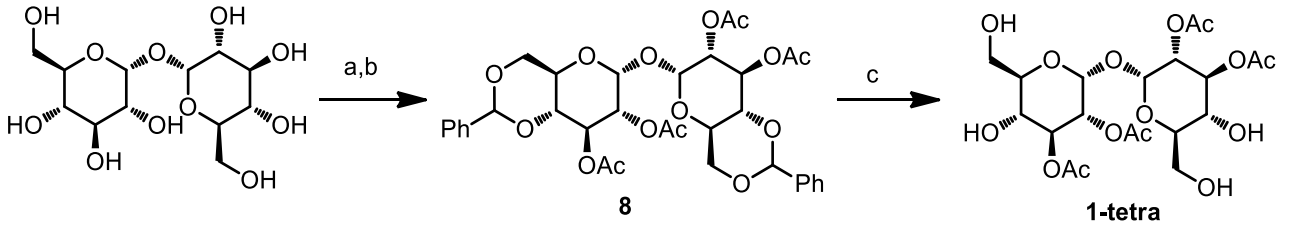

a) $PhCH(OMe)_2$ 2.2eq, cat PTSA, DMF, 105°C, 80min; b) Ac_2O, Py, RT, 16hrs, **80%** over two steps; c) H_2, Pd-C, MeOH/THF 4:1, RT, 16hrs, **99%**.

Scheme 2. Synthesis of **1-tetra** from trehalose **1**.

The simultaneous protection of trehalose hydroxy groups in position six and four was performed as described in literature using benzaldehyde dimethyl acetal and a catalytic toluene-4-sulfonic acid in DMF at 100℃ (step a, Scheme 2) [61]. The reaction crude, after solvent evaporation at reduced pressure, was acetylated in standard conditions (step b) to yield the fully protected intermediate **8** after chromatographic purification in very good yield. Full benzylidene deprotection was performed in hydrogenolytic conditions (step c), yielding compound **1-tetra** in quantitative yield.

The synthetic pathway used for the synthesis of bis-acetylated **1-bis** is reported in Scheme 3.

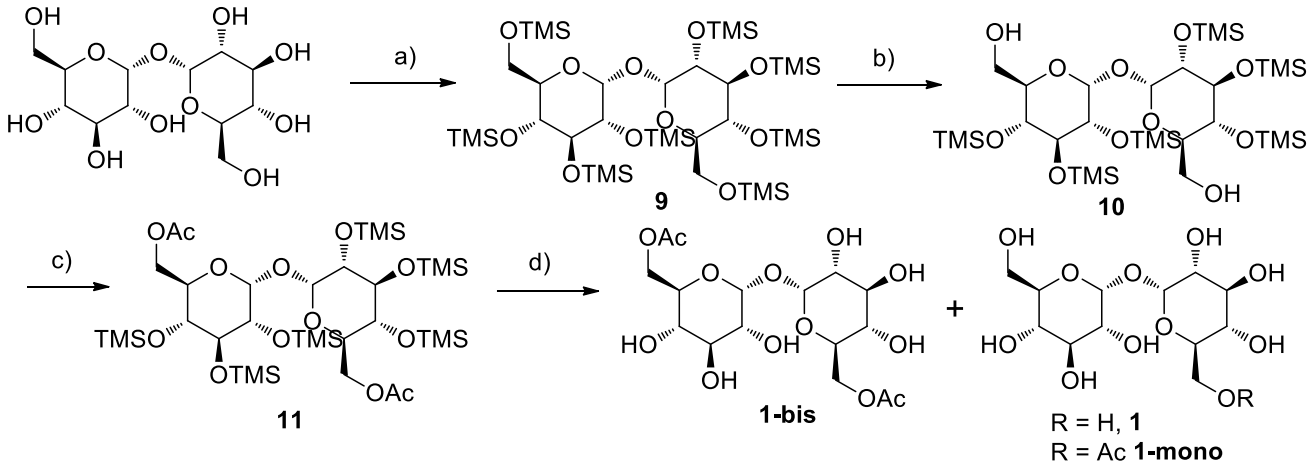

a) TMSCl, Py, 0°C to RT, 16hrs; b) cat. K_2CO_3, MeOH/DCM (3:1) 0°C to RT, 1hr, **75%** over two steps; c) Ac_2O, TEA, DMAP, DCM, RT, 4hrs, **91%**; d) de-silylation reaction **0-99%** (**1-bis**).

Scheme 3. Synthesis of **1-bis** from trehalose **1**.

The synthetic pathway was executed similarly to what reported in a patent [63], per-silylation (step a, Scheme 3), selective desilylation (step b) and acetylation (step c) were carried smoothly. As to desilylation of intermediate **11** (step d), we performed some optimization. The experimental conditions used in [63] (Table 1, entry 1) led to the formation of side-products trehalose **1** and mono-acetylated **1-mono** (Scheme 3); purification of **1-bis** from them required tricky direct phase chromatographic purification with a polar eluant mixture. Thus, we screened alternative, well-known desilylation protocols (Table 1, entries 2-6), looking for high yielding conditions devoid of chromatographic purification.

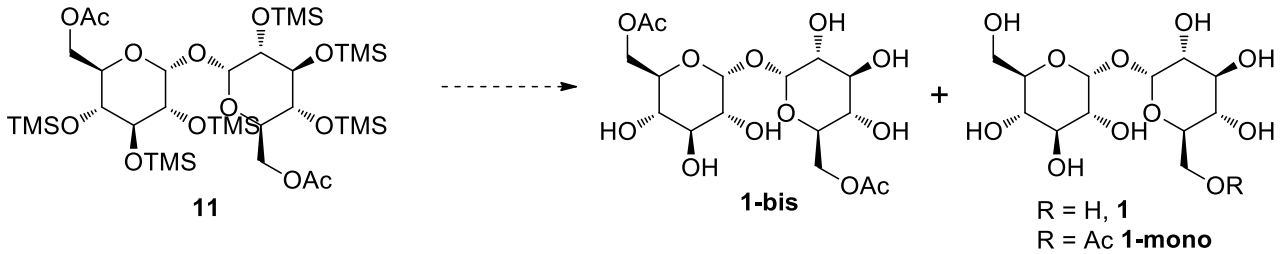

#	Desilylation conditions*	T °C	Time	Results
1	Dowex 50W-X8, MeOH	RT	1hr	> 90% **1-bis**[c], requiring chromatography
2	EtOCOCl (0.1eq), dry MeOH	0°C	5min	>95% **1**
3	4:1:6 THF/TFA/H_2O	0°C to RT	30min	60% **1-bis**, 30% **1-mono** and 10% **1**[c].
4	3:3:1 AcOH/THF/H_20	RT	4hrs	75% **1-bis**, 25% **1-mono**[c].
5	H_2 (1atm), 20% $Pd(OH)_2$/C, MeOH	RT	1hr	90% **1-bis**, 10% **1-mono**[c].
6	AcOH (0.2eq), dry MeOH	75°C	2hrs	> 98% **1-bis**[c, d].

Table 1.[a] Each entry/attempt was performed on a 50 mg scale, [b] TLC monitoring: $CHCl_3$/MeOH/H_2O 60:35:5 as eluants, H_2SO_4 as reagent. Rf **1-bis**: 0.5, **1-mono**: 0.2, trehalose: 0.1, [c] Determined by NMR, [d] Same results on a 500 mg scale with longer reaction time (8hrs).

By generating HCl in situ (entry 2) [70], fully deprotected trehalose **1** was rapidly obtained due to trans-esterification of acetates with MeOH/solvent. The same side reaction, albeit in lower yields (**1-bis** as major reaction product) was observed also in entries 3 and 4 [71,72], using other acids in large excess. Slightly worse yields, when compared to entry 1, were obtained by hydrogenolytic desilylation (entry 5 [73]; and chromatographic purification was still required.

We identified suitable desilylation conditions (entry 6, Table 1) by using sub-stoichiometric AcOH in refluxing MeOH [74]. Highly pure **1-bis** was obtained without need for a chromatography, and similar results were obtained by scaling up to a 500 mg scale.

Trehalose-based prodrugs **1-hexa**, **1-tetra** and **1-bis** were tested at the University of Trento as autophagy inducers at low millimolar concentration either as such, or as prodrugs of trehalose **1** (see Section 3.3). In future, they will be tested for their affinity for trehalases, and their ability to regenerate the parent trehalose **1** will be determined in cellular media.

3.2.2. Synthesis of 6-azido acetylated trehaloses 2a and 2b

Mono-6-azido acetylated trehalose **2a** and bis-6-azido acetylated trehalose **2b** were obtained in low (**2b**) to moderate yields (**2a**) starting from trehalose, according with the synthetic strategy reported in Scheme 4.

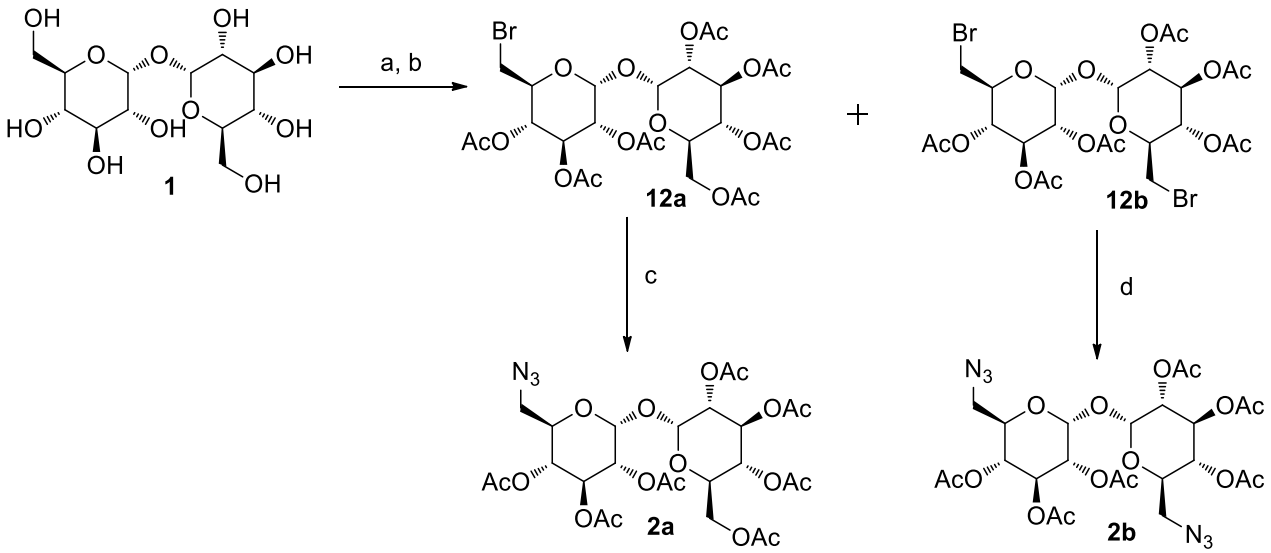

a) NBS 2eq, PPh_3 2eq, DMF, RT 16hrs then 60°C 24hrs; b) Ac_2O, Pyridine RT, 24hrs **30% (12a), 18% (12b)**; c) NaN_3 5 eq, DMF, 55°C, 16hrs, **80%**.d) NaN_3 10eq, DMF, 55°C, 16hrs, **79%**.

Scheme 4. Synthesis of mono 6-azido acetylated trehalose **2a** and bis 6-azido acetylated trehalose **2b**.

By treating trehalose with two equivalents of NBS and PPh_3 we obtained a mixture of mono- and bis-brominated trehalose derivatives (step a, Scheme 4). The mixture was separated after per-acetylation (step b) by direct phase chromatography, yielding mono- (**12a**) and bis-6-bromo per-acetylated trehalose (**12b**). Both compounds were submitted to nucleophilic substitution with NaN_3 (Scheme 4, respectively step c and d), affording compounds **2a** and **2b** respectively with moderate and low yields. Although reaction conditions could be optimized to increase the yields and to direct the synthesis towards either one of the two target compounds, this route led to enough material to proceed further in trehalose-sephin-1 based DAC synthesis (see Paragraph 3.2.5).

3.2.3. Synthesis of 4-azido acetylated trehalose 3

The first conceived synthetic pathway to obtain 4-azido acetylated trehalose **3** from trehalose is reported in Scheme 5.

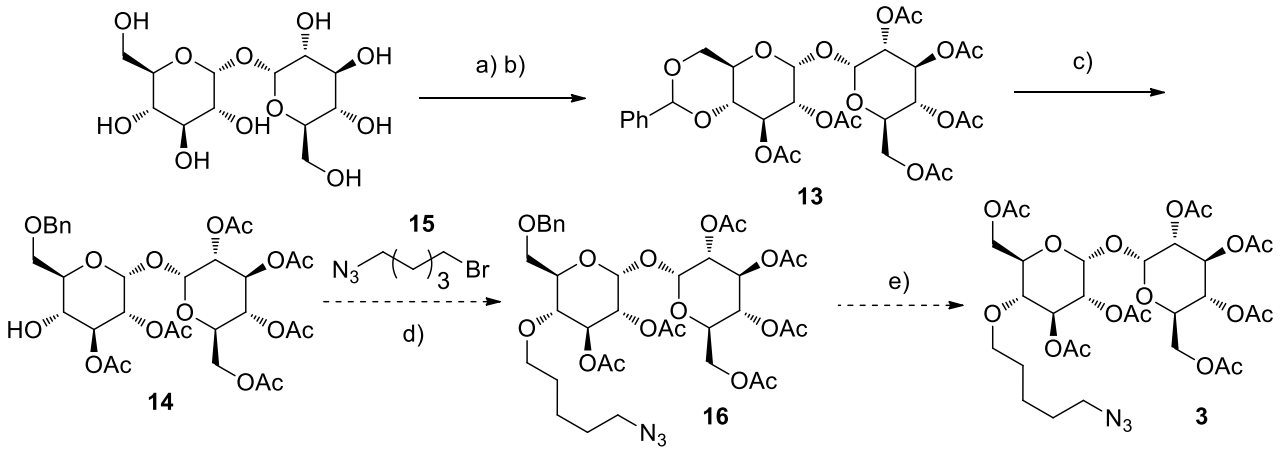

a) $PhCH(OMe)_2$ 1eq, PTSA 0.05eq, DMF, 105°C, 80min; b) Ac_2O, Py, RT, 16hrs, **51%** over two steps; c) Et_3SiH 5eq, TFA 5eq, DCM [0.1M], 0°C, 24hrs, **77%**

Scheme 5. Attempted synthesis of 4-azido acetylated trehalose **3.**

Desymmetrization of trehalose was achieved by working with strict trehalose-protecting reagent 1:1 stoichiometry, thus mostly introducing the latter on one of the two glucose rings (step a, Scheme 5). Per-acetylation (step b) was followed by direct phase chromatography, removing unreacted trehalose and bis-benzylidene acetal trehalose, and obtaining in overall good yields the hexa-acetyl, benzylidene acetal **13** The benzylidene moiety was then selectively opened with good yields in literature reported reducing conditions, leaving a benzyl protecting group on the primary alcohol (compound **12**) using Et_3SiH/TFA in dry DCM (Scheme 5, step c) [75].

The next attempted step (step d, Scheme 5) required the preparation of 1-azido-5-bromopentane **15**, that was prepared from commercially available 5-azido-pentan-1-ol as reported in Scheme 6.

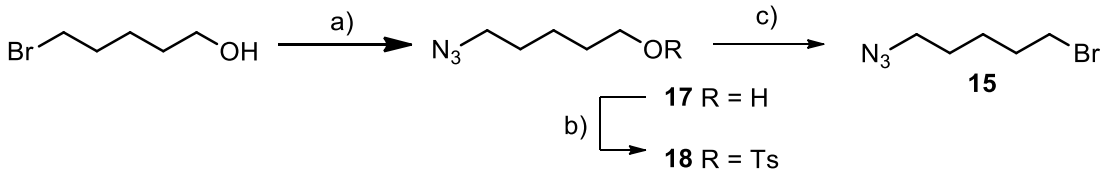

a) NaN_3 2eq, H_2O, 80°C, 18hrs, **90%**; b) TsCl 1.5eq, TEA 2eq, DMAP 0.1eq, CH_2Cl_2, 0°C to rt, 16hrs, **75%**, c) LiBr 3eq, acetone, 70°C, 18 hrs, **82%**

Scheme 6. Synthesis of 1-azido-5-bromopentane **15.**

We tried unsuccessfully to alkylate the free 4-OH in compound **14**, as reported below in Table 2.

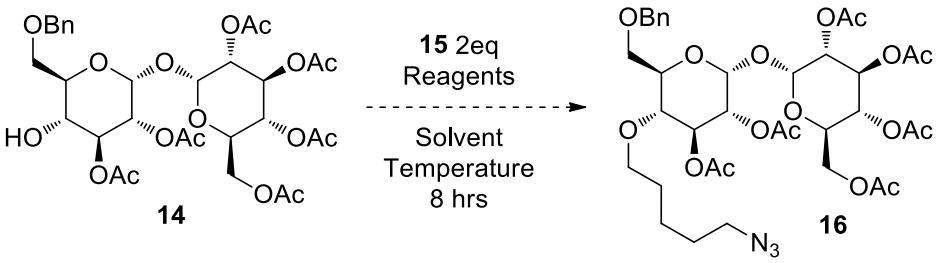

entry	Solvent (dry)	Reagents	T (°C)	Results
1	DMF	NaH 1.5eq	0°C	CM.
2	THF	Ag_2O 2eq	RT	Recovery of SM.
3	DMF	Ag_2O 2eq	RT to 80°C	Recovery of SM.
4	DMF	Ag_2O 2eq, KI 0.2eq	80°C	CM.
5	Toluene	Ag_2O 2eq, TBAI 0.2eq	110°C, TBAI	Recovery of SM.
6	DCM	AgOTf 3eq, TMU 3eq	0°C to RT	Recovery of SM.

Table 2. Alkylation attempts on compound **14**. SM: starting material, CM: complex mixture of products.

As expected, the used of a strong base as NaH led to the formation of an uncharacterizable, complex mixture of products (entry 1). We tried well known benzylation conditions [76-78] for carbohydrates, in presence of silver oxide with varying solvents, temperature and additional reagents (entries 2-5), mostly recovering unreacted compound **14**. The same was observed replacing silver oxide with silver triflate (entry 6).

We reasoned that instability of the acetate group in "hard" alkylation conditions (i.e., entries 1, 4) could have led to complex reaction mixtures, and we decided to change the protecting group to the more alkylation-stable benzyl ether. A revised synthetic strategy to 4-azido benzylated trehalose **19** from mono-benzylidene acetal hexa-acetate **13** is shown in Scheme 7.

First, the acetyl groups in compound **13** were removed using catalytic NaOMe (step a, Scheme 7) and the hydroxyl groups were alkylated with BnBr in basic conditions (step b) in high yield over two steps. Previously used reducing conditions (step c) led to 4-OH-free per-benzylated compound **19** in high yields, that was successfully alkylated with 1-azido-5-bromopentane **15** in good yields (step d, Scheme 7).

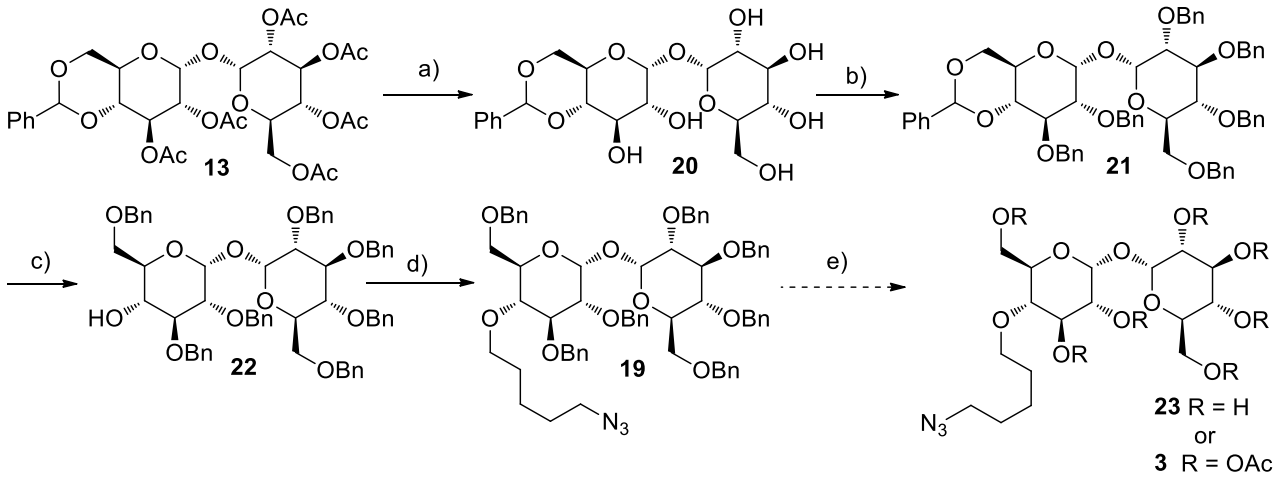

a) MeONa 0.15eq, MeOH, RT, 16hrs; b) BnBr 9eq, NaH 7.5eq, dry DMF, RT, 24hrs, **84%** over two steps; c) Et_3SiH 7.5eq, TFA 7.5eq, dry DCM, 0°C to RT, 4hrs, **80%**; d) 1-azido-5-bromopentane 3eq, NaH, DMF, 55°C, 8hrs, **75%.**

Scheme 7. Synthesis of 4-azido benzylated trehalose **19**.

As the presence of an azide moiety was not compatible with the common hydrogenolytic debenzylation conditions (H_2 or homogeneous H_2 transfer reagents), we attempted benzyl deprotection in acidic conditions by Lewis acids. Table 3 describes six attempts towards debenzylation (entries 1-3) or towards protecting group switch (acetylation, entries 4-6) promoted by several Lewis acids and performed as reported in literature [79-85].

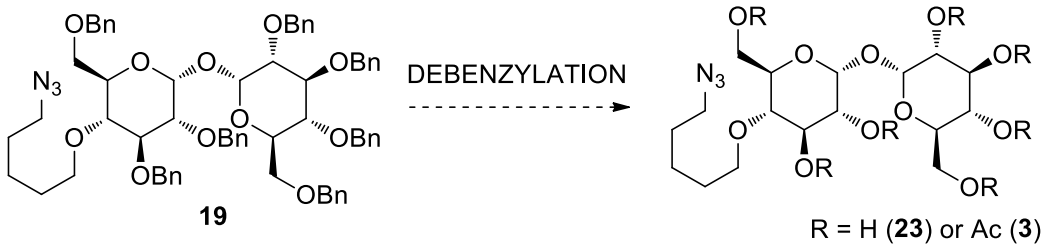

Table 3. Debenzylation attempts on compound **19**.

#	R	Reagents, [Ref.]	Solvent	T (°C)	Results
1	H	BCl_3 [79]	dry DCM	-78°C to 0°C	CM
2	H	Me_3SiI [80]	dry DCM	0°C	CM
3	H	Anhydrous $FeCl_3$ [81]	dry DCM	0°C to RT	CM
4	Ac	Anhydrous $FeCl_3$ [82]	Ac_2O	RT	CM
5	Ac	Anhydrous $FeCl_3$, cat H_2SO_4 [83]	Ac_2O	RT	CM
6	Ac	TMSOTf [84, 85]	Ac_2O	10-15°C	CM

CM: complex mixture of products.

Unfortunately, none among the attempted trials provided high yields in either debenzylated (**23**) or acetylated (**3**) reaction products. Namely, full conversion to either **23** or **3** was never observed. Partial

debenzylation and/or acetylation was observed in each entry, and the complex reaction mixtures (TLC monitoring) could not be separated or characterized.

Thus, we slightly modified the strategy employed in Scheme 6 by coupling bis-bromopentane with polybenzylated trehalose **22** in good yields (step a, Scheme 8; large excess of dibromo compound to avoid dialkylation).

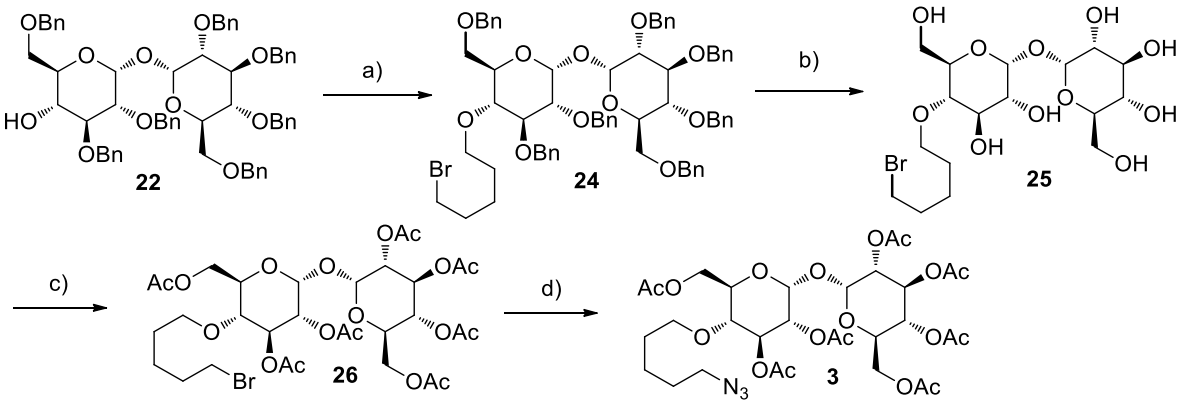

a) $Br(CH_2)_5Br$ 10eq, NaH 2eq, DMF, 55°C, 8hrs, **70%;** b) H_2, Pd/C 10%, MeOH/THF 4:1, RT, 16hrs; c) Ac_2O, cat DMAP, DCM/Py 4:1, RT, 16hrs; d) NaN_3, DMF 65°C, 16hrs, **60%** over three steps.

Scheme 8. Synthesis of 4-azido acetylated trehalose **3**.

Hydrogenolytic benzyl deprotection (step b, **25**) was achieved without significant dehalogenation by minimizing the catalyst. Acetylation (**26**) and azide substitution in standard conditions (respectively steps c and d, Scheme 8) successfully led to target 4-azido acetylated trehalose **3** in good yields over three steps.

3.2.4. Synthesis of 2-azido acetylated trehalose 4

2-Azido acetylated trehalose **4** was prepared according with the 7-step synthetic strategy depicted in Scheme 9.

The sequential introduction of two benzylidene acetals and four TMS groups on trehalose (step a, Scheme 9) was performed with the same logic used for the preparation of compound **8**. Acetic anhydride was replaced with TMSCl and this methodology led with good yields to fully protected compound **27**. One-pot TMS deprotection and 3-OH benzylation with PhCHO and Et_3SiH in Lewis acid conditions as reported in literature [86] (step b) led to 2-OH-free compound **28**, which was mono-benzylated further with 0.75 eq of BnBr as alkylating agent (step c), leading to mono-OH trehalose **29** in moderate yields. Steps d to g in Scheme 9 were carried out exactly as previously seen for steps a to d, Scheme 8, leading to target 2-azido acetylated trehalose **4** in moderate yields.

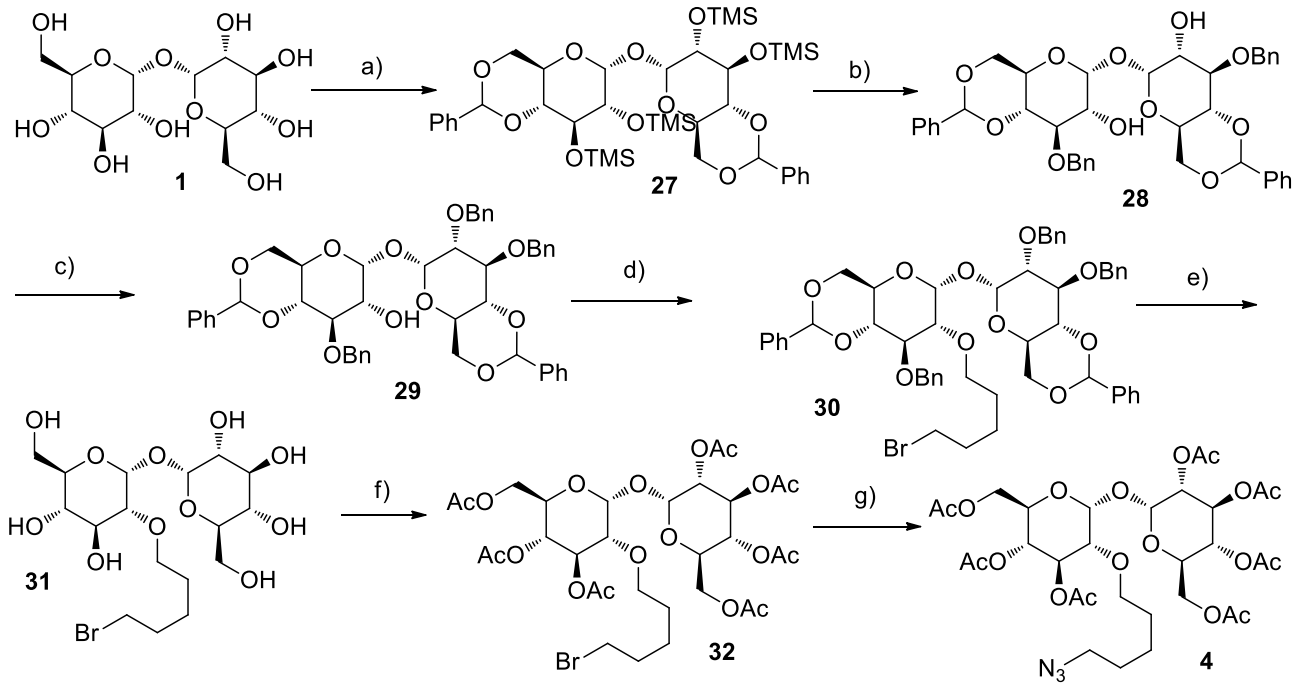

a) $PhCH(OMe)_2$ 2.2eq, cat PTSA, DMF, 105°C, 80min, then TMSCl, 1H-Imidazole, 0° to RT, 16hrs, **76%**; b) cat TMSOTf, PhCHO, Et_3SiH, DCM -78°C to 0°C, 4hrs, **80%**; c) BnBr 0.75eq, NaH, THF, 0°C to RT, 6hrs, **49%;** d) $Br(CH_2)_5Br$ 10eq, NaH 2eq, DMF, 55°C, 8hrs, **71%** e) H_2, Pd-C, MeOH/THF 4:1, RT, 24hrs; f) Ac_2O, Py, cat DMAP, DCM/Py, RT, 4hrs, **78%** over two steps; g) NaN_3, DMF 65°C, 16hrs, **90%.**

Scheme 9. Synthesis of 2-azido acetylated trehalose **4**.

3.2.5. Synthesis of sephin1-trehalose DACs 5 and 6

We selected as first DAC targets the conjugates between sephin-1 and 6-azido trehaloses **2a,b**, respectively in a 1:1 (compound **5**) or in a 2:1 ratio (compound **6**, Figure 9).

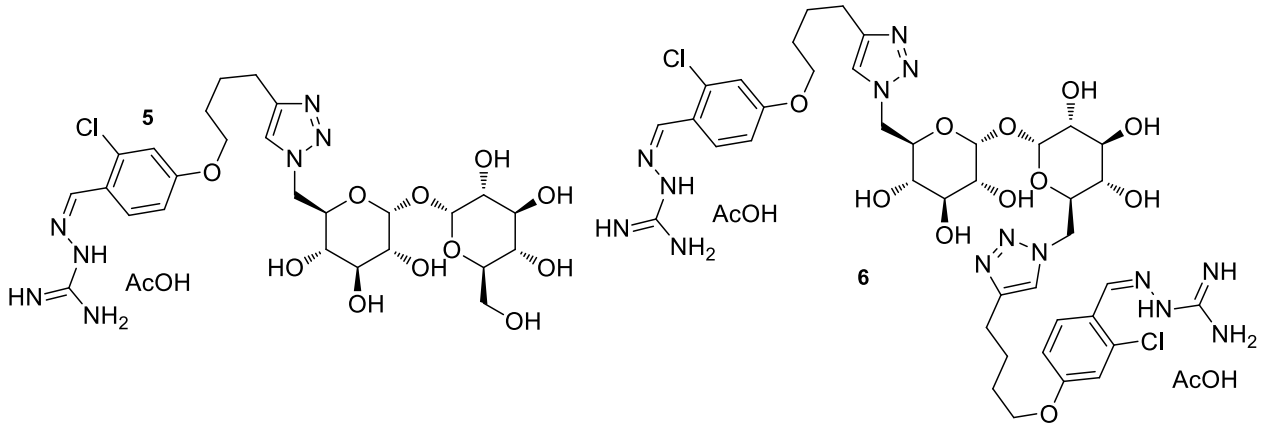

Figure 9. Chemical structure of sephin1-trehalose DACs **5** and **6**.

The retrosynthetic pathway to 1:1 DAC **5** is depicted in Scheme 10.

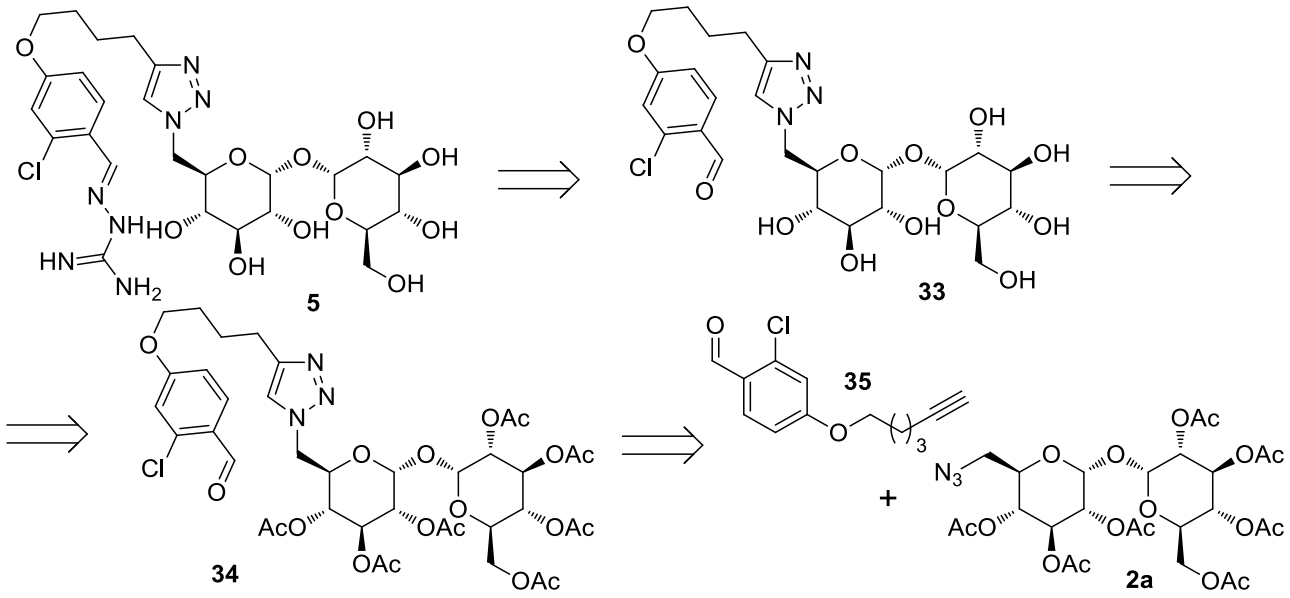

Scheme 10. Retrosynthetic pathway for the synthesis of monomeric sephin1-trehalose DAC **5**.

The retrosynthetic scheme relies upon two key synthons: triple bond-containing, para-substituted sephin1-linker construct **35** and mono 6-azido acetylated trehalose **2a**. While the synthesis of the latter was described in Scheme 4, the sephin1-linker construct **35** was obtained from commercially available 5-hexyn-1-ol, as shown in Scheme 11.

Introduction of a tosyl leaving group on 5-hexyn-1-ol (step a, Scheme 11) was followed by its use in a nucleophilic substitution on 2-Cl-4-hydroxybenzaldehyde (step b). Target construct **35** was obtained in excellent yields.

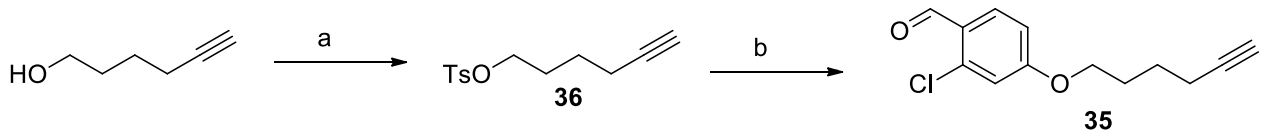

a) TsCl, TEA, cat DMAP, DCM, 0°C to RT 20hrs, **95%**; b) 2-chloro-4-hydroxybenzaldehyde, K_2CO_3, DMF, 95°C, 24hrs, **83%**

Scheme 11. Synthesis of tri-substituted benzaldehyde **35.**

The Click reaction between sephin-1-based alkyne **35** and acetylated trehalose monoazide **2a** is graphically depicted in Scheme 12.

In situ-generated copper (I), produced by ascorbate reduction of copper (II), smoothly led to acetylated, triazole-linked benzaldehyde construct **34** (step a, Scheme 12) in excellent yields after column chromatography. Deacetylation with catalytic NaOMe (step b) and condensation with aminoguanidine hydrochloride in catalytic acid conditions (step c, Scheme 12) led, after reverse phase chromatography, to pure 1:1 target DAC **2a** as an acetate, in good purity and yields.

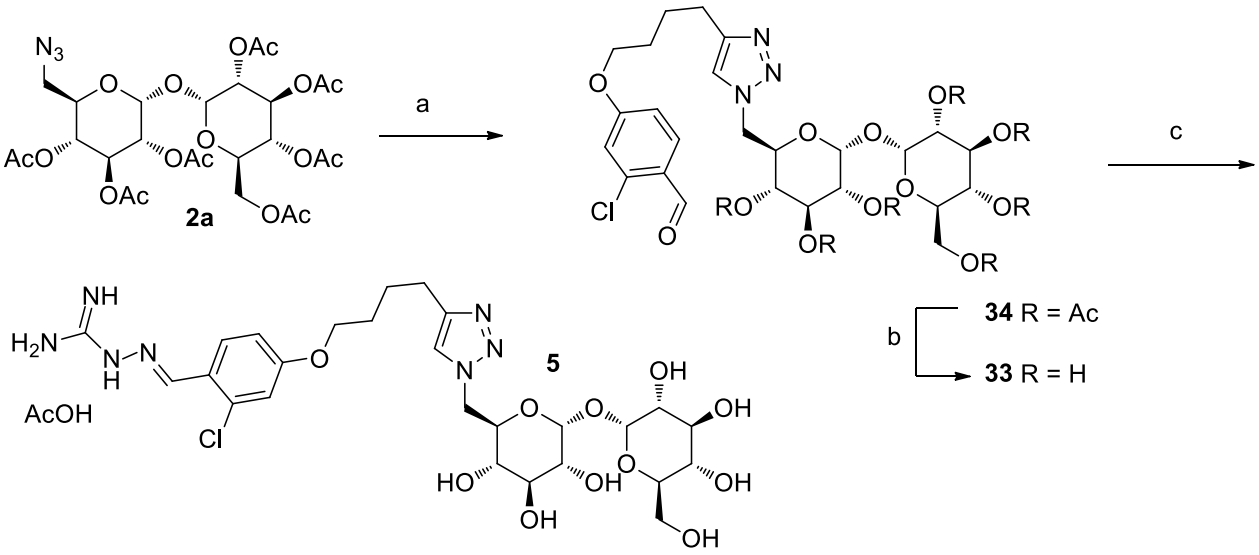

a) **35** 1eq, $CuSO_4$ $5H_2O$, Na Ascorbate, THF:H_2O 1:1, RT, 6hrs, **88%**; b) NaOMe, MeOH, RT, 20hrs; c) aminoguanidine HCl, cat. HCl_{aq}, EtOH, H_2O, 70°C, 6hrs, **80%** over two steps.

Scheme 12. Synthesis of 1:1 trehalose-sephin-1 DAC **5.**

The synthesis of 1:2 trehalose-sephin-1 DAC **6** was carried out according to Scheme 13, similarly to what presented for 1:1 DAC **5**.

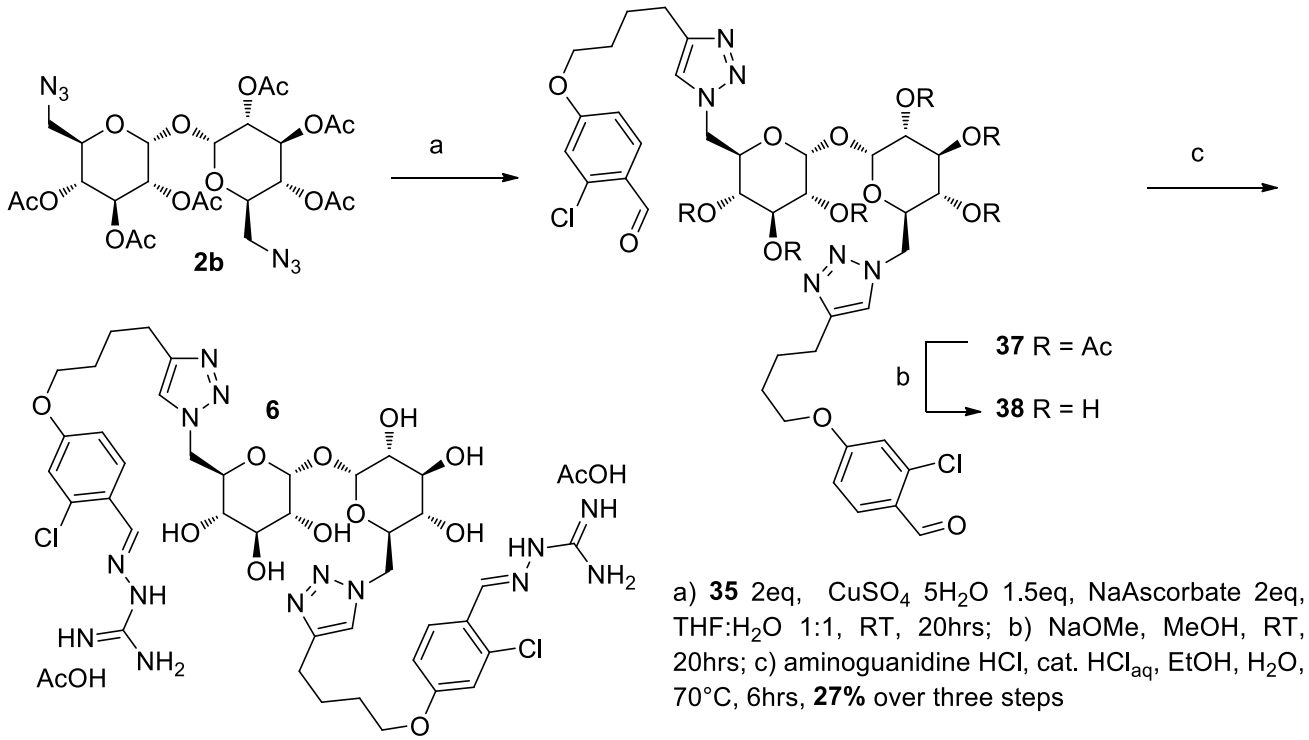

a) **35** 2eq, $CuSO_4$ $5H_2O$ 1.5eq, NaAscorbate 2eq, THF:H_2O 1:1, RT, 20hrs; b) NaOMe, MeOH, RT, 20hrs; c) aminoguanidine HCl, cat. HCl_{aq}, EtOH, H_2O, 70°C, 6hrs, **27%** over three steps

Scheme 13. Synthesis of 1:2 trehalose-sephin-1 DAC **6.**

The Click reaction between bis-6-azido acetylated trehalose **2b** and triple bond-containing sephin1-linker construct **35** (step a, Scheme 13), catalytic deprotection (step b) and condensation with aminoguanidine hydrochloride (step c) were performed similarly to the same steps in Scheme 12. After reverse phase chromatography, pure 1:2 target DAC **6** was obtained as a bis-acetate, in good purity and low, unoptimized yields.

3.3. BIOLOGICAL PROFILING

Trehalose-based prodrugs **1-hexa**, **1-tetra** and **1-bis** were tested at the University of Trento as autophagy inducers at low millimolar concentration either as such, or as prodrugs of trehalose **1**. This was set up to check a putative increase of cell penetration for the lipophilic prodrugs, leading then – after intracellular delivery – to the regeneration of trehalose **1**, and to a stronger induction of autophagy. Namely, HEK293 cells were treated with a buffer solution (first two-columns, Western blot a, Figure 10, left), with a 100 mM solution of trehalose **1** (third and fourth column), or with a 2.5 mM solution of prodrugs **1-bis**, **1-tetra** and **1-hexa** (fifth to tenth column) for 24hrs. As already described, autophagy induction was measured by the LC3B-I/LC3B-II ratio; prodrugs **1-bis**, **1-tetra** and **1-hexa** were tested at a much lower concentration than trehalose 1, hoping to see at least similar autophagy induction, due to better cell penetration.

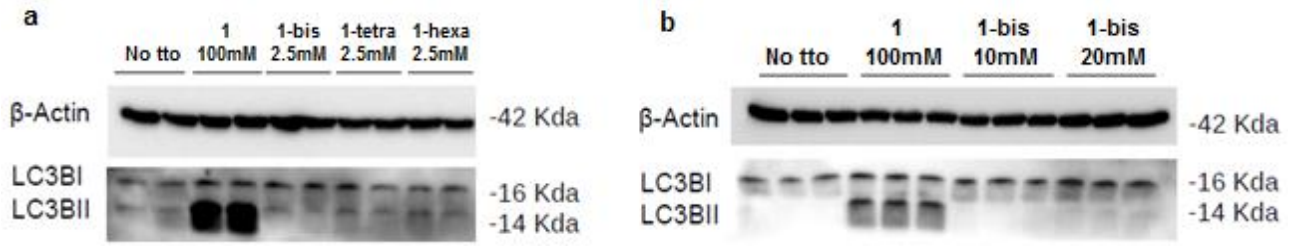

Figure 10. Trehalose prodrugs **1-hexa**, **1-tetra** and **1-bis**: induction of autophagy.

Unfortunately, even highly lipophilic hexa-acetylated **1-hexa** did not show any induction of autophagy at 2.5 mM. Additionally, we tested most water-soluble prodrug **1-bis** at higher concentration (Figure 10, Western blot b, right) but again no autophagy induction was observed up to 20 mM.

These negative results suggest that the poor biological activity of trehalose, requiring extremely high concentrations, does not depend only from its high polarity and poor cell-permeability. In future, prodrugs **1-bis**, **1-tetra** and **1-hexa** will be tested for their affinity for trehalases, and for their ability to regenerate parent trehalose **1** will be determined in cellular media. After such tests, their potential as prodrugs to decrease the dose of trehalose in humans as a putative drug against neurodegenerative diseases will be determined.

Autophagy induction was tested also for sephin1-trehalose DACs **5** and **6**; they were expected to be active also due to the previously shown activity of sephin1 (see Figure 8, Paragraph 3.1.4). As to 1:1 DAC **5**, we were delighted to observe autophagy induction (i.e., increase of LC3B-II) at 1 mM (Figure 11, Western blot a and tabulation b). Unfortunately, a cytotoxicity test (tabulation c) showed limited but significant toxicity for DAC **5** at 2.5 mM, i.e. close to its efficacy concentration.

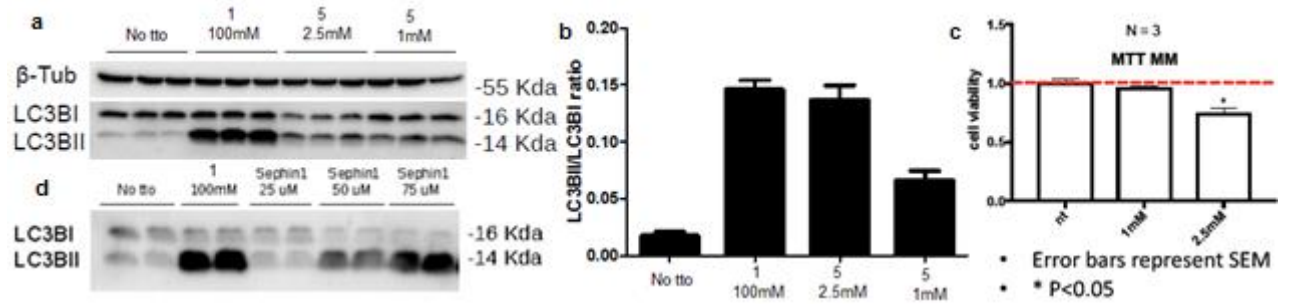

Figure 11. 1:1-sephin1-trehalose DAC **5**: induction of autophagy and cytotoxicity profile.

The autophagy induction and tolerability profile of 1:2 trehalose/sephin1 DAC **6** is shown in Figure 12. Compared to its 1:1 DAC counterpart **5**, it is more potent, inducing autophagy at concentrations around 50 μM (Western blot a and tabulation b, Figure 12); such value is similar to sephin1 itself (Figure 8, Paragraph 3.1.4). Once more, its cytotoxicity profile (tabulation c, Figure 12) shows toxicity at concentrations close to the efficacy of DAC **6** as an autophagy inducer, mirroring the behavior of sephin1.

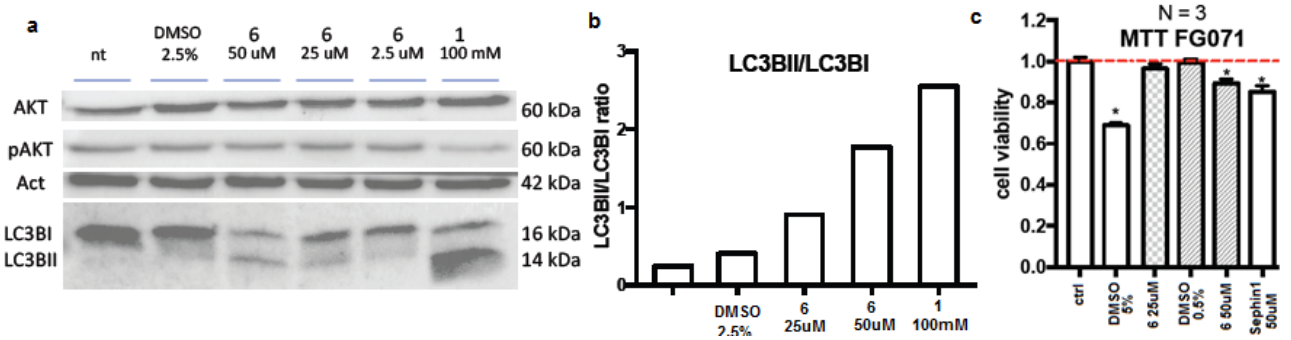

Figure 12. 2:1-sephin1-trehalose DAC **6**: induction of autophagy and cytotoxicity profile.

Thus, we concluded that the observed activity for DACs **5** (limited) and **6** (similar to sephin1) is likely exclusively due to its sephin1 portion. In future, the research group where I carried out my Ph. D. thesis plans to investigate the potential of novel, patentable sephin1 analogues as autophagy inducers against neurodegenerative diseases; and plans to rationally design and synthesize sephin1-based chemical probes, in order to identify its autophagy-related molecular target.

3.4 CONCLUSIONS AND FUTURE PERSPECTIVES

Trehalose-based prodrugs **1-hexa**, **1-tetra** and **1-bis** were synthesized, by refining existing synthetic routes, and were tested at the University of Trento as autophagy inducers at low millimolar concentrations. They will be tested in future for their affinity for trehalases, and for their prodrug efficiency, i.e. for their kinetics and stoichiometry in the regeneration process of parent trehalose **1** in cellular media. The research group where I carried out my Ph.D. internship is also considering the synthesis of either organic (i.e., liposomes) and inorganic (i.e., iron- or gold-based) trehalose-decorated nanoparticles (NPs) to determine their biological profiles.

Four different trehalose-azide compounds **2a**-**4** were prepared, and two of them (**2a**, **b**) were used for the synthesis of two sephin1-trehalose DACs (compounds **5** and **6**), that were tested for their ability to induce autophagy. Trehalose-azides **3** and **4** will also be coupled to sephin1 (only in a 1:1 ratio, due to the results of testing for DAC **5**), to provide the two corresponding DACs **39** and **40** (Figure 13).

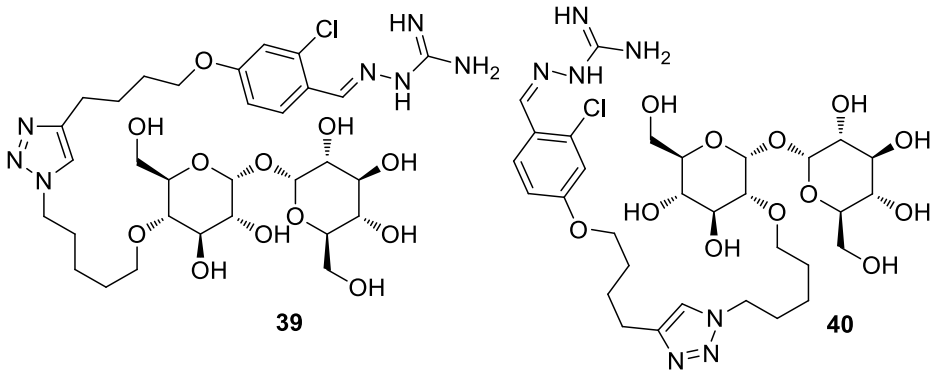

Figure 13. 4-connected (**39**) and 2-connected (**40**) 1:1 sephin1-trehalose DACs.

3.5. EXPERIMENTAL PART: Synthesis and analytical characterization of intermediates and final compounds

3.5.1. Synthesis of 2,3,4,2',3',4'-hexa-O-acetyl-α,α'-trehalose 1-hexa

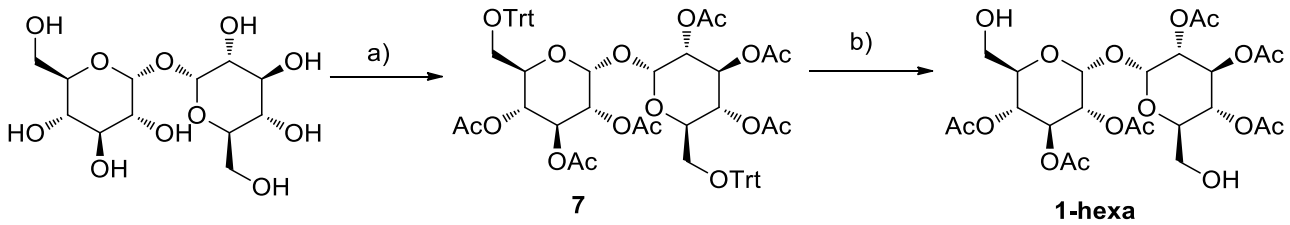

a) TrtCl, Py, 90°C, 24hrs then Ac_2O, RT, 16hrs, **72%**; b) DCA/DCM 1:1, RT, 30min, **90%**

2,3,4,2',3',4'-hexa-O-acetyl-6,6'-di-O-trityl-α,α-trehalose 7

Anhydrous trehalose **1** (501.2 mg, 1.460 mmol, 1eq) was stirred under N_2 atmosphere in dry pyridine (5 mL) for 30 minutes at 50°C. Trityl chloride (TrCl, 1.4260 g, 5.116 mmol, 3.5 eq) was then added, and the reaction mixture was stirred at 90°C (TLC monitoring, eluant mixture: EtOAc/MeOH 8:2). After 24hrs the solution was cooled at RT, Ac_2O (1.25 ml, 13.14 mmol, 9 eq) was slowly added, and the reaction mixture was stirred under N_2 for 16hrs (TLC monitoring, eluant mixture: EtOAc/n-hexane 3:7). Then the solvent was removed under reduced pressure. The crude solid was dissolved in EtOAc (30 mL), the organic layer was then sequentially washed with 5% HCl (20 mL), sat. $NaHCO_3$ (20 mL), and brine (10 mL). The organic layer was then dried with Na_2SO_4 and concentrated under reduced pressure. The crude was purified by flash chromatography (eluant mixture: EtOAc/n-hexane 3:7) yielding 1134 mg of pure **7** as a white solid (1.051 mmol, **72%** yield). For technical inconvenient this intermediate was not characterized.

2,3,4,2',3',4'-hexa-O-acetyl-α,α'-trehalose 1-hexa

Compound **7** (300 mg, 0.280 mmol, 1eq) was dissolved in DCM (1.5 mL), then dichloroacetic acid (DCA, 1.5 mL) was added and the yellow solution was stirred at RT for 30 min (TLC monitoring, eluant mixture: DCM/EtOAc 7:3). The crude mixture was diluted with DCM (25 mL), washed with water (20 mL), and then with sat. $NaHC0_3$ (2 x 20 mL). The organic layer was then dried with Na_2SO_4 and concentrated under reduced pressure. The light yellow solid crude (300 mg) was purified by flash chromatography (eluant mixture: EtOAc/DCM 6:4) yielding 133.2 mg of pure **1-hexa** as a white solid (0.224 mmol, **80%** yield).

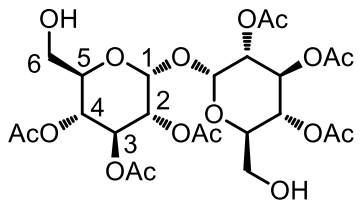

Characterization:

^1H NMR (300 MHz, $CDCl_3$): δ (ppm) 5.50 (t, J=10.0 Hz, 2H, H3), 5.29 (d, J=3.9 Hz, 2H, H1), 5.01-4.93 (m, 4H, H4, H2), 3.92 (m, 2H, H5), 3.59 (m, 4H, H6), 2.10 (s, 12H, Ac), 2.02 (s, 6H, Ac), 1.24 (bs, 2H, OH).

ESI MS: Calcd $[C_{24}H_{34}O_{17}]$:594.52, found: 617.60 $(M+Na^+)$.

3.5.2. Synthesis of 2,3,2',3'-tetra-O-acetyl-α,α'-trehalose 1-tetra

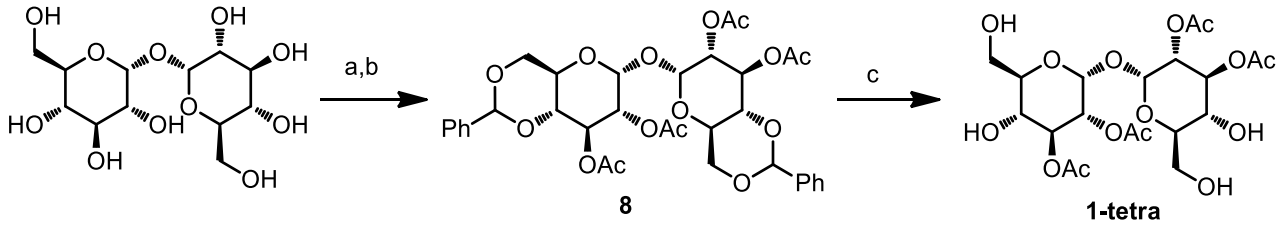

a) $PhCH(OMe)_2$ 2.2eq, cat PTSA, DMF, 105°C, 80min; b) Ac_2O, Py, RT, 16hrs, **80%** over two steps; c) H_2, Pd-C, MeOH/THF 4:1, RT, 16hrs, **99%**.

2,3,2',3'-tetra-O-acetyl-4,6:4',6'-di-O-benzylidene-α,α'-trehalose 8

Trehalose dihydrate (1000 mg, 2.922 mmol, 1 eq) was dried under vacuum at 96°C overnight. Then it was transferred in a two-neck round bottom flask and dissolved under argon atmosphere in dry DMF (8 mL). The mixture was heated at 105°C for 5 minutes, then solid p-toluenesulfonic acid monohydrate (PTSA, 25.2 mg, 0.146 mmol, 0.05 eq) was added. The resulting solution was stirred for additional 5 minutes. Benzaldehyde dimethyl acetal (0.940 µL, 6.428 mmol, 2.2 eq) was then added in three equal portions in 1 hour, while maintaining the reaction temperature at 100°C. After the third addition the solution was stirred for additional 40 minutes, while monitoring by TLC (eluant mixture: DCM/MeOH 95:5). The solvent was removed at reduced pressure, the brown oily residue was dissolved in pyridine (10 mL) and cooled at 0°C under stirring. Then Ac_2O (2.8 mL, 14.61 mmol, 10 eq) was slowly added and the solution was stirred at RT for 16 hrs (TLC monitoring, eluant mixture: n-hexane/EtOAc 6:4). After reaction completion, the solvent was removed at reduced pressure. The crude solid was dissolved in EtOAc (50 mL), and was sequentially washed with 5% HCl (25 mL), sat. $NaHC0_3$ (25 mL), and brine (15 mL). The organic layer was then dried with Na_2SO_4 and concentrated under reduced pressure. The crude (2.3g) was purified by flash chromatography (eluant mixture: n-hexane/EtOAc from 7:3 to 1:1), yielding 1.65 g of pure **8** as a white solid (2.338 mmol, **80%** yield).

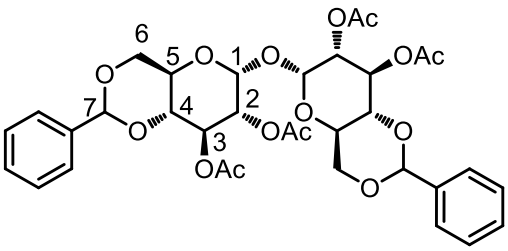

Characterization:

^{1}H NMR (300 MHz, $CDCl_3$): δ (ppm) 7.50-7.31 (m, 10H, Ph), 5.62 (t, J=9.8 Hz, 2H, H3), 5.51 (s, 2H, H7), 5.32 (d, J=4.0 Hz, 2H, H1), 5.00 (dd, 2H, J=9.8 Hz, J=4.0 Hz, H2), 4.18 (m, 2H, H6), 4.00 (m, 2H, H5), 3.75 (m, 4H, H6, H4), 2.18 (s, 6H, Ac), 2.07 (s, 6H, Ac).

2,3,2',3'-tetra-O-acetyl-α,α'-trehalose 1-tetra

A stirred solution of compound **8** (300.8 mg, 0.439 mmol) in a 4:1 mixture of MeOH/THF (9 mL) at RT was treated with 10% Pd-C (30 mg) under nitrogen atmosphere. The reaction mixture was degassed and flushed with H_2 (three times), and then stirred vigorously for 6 hrs under hydrogen atmosphere at RT (TLC monitoring, eluant mixture: DCM/MeOH 8:2). After reaction completion, the mixture was filtered through a Celite pad, washing it afterwards with MeOH (30 mL). The colourless solution was concentrated *in vacuo* to give 223.4 mg of pure **1-tetra** as a white solid (0.436 mmol, **99%** yield).

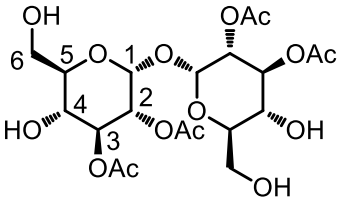

Characterization:

^{1}H NMR (300 MHz, CD_3CN): δ (ppm) 5.28 (t, J=10.2 Hz, 2H, H3), 5.19 (d, J=3.7 Hz, 2H, H1), 4.78 (dd, 2H, J=10.2 Hz, J=3.7 Hz, H2), 3.70 (m, 2H, H5), 3.68 (m, 6H, H6, H4), 2.80 (m, 4H, OH), 2.08 (s, 6H, Ac), 2.00 (s, 6H, Ac).

ESI MS: Calcd [$C_{20}H_{30}O_{15}$]:510.44, found: 533.34 (M + Na).

3.5.3. Synthesis of 6,6'-bis-O-acetyl-α,α'-trehalose 1-bis

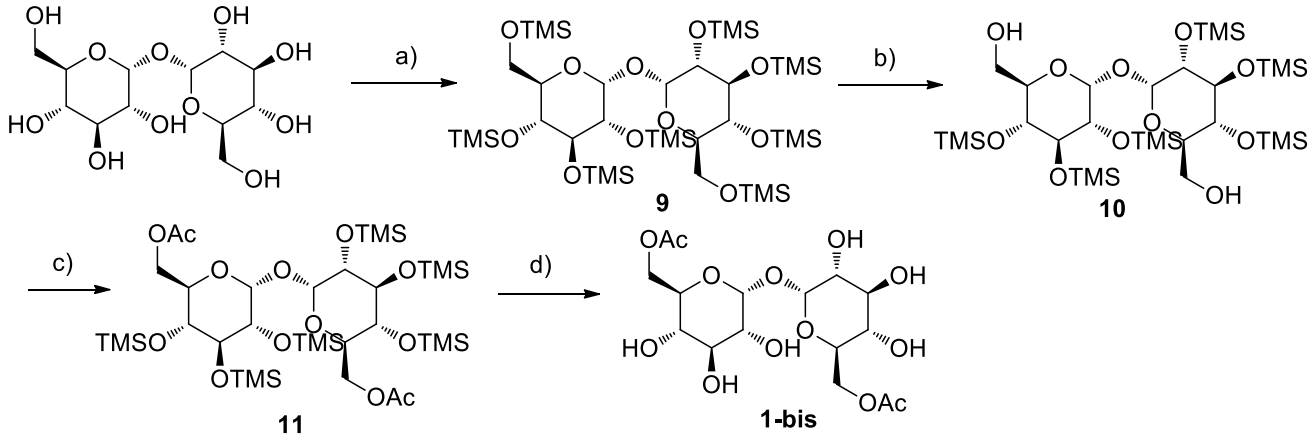

a) TMSCl, Py, 0°C to RT, 16hrs; b) cat. K_2CO_3, MeOH/DCM (3:1) 0°C to RT, 1hr, **75%** over two steps; c) Ac_2O, TEA, DMAP, DCM, RT, 4hrs, **91%**; d) cat. AcOH, MeOH, 70°C, 6hrs, **99%**.

2,3,4,2',3',4'-hexa-O-trimetylsilyl-α,α'-trehalose 10

Trehalose **1** (471.4 mg, 1.246 mmol, 1eq) was dissolved in pyridine (12 mL) and stirred for 20 minutes at RT, until complete dissolution. The reaction was cooled to 0 °C and chlorotrimethyl silane (1.6 mL, 12.46 mmol, 10 eq) was added dropwise. The reaction was stirred for additional 30 minutes at 0 °C and warmed to RT. After 16 hours the solvent was concentrated at reduced pressure. The white solid residue was dissolved in water (35 mL) and extracted with n-hexane (4 x 30 mL). The combined organic layers were dried over Na_2SO_4 and concentrated in vacuum to yield crude **9** (1.1 g) as a white solid that was used without purification in the next reaction step.

Crude **9** (1.1 g, theoretically 1.24 mmoles) was dissolved in 3:1 MeOH/DCM (8 mL), cooled at 0°C under stirring, and solid K_2CO_3 (20.7 mg, 0.150 mmol, 0.12 eq) was added. The reaction was stirred for 15 minutes at 0°C, then at RT for 1 hour (TLC monitoring, eluant mixture: n-hexane/AcOEt 8:2). After reaction completion the reaction was quenched by addition of acetic acid (0.025 mL). The solvent was removed at reduced pressure, and the crude was purified by flash chromatography (eluant mixture: EtOAc/ n-hexane from 2:8 to 4:6), yielding 724.6 mg of pure **10** as a white solid (0.935 mmol, **75%** yield over two steps).

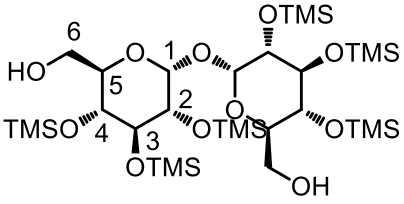

Characterization:

^{1}H NMR (300 MHz, $CDCl_3$): δ (ppm) 4.85 (d, J=3.6 Hz, 2H, H1), 3.92 (m, 4H, H3, H5), 3.70 (m, 4H, H6), 3.40 (m, 4H, H2, H4), 1.61 (bs, 2H, OH), 0.15 (s, 54H, TMS).

2,3,4,2',3',4'-hexa-O-trimetylsilyl-6,6'-bis-O-acetyl-α,α'-trehalose 11

2,3,4,2',3',4'-hexa-O-trimetylsilyl-α,α'-trehalose **10** (700 mg, 0.903 mmol, 1 eq) was dissolved in DCM (5 mL), and TEA (456.9 mg, 4.515 mmol, 5 eq) was added under stirring at RT. Acetic anhydride (260 µL, 2.708 mmol, 3eq) was slowly added, followed by a catalytic amount of DMAP. The reaction mixture was stirred at RT for 4 hours (TLC monitoring, eluant mixture: n-hexane/EtOAc 8:2). Then the reaction mixture was diluted with DCM (30 mL), and sequentially washed with water (10 mL) and brine (10 mL). The organic layer was then dried with Na_2SO_4 and concentrated under reduced pressure to give a solid which was purified by column chromatography (eluant mixture: n-hexane/EtOAc 9:1) to obtain 706.2 mg of pure **11** as a white solid (0.821 mmol, **91%** yield).

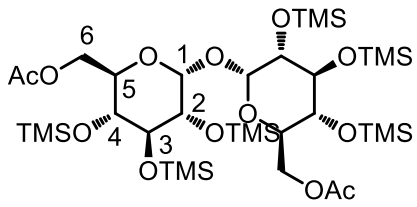

Characterization:

^{1}H NMR (300 MHz, $CDCl_3$): δ (ppm) 4.85 (d, J=3.6 Hz, 2H, H1), 4.27 (dd, J=8.9 Hz, J=3.6 Hz, 2H, H2), 4.19 (t, J=8.9 Hz, 2H, H3), 4.07 (m, 2H, H5), 3.90 (t, J=8.9 Hz, 2H, H4), 3.48 (m, 4H, H6), 2.05 (s, 6H, Ac), 0.15 (s, 54H, TMS).

6,6'-bis-O-acetyl-α,α'-trehalose 1-bis

AcOH (5 drops) was added under nitrogen atmosphere at RT to a solution of compound **11** (500 mg, 0.582 mmol, 1 eq) in dry MeOH (20 mL). The reaction was stirred at 70°C for 8 hrs, and monitored by TLC (eluant mixture: $CHCl_3$/MeOH/water 60:35:5). Then, the solvent was evaporated at reduced pressure yielding 247.3 mg of pure **1-bis** as a white solid (0.580 mmol, **99%** yield).

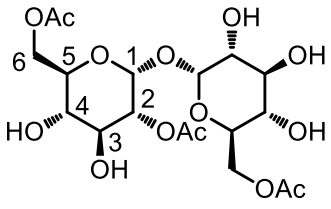

Characterization:

^{1}H NMR (300 MHz, D_2O): δ (ppm) 5.19 (d, J=3.6 Hz, 2H, H1), 4.51-4.27 (m, 4H, H6), 4.19 (m, 2H, H5), 3.85 (t, J=9.5 Hz, 2H, H3), 3.68 (dd, J=9.5 Hz, J=3.6 Hz, 2H, H2), 3.51 (t, J=9.5 Hz, 2H, H4), 2.12 (s, 6H, Ac).

ESI MS: Calcd [$C_{16}H_{26}O_{13}$]:426.37, found: 449.50 (M + Na).

3.5.4. Synthesis of fully acetylated mono and bis 6-azido-6-deoxy-α,α-trehalose 2a and 2b

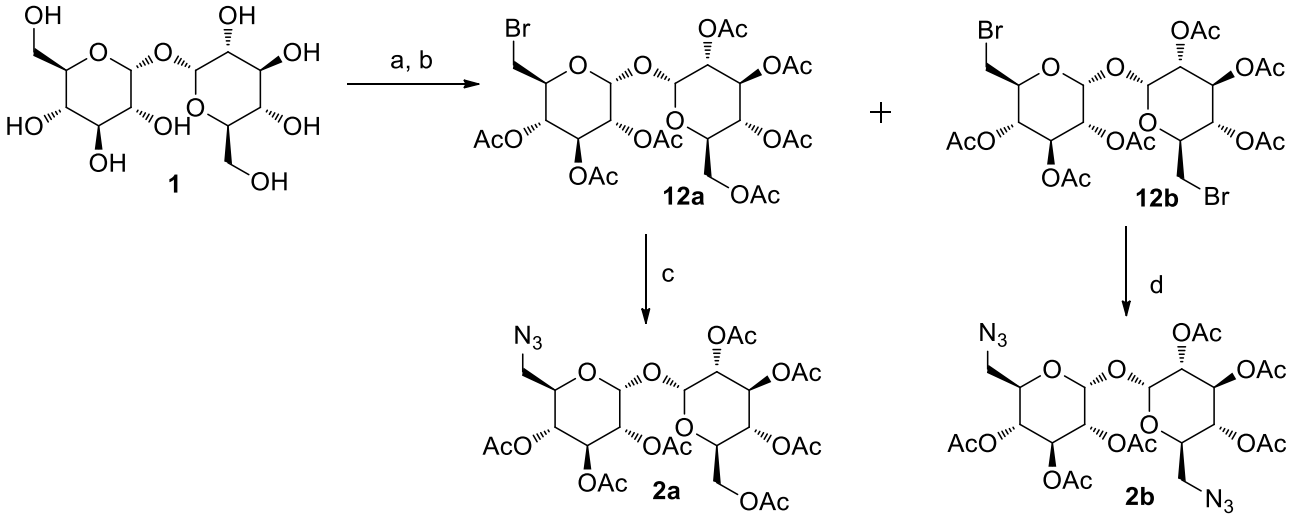

a) NBS 2eq, PPh_3 2eq, DMF, RT 16hrs then 60°C 24hrs; b) Ac_2O, Pyridine RT, 24hrs **30%** (**12a**), **18%** (**12b**); c) NaN_3 5 eq, DMF, 55°C, 16hrs, **80%**.d) NaN_3 10eq, DMF, 55°C, 16hrs, **79%**.

2,3,4,2',3',4',6'-hepta-O-acetyl-6-bromo-6-deoxy-α,α-trehalose 12a and 2,3,4,2',3',4',-hexa-O-acetyl-6,6'-bromo-6,6'-deoxy-α,α-trehalose 12b

Trehalose dihydrate (950.1 mg, 2.775 mmol, 1 eq) was dehydrated in vacuum at 100° overnight. Then it was dissolved under nitrogen atmosphere in l dry DMF (9 mL), and solid Ph_3P (1455.6 mg, 5.55 mmol, 2 eq) was added under stirring at RT. After 15 minutes, solid N-bromosuccinimide (NBS, 988.0 mg, 5.551 mmol, 2 eq) was added in small portions over 1 hour while stirring. The mixture was stirred at RT overnight, warmed to 60°C and stirred for additional 24 hrs (TLC monitoring, eluant mixture: $CHCl_3$/MeOH/H_2O 60:35:5). MeOH (10 mL) was then added to quench the reaction, and the solvents were removed under reduced pressure to give a yellow-brown solid (1.2 g). The residue was dissolved in water (50 mL), and the solution was washed with DCM (4 x 20 mL). The aqueous phase was then concentrated at reduced pressure. The resulting brown oil was dissolved in pyridine (9 mL), cooled at 0°C under stirring and Ac_2O (3.7 mL, 38.85 mmol, 2 eq) was added dropwise. The reaction was stirred overnight at RT (TLC monitoring, eluant mixture; DCM/AcOEt 8:2). After solvent removal at reduced pressure, the crude was dissolved in AcOEt (60 mL) and washed sequentially with 5%aq HCl (30mL), saturated aq. $NaHCO_3$ (30 mL) and brine (30 mL). The organic phase was dried with Na_2SO_4. After solvent concentration at reduced pressure, column chromatography on silicagel (eluant mixture: DCM/AcOEt 9:1 to 8:2) led to pure 485.3 mg of **12b** as a white solid (0.694 mmol, **18**% yield) and 400 mg of **12a** as a white solid (0.555 mmol, **30**% yield).

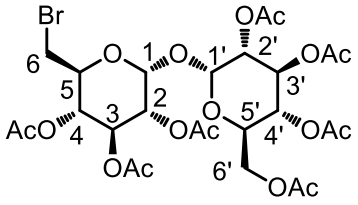

Characterization – 12a:

^{1}H NMR (400 MHz, $CDCl_3$): δ (ppm) δ 5.51 (m, 2H, H3), 5.535 (m, 2H, H1, H1'), 5.16 (dd, J = 10.3, 3.9 Hz, 1H, H2), 5.06 (m, 2H, H4', H2'), 4.98 (t, J = 9.7 Hz, 1H, H4), 4.23 (dd, J = 12.2, 5.9 Hz, 1H, H5'), 4.18 – 4.08 (m, 1H, H6'), 4.08 – 3.98 (m, 2H, H5, H6'), 3.37 (ddd, J = 18.9, 11.2, 5.2 Hz, 2H, H6), 2.18 – 1.97 (m, 21H, Ac).

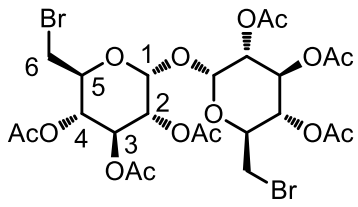

Characterization – 12b:

^{1}H NMR (400 MHz, $CDCl_3$): δ (ppm) 5.48 (t, J = 8.9 Hz, 2H, H3), 5.33 (d, J = 4.1 Hz, 2H, H1), 5.12 (dd, J = 8.9Hz, J = 4.1Hz, 2H, H2), 4.95 (t, J = 8.9Hz, 2H, H4), 4.11(m, 2H, H5), 3.31 (m, 4H, H6), 2.12 (s, 6H, Ac), 2.07 (s, 6H, Ac), 2.01 (s, 6H, Ac).

2,3,4,2',3',4',6'-hepta-O-acetyl-6-azido-6-deoxy-α,α-trehalose 2a

Compound **12a** (290.4 mg, 0.415 mmol, 1 eq) was dissolved in anhydrous DMF (4 mL) while stirring under a nitrogen atmosphere. Solid NaN_3 (134.9 mg, 2.076 mmol, 5eq) was added, the reaction mixture was heated at 55°C and stirred for 16 hours (TLC monitoring, eluant mixture: DCM/ EtOAc 4:1). Then the solvent was removed at reduced pressure. The crude was dissolved in EtOAc (30 mL), and the solution was sequentially washed with water (20 mL) and brine (15 mL). The organic layer was then dried with Na_2S0_4 and concentrated at reduced pressure. The brown-solid crude (280 mg) was purified by column chromatography on silicagel (eluant mixture: DCM/EtOAc 85:15) to obtain 219.7 mg of pure **2a** as a white solid (0.332 mmol, **80**% yield).

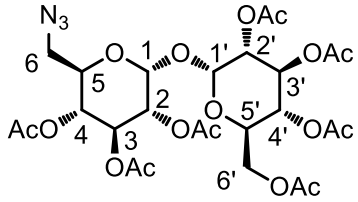

Characterization:

^{1}H NMR (300 MHz, $CDCl_3$): δ (ppm) 5.46 (m, 2H, H3, H3'), 5.31 (m, 2H, H1, H1'), 5.02 (m, 4H, H4, H4', H2, H2'), 4.24 (m, 1H, H5), 4.06 (m, 3H, H5', H6'), 3.25 (m, 2H, H6), 2.04 (m, 21H, Ac).

2,3,4,2',3',4'-hexa-O-acetyl-6,6'-azido-6,6'-deoxy-α,α-trehalose 2b

Compound **12b** (338 mg, 0.470 mmol, 1 eq) was dissolved in dry DMF (5 mL) at RT, then NaN_3 (305.3 mg, 4.70 mmol, 10 eq) was added while stirring under a nitrogen atmosphere. The reaction mixture was heated to 55°C and stirred for 16 hours (TLC monitoring, eluant mixture: DCM/EtOAc 8:2). Then, the solvent was evaporated at reduced pressure and the crude was dissolved in AcOEt (40 mL), washed with water (20 mL) and brine (15 mL). The organic phase was dried with Na_2SO_4, filtered and the solvent removed under reduced pressure. The crude residue (295.3 mg) was purified by flash chromatography on silicagel (eluant mixture: DCM/EtOAc 8:2), yielding 240 mg of pure **2b** as a white solid (0.371 mmol, **75**% yield).

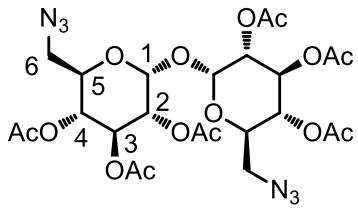

Characterization:

^{1}H NMR (400 MHz, $CDCl_3$): δ (ppm) 5.41 (t, J = 8.9 Hz, 2H, H3), 5.27 (d, J = 4.1 Hz, 2H, H1), 5.02 (dd, J = 8.9Hz, J = 4.1Hz, 2H, H2), 4.92 (t, J = 8.9Hz, 2H, H4), 4.04 (m, 2H, H5), 3.30 (dd, J = 13.3 Hz, J = 7.3 Hz, 2H, H6), 3.09 (dd, J = 2.4Hz, J = 13.3 Hz, 2H, H6), 2.06 (s, 6H, Ac), 2.00 (s, 6H, Ac), 1.97 (s, 6H, Ac)

3.5.5. Synthesis of 2,3,6,2',3',4',6'-hepta-O-acetyl-4-O-(5-azidopentyl)-α,α-trehalose 3

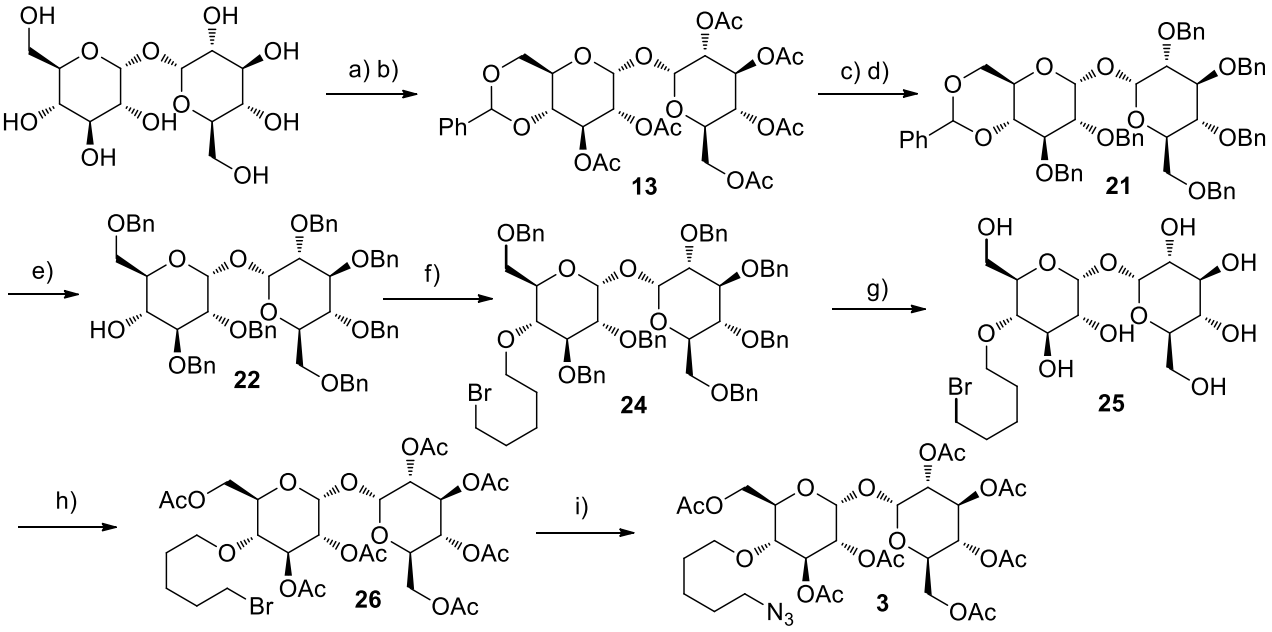

a) $PhCH(OMe)_2$ 1eq, PTSA 0.05eq, DMF, 105°C, 80min; b) Ac_2O, Py, RT, 16hrs, **51%** over two steps; c) MeONa 0.15eq, MeOH, RT, 16hrs; d) BnBr 9eq, NaH 7.5eq, dry DMF, RT, 24hrs, **84%** over two steps; e) Et_3SiH 7.5eq, TFA 7.5eq, dry DCM, 0°C to RT, 4hrs, **80%**; f) $Br(CH_2)_5Br$ 10eq, NaH 2eq, DMF, 55°C, 8hrs, **70%;** g) H_2, Pd/C 10%, MeOH/THF 4:1, RT, 16hrs; h) Ac_2O, cat DMAP, DCM/Py 4:1, RT, 16hrs; i) NaN_3, DMF 65°C, 16hrs, **60%** over three steps.

2,3,2',3',4',6'-hexa-O-acetyl-4,6-O-benzylidene-α,α-trehalose 13

Trehalose dihydrate (1.43 g, 3.789 mmol, 1 eq) was dried under vacuum at 100°C overnight. Then was transferred in a two-neck round bottom flask and dissolved under argon atmosphere in dry DMF (13 mL). The mixture was heated at 105°C for 5 minutes, then p-toluenesulfonic acid monohydrate (PTSA, 36.1 mg, 0.190 mmol, 0.05 eq) was added as solid and the solution was stirred for additional 5 minutes. Benzaldehyde dimethyl acetal (0.627 µL, 4.178 mmol, 1.1 eq) was added in three equal portions in an hour, while maintaining the reaction temperature at 100°C. After the third addition the solution was stirred for additional 40 minutes (TLC monitoring, eluant mixture: DCM/MeOH 95:5). The solvent was removed under high vacuum, the resulting brown oil was dissolved in pyridine (12 mL) and cooled at 0°C. Then Ac_2O (3.5 mL, 37.89 mmol, 10 eq) was slowly added and the solution was stirred at RT for 16 hrs (TLC monitoring, eluant mixture: n-hexane/ EtOAc 1:1). Then the solvent was removed under high vacuum. The crude solid was dissolved in EtOAc (50 mL), the organic layer was then sequentially washed with 5% HCl (25 mL), sat. $NaHC0_3$ (25 mL), and brine (15 mL). The organic layer was then dried with Na_2SO_4 and concentrated under reduced pressure. The crude (≈3 g) was purified by flash chromatography (eluant mixture: EtOAc/n- hexane from 4:6 to 6:4) yielding 1.25 g of pure **13** as a white solid (1.831 mmol, **51**% yield).

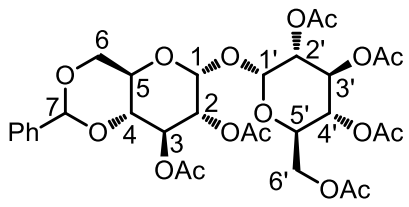

Characterization:

^1H NMR (400 MHz, $CDCl_3$): δ (ppm) 7.42-7.33 (m, 5H, Ph), 5.58 (m, 1H, H3'), 5.45 (m, 2H, H3, H7), 5.40 (d, J = 4.09 Hz, 1H, H1), 5.22 (d, J = 4.07 Hz, 1H, H1'), 5.00 (m, 3H, H4', H2, H2'), 4.25-3.90 (m, 5H, H4, H5, H5', H6'), 3.70 (m, 2H, H6), 2.05 (m, 18H, Ac).

2,3,2',3',4',6'-hexa-O-benzyl-4,6-O-benzylidene-α,α-trehalose 21

Fully protected trehalose **13** (1.0 g, 1.465 mmol, 1 eq) was suspended in dry MeOH (20 mL). Then, sodium methoxide (80.0 mg, 1.465 mmol, 1 eq) was added under stirring. The reaction mixture was stirred at RT for 24 hrs (TLC monitoring, eluant mixture: DCM/MeOH 95:5). Then, Amberlite IR120 H^+ resin was added under stirring until neutral pH. The reaction mixture was filtered, and the solvent evaporated. The white solid residue was dissolved in dry DMF (14 mL) and benzyl bromide (BnBr, 1.566 mL, 13.185 mmol, 9 eq) was added. Then, sodium hydride (60% dispersion in mineral oil, 470 mg, 11.72 mmol, 8 eq) was slowly added. The resulting mixture was stirred at 25°C for 24 hours (TLC monitoring, eluant mixture: n-hexane/EtOAc 75:25). Then, the excess of sodium hydride was quenched with methanol (3 mL). After further stirring for 30 minutes, the reaction mixture was concentrated at reduced pressue,and the residue was diluted with EtOAc (30 mL). The organic phase was washed with saturated $NaHCO_3$ (20 mL) and brine (15 mL), dried with Na_2SO_4 and concentrated under reduced pressure. The crude yellow oil was purified by flash chromatography (eluant mixture: EtOAc/ n-hexane 2:8) yielding 1.20 g of pure **21** as a colorless oil (1.23 mmol, **84**% yield).

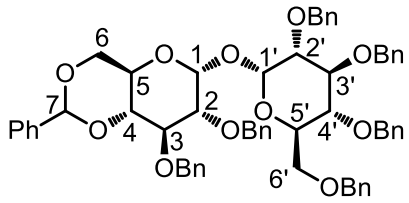

Characterization:

^{1}H NMR (400 MHz, $CDCl_3$): δ (ppm) δ 7.51-7.49 (m, 2H, Ph), 7.40-7.20 (m, 31H, Ph), 7.14-7.12 (m, 2H, Ph), 5.55 (s, 1H, H7), 5.18-5.17 (m, 2H, H1, H1'), 4.97 (d, J = 14.7 Hz, 1H, $PhCH_2$), 4.95 (d, J = 14.5 Hz, 1H, $PhCH_2$), 4.86-4.66 (m, 7H, $PhCH_2$), 4.53 (d, J = 11.8 Hz, 1H, $PhCH_2$), 4.46 (d, J = 11.5 Hz, 1H, $PhCH_2$), 4.38 (d, J = 12.4 Hz, 1H, $PhCH_2$), 4.27 (dt, J = 9.7, 4.7 Hz, 1H, H5), 4.17-4.10 (m, 3H, H4', H5', H6), 4.03 (t, J = 7.4 Hz, 1H, H3), 3.69-3.57 (m, 5H, H2, H2', H3', H4, H6), 3.50 (dd, J = 10.7, 2.9 Hz, 1H, H6'), 3.37 (d, J = 10.7 Hz, 1H, H6').

2,3,4,2',3',4',6'-hepta-O-benzyl-α,α-trehalose 22

Protected trehalose derivative **21** (1.07 g, 1.086 mmol, 1eq) was dissolved in dry DCM (20 mL), cooled at 0°C and stirred under Ar atmosphere. Triethylsilane (TESH, 1.3 mL, 8.148 mmol, 7.5 eq) and trifluoroacetic acid (TFA, 0.623 mL, 8.148 mmol, 7.5 eq) were sequentially added under stirring. The reaction mixture was slowly warmed to RT, and stirred for additional 4 hours (TLC monitoring, eluant mixture: n-hexane/ EtOAc 7:3). Then, the solution was diluted with DCM (20 mL) and neutralized with a sat aqueous $NaHCO_3$ solution (20 mL). The organic layer was washed with brine (20 mL), dried over Na_2SO_4 and concentrated in vacuum. The crude (1.06 g) was purified by flash chromatography (eluant mixture: n-hexane/ EtOAc from 75:25 to 65:35), yielding 831 mg of pure **22** as a colorless oil (0.853 mmol, **78**% yield).

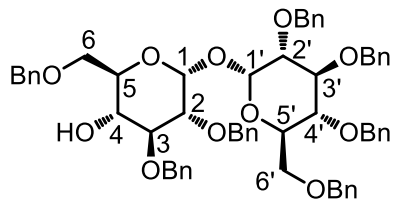

Characterization:

^{1}H NMR (400 MHz, $CDCl_3$): δ (ppm) 7.37-7.20 (m, 33H, Ph), 7.13-7.11 (m, 2H, Ph), 5.26 (m, 2H, H1, H1'), 5.00 (m, 2H, $PhCH_2$), 4.85 (m, 3H, $PhCH_2$), 4.70 (m, 4H, $PhCH_2$), 4.60-4.40 (m, 5H, $PhCH_2$), 4.15 (m, 2H, H5, H5'), 4.03 (t, J=9.4 Hz, 1H, H3), 3.87 (t, J=9.4 Hz, 1H, H3'), 3.63 (m, 2H), 3.56-3.44 (m, 5H), 3.36 (d, J=10.1 Hz, 1H), 2.38 (d, J=2.3 Hz, 1H, OH).

2,3,6,2',3',4',6'-hepta-O-benzyl-4-O-(5-bromopentyl)-α,α-trehalose 24

A stirred solution of benzylated trehalose **22** (800 mg, 0.822 mmol, 1 eq) in dry DMF (8 mL) was treated with 1,5-dibromopentane (1.12 mL, 8.223 mmol, 10 eq) under Ar atmosphere. Then, sodium hydride (60% dispersion in mineral oil, 65.7 mg, 1.644 mmol, 2 eq) was slowly added, the resulting mixture was heated at

55°C and stirred for 4 hours (TLC monitoring, eluant mixture: n-hexane/EtOAc 75:25). Then, the excess of sodium hydride was quenched with 5% aqueous citric acid (3 mL). After further stirring for 30 minutes, the reaction mixture was concentrated at reduced pressure and the residue was diluted with EtOAc (30 mL). The organic layer was washed with saturated aqueous $NaHCO_3$ (20 mL), brine (15 mL), dried with Na_2SO_4 and concentrated under reduced pressure. The crude yellow oil was purified by flash chromatography (eluant mixture: EtOAc/ n-hexane 2:8), yielding 645.7 mg of pure **24** as a colorless oil (0.575 mmol, 70% yield).

Characterization:

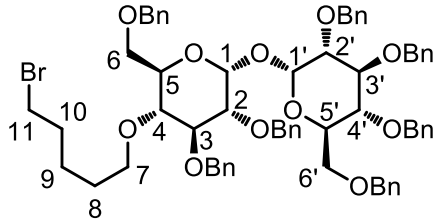

^{1}H NMR (400 MHz, $CDCl_3$): δ (ppm) 7.37-7.20 (m, 33H, Ph), 7.13-7.11 (m, 2H, Ph), 5.15 (d, J = 4.1 Hz, 1H, H1), 5.13 (d, J = 4.2 Hz, 1H, H1'), 4.86 (m, 2H, $PhCH_2$), 4.81 (d, 1H, $PhCH_2$), 4.73 (m, 2H, $PhCH_2$), 4.60-4.58 (m, 4H, $PhCH_2$), 4.48 (m, 2H, $PhCH_2$), 4.45 (d, 1H, $PhCH_2$), 4.31 (m, 2H, $PhCH_2$), 4.05 (m, 1H, H5), 3.96 (m, 2H, H5', H3), 3.83 (t, J=9.4 Hz, 1H, H3'), 3.61 (m, 2H, H4, H7), 3.56 (m, 1H, H2), 3.50-3.22 (m, 9H, H11, H7, H6, H6', H4', H2'), 1.68 (m, 2H, H10), 1.36-1.17 (m, 4H, H9, H8).

^{13}C NMR (100 MHz, $CDCl_3$): 138.9, 138.4, 138.3, 137.8, 128.3, 128.0, 127.8, 127.7, 127.4, 94.5, 81.7,79.4, 79.3, 78.2, 75.6, 75.0, 73.5, 72.7, 70.7, 70.6, 68.1, 33.7, 32.6, 29.6, 24.8, 14.2.

4-O-(5-bromopentyl)-α,α-trehalose 25

A stirred solution of bromobenzyl trehalose **24** (597.2 mg, 0.534 mmol) in a 4:1 mixture of MeOH/THF (11 mL) was treated at RT with 10% Pd-C (60 mg) under nitrogen atmosphere. The reaction mixture was degassed and flushed with H_2 (three times), and then stirred vigorously for 16 hrs under hydrogen atmosphere at RT (TLC monitoring, eluant mixture: $CHCl_3$/MeOH/H_2O 60:35:5). After reaction completion, the mixture was filtered through a Celite pad, washing it afterwards with MeOH (30 mL). The colourless solution was concentrated *in vacuo* to give 240.1 mg of pure **25** as a white solid, which was used for the next step without further purification.

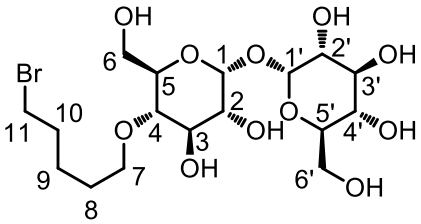

Characterization:

^{1}H NMR (400 MHz, D_2O): δ (ppm) 5.13 (m, 2H, H1, H1'), 3.87-3.57 (m, 12H, H2, H2', H3, H3', H5, H5', H6, H6', H7), 3.48 (t, J = 9.1 Hz, 2H, H11), 3.40 (t, J = 8.5 Hz, 1H, H4'), 3.31 (t, J = 7.8 Hz, 1H, H4), 1.84 (m, 2H, H10), 1.57 (m, 2H, H8), 1.46 (m, 2H, H9).

^{13}C NMR (from HSQC, D_2O): δ (ppm) 93.1, 93.0, 77.9, 73.1, 72.5, 72.0, 71.6, 71.3, 71.1, 69.3, 60.3, 34.5, 31.7, 28.3, 23.9.

ESI MS: Calcd [$C_{17}H_{31}BrO_{11}$]:490.1, found: 513.33 ($M+Na^+$).

2,3,6,2',3',4',6'-hepta-O-acetyl-4-O-(5-bromopentyl)-α,α-trehalose 26

Bromo trehalose **25** was suspended in DCM (5.5 mL), and pyridine (973 mg, 13.884 mmol, 28 eq) was added under stirring at RT. Acetic anhydride (656 µL, 6.942 mmol, 13 eq) was slowly added, followed by a catalytic amount of DMAP. The reaction mixture was stirred at RT for 16 hrs (TLC monitoring, eluant mixture: DCM/EtOAc 4:1). Then, the solvent was removed under vacuum, the brown oil was dissolved in EtOAc (2 0mL) and the organic layer was sequentially washed with 5% HCl (10 mL), sat. $NaHCO_3$ (10 mL) and brine (10

mL). The organic layer was then dried with Na_2SO_4 and concentrated under reduced pressure to give the crude acetylated product **26** (370.1 mg) which was used for the next step without further purification.

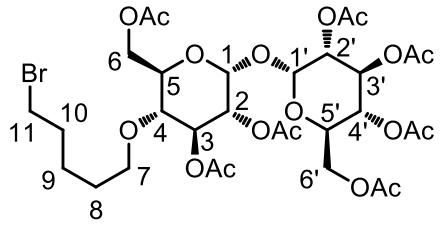

Characterization:

^{1}H NMR (400 MHz, $CDCl_3$): δ (ppm) 5.41 (m, 2H, H3, H3'), 5.20 (d, J = 4.1 Hz, 1H, H1'), 5.13 (d, J = 4.1 Hz, 1H, H1), 4.96 (m, 2H, H4', H2'), 4.89 (dd, J = 8.9 Hz, J = 4.1 Hz, 1H, H2), 4.16 (m, 3H, H6, H6'), 4.00 (m, 1H, H5'), 3.95 (m, 1H, H6'), 3.86 (m, 1H, H5), 3.46 (m, 2H, H7), 3.31 (m, 3H, H11, H4), 2.03-1.95 (m, 21H, Ac), 1.78 (m, 2H, H10), 1.43 (m, 2H, H8), 1.38 (m, 2H, H9).

^{13}C NMR (100 MHz, $CDCl_3$): δ (ppm) 170.6, 169.7, 169.6, 92.4, 92.1, 76.6, 72.7, 71.7, 70,2, 69.9, 69.7, 69.4, 68.5, 68.0, 62.5, 61.8, 33.5, 32.4, 29.3, 24.7, 20.9, 20.6.

2,3,6,2',3',4',6'-hepta-O-acetyl-4-O-(5-azidopentyl)-α,α-trehalose 3

In a round bottom flask, under argon atmosphere, bromo trehalose **26** was dissolved in dry DMF (5 mL). Sodium azide (173.5 mg, 2.67 mmol, 5 eq) was added, the reaction mixture was heated at 65°C and stirred for 16 hours (TLC monitoring, eluant mixture: DCM/ EtOAc 4:1). Then, the solvent was removed under high vacuum. The crude residue was diluted with EtOAc (20 mL), washed with water (20 mL) and brine (15 mL). The organic layer was then dried with Na_2SO_4 and concentrated under reduced pressure. The crude (400 mg) was purified by column chromatography (eluant mixture: toluene/EtOAc 7:3) to obtain 240 mg of pure 2,3,6,2',3',4',6'-hepta-O-acetyl-4-O-(5-azidopentyl)-α,α-trehalose **3** as a white solid (0.322 mmol, **60**% yield over three steps).

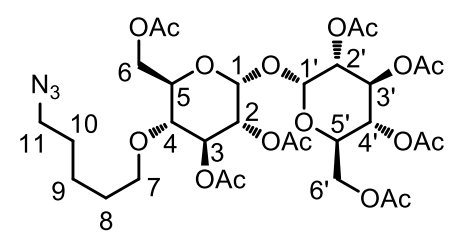

Characterization:

^{1}H NMR (400 MHz, $CDCl_3$): δ (ppm) 5.51 (m, 2H, H3, H3'), 5.30 (d, J = 4.1 Hz, 1H, H1'), 5.21 (d, J = 4.1 Hz, 1H, H1), 5.04 (m, 2H, H4', H2'), 4.96 (dd, J = 8.9 Hz, J = 4.1 Hz, 1H, H2), 4.27 (m, 3H, H6, H6'), 4.09 (m, 1H, H5'), 4.02 (m, 1H, H6'), 3.95 (m, 1H, H5), 3.54 (m, 2H, H7), 3.40 (t, J = 8.9 Hz, 1H, H4), 3.30 (t, J = 4.5 Hz, 2H, H11), 2.12-2.05 (m, 21H, Ac), 1.59 (m, 4H, H9, H10), 1.41 (m, 2H, H8).

^{13}C NMR (100 MHz, $CDCl_3$): δ (ppm) 170.6, 170.5, 169.9, 169.8, 169.7, 169.6, 169.4, 92.3, 92.0, 76.5, 72.6, 71.7, 70,2, 69.9, 69.7, 69.4, 68.5, 68.0, 62.4, 61.7, 51.2, 29.6, 28.6, 23.2, 20.9, 20.5.

ESI MS: Calcd [$C_{31}H_{45}N_3O_{18}$]:747.70, found: 770.45 ($M+Na^+$).

3.5.6. Synthesis of 3,4,6,2',3',4',6'-hepta-O-acetyl-2-O-(5-azidopentyl)-α,α-trehalose 4

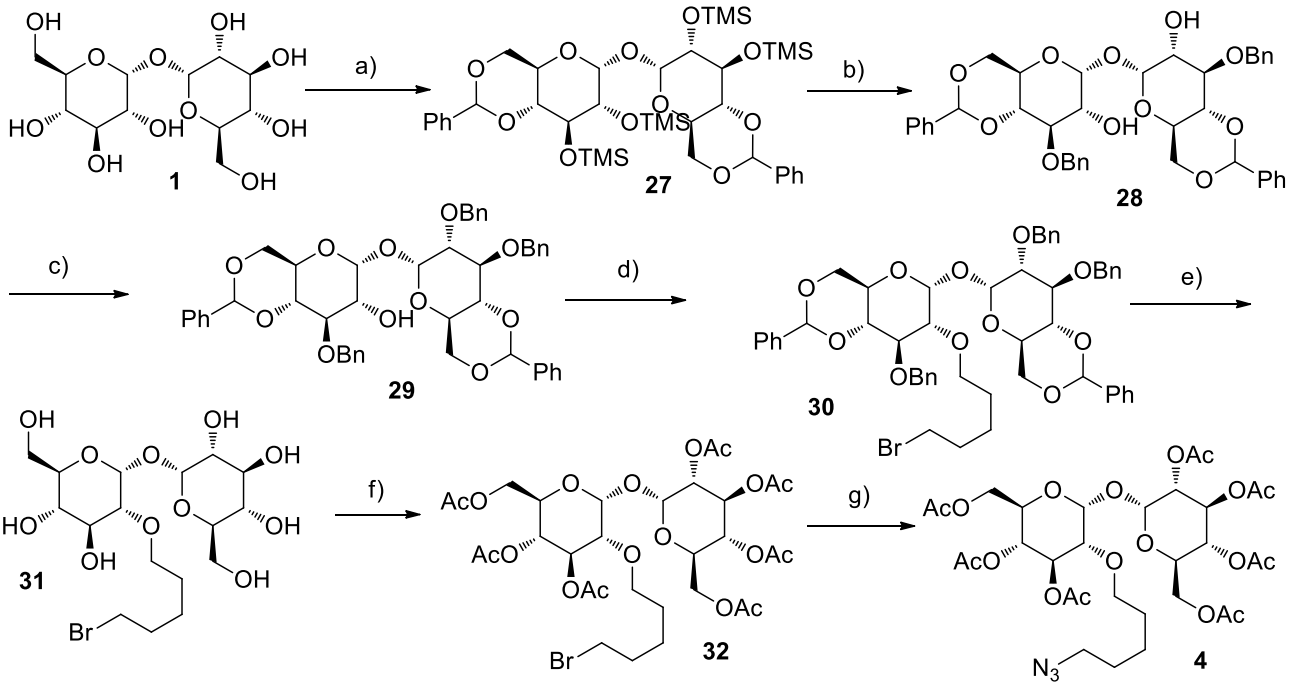

a) $PhCH(OMe)_2$ 2.2eq, cat PTSA, DMF, 105°C, 80min, then TMSCl, 1H-Imidazole, 0° to RT, 16hrs, **76%**; b) cat TMSOTf, PhCHO, Et_3SiH, DCM -78°C to 0°C, 4hrs, **80%**; c) BnBr 0.75eq, NaH, THF, 0°C to RT, 6hrs, **49%;** d) $Br(CH_2)_5Br$ 10eq, NaH 2eq, DMF, 55°C, 8hrs, **71%** e) H_2, Pd-C, MeOH/THF 4:1, RT, 24hrs; f) Ac_2O, Py, cat DMAP, DCM/Py, RT, 4hrs, **78%** over two steps; g) NaN_3, DMF 65°C, 16hrs, **90%.**

2,3,2',3'-tetra-O-trimetylsilyl-4,6:4',6'-di-O-benzylidene-α,α'-trehalose 27

Trehalose dihydrate (1.43 g, 3.789 mmol, 1 eq) was dried under vacuum at 100°C overnight. Then, it was transferred in a two-neck round bottom flask and dissolved under argon atmosphere in dry DMF (9 mL). The mixture was heated at 105°C for 5 minutes, then solid p-toluenesulfonic acid monohydrate (PTSA, 36.1 mg, 0.190 mmol, 0.05 eq) was added and the solution was stirred for additional 5 minutes. Benzaldehyde dimethyl acetal (1.251 ml, 8.336 mmol, 2.2 eq) was added in three equal portions during 1 hour while maintaining the reaction temperature at 100°C. Then, the solution was stirred for additional 40 minutes (TLC monitoring, eluant mixture: DCM/MeOH 95:5).

The brown solution was cooled at 0°C, and a solution of 1H-Imidazole (2.06 g, 30.312 mmol, 8 eq) in dry DMF (4 mL) was added dropwise. Then, TMSCl (2.9 mL, 22.716 mmol, 6 eq) was slowly added dropwise, and the solution was stirred at RT for 48 hrs (TLC monitoring, eluant mixture: n-hexane/ EtOAc 9:1). The solvent was removed under high vacuum, and the crude solid was dissolved in EtOAc (70 mL). The organic layer was then sequentially washed with water (2 x 40 mL) and brine (30 mL). The organic layer was then dried with Na_2SO_4 and concentrated under reduced pressure. The crude (3 g) was purified by flash chromatography (eluant mixture: n-hexane/ EtOAc from 95:5 to 85:15) yielding 2.32 g of pure **27** as a white solid (2.879 mmol, **76**% yield).

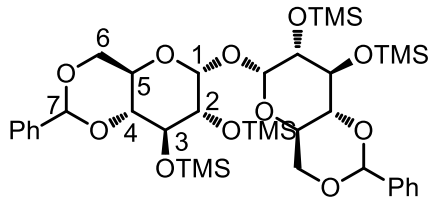

Characterization:

^{1}H NMR (300 MHz, $CDCl_3$): δ (ppm) 7.48 (m, 4H, Ph), 7.37 (m, 6H, Ph), 5.45 (s, 2H, H7), 4.92 (d, J=3.5 Hz, 2H, H1), 4.21-4.00 (m, 6H, H2, H3, H5), 3.70-3.52 (m, 4H, H4, H6), 3.41 (t, J=4.7 Hz, 2H, H6), 0.2 (s, 18H, TMS), 0.1 (s, 18H, TMS).

3,3'-bis-O-benzyl-4,6:4',6'-di-O-benzylidene-α,α'-trehalose 28

A mixture of fully protected trehalose **27** (880 mg, 1.09 mmol, 1 eq), benzaldehyde (0.244 mL, 2.289 mmol, 2.1 eq), triethylsilane (0.418 mL, 2.616 mmol, 2.4 eq) in dry DCM (10 mL) was stirred at 0°C for 30 minutes under argon atmosphere. The mixture was then cooled to -78°C, trimethylsilyl trifluoromethanesulfonate (18 µL, 0.101 mmol, 0.1 eq) was added, and the reaction was stirred at the same temperature for 6 hours (TLC monitoring, eluant mixture: n-hexane/AcOEt 8:2). The solution was then diluted with DCM (25 mL) and sequentially washed with saturated aqueous $NaHCO_3$ (20 mL), 1M aqueous HCl (20 mL) and brine (15 mL) The organic layer was dried over Na_2SO_4, filtered and concentrated *in vacuo*. The crude was purified by flash chromatography (eluant mixture: n-hexane/EtOAc from 75:25 to 7:3) yielding 609 mg of pure **28** as a colorless oil (0.872 mmol, **80**% yield).

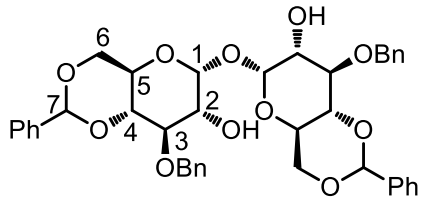

Characterization:

^{1}H NMR (400 MHz, $CDCl_3$): δ (ppm) 7.53-7.21 (m, 20H, Ph), 5.98 (s, 2H, H7), 5.22 (d, J = 3.8 Hz, 2H, H1), 5.18 (d, J = 9.2 Hz, 2H, $PhCH_2$), 4.96 (d, J = 9.2, Hz, 2H, $PhCH_2$), 4.36 (m, 2H, H6),4.18 (m, 2H, H5), 3.92 (t, J = 8.8 Hz, 2H, H3), 3.83 (m, 2H, H2), 3.79-3.62 (m, 4H, H4, H6), 2.98 (bd, 2H, OH).

2',3,3'-tri-O-benzyl-4,6:4',6'-di-O-benzylidene-α,α'-trehalose 29

2' Dihydroxyl trehalose **28** (601 mg, 0.858 mmol, 1 eq) in dry THF (9 mL) was cooled at 0°C under argon atmosphere, then sodium hydride (60% in mineral oil, 41.2 mg, 1.029 mmol, 0.6 eq) was added and the suspension was stirred for 15 minutes. Then, benzyl bromide (BnBr, 0.153 mL, 1.287 mmol, 0.75 eq) was added and the resulting mixture was stirred at RT for 6 hrs (TLC monitoring, eluant mixture: n-hexane/EtOAc 75:25). Then, the excess of NaH was quenched with 5% aqueous citric acid (2 mL). After stirring for 10 minutes, the reaction mixture was concentrated at reduced pressure and the residue diluted with EtOAc (30 mL). The organic solution was washed with saturated $NaHCO_3$ (20 mL) and brine (15 mL), dried with Na_2SO_4 and concentrated under reduced pressure. The crude yellow oil was purified by flash chromatography (eluant mixture: n-hexane/ EtOAc from 75:25 to 65:35), yielding 331.6 mg of pure **29** as a colorless oil (0.420 mmol, **49**% yield).

Characterization:

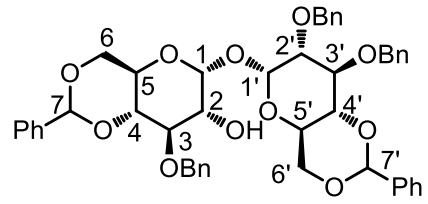

^{1}H NMR (400 MHz, $CDCl_3$): δ (ppm) 7.53-7.28 (m, 25H, Ph), 5.60 (s, 2H, H7, H7'), 5.19 (d, 1H, H1'), 5.16 (d, 1H, H1), 5.02 (m, 2H, $PhCH_2$), 4.90 (m, 2H, $PhCH_2$), 4.78 (m, 2H, $PhCH_2$), 4.32 (m, 2H, H5, H5'), 4.20 (m, 2H, H6, H6'), 4.17 (t, 1H, H3'), 3.98 (t, 1H, H3), 3.82-3.65 (m, 6H, H6, H6', H4, H4', H2, H2'), 2.24 (bs, 1H, OH).

2',3,3'-tri-O-benzyl-4,6:4',6'-di-O-benzylidene-2-O-(5-bromopentyl)-α,α'-trehalose 30

1,5-Dibromopentane (0.933 mL, 6.850 mmol, 10 eq) was added to a solution of 2-hydroxy trehalose **29** (540.4 mg, 0.685 mmol, 1 eq) in dry DMF (7 mL), under nitrogen atmosphere. Then, sodium hydride (60% dispersion in mineral oil, 54.8 mg, 1.37 mmol, 2 eq) was slowly added, the resulting mixture was heated at 55°C and stirred for 4 hours (TLC monitoring, eluant mixture: n-hexane/EtOAc 75:25). Then, the excess of sodium hydride was quenched with 5% aqueous citric acid (3 mL). After further 30 minutes' stirring, the reaction mixture was concentrated under high vacuum and the residue diluted with EtOAc (35 mL). The organic phase was washed with saturated aqueous $NaHCO_3$ (20 mL), brine (15 mL), dried with Na_2SO_4 and concentrated under reduced pressure. The crude yellow oil was purified by flash chromatography (TLC monitoring, eluant mixture: EtOAc/ n-hexane 2:8), yielding 455 mg of pure **30** as a colorless oil (0.486 mmol, **71**% yield).

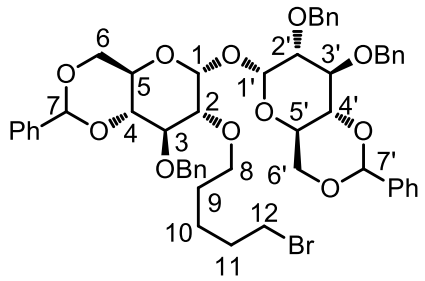

Characterization:

^{1}H NMR (400 MHz, $CDCl_3$): δ (ppm) 7.54-7.29 (m, 25H, Ph), 5.60 (m, 2H, H7, H7'), 5.22 (d, 1H, H1'), 5.16 (d, 1H, H1), 5.01-4.74 (m, 6H, $PhCH_2$), 4.29-4.12 (m, 5H, H5, H5', H6, H6', H3), 4.06 (t, 1H, H3'), 3.76-3.63 (m, 7H, H6, H6', H4, H4', H2, H8), 3.49 (dd, 1H, H2'), 3.29 (t, 2H, H12), 1.85 (m, 2H, H11), 1.65 (m, 2H, H9), 1.42 (m, 2H, H10).

^{13}C NMR (100 MHz, $CDCl_3$): δ (ppm) 138.9, 138.8, 138.0, 137.5, 137.5, 128.9, 128.5, 128.3, 128.3, 128.2, 128.2, 128.0, 127.8, 127.8, 127.6, 127.5, 126.1, 126.0, 101.3, 101.3, 94.8, 94.4, 82.3, 80.0,78.8, 78.7, 78.4, 75,3, 75.2, 73.8, 71.9, 69.1, 69.0, 63.0, 62.8, 33.7, 32.7, 29.4, 24.9.

2-O-(5-bromopentyl)-α,α-trehalose 31

A vigorously stirred solution of bromopentyl protected trehalose **30** (451 mg, 0.534 mmol, 1 eq) in a 4:1 MeOH/THF mixture (10 mL) was treated 10% Pd-C (40 mg) under nitrogen atmosphere at RT. The reaction mixture was degassed and flushed with hydrogen (three times), then stirred vigorously under hydrogen atmosphere for 24 hours (TLC monitoring, eluant mixture: $CHCl_3$/MeOH/H_2O 60:35:5). The reaction mixture was then filtered through a celite pad, that was washed with MeOH (30 mL). The colourless solution was concentrated *in vacuo* to give crude bromopentyl trehalose **31** (235.1 mg), which was used for the next step without further purification.

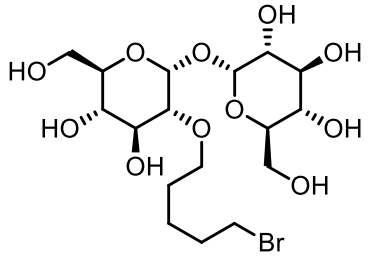

Characterization:

ESI MS: Calcd [$C_{17}H_{31}BrO_{11}$]: 490.1, found: 513.33 ($M+Na^+$).

3,4,6,2',3',4',6'-hepta-O-acetyl-2-O-(5-bromopentyl)-α,α-trehalose 32

Bromopentyl trehalose **31** (235.1 mg) was suspended in DCM (5 mL), and pyridine (1.9 g, 27.16 mmol, 56 eq) was added under stirring at RT. Acetic anhydride (656 µL, 6.305 mmol, 13 eq) was slowly added, followed by a catalytic amount of DMAP. The reaction mixture was stirred at for 4 hours (TLC monitoring, eluant mixture: DCM/EtOAc 4:1). Volvents were removed under high vacuum, the resulting brown oil was dissolved in EtOAc (20 mL), and the organic layer was sequentially washed with 5% aqueous HCl (10 mL), saturated aqueous $NaHC0_3$ (10 mL) and brine (10 mL). The organic layer was then dried with Na_2SO_4 and concentrated under

reduced pressure to give a solid (330 mg) which was purified by column chromatography (eluant mixture: toluene/EtOAc 7:3) to obtain 297.2 mg of pure **32** as a white solid (0.378 mmol, **78**% yield over two steps).

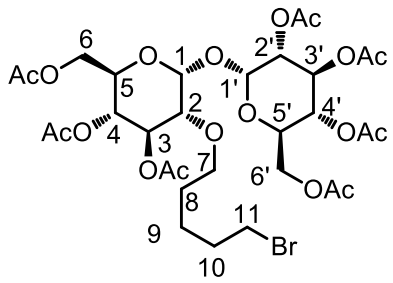

Characterization:

^{1}H NMR (400 MHz, $CDCl_3$): δ (ppm) 5.42 (t, J = 9.8 Hz, 1H, H3'), 5.31 (t, *J* = 9.7 Hz, 1H, H3), 5.22 (d, *J* = 3.9 Hz, 1H, H1'), 5.14 (d, *J* = 3.7 Hz, 1H, H1), 5.05 (t, *J* = 9.8 Hz, 1H, H4'), 4.96 (dd, J = 10.2, 3.9 Hz, 1H, H2'), 4.90 (t, *J* = 9.8 Hz, 1H, H4), 4.20 (m, 3H, H6, H6'), 3.97 (m, 2H, H5, H5'), 3.89 (dd, *J* = 12.1, 2.0 Hz, 1H, H6), 3.57 (m, 1H, H7), 3.49 (dd, *J* = 10.0, 3.7 Hz, 1H, H2), 3.43 (m, 1H, H7), 3.34 (t, *J* = 6.6 Hz, 2H, H11), 2.00-1.95 (m, 21H, Ac), 1.80 (m, 2H, H10), 1.43 (m, 4H, H9, H8).

^{13}C NMR (100 MHz, $CDCl_3$): δ (ppm) 170.6, 169.7, 169.6, 93.2, 92.7, 77.5, 72.7, 71.8, 70,2, 68.9, 67.8, 67.5, 67.0, 62.0, 61.5, 33.5, 32.4, 29.3, 24.8, 19.9, 19.6.

3,4,6,2',3',4',6'-hepta-O-acetyl-2-O-(5-azidopentyl)-α,α-trehalose 4

In a round bottom flask, under argon atmosphere, crude bromopentyl acetate **32** (294.3 mg, 0.342 mmol, 1 eq) was dissolved in dry DMF (4 mL). Sodium azide (140.1 mg, 1.718 mmol, 5 eq) was added, the reaction mixture was heated at 65°C and stirred for 16 hours (TLC monitoring, eluant mixture: DCM/ EtOAc 4:1). Then the solvent was removed under high vacuum. The crude mixture was diluted with EtOAc (25 mL) and washed with water (20 mL) and brine (15 mL). The organic layer was then dried with Na_2SO_4 and concentrated under reduced pressure. The crude (400 mg) was purified by column chromatography (eluant mixture: toluene/EtOAc from 7:3 to 6:4) to obtain 230.1 mg of pure 3,4,6,2',3',4',6'-hepta-O-acetyl-2-O-(5-azidopentyl)-α,α-trehalose **4** as a white solid (0.308 mmol, **90**% yield).

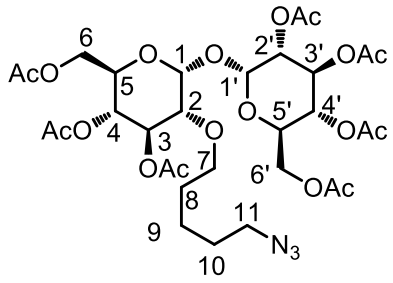

Characterization:

^{1}H NMR (400 MHz, $CDCl_3$): δ (ppm) 5.42 (t, J = 9.8 Hz, 1H, H3'), 5.31 (t, *J* = 9.7 Hz, 1H, H3), 5.22 (d, *J* = 3.9 Hz, 1H, H1'), 5.14 (d, *J* = 3.7 Hz, 1H, H1), 5.05 (t, *J* = 9.8 Hz, 1H, H4'), 4.96 (dd, J = 10.2, 3.9 Hz, 1H, H2'), 4.90 (t, *J* = 9.8 Hz, 1H, H4), 4.20 (m, 3H, H6, H6'), 3.97 (m, 2H, H5, H5'), 3.89 (dd, *J* = 12.1, 2.0 Hz, 1H, H6), 3.57 (m, 1H, H7), 3.49 (dd, *J* = 10.0, 3.7 Hz, 1H, H2), 3.43 (m, 1H, H7), 3.22 (t, *J* = 6.6 Hz, 2H, H11), 2.00-1.95 (m, 21H, Ac), 1.58-1.43 (m, 4H, H10, H8), 1.32 (m, 2H, H9).

^{13}C NMR (300 MHz, DMSO-d_6): δ (ppm) 168.3, 167.6, 167.4, 91.3, 90.7, 75.2, 69.8, 69.5, 67.9, 66.5, 65.9, 65.5, 59.7, 59.2, 49.0, 27.3, 26.4, 21.0, 18.6, 18.4,

ESI MS: Calcd [$C_{31}H_{45}N_3O_{18}$]:747.70, found: 770.45 ($M+Na^+$).

3.5.7. Synthesis of 1:1 sephin1-trehalose DAC 5

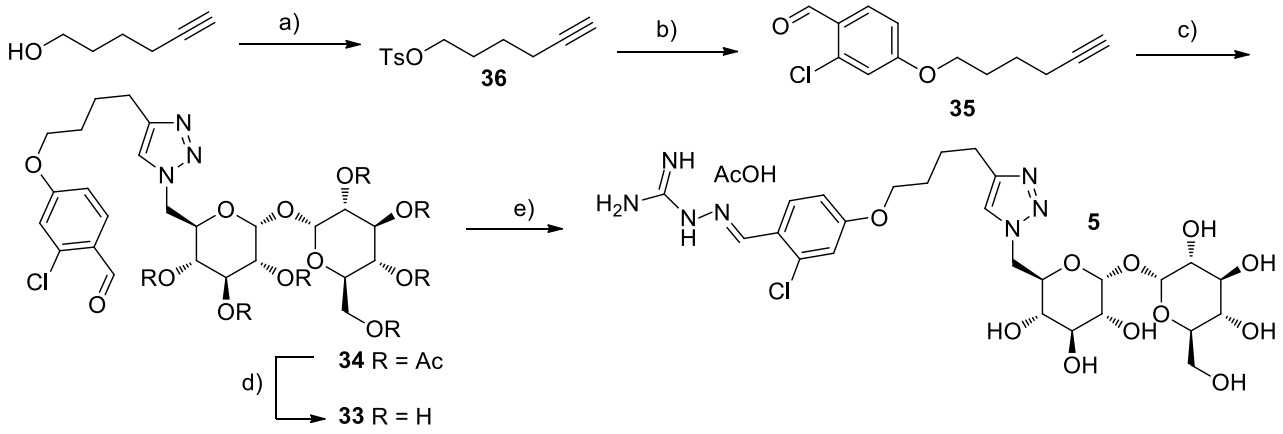

a) TsCl, TEA, cat DMAP, DCM, 0°C to RT 20hrs, **95%**; b) 2-chloro-4-hydroxybenzaldehyde, K_2CO_3, DMF, 95°C, 24hrs, **83%;** c) **2a** 1eq, $CuSO_4$ $5H_2O$, Na Ascorbate, THF:H_2O 1:1, RT, 6hrs, **88%**; d) NaOMe, MeOH, RT, 20hrs; e) aminoguanidine HCl, cat. HCl_{aq}, EtOH, H_2O, 70°C, 6hrs, **80%** over two steps.

hex-5-yn-1-yl 4-methylbenzenesulfonate 36

5-Hexyn-1-ol (750 mg, 7.64 mmol, 1 eq) was dissolved in dry DCM (25 mL) under nitrogen atmosphere. TEA (1.59 mL, 1.5 eq) was added under stirring at RT, then after cooling to 0°C tosyl chloride (2.185 g, 11.46 mmol, 1.5 eq) and a catalytic amount of DMAP were added. . The resulting solution was stirred for 20 hours at RT (TLC monitoring, eluant mixture: n-hexane/EtOAc 85:15). Then, the reaction mixture was diluted with DCM (50 mL) and sequentially washed with water (25 mL) and brine (20 mL). The organic phase was dried with Na_2SO_4, filtered and the solvent removed under reduced pressure. The crude product (2.38 g) was purified by flash chromatography (eluant mixture: n-hexane/EtOAc 85:15), yielding 1.735 g of pure **51** as a colourless oil (6.88 mmol, **95%** yield).

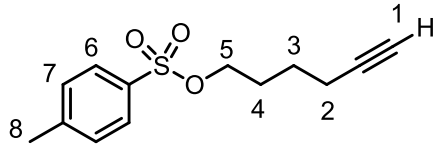

Characterization:

^{1}H NMR (300 MHz, $CDCl_3$): δ (ppm) 7.78 (d, 2H, J = 8.3 Hz, H6), 7.34 (d, 2H, J = 8.2 Hz, H7), 4.04 (t, 1H, J = 6.2 Hz, H1), 2.44 (s, 3H, H8), 2.15 (dt, J = 6.9, 2.6 Hz, H4), 1.91 (t, 1H, J = 2.6 Hz, H5), 1.77 (m, 2H, H2), 1.54 (m, 2H, H3).

2-chloro-4-(hex-5-yn-1-yloxy)benzaldehyde 35

Alkynyl tosylate **36** (590.2 mg, 2.34 mmol, 1 eq) was dissolved in dry DMF (5 mL) under nitrogen atmosphere. Then, chlorohydroxy benzaldehyde (366.5 mg, 2.34 mmol, 1 eq) and solid K_2CO_3 (670 mg, 4.84 mmol, 2 eq) were sequentially added. The reaction mixture was heated to 95°C and stirred for 24 hrs (TLC monitoring, eluant mixture: n-hexane/EtOAc 9:1). After solvent evaporation under high vacuum, the crude was dissolved in AcOEt (30 mL). The organic phase was sequentially washed with water (15 mL) and brine (10 mL). The organic phase was dried with Na_2SO_4, filtered and the solvent removed under reduced pressure. The crude product (680 mg) was purified by flash chromatography (TLC monitoring, eluant mixture: hexane/EtOAc 9:1), yielding 462.1 mg of pure **35** as a yellow solid (1.95 mmol, **83%** yield).

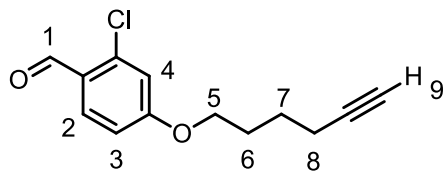

Characterization:

^{1}H NMR (300 MHz, $CDCl_3$): δ (ppm) 10.32 (s, 1H, H1), 7.87 (d, 1H, J = 8.7 Hz, H2), 6.91 (d, 1H, J = 2.4 Hz, H4), 6.87 (dd, 1H, J = 8.7, J = 2.4 Hz, H3), 4.05 (t, 2H, J = 6.2 Hz, H5), 2.28 (dt, 2H, J = 7.0, J = 2.6 Hz, H8), 1.94 (m, 3H, H9, H6), 1.72 (m, 2H, H7).

(2R,3R,4S,5R,6R)-2-(Acetoxymethyl)-6-(((2R,3R,4S,5R,6R)-3,4,5-triacetoxy-6-((4-(4-(3-chloro-4-formyl phenoxy)butyl)-1H-1,2,3-triazol-1-yl)methyl)tetrahydro-2H-pyran-2-yl)oxy)tetrahydro-2H-pyran-3,4,5-triyl triacetate 34

Chloroalkynyl benzaldehyde **35** (111.0 mg, 0.468 mmol, 1 eq) was dissolved in a 1:1 H_2O/THF mixture (18 mL). Then, protected azido trehalose **2a** (310.0 mg, 0.468 mmol, 1 eq) was added. The mixture was stirred at RT for 10 minutes, then $CuSO_4$*$5H_2O$ (116.85 mg, 0.468 mmol, 1 eq) and Na ascorbate (190.0 mg, 0.936 mmol, 2 eq) were added under stirring. The reaction mixture was stirred for 6 hrs at RT (TLC monitoring, eluant mixture: 7:3 DCM/AcOEt). After solvent evaporation, the crude (158.3 mg) was purified by flash chromatography (eluant mixture: DCM/AcOEt 4:6), yielding 370 mg of pure **34** as a white solid (0.412 mmol, **88%** yield).

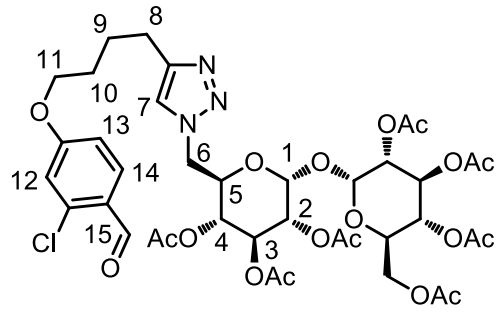

Characterization:

^{1}H NMR (400 MHz, $CDCl_3$): δ (ppm) 10.34 (s, 1H, H15), 7.91 (d, 1H, J = 8.9 Hz, H14), 7.45 (bs, 1H, H7), 6.96 (d, 1H, J = 2.3 Hz, H12), 6.92 (dd, 1H, J = 8.9 Hz, J = 2.3 Hz, H13), 5.54 (t, 1H, H3'), 5.43 (t, 1H, H3), 5.32 (d, 1H, H1'), 5.12 (dd, 1H, H2'), 4.91 (m, 4H, H4, H4', H2, H1), 4.62 (bs, 1H, H6), 4.30 (bs, 1H, H6), 4.25 (m, 2H, H5', H6'), 4.10 (bs, 2H, H11), 3.99 (m, 2H, H5, H6'), 2.88 (m, 2H, H8), 2.05 (m, 21H, Ac), 2.04 (m, 4H, H9, H10).

^{13}C NMR (400 MHz, $CDCl_3$): δ (ppm) 188.6, 170.9, 169.6, 131.0, 115.7, 114.0, 92.1, 91.6, 69.7, 69.2, 69.1, 68.4, 61.7, 51.0, 28.4, 25.6, 24.8, 20.6.

ESI MS: Calcd [$C_{39}H_{48}ClN_3O_{19}$]:897.26, found: 921.04 ($M+Na^+$).

2-Chloro-4-(4-(1-(((2R,3S,4S,5R,6R)-3,4,5-trihydroxy-6-(((2R,3R,4S,5S,6R)-3,4,5-trihydroxy-6-(hydroxy methyl)tetrahydro-2H-pyran-2-yl)oxy)tetrahydro-2H-pyran-2-yl)methyl)-1H-1,2,3-triazol-4-yl)butoxy) benzaldehyde 33

Acetylated 1:1 sephin1-trehalose adduct **34** (370.0 mg, 0.412 mmol, 1 eq) was dissolved in dry MeOH (12 mL). Then, sodium methoxide (22.3 mg, 0.412 mmol, 1 eq) was added under stirring. The reaction mixture was stirred at RT for 20 hours (TLC monitoring, eluant mixture: $CHCl_3$/MeOH/H_2O 60:35:5). Then, Amberlite IR120 H^+ resin was added under stirring until neutral pH. The reaction mixture was filtered, the solvent was evaporated at reduced pressure, and 241.4 mg of crude **33** was obtained as a white solid, that was used without further purification.

1:1 Sephin1- trehalose DAC 5

1:1 Sephin1-trehalose adduct **33** (241.4 mg, 0.400 mmol, 1 eq) was suspended in absolute EtOH (7 mL), and water (1 mL) was added. Then, aminoguanidine hydrochloride (48.6 mg, 0.440 mmol, 1,1 eq) was added

under vigorous stirring. After the addition of cat. [1M] HCl (2 drops), the reaction mixture was heated to 70°C and stirred for 8 hours (TLC monitoring, eluant mixture: $CHCl_3$/MeOH/H_2O 60:35:5). After solvent evaporation at reduced pressure, the crude (290 mg) was purified by reverse phase chromatography (TLC monitoring, eluant mixture: H_2O/MeOH + 0.5% AcOH from 95:5 to 0:100), yielding 229.3 mg of pure sephin1-mono-trehalose DAC acetate **5** as a white solid (0.320 mmol, **80**% yield).

Characterization:

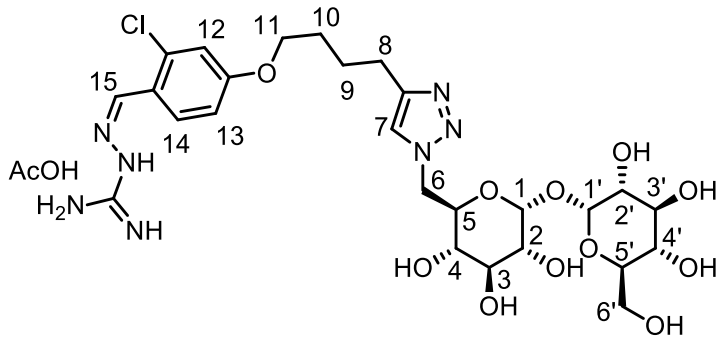

^{1}H NMR (300 MHz, D_2O); δ (ppm) 8.20 (s, 1H, H15), 7.75 (d, 1H, *J* = 8.8 Hz, H14), 7.70 (s, 1H, H7), 6.84 (d, 1H, *J* = 2.4 Hz, H12), 6.78 (dd, 1H, *J* = 8.9, 2.3 Hz, H13), 4.98 (d, 1H, *J* = 3.8 Hz, H1), 4.67 (m, 1H, H6), 4.50 (d, 1H, *J* = 3.8 Hz, H1'), 4.42 (dd, 1H, *J* = 14.6, 8.3 Hz, H6), 3.99 (m, 1H, H5), 3.90 (t, 2H, *J* = 5.9 Hz, H11), 3.74 (t, 1H, J = 8.7 Hz, H3), 3.65 (m, 3H, H3', H6', H5'), 3.49 (m, 2H, H6', H2), 3.31 (dd, 1H, *J* = 9.9, 3.8 Hz, 1H, H2'), 3.16 (m, 2H, H4, H4'), 2.67 (t, 2H, *J* = 6.7 Hz, H8), 1.64 (m, 4H, H10, H9).

^{13}C NMR (300 MHz, DMSO-d_6): δ (ppm) 178.6, 164.8, 163.6, 151.7, 145.4, 138.3, 133.3, 130.3, 127.4, 119.9, 119.6, 98.2, 77.8, 77.7, 77.5, 76.5, 76.3, 75.1, 74.9, 73.0, 65.8, 55.9, 33.6, 30.6, 29.7, 27.2.

HPLC/MS (ESI$^+$): 661.52 $[M+H]^+$ (mass calculated for $C_{26}H_{38}ClN_7O_{11}$: 660.07). Purity measured: 99.8 %.

3.5.8. Synthesis of 2:1 sephin1 trehalose DAC 6

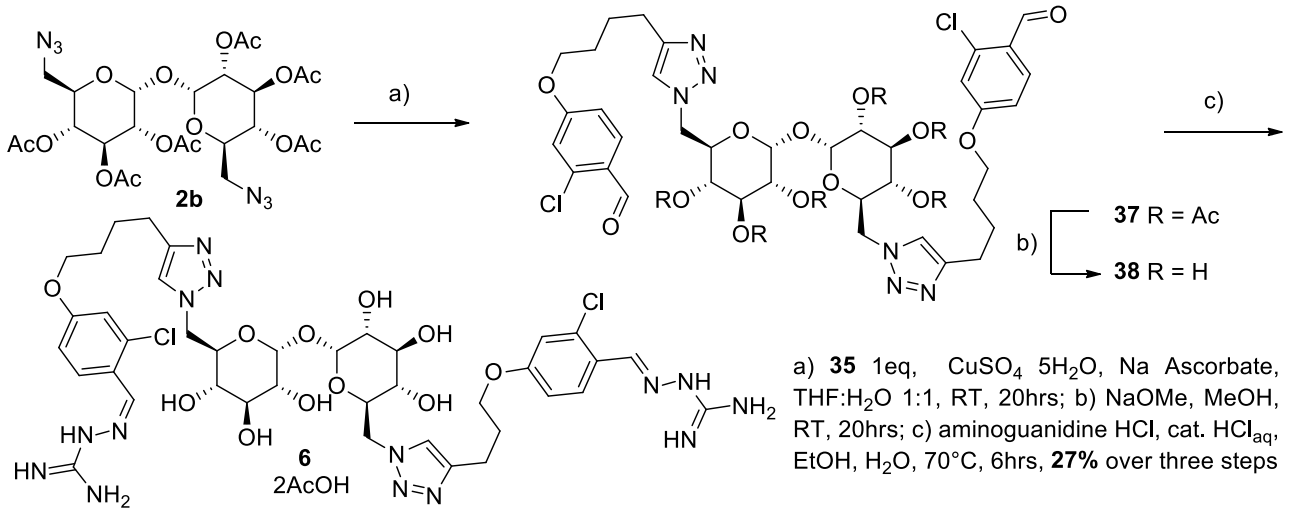

4,4'-(((1,1'-(((2R,2'R,3S,3'S,4S,4'S,5R,5'R,6R,6'R)-6,6'-oxybis(3,4,5-triacetoxytetrahydro-2H-pyran-6,2-diyl))bis(methylene))bis(1H-1,2,3-triazole-4,1-diyl))bis(butane-4,1-diyl))bis(oxy))bis(2-chlorobenzaldehyde) 37

Protected 6-diazido trehalose **2b** (231 mg, 0.358 mmol, 1 eq) and chloroalkynyl benzaldehyde **35** (186.5 mg, 0.787 mmol, 1.1 eq) were dissolved in a 1/1 H_2O/THF mixture (10 mL). The reaction mixture was stirred for 10 minutes, then $CuSO_4$*$5H_2O$ (58.4 mg, 0.234 mmol, 0.33 eq) and Na ascorbate (61.6 mg, 0.312 mmol, 0.44 eq) dissolved in H_2O (10 mL) were added under stirring. The reaction mixture was stirred for 20 hours at rt (TLC monitoring, eluant: AcOEt). Then, the solvent was evaporated, and the crude was suspended in AcOEt/MeOH 1:1. The mixture was filtered through a celite pad to remove the residual salts, the filtrate was concentrated at reduced pressure and crude **37** was used for the next reaction step without further purification.

4,4'-(((1,1'-(((2R,2'R,3S,3'S,4S,4'S,5R,5'R,6R,6'R)-6,6'-oxybis(3,4,5-trihydroxytetrahydro-2H-pyran-6,2-diyl))bis(methylene))bis(1H-1,2,3-triazole-4,1-diyl))bis(butane-4,1-diyl))bis(oxy))bis(2-chlorobenzaldehyde) 38

Acetylated 2:1 sephin1-trehalose **37** was dissolved in dry MeOH (8 mL). Then, sodium methoxide (67.5 mg) was added. The reaction mixture was stirred at RT for 20 hours (TLC monitoring, eluant mixture: $CHCl_3$/MeOH/H_2O 60:35:5). Then, Amberlite IR 120 H^+ resin was added under stirring until neutral pH. The mixture was filtered through a celite pad to remove the residual salts. The solvent was evaporated under reduced pressure, and crude Sephin1-bis-trehalose dialdehyde adduct **38** (106.7 mg, **35%** theoretical yield over two steps) was used as such without further purification in the next reaction step.

2:1 sephin1 trehalose DAC 6

2:1 Sephin1-trehalose adduct **38** (106.7 mg, 0.123 mmol, 1 eq) was dissolved in absolute EtOH (5 mL). Then, aminoguanidine hydrochloride (29.8 mg, 0.269 mmol, 2.2 eq) was added. After the addition of cat. [1M] HCl (2 drops), the mixture was heated to 70°C and the homogeneous solution was stirred for 6 hours (2:1 sephin1-trehalose $CHCl_3$/MeOH/H_2O 60:35:5). After solvent evaporation, the crude was purified by reverse phase chromatography (eluant mixture: H_2O/MeOH from 95:5 to 0:100, 0.5% AcOH), yielding 104.2 mg of pure sephin1-bis-trehalose DAC **6** as a white solid (0.098 mmol, **27%** yield over three steps).

Characterization:

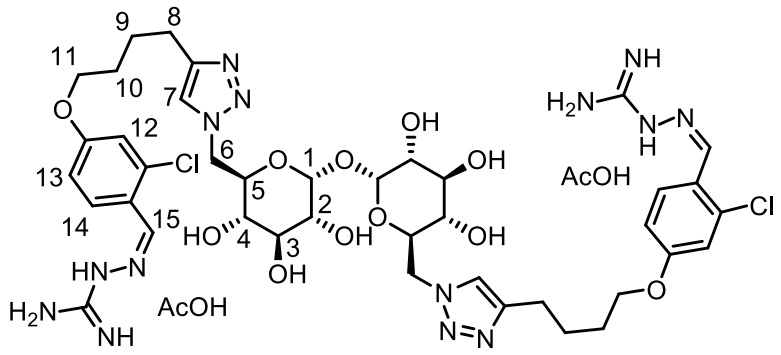

^{1}H NMR (400 MHz, DMSO-d_6 + D_2O): δ (ppm) 8.26 (s, 2H, H15), 8.05 (d, 2H, J = 8.9 Hz, H14), 7.73 (s, 2H, H7), 6.98 (d, 2H, J = 2.3 Hz, H12), 6.88 (dd, 2H, J = 8.8 Hz, J = 2.3 Hz, H13), 4.54 (m, 4H, H6, H1), 4.34 (m, 2H, H6), 4.13 (m, 2H, H5), 3.99 (m, 4H, H11), 3.55 (m, 2H, H3), 3.18 (m, 2H, H2), 2.95 (m, 2H, H4), 2.64 (m, 4H, H8), 1.87 (s, 6H, AcOH), 1.69 (m, 8H, H10, H9).

^{13}C NMR (100 MHz, DMSO-d*6*): δ (ppm) 173.0, 159.6, 159.1, 146.6, 140.1, 133.1, 128.1, 125.5, 122.3, 114.8, 114.5, 93.7, 72.6, 71.2, 70.0, 67.9, 50.8, 28.0, 25.6, 24.6, 21.9.

HPLC/MS (ESI+): 979.37 [M+H^+] (mass calculated for $C_{40}H_{54}Cl_2N_{14}O_{11}$: 977.85). Purity measured 98.8%.

3.6 BIBLIOGRAPHY

[1]. Bossy-Wetzel, E.; Scharzenbacher, R.; Lipton, S.A. Molecular pathways to neurodegeneration. *Nat. Med.* **2014**, 10, S2-S9.

[2]. Forman, M.S.; Trojanowski, J.Q.; Lee V.M.-Y. Neurodegenerative diseases a decade of discoveries paves the way for therapeutic breakthroughs. *Nat. Med.* **2004**, 10, 1055-1063.

[3]. Debès, C.; Wang, M.; Caetano-Anollés, G.; Gräter, F. Evolutionary optimization of protein folding. *PLoS Comput. Biol.* **2013**, 9, e1002861.

[4]. Junker, M.; Besingi, R.N.; Clark, P.L. Vectorial transport and folding of an autotransporter virulence protein during outer membrane secretion. *Mol. Microbiol*. **2009**, 71, 1323-1332.

[5]. Ellis, R.J.; Minton, A.P. Protein aggregation in crowded environments. *Biol. Chem.* **2006**, 387, 5, 485-497.

[6]. Young, J.C.; Agashe, V.R.; Siegers, K.; Hartl, F.U. Pathways of chaperone-mediated protein folding in the cytosol. *Nat. Rev. Mol. Cell. Biol.* **2004**, 5, 81-791.

[7]. Uversky, V.N. Flexible nets of malleable guardians: intrinsically disordered chaperones in neurodegenerative diseases. *Chem. Rev.* **2011**, 111, 1134–1166.

[8]. Drummond, D.A.; Wilke, C.O. Mistranslation-induced protein misfolding as a dominant constraint on coding-sequence evolution. *Cell* **2008**, 134, 341-352.

[9]. Tyedmers, J.; Mogk, A.; Bukau, B. Cellular strategies for controlling protein aggregation. *Nat. Rev. Mol. Cell. Biol*. **2010**, 11, 777-788.

[10]. Hegde, A.N.; Upadhya, S.C. Role of ubiquitin-proteasome-mediated proteolysis in nervous system disease. *Biochim. Biophys. Acta* **2011**, 1809, 128-140.

[11]. Sawkar, A.R.; D'Haeze, W.; Kelly, J.W. Therapeutic strategies to ameliorate lysosomal storage disorders- a focus on Gaucher disease. *Cell. Mol. Life Sci*. **2006**, 63, 1179-1192.

[12]. Gidalevitz, T.; Ben-Zvi, A.; Ho, K.H.; Brignull, H.R.; Morimoto, R.I. Progressive disruption of cellular protein folding in models of polyglutamine diseases. *Science* **2006**, 3111, 471-474.

[13]. Codogno, P.; Mehrpour, M.; Proikas-Cezanne. Canonical and non-canonical autophagy: variations on a common theme of self-eating? *Nat. Rev. Mol. Cell Biol*. **2012**, 13, 7-12.

[14]. Korolchuk, V.I.; Rubinsztein, D.C. On signals controlling autophagy: It's time to eat yourself healthy. *Biochemist* **2012**, 34, 8-13.

[15]. Mizushima, N.; Levine, B.; Cuervo, A.M.; Klionsky, D.J. Autophagy fights disease through cellular self-digestion. *Nature* **2008**, 451, 1069–1075.

[16]. He, C.; Klionsky, D.J. Regulation mechanisms and signalling pathways of autophagy. *Annu. Rev. Genet*. **2009**, 43, 67-93.

[17]. Kroemer, G.; Marino, G.; Levine, B. Autophagy and the integrated stress response. *Mol. Cell* **2010**, 40, 280-293.

[18]. Ravikumar, B.; *et al.* Regulation of mammalian autophagy in physiology and pathophysiology. *Physiol. Rev.* **2010**, 90, 1383–1435.

[19]. Li, W.W.; Li, J.; Bao, J.K. Microautophagy: lesser-known self-eating. *Cell. Mol. Life Sci*. **2012**, 69, 1125-1136.

[20]. Mijaljica, D.; Prescott, M.; Devenish, R.J. Microautophagy in mammalian cells: revisiting a 40-year-old conundrum. *Autophagy* **2011**, 7, 673-682.

[21]. Puyal, J.; Ginet, V.; Grishchuk, Y.; Truttmann, A.C.; Clarke, P.G.H. Neuronal autophagy as a mediator of life and death. *The Neuroscientist* **2012**, 18, 224–236.

[22]. Choi, A.M.K.; Ryter, S.W.; Levine, B. N. Autophagy in human health and disease. *Engl. J. Med*. **2013**, 368, 651-662.

[23]. Suzuki, K.; Ohsumi, Y. Current knowledge of the pre-autophagosomal structure (PAS). *FEBS Lett*. **2010**, 584, 1280–1286.
[24]. Mizushima, N. The role of the Atg1/ULK1 complex in autophagy regulation. *Cell Biol*. **2010**, 22, 132 139.
[25]. Backer, J.M. The regulation and function of Class III PI3Ks: novel roles for Vps34. *Biochem. J.* **2008**, 410, 1-17.
[26]. He, C.; Levine, B. The Beclin 1 interactome. *Cell Biol.* **2010**, 22, 140-149.
[27]. Orsi, A.; et al. Dynamic and transient interactions of Atg9 with autophagosomes, but not membrane integration, are required for autophagy. *Mol. Biol. Cell* **2012**, 23, 1860-1873.
[28]. Young, A.R.J.; *et al.* Starvation and ULK1-dependent cycling of mammalian Atg9 between the TGN and endosomes. *J. Cell Sci*. **2006**, 119, 3888-3900.
[29]. Esclatine, A.; Chaumorcel, M.; Codogno, P. Macroautophagy signaling and regulation. *Curr. Top. Microbiol. Immunol.* **2009**, 335, 33-70.
[30]. Kihara, A.; Noda, T.; Ishihara, N.; Ohsumi, Y. Two distinct Vps34 Phosphatidylinositol 3–Kinase complexes function in autophagy and Carboxypeptidase Y sorting in Saccharomyces cerevisiae. *J. Cell Biol.* **2001**, 152, 519–530.
[31]. Rogov, V.; Doetsch, V.; Johansen, T.; Kirkin, V. Interactions between autophagy receptors and ubiquitin-like proteins form the molecular basis for selective autophagy. *Mol. Cell* **2014**, 53, 167-178.
[32]. Shpilka, T.; Weidberg, H.; Pietrokovski, S.; Elazar, Z. Atg8: an autophagy-related ubiquitin-like protein family. *Genome Biol*. **2011**, 12, 226.
[33]. Ichimura, Y.; *et al*. A ubiquitin-like system mediates protein lipidation. *Nature* **2000**, 408, 488-492.
[34]. Tanida, I.; Sou, Y.S.; Ezaki, J.; Minematsu-Ikeguchi, N.; Ueno, T.; Kominami, E. HsAtg4B/HsApg4B/ Autophagin-1 cleaves the carboxyl termini of three human Atg8 homologues and delipidates microtubule-associated protein light chain 3- and GABAA receptor-associated protein-phospholipid conjugates. *J. Biol. Chem.* **2004**, 279, 36268–36276.
[35]. Longatti, A.; Tooze, S.A. Vesicular trafficking and autophagosome formation. *Cell Death Differ*. **2009**, 16, 956–965.
[36]. Fengsrud, M.; Lunde Sneve, M.; Øverbye, A.; Seglen, P.O. Structural aspects of mammalian autophagy, *Autophagy* **2009**, 11–25.
[37]. Birch, G.G. Trehaloses. *Adv. Carbohydr. Chem*. **1963**, 18, 201-225.
[38]. Harding, T.S. History of trehalose, its discovery and methods of preparation. *Sugar*, **1923**, 25, 476–478.
[39]. Richards, A.B., et al. Trehalose: a review of properties, history of use and human tolerance, and results of multiple safety studies. *Food Chem. Toxicol.* **2003**, 40, 871–898
[40]. Elbein, A.D. The metabolism of α,α-trehalose. *Adv. Carbohydr. Chem. Biochem.* **1974**, 30, 227-256
[41]. Sussman, A.S.; Lingappa, B.T. Role of trehalose in ascaspores of Neurospora tetrasperma. *Science* **1959**, 130, 1343.
[42]. Wyatt, G.R.; Kalf, G.F. The chemistry of insect hemolymph. II. Trehalose and other carbohydrates. *J. Gen. Phys.* **1957**, 40, 833–847.
[43]. Clegg, J.S.; Evans, D.R. The physiology of blood trehalose and its function during flight in the blowfly. *J. Exp. Biol.* **1961**, 38, 771–792.
[44]. Elbein, A.D.; Mitchell, M. Levels of glycogen and trehalose in Mycobacterium smegmatis and the purification and properties of the glycogen synthetase. *J. Bacter.* **1973**, 113, 863–873.
[45]. Paiva, C.L.; Panek, A.D. Biotechnological applications of the disaccharide trehalose. *Biotech. Ann. Rev*. **1996**, 2, 293–314.
[46]. McBride, M.J.; Ensign, J.C. Effects of intracellular trehalose content on Streptomyces griseus spores. *J. Bacter*. **1987**, 169, 4995–5001.

[47]. Van Dijck, P.; Colavizza, D.; Smet, P.; Thevelein, J.M. Differential importance of trehalose in stress resistance in fermenting and nonfermenting Saccharomyces cerevisiae cells. *App. Env. Microbiol.* **1995**, 61, 109–115.

[48]. Komes, D., Lovric´, T.; Ganic´, K.K.; Gracin, L. Study of Trehalose Addition on Aroma Retention in Dehydrated Strawberry Puree*Food Technol. Biotechnol.*, **2003**, 41, 111–119.

[49]. Tanaka, M.; *et al*. Trehalose alleviates polyglutamine-mediated pathology in a mouse model of Huntington disease. *Nat. Med.* **2004**, 10, 148–154.

[50]. Jain, N.K.; Roy, I. Effect of trehalose on protein structure. *Protein Sci.* **2009**, 18, 24-36

[51]. Liu, R.; Barkhordarian, H.; Emadi, S.; Park, C.B.; Sierks, M.R. Trehalose differentially inhibits aggregation and neurotoxicity of beta-amyloid 40 and 42. *Neurobiol. Dis.* **2005**, 20, 74–81.

[52]. Xu, C.; Li, X.; Wang, F.; Weng, H.; Yang, P. Trehalose prevents neural tube defects by correcting maternal diabetes-suppressed autophagy and neurogenesis. *Am. J. Physiol. Endocrinol. Metab.* **2013***,* 305, 667–678

[53]. Castillo, K.; *et al*. Trehalose delays the progression of amyotrophic lateral sclerosis by enhancing autophagy in motoneurons. *Autophag*, **2013**, 9, 1308-1320.

[54]. Krüger, U.; Wang, Y.; Kumar, S.; Mandelkow, E.M. Autophagic degradation of tau in primary neurons and its enhancement by trehalose. *Neurobiol. Aging* **2012**, 33, 2291-2305.

[55]. Beranger, F.; Crozet, C.; Goldsborough, A.; Lehmann, S. Trehalose impairs aggregation of PrPSc molecules and protects prion-infected cells against oxidative damage. *Biochem. Biophys. Res. Commun.* **2008**, 334, 44–48.

[56]. Sarkar, S.; Davies, J.E.; Huang, Z.; Tunnacliffe, A.; Rubinsztein, D.C. Trehalose, a novel Mtor independent autophagy enhancer, accelerates the clearance of mutant Huntingtin and α-synuclein*. J. Biol. Chem.* **2007**, 282, 5641-5652.

[57]. Chen, X.; *et al.* Trehalose, sucrose and raffinose are novel activators of autophagy in human keratinocytes through an mTOR-independent pathway. *Sci. Rep.,* **2016**, 6, 28423.

[58]. Mardones, D.; Rubinsztein, C.; Hetz C. Mystery solved: Trehalose kickstarts autophagy by blocking glucose transport. *Sci. Signal.* **2016**, 9, fs2.

[59]. Myrbäck, K.; Örtenblad, B. Trehalose und Hefe. II. Trehalasewirkung von hefepräparaten. *Biochem. Z*. **1937**, 291, 61–69.

[60]. Kalf, G.F.; Rieder, S.V. The purification and properties of trehalase. *J. Biol. Chem.* **1958**, 230, 691–698.

[61]. Abazari, A.; et al. Engineered trehalose permeable to mammalian cells. *PLoS ONE* **2015**, 10(6): e0130323.

[62]. Baddeley, T.C., Wardell J.L. Synthesis of per- and poly-substituted trehalose derivatives: studies of properties relevant to their use as excipients for controlled drug release. *J. Carbohydr. Chem*. **2009**, 28, 198–221.

[63]. Paulick, Margot G. Cell-permeable variants of trehalose and methods for the protection of living cells. US2013/331353, **2013.**

[64]. Shaul, P.; *et al.* Synthesis and evaluation of membrane permeabilizing properties of cationic amphiphiles derived from the disaccharide trehalose. *Org. Biomol. Chem*. **2016,** 3012- 3015.

[65]. Huisgen, R. Centenary Lecture. *Proc. Chem. Soc*. **1961**, 357-396.

[66]. Kolb, H.C.; Finn, M.G.; Sharpless, K.B. Click chemistry: diverse chemical function from a few good reactions. *Angew. Chem. Int. Ed*. **2001**, 40, 2004 – 2021.

[67]. Staudinger, H.; Meyer, J. Über neue organische Phosphorverbindungen III. Phosphinmethylenderivate und Phosphinimine. *Helv. Chim. Acta* **1919**, 2, 635-646.

[68]. Cartwright, I.L.; Hutchinson, D.W.; Armstrong, V.W. The reaction between thiols and 8-azidoadenosine derivatives. *Nucleic Acids Res*. **1976**, 3, 2331.
[69]. Maynard, H.D. Biodegradable trehalose glycopolymers. WO2016/25668, **2016.**
[70]. Yeom, C.E.; Kim, Y.J.; Lee, S.Y.; Kim, B.M. Chemoselective deprotection of triethylsilyl ethers. *Tetrahedron* **2005,** 61, 12227–12237.
[71]. Pässler, U.; Gruner, M.; Penkov, S., Kurzchalia, T.V., Knölker, H.J. Synthesis of ten members of the maradolipid family; novel diacyltrehalose glycolipids from caenorhabditis elegans. *Synlett* **2011**, 17, 2482-2486.
[72]. Toshima, K.; Tatsuta, K.; Kinoshita, M. Total synthesis of elaiophylin (azalomycin B). *Tetrahedron Lett.* **1986**, 27, 4741-4744.
[73]. Hsieh, H.-W.; Schombs, M.W.; Gervay, J. Integrating ReSET with glycosyl iodide glycosylation in step economy syntheses of tumor-associated carbohydrate antigens and immunogenic glycolipids *J. Org. Chem*. **2014**, 79, 1736−1748.
[74]. Bundy, G.L.; Peterson, D.C. The synthesis of 15-deoxy-9,11-(epoxyimino)prostaglandins - potent thromboxane synthetase inhibitors. *Tetrahedron Lett*. **1978**, 19, 41-44.
[75]. DeNinno, M.P.; Etienne, J.B.; Duplantier, K.C. A method for the selective reduction of carbohydrate 4,6 O-benzylidene acetals. *Tetrahedron Lett.* **1995**, 36, 669-672
[76]. Kuhn, R.; Low, I.; Trishmann, H. Die Konstitution der Lycotetraose. *Chem. Ber.* **1957**, 90, 203-218.
[77]. Van Hijfte, L.; Little, R.D. Intramolecular 1,3-diyl trapping reactions. A formal total synthesis of (.+-.) coriolin. *J. Org. Chem.* **1985**, 50, 3940-3942.
[78]. Bouzide, A.; Sauv, G. Highly selective silver(I) oxide mediated monoprotection of symmetrical diols. *Tetrahedron Lett.* **1997**, 38, 5945-5948.
[79]. Williams, D.R.; Brown, D.L.; Benbow, J.W. Studies of Stemona alkaloids. Total synthesis of (+) croomine *J. Am. Chem. Soc.* **1989**, 111, 1923-1925.
[80]. Jung, M.E.; Lyster, M.A. Quantitative dealkylation of alkyl ethers via treatment with trimethylsilyl iodide. A new method for ether hydrolysis. *J. Org. Chem.* **1977**, 42, 3761-3764.
[81]. Rodebaugh, R.; Debenham, J.S.; Fraser-Reid, B. Debenzylation of complex oligosaccharides using ferric chloride. *Tetrahedron Lett*. **1996**, 37, 5477-5478.
[82]. Kartha, K.P.R.; Dasgupta, F.; Singh, P.P.; Srivastava, H.C. Use of ferric chloride in carbohydrate reactions. IV. Acetolysis of benzyl ethers of sugars. *J. Carbohydr. Chem*. **1986**, 5, 437-444.
[83]. Sakai, J.; Takeda, T.; Ogihara, Y. Selective acetolysis of benzyl ethers of methyl d-glucopyranosides. *Carbohydr. Res.* **1981**, 95, 125-131.
[84]. Alzeer, J.; Vasella, A. Oligosaccharide analogues of polysaccharides. Part 2. Regioselective deprotection of monosaccharide-derived monomers and dimers. *Helv. Chim. Acta* **1995**, 78, 177-193.
[85]. Angibeaud, P.; Utille, J.P. Cyclodextrin chemistry; Part I. Application of a regioselective acetolysis method for benzyl ethers. *Synthesis* **1991**, 737-738.
[86]. Wang, C.C.; *et al*. Synthesis of biologically potent α1→2-linked disaccharide derivatives via regioselective one-pot protection glycosylation. *Angew. Chem. Int. Ed*. **2002**, 41, 2360 – 2362.

Chapter IV

Aminoguanidyl hydrazones as ASIC channel modulators

INDEX

4.1. INTRODUCTION

4.1.1 Acid-Sensing Ion Channels (ASICs)

Ion currents initiated by acidification were observed in neurons as early as the 1980s [1]. A protein producing an acid-gated current was cloned and identified as an Acid-Sensing Ion Channel (ASIC) [2]. Following this discovery, a few related channel family members were found to be also pH-sensitive [3] and were attributed to the ASICs family due to similarity in structure, function and pH sensitivity [4]. ASICs have widespread distribution to many nervous system (NS) regions, including dorsal root ganglia, cortex, hippocampus, basal ganglia, amygdale, olfactory bulb, and cerebrum [2,5-7]. ASICs are primarily neuron-specific, as their expression in non-neuronal tissues is weak or negligible [8]. They are involved in several neuronal functions, including modulation of synaptic plasticity [5], sour-taste perception [9], modulation of retinal functions [10], autonomic control of the circulation [11], fear conditioning and learning [12].

In mammals, four ASIC subunits can assemble into functional homomeric channels made by three identical subunits - ASIC1a, ASIC1b, ASIC2a, and ASIC3 [2,7,13]. Alternatively, the same subunits in addition to ASIC2b can co-assemble into heterotrimeric ASICs, in many combinations [14]. In central nervous system (CNS) neurons, ASICs are mainly either homomeric ASIC1a, or heteromeric ASIC1a/2a and ASIC1a/2b [15-17]. In the peripheral nervous system (PNS), ASIC3-containing channels are most important [18,19]. ASIC1a/2a heteromers contain either 2 ASIC1a and 1 ASIC2a subunit, or vice versa [20]. Their activation induces neuronal depolarization, sometimes associated with direct and indirect Ca^{2+} entry as for homomeric ASIC1a channels. Neurons may use the flexible stoichiometry to fine-tune their ASICs, as subunits vary in their apparent proton affinity / pH sensitivity, their desensitization kinetics and rate of recovery [20].

Individual ASIC subunits consist of 500 to 560 amino acids (AAs). They contain two transmembrane domains (TMDs), short cytoplasmic amino- and carboxyl-termini (35 to 90 AAs) and a large (≈370 AAs) extracellular domain (ECD) [21]. The ECD is where most exogenous and endogenous ligands most likely bind. The crystal structure of chicken ASIC1 (cASIC1) in its desensitized conformation revealed the 3D organization of the ECD in 12 β-sheets and 7 α-helices, two of which form the TMDs that line the ion pore [22]. Based on this structure, a proposed model (Figure 1) entails subunits represented as a hand holding a ball and divided into finger, thumb, palm, knuckle, β-ball, wrist, and forearm as the transmembrane domains TM1 and TM2. An “acidic pocket” containing several pairs of acidic amino acids lies at the interface between two subunits should be a pH-sensor of ASIC channels. Cations may access the ion channel also by lateral fenestrations in the wrist region, then moving into a broad extracellular vestibule.

At sensory neuron terminals, protons and other endogenous (or exogenous) chemicals should activate ASICs by binding to specific ASIC subunit epitopes (Figure 1) [23]. It has been suggested that ASICs respond to mechanical stimuli at these terminals [24]. Homomeric ASIC1a and ASIC3 have the highest sensitivity for protons [25]. They are activated when the pH falls below 6.9 and are strongly activated at pH = 6.0 or slightly lower pH. Half-maximal activation happens at pH ≈6.5, with cooperative binding of more than one proton during activation of ASICs [26].

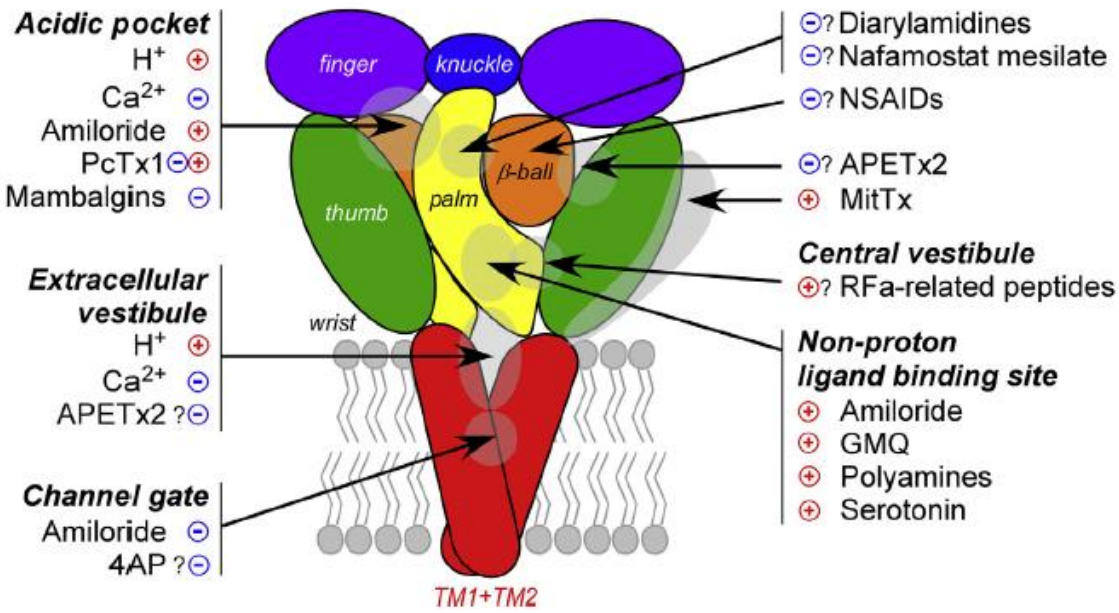

Figure 1. Structure of ASIC1a: X-ray-extracted structural model, and binding site for exogenous and endogenous ligands. (+), Activators; (-), antagonists; ?, hypothetical / not fully validated binding site.

ASIC activation takes place with activation time constants t_{act} at pH 6.0 of 6-14 ms for ASIC1a and <5 ms for ASIC3 [13], [27]. If protons / acidic pH persists in the medium after activation, ASICs desensitize. The time constant of desensitization t_{desens} is 1.2-3.5 s for ASIC1a [13] and ≈0.3 s for ASIC3 [27] and is pH-independent at pH <6.0 [28]. ASIC1a recovers from desensitization with a time constant t≈10 s and ASIC3 with t≈0.5 s [29].

The mechanisms by which ASICs are activated in the brain are not fully clarified. Protons released during neurotransmission by acidic (pH ≈5.5) neurotransmitter-containing vesicles may be involved [30], but post-synaptic ASIC-dependent currents were not detected during neurotransmission [31]. Protons generated by localized energy metabolism might also contribute to ASIC activation [32], as might a list of ASIC modulators (see Section 1.3). The downstream mechanisms by which ASIC1A activation produces its effects also needs further clarification. ASICs should influence neuronal function through membrane depolarization [33], Ca^{2+} entry [34] and multiple downstream signalling cascades [35]. Its graphical description is reported in Figure 2. Despite the potential importance of ASIC channels in brain disorders, their location on the axo-somato-dendritic surface of neurons is still unknown. Furthermore, it is also unknown whether their chronic activation in specific neuronal population can induce broad alterations involving large networks of functionally assembled neurons.

Therefore, the generation of new and isoform-selective modulators to get the fine tuning of each specific ASICs isoforms, and possibly a fine dissection of their expression and localization in neurons under physiological and pathological conditions (i.e., synaptic plasticity, learning, memory and behaviour) is a major need in that field.

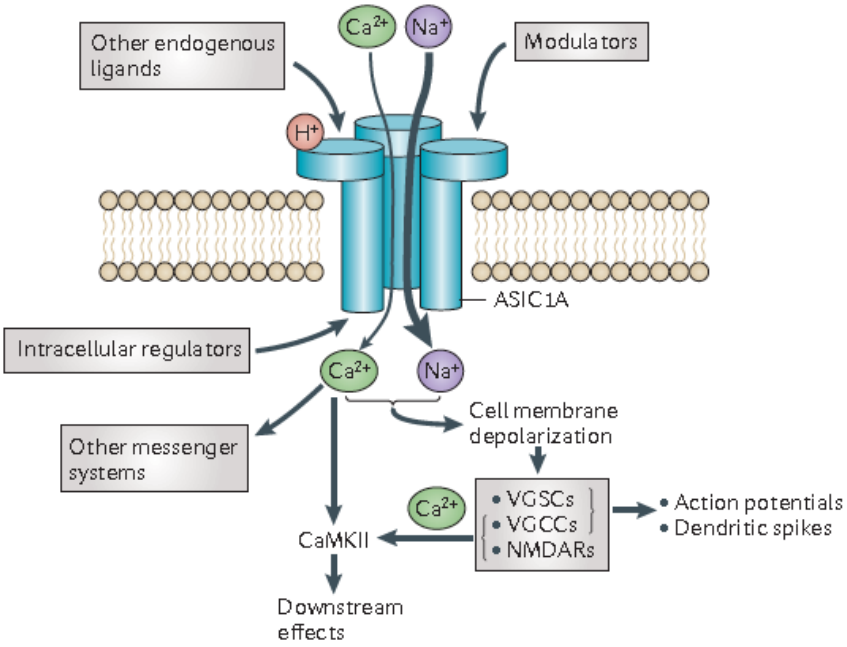

Figure 2. Downstream effects of ASIC1a activation, and modulators of downstream effects.

4.1.2 Therapeutic applications for modulators of ASICs

Most data on the physiological and pathological roles of ASIC channels came from pharmacological approaches using ASIC-targeting compounds in vivo in animal models as well as in rare, small clinical studies in humans [36]. While ASICs modulators are covered in the next Section, a non-exhaustive list of PNS (top left), CNS (bottom left) and diseases unrelated to the nervous system (right) where the influence of ASICs has been confirmed in vivo is graphically depicted in Figure 3. Several neurological diseases involve acidosis, including ischaemia, inflammation, metabolism and synaptic transmission [37]. Extreme or prolonged acidosis kills neurons, and there is growing evidence that ASICs mediate acid-induced toxicity in the CNS [38]. Pharmacological inhibition and modulation of ASICs represents a valuable approach to reduce neuronal degeneration and tissue damage in different neuronal disorders as suggested by several works in animal models [39,40]. Indeed, preclinical studies of ASIC1a inhibitors, have largely predicted clinical benefit in MS and brain ischemia [41,42]. Accordingly, extracellular acidosis and ASICs activation participate in ischemic death of neurons, indicating that tissue acidosis *per se*, affects neuronal survival [43]. A step toward the development of therapies based on ASICs inhibitors has been recently conducted in patients with a progressive form of MS [44]. Although not conclusive, this clinical trial is a suggestive attempt that strives toward the goal of finding new neuroprotective therapies for the treatment of progressive MS.

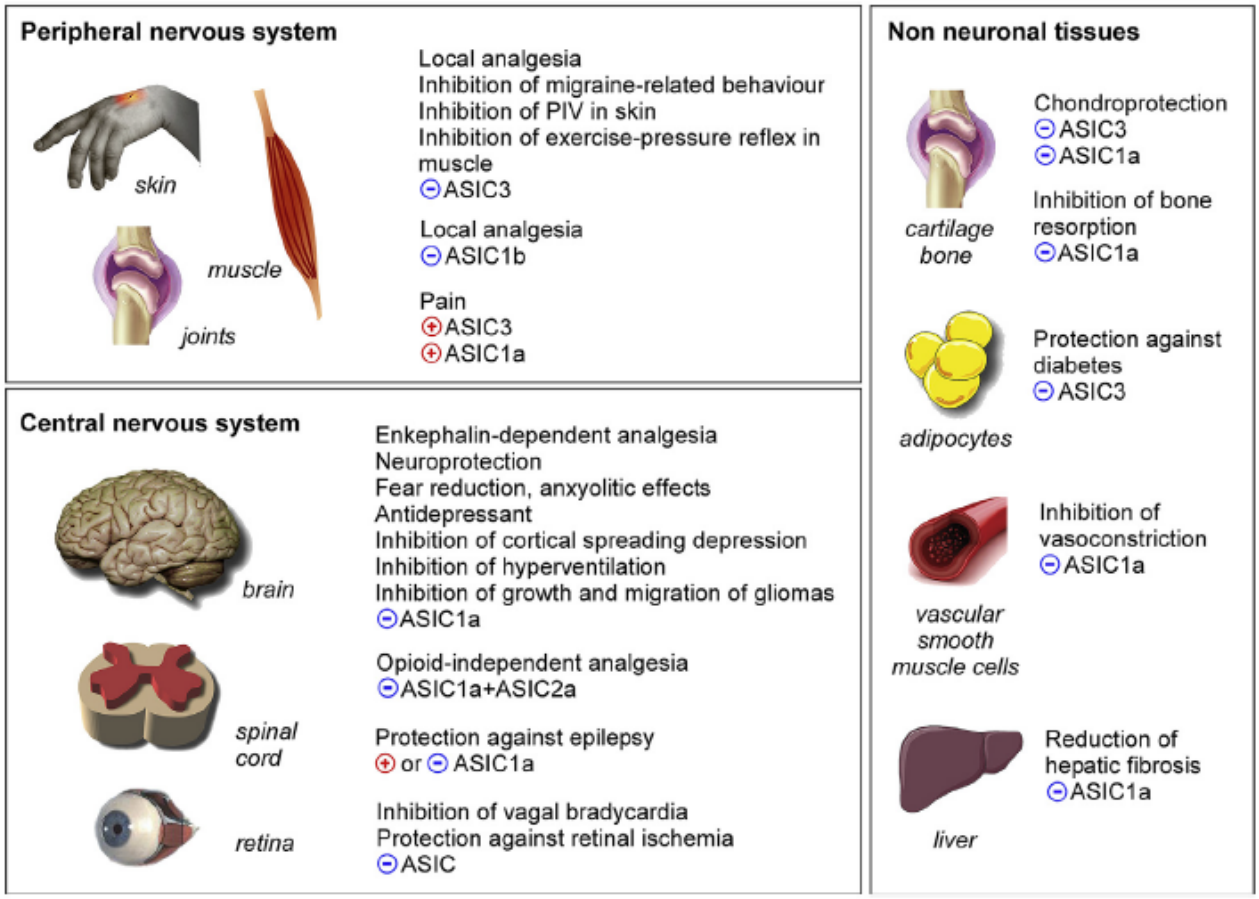

Figure 3. Therapeutic potential of ASICs modulators: diseases, tissues and organs, therapeutic effects. (+), ASICs activators needed; (-), ASICs antagonists needed; ?, hypothetical / not fully validated applications.

As to neuroprotection, ASIC1a channels in the CNS participate to acido-toxicity and neuronal death associated with ischemia or traumatic injury [43], [45]. In addition to acidosis, brain injury releases a number of endogenous chemicals that can modulate ASICs, and may boost ASIC currents and their associated toxicity [46,47]. In rodents, i.c.v. [42,43] or intraperitoneal injection [48] of ASICs modulators protects against severe focal ischemia by reducing the infarct volume by more than 50%. In rat spinal cord, i.t. injection of a natural ASIC1a-targeted toxin reduces the lesion volume induced by traumatic injury and increases locomotor recovery [49]. ASICs modulators significantly decreased ischemia-induced retinal degeneration in rats [50], and are also neuroprotective in animal models of neurodegenerative diseases – Huntington's disease, where depletion of ASIC1a activity reduced polyglutamine aggregation [51]; Parkinson Disease, where ASICs-targeted traditional medicine remedies are neuroprotective [52].

As indicated by many pre-clinical studies, the inhibition of ASICs may represent a successful strategy in a large spectrum of neuroinflammatory disorders, although some controversial data limit the direct use of available ASICs inhibitors to treat patients. If we consider the tissue acidosis associated with epilepsy, experimental data suggest that a local drop of pH limits seizure duration and exert protective effects that rely on ASICs recruitment [33]. ASICs inhibition reduces innate fear-related behaviour [53], and overexpression of ASIC1a in transgenic mice increases fear conditioning [54]. Anxiolytic-like effects of ASICs modulators have been described [55]. An i.c.v. injection of ASICs toxins or small molecule modulators [56] has antidepressant effects through inhibition of ASIC1a channels.

ASICs activation is also involved in synaptic remodelling, a basic process in neuronal physiology. ASIC1a is mainly located in dendritic spines of neurons, although such channels are also identified on neuronal cell

bodies [5]. Reducing or increasing ASIC1a expression levels in neurons increases or decreases spine density, respectively [34]. Unexpectedly, a long-term acidic treatment in neurons activates ASICs and reduces pre-synaptic terminals in these cells, while it does not affect post-synaptic terminals [40]. The proton sensitivity of ASICs is also centrally involved in their function. Indeed, a mild acidosis (pH ≈ 6.9) causes ASIC1a homotrimers to undergo steady state desensitization, rendering such channels unavailable for subsequent activations when pH levels further drop [25]. This complete desensitization of homotrimeric channels, is appropriate for a physiological role of ASIC1a at the synaptic level, where pH levels rapidly fluctuate during synaptic transmission, but is hardly reconciled with long term pathological phenomena, in which a persisting acidosis affects the brain [40]. ASIC1a can form heterotrimeric channels that include the presence of ASIC2a subunits [15], [57]. Furthermore, the expression levels of ASICs and their ability to influence neuronal functioning is also modulated in the inflamed CNS both at mRNA and at protein levels, as shown in axons during inflammatory episodes [41] and also in spinal cord slices treated with kainate [58].

4.1.3. Pharmacology of known ASICs modulators

4.1.3.1. Endogenous modulators

Extracellular divalent cations (Ca^{2+} and Mg^{2+}) play a key role in ASIC1a and ASIC3 gating [25], [59]. At low [Ca^{2+}], smaller ASICs activation constants and desensitization times are observed (higher apparent affinity). High [Ca^{2+}] has the opposite effect [46]. These observations are expected when Ca^{2+} and protons compete for a common binding site. Increasing [Ca^{2+}] also reduces single channel amplitude, in accordance with a binding site in the ion pore [60]. A model was proposed that explains modulation of proton sensitivity and Ca^{2+} blockage with a single Ca^{2+} binding site in the ion pore [59].

Extracellular Zn^{2+} shows multiple effect on ASICs when co-applied with acidic pH: a moderate potentiating effect (IC_{50} ≈ 120 μM) on ASIC2a channels [61], and a potent inhibitory effect (IC_{50} ≈ 10 nM) on both homomeric ASIC1a and heteromeric ASIC1a - ASIC2a channels [62]. High concentration of Zn^{2+} (IC_{50} ≈ 61 μM) was also reported to inhibit ASIC3 currents [63]. ASICs are inhibited by heavy metal ions (Gd^{3+}, Pb^{2+}, Ni^{2+}, Cd^{2+}, Cu^{2+}) [16, 46, 64, 65]. Cu^{2+} inhibits ASIC currents in central neurons with a μM IC_{50} [66], and the neurotoxic ion Pb^{2+} strongly blocks ASIC1a-containing trimers (IC_{50} ≈ 5 μM) [65].

Polyamines agmatine **1** and arcaine **2**, inhibitors of NMDA receptors, weakly activate homomeric ASIC3 channels and heteromeric ASIC3/1b channels (EC_{50} ≈ 10 mM and 1.2 mM, respectively) through direct interaction with the palm region [67] (Figure 1). Spermine **3**, a polyvalent cation agonist of NMDA receptors, increases ASIC1a, ASIC1b, and ASIC1a + ASIC2a currents in neurons by shifting their pH dependence of inactivation [45]. Its potent activating effect on ASIC currents in rat hippocampal neurons (EC_{50} = 495 nM) [45] could justify its neurotoxicity in brain ischemia. The structures of polyamines **1**-**3** are shown in Figure 4.

Neuropeptide enhancers of ASIC currents include FMFRamides such as **4** [68,69], and dynorphins, such as **5** [36]. The former bind with good potency (EC_{50} = 10-50 μM) to ASIC1a regions of the extracellular palm domain and the β11-12 linker, belonging to the central vestibule, which are important for inactivation and steady-state desensitization of ASIC1a [70]. Dynorphins potently prevent steady-state desensitization and enhance ASIC1a and ASIC1b currents (EC_{50} ≈ 30 nM), likely binding at the acidic pocket [71]. The structures of neuropeptides **4**, **5** are shown in Figure 4.

Miscellaneous endogenous ASIC modulators include serotonin / 5-hydroxytryptamine / 5-HT **6** [72], that increases the homotrimeric ASIC3-mediated current in neurons and binds with moderate potency (EC_{50} ≈ 41 μM) to the palm region of ASIC3; the phospholipid metabolite arachidonic acid **7** [73], that potentiates ASIC1a, ASIC2a and ASIC3 currents at low μM; the cannabinoid anandamide **8** [18], that shifts the activation of ASIC3 in neurons toward less acidic pH and contributes to inflammatory pain sensations; and nitric oxide donors [74], that potentiates ASIC currents in brain ischemia (> neurotoxicity [75]) by S-nitrosylation of Cys residues in the extra-cellular loop of the channels. The structures of miscellaneous endogenous ASIC modulators **6**-**8** are shown in Figure 4.

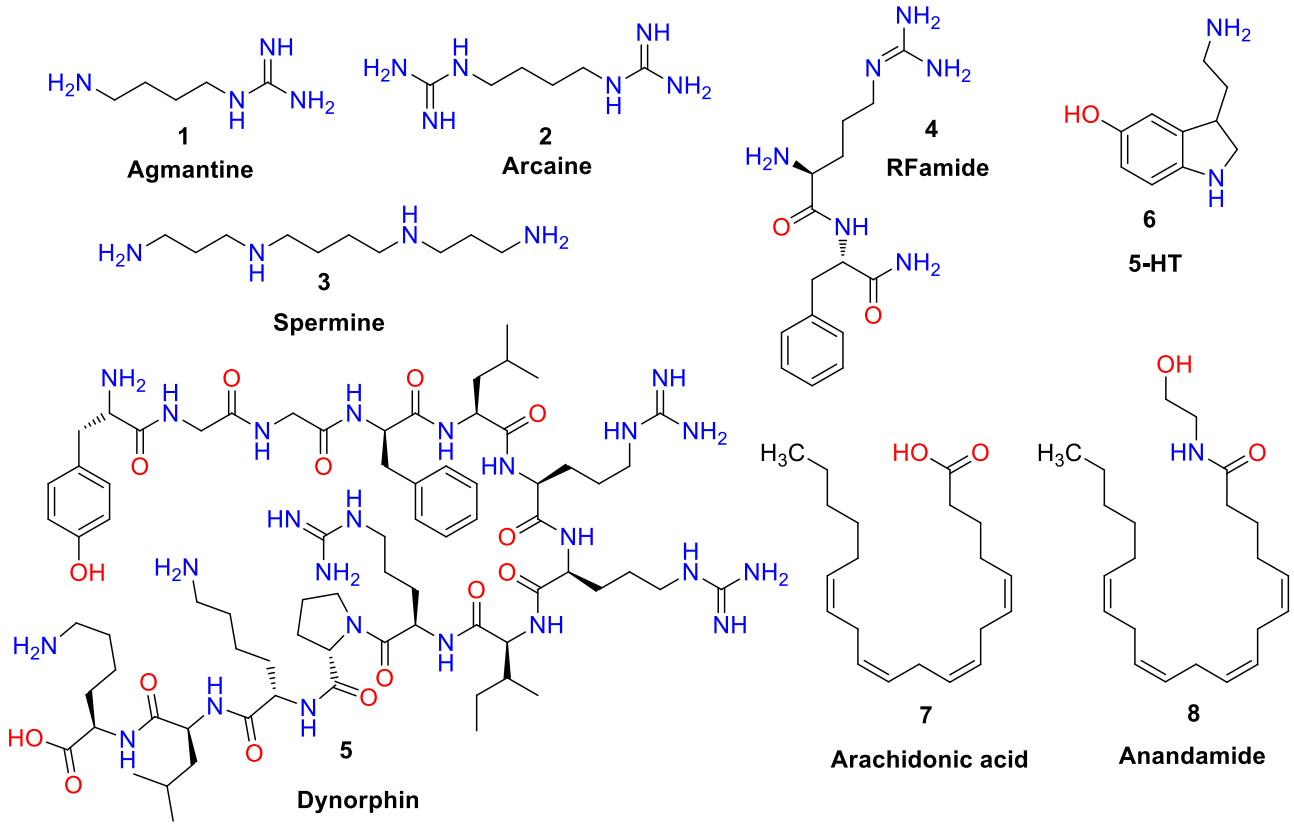

Figure 4. Endogenous ASICs modulators **1**-**8**: chemical structures.

4.1.3.2. Exogenous modulators from natural sources

Animal venoms from different predators contain several peptide toxins acting as exquisitely selective antagonists of ASIC subunits, with partially overlapping pharmacological profiles [76]. The most studied peptide toxins were found in spiders (plasmotoxin-1, PcTx-1 [77], from South American tarantulas), in marine organisms (APETx2 [78], from a sea anemone) and in snakes (three mambalgins [79] from African mamba snakes, and MitTx [80] from the Texas coral snake). Their primary sequence, with S-S bonds highlighted in red, is shown in Figure 5.

At pH = 7.4, PcTx-1 is a potent inhibitor of ASIC1a either in homo- and heterotrimeric complexes (EC_{50} ≈ 1 nM), while it opens ASIC1b channels at higher concentrations (EC_{50} ≈ 100 nM) [77]. Its binding to the acidic pocket of ASIC1a was determined by X-ray crystallography [81] (Figure 1). APETx2 is ASIC3-specific (either in homo- and heterotrimers) and potent (EC_{50} between 30 nM and 2μM). It also inhibits other ion channels with similar potencies [78], [82]. Two putative binding sites (respectively the thumb, and between the wrist and the palm regions) were proposed by a computer simulation [83].

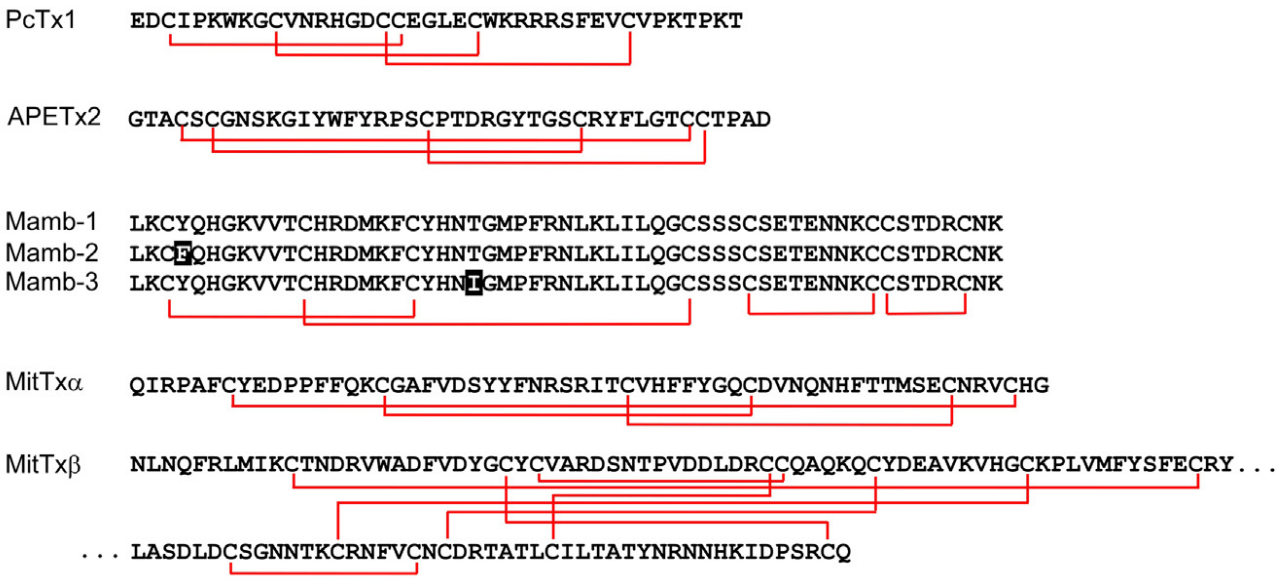

Figure 5. Exogenous ASICs modulators from animal sources: primary structures.

MitTx is made by two α and β subunits, and strongly potentiates ASIC1a and ASIC1b currents in neurons (respectively EC_{50} = 9 and 23 nM), with a weaker effect on ASIC3 (EC_{50} ≈ 830 nM) and ASIC1a + ASIC2a heterotrimers [80], [84]. Its binding to regions of ASIC1a including the wrist, knuckle and thumb was determined by X-ray crystallography [85] (Figure 1). Closely related mambalgins 1-3 potently inhibit either homomeric ASIC1a/1b channels, or heterotrimeric ASIC1a/1b-containing channels (EC_{50} varying between 11 and 252 nM) [76]. A computational model suggested a stimulatory binding of mambalgins to the upper part of the thumb domain, overwhelmed by an inhibitory interaction with the palm domain of an adjacent subunit and with the β-ball domain that prevent the conformational changes of the palm and β-ball regions following proton activation [86] (Figure 1).

ASICs modulators from plants are less characterized. Among them, sub-nM potency on ASICs currents in neurons was observed with the polyphenol chlorogenic acid **9** (Figure 6) from traditional medicinal plants (inhibition, EC_{50} ≈ 200 nM [87]), and with the analgesic gastrodin **10** from chinese Tianma (inhibition, EC_{50} ≈ 200 nM [87]). Low μM potency was attributable to the plant flavonoid quercetin **11** (inhibition, EC_{50} ≈ 2 μM [88]), to the monoterpene glycoside paeoniflorin **12** from anti-inflammatory *Peonia lactiflora* (ASIC1a inhibition, EC_{50} ≈ 5 μM [52]) and to the isoflavone puerarin **13** from *Pueraria lobata* (ASIC1a inhibition, EC_{50} = 9.31 μM [89]). Weaker inhibitors included the sulphated flavone isoglycoside thalassiolin B **14** from sea grass (inhibition, EC_{50} ≈ 27 μM [90]) and the lignin sevanol **15** from armenian thyme (ASIC3 inhibition, EC_{50} ≈ 300 μM [91]). The antioxidant curcumin **16** (Figure 6) from turmeric showed ASICs inhibition-mediated *in vivo* potency at 50 mg / Kg in a model of inflammation [92]. The structures of exogenous ASIC modulators **9**-**16** from vegetal sources are shown in Figure 6.

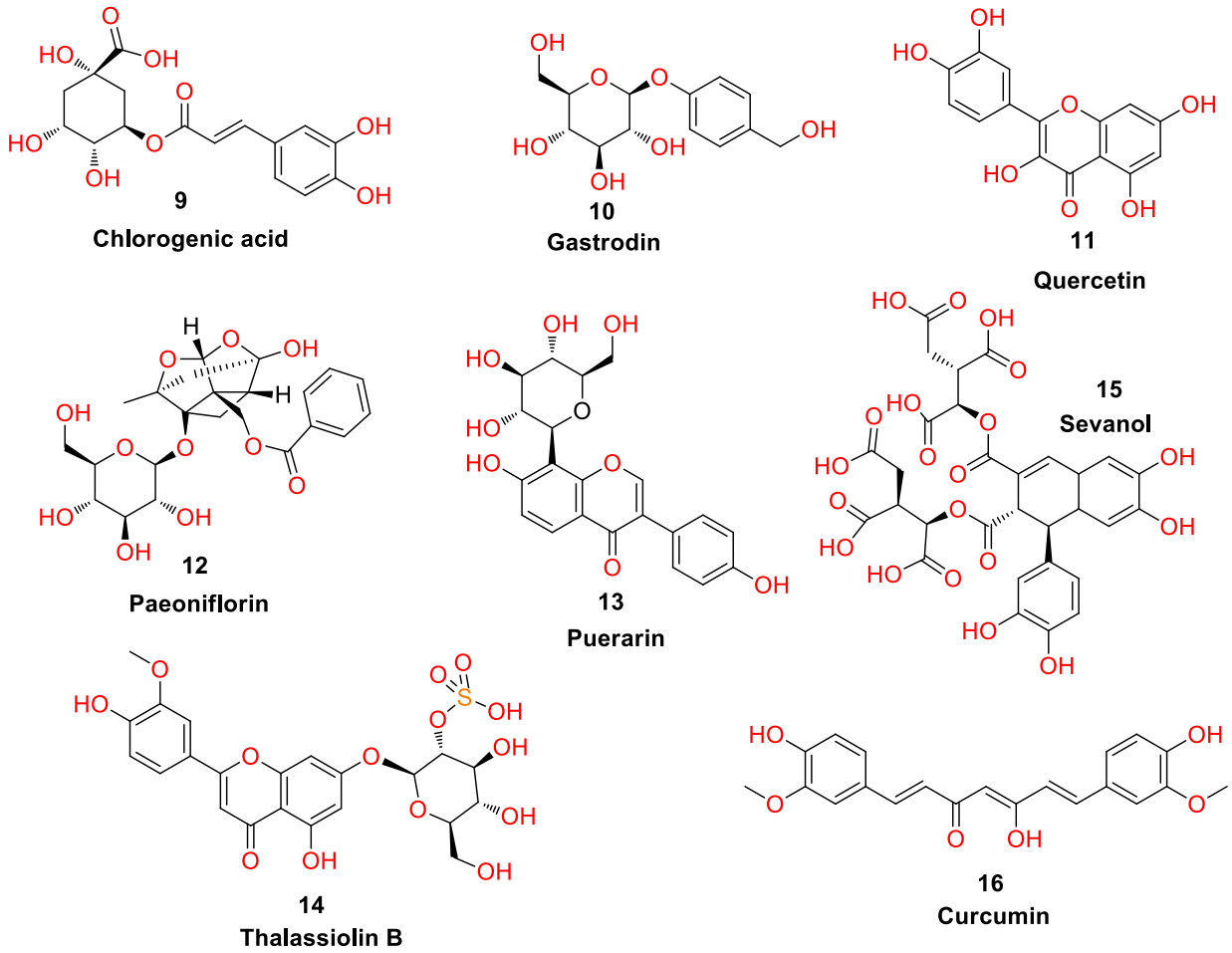

Figure 6. Exogenous ASICs modulators **9**-**16** from vegetal sources: chemical structures.

4.1.3.3. Synthetic exogenous modulators

Synthetic ASIC modulators – mostly inhibitors – belonging to multiple chemical classes were published in the past decades [36]. Their structures are depicted in Figures 7 and 8.

Non-steroid anti-inflammatory drugs (NSAIDs), such as diclofenac **17** (Figure 7), inhibit most homo- and heterotrimeric ASICs with potencies ranging between 90 and 500 μM [93]. Structurally related CHF5074 **18**, a neuroprotective agent lacking NSAID-typical cyclooxygenase inhibitory activity, showed significantly higher potency (EC_{50} ≈ 50 nM [94]) on ASICs currents in neurons. CHF5074, and possibly other NSAIDs, were suggested by computational simulations to bind to the β-ball region of ASIC1a [94] (Figure 1).

Amine-containing ASICs modulators include the non-specific inhibitors of voltage-gated K^+ channels 4-aminopyridine (4-AP **19**) and tetraethyl ammonium (TEA **20**). They showed high μM to low mM potency, with partial ASIC subunit selectivity [71]. 4-AP, clinically used against multiple sclerosis, showed activity on ASIC1a and on heterotrimeric channels containing ASIC1a, ASIC1b and ASIC2 subunits, losing potency on ASIC3-containing heterotrimers up to inactivity against ASIC3 [95]. TEA blocked heteromeric ASIC1a + ASIC2a/2b channels without affecting homomeric ASIC1a channels [71].

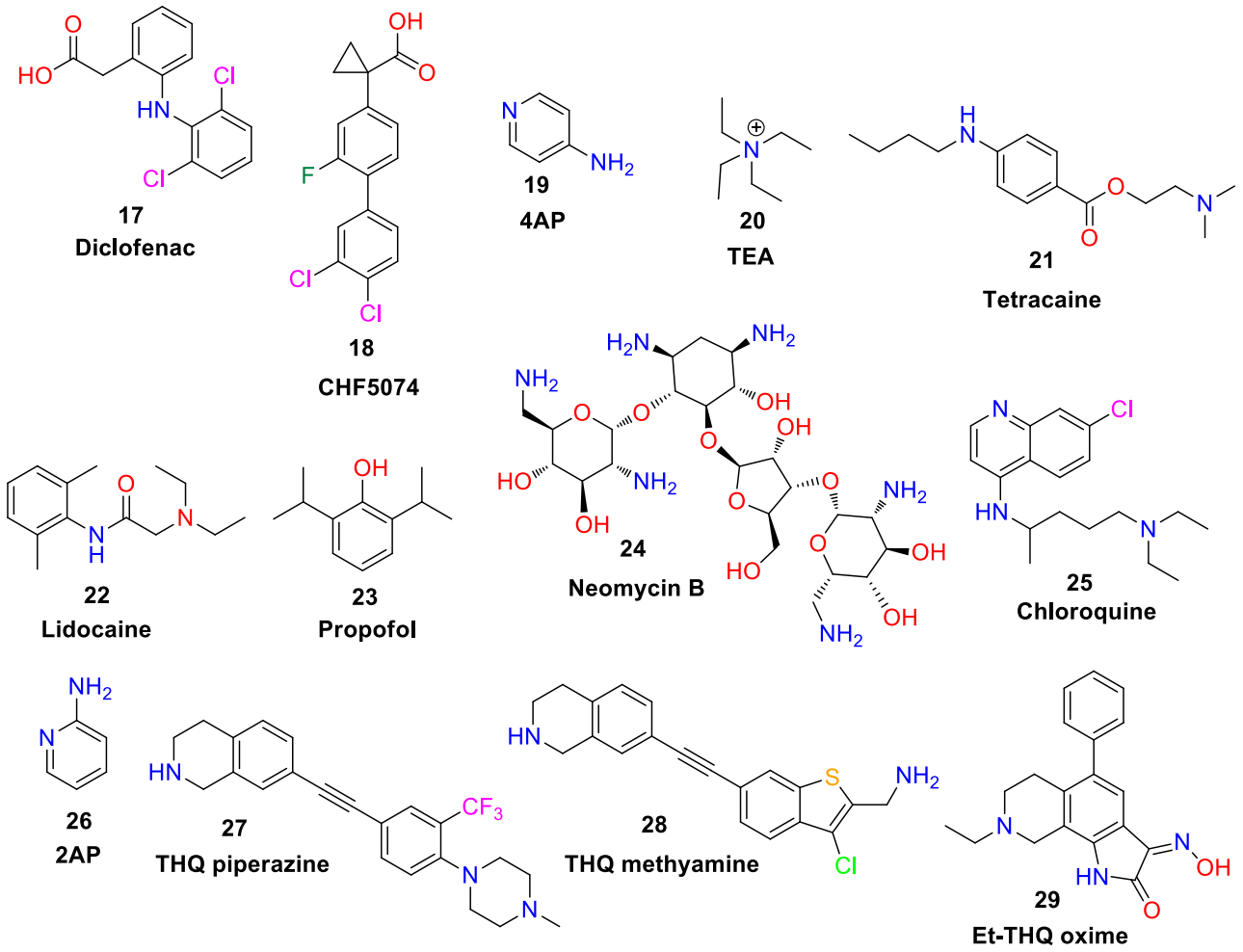

Figure 7. Amine-containing synthetic ASICs modulators **17**-**29**: chemical structures.

Local anesthetics show moderate ASIC inhibition. Tetracaine **21** showed low mM inhibition of ASIC1b and ASIC3 currents, without acting on ASIC2b channels [96]; lidocaine **22** showed similar potency on ASIC1a and lack of activity against ASIC2a [97]. Structurally related, amine-missing propofol **23** partially inhibited ASIC1a and ASIC3 currents in neurons [98], with different subunit specificity. Clinically used aminoglycoside antibiotics, such as neomycin B **24**, showed μM potency on ASICs currents in neurons, on ASIC1a homotrimers [99] and ASIC-dependent analgesia in vivo [100]. The antimalarial chloroquine **25** inhibited homotrimeric ASIC1a channels and ASIC currents in retinal neurons with EC_{50} ≈ 600 μM [101]. 2-Aminopyridine **26**, tetrahydroisoquinoline / THQ piperazine **27** [102] and THQ methylamine **28** [103] were rationally designed and structurally optimized by Merck for ASIC3 inhibition (respectively EC_{50} = 9 μM, 3.1 μM and 220 nM). They were active on recombinant ASIC3 channels and on cellular assays, and showed appropriate PK, although they were not pursued further due to early ADMET issues (**26**, **27**) and off-side effects (**28**). Finally, ethyl THQ oxime **29** (Figure 7) showed sub-micromolar effects (EC_{50} varying between 120 and 690 nM) on homomeric ASIC1a and ASIC3, and heteromeric ASIC1a-containing channels. It also showed activity on ASIC currents in neurons, a good PK profile and efficacy in rat pain models between 30 and 60 mg / Kg [104].

Guanidine-containing ASICs modulators include the acyl-guanidine amiloride **30** (Figure 8), a diuretic drug that was the first identified small molecule ASIC modulator [2], [105]. Amiloride is neither subunit- nor target-specific, as it blocked other ion channels with similar potency (EC_{50} varying between 5 and 100 μM) [106]. At higher, >500 μM concentrations amiloride stimulated homomeric ASIC3 and heteromeric ASIC1b + ASIC3 channels [107]. The ASIC-blocking effect was attributed to the occlusion of the channel pore in the

extracellular vestibule [108], while the paradoxical stimulating effect was linked both to the acidic pocket and to the non-proton binding site [85, 109-111] (Figure 1). Amiloride analogues include its benzylated (benzamil, **31**) and its dialkylated derivative (EIPA, **32**), that showed similar potencies and selectivity / aspecificity [112]; and biphenylic compound **33** [113], showing potent sub-micromolar potency on ASIC3 and in vivo activity against inflammatory pain at 30 mg / Kg.

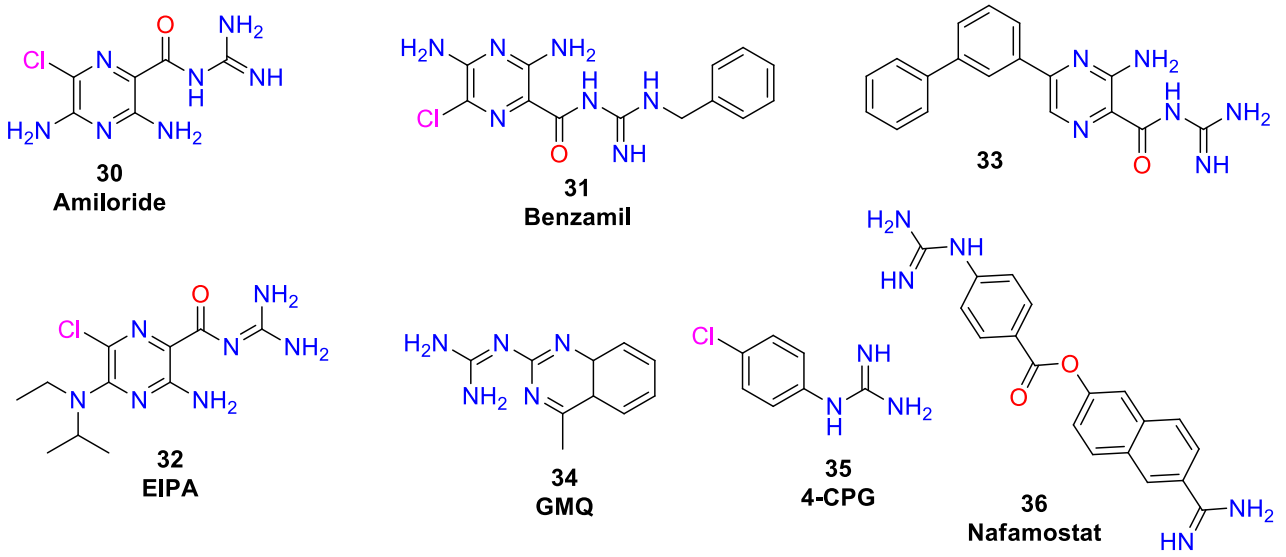

Figure 8. Guanidine-containing synthetic ASICs modulators **30**-**36**: chemical structures.

2-Guanidino-4-methylquinazoline (GMQ, **34**) was found to be a guanidine-containing ASICs' channel stimulator at similar concentrations as amiloride (EC_{50} ≈ 1 mM) [114]. Its stimulation at pH 7.4 was subunit-selective / effective only on ASIC3 [115, 116], and its binding to the non-proton binding site was proposed [116] (Figure 1). 4-Chlorophenyl guanidine (4-CPG, **35**) showed a similar activity profile, but lower ASIC3 activation currents [117]. Finally, the di-cationic protease inhibitor nafamostat **36** (Figure 8), containing a guanidine and an amidine moiety, inhibited most ASIC subunits with good to moderate potencies (EC_{50} varying between 2 and 70 μM) [118].

4.1.3.4. Aryl mono- and diamidines

While nafamostat **36** already contained an amidine moiety, the first identified mono-amidine small molecule ASIC inhibitor was A-317567 (**37**, Figure 9) [119]. Possibly selected out of an optimization project, A-317567 showed good inhibition of ASIC3 and ASIC1a channels (EC_{50} varying between 1 and 30 μM), both in CNS [120] and peripheral neurons [119]. It showed in vivo efficacy on peripheral pain models after i.p. administration, but was not BBB-permeable preventing its CNS applications [120]. A more potent, closely related analogue (**38**, EC_{50} = 356 and 450 nM respectively on ASIC3 and ASIC1a) showed in vivo efficacy in a rat model of osteoarthritis, but remained BBB-impermeable and showed multiple off-site activities (EC_{50} < 10 μM, ≈40 targets) [121]. In both compounds, the amidine group was essential for ASICs inhibition.

Subsequently, two research groups independently identified aryl diamidines as potent ASICs inhibitors. The screening of a large compound collections for amidine-containing small molecules, and their testing in a low throughput electrophysiology ASIC3 assay led to the identification of indole-based diamidine **39** [122]. A preliminary SAR, carried out through parallel synthesis, identified the essential nature of the amidine group on the indolic ring (position 6 preferred), while the other amidine could be replaced – also to improve bioavailability – with more lipophilic groups in several ring positions. The most potent mono-amidine

analogue **40** showed nM potency on ASIC3 (EC_{50} = 133 nM) and in vivo efficacy on rat inflammatory pain models [122].

A structure-based approach focused the search of novel ASICs inhibitors onto di-cationic molecules, due to the large percentage of charged aminoacids in their structure [123]. Out of them, known anti-protozoal aryl diamidine DNA minor groove binders used as drugs and / or veterinary treatments were tested. Cyclic imidocarb **41** and linear hydroxystilbamidine / HSB **42** showed respectively weak (EC_{50} ≈ 200 μM) and good inhibition (EC_{50} ≈ 1.5 μM) of ASIC currents in neurons. Triazene-connected diminazene **43** showed the strongest effect (EC_{50} ≈ 0.3 μM) on neurons, with limited selectivity among ASIC subunits (% inhibition at 3 μM concentration: 39% ASIC1a, 92%, ASIC1b, 51% ASIC2a, 74% ASIC3) [123]. Due to its lack of BBB penetration, diminazene was administered intrathecally to mice in an experimental autoimmune encephalomyelitis model of MS, showing ASICs-driven neuroprotective effects at 30 mg / Kg [40]. Molecular docking initially suggested for diminazene – and possibly any other aryl diamidine – a binding pocket spanning through the β-ball and the palm domains [123]; more recently, a competition with amiloride / binding within the ion pore was proposed, being supported also by mutagenesis data [124].

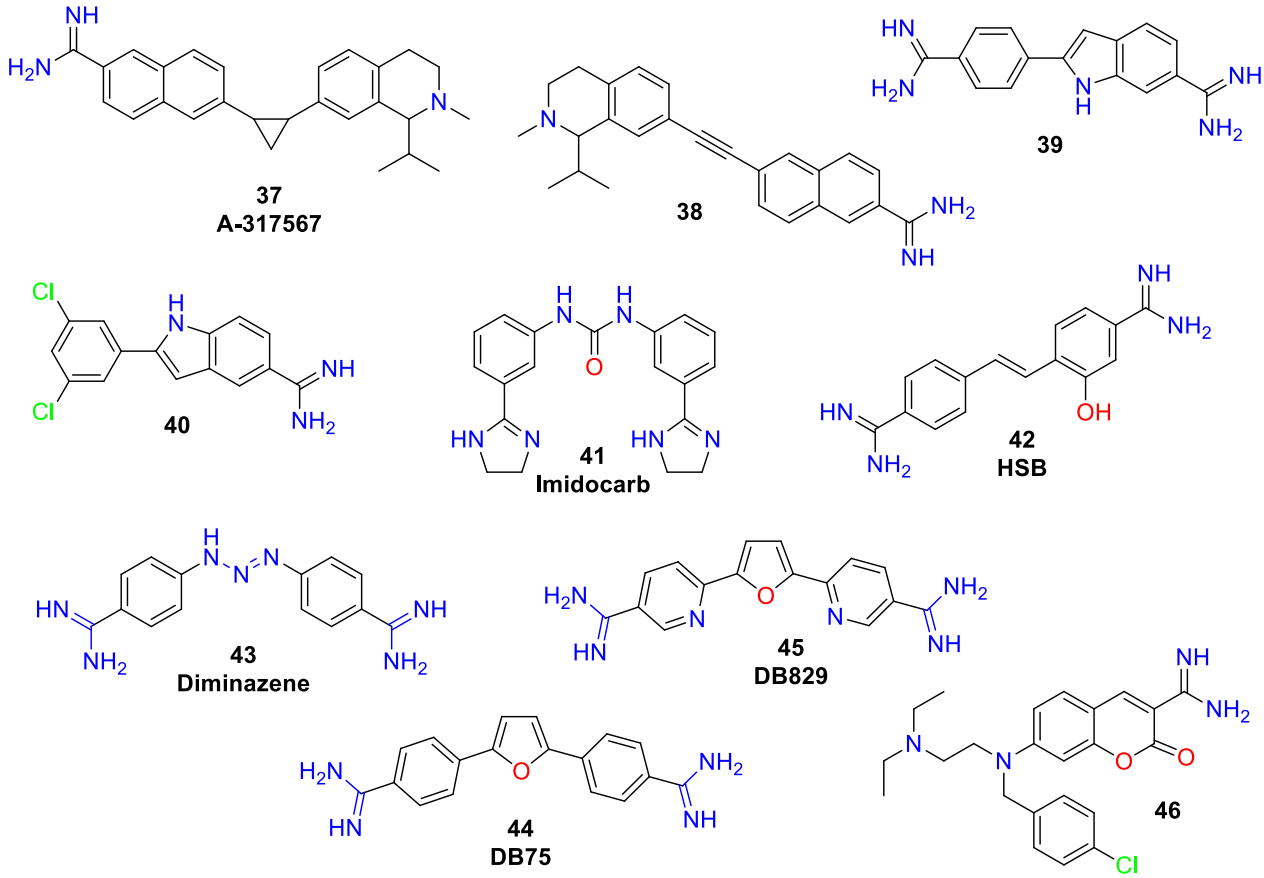

Figure 9. Amidine-containing synthetic ASICs modulators **37-46**: chemical structures.

Furan-connected aryl diamidines such as furamidine /DB75 44 were recently published, following their synthesis and clinical development as treatments against tropical diseases [125,126]. In particular, BBB-compliant DB829 45 and its prodrugs were suggested as potential CNS-targeted ASIC inhibitors [127]. To my knowledge, furan-connected aryl diamidines have not been tested yet against ASICs. Finally, a structure-based approach led to the identification and biological characterization of 2-oxo-chromene mono-amidine 46 (Figure 9). Compound 46 resulted to be potent (nM activity) both on ASIC1a channels and currents in neurons and on hippocampal slices.

4.2. CHEMISTRY

4.2.1. Rationale of the project

We selected aryl amidines in general, and diminazene **43** in particular (Figure 10, left) as the scaffold onto which to build innovative and potent ASICs channel antagonists (Figure 10, right).

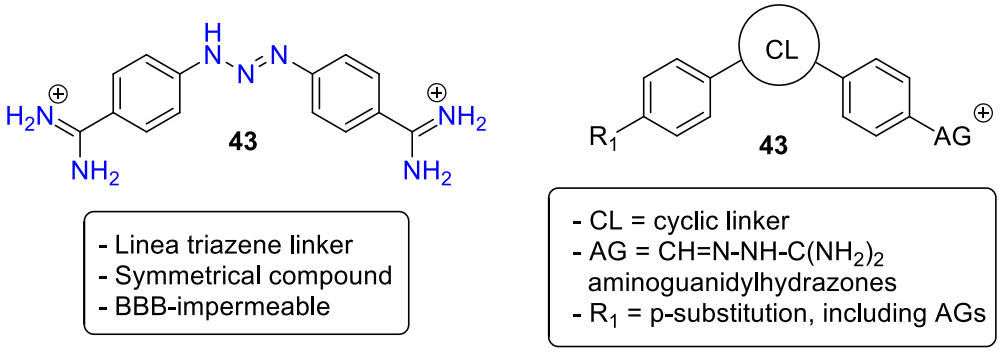

Figure 10. Diminazene **43** and general structure of novel ASICs antagonists: structural comparison.

We decided to keep two substituted phenyl groups spaced with a rigid, conformation-constraining cyclic linker with the same length as triazene (CL, either a 3,5-substituted 5-member ring, or a m-substituted 6-member ring).

We decided to replace the charged amidine groups with aminoguanidines, another drug-recurring ionisable moiety with pKa as close as possible to neutrality, so to ensure a significant percentage of non-ionized molecules at physiological pH and BBB penetrance. Either unsubstituted or substituted aminoguanidyl hydrazones (AGs) were considered.

Finally, we decided to explore the substitution pattern on the second phenyl ring by introducing either another AG (symmetrical, p-disubstituted aryl diAGs), or a more lipophilic substitution pattern (i.e., alkyls, halogens) to optimize affinity for ASICs and to increase BBB permeability.

We expected that both aryl mono- and di-AGs should have been able to interact with the diamidine binding site on trimeric ASIC channels, providing that the diamidine-aminoguanidyl hydrazine substitution would be tolerated. We expected, due to preliminary molecular modelling experiments, that di-AGs would be more potent in terms of target affinity, while mono-AGs bearing lipophilic p-substituents on the other phenyl ring could be more bioavailable / BBB-permeable. The next Sections in this Chapter will detail my efforts towards the rational design of targeted aryl mono- and di- AGs, and the synthetic routes leading to them.

4.2.2. Synthesis of m-substituted phenyl linker connected, non-symmetrical aryl mono-aminoguanidyl hydrazones 47a, 47b and symmetrical aryl di-aminoguanidyl hydrazone 47c

We started the exploration of rigid, cyclic linkers between the diminazene-inspired substituted phenyl ring with a meta-substituted phenyl ring. Such linker was to be connected either to two AG-bearing phenyls (symmetrical aryl di-AG), or to asymmetrically substituted phenyl rings (non-symmetrical aryl mono-AGs). The general retrosynthetic scheme is shown in **Scheme 1**.

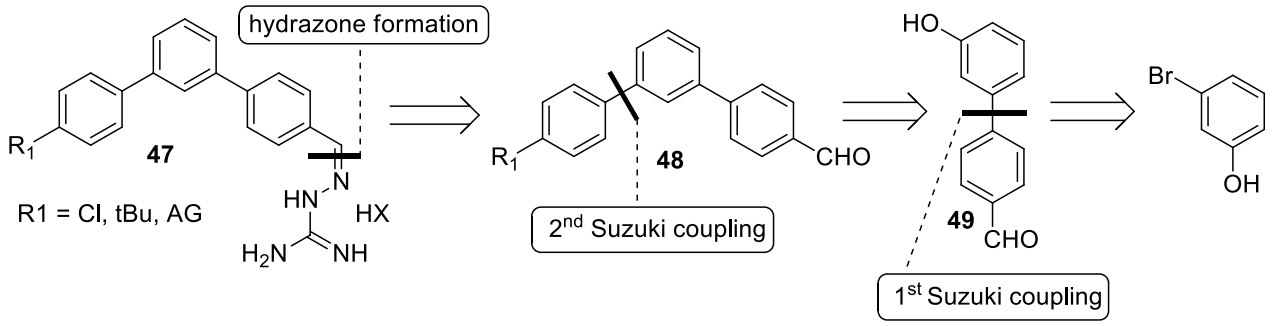

Scheme 1. Retrosynthetic scheme for non-symmetrical and symmetrical, m-phenyl-connected aryl mono-bis AGs **47**.

We reasoned that any targeted aryl mono- and bis-AG (general structure **47**, Scheme 1) could have been obtained from the corresponding aldehydes **48** by standard condensation with aminoguanidine HCl. Aldehydes **48** should derive from the Suzuki coupling between phenoxy aldehyde **49** (after activation of the OH function as a triflate) and a variety of p-substituted arylboronic acids. Finally, phenoxy aldehyde **49** could be synthesized by Suzuki coupling between commercially available 3-bromo phenol – that contains two different groups suitable for Suzuki coupling either directly (Br) or after activation (OH) - and p-formyl phenylboronic acid (Scheme 1). The synthesis of key triflate intermediate **50** is shown in Scheme 2.

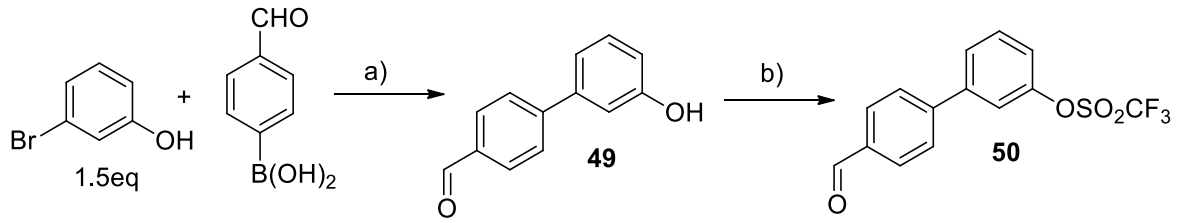

a) $Pd(PPh_3)_4$ (0.1eq), 2.0M aq.Na_2CO_3 (2 eq), dry 1,4-dioxane, N_2, 90°C, 4hrs, **73%**; b) Tf_2O (1.3 eq), TEA (1.5 eq), dry DCM, 0°C to RT, 1hr, **95%**.

Scheme 2. Synthesis of aryltriflate **50** from m-bromophenol.

The Suzuki coupling between m-bromophenol and p-formylphenylboronic acid was carried out in standard conditions (step a, Scheme 2). The reaction is very sensitive to the presence of oxidant species as atmospheric O_2, due to the easy oxidation of the Pd(0) catalyst that would prevent its catalytic action. Thus, we performed it under inert N_2 atmosphere; furthermore, we used degassed, oxygen-free distilled water to prepare the basic Na_2CO_3 solution. This experimental protocol led to phenoxy aldehyde **49** in good yields. The phenoxy group in the intermediate **49**, was converted into a triflate (step b).

We then submitted the triflate intermediate **50** to a second Suzuki coupling, with boronic acids containing two unreactive (to avoid aspecific reactivity in biological systems) and lipophilic substituents (to increase the affinity for biological membranes, i.e. the BBB) for the synthesis of non-symmetrical aldehydes **48a,b**, and with another p-formylphenylboronic acid unit to obtain symmetrical dialdehyde **48c** (step a, Scheme 3).

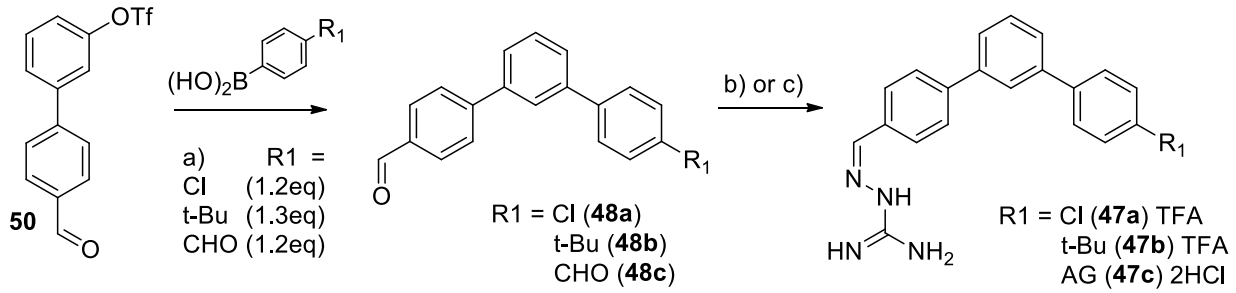

a) $Pd(PPh_3)_4$ (0.1 eq), 2.0M aq.Na_2CO_3 (2.0 eq.), dry 1,4-dioxane, 90°C, 3 hrs, N_2, **91%** (**48a**), **81%** (**48b**), **78%** (**48c**); b) aminoguanidine HCl (1.2 eq), cat. [1N] HCl, EtOH, 80°C, 3 hrs, **92%** (**47a**), **96%** (**47b**); c) aminoguanidine HCl (2.1 eq), cat. [1N] HCl, EtOH, 80°C, 4 hrs, **90%** (**47c**).

Scheme 3. Synthesis of non-symmetrical aryl mono-AGs **47a,b** and symmetrical aryl di-AG **47c** from bis-aryltriflate **50**.

The same experimental procedure for a Suzuki coupling described in Scheme 2 was used. The target, non-symmetrical aryl mono-AGs **47a,b** were finally obtained by treatment of **48a,b** with aminoguanidine HCl in presence of acid catalysis (step b, Scheme 3) in high yield and purity after reverse phase chromatography as trifluoroacetate salts. The symmetrical, aryl di-AG **47c** was obtained after condensation of two equivalents of aminoguanidine HCl onto dialdehyde **48c** (step c, Scheme 3). The solid bis-hydrochloride salt **47c** was formed in the reaction mixture in excellent yields and purity, and was recovered after simple filtration and repeated washings with EtOH/H_2O 95:5.

4.2.3. Synthesis of 3,5-substituted pyrazole connected, non-symmetrical aryl mono-aminoguanidyl hydrazones 51, 58a,b, 61a,b and 62

We selected 3,5-substituted pyrazole as a heterocyclic linker, allowing a further substitution on the 1-nitrogen atom (we selected the unsubstituted N_1-H; the N_1-methylated / small substituent; and the N_1-p-methoxybenzyl / large substituent pattern). We focused our efforts on eight synthetic targets bearing either a p-F- or a p-Br substitution on a phenyl (non-symmetrical aryl mono-AG), or two AGs on both phenyl rings (symmetrical aryl di-AG); one among the symmetrical aryl di-AGs was made with a disubstituted, cyclic AG. We elected to prepare a homogeneous series of p-F-bearing non-symmetrical mono-AG connected via a 3,5-pyrazole cyclic linker, and a single p-Br analogue to evaluate the influence of its bulk on potency. The retrosynthetic pathway conceived for NH, non-symmetrical aryl fluoro mono-AG **51** is reported in Scheme 4.

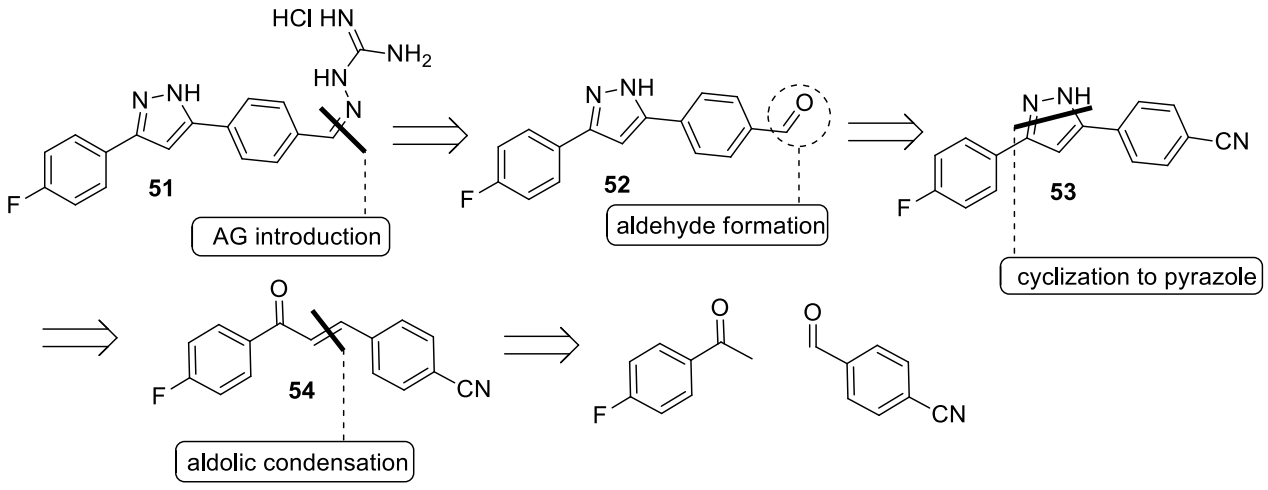

Scheme 4. Retrosynthetic scheme for NH, non-symmetrical aryl fluoro mono-AGs **51.**

The initial aldolic condensation between 4-fluoro acetophenone and p-cyanobenzaldehyde (standard basic conditions, step a, Scheme 5) led to target fluoro cyano chalcone **54** in good yields.

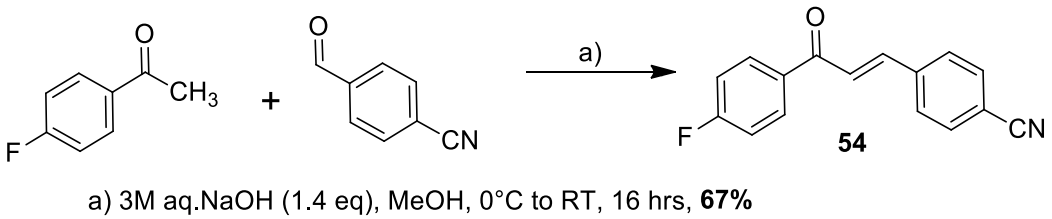

Scheme 5. Synthesis of fluoro cyano chalcone **54** from 4-fluoro acetophenone and p-cyanobenzaldehyde**.**

The cyclization between tosyl-hydrazine and chalcone **54** (Scheme 6) was tried in 4 experimental conditions, listed in Table 1.

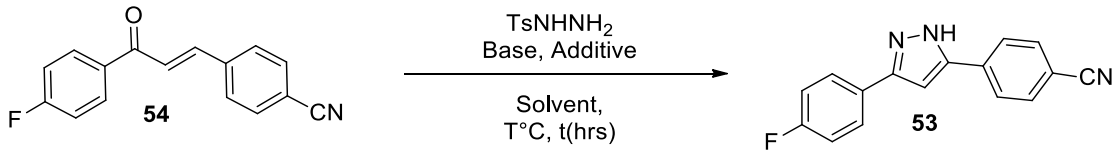

Scheme 6. Synthesis of N_1-unsubstituted fluoro cyano pyrazole **53** from fluoro cyano chalcone **54**.

#	SM	Reagents	T (°C)	Solvent	Time	Results
1	**54** (1 eq)	$TsNHNH_2$ (1.1eq), NaOH (2eq), TBAB (1.5eq)	80°C	H_2O	16 hrs	≈95% recovery of SM, target **53** observed in trace amounts
2	**54** (1 eq)	$TsNHNH_2$ (1.1eq), K_2CO_3 (2eq), I_2 (2%mol)	80°C	EtOH	4 hrs	Major product derived from reduction of α,β-conjugated double bond of SM, target **53** not found
3	**54** (1 eq)	$TsNHNH_2$ (1.1eq), HCl_{aq} (cat.) then NaOH (2eq)	80°C	EtOH	20 hrs	**70**% yield of targets **53**
4	**54** (1 eq)	$TsNHNH_2$ (1.1eq), HCl_{aq} (cat.) then K_2CO_3 (2eq)	80°C	EtOH	20 hrs	**87**% yield of target **53**

Table 1. Experimental conditions for the synthesis of N_1-unsubstituted fluoro cyano pyrazole **53**.

At first, we tried the phase-transfer catalyst conditions (entry 1, Table 1) unfortunately, only trace amounts of target pyrazole **53** was found. Then, we tried to use catalytic iodine (entry 2, Table 1); in this case, we only observed the reduction of the α,β-conjugated double bond in the starting chalcone **54.** Finally, we tried HCl / base-promoted cyclization (entries 3 and 4, Table 1) To our delight, both reactions were successful, and the desired N_1-unsubstituted fluoro cyano pyrazole **53** was obtained either in good (NaOH as base, entry 3) or excellent yields (K_2CO_3 as base, entry 4).

Initially, we tried to directly reduce the cyano group in compound **53** using DIBAL-H (step a, Scheme 7). Unfortunately, due to the incompatibility of the acidic N-H function with DIBAL-H, we could not control the reaction conditions to avoid over-reduction. The same degradation pattern was observed when we tried the DIBAL-H reduction (step c) of the cyano group on N_1-acetyl fluoro cyano pyrazoles **55a,b,** obtained by

acetylation of the N_1-unsubstituted fluoro cyano pyrazole **53** (step b); we presume that N-acetyl removal by DIBAL-H led to this negative outcome.

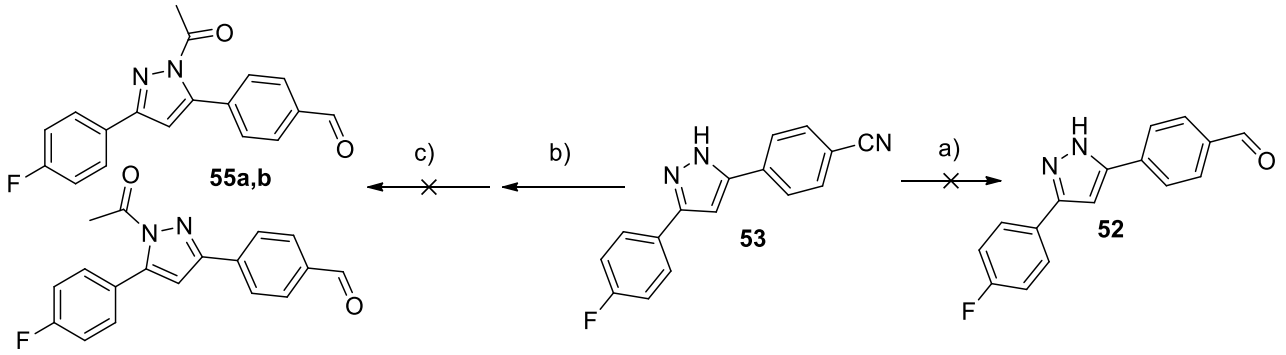

a) 1M DIBAL-H in hexane (2.1 eq), dry DCM, $Ar_{(g)}$, 0°C to RT, 1hr; b) Ac_2O (1.2 eq), DMAP (0.2 eq), DCM/TEA 4:1, RT, 2hrs **95%**; c) 1M DIBAL-H in hexane (1.2 eq), dry DCM, $Ar_{(g)}$, 0°C to RT, 1hr.

Scheme 7. Attempted synthesis of N_1-unsubstituted fluoro formyl pyrazole **52** and of N_1-acetyl fluoro formyl pyrazoles **55a,b** from fluoro cyano pyrazole **53**.

Due to these results, we looked for a reduction-stable protecting group for the N_1 position. We alkylated the N_1 position of the N_1-unsubstituted fluoro cyano pyrazole **53** with a para-methoxybenzyl (PMB) group (step a, Scheme 8). We reasoned that the PMB group should be stable in most reaction conditions, and removable in pyrazole-compatible strong acidic conditions.

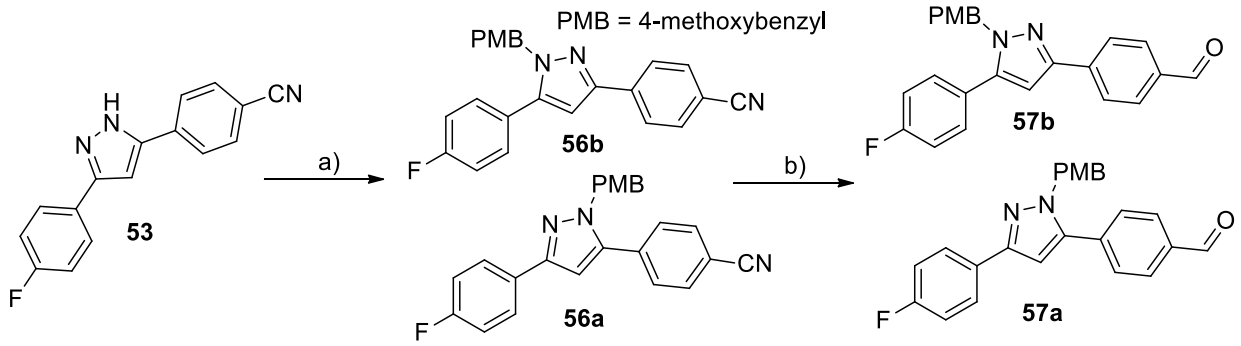

a) PMBCl (1.3 eq), K_2CO_3 (1.5 eq), dry DMF, $Ar_{(g)}$, RT, 16 hrs; b) 1M DIBAL-H in hexane (1.2 eq), dry DCM, $Ar_{(g)}$, 0°C to rt, 1 hr.

Scheme 8. Synthesis of N_1-PMB fluoro formyl pyrazoles **57a,b** from fluoro cyano pyrazole **53**.

The crude, resulting ≈1:1 regioisomeric mixture of N_1-PMB fluoro cyano pyrazoles **56a,b** was submitted without purification to DIBAL-H reduction (step b, Scheme 8). The ≈1:1 regioisomeric mixture of N_1-PMB fluoro formyl pyrazoles **57a,b** was then submitted to acidic deprotection conditions (step a, Scheme 9). According to our expectations, the PMB group was removed smoothly, yielding the N_1-unsubstituted fluoro formyl pyrazoles **52** in good yields over three steps from pyrazole **53**. Target N_1-unsubstituted fluoropyrazole mono-AG **51** was then obtained in high yield and purity by standard condensation of fluoro formyl pyrazole **52** with aminoguanidine HCl (step b, Scheme 9), after purification by reverse phase chromatography.

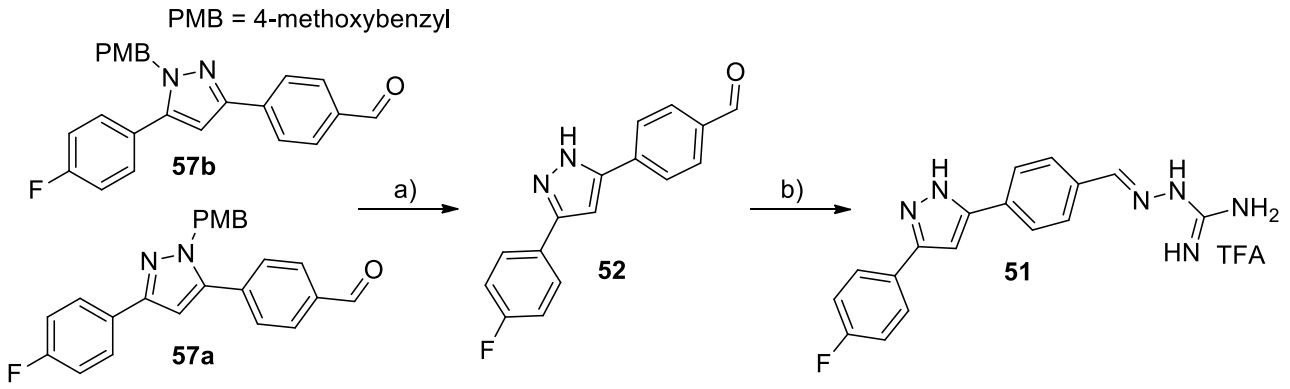

a) TFA [0.1 M], 70°C, 6hrs, **40%** over 3 steps from **53** (Scheme 8); b) aminoguanidine hydrochloride (1 eq), cat. [1N] HCl, EtOH, 80°C, 6hrs, **91%**.

Scheme 9. Synthesis of N_1-unsubstituted pyrazole-connected aryl fluoro mono-AG **51**.

We reasoned the PMB-alkylated product could also be useful to establish a SAR around the N_1 position (bulky PMB group). Thus, pyrazole-connected N_1-PMB, aryl fluoro mono-AGs **58a,b** were then obtained by standard condensation of the N_1-PMB fluoro formyl pyrazole mixture **57a,b** with aminoguanidine HCl (step a, Scheme 10).

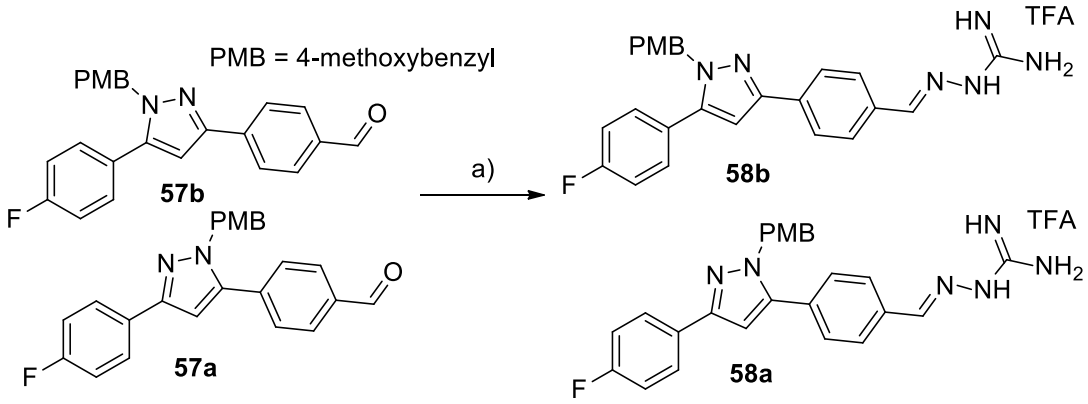

a) aminoguanidine hydrochloride (1 eq), 1M aq.HCl (cat.), EtOH [0.05 M], 80°C, 6 hrs, **82%** over 3 steps from **53** (Scheme 8).

Scheme 10. Synthesis of N_1-PMB pyrazole-connected aryl fluoro mono-AG **58a,b** from N_1-PMB fluoro formyl pyrazoles **57a,b**.

The ≈1:1 relative abundance of the regioisomers confirmed once more the stability / lack of interconversion among N-regioisomers during the whole synthesis.

To continue the SAR exploration around the N_1 position we decided to insert a small methyl group. Pyrazole **53** was thus methylated with MeI (step a, Scheme 11), yielding a ≈1:1 regioisomeric N_1-methyl fluoro cyano pyrazole mixture **59a,b** in good yields. Then, the nitrile group was reduced to aldehyde with DIBAL-H as seen in Scheme 8 (step b, Scheme 11). The regioisomeric 1:1 N_1-methyl fluoro formyl pyrazole mixture **60a,b** was used without purification (see Scheme 12 for a two step yield).

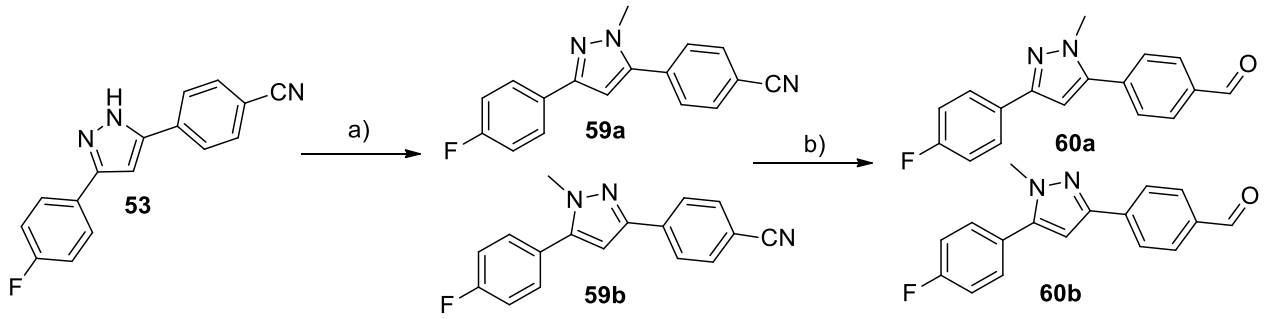

a) MeI (1.3 eq), K_2CO_3 (1.5 eq), dry DMF [0.2 M], $Ar_{(g)}$, rt, 16 hrs, **70%** yield; b) 1M DIBAL-H in hexane (1.2 eq), dry DCM [0.2 M], $Ar_{(g)}$, 0°C to rt, 1 hr.

Scheme 11. Synthesis of N_1-methyl fluoro formyl pyrazoles **60a,b** from fluoro cyano pyrazole **53**.

Finally, the target N_1-methyl fluoro pyrazole di-AGs **61a,b** were obtained as trifluoroacetate salts by treatment of the **60a,b** mixture with aminoguanidine HCl (step a, Scheme 12) and reverse phase chromatography. The ≈1:1 relative abundance of the regioisomers confirmed their insensitivity to the group introduced onto the N_1 position.

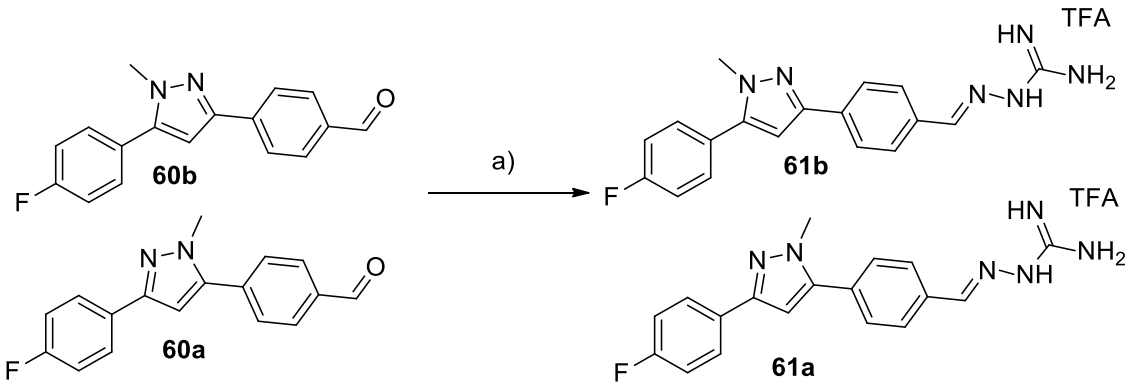

a) aminoguanidine hydrochloride (1 eq), 1M aq.HCl (cat.), EtOH, 80°C, 6hrs, **74%** over 2 steps from pure **59a,b** (Scheme 11).

Scheme 12. Synthesis of N_1-methyl fluoro pyrazole mono-AG **61a,b** from N_1-methyl fluoro formyl pyrazoles **60a,b**.

Taking advantage of the synthetic protocols assessed for the synthesis of N_1-unsubstituted pyrazole-connected fluoro mono-AG **51**, we prepared its bromo analogue **62** (Scheme 13). The ruse of para-bromo acetophenone in step a) did not significantly alter the success and the yields of each synthetic step, when compared to fluoro mono AG **51**. Thus, aldolic condensation (step a, Scheme 13; bromo cyano chalcone **63**), cyclization with tosyl hydrazide (step b; N_1-unsubstituted bromo cyano pyrazole **64**), alkylation with PMB-Cl (step c; N_1-PMB bromo cyano pyrazoles **65a,b**), DIBAL-H reduction (step d; N_1-PMB bromo formyl pyrazoles **66a,b**), PMB deprotection (step e; N-unsubstituted bromo formyl pyrazole **67**), and finally condensation with aminoguanidine HCl (step f, Scheme 13) led after simple filtration and EtOH washing to pure, target N_1-unsubstituted pyrazole-connected bromo mono-AG **62** as a hydrochloride salt in moderate yields.

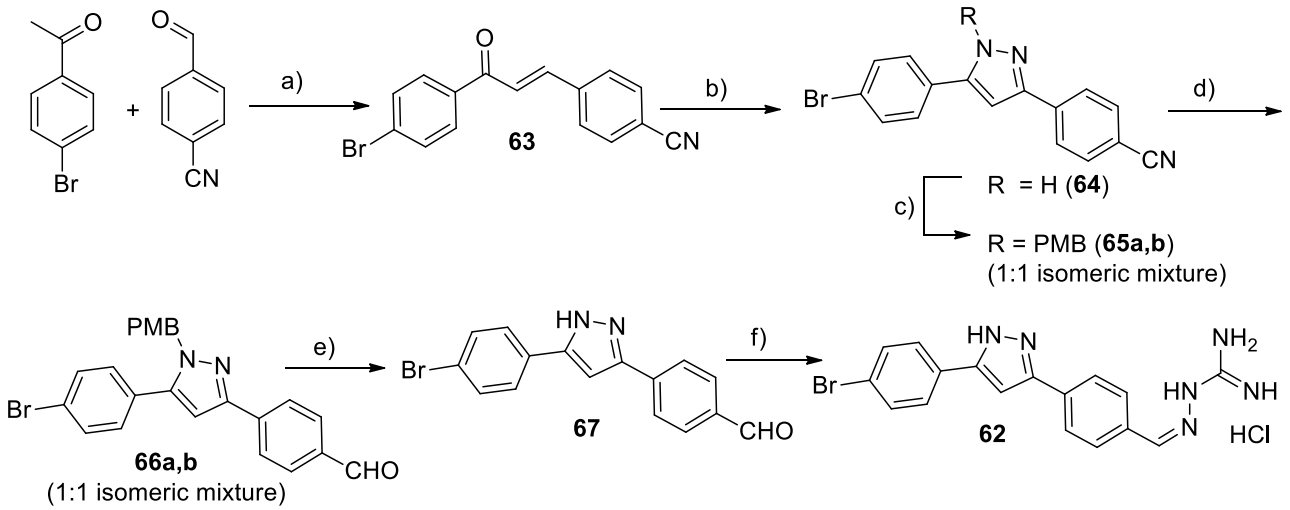

a) 3M aq.NaOH (1.5 eq), MeOH, 0°C to RT, 16 hrs, **63%** yield; b) $TsNHNH_2$ (1.05 eq), cat. 2M HCl, then K_2CO_3 (2.1 eq), EtOH, 80°C, 20 hrs, **87%** yield; c) 4-methoxybenzyl chloride (1.3 eq), K_2CO_3 (1.5 eq), dry DMF, $Ar_{(g)}$, RT, 16 hrs, **77%** yield; d) 1M DIBAL-H in hexane (1.2 eq), dry DCM, $Ar_{(g)}$, 0°C to RT, 1 h, **75%** yield; e) TFA, 70°C, 6 hrs, **69%** yield; f) aminoguanidine hydrochloride (1.1 eq), cat. [1N] HCl, EtOH, 4 hrs, **89%** yield.

Scheme 13. Synthesis of target N_1-unsubstituted pyrazole-connected aryl bromo mono-AG **62** from para-bromo acetophenone and para-cyano benzaldehyde.

4.2.4 Synthesis of 3,5-substituted pyrazole connected, symmetrical aryl di-aminoguanidylhydrazones 68, 69, 76 and 77

The assessed chemical routes for the synthesis of non-symmetrical, pyrazole-connected aryl fluoro mono AGs were successfully used – in simpler reaction pathways – to obtain four symmetrical pyrazole-connected aryl bis-AGs. Our first targets, N_1-methyl pyrazole aryl bis-AG **68** and N_1-PMB pyrazole aryl bis-AG **69,** were synthesized as shown in Scheme 14. Please note that the symmetrical substitution pattern on the two phenyls leads to single pure target compounds.

Bis cyanochalcone **70** was obtained in good yield by aldolic condensation between p-cyano acetophenone and p-cyano benzaldehyde after simple filtration (step a, Scheme 14). Then, cyclization with tosyl hydrazide (step b; N_1-unsubstituted dicyano pyrazole **71**), alkylation with MeI (step c_1; N_1-methyl dicyano pyrazole **72**) or with PMB-Cl (step c_2 li devi differenziare; N_1-PMB dicyano pyrazole **73**), DIBAL-H reduction (step d_1; N_1-methyl diformyl pyrazole **74**, step d_2; N_1-PMB diformyl pyrazole **75**), and finally condensation with aminoguanidine hydrochloride (2 equivalents, step e_1 and e_2, Scheme 14) led after purification by reverse phase chromatography respectively to target N_1-methyl pyrazole-connected aryl bis-AG **68** and N_1-PMB pyrazole-connected aryl bis-AG **69** as bis-trifluoroacetate salts in moderate to good yields.

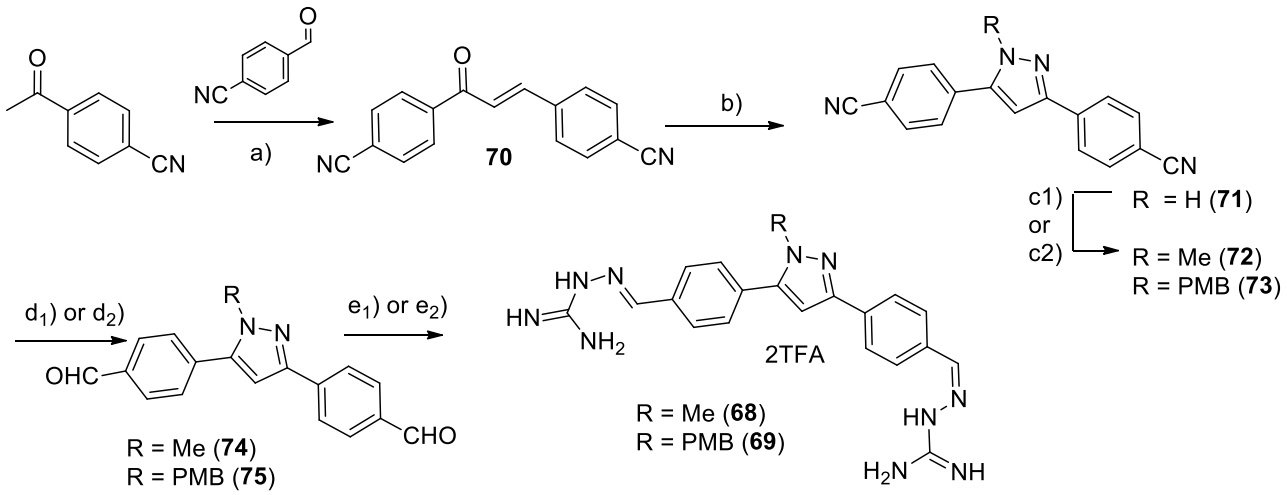

a) cat. aq.NaOH, dry MeOH, 70°C, 45min **66%;** b) $TsNHNH_2$ (1.05 eq), [2N] HCl, then K_2CO_3 (2.1 eq), EtOH, 80°C, 20hrs, **87%**; c) MeI (1.3eq) or PMBCl (1.3 eq), K_2CO_3 (1.5 eq), dry DMF, $Ar_{(g)}$, RT, 16hrs, **95%**(**72**), **87%**(**73**); d) 1M DIBAL-H in hexane (1.1 eq), dry DCM, $Ar_{(g)}$, 0°C to RT, 1 hr, **80%**(**74**), **82%**(**75**); e) aminoguanidine HCl (1.1 eq), cat. [1N] HCl (cat.), EtOH, 4hrs, **89%**(**68**), **87%**(**69**).

Scheme 14. Synthesis of N_1-methyl pyrazole-connected aryl bis-AG **68** and **69** from dinitrile chalcone **70**.

Finally, the N_1-PMB diformyl pyrazole **75** was used to prepare target N_1-unsubstituted pyrazole-connected aryl bis-AGs **76**, and its cyclic AG analogue **77** (Scheme 15).

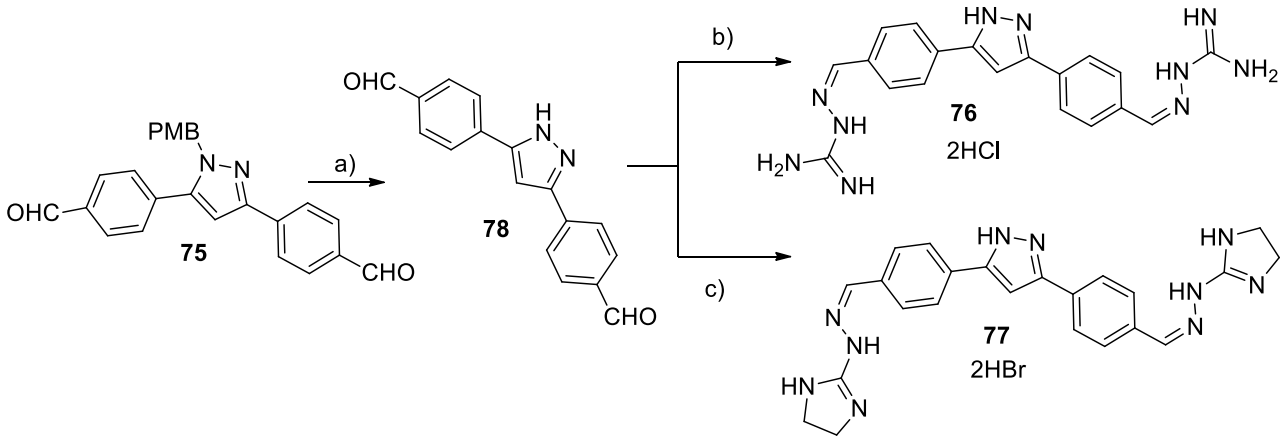

a) TFA, 70°C, 6hrs, **71%**; b) aminoguanidine HCl (1.1 eq), cat. [1N] HCl, EtOH, 2hrs, **53%**; c) 2-hydrazino-2-imidazoline HBr (1.03 eq), 1M aq.HCl (cat.), EtOH, 6hrs, **76%**.

Scheme 15. Synthesis of N_1-unsubstituted pyrazole-connected aryl bis-AG **76** and N_1-unsubstituted pyrazole-connected aryl bis-cyclic AG **77** from N_1-PMB diformyl pyrazole**78**.

Namely, PMB deprotection (step a; N_1-unsubstituted diformyl pyrazole **78**) was followed by condensation with aminoguanidine HCl (two equivalents, step b, Scheme 15) to yield, after filtration and washings with 5:1 MeCN/H_2O, pure target N_1-unsubstituted pyrazole-connected bis-AGs **76** as a poorly soluble dihydrochloride salt in moderate yields. Alternatively, N_1-unsubstituted diformyl pyrazole **78** was condensed with 2-hydrazino-2-imidazoline HBr / cyclic AG (two equivalents, step c, Scheme 15) to yield, after filtration and repeated washings with 95:5 EtOH/H_2O and Et_2O, pure target N_1-unsubstituted pyrazole-connected bis-cyclic AGs **77** as a poorly soluble dihydrobromide salt in good yields.

4.3. ACTIVITY PROFILING: BIOLOGICAL AND VIRTUAL ASSAYS

4.3.1. Biological testing: Patch Clamp experiments

The whole set of putative ASICs inhibitors bearing either one (non-symmetrical mono-AGs) or two aminoguanidyl hydrazone groups (symmetrical di-AGs) connected by two types of cyclic linkers / CLin (1,3-phenyl CLin, **47a-c**; N_1-substituted 3,5-pyrazole CLin, **51**, **58**, **61**, **62**, **68**, **69**, **76**, **77**) reported in Figure 11 were sent for biological profiling to the University of Naples "Federico II" – Neuroscience Department (Prof. L. Annunziato).

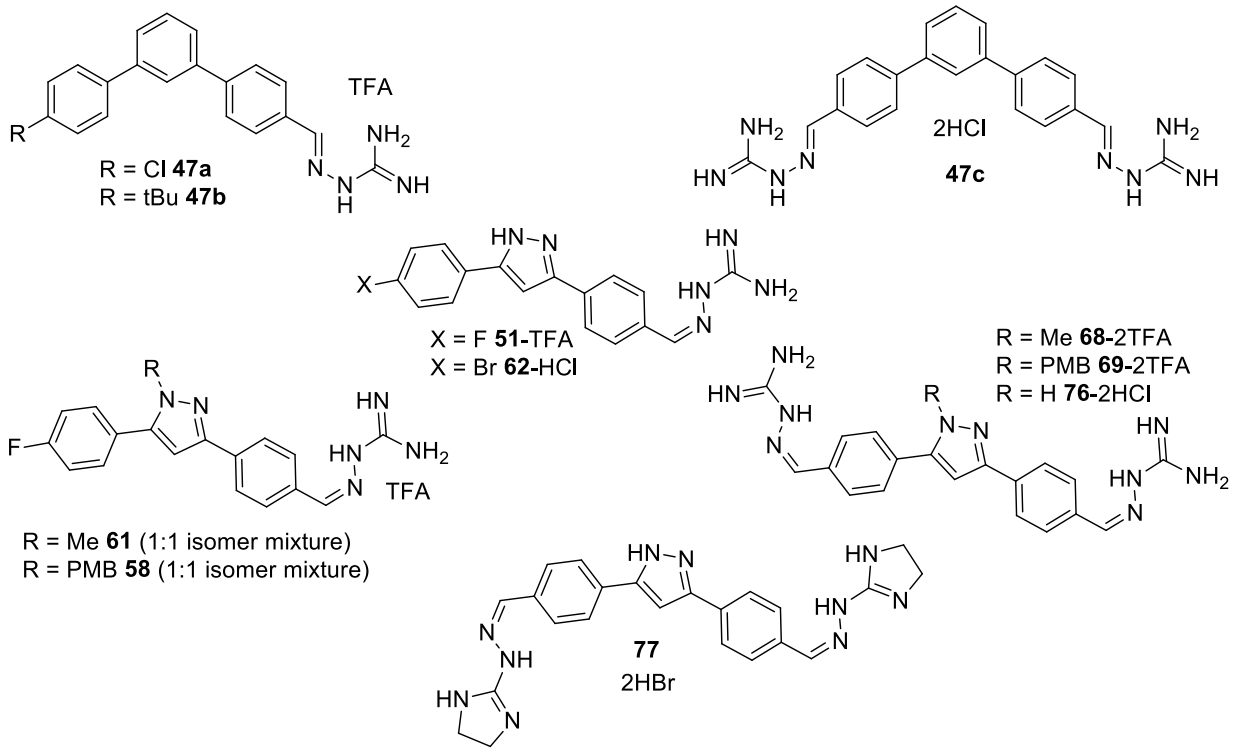

Figure 11. Structure of tested phenyl-connected and pyrazole-connected mono- and di-AGs.

Planned in vitro profiling consisted in the determination of their biological potency against ASIC1a channels (the most relevant isoform in CNS) through a cellular assay named **patch clamp** [128]. A more detailed profiling should have followed, if one or more of them would have resulted to be either more active, or prospectively more bioavailable than standard, amidine-based diminazene **43** (Figure 9).

The patch clamp is a laboratory technique in electrophysiology discovered in late '70s [129], used to study ionic currents in individual isolated living cells, tissue sections, or patches of cell membrane. Its discovery made it possible to record the currents of single ion channel molecules (i.e., ASIC isoforms) for the first time, which improved understanding of the involvement of ion channels in fundamental cell processes such as action potentials and nerve activity. The technique is especially useful in the study of excitable cells; among them, neurons have been studied repeatedly [130].

As to our experiments, they were run on human embryonic kidney 293 (HEK293) cells [131], that functionally express an endogenous proton-gated conductance attributable to the activity of human ASIC1a [132]. We used genetically unmodified HEK293 cells seeded on coated glass coverslips and used after 24-72 hours in

culture. Whole-cell patch-clamp experiments were carried out at room temperature, with a holding voltage / potential set at -70 mV.

ASIC1a channels were activated by shifting the pH of the extracellular solution from pH 7.4 to pH 6.0. The pH 7.4 extracellular solutions contained (in mM): 140 NaCl, 5 KCl, 2 $CaCl_2$, 2 $MgCl_2$, 10 HEPES, adjusted to 7.4 using NaOH or HCl. The solution with pH 6.0 – needed to activate the ASIC1a channels - contained 10mM glycine and MES replacing HEPES, for more reliable pH buffering. Micropipettes were filled with the intracellular solution, which contained (in mM): 30 NaCl, 120 KCl, 2 $MgCl_2$, 10 HEPES with or without EGTA, adjusting the pH to 7.3 using NaOH or HCl. The application of mono- and di-AGs (as single compounds, in independent experiments) to extracellular solutions, and the alterations in extracellular pH were carried out using commercially available automated fast solution exchange systems able to generate precisely timed alterations in extracellular solutions.

First, we activated ASIC1a repeatedly by pH decreases from pH 7.4 to pH 6.0 in the absence of our mono- and di-AGs. After that, AGs were pre-applied in extracellular solution at pH 7.4 for 40 seconds and co-applied in extracellular solution at pH 6.0 for 10 seconds (approximately 50 seconds between pH stimulations). In these conditions we measured ASIC1a peak current amplitudes. Diminazene **43**, used as its aceturate salt, and/or each AG were dissolved at the final, desired concentration in both pH 7.4 and pH 6.0 extracellular solutions; typically, 3 or 4 concentrations / time points per compound were determined (varying between 100 nM and 30 µM). The available results related to diminazene **43** are summarized in Figure 12; the standard, reference compound showed low micromolar potency (IC_{50} ≈ 1.2 µM).

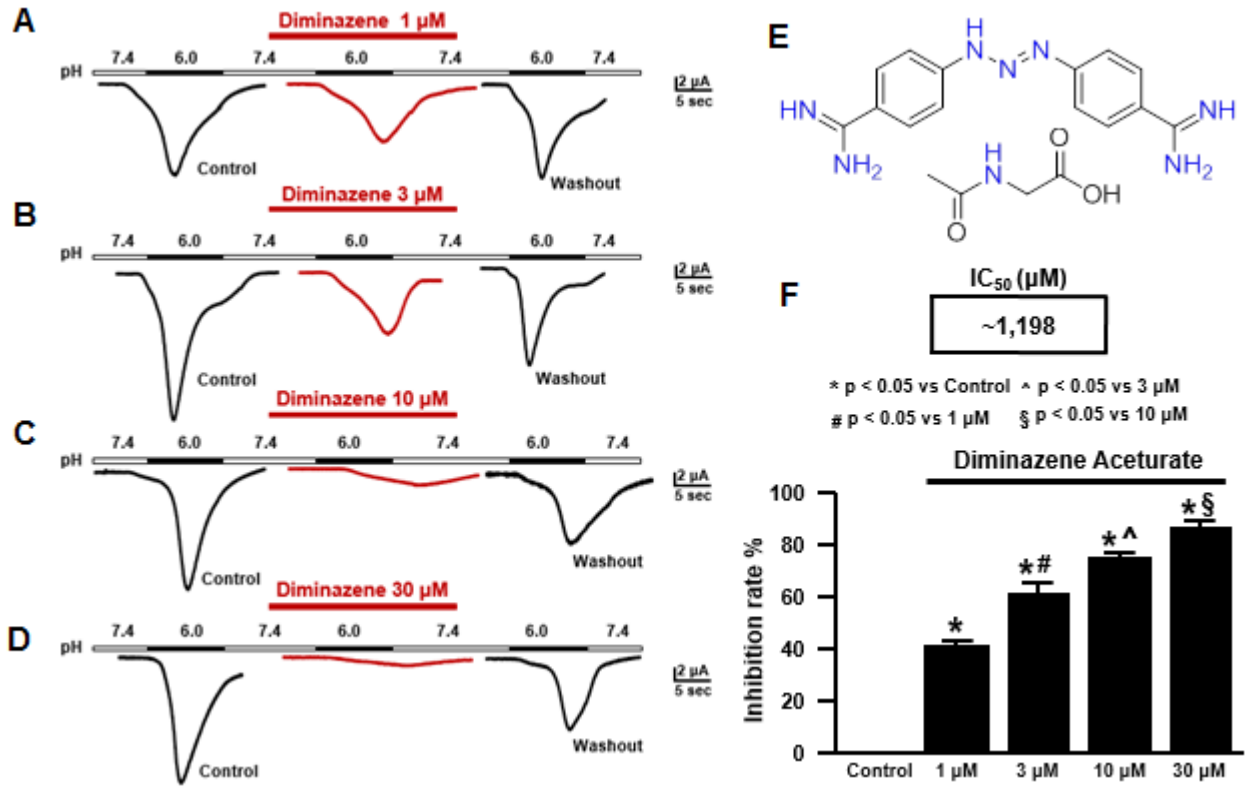

Figure 12. Representative ASIC1a currents elicited by pH 6.0 in HEK-293 cells in the absence (black) or presence of diminazene aceturate **43** (red). (**A**) The left part represents the control current; the middle part shows inhibitory action of 1µM of **43**, and the right part shows the current after 5min washout with normal extracellular solution. (**B**) as **A**, with 3 µM of **43**. (**C**) as **A**, with 10 µM of **43**. (**D**) as **A**, with 30 µM of **43**. (**E**) Structure of diminazene aceturate **43** (**F**) Percentage quantification of ASIC1a currents inhibition from A-D.

The experimental inhibition constants (IC_{50s}) calculated for our AGs are reported in Figure 13.

Name	IC_{50} (μM)	Name	IC_{50} (μM)
Diminazene	1.20	**61a/b**	2.51
47a	1.27	**62**	1.43
47b	1.50	**68**	1.41
47c	0.41	**69**	0.52
51	2.59	**76**	0.36
58a/b	1.99	**77**	0.14

Figure 13. Left: Inhibition (IC_{50s}) of ASIC1a currents by selected mono- and di-AGs: IC_{50} values.

To our delight, the eleven tested compounds showed ASIC1a modulation, with IC_{50} values ranging between sub-micromolar (**77**) and low micromolar potency (**51**). The data collected for these compounds allow us to extract some preliminary structure-activity relationship (SAR) regarding mono- and di-AGs.

1) As already mentioned, the replacement of diamidines, as in diminazene standard **43**, with AGs is compatible with biological activity on ASIC1a channels.

2) As to mono-AGs, it appears that larger para-substituents may be preferable to their smaller counterparts – compare fluoro-substituted, N_1-unsubstituted 3,5-pyrazole-connected mono-AG **51** with its larger bromo analogue **62.**

3) As to di-AGs, it appears that they could be more potent than their mono-AG counterparts - compare fluoro-substituted mono-AGs **51**, **58a,b** and **61a,b,** with the corresponding di-AGs **76**, **68 and 69** – although larger substituents than F could partially compensate in terms of ASIC1a current inhibition.

4) As to N_1-substituted 3,5-pyrazole linkers, bulky N_1 substituents appear to be preferable than either smaller ones, or N_1-unsubstituted pyrazoles – compare bulky fluoro-substituted, N_1-PMB 3,5-pyrazole-connected mono-AG mixture **58a,b** with the corresponding N_1-methyl and N_1-unsubstituted analogues (respectively **61a,b** and **51**). The same trend was partially observed compared N_1-PMB 3,5-pyrazole-connected di-AG mixture **69** with the corresponding N_1-methyl analogue **68**. Curiously in N_1-unsubstituted analogue **76** was the most potent in this serie.

5) As to 1,3-phenyl linkers; **47a** and **47b** appear more active than the corresponding 3,5-pyrazole-mono-AGs. Compound **47c** shown the same activity of N_1-unsubstituted analogue **76** but offer the possibility to added different groups on the phenyl linker suitable for the synthesis of more active and bioavailable compounds

6) Compound **77**, the only molecule that bear a Cyclization on the AGs moiety shown the best potency leads open the possibility to add substituent on the charged moiety.

4.3.2. Virtual testing: In-silico docking

The whole set of putative ASICs inhibitors present in this Chapter was docked *in-silico* within the extracellular domain (ECD) of chicken ASIC1a trimer (ECD-ASIC1a), built accordingly with literature [132, 133] and with the results of our own experiments. Namely, IBF-CNR (Dr. Milani) run a molecular dynamics (MD) simulation on the ECD of chicken ASIC1a trimer in presence of three molecules of diminazene **43** placed around the trimer. During the simulation, one of them migrate inside the pH sensor region (also named "acidic pocket") shown in Figure 14; thus, we chose this pocket as a putative binding site also for the virtual testing of our AGs.

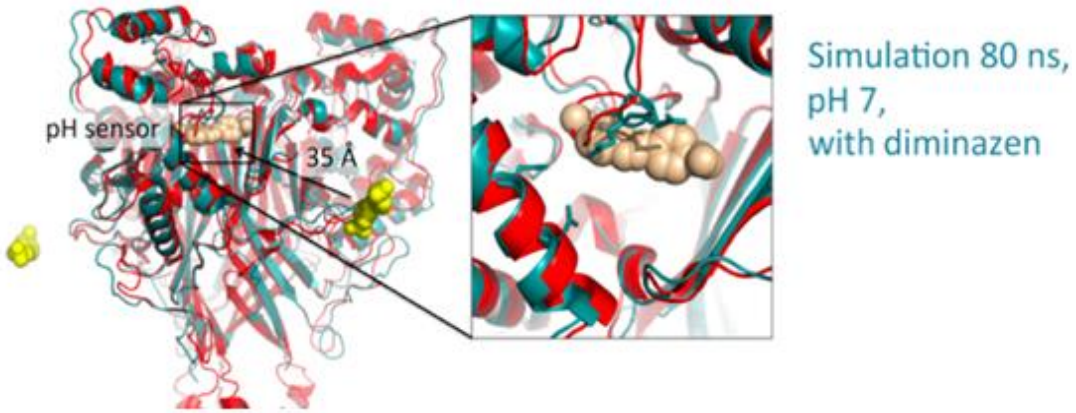

Figure 14. Molecular Dynamics Simulation (MDS) on chicken ASIC1a in presence of DA **43** (three molecules). The migration of one copy of **43** along the ECD of ASIC1a is shown in details. The initial and the final structure of ASIC1a trimer after 80 ns of MD simulation are shown in red and blue, respectively

The calculated energy binding for standard diminazene **43**, and for our mono- and di-AGs is reported in Table 1 (third and sixth columns), and is compared with previously reported experimental IC_{50} (second and fifth columns). Asymmetric/ mono AG compounds are reported in the left part of the Table, while symmetric / di-AG compounds are shown in the right part. To our delight, di-AGs were predicted to be more potent than their mono-AG counterparts (a higher Eb in absolute value indicates a higher interaction energy between AGs and ASIC1a). Please note that diminazene, in our virtual model, scores very poorly, while its biological activity is significant; this discrepancy may be due to poor cellular bioavailability of our compounds, and will be further investigated in future.

mono-AGs	IC_{50} (μM)	Eb (Kcal/mol)	di-AGs	IC_{50} (μM)	Eb (Kcal/mol)
47a	1.27	-10.72	**43(diminazene)**	1.20	-5.84
47b	1.50	- 10.62	**47c**	0.41	-13.78
51	2.59	-9.23	**68**	1.41	-11.11
58a/b	1.99	-10.00	**69**	0.52	-13.07
61a/b	2.51	-9.46	**76**	0.36	-12.93
62	1.43	-9.70	**77**	0.14	-12.30

Table 2. Comparison of docking results (Eb, third, sixth column) and affinity values (IC_{50}, second, fifth column) for mono- (first column) and di-AGs (fourth column). The free energy of binding (Eb) is represented by ΔG values (Kcal/mol) calculated by Autodock4. N.A.: not yet tested.

4.4. CONCLUSIONS AND FUTURE PERSPECTIVES

In conclusion, a new class of diminazene **43**-inspired ASIC1a antagonists (mono- and di-aminoguanidine hydrazones, AGs) was rationally designed, and synthetic accessibility was planned through several chemical routes. After chemical assessment, six mono-AGs (two with a 1,3-phenyl CLin, four with a 3,5-pyrazole CLin) and five di-AGs (one with a 1,3-phenyl CLin, four with a 3,5-pyrazole CLin) were synthetized and purified.

Biological testing (patch clamp experiments) were completed for all the AGs, and ASIC1a inhibition – in most of the cases better than standard diminazene **43** – was observed. The best leads (at least one mono-AG and one di-AG) will be selected for more detailed biological profiling in Naples/Prof. Annunziato's group (further cellular/ex vivo assays, physico-chemical assays, etc.).

The validated computational assay/in silico docking will be used to rationally propose some new substitution patterns and CLin structures. The selected virtual leads will be synthesized, and their biological activity against ASIC1a will be determined.

Once a first wave of synthesis and testing (virtual and biological) will be completed, at least a first potent and bioavailable lead will be resynthesized in larger amounts, and tested for efficacy testing in vivo (rodent models of cerebral ischaemia, i.v. or intracerebroventricular / i.c.v. route of administration).

4.5 EXPERIMENTAL PART: Synthesis and analytical characterization of intermediates and final compounds

4.5.1 General Procedures

4.5.1.1 General Procedure for the Suzuki cross coupling on triflate 50

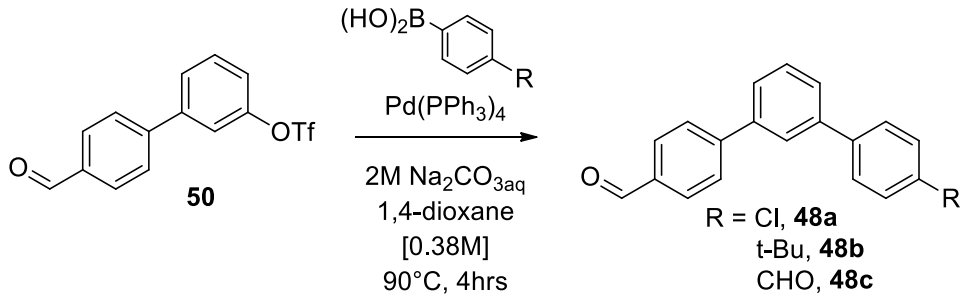

2M aq. Na_2C0_3 (2 eq) was added to a stirred mixture of triflate **50** (1.0 eq), 4-substituted phenyl boronic acid (1.2-1.3 eq), and $Pd(PPh_3)_4$ (0.1 eq) in 1 ,4-dioxane (5-10 mL/mmol) under nitrogen atmosphere at RT. The reaction mixture was then heated at 90°C for 3 hrs, until disappearance of **50** (TLC monitoring, eluant mixture: DCM/hexane). Then, the solvent was removed under reduced pressure, and the crude (brown solid) was taken up with AcOEt (25 mL). The resulting suspension was sequentially washed with water (20 mL), with saturated $NaHCO_3$ (10 mL) and brine (10 mL). The collected organic phase was dried over Na_2SO_4, and the solvent was removed under reduced pressure. The pure aldehydes **48a-c** were obtained after column chromatography on silicagel (eluant mixture: DCM/n-hexane).

4.5.1.2 General procedure for the synthesis of N_1-H cyano pyrazoles 53, 64, 71 from chalcones 54, 63, 70

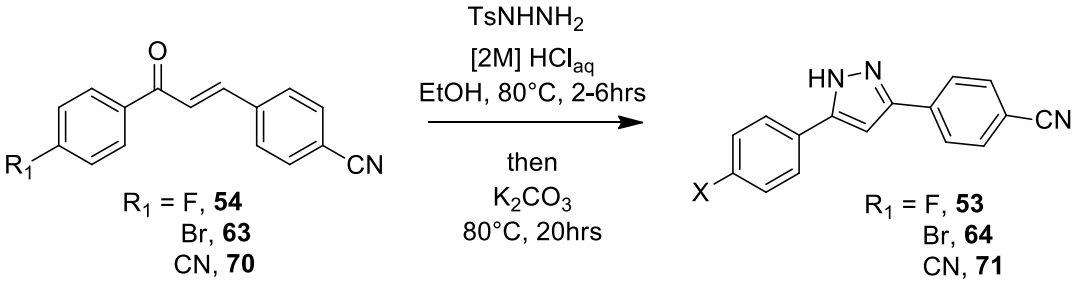

Chalcones **54**, **63** or **70** (1.0 eq) were suspended in absolute EtOH (7.5 mL/mmol) and stirred at RT for 5 minutes. Then, tosylhydrazide (1.05 eq) was added as a single portion, followed by a few drops of 2M aq. HCl. The resulting suspension was stirred at 80°C for 6 hrs, observing complete dissolution of the solid (TLC monitoring, eluant mixture: AcOEt/n-hexane). Then, solid K_2CO_3 (2.1 eq) was added and the reaction mixture was stirred at 80°C for additional 20hrs. The reaction mixture was then cooled to RT, diluted with water (10 mL/mmol) and brought to pH = 3-4 with 2N HCl. The resulting suspension was filtered, and the solid was repeatedly washed with water and MeOH. After drying in the oven, pure N_1-H cyano pyrazoles **53**, **64** or **71** were obtained as white solids, that were used as such in the following reaction steps.

4.5.1.3 General procedure for the N-alkylation of pyrazoles 53, 64, 71 to N_1-methyl and N_1- PMB cyano pyrazoles 56a,b, 59a,b, 65a,b, 72, 73

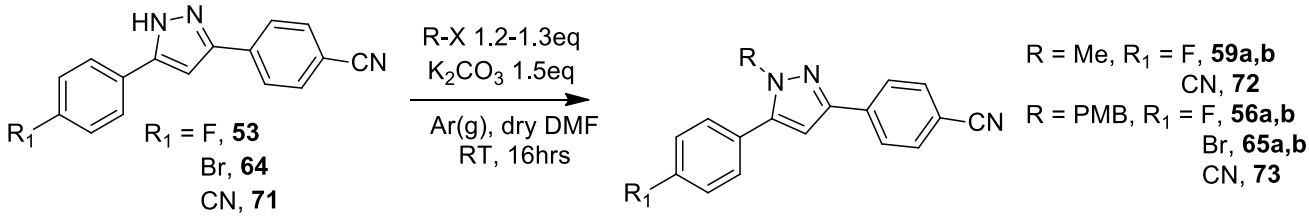

N_1-H cyano pyrazoles **53**, **64** or **70** (1.0 eq) were dissolved in dry DMF (5 mL/mmol) at RT under stirring in an Ar atmosphere. Solid K_2CO_3 (1.5 eq) was added, and the colourless solution became a dark orange-red suspension. After 15 minutes, the corresponding alkyl halide (PMB-Cl or MeI, 1.2-1.3 eq) was added, the solution was stirred at RT for 16hrs and monitored by TLC (eluant mixture: n-hexane/AcOEt). After reaction completion, the solvent was removed under reduced pressure. The residue was diluted with AcOEt (30-60 mL) and washed with water (20-30 mL) and brine (20-30 mL). The organic phase was dried over Na_2SO_4 filtered and concentrated. The crude was often purified by flash chromatography (eluant mixture: n-hexane/AcOEt) to give pure N_1-alkylated cyano pyrazoles **56a,b, 59a,b, 65a,b, 72** or **73** as white solids.

4.5.1.4 General procedure for the reduction of asymmetric N_1-methyl and N_1- PMB cyano pyrazoles 56a,b, 59a,b, 65a,b to the corresponding asymmetric N_1-methyl and N_1-PMB formyl pyrazoles 57a,b, 60a,b, 66a,b

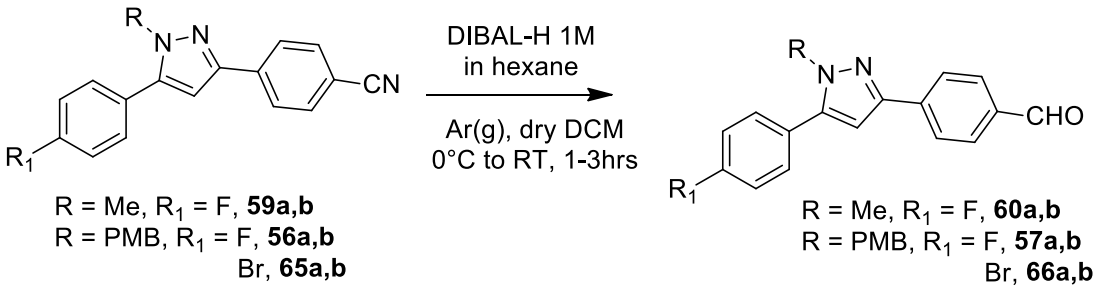

Asymmetric N_1-methyl and N_1- PMB cyano pyrazoles **56a,b, 59a,b** or **65a,b** (1.0 eq) were dissolved at RT in dry DCM (5 mL/mmol) under Ar atmosphere and stirred for 2 minutes. The reaction mixture was then cooled at 0°C, and a 1M DIBAL-H solution in n-hexane (1.2 eq) was added dropwise in 15 minutes. The yellow reaction mixture was cooled at RT and stirred for 2.30 hrs (TLC monitoring, eluant mixture: n-hexane/AcOEt). After reaction completion, water (2 mL) was added at 0°C dropwise, followed by HCl 10% V/V (15 mL) and DCM (15 mL). The reaction mixture was then stirred for 2 hrs at RT, observing a clear phase separation. The aqueous phase was extracted DCM (2 x 15 mL). The collected organic phase was dried over Na_2SO_4 and the solvent was removed under reduced pressure. The crude was often purified by column chromatography (eluant mixture: n-hexane/AcOEt), yielding pure asymmetric N_1-methyl and N_1- PMB formyl pyrazoles **57a,b, 60a,b** or **66a,b** as white solids.

4.5.1.5 General procedure for the reduction of symmetric N_1-methyl and N_1- PMB cyano pyrazoles 72, 73 to the corresponding symmetric N_1-methyl and N_1-PMB formyl pyrazoles 74, 75

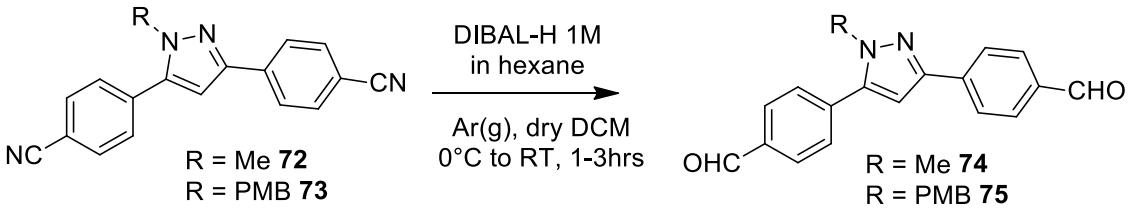

Symmetric N_1-methyl and N_1-PMB cyano pyrazoles **72, 73** (1.0 eq) were dissolved in dry DCM (7.5 mL/mmol) under Ar atmosphere and stirred for 2 minutes. The reaction mixture was then cooled at 0°C, and a 1M DIBAL-H solution in n-hexane (1.15 eq) was added dropwise in 15 minutes. The yellow reaction mixture was cooled at RT and stirred for 40 minutes (TLC monitoring, eluant mixture: n-hexane/AcOEt). After reaction completion, water (5 mL) was added at 0°C dropwise, followed by HCl 10% v/v (20 mL) and DCM (20 mL). The reaction mixture was then stirred for 2 hrs at RT, observing a clear phase separation. The aqueous phase was extracted with DCM (2 x 20 mL). The collected organic phase was dried over Na_2SO_4 and the solvent was removed under reduce pressure. The crude was purified by column chromatography (eluant mixture: n-hexane/AcOEt), yielding pure symmetric N_1-methyl and N_1- PMB formyl pyrazoles **74** or **75** as white solids.

4.5.1.6 General procedure for PMB deprotection of N_1-PMB formyl pyrazoles 57a,b, 66a,b, 75 to N_1-unsubstituted formyl pyrazoles 52, 67, 78

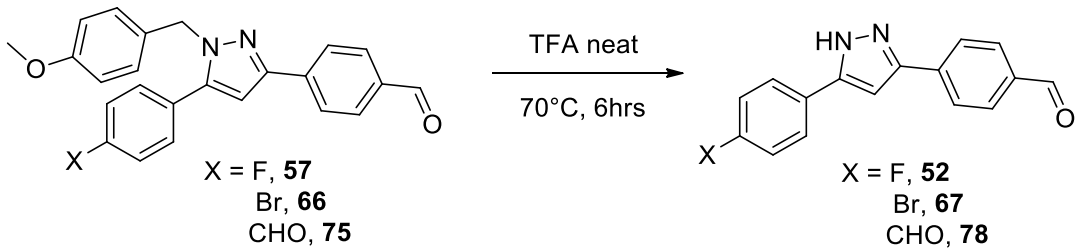

N_1-PMB formyl pyrazoles **57a,b, 66a,b** or **75** (1.0 eq) were dissolved in TFA (10 ml/mmol) and stirred at 70°C until TLC monitoring (eluant mixture:: n-hexane/AcOEt 6:4) showed reaction completion. Then, TFA was removed under high vacuum with toluene stripping, and the crude brown solid was diluted with DCM (5 mL) and centrifugated (5000 RPM, 5 minutes), then carefully removing the solvent with a syringe. DCM dilution, centrifugation and DCM removal was repeated four times. The resulting, crude N_1-unsubstituted formyl pyrazoles **52, 67** or **78** were used without further purification in the next, final reaction step.

4.5.1.7 General procedure for the synthesis of non-symmetrical aryl mono-AGs 47a, 47b, 51, 58a,b, 61a,b, 62 and symmetrical aryl di-AGs 47c, 68, 69, 76

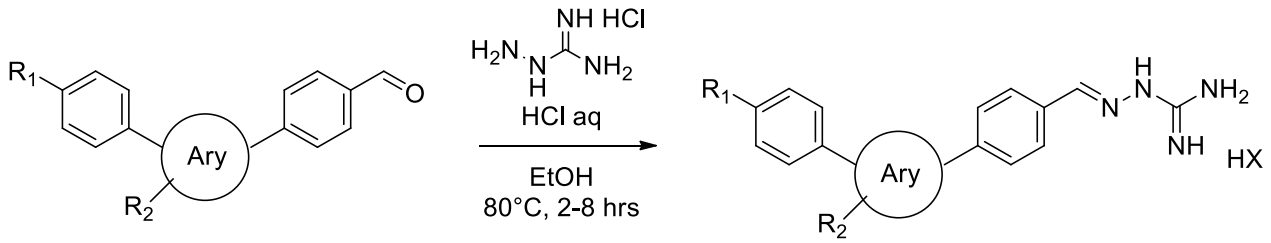

Ary = Ph, R_1 = Cl, R_2 = H, **48a**
Ary = Ph, R_1 = tBu, R_2 = H, **48b**
Ary = Ph, R_1 = CHO, R_2 = H, **48c**
Ary = Pyraz, R_1 = F, R_2 = H, **52**
Ary = Pyraz, R_1 = F, R_2 = PMB, **57a,b**
Ary = Pyraz, R_1 = F, R_2 = Me, **60a,b**
Ary = Pyraz, R_1 = Br, R_2 = H, **67**
Ary = Pyraz, R_1 = CHO, R_2 = Me, **74**
Ary = Pyraz, R_1 = CHO, R_2 = PMB, **75**
Ary = Pyraz, R_1 = CHO, R_2 = H, **78**

Ary = Ph, R_1 = Cl, R_2 = H, **47a**
Ary = Ph, R_1 = tBu, R_2 = H, **47b**
Ary = Ph, R_1 = AG, R_2 = H, **47c**
Ary = Pyraz, R_1 = F, R_2 = H, **51**
Ary = Pyraz, R_1 = F, R_2 = PMB, **58a,b**
Ary = Pyraz, R_1 = F, R_2 = Me, **61a,b**
Ary = Pyraz, R_1 = Br, R_2 = H, **62**
Ary = Pyraz, R_1 = AG, R_2 = Me, **68**
Ary = Pyraz, R_1 = AG, R_2 = PMB, **69**
Ary = Pyraz, R_1 = AG, R_2 = H, **76**

Aminoguanidine hydrochloride (1.1 eq.) and 1N aq. HCl (3-5 drops, catalytic) were sequentially added to a warm, vigorously stirred suspension of 1 eq. of mono-formyl (**48a**, **48b**, **52**, **57a,b**, **60a,b**, **66a,b** or **67**) or di-formyl compounds (**48c**, **74**, **75** or **78**) in absolute EtOH. After the addition of the catalytic acid, the suspension became a solution. The reaction mixture was refluxed at 80°C, with periodical TLC monitoring (eluant mixtures: 100% EtOAc and 8:2 DCM/MeOH with a few AcOH drops).

Precipitation of a white solid was sometimes observed in 2-4 hours**.** Then, the reaction mixture was cooled to RT, the precipitate was filtered, washed with various solvents (vide infra), and dried in vacuum to yield the corresponding pure mono- or di-AGs as white solids. Namely, mono-AG **62** and bis-AGs **47c** and **76** were obtained using this procedure.

When precipitation was not observed, the reaction mixture was cooled to RT, and concentrated under reduce pressure. The crude solid was purified with reverse phase chromatography (H_2O:MeCN from 95/5 to 0/100, + 0.2% TFA as eluant mixture), obtaining the corresponding pure mono- or di-AGs as white solids. Namely, mono-AGs **47a, 47b, 51, 58a,b** and **61a,b** and bis-AGs **68** and **69** were obtained using this procedure.

4.5.2 Mono- and di-AG synthesis: Final compounds

4.5.2.1 Synthesis of 1,3-phenyl-connected mono-AGs 47a, 47b, and di-AG 47c

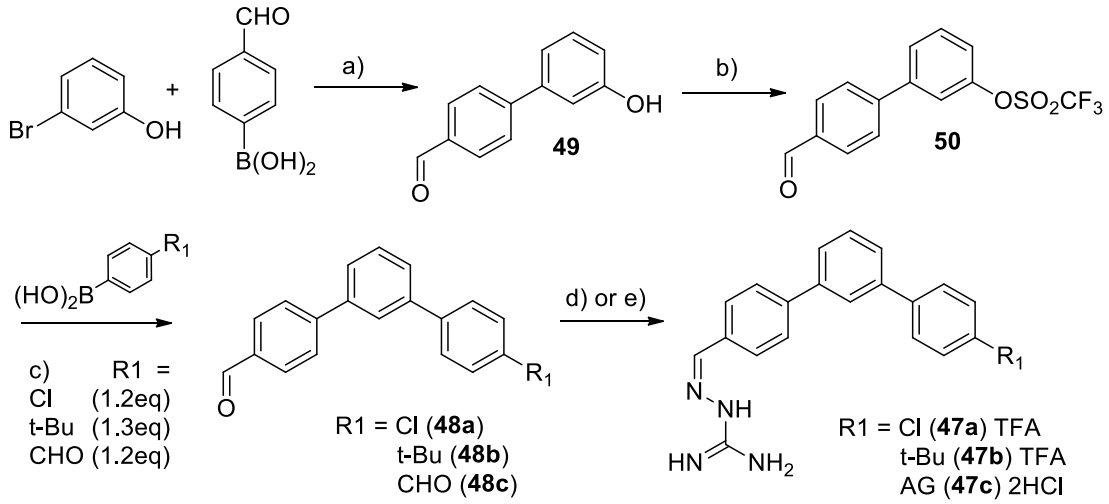

a) $Pd(PPh_3)_4$ (0.1eq), 2.0M aq.Na_2CO_3 (2 eq), dry 1,4-dioxane, N_2, 90°C, 4hrs, **73%**; b) Tf_2O (1.3 eq), TEA (1.5 eq), dry DCM, 0°C to RT, 1hr, **95%**; c) $Pd(PPh_3)_4$ (0.1 eq.), 2.0M aq.Na_2CO_3 (2.0 eq), dry 1,4-dioxane, 90°C, 3 hrs, N_2, **91%** (**48a**), **81%** (**48b**), **78% (48c)**; d) aminoguanidine HCl (1.1 eq), cat. [1N] HCl, EtOH, 80°C, 3 hrs, **92%** (**47a**), **96%** (**47b**); e) aminoguanidine HCl (1.1 eq.), cat. [1 N] HCl, EtOH, 80°C, 4 hrs, **90%** (**47c**).

3'-hydroxy-[1,1'-biphenyl]-4-carbaldehyde 49

2M aq. Na_2C0_3 (2.4 mL, 4.873 mmol, 2.0 eq) was added dropwise at RT under nitrogen atmosphere to a solution of 3-bromophenol (626.0 mg, 3.618 mmol, 1.48 eq), 4-formylphenylboronic acid (366.0 mg, 2.441 mmol, 1.0 eq), and $Pd(PPh_3)_4$ (220.0 mg, 0.190 mmol, 0.08 eq) in 1 ,4-dioxane (6.5 mL). The yellow mixture was heated at reflux (90°C) for 4 hours, until reaction completion (TLC monitoring, eluant mixture: DCM/AcOEt 95:5). The reaction was then cooled to RT, and the solvent was removed under reduced pressure. The crude was diluted with EtOAc (40 mL) and was washed with 5% m/m aq. citric acid (40 mL). The organic layer was dried over Na_2SO_4, concentrated at reduced pressure, and the crude was purified by flash chromatography (eluant mixture: DCM/EtOAc from 10:0 to 9:1) to yield 355.2 mg of pure **49** as a white solid (1.792 mmoles, **73%** yield).

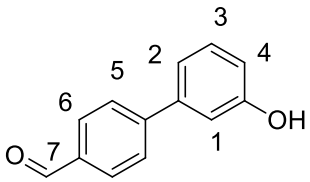

Characterization:

^{1}H-NMR (400 MHz, acetone-d_6) δ ppm 10.09 (s, 1H, H7), 8.53 (s, 1H, OH), 8.00 (m, 2H, H5), 7.85 (m, 2H, H6), 7.34 (t, J = 7.8 Hz, 1H, H3), 7.21 (m, 2H, H1, H4), 6.92 (ddd, J = 8.1, 2.4, 1.0 Hz, 1H, H2).

4'-formyl-[1,1'-biphenyl]-3-yl trifluoromethanesulfonate 50

TEA (100 µL, 0.718 mmol, 1.54 eq) was added at RT to a stirred suspension of hydroxyaldehyde **49** (92.1 mg, 0.465 mmol, 1.0 eq) in dry DCM (3 mL). The solution was cooled at 0°C and trifluoromethansulfonic-anhydride ($(CF_3SO_2)_2O$, 100 µL, 0.594 mmol, 1.28 eq) was added dropwise in 5 minutes. The brown solution was stirred for 30 minutes at 0°C, then warmed to RT and stirred for 30 minutes (TLC monitoring, eluant: DCM). The reaction mixture was then diluted with DCM (20 mL), and washed with 5% aqueous citric acid (15 mL) and saturated aqueous $NaHCO_3$ (15 mL). The organic phase was dried over Na_2SO_4 and the solvent removed under pressure. The crude was purified by column chromatography (eluant mixture: DCM/n-hexane 7:3) to give

146.0 mg of **50** as a yellow oil (0.442 mmol, **95%** yield). Its NMR spectra went lost, and could not be reported here.

4''-chloro-[1,1':3',1''-terphenyl]-4-carbaldehyde 48a

The reaction was performed according to **Paragraph 4.5.1.1**, using **50** (453.8 mg, 1.374 mmol, 1.0 eq), 4-chloro-phenylboronic acid (250 mg, 1.599 mmol, 1.2 eq), $Pd(PPh_3)_4$ (158.8 mg, 0.137 mmol, 0.1 eq), 2M aqueous Na_2CO_3 (1.3 mL, 2.74 mmol, 2.0 eq), and dry 1,4 dioxane (7 mL). After work up and chromatographic purification (eluant mixture: DCM/n-hexane 1:1) pure **48a** was obtained as a colourless oil (362.1 mg, 1.237 mmol, **91%** yield).

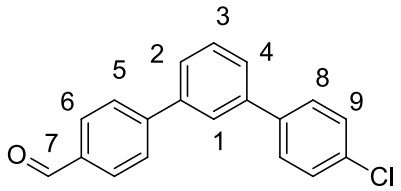

Characterization:

^{1}H-NMR (400 MHz, $CDCl_3$) δ ppm 10.01 (s, 1H, H7), 7.91 (d, J = 8.1 Hz, 2H, H5), 7.73 (m, 3H, H6, H1), 7.57-7.46 (m, 5H, H2, H3, H4, H9), 7.72 (d, J = 8.2 Hz, 2H, H8).

^{13}C-NMR (from HSQC, $CDCl_3$) δ ppm 191.8, 130.2, 129.3, 128.4, 128.1, 127.7, 127.4, 127.1, 126.5.

4''-(tert-butyl)-[1,1':3',1''-terphenyl]-4-carbaldehyde 48b

The reaction was performed according to **Paragraph 4.5.1.1**, using **50** (146.0 mg, 0.442 mmol, 1.0 eq), (4-(tert-butyl)phenyl)boronic acid (102.3 mg, 0.575 mmol, 1.3 eq), $Pd(PPh_3)_4$ (55.2 mg, 0.049 mmol, 0.1 eq), Na_2CO_3 [2.0 M] (500.0 µL, 1.0 mmol, 2.26 eq), and dry 1,4 dioxane (4.0 mL). After work up and chromatographic purification (eluant mixture: DCM/n-hexane 1:1) pure **48b** was obtained as a pale-yellow oil (113.1 mg, 0.359 mmol, **81%** yield).

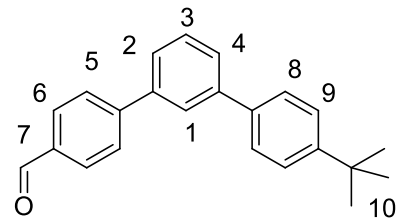

Characterization:

^{1}H-NMR (400 MHz, $CDCl_3$) δ ppm 10.08 (s, 1H, H7), 7.91 (d, J = 8.1 Hz, 2H, H5), 7.84 – 7.80 (m, 3H, H6, H1), 7.66–7.49 (m, 7H, H2, H3, H4, H8, H9), 1.38 (s, 9H, H10).

^{13}C-NMR (from HSQC, $CDCl_3$) δ ppm 191.8, 130.1, 129.2, 128.7, 127.7, 127.1, 126.5, 126.3, 125.9, 31.3.

[1,1':3',1''-terphenyl]-4,4''-dicarbaldehyde 48c

The reaction was performed according to **Paragraph 4.5.1.1**, using **50** (203.1 mg, 0.615 mmol, 1.0 eq), (4-formylphenyl) boronic acid (110.7 mg, 0.738 mmol, 1.2 eq), $Pd(PPh_3)_4$ (71.6 mg, 0.062 mmol, 0.1 eq), Na_2CO_3 [2.0 M] (0.615 mL, 1.230 mmol, 2.0 eq), and dry 1,4 dioxane (5.0 mL). After work up and chromatographic purification (eluant mixture: DCM/n-hexane 7:3) pure **48c** was obtained as a colourless oil (137.3 mg, 0.479 mmol, **78%** yield).

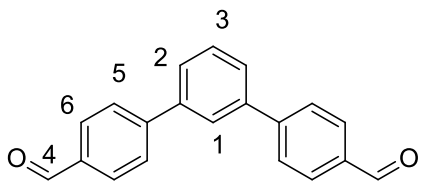

Characterization:

^{1}H-NMR (400 MHz, $CDCl_3$) δ ppm 10.11 (s, 2H, H4), 8.02 (d, J = 8.1Hz, 4H, H5), 7.90 (bs, 1H, H1), 7.84 (d, J = 8.1Hz, 4H, H6), 7.72 (d, J = 8.4Hz, 2H, H2), 7.65 (t, J = 8.4Hz, 1H, H3).

(E)-2-((4''-chloro-[1,1':3',1''-terphenyl]-4-yl)methylene)hydrazinecarboximidamide trifluoroacetate 47a

The reaction was performed according to **Paragraph 4.5.1.7 – no precipitation**, using **48a** (55.7 mg, 0.190 mmol, 1eq), aminoguanidine hydrochloride (21.3 mg, 0.190 mmol, 1.0 eq), 2 drops of aqueous 1N HCl and absolute EtOH (4.0 mL). After work up and reverse phase chromatography purification, pure **47a** (81. 0 mg, 0.175 mmol) was obtained as a white solid in **92%** yield.

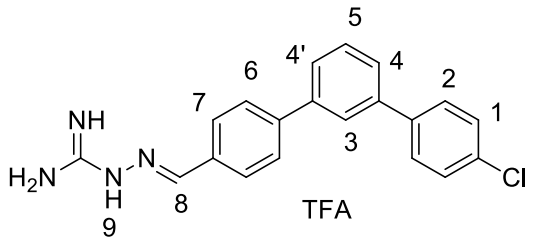

Characterization:

^{1}H-NMR (400 MHz, DMSO-d_6) δ ppm 11.77 (bs, 1H, H9), 8.22 (s, 1H, H8), 8.00-7.50 (bs, 3H, NH), 7.90 (m, 3H, H7, H3), 7.84 (m, 2H, H6), 7.79 (m,2H, H2), 7.78-7.71 (m, 2H, H4, H4'), 7.59 (m, 1H, H5), 7.55 (m, 2H, H1).

^{13}C-NMR (100 MHz, DMSO-d_6) δ ppm 155.4, 146.8, 142.0, 140.3, 139.9, 139.0, 132.9, 132.8, 129.9, 129.1, 129.0, 128.4, 127.4, 126.5, 126.4, 125.3.

HPLC-MS (ESI+): 349.14 (M+H$^+$), calculated for $C_{20}H_{17}ClN_4$: 348.11. Purity measured by HPLC-MS: 99.72 %.

(E)-2-((4''-(tert-butyl)-[1,1':3',1''-terphenyl]-4-yl)methylene)hydrazinecarboximidamide trifluoroacetate 47b

The reaction was performed according to **Paragraph 4.5.1.7 – no precipitation**, using **48b** (101.3 mg, 0.322 mmol, 1eq), aminoguanidine hydrochloride (51.3 mg, 0.464 mmol, 1.3eq), 5 drops of aqueous 1N HCl and absolute EtOH (6.0 mL).After work up and reverse phase chromatography purification, pure **47b** (150. 2 mg, 0.310 mmol) was obtained as a white solid in **96%** yield.

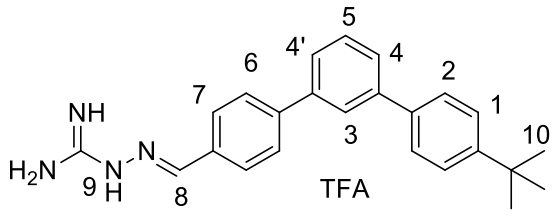

Characterization:

^{1}H-NMR (400 MHz, DMSO-d_6) δ ppm 11.82 (bs, 1H, H9), 8.22 (s, 1H, H8), 8.00-7-50 (bs, 3H, NH), 7.99 (m, 2H, H7), 7.94 (s, 1H, H3), 7.88 (m, 2H, H6), 7.70 (m, 4H, H2, H4, H4'), 7.58 (m, 1H, H5), 7.52 (m, 2H, H1), 1.34 (s, 9H, H10).

^{13}C-NMR (100 MHz, DMSO-d_6) δ ppm 155.7, 150.6, 147.1, 142.5, 141.4, 140.4, 137.7, 133.1, 130.1, 128.7, 127.6, 127.1, 126.7, 126.2, 126.1, 125.5, 34.7, 31.6.

HPLC-MS (ESI+): 371.36 (M+H$^+$), calculated for $C_{24}H_{26}N_4$: 370.22. Purity measured by HPLC-MS: 99.95 %

(2E,2'E)-2,2'-([1,1':3',1''-terphenyl]-4,4''-diylbis(methanylylidene))bis(hydrazinecarboximidamide) dihydrochloride 48c

The reaction was performed according to **Paragraph 4.5.1.7 –precipitate formation**, using **48c** (91.1 mg, 0.328 mmol, 1eq), aminoguanidine hydrochloride (72.6 mg, 0.657 mmol, 1.0eq), 3 drop of aqueous 1N HCl and absolute EtOH (6 mL). The precipitate was filtered and washed with a 95:5 mixture of EtOH/H_2O (20mL), to give after drying 139.0 mg of **48c** as a white solid (0.295 mmol, **90%** yield).

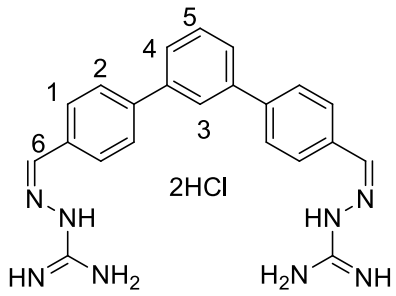

Characterization:

^{1}H-NMR (400 MHz, DMSO-d_6 + D_2O) δ ppm 8.24 (s, 2H, H6), 8.02 (s, 1H, H3), 7.98 (d, J = 8.2Hz, 4H, H1), 7.88 (d, J = 8.2Hz, 4H, H2), 7.76 (d, J = 8.1Hz, 2H, H4), 7.62 (t, J = 8.1Hz, 1H, H5).

^{13}C-NMR (100 MHz, DMSO-d_6) δ ppm 155.3, 147.3, 142.3, 140.6, 133.1, 130.3, 128.7, 127.7, 127.0, 125.6.

HPLC-MS (ESI+): 399.13 ($M + H^+$) calculated for $C_{22}H_{22}N_8$: 398.20. Purity measured by HPLC-MS: 97.3 %

4.5.2.2. Synthesis of 3,5-pyrazole-connected mono-AG 51

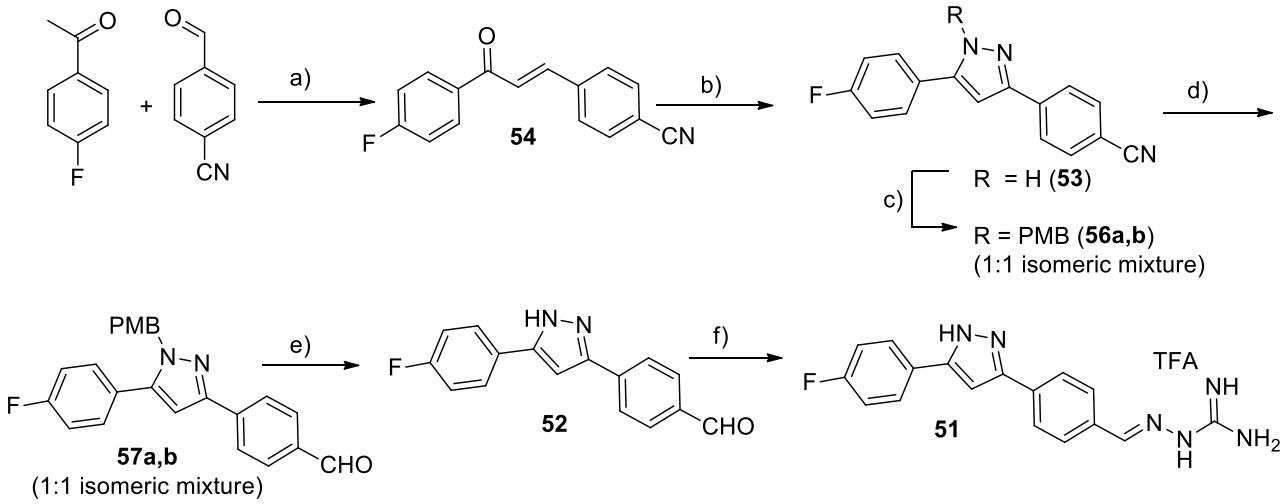

a) 3M aq.NaOH (1.5 eq), MeOH [0.5 M], 0°C to RT, 16 hrs, **67%**; b) $TsNHNH_2$ (1.05 eq), 2M aq.HCl (cat.), then K_2CO_3 (2.1 eq), EtOH [0.15 M], 80°C, 20hrs, **87%**; c) PMBCl (1.3 eq), K_2CO_3 (1.5 eq), dry DMF [0.2 M], $Ar_{(g)}$, RT, 16hrs; d) 1M DIBAL-H in hexane (1.2 eq), dry DCM [0.2 M], $Ar_{(g)}$, 0°C to RT, 1 hr; e) TFA [0.1 M], 70°C, 6 hrs, **40%** over three steps; f) aminoguanidine HCl(1.1 eq), 1M aq.HCl (cat.), EtOH [0.05 M], 4hrs, **91%**.

(E)-4-(3-(4-fluorophenyl)-3-oxoprop-1-en-1-yl)benzonitrile 54

3M NaOH (4.0 mL, 10.86 mmol, 1.5 eq) was slowly added dropwise in 30 minutes at 0°C to a solution of 4-formylbenzonitrile (950 mg, 7.24 mmol, 1 eq) and 4-fluoroacetophenone (1.0 g, 7.24 mmol, 1eq) in MeOH (14 mL). The reaction mixture was warmed at RT and stirred for 16 hours (TLC monitoring, eluant mixture: n-hexane/EtOAc 8:2). Then, the formed precipitate was filtered and sequentially washed with water (multiple washings until pH = 7, 50 mL) and methanol (10 mL). After drying, pure **54** was obtained as a white solid (1.205 g, **67%** yield) that was used without further purification.

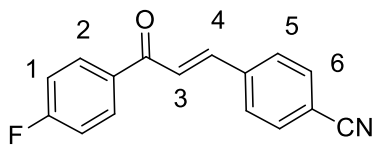

Characterization:

^{1}H-NMR ($CDCl_3$, 300 MHz) δ ppm 8.07 (dd, J = 8.8, 5.4 Hz, 2H, H2), 7.78 (d, J = 15.7 Hz, 1H, H3 or H4), 7.74-7.70 (m, 4H, H5, H6), 7.58 (d, J = 15.6 Hz, 1H, H4 or H3), 7.20 (m, 2H, H1).

4-(5-(4-fluorophenyl)-1H-pyrazol-3-yl)benzonitrile 53

The reaction was performed according to **Paragraph 4.5.1.2** using **54** (520 mg, 2.07 mmol, 1eq), tosylhydrazide (424.8 mg, 2.277 mmol, 1.05 eq), 4 drops of aqueous 2N HCl, K_2CO_3 (572 mg, 4.14 mmol, 2.1eq) and absolute EtOH (15 mL). After work up and filtration, pure **53** was obtained as a white solid (475 mg, 1.8 mmol, **87%** yield) and used without further purification.

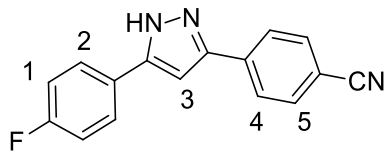

Characterization:

^{1}H-NMR (400 MHz, DMSO-d_6) δ ppm 13.70 (bs, 1H,NH), 8.04 (d, J = 7.8Hz, 2H, H5), 7.90 (d, J = 7.8Hz, 2H, H4), 7.90 (dd, J = 5.2Hz, J = 8.4Hz, 2H, H2), 7.37 (s, 1H, H3), 7.33 (t, J = 8.4Hz, 2H, H1).

4-(5-(4-fluorophenyl)-1-(4-methoxybenzyl)-1H-pyrazol-3-yl)benzonitrile 56a,b

The reaction was performed accordind to **Paragraph 4.5.1.3** using **53** (315mg, 1.198 mmol, 1 eq), K_2CO_3 (247.5 mg, 1.79 mmol, 1.5 eq) and 4-methoxybenzyl chloride (PMBCl, 210 µL, 1.558 mmol, 1.3 eq) in dry DMF (6 mL). After work up the reaction crude (410.0 mg) was used without further purification.

4-(5-(4-fluorophenyl)-1-(4-methoxybenzyl)-1H-pyrazol-3-yl)benzaldehyde 57a,b

The reaction was performed according to **Paragraph 4.5.1.4** using **56a,b** as ≈1:1 isomeric mixture (410 mg, 1.069 mmol, 1 eq), and 1M DIBAL-H in n-hexane (1.28 mL, 1.28 mmol, 1.2 eq) in dry DCM (3.3 mL). After work up, the reaction mixture was filtered on a small path of silica gel using AcOEt/hexane 1:1. After concentration under reduced pressure, crude **57a,b** (342 mg) used without further purification.

4-(5-(4-fluorophenyl)-1H-pyrazol-3-yl)benzaldehyde 52

The reaction was performed in 7 hours according to **Paragraph 4.5.1.6** using crude **57a,b** as ≈1:1 isomeric mixture (221 mg, 0.569 mmol, 1 eq) and TFA (6 mL). After work up, 102.8 mg of pure **52** was obtained as a beige solid (0.386 mmol, **40%** yield over three steps).

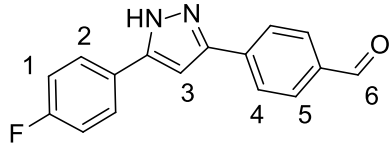

Characterization:

^{1}H-NMR (400 MHz, DMSO-d_6) δ ppm 13.88 (s, 1H, NH), 10.03 (s, 1H, H6), 8.08 (d, J = 8.0 Hz, 2H, H5), 8.00 (d, J = 8.0Hz, 2H, H4), 7.90 (dd, J = 8.2 Hz, J = 4.1 Hz, 2H, H2), 7.37 (s, 1H, H3), 7.69 (t, J = 8.2 Hz, 2H, H1).

^{13}C-NMR (from HSQC, DMSO-d_6) δ ppm: 192.8, 130.7, 125.9, 116.3, 101.3.

(E)-2-(4-(5-(4-fluorophenyl)-1H-pyrazol-3-yl)benzylidene)hydrazinecarboximidamide trifluoroacetate 51

The reaction was performed according to **Paragraph 4.5.1.7 – no precipitation**, using **52** (93.1 mg, 0.349 mmol, 1eq), aminoguanidine hydrochloride (38.6 mg, 0.349 mmol, 1.0eq), 4 drops of aqueous 1N HCl and absolute EtOH (7.0 mL). After work up and reverse phase chromatography purification, 138.6 mg of pure **51** were obtained as a white solid (0.318 mmol, **91%** yield).

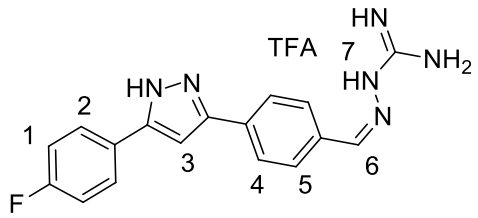

Characterization:

^{1}H-NMR (400 MHz, DMSO-d_6) δ ppm 11.81 (bs, 1H, H7), 8.18 (s, 1H, H6), 7.98-7.87 (m, 6H, H2, H4, H5), 7.78-7.55 (bs, 3H, NH), 7.34-7.30 (m, 3H, H1, H3).

^{13}C-NMR (100 MHz, DMSO-d_6) δ ppm 163.0, 160.6, 158.6, 158.3, 155.2, 146.5, 132.7, 128.2, 127.2, 125.2, 115.9, 115.6, 100.2.

HPLC-MS (ESI+): 323.06 ($M+H^+$) calculated for $C_{17}H_{15}FN_6$: 322.13. Purity measured by HPLC-MS: 99.75%.

4.5.2.3. Synthesis of 3,5-pyrazole-connected mono-AG 58a,b

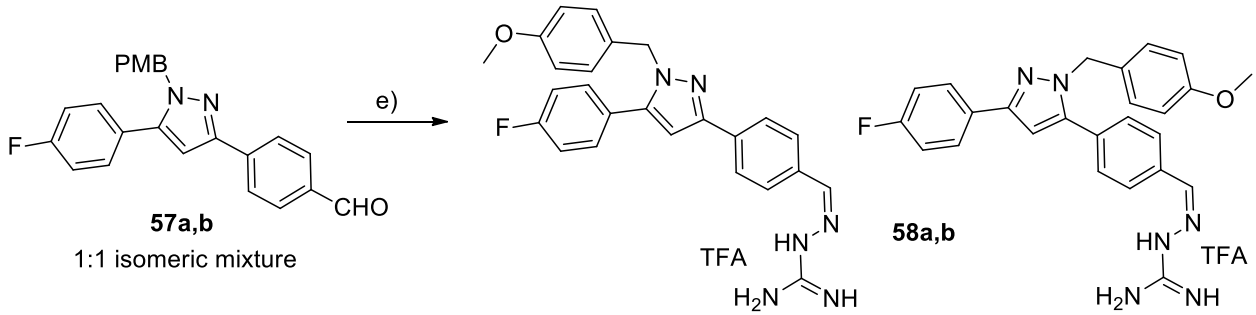

a) aminoguanidine HCl (1.1 eq), 1M aq.HCl (cat.), EtOH [0.05 M], 4hrs, **82%**.

The reaction was performed according to **Paragraph 4.5.1.7 – no precipitation**, using **57a,b** as ≈1:1 isomeric mixture (120 mg, 0.311 mmol, 1eq), aminoguanidine hydrochloride (38.9 mg, 0.353 mmol, 1.15 eq), 4 drops of aqueous 1N HCl and absolute EtOH (7 mL). After work up and reverse phase chromatography purification 142 mg of pure **58a,b (**≈1:1 isomeric mixture) were obtained as a white solid (0.255 mmol, **82%** yield).

Characterization:

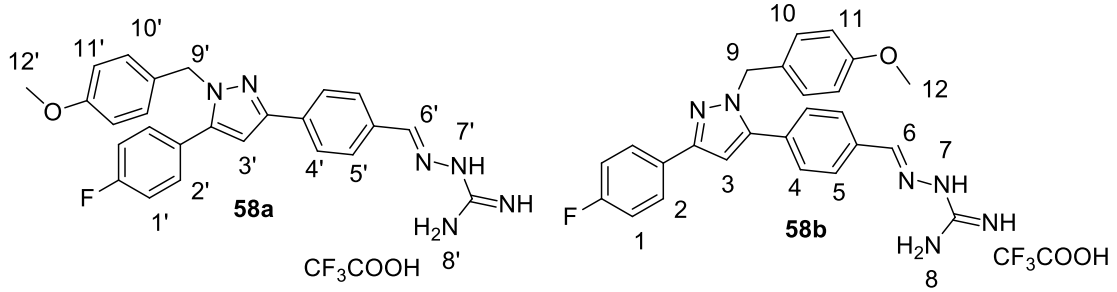

^{1}H-NMR (400 MHz, DMSO-d_6) – attributed to **58a** δ ppm 11.81 (bs, 1H, H7), 8.17 (s, 1H, H6), 7.93 (s, 4H, H4, H5), 7.81 (bs, 3H, H8), 7.57-7.51 (m, 2H, H2), 7.35 (t, J = 8.1 Hz, 2H, H1), 7.05-6.97 (m, 3H, H3, H10), 6.87-6.85 (m, 2H, H11), 5.36 (s, 2H, H9), 3.70 (s, 3H, H12).

^{1}H-NMR (400 MHz, DMSO-d_6) – attributed to **58b** δ ppm 11.91 (bs, 1H, H7'), 8.19 (s, 1H, H6'), 8.00-7.98 (m, 2H, H5'), 7.91-7.89 (m, 2H, H2'), 7.81 (bs, 3H, H8'), 7.57-7.51 (m, 2H, H4'), 7.27 (t, J = 8.1 Hz, 2H, H1'), 7.05-6.97 (m, 3H, H3', H10') , 6.87-6.85 (m, 2H, H11'), 5.40 (s, 2H, H9'), 3.70 (s, 3H, H12').

^{13}C-NMR (100 MHz, DMSO-d_6) δ ppm 161.0, 160.6, 158.5, 149.0, 148.9, 144.2, 143.9, 134.9, 133.6, 132.6, 131.6, 130.9, 130.8, 129.6, 129.5, 129.3, 128.6, 128.1, 128.0, 127.9, 127.2, 127.1, 126.4, 125.2, 116.0, 115.8, 115.7, 115.5, 114.0, 104.5, 104.1, 99.5, 55.1, 52.4.

HPLC-MS (ESI+): 443.31 ($M+H^+$) calculated for $C_{25}H_{23}FN_6$: 442.19. Purity measured by HPLC-MS: 99.80%

4.5.2.4. Synthesis of 3,5-pyrazole-connected mono-AG 61a,b

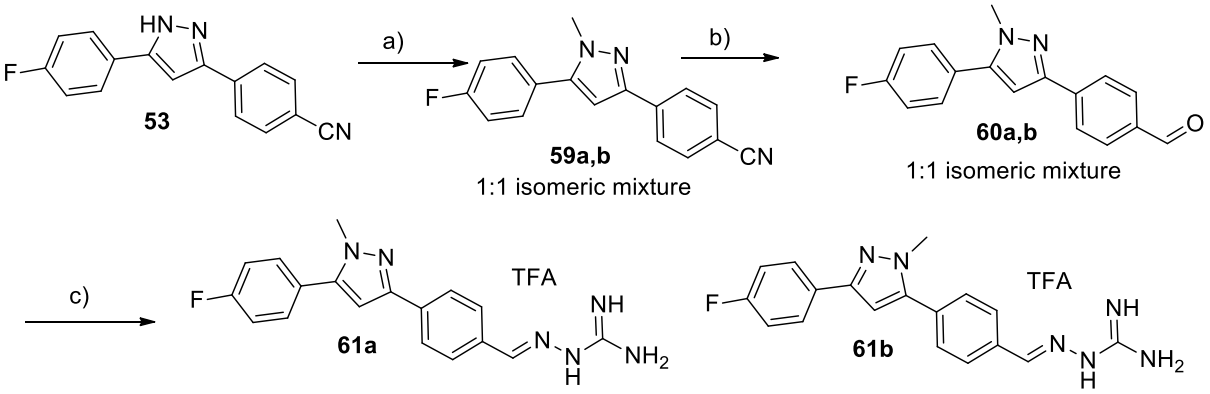

a) MeI (1.2 eq), K_2CO_3 (1.5 eq), dry DMF [0.2 M], $Ar_{(g)}$, RT, **70%**; b) 1M DIBAL-H in hexane (1.2 eq), dry DCM [0.2 M], $Ar_{(g)}$, 0°C to RT, 1 hr; c) aminoguanidine HCl (1.1 eq), 1M aq.HCl (cat.), EtOH [0.05 M], 4hrs, **74%** over two steps.

4-(5-(4-fluorophenyl)-1-methyl-1H-pyrazol-3-yl)benzonitrile 59a,b

The reaction was performed according to **Paragraph 4.5.1.3** using **53** (200.1 mg, 0.769 mmol, 1 eq), K_2CO_3 (159.4 mg, 1.154 mmol, 1.5 eq) and MeI (58 µL, 0.923 mmol, 1.2 eq) in dry DMF (4 mL). After work up the crude was purified by direct phase flash chromatography (eluant mixture: n-hexane/AcOEt 7:3) to give 149.3 mg of pure **59a,b** as a white solid (≈1:1 isomeric mixture, 0.538 mmol, **70%** yield).

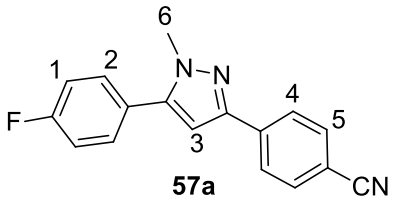

Characterization:

^{1}H-NMR (400 MHz, $CDCl_3$) presumed **59a** δ ppm 7.93-7.91 (m, 2H, H5), 7.80-7.77 (m, 2H, H2), 7.70-7.68 (m, 2H, H4), 7.13-7.08 (m, 2H, H1), 6.63 (s, 1H, H3), 3.94 (s, 3H, H6).

^{1}H-NMR (400 MHz, $CDCl_3$) presumed **59b** δ ppm 7.80-7.77 (m, 2H, H5'), 7.61-7.58 (m, 2H, H4'), 7.45-7.42 (m, 2H, H1'), 7.21-7.17 (m, 2H, H2'), 6.63 (s, 1H, H3'), 3.94 (s, 3H, H6').

^{13}C-NMR (from HSQC, $CDCl_3$) δ ppm: 132.4, 130.7, 129.2, 127.3, 125.8, 116.0, 115.6, 115.5, 103.9, 37.8, 37.7.

4-(5-(4-fluorophenyl)-1-methyl-1H-pyrazol-3-yl)benzaldehyde 60a,b

The reaction was performed according to **Paragraph 4.5.1.4** using **59a,b** as ≈1:1 isomeric mixture (140 mg, 0.504 mmol, 1 eq), 1M DIBAL-H in hexane (0.61 mL, 0.605 mmol, 1.2 eq) in dry DCM (2.5 mL) and followed by TLC analysis using 7:3 Hex/AcOEt as eluent. After work up, the reaction mixture was filtered on a small path of silica gel using AcOEt/hexane 1:1. After concentration under reduced pressure, crude **60a,b** (110.8 mg) was used without further purification.

(E)-2-(4-(5-(4-fluorophenyl)-1-methyl-1H-pyrazol-3-yl)benzylidene)hydrazine carboximidamide trifluoroacetate 61a,b

The reaction was performed according to **Paragraph 4.5.1.7 – no precipitation**, using crude **60a,b** as ≈1:1 isomeric mixture (110.8 mg, 0.395 mmol, 1eq), aminoguanidine hydrochloride (32.5 mg, 0.295 mmol, 1.1eq), 4 drops of aqueous 1N HCl and absolute EtOH (6 mL). After work up and reverse phase chromatography purification, 168.4 mg of pure **61a,b** (≈1:1 isomeric mixture, 0.373 mmol, **74%** yield over two steps) was obtained as a white solid.

Characterization:

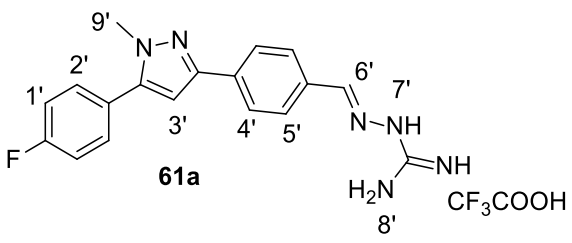

61a

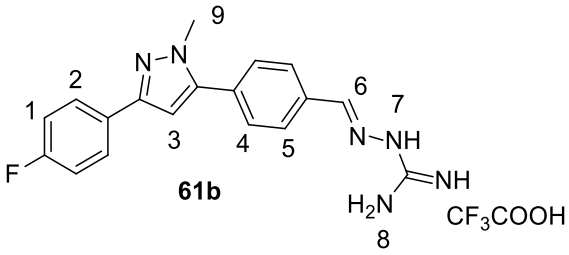

61b

^{1}H-NMR (400 MHz, DMSO-d_6) - attributed to **61a** δ ppm 11.90 (bs, 1H, H7'), 8.22 (s, 1H, H6'), 8.05-8.02 (m, 2H, H5'), 7.90-7.86 (m, 2H, H2'), 7.86-7.72 (bs, 3H, H8'), 7.66 (m, 2H, H4'), 7.28-7.24 (m, 2H, H1'), 6.98 (s, 1H, H3'), 3.95 (s, 3H, H9').

^{1}H-NMR (400 MHz, DMSO-d_6) – attributed to **61b** δ ppm 11.79 (bs, 1H, H7), 8.17 (s, 1H, H6), 7.92 (s, 4H, H5, H4), 7.86-7.72 (bs, 3H, H8), 7.69 (m, 2H, H2),7.41-7.37 (m, 2H, H1), 7.00 (s, 1H, H3), 3.91 (s, 3H, H9).

^{13}C-NMR (100 MHz, DMSO-d_6) δ ppm 155.2, 148.3, 148.2, 146.7, 146.2, 143.9, 143.6, 135.0, 133.5, 132.4, 131.6, 130.8, 130.7, 128.6, 128.1, 128.0, 127.0, 126.9, 126.4, 125.1, 115.9, 115.7, 115.4, 103.8, 103.8, 103.4, 38.0, 37.7.

HPLC-MS (ESI+): 337.18 ($M+H^+$) calculated for $C_{18}H_{17}FN_6$: 336.15. Purity measured by HPLC-MS: 99.80%

4.5.2.5. Synthesis of 3,5-pyrazole-connected mono-AG 62

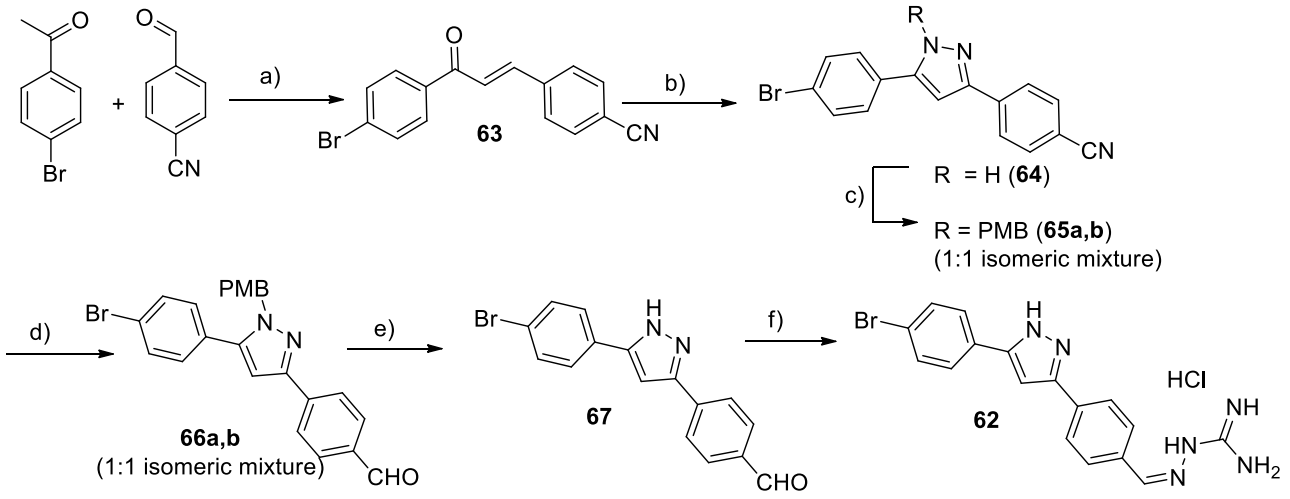

a) 3M aq.NaOH (1.5 eq), MeOH [0.5 M], 0°C to RT, 16 hrs, **63%**; b) $TsNHNH_2$ (1.05 eq), 2M aq.HCl (cat.), then K_2CO_3 (2.1 eq), EtOH [0.15 M], 80°C, 20hrs, **87%**; c) PMBCl (1.3 eq), 1.5eq K_2CO_3 (1.5 eq), dry DMF [0.2 M], $Ar_{(g)}$, RT, 16hrs, **77%**; d) 1M DIBAL-H in hexane (1.2 eq), dry DCM [0.2 M], $Ar_{(g)}$, 0°C to RT, 1 h, **75%**; e) TFA [0.1 M], 70°C, 6 hrs, **69%**; f) aminoguanidine HCl (1.1 eq), 1M aq.HCl (cat.), EtOH [0.05 M], 4hrs, **89%**.

(E)-4-(3-(4-bromophenyl)-3-oxoprop-1-en-1-yl)benzonitrile 63

3M NaOH (2.5 mL, 7.5 mmol, 1.5 eq) was slowly added dropwise in 30 minutes at 0°C to a solution of 4-formylbenzonitrile (692 mg, 5.28 mmol, 1 eq) and 4-bromoacetophenone (1.0 g, 5.28 mmol, 1eq) in MeOH (10 mL). The reaction mixture was warmed at RT and stirred for 16 hours (TLC monitoring, eluant mixture: n-hexane/EtOAc 8:2). Then, the formed precipitate was filtered and sequentially washed with water (multiple washings until pH = 7, 50 mL) and methanol (10 mL). After drying, pure **63** was obtained as a pale-yellow solid (1.015 g, **63%** yield) that was used without further purification.

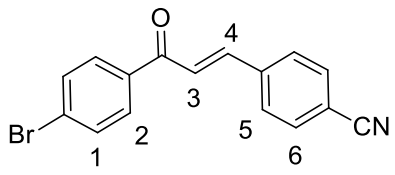

Characterization:

^{1}H-NMR ($CDCl_3$, 300 MHz) δ ppm 7.87–7.90 (m, 2H, H2), 7.78 (d, J =15.7 Hz, 1H, H3 or H4), 7.70–7.72 (m, 4H, H5, H6), 7.64–7.67 (m, 2H, H1), 7.54 ppm (d, J =15.7 Hz, 1H, H4 or H3).

4-(5-(4-bromophenyl)-1H-pyrazol-3-yl)benzonitrile 64

The reaction was performed according to **Paragraph 4.5.1.2** using **63** (359.7 mg, 1.153 mmol, 1 eq), tosyl hydrazide (235.9 mg, 1.27 mmol, 1.05 eq), 4 drops of aqueous 2N HCl, solid K_2CO_3 (334.7 mg, 2.421 mmol, 2.1eq) and absolute EtOH (8.0 mL). After work up and filtration, pure **64** was obtained as a white solid (322.2 mg, 0.994 mmol, **87%** yield) and used without further purification.

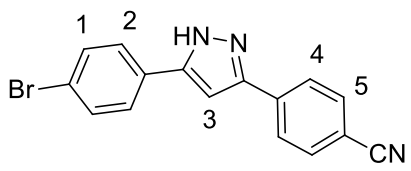

Characterization

^{1}H-NMR (400 MHz, DMSO-d_6) δ ppm 13.70 (bs, 1H, NH), 8.07–7.64 (m, 8H, H1, H2, H4, H5), 7.42 (s, 1H, H3).

4-(5-(4-bromophenyl)-1-(4-methoxybenzyl)-1H-pyrazol-3-yl)benzonitrile 65a,b

The reaction was performed according to **Paragraph 4.5.1.3** using **64** (309.1 mg, 0.953 mmol, 1 eq), K_2CO_3 (278.2 mg, 1.483 mmol, 1.5 eq) and 4-methoxybenzyl chloride (PMBCl) (162 µL, 1.208 mmol, 1.3 eq) in dry DMF (5 mL). After work up the crude was purified by direct phase flash chromatography (eluant mixture: n-hexane/AcOEt from 9:1 to 8:2) to give 326.1 mg of pure **65a,b** as a white solid (≈1:1 isomeric mixture, 0.734 mmol, **77%** yield).

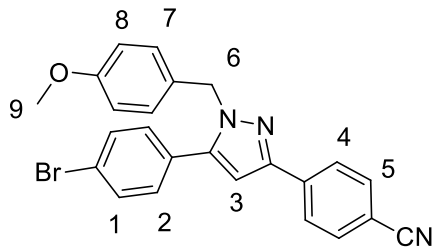

Characterization:

^{1}H-NMR (400 MHz, $CDCl_3$) - attributed to **65a** δ ppm 7.89-7.87 (m, 2H, H5), 7.67-7.60 (m, 2H, H4), 7.49-7.46 (m, 2H, H2), 7.14-7.12 (m, 2H, H1), 6.97-6.93 (m, 2H, H7), 6.76-6.73 (m, 2H, H8), 6.60 (s, 1H, H3), 5.25-5.22 (m, 2H, H6), 3.70 (s, 3H, H9).

^{1}H-NMR (400 MHz, $CDCl_3$) – attributed to **65b** δ ppm 7.70-7.60 (m, 4H, H5', H2'), 7.49-7.46 (m, 2H, H4'), 7.39-7.37 (m, 2H, H1'), 6.97-6.93 (m, 2H, H7'), 6.76-6.73 (m, 2H, H8'), 6.60 (s, 1H, H3'), 5.25-5.22 (m, 2H, H6'), 3.70 (s, 3H, H9').

^{13}C-NMR (from HSQC, $CDCl_3$) δ ppm 132.5, 131.9, 130.5, 129.4, 128.1, 127.1, 126.0, 114.1, 104.4, 55.3, 53.3.

4-(5-(4-bromophenyl)-1-(4-methoxybenzyl)-1H-pyrazol-3-yl)benzaldehyde 66a and 66b

The reaction was performed according to **Paragraph 4.5.1.4** using **65a,b** as ≈1:1 isomeric mixture (301.2 mg, 0.675 mmol, 1 eq), 1M DIBAL-H in n-hexane (0.81 mL, 0.81 mmol, 1.2 eq) in dry DCM (3 mL). After work up and chromatographic purification (eluant mixture: n-hexane/AcOEt 85:15), 195.1 mg of pure **66a,b (**≈1:1 isomeric mixture, 0.436 mmol, **65%** yield) were obtained as a white solid().

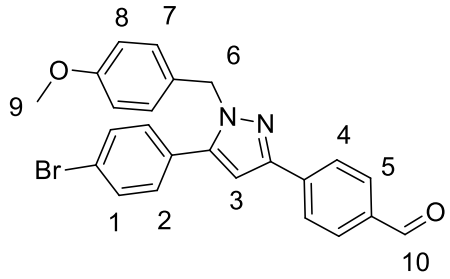

Characterization:

^{1}H-NMR (400 MHz, $CDCl_3$) – attributed to **66a** δ ppm 9.96 (s, 1H, H10), 7.97-7.95 (m, 2H, H5), 7.86-7.84 (m, 2H, H4), 7.50-7.45 (m, 2H, H2), 7.16-7.13 (m, 2H, H1), 6.98-6.94 (m, 2H, H7), 6.76-6.73 (m, 2H, H8), 6.64 (s, 1H, H3), 5.24 (s, 2H, H6), 3.71 (s, 3H, H9).

^{1}H-NMR (400 MHz, $CDCl_3$) – attributed to **66b** δ ppm 9.99 (s, 1H, H10'), 7.86-7.84 (m, 2H, H4'), 7.69-7.66 (m, 2H, H1'), 7.50-7.45 (m, 4H, H2', H5'), 6.98-6.94 (m, 2H, H7'), 6.76-6.73 (m, 2H, H8'), 6.62 (s, 1H, H3'), 5.28 (s, 2H, H6'), 3.70 (s, 3H, H9').

^{13}C-NMR (from HSQC, $CDCl_3$) δ ppm 191.8, 191.5, 132.0, 130.4, 130.1, 129.3, 128.2, 127.2, 125.9, 114.2, 104.5, 55.2, 53.3.

4-(5-(4-bromophenyl)-1H-pyrazol-3-yl)benzaldehyde 67

The reaction was performed according to **Paragraph 4.5.1.6** using **66a,b** as ≈1:1 isomeric mixture (140.1 mg, 0.313 mmol, 1 eq) and TFA (3mL). After work up, 70.7 mg of pure **67** were obtained as a pale brown solid (0.216 mmol, **69%** yield).

Characterization:

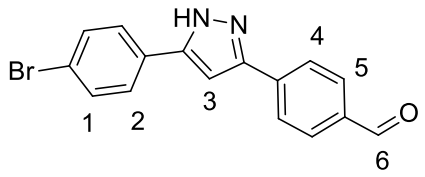

^{1}H-NMR (400 MHz, DMSO-d_6) δ 13.88 (s, 1H, H4), 10.03 (s, 1H, H7), 8.07 (d, J = 8.0 Hz, 2H, H6), 8.00 (d, J = 8.0 Hz, 2H, H5), 7.81 (d, J = 8.4Hz, 2H, H2), 7.69 (d, J = 8.4Hz, 2H, H1) 7.43 (s, 1H, H3).

^{13}C-NMR (from HSQC, DMSO-d_6) δ ppm 192.8, 132.3, 130.7, 127.6, 126.0, 101.7.

(E)-2-(4-(5-(4-fluorophenyl)-1H-pyrazol-3-yl)benzylidene)hydrazinecarboximidamide hydrochloride 62

The reaction was performed according to **Paragraph 4.5.1.7 –precipitate formation**, using **67** (46.0 mg, 0.141 mmol, 1eq), aminoguanidine hydrochloride (17.1 mg, 0.155 mmol, 1.1eq), 2 drops of aqueous 1N HCl and absolute EtOH (3 mL).The precipitate was filtered, and washed with cold EtOH (3 x 5 mL) and Et_2O (15 mL). After drying pure **62** was obtained as a white solid (52.7 mg, 0.126 mmol, **89%** yield).

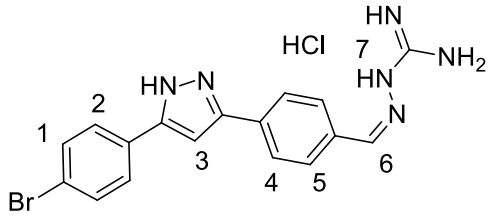

Characterization:

^{1}H-NMR (400 MHz, DMSO-d_6) δ ppm 13.60 (bs, 1H, NH), 11.97 (bs, 1H, H7), 8.20 (s, 1H, H6), 7.98-7.68 (m, 8H, H1, H2, H4, H5), 7.78-7.55 (bs, 3H, NH), 7.36 (s, 1H, H3).

^{13}C-NMR (100 MHz, DMSO-d_6) δ ppm 155.8, 146.8, 132.2, 128.6, 127.6, 125.7, 101.0.

HPLC-MS (ESI+): 383.15 ($M+H^+$) calculated for $C_{17}H_{15}BrN_6$: 382.05. Purity measured by HPLC-MS: 98.95%

4.5.2.6. Synthesis of 3,5-pyrazole-connected di-AGs 68 and 69

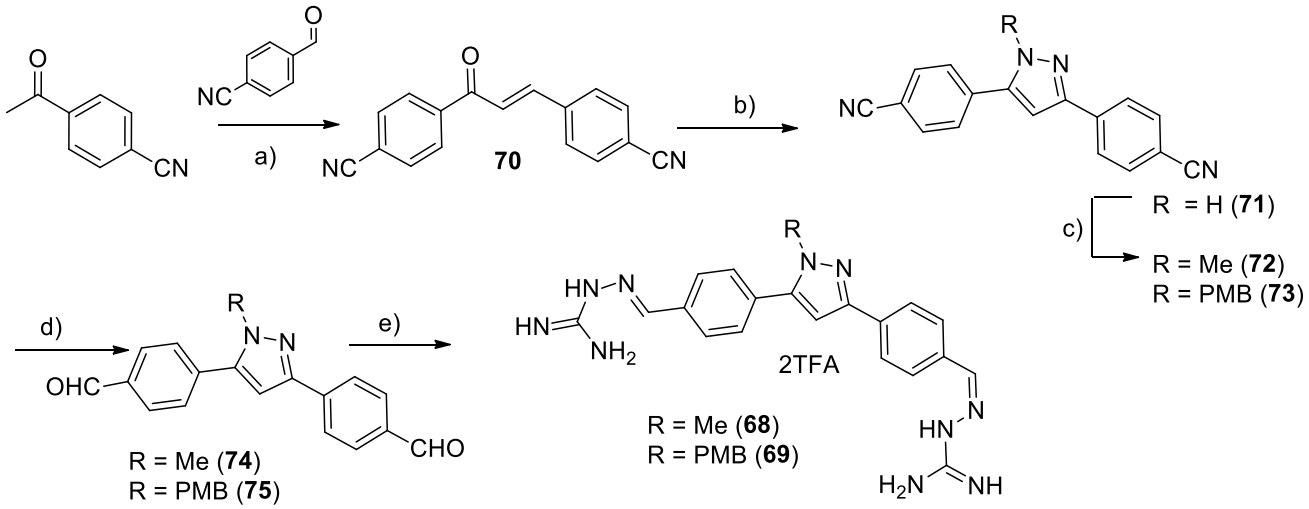

a) 0.03eq aq.NaOH, dry MeOH [0.5 M], 70°C, 45min **66%;** b) $TsNHNH_2$ (1.05 eq), 2M aq.HCl (cat.), then K_2CO_3 (2.1 eq), EtOH [0.15 M], 80°C, 20hrs, **91%**; c) MeI (1.3eq) or PMBCl (1.3 eq), K_2CO_3 (1.5 eq), dry DMF [0.2 M], $Ar_{(g)}$, RT, 16hrs, **95%**(**72**), **87%**(**73**); d) 1M DIBAL-H in hexane (2.2 eq), dry DCM [0.2 M], $Ar_{(g)}$, 0°C to RT, 1 hr, **80%**(**74**), **82%**(**75**);e) aminoguanidine HCl (2.1 eq), 1M aq.HCl (cat.), EtOH [0.05 M], 4hrs, **89%**(**68**), **87%** (**69**)

(E)-4,4'-acryloyldibenzonitrile 70

4-Acetylbenzonitrile (1.0 g, 6.886 mmol, 1 eq) was dissolved in dry MeOH (14 mL) while stirring under nitrogen atmosphere. Upon complete dissolution of the reagent, solid 4-formylbenzonitrile (905 mg, 6.897 mmol, 1 eq) was added. The solution was heated at reflux, and stirred for 30 minutes. Then, 1M aqueous NaOH (230 µL, 0.23 mmol, 0.03 eq) was added until the formation of a yellow precipitate. After stirring for additional 15 minutes, the precipitate was filtered and washed with Et_2O (30 mL). After drying, pure **70** was obtained as a yellow solid (1.165 g, **66%** yield) that was used without further purification.

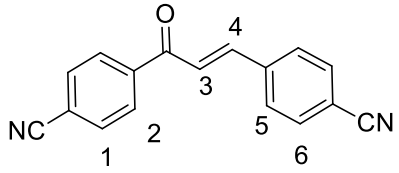

Characterization:

^{1}H-NMR ($CDCl_3$) δ ppm 8.10 (d, 2H, J = 8.4 Hz), 7.81 (d, 2H, J = 8.4 Hz), 7.78 (d, 1H, J = 15.3 Hz H4 or H3), 7.74 (s, 4H, H5-H6) 7.48 (d, 1H, J = 15.6 Hz, H3 or H4).

4,4'-(1H-pyrazole-3,5-diyl)dibenzonitrile 71

The reaction was performed according to **Paragraph 4.5.1.2** using **70** (1.16 g, 4.502 mmol, 1 eq), tosyl hydrazide (880.4 mg, 4.728 mmol, 1.05 eq), 6 drops of aqueous 2N HCl), K_2CO_3 (1278.7 mg, 9.252 mmol, 2.1 eq) and absolute EtOH (33 mL). After work up and filtration, pure **71** (1.11 g, 4.107 mmol, **91**% yield) was obtained as a white solid that was used without further purification.

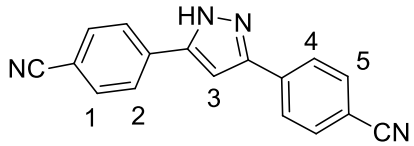

Characterization:

^{1}H-NMR (400 MHz, DMSO-d_6) δ ppm 13.90 (bs, 1H, NH), 8.04 (d, J = 4.0 Hz, 4H, H1, H5), 7.95 (d, J = 4.0 Hz, 2H, H2, H4), 7.57 (s, 1H, H3).

4,4'-(1-methyl-1H-pyrazole-3,5-diyl)dibenzonitrile 72

The reaction was performed according to **Paragraph 4.5.1.3** using **71** (205 mg, 0.758 mmol, 1 eq), K_2CO_3 (158 mg, 1.137 mmol, 1.5 eq) and MeI (57 µL, 0.910 mmol, 1.2 eq) in dry DMF (4 mL). After work up the crude was purified by direct phase flash chromatography (eluant mixture: n-hexane/AcOEt from 6:4 to 4:6) to give pure **72** (228.6 mg, 0.720mmol, **95%** yield) as a white solid.

Characterization:

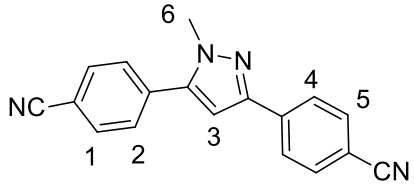

^{1}H-NMR (400 MHz, $CDCl_3$) δ ppm 7.93 (d, J = 8.3 Hz, 2H, H4), 7.80 (d, J = 8.3 Hz, 2H, H2), 7.70 (d, J = 8.3 Hz, 2H, H5), 7.60 (d, J = 8.3 Hz, 2H, H1), 6.73 (s, 1H, H3), 3.98 (s, 3H, H6).

^{13}C-NMR (from HSQC, $CDCl_3$) δ ppm 132.7, 132.6, 129.3, 125.9, 104.6, 38.11.

4,4'-(1-(4-methoxybenzyl)-1H-pyrazole-3,5-diyl)dibenzonitrile 73

The reaction was performed according to **Paragraph 4.5.1.3** using **71** (1.11 g, 4.107 mmol, 1 eq), K_2CO_3 (852 mg, 6.1656 mmol, 1.5 eq) and 4-methoxybenzyl chloride (PMBCl) (700 µL, 5.163 mmol, 1.3 eq) in dry DMF (20 mL). After work up the crude was purified by direct phase flash chromatography (eluant mixture: n-hexane/AcOEt from 6:4 to 4:6) to give pure **73** (1.39 g, 3.573 mmol, **87%** yield) as a white solid.

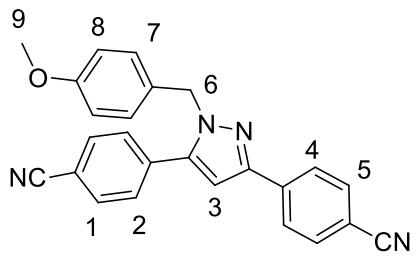

Characterization:

^{1}H-NMR (400 MHz, $CDCl_3$) δ ppm 7.97 (d, J = 8.4 Hz, 2H, H4), 7.72 – 7.69 (m, 4H, H2, H5), 7.46 (d, J = 8.4 Hz, 2H, H1), 7.01 (d, J = 8.7 Hz, 2H, H7), 6.82 (d, J = 8.7 Hz, 2H, H8), 6.74 (s, 1H, H3), 5.33 (s, 2H, H6), 3.78 (s, 3H, H9).

^{13}C-NMR (100 MHz, $CDCl_3$) δ ppm 159.4, 149.3, 143.8, 137.5, 134.8, 132.7, 129.6, 128.7, 128.2, 126.1, 119.1, 118.3, 114.4, 112.9, 111.3, 105.2, 55.4, 53.7.

4,4'-(1-methyl-1H-pyrazole-3,5-diyl)dibenzaldehyde 74

The reaction was performed according to **Paragraph 4.5.1.5** using **72** (228 mg, 0.802 mmol, 1 eq), 1M DIBAL-H in n-hexane (1.9 mL, 1.9 mmol, 1.15 eq) in dry DCM (6.2 mL). After work up and chromatographic purification (eluant mixture: n-hexane/AcOEt from 6:4 to 1:1) pure **74** (186.3 mg, 0.642 mmol, **80%** yield) was obtained as a white solid.

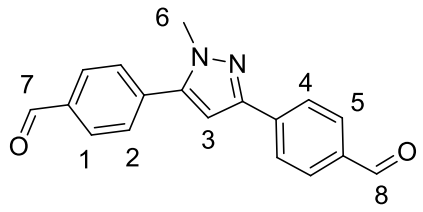

Characterization:

^{1}H-NMR (400 MHz, $CDCl_3$) δ ppm 10.03 (s, 1H, H7), 9.97 (s, 1H, H8), 7.97-7.93 (m, 4H, H2, H5), 7.87 (d, J= 8.4 Hz, 2H, H4), 7.60 (d, J= 8.4 Hz, 2H, H1), 6.73 (s, 1H, H3).

^{13}C-NMR (from HSQC, $CDCl_3$) δ ppm: 191.7, 191.2, 130.3, 130.1, 129.2, 125.8, 104.7, 38.0.

4,4'-(1-(4-methoxybenzyl)-1H-pyrazole-3,5-diyl)dibenzaldehyde 75

The reaction was performed according to **Paragraph 4.5.1.5** using **73** (336.4 mg, 0.862 mmol, 1 eq),1M DIBAL-H in n-hexane (2.0 mL, 2 mmol, 1.15 eq) in dry DCM (6.4 mL). After work up and chromatographic purification (eluant mixture: n-hexane/AcOEt from 6:4 to 1:1) pure **75** (280 mg, 0.707 mmol, **82%** yield) was obtained as a white solid.

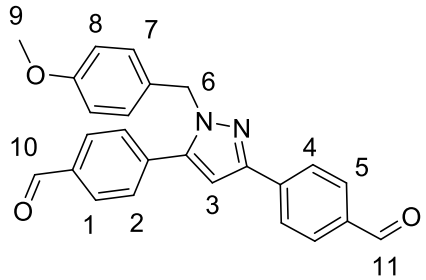

Characterization:

^{1}H-NMR (400 MHz, $CDCl_3$) δ ppm 10.07 (s, 1H, H11), 10.04 (s, 1H, H10), 8.05 (d, J = 8.3 Hz, 2H, H5), 7.95 – 7.93 (m, 4H, H1, H4), 7.55 – 7.53 (m, 2H, H2), 7.05 (d, J = 8.8 Hz, 2H, H7), 6.83- 6.81 (m, 3H, H3, H8), 5.37 (s, 2H, H6), 3.78 (s, 3H, H9).

^{13}C-NMR (100 MHz, $CDCl_3$) δ ppm:191.9, 191.5, 159.2, 149.7, 144.3, 138.9, 136.2, 136.1, 135.6, 130.3, 130.0, 129.4, 128.8, 128.2, 126.0, 114.2, 105.2, 55.3, 53.5.

2,2'-(((1-methyl-1H-pyrazole-3,5-diyl)bis(4,1-phenylene))bis(methanylylidene))bis(hydrazine carboximidamide) bis(trifluoroacetate) 68

The reaction was performed according to **Paragraph 4.5.1.7 – no precipitation**, using **74** (61.1 mg, 0.210 mmol, 1 eq), aminoguanidine hydrochloride (47 mg, 0.42 mmol, 1.0 eq), 3 drop of aqueous 1N HCl and absolute EtOH (4.0 mL). After work up and reverse phase chromatography purification, pure **68** (118.3 mg, 0.188 mmol, **89%** yield) was obtained as a white solid.

Characterization:

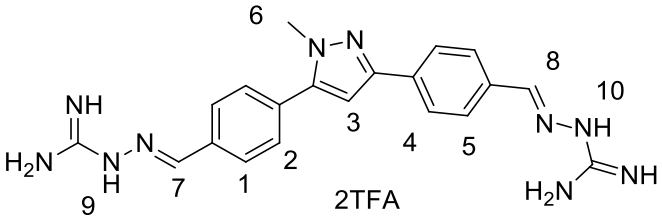

^{1}H-NMR (400 MHz, DMSO-d_6) δ ppm 12.06 (s, 1H, H9), 11.94 (s, 1H, H10), 8.25-7.75 (bs, 6H, NH), 8.22 (s, 1H, H7), 8.17 (s, 1H, H8), 8.04 (d, J = 8.3Hz, 2H, H1), 7.93 (s, 4H, H4, H5), 7.70 (d, J = 8.3Hz, 2H, H2), 7.10 (s, 1H, H3), 3.97 (s, 3H, H6).

^{13}C-NMR (100 MHz, DMSO-d_6) δ ppm 159.4, 159.1, 155.8, 155.7, 148.9, 147.1, 146.5, 144.4, 135.4, 134.0, 132.9, 132.0, 129.1, 128.5, 128.4, 125.6, 104.5, 38.5.

HPLC-MS (ESI+): 403.25 ($M+H^+$) calculated for $C_{20}H_{22}N_{10}$: 402.20. Purity measured by HPLC-MS: 98.39%.

2,2'-(((1-(4-methoxybenzyl)-1H-pyrazole-3,5-diyl)bis(4,1-phenylene))bis(methanylylidene))bis(hydrazine carboximidamide) bis(trifluoroacetate) 69

The reaction was performed according to **Paragraph 4.5.1.7 – no precipitation**, using **75**(80.9 mg, 0.204 mmol, 1 eq), aminoguanidine hydrochloride (47.6 mg, 0.431 mmol, 1.05eq), 4 drops of aqueous 1N HCl and absolute EtOH (4.0 mL). After work up and reverse phase chromatography purification, pure **69** (131 mg, 0.178mmol, **87**% yield) was obtained as a white solid.

Characterization:

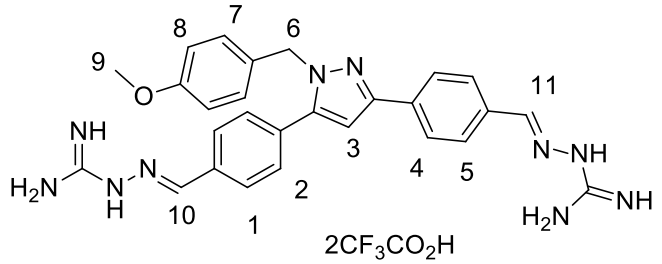

^{1}H-NMR (400 MHz, DMSO-d_6 + D_2O) δ ppm 8.18 (s, 1H, H11), 8.16 (s, 1H, H10), 7.98 – 7.90 (m, 6H, H2, H4, H5), 7.57 (d, J = 8.3 Hz, 2H, H1), 7.11 (s, 1H, H3), 6.97 (d, J = 8.7 Hz, 2H, H7), 6.85 (d, J = 8.7 Hz, 2H, H8), 5.42 (s, 2H, H6), 3.68 (s, 3H, H9).

^{13}C-NMR (100 MHz, DMSO-d_6) δ ppm 158.8, 155.2, 155.1, 149.5, 147.3, 146.7, 144.7, 135.1, 133.9, 132.9, 131.7, 129.6, 128.9, 128.4, 128.3, 128.2, 125.7, 114.3, 105.0, 55.4, 52.8.

HPLC-MS (ESI+): 509.23 ($M+H^+$) calculated for $C_{27}H_{28}N_{10}O$: 508.24. Purity measured by HPLC-MS: 99.66%

4.5.2.7. Synthesis of 3,5-pyrazole-connected di-AGs 76 and 77

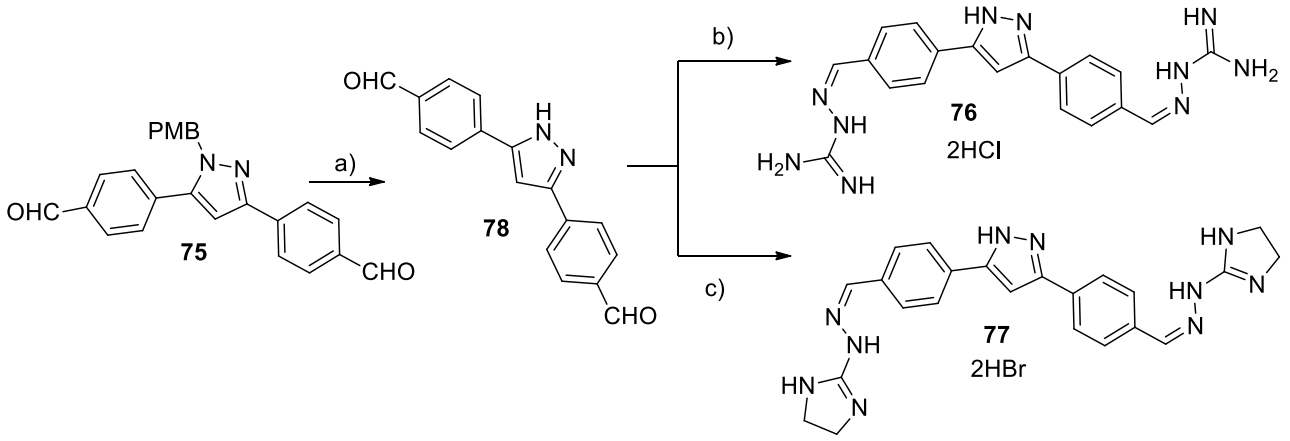

a) TFA [0.1 M], 70°C, 6hrs, **71%** yield; b) aminoguanidine HCl (2.2 eq), 1M aq.HCl (cat.), EtOH [0.05 M], 2hrs, **53%**; c) 2-hydrazino-2-imidazoline HBr (2.05 eq), 1M aq.HCl (cat.), EtOH [0.05 M], 6hrs, **76%**.

4,4'-(1H-pyrazole-3,5-diyl)dibenzaldehyde 78

The reaction was performed according to **Paragraph 4.5.1.6** using **75** (426.7 mg, 1.078 mmol, 1 eq), TFA (11 mL). After work up, 211.4 mg of pure **78** were obtained as a pale brown solid (0.713 mmol, **71%** yield).

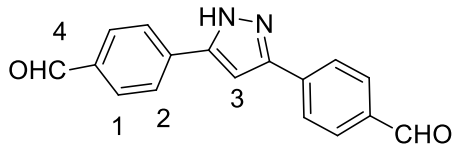

Characterization:

^{1}H-NMR (400 MHz, DMSO-d_6) δ 13.88 (bs, 1H, NH), 10.03 (s, 2H, H4), 8.09 – 8.01 (m, 8H, H1, H2), 7.57 (s, 1H, H3).

2,2'-(((1H-pyrazole-3,5-diyl)bis(4,1-phenylene))bis(methanylylidene))bis(hydrazinecarboximidamide) dihydrochloride 76

The reaction was performed according to **Paragraph 4.5.1.7 –precipitate formation**, using **78** (91.1 mg, 0.330 mmol, 1eq), aminoguanidine hydrochloride (81.1 mg, 0.734 mmol, 2.2eq), 3 drop of aqueous 1N HCl and absolute EtOH (6.0 mL). The precipitate was filtered, and washed with EtOH (15 mL) and 5:1 MeCN/H_2O (15 mL). After drying, pure **76** (80 mg, 0.173 mmol, **53%** yield) was obtained as a white solid.

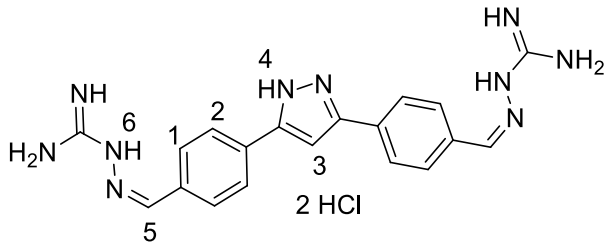

Characterization:

^{1}H-NMR (400 MHz, DMSO-d_6) δ ppm 13.66 (s, 1H, H4), 12.08 (bs, 2H, H6), 8.21 (s, 2H, H5), 7.94-7.53 (m, 16H, H1, H2, NH), 7.41 (s, 1H, H3).

^{13}C-NMR (100 MHz, DMSO-d_6) δ ppm 155.2, 147.4, 147.0, 133.4, 132.8, 131.1, 128.7, 128.5, 125.7, 101.2.

HPLC-MS (ESI+): 389.27 (M + H^+) calculated for $C_{19}H_{20}N_{10}$: 388.19. Purity measured by HPLC-MS: 98.4 %

2,2'-(((1H-pyrazole-3,5-diyl)bis(4,1-phenylene))bis(methanylylidene))bis(hydrazin-1-yl-2-ylidene))bis(4,5-dihydro-1H-imidazole) dihydrobromide 77

2-Hydrazino-2-imidazoline hydrobromide (79 mg, 0.436 mmol, 1.03 eq) and 1N aq. HCl (5 drops, catalytic) were sequentially added to a warm, vigorously stirred suspension of **78** (58.8 mg, 0.213 mmol ,1 eq) in abs EtOH (4mL). After the addition of the catalytic acid, the suspension became a solution. The reaction mixture was refluxed at 80°C for 2 hrs, till the formation of a white precipitate, and then for additional 4 hrs.Then, the reaction mixture was cooled to RT, the precipitate was filtered and washed with EtOH/H_2O 95:5 (20 mL) and Et_2O (20 mL), to give after drying pure **77** (97.2 mg, 0.162 mmol, **76%**) as a white solid.

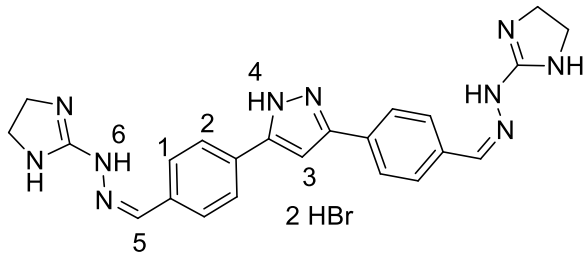

Characterization:

^{1}H-NMR (400 MHz, DMSO-d_6 + D_2O) δ ppm 8.18 (s, 2H, H5), 7.94 – 7.88 (m, 8H, H1, H2), 7.37 (s, 1H, H3), 3.74 (s, 8H, H6).

^{13}C-NMR (100 MHz, DMSO-d_6) δ ppm 158.0, 148.1, 133.0, 128.5, 125.8, 101.3, 94.1, 87.5, 43.0

HPLC-MS (ESI+): 441.42 ($M+H^+$) (calculated for $C_{23}H_{24}N_{10}$: 440.22). Purity measured by HPLC-MS: 98.69 %.

4.6.BIBLIOGRAPHY

[1]. Gruol, D.L.; Barker, J.L.; Huang, L.Y.; MacDonald, J.F.; Smith, T.G. Jr. Hydrogen ions have multiple effects on the excitability of cultured mammalian neurons. *Brain Res.* **1980***,* 183, 247–252.

[2]. Waldmann, R.; Champigny, G.; Bassilana, F.; Heurteaux, C.; Lazdunski, M. A proton-gated cation channel involved in acid-sensing. *Nature* **1997**, 386, 173–177.

[3]. Lingueglia, E. *et al.* A modulatory subunit of acid sensing ion channels in brain and dorsal root ganglion cells. *J. Biol. Chem.* **1997**, 272, 29778–29783.

[4]. Waldmann, R.; Lazdunski, M. H^+-gated cation channels: neuronal acid sensors in the NaC/DEG family of ion channels. *Curr. Opin. Neurobiol.* **1998**, 8, 418–424.

[5]. Wemmie, J.A. *et al*. The acid-activated ion channel ASIC contributes to synaptic plasticity, learning, and memory. *Neuron* **2002**, 34, 463–477.

[6]. Wemmie, J.A. *et al*. Acid-sensing ion channel 1 is localized in brain regions with high synaptic density and contributes to fear conditioning. *J. Neurosci*. **2003**, 23, 5496–550.

[7]. Chen, C.C.; England, S.; Akopian, A.N.; Wood, J.N. A sensory neuron-specific, proton-gated ion channel. *Proc. Natl Acad. Sci. USA* **1998***,* 95, 10240–10245.

[8]. Grunder, S.; Chen, X. Structure, function, and pharmacology of acid-sensing ion channels (ASICs): focus on ASIC1a. *Int J. Physiol. Pathophysiol. Pharmacol*. **2010**, 2, 73–94.

[9]. Ugawa, S. *et al*. Receptor that leaves a sour taste in the mouth. *Nature* **1998**, 395, 555–556.

[10]. Ettaiche, M.; Guy, N.; Hofman, P.; Lazdunski, M.; Waldmann, R. Acid-sensing ion channel 2 is important for retinal function and protects against light-induced retinal degeneration. *J. Neurosci.* **2004**, 24, 1005–1012.

[11]. Lu, Y. *et al*. The ion channel ASIC2 is required for baroreceptor and autonomic control of the circulation. *Neuron* **2009**, 64, 885–897.

[12]. Wemmie, J.A.; Price, M.P.; Welsh, M.J. Acid-sensing ion channels: advances, questions and therapeutic opportunities. *Trends Neurosci*. **2006**, 29, 578–586.

[13]. Bassler, E.L.; Ngo-Anh, T.J.; Geisler, H.S.; Ruppersberg, J.P.; Gründer, S. Molecular and functional characterization of acid-sensing ion channel (ASIC) 1b. *J. Biol. Chem*. **2001**, 276, 33782-33787.

[14]. Hesselager, M.; Timmermann, D.B.; Ahring, P.K. pH dependency and desensitization kinetics of heterologously expressed combinations of acidsensing ion channel subunits. *J. Biol. Chem.* **2004**, 279, 11006-11015.

[15]. Baron, A.; Waldmann, R.; Lazdunski, M. ASIC-like, proton-activated currents in rat hippocampal neurons. *J. Physiol*. **2002**, 539, 485-494.

[16]. Sherwood, T.W.; Lee, K.G.; Gormley, M.G.; Askwith, C.C. Heteromeric acid-sensing ion channels (ASICs) composed of ASIC2b and ASIC1a display novel channel properties and contribute to acidosis-induced neuronal death. *J. Neurosci*. **2011**, 31, 9723-9734.

[17]. Wu, L.J. *et al*. Characterization of acid-sensing ion channels in dorsal horn neurons of rat spinal cord. *J. Biol. Chem*. **2004**, 279, 43716-43724.

[18]. Deval, E. *et al*. ASIC3, a sensor of acidic and primary inflammatory pain. *Embo J.* **2008**, 27, 3047-3055

[19]. Hattori, T. *et al.* ASIC2a and ASIC3 heteromultimerize to form pH-sensitive channels in mouse cardiac dorsal root ganglia neurons. *Circ. Res*. **2009**, 105, 279-286.

[20]. Bartoi, T.; Augustinowski, K.; Polleichtner, G.; Gründer, S.; Ulbrich, M.H. Acid sensing ion channel (ASIC) 1a/2a heteromers have a flexible 2:1/1:2 stoichiometry. *Proc. Natl. Acad. Sci. USA* **2014***,* 111, 8281-8286.

[21]. Saugstad, J.A.; Roberts, J.A.; Dong, J.; Zeitouni, S.; Evans, R.J. Analysis of the membrane topology of the acid-sensing ion channel 2a. *J. Biol. Chem*. **2004**, 279, 55514-55519.

[22]. Jasti, J.; Furukawa, H.; Gonzales, E.B.; Gouaux, E. Structure of acid-sensing ion channel 1 at 1.9 Å resolution and low pH. *Nature* **2007**, 449, 316-323.

[23]. Deval, E. *et al.* Acid-sensing ion channels (ASICs): pharmacology and implication in pain. *Pharmacol. Ther.* **2010**, 128, 549–558.

[24]. Price, M.P. *et al.* The DRASIC cation channel contributes to the detection of cutaneous touch and acid stimuli in mice. *Neuron* **2001**, 32, 1071–1083.

[25]. Babini, E.; Paukert, M.; Geisler, H.S.; Gründer, S. Alternative splicing and interaction with di- and polyvalent cations control the dynamic range of acid-sensing ion channel 1 (ASIC1). *J. Biol. Chem.* **2002**, 277, 41597-41603.

[26]. Gründer, S.; Pusch, M. Biophysical properties of acid-sensing ion channels (ASICs). *Neuropharmacology* **2015**, 94, 9–18.

[27]. Sutherland, S.P.; Benson, C.J.; Adelman, J.P.; McCleskey, E.W. Acid-sensing ion channel 3 matches the acid-gated current in cardiac ischemia-sensing neurons. *Proc. Natl. Acad. Sci. USA* **2001**, 98, 711-716.

[28]. Roy, S.; Boiteux, C.; Alijevic, O.; Liang, C.; Berneche, S.; Kellenberger, S. Molecular determinants of desensitization in an ENaC/degenerin channel. *Faseb J.* **2013**, 27, 5034-5045.

[29]. Benson, C.J.; Xie, J.; Wemmie, J.A.; Price, M.P.; Henss, J.M.; Welsh, M.J.; Snyder, P.M. Heteromultimers of DEG/ENaC subunits form Hþ-gated channels in mouse sensory neurons. *Proc. Natl. Acad. Sci. USA.* **2002**, 99, 2338-2343.

[30]. Wemmie, J.A., Zha, X.; Welsh, M. J. Acid-sensing ion channels (ASICs) and pH in synapse physiology, in *Structural and Functional Organization of the Synapse*, 661-681. Editors: Hell, J.W.; Ehlers, M. D. Springer, Philadelphia, **2008**.

[31]. Alvarez de la Rosa, D. *et al.* Distribution, subcellular localization and ontogeny of ASIC1 in the mammalian central nervous system. *J. Physiol.* **2003**, 546, 77–87.

[32]. Wemmie, J. A. Neurobiology of panic and pH chemosensation in the brain. *Dialogues Clin. Neurosci.* **2011**, 13, 475–483.

[33]. Ziemann, A.E. *et al.* Seizure termination by acidosis depends on ASIC1a. *Nat. Neurosci.* **2008**, 11, 816-822.

[34]. Zha, X.M.; Wemmie, J.A.; Green, S.H.; Welsh, M.J. Acid-sensing ion channel 1a is a postsynaptic proton receptor that affects the density of dendritic spines. *Proc. Natl. Acad. Sci. USA* **2006**, 103, 16556-16561.

[35]. Gao, J. *et al.* Coupling between NMDA receptor and acid-sensing ion channel contributes to ischemic neuronal death. *Neuron* **2005**, 48, 635–646.

[36]. Baron, A.; Lingueglia, E. Pharmacology of acid-sensing ion channels: Physiological and therapeutical perspectives. *Neuropharmacology* **2015**, 94, 19–35.

[37]. Zeng, W.Z.; Xu, T.L. Proton production, regulation and pathophysiological roles in the mammalian brain. *Neurosci. Bull.* **2012**, 28, 1–13.

[38]. Wemmie, J.A.; Taugher, R.J.; Kreple, C.J. Acid-sensing ion channels in pain and disease. *Nat. Rev. Neurosci*. **2013**, 14, 461-471.

[39]. Friese, M.A. *et al.* Acid-sensing ion channel-1 contributes to axonal degeneration in autoimmune inflammation of the central nervous system. *Nat. Med.* **2007**, 13, 1483-1489.

[40]. de Ceglia, R. *et al.* Down-sizing of neuronal network activity and density of presynaptic terminals by pathological acidosis are efficiently prevented by Diminazene Aceturate. *Brain Behav. Immun.* **2015**, 45, 263-276.

[41]. Vergo, S. *et al.* Acid-sensing ion channel 1 is involved in both axonal injury and demyelination in multiple sclerosis and its animal model. *Brain* **2011**, 134, 571-584.

[42]. Pignataro, G.; Simon, R.P.; Xiong, Z.G. Prolonged activation of ASIC1a and the time window for neuroprotection in cerebral ischaemia. *Brain* **2007**, 130, 151-158.

[43]. Xiong, Z.G. *et al.* Neuroprotection in ischemia: blocking calcium-permeable acid-sensing ion channels. *Cell* **2004**, 118, 687-698.
[44]. Arun, T. *et al.* Targeting ASIC1 in primary progressive multiple sclerosis: evidence of neuroprotection with amiloride. *Brain* **2013**, 136, 106-115.
[45]. Duan, B. *et al*. Extracellular spermine exacerbates ischemic neuronal injury through sensitization of ASIC1a channels to extracellular acidosis. *J. Neurosci*. **2011**, 31, 2101-2112.
[46]. Immke, D.C.; McCleskey, E.W. Lactate enhances the acid-sensing Na^+ channel on ischemia-sensing neurons. *Nature Neurosci.* **2011**, 4, 869–870.
[47]. Allen, N.J.; Attwell, D. Modulation of ASIC channels in rat cerebellar Purkinje neurons by ischaemia-related signals. *J. Physiol.* **2002**,543, 521–529.
[48]. Mishra, V.; Verma, R.; Raghubir, R. Neuroprotective effect of flurbiprofen in focal cerebral ischemia: the possible role of ASIC1a. *Neuropharmacology* **2010**, 59, 582-588.
[49]. Hu, R. *et al*. Role of acid-sensing ion channel 1a in the secondary damage of traumatic spinal cord injury. *Ann. Surg*. **2011**,254, 353-362.
[50]. Miyake, T.; Nishiwaki, A.; Yasukawa, T.; Ugawa, S.; Shimada, S.; Ogura, Y. Possible implications of acid-sensing ion channels in ischemia-induced retinal injury in rats. *Jpn. J. Ophthalmol*. **2013**, 57, 120-125.
[51]. Wong, H.K. *et al*. Blocking acid-sensing ion channel 1 alleviates Huntington's disease pathology via an ubiquitin-proteasome system-dependent mechanism. *Hum. Mol. Genet*. **2008**,17, 3223-3235.
[52]. Sun, X.; Cao, Y.B.; Hu, L.F.; Yang, Y.P.; Li, J.; Wang, F.; Liu, C.F. ASICs mediate the modulatory effect by paeoniflorin on alpha-synuclein autophagic degradation. *Brain Res*. **2011**,1396, 77-87.
[53]. Coryell, M.W. *et al*. Targeting ASIC1a reduces innate fear and alters neuronal activity in the fear circuit. Biol. *Psychiatry* **2007**,62, 1140-1148.
[54]. Wemmie, J.A. *et al*. Overexpression of acid-sensing ion channel 1a in transgenic mice increases acquired fear-related behavior. *Proc. Natl. Acad. Sci. USA* **2004**, 101, 3621-3626.
[55]. Dwyer, J.M. *et al*. Acid sensing ion channel (ASIC) inhibitors exhibit anxiolytic-like activity in preclinical pharmacological models. *Psychopharmacol*. **2009**, 203, 41e52.
[56]. Coryell, M.W. *et al*. Acid-sensing ion channel-1a in the amygdala, a novel therapeutic target in depression-related behavior. *J. Neurosci*. **2009**, 29, 5381-5388.
[57]. Joeres, N.; Augustinowski, K.; Neuhof, A.; Assmann, M.; Grunder, S. Functional and pharmacological characterization of two different ASIC1a/2a heteromers reveals their sensitivity to the spider toxin PcTx1. *Sci. Rep.* **2016**, 6, 27647.
[58]. Mazzone, G.L.; Veeraraghavan, P.; Gonzalez-Inchauspe, C.; Nistri, A.; Uchitel, O.D. ASIC channel inhibition enhances excitotoxic neuronal death in an in vitro model of spinal cord injury. *Neuroscience* **2017**, 343, 398-410.
[59]. Immke, D.C.; McCleskey, E.W. Protons open acid-sensing ion channels by catalyzing relief of Ca(2þ) blockade. *Neuron* **2003**, 37, 75-84.
[60]. Paukert, M.; Babini, E.; Pusch, M.; Gründer, S. Identification of the Ca2þ blocking site of acid-sensing ion channel (ASIC) 1: implications for channel gating. *J. Gen. Physiol*. **2004**, 124, 383-394.
[61]. Baron, A.; Schaefer, L.; Lingueglia, E.; Champigny, G.; Lazdunski, M. Zn^{2+} and H^+ are coactivators of acid-sensing ion channels. *J. Biol. Chem*. **2001**, 276, 35361-35367.
[62]. Chu, X.P. *et al*. Subunit-dependent high-affinity zinc inhibition of acid-sensing ion channels. *J. Neurosci*. **2004**, 24, 8678-8689.
[63]. Jiang, Q.; Papasian, C.J.; Wang, J.Q.; Xiong, Z.G.; Chu, X.P. Inhibitory regulation of acid-sensing ion channel 3 by zinc. *Neuroscience* **2010**, 169, 574-583.
[64]. Staruschenko, A.; Dorofeeva, N.A.; Bolshakov, K.V.; Stockand, J.D. Subunit-dependent cadmium and nickel inhibition of acid-sensing ion channels. *Dev. Neurobiol*. **2007**, 67, 97-107.

[65]. Wang, W.; Duan, B.; Xu, H.; Xu, L.; Xu, T.L. Calcium-permeable acid-sensing ion channel is a molecular target of the neurotoxic metal ion lead. *J. Biol. Chem*. **2006**, 281, 2497-2505.

[66]. Wang, W.; Yu, Y.; Xu, T.L. Modulation of acid-sensing ion channels by Cu^{2+} in cultured hypothalamic neurons of the rat. *Neuroscience* **2007**, 145, 631-641.

[67]. Li, W.G.; Yu, Y.; Zhang, Z.D.; Cao, H.; Xu, T.L. ASIC3 channels integrate agmatine and multiple inflammatory signals through the nonproton ligand sensing domain. *Mol. Pain* **2010**, 6, 88.

[68]. Deval, E.; Baron, A.; Lingueglia, E.; Mazarguil, H.; Zajac, J.M.; Lazdunski, M. Effects of neuropeptide SF and related peptides on acid sensing ion channel 3 and sensory neuron excitability. *Neuropharmacology* **2003**, 44, 662-671.

[69]. Sherwood, T.W.; Askwith, C.C. Endogenous arginine-phenylalanine-amide related peptides alter steady-state desensitization of ASIC1a. *J. Biol. Chem*. **2008**, 283, 1818-1830.

[70]. Frey, E.N.; Pavlovicz, R.E.; Wegman, C.J.; Li, C.; Askwith, C.C. Conformational changes in the lower palm domain of ASIC1a contribute to desensitization and RFamide modulation. *PLoS One* **2013**, 8, e71733.

[71]. Sherwood, T.W.; Askwith, C.C. Dynorphin opioid peptides enhance acid-sensing ion channel 1a activity and acidosis-induced neuronal death. *J. Neurosci*. **2009**, 29, 14371-14380.

[72]. Wang, X. *et al*. Serotonin facilitates peripheral pain sensitivity in a manner that depends on the nonproton ligand sensing domain of ASIC3 channel. *J. Neurosci*. **2013**, 33, 4265-4279.

[73]. Smith, E.S.; Cadiou, H.; McNaughton, P.A. Arachidonic acid potentiates acidsensing ion channels in rat sensory neurons by a direct action. *Neuroscience* **2007**, 145, 686-698.

[74]. Cadiou, H. *et al.* Modulation of acid-sensing ion channel activity by nitric oxide. *J. Neurosci*. **2007**, 27, 13251-13260.

[75]. Jetti, S.K.; Swain, S.M.; Majumder, S.; Chatterjee, S.; Poornima, V.; Bera, A.K. Evaluation of the role of nitric oxide in acid sensing ion channel mediated cell death. *Nitric Oxide* **2010**, 22, 213-219.

[76]. Cristofori-Armstrong, B.; Rash, L.D. Acid-sensing ion channel (ASIC) structure and function: Insights from spider, snake and sea anemone venoms. *Neuropharmacology* **2017**, 127, 173-184.

[77]. Escoubas, P. *et al*. Isolation of a tarantula toxin specific for a class of proton-gated Na^+ channels. *J. Biol. Chem*. **2000**, 275, 25116-2512.

[78]. Diochot, S. *et al*. A new sea anemone peptide, APETx2, inhibits ASIC3, a major acid-sensitive channel in sensory neurons. *EMBO J.* **2004**, 23, 1516-1525.

[79]. Bohlen, C.J. *et al*. A heteromeric Texas coral snake toxin targets acid-sensing ion channels to produce pain. *Nature* **2011**, 479, 410-414.

[80]. Diochot, S. *et al*. Black mamba venom peptides target acid-sensing ion channels to abolish pain. *Nature* **2012**, 490, 552-555.

[81]. Baconguis, I.; Gouaux, E. Structural plasticity and dynamic selectivity of acid-sensing ion channel-spider toxin complexes. *Nature* **2012**, 489, 400-405.

[82]. Jensen, J.E. *et al*. Understanding the molecular basis of toxin promiscuity: the analgesic sea anemone peptide APETx2 interacts with acid-sensing ion channel 3 and hERG channels via overlapping pharmacophores. *J. Med. Chem*. **2014**, 57, 9195-9203.

[83]. Rahman, T.; Smith, E.S. In silico assessment of interaction of sea anemone toxin APETx2 and acid sensing ion channel 3. *Biochem. Biophys. Res. Commun*. **2014**, 450, 384-389.

[84]. Bohlen, C.J.; Julius, D. Receptor-targeting mechanisms of pain-causing toxins: how ow? *Toxicon* **2012**, 60, 254-264.

[85]. Baconguis, I.; Bohlen, C.J.; Goehring, A.; Julius, D.; Gouaux, E. X-ray structure of acid-sensing ion channel 1-snake toxin complex reveals open state of a Na^+-selective channel. *Cell* **2014**, 156, 717-729.

[86]. Salinas, M. *et al.* Binding site and inhibitory mechanism of the mambalgin-2 pain-relieving peptide on acid-sensing ion channel 1a. *J. Biol. Chem*. **2014**, 289, 13363-13373.

[87]. Qu, Z.W.; Liu, T.T.; Qiu, C.Y.; Li, J.D.; Hu, W.P. Inhibition of acid-sensing ion channels by chlorogenic acid in rat dorsal root ganglion neurons. *Neurosci. Lett*. **2014**, 567, 35-39.

[88]. Mukhopadhyay, M.; Singh, A.; Sachchidanand, S.; Bera, A.K. Quercetin inhibits acid-sensing ion channels through a putative binding site in the central vestibular region. *Neuroscience* **2017**, 348, 264-272.

[89]. Zhou, Y.X.; Zhang, H.; Peng, C. Puerarin: a review of pharmacological effects. *Phytother. Res*. **2013**, 28, 961-975.

[90]. Garateix, A. *et al*. Antinociception produced by Thalassia testudinum extract BM-21 is mediated by the inhibition of acid sensing ionic channels by the phenolic compound thalassiolin B. *Mol. Pain* **2011**, 7, 10.

[91]. Dubinnyi, M.A. *et al.* Lignan from thyme possesses inhibitory effect on ASIC3 channel current. *J. Biol. Chem*. **2012**, 287, 32993-33000.

[92]. Wu, Y.; Qin, D.; Yang, H.; Fu, H. Evidence for the participation of Acid-Sensing Ion Channels (ASICs) in the antinociceptive effect of curcumin in a formalin-induced orofacial inflammatory model. *Cell. Mol. Neurobiol.* **2017**, 37, 635-642.

[93]. Dorofeeva, N.A.; Barygin, O.I.; Staruschenko, A.; Bolshakov, K.V.; Magazanik, L.G. Mechanisms of non-steroid anti-inflammatory drugs action on ASICs expressed in hippocampal interneurons. *J. Neurochem*. **2008**, 106, 429-441.

[94]. Mango, D. *et al*. Electrophysiological and metabolic effects of CHF5074 in the hippocampus: protection against in vitro ischemia. *Pharmacol. Res*. **2014**, 81, 83-90.

[95]. Boiko, N.; Kucher, V.; Eaton, B.A.; Stockand, J.D. Inhibition of neuronal degenerin/epithelial Naþ channels by the multiple sclerosis drug 4-aminopyridine. *J. Biol. Chem*. **2013**, 288, 9418-9427.

[96]. Leng, T.; Lin, J.; Cottrell, J.E.; Xiong, Z.G. Subunit and frequency-dependent inhibition of Acid Sensing Ion Channels by local anesthetic tetracaine. *Mol. Pain* **2013**, 9, 27.

[97]. Lin, J. *et al*. Inhibition of acid sensing ion channel currents by lidocaine in cultured mouse cortical neurons. *Anesth. Analg*. **2011**, 112, 977-981.

[98]. Lei, Z. *et al*. Inhibition of acidsensing ion channel currents by propofol in rat dorsal root ganglion neurons. *Clin. Exp. Pharmacol. Physiol.* **2014**, 41, 295-300.

[99]. Garza, A.; Lopez-Ramirez, O.; Vega, R.; Soto, E. The aminoglycosides modulate the acid-sensing ionic channel currents in dorsal root ganglion neurons from the rat. *J. Pharmacol. Exp. Ther*. **2010**, 332, 489-499.

[100]. Mercado, F. *et al*. Inhibition of peripheral nociceptors by aminoglycosides produces analgesia in inflammatory pain models in the rat. *Inflammation* **2015**, 38, 649-657.

[101]. Li, X. *et al*. Chloroquine impairs visual transduction via modulation of acid sensing ion channel 1a. *Toxicol. Lett*. **2014**, 228, 200-206.

[102]. Wolkenberg, S.E. *et al*. High concentration electrophysiology-based fragment screen: Discovery of novel acid-sensing ion channel 3 (ASIC3) inhibitors. *Bioorg. Med. Chem. Lett*. **2011**, 21, 2646-2649.

[103]. Kuduk, S.D. *et al*. Identification of non-amidine inhibitors of acid-sensing ion channel-3 (ASIC3). *Bioorg. Med. Chem. Lett*. **2011**, 21, 4255-4258.

[104]. Munro, G. *et al*. NS383 selectively inhibits Acid-Sensing Ion Channels containing 1a and 3 subunits to reverse inflammatory and neuropathic hyperalgesia in rats. *CNS Neurosci. Ther*. **2016**, 22, 135-145.

[105]. Waldmann, R.; Champigny, G.; Voilley, N.; Lauritzen, I.; Lazdunski, M. The mammalian degenerin MDEG, an amiloride-sensitive cation channel activated by mutations causing neurodegeneration in Caenorhabditis elegans. *J. Biol. Chem*. **1996**, 271, 10433-10436.

[106]. Kleyman, T.R.; Cragoe Jr., E.J. Amiloride and its analogs as tools in the study of ion transport. *J. Membr. Biol*. **1988**, 105, 1-21.

[107]. Adams, C.M.; Snyder, P.M.; Welsh, M.J. Paradoxical stimulation of a DEG/ENaC channel by amiloride. *J. Biol. Chem*. **1999**, 274, 15500-15504.
[108]. Kellenberger, S.; Gautschi, I.; Schild, L. Mutations in the epithelial Na^+ channel ENaC outer pore disrupt amiloride block by increasing its dissociation rate. *Mol. Pharmacol*. **2003**, 64, 848-856.
[109]. Li, W.G.; Yu, Y.; Huang, C.; Cao, H.; Xu, T.L. Nonproton ligand sensing domain is required for paradoxical stimulation of acid-sensing ion channel 3 (ASIC3) channels by amiloride. *J. Biol. Chem*. **2011**, 286, 42635-42646.
[110]. Arun, T. *et al*. Targeting ASIC1 in primary progressive multiple sclerosis: evidence of neuroprotection with amiloride. *Brain* **2013**, 136, 106–115.
[111]. McKee, J.B. *et al*. Amiloride clinical trial in optic neuritis (ACTION) protocol: a randomised, double blind, placebo controlled trial. *BMJ Open* **2015**, 5, e009200.
[112]. Jeong, S.; Lee, S.H.; Kim, Y.O.; Yoon, M.H. Antinociceptive effects of amiloride and benzamil in neuropathic pain model rats. *J. Korean Med. Sci*. **2013**, 28, 1238-1243.
[113]. Kuduk, S.D. *et al*. G. Amiloride derived inhibitors of acid-sensing ion channel-3 (ASIC3). *Bioorg. Med. Chem. Lett*. **2009**, 19, 2514-2518.
[114]. Yu, Y. *et al.* A nonproton ligand sensor in the acid-sensing ion channel. *Neuron* **2010**, 68, 61-72.
[115]. Yu, Y. *et al*. Atomic level characterization of the nonproton ligand-sensing domain of ASIC3 channels. *J. Biol. Chem*. **2011**, 286, 24996-25006.
[116]. Alijevic, O.; Kellenberger, S. Subtype-specific modulation of acid-sensing ion channel (ASIC) function by 2-guanidine-4-methylquinazoline. *J. Biol. Chem*. **2012**, 287, 36059-36070.
[117]. Agharkar, A.S.; Gonzales, E.B. 4-Chlorophenylguanidine is an ASIC3 agonist and positive allosteric modulator. *J. Pharm. Sci*. **2017**, 133, 184-186.
[118]. Ugawa, S.; Ishida, Y.; Ueda, T.; Inoue, K.; Nagao, M.; Shimada, S. Nafamostat mesilate reversibly blocks acid-sensing ion channel currents. *Biochem. Biophys. Res. Commun*. **2007**, 363, 203-208.
[119]. Dube, G.R. *et al*. Electrophysiological and in vivo characterization of A-317567, a novel blocker of acid sensing ion channels. *Pain* **2005**, 117, 88-96.
[120]. Coryell, M.W. *et al*. Acid-sensing ion channel-1a in the amygdala, a novel therapeutic target in depression-related behavior. *J. Neurosci*. **2009**, 29, 5381-5388.
[121]. Kuduk, S.D. *et al*. Synthesis, structure-activity relationship, and pharmacological profile of analogs of the ASIC-3 inhibitor A-317567. *ACS Chem. Neurosci*. **2010**, 1, 19-24.
[122]. Kuduk, S.D. *et al*. Amidine derived inhibitors of acidsensing ion channel-3 (ASIC3). *Bioorg. Med. Chem. Lett*. **2009**, 19, 4059-4063.
[123]. Chen, X. *et al*. Diarylamidines: high potency inhibitors of acid-sensing ion channels. *Neuropharmacology* **2010**, 58, 1045-1053.
[124]. Schmidt, A.; Rossetti, G.; Joussen, S.; Grunder, S. Diminazene is a slow pore blocker of Acid-Sensing Ion Channel 1a (ASIC1a). *Mol. Pharmacol*., **2017**, 92, 665-675.
[125]. Werbovetz, K. Diamidines as antitrypanosomal, antileishmanial and antimalarial agents. *Curr. Opin. Investig. Drugs* **2006**, 7, 147–157.
[126]. Wenzler, T.; Boykin, D.W.; Ismail, M.A.; Hall, J.E.; Tidwell, R.R.; Brun, R. New treatment option for second-stage African sleeping sickness: in vitro and in vivo efficacy of aza analogs of DB289. *Antimicrob. Agents Chemother*. **2009**, 53, 4185–4192.
[127]. Chen, X.; Orser, B.A.; MacDonald, J.F. Design and screening of ASIC inhibitors based on aromatic diamidines for combating neurological disorders. *Eur. J. Pharmacol*. **2010**, 648, 15−23.
[128]. "The Nobel Prize in Physiology or Medicine 1991 was awarded jointly to Erwin Neher and Bert Sakmann "*for their discoveries concerning the function of single ion channels in cells*". nobelprize.org. Nobel Media AB.

[129]. Neher, E.; Sakmann, B.; Steinbach, J.H. The extracellular *patch clamp*: A method for resolving currents through individual open channels in biological membranes. *Pfluegers Arch*., **1978**, 375, 219–228.

[130]. Kodandaramaiah, S.B.; Talei Franzesi, G.; Chow, B.Y.; Boyden, E.S.; Forest, C.R. Automated whole-cell patch clamp electrophysiology of neurons in vivo. *Nat. Methods* **2012**, 9, 585-587.

[131]. Thomas, P.; Smart, T.G. HEK293 cell line: a vehicle for the expression of recombinant proteins. *J. Pharmacol. Toxicol. Methods*, **2005**, 51, 187-200.

[132]. Gunthorpe, M.J.; Smith, G.D.; Davis, J.B.; Randall, A.D. Characterisation of a human acid-sensing ion channel (hASIC1a) endogenously expressed in HEK293 cells. *Pflugers Arch*., **2001**, 442, 668-674.

[133]. Gonzales, E.B.; Kawate, T.; Gouaux, E. Pore architecture and ion sites in acidsensing ion channels and P2X receptors. *Nature* **2009**, 460, 599-604.